EMERGING INFECTIOUS DISEASES®

EDITOR-IN-CHIEF
D. Peter Drotman

EMERGING INFECTIOUS DISEASES®

Zoonotic Infections

December 2024

Research

On the Cover

Unknown artist, *Tomb painting identified as Nebamun Fowling in the Marshes* **fragment (circa 1350 BCE).** Painted plaster, 38.6 in × 38.6 in × 8.7 in/98 cm × 98 cm × 22 cm. © Trustees of the British Museum, London, United Kingdom. Shared under a Creative Commons Attribution-NonCommercial-ShareAlike 4.0 International (CC BY-NC-SA 4.0) license.

About the Cover p. 2706

Perspective

Synopses

2459

Dogs as Reservoirs for *Leishmania donovani*, Bihar, India, 2018–2022

A.K. Kushwaha et al.

Dispatches

2513

Research Letters

Comment Letter

EMERGING INFECTIOUS DISEASES®

December 2024

Emerging Infections Network Letter

Books and Media

About the Cover

Online Report

Thank You EID Reviewers
We couldn't do it without your support.

We only maintain high standards because of your support.

EID's 2024 Impact Factor of 7.2 ranked it 10th among open-access infectious disease journals and 4th out of 132 infectious disease journals.

The Google Scholar h-Index is 114; 2nd of top 20 publications in Epidemiology and 2nd among open-access journals; ranked 6th among top 20 publications in Communicable Diseases and 2nd among open-access journals.

The electronic table of contents goes to 53,109 subscribers each month.

All articles published in the *Emerging Infectious Diseases* journal are peer-reviewed by volunteers from around the globe, enabling us to bring you high-quality content about new and emerging infectious diseases and trends world-wide.

A list of reviewers is posted at
http://wwwnc.cdc.gov/eid/page/reviewers

●DPDx
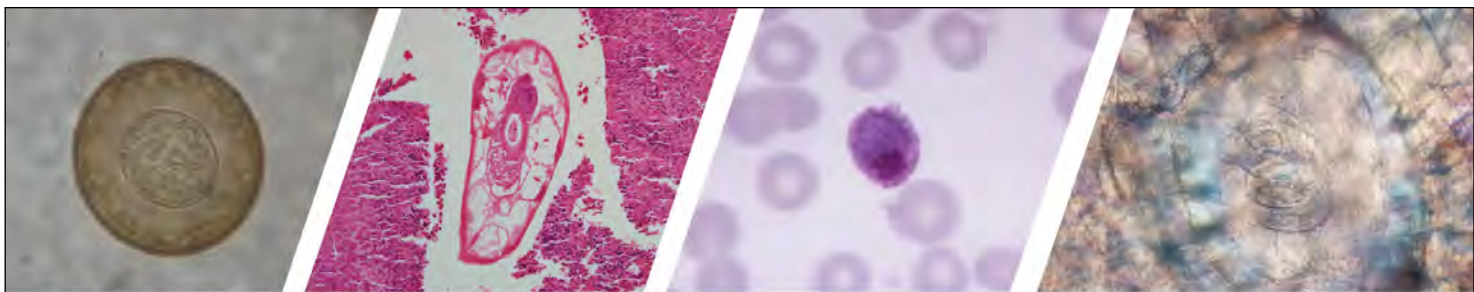
Diagnostic Assistance and Training in Laboratory Identification of Parasites

A free service of CDC available to laboratorians, pathologists, and other health professionals in the United States and abroad

Diagnosis from photographs of worms, histological sections, fecal, blood, and other specimen types

Expert diagnostic review

Formal diagnostic laboratory report

Submission of samples via secure file share

Visit the DPDx website for information on laboratory diagnosis, geographic distribution, clinical features, parasite life cycles, and training via Monthly Case Studies of parasitic diseases.

www.cdc.gov/dpdx
dpdx@cdc.gov

U.S. Department of Health and Human Services
Centers for Disease
Control and Prevention

Homelessness and Organ Donor–Derived *Bartonella quintana* Infection

Rachel Henderson, Emily Mosites, Jane E. Koehler, Carl Boodman, Grace E. Marx

Louseborne *Bartonella quintana* infections in the United States occur almost exclusively among persons experiencing homelessness because of inadequate access to hygiene resources. Homelessness is increasing, and persons experiencing homelessness can be organ donors, despite barriers to receiving donated organs themselves. Recent reports have documented *B. quintana* transmission via organs transplanted from donors who had recently experienced homelessness. Those reports demonstrate the threat of severe bartonellosis in immunosuppressed organ transplant recipients after donor-derived *B. quintana* infection. Addressing the root causes of *B. quintana* transmission could improve the quality of life for persons experiencing homelessness and simultaneously mitigate risk for donor-derived *B. quintana* transmission. Interventions include improved access to housing, consistent access to hot water for showers and laundry, early treatment of body lice infestation and *B. quintana* infection, and *B. quintana* testing and prophylactic treatment of recipients of organs from donors who have experienced risk factors for *B. quintana*, including homelessness.

*B*artonella quintana is a re-emerging, louseborne pathogen that can be insidious because of diverse clinical manifestations, laboratory diagnostic challenges, and disproportionate effects on marginalized populations that face substantial barriers to obtaining adequate healthcare. After *B. quintana* infection is diagnosed, treatment can be complex and costly, consisting of extended courses of antimicrobial drugs and sometimes requiring surgical intervention (e.g., cases of infective endocarditis). With increasing availability of molecular diagnostic tests that can identify *B. quintana*, outbreaks and infections have been detected with increasing frequency (1–7) among persons experiencing homelessness (PEH) and, more recently, among organ transplant recipients (8).

B. quintana is transmitted by human body lice (Figure 1), which can live in the clothing of persons who lack regular access to hygiene resources. In the United States, *B. quintana* infection occurs almost exclusively among PEH. Because the number of persons experiencing housing instability is increasing (9,10), the number of organ donors recently or currently experiencing homelessness at the time of death is also likely to rise (11). Housing status is not included in donor registries (12); thus, the frequency of homelessness among deceased organ donors is unknown. However, organ donors are often young persons who have experienced sudden and traumatic deaths; and because persons with housing instability experience disproportionate rates of physical trauma, opioid overdose, and early death (13), they may also be more likely than members of the general population to become organ donors.

Beeson et al. describe an intensive investigation into *B. quintana* infections resulting from donor organ–derived transmission to 2 kidney recipients (14). In Canada, 6 confirmed cases of donor organ–derived transmission of *B. quintana* from donors with a history of experiencing homelessness were also recently reported (8). Those cases show that *B. quintana* transmission via organ donation can cause severe disease, probably because of the high level of immunocompromise resulting from medications designed to prevent organ rejection.
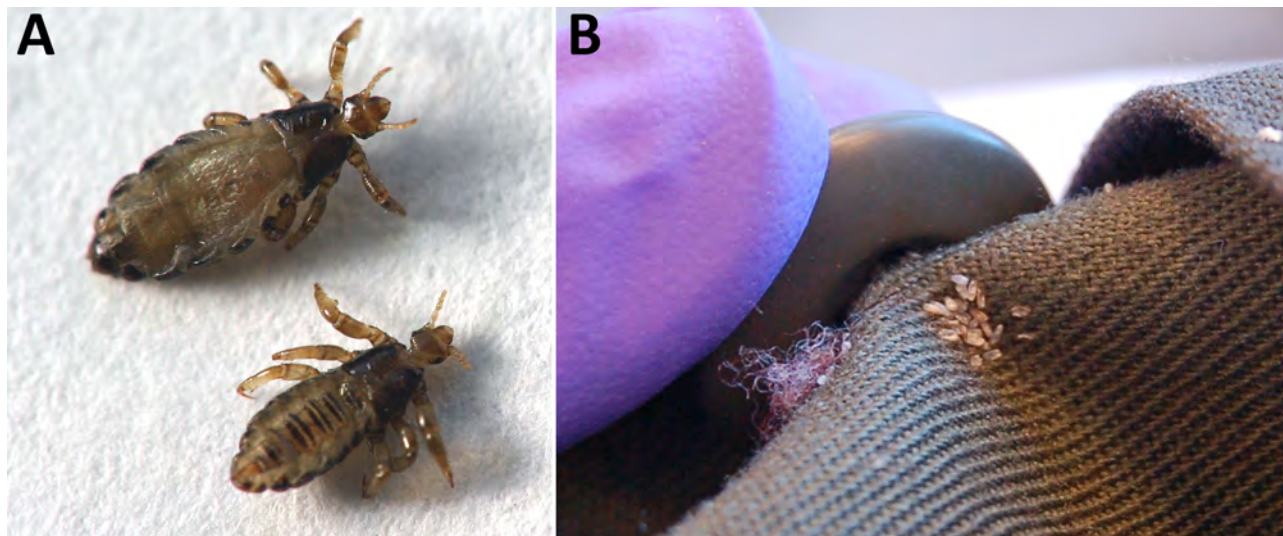
Figure 1. Dimorphous *Pediculus humanus humanus* (human body louse). A) The female adult (top) is larger than the male adult (bottom). B) Eggs, also known as nits, observed behind a coat button. Photographs courtesy of Denise Bonilla and the California Department of Public Health.

Opportunities for prevention and early diagnosis can be identified by analysis of homelessness epidemiology, body lice ecology, and *B. quintana* transmission dynamics. We closely examined those factors to determine specific strategies to reduce body louse infestation among PEH; promote early recognition, detection, and treatment of *B. quintana* infection among PEH; and mitigate transmission risk to organ recipients.

Epidemiology of Homelessness in the United States

Since 2016, homelessness has increased in the United States, driven in part by increasing housing costs, the COVID-19 pandemic, and the opioid epidemic. The US Department of Housing and Urban Development (HUD) estimates that, on a single night in 2022, approximately 582,500 persons in the United States were experiencing homelessness; 40% of those were experiencing unsheltered homelessness in cars, tents, abandoned buildings, the street, or in other places not intended for human habitation (10). The HUD estimate of homelessness prevalence does not include persons with unstable housing who were able to stay with friends or relatives, sometimes called doubling up or couch-surfing, which has also been on the rise (9).

Homelessness is a nationwide issue; however, ≈20% of PEH in the United States live in New York, New York, or Los Angeles, California (10). The experience of homelessness differs by geographic area; sheltered homelessness is most common in New York, and unsheltered homelessness is more common in Los Angeles (10).

In the United States, PEH are most often cisgender men; rates of homelessness are almost twice as high among men than women (9). In 2022, approximately 1.1% of all PEH reported a gender other than cisgender (10,15); proportions among youth experiencing homelessness were higher (15). Rates of homelessness among many minority groups in the United States are disproportionate. The highest rates of homelessness among persons of any race/ethnicity are among persons who identify as Native Hawaiian/Pacific Islander (160/10,000 population), American Indian/Alaska Native (67/10,000 population), or Black/African American (55/10,000 population); nearly 40% of PEH identify as Black/African American (9). Hispanic/Latinx persons are also disproportionately affected, representing nearly one quarter of PEH in 2022, an increase from prior years (10). Barriers to adequate housing may be further amplified by intersectionality of those characteristics (e.g., when an individual's race/ethnicity coincides with nonconforming gender or sexual orientation).

Homelessness is strongly associated with substance use (16). In the ongoing opioid epidemic, driven by readily available, highly potent synthetic opioids (e.g., fentanyl), drug overdose has become the leading cause of death among PEH (17). In Los Angeles, drug overdose accounted for 37% of all deaths among PEH in 2020 and 2021, outpacing other causes (e.g., coronary artery disease) (18).

Homelessness has well-documented adverse effects on health (19–21), resulting from structural and social barriers to healthcare, nutrition, and safe

environments. Barriers are exacerbated by discrimination and stigma against PEH. Lack of consistent access to basic services, resources, and safety can result in inconsistent showering and laundering, which creates a risk for body lice infestation (*22,23*), which directly contributes to the greatly disproportionate rate of *B. quintana* infection and disease in PEH.

Body Lice Ecology and Transmission Dynamics

Body lice (*Pediculus humanus humanus*), unlike the more common head lice, are not found directly attached to the human host; instead, body lice live on clothing, which provides easy proximity to human skin for frequent blood meals. Ideal conditions for body lice are 79%–90% humidity and 29°C–32°C (84.2°F –89.6°F) temperature, conditions that are often found in clothing next to human skin. Body lice cannot survive humidity <40% or temperatures >50°C (122°F) (*24*) and thus are easily killed when clothing is laundered in hot water (typically 60°C [160°F]). Adult body lice (Figure 1, panel A) live for weeks to months but can survive for only 2 days without a blood meal (*24*). They cement their eggs, also known as nits, to clothing fibers or seams (Figure 1, panel B), and the eggs hatch after 8–10 days (*24*). Body lice spread person to person through direct close contact or by shared infested clothing or bedding; dense living quarters with infrequent showering and clothes laundering present an ideal setting for body lice transmission.

Body lice are competent vectors of several bacterial pathogens, including *B. quintana*, *Rickettsia prowazekii* (the cause of epidemic typhus), and *Borrelia recurrentis* (the cause of louseborne relapsing fever). Humans are the primary reservoirs of *B. quintana*; a body louse becomes infected after taking a blood meal from a bacteremic human host. After infection, exponential replication occurs in the louse gut; up to 10^7 *B. quintana* bacteria have been shown to be excreted in the feces of 1 louse in 1 day (*25*). An infected body louse remains infectious for its lifespan; louse feces can remain infectious for up to 1 year (*26*). When the infected body louse takes blood meals, which they do 1–5 times each day, they defecate and leave feces with high quantities of viable *B. quintana* near the bite site (*25*). A person becomes infected from inoculation of infectious louse feces through skin lesions or mucosal surfaces (*24,27*). The bite of a human body louse causes an intensely pruritic rash; scratching increases inoculation risk via the introduction of infected feces into abraded skin. *B. quintana* bacteremia in humans is often asymptomatic and chronic; durations of up to

8 years have been documented (*26*). Asymptomatic *B. quintana* bacteremia can result in further transmission to biting body lice and subsequent transmission to other persons, as well as increased risk of developing end-organ damage, including endocarditis (*28*).

Asking patients about itchy skin and bug bites can be helpful questions when screening for body lice infestation. Careful inspection of clothing may reveal visible body lice, nymphs, nits, or feces in the interior seams of clothing. A thorough dermatologic examination often reveals erythematous papules and papular urticaria, typically concentrated on the trunk where lice-infested clothing is in direct contact with the skin. Because of the severe pruritis, extensive excoriations are common and severe, and chronic infestation can lead to postinflammatory increased pigmentation and skin thickening (*24*). In addition to bacterial infections transmitted by body lice, severe infestation can also result in iron deficiency anemia and eosinophilia (*24,29*).

Body lice infestations occur among persons in crowded living situations who lack access to hygiene resources. PEH often lack consistent access to hot water for bathing and laundry, which are the primary tools for preventing and treating body lice infestation (*30–32*). Homeless shelters are often crowded, increasing risk for close person-to-person contact, which promotes body lice transmission. Some PEH may receive donated clothing and bedding, which are not always washed with hot water before distribution (*31*). Sharing of resources such as clothing and bedding by PEH further increases risk for spread of body lice. Mental health and substance use conditions may also be barriers to accessing laundry and bathing facilities, even when they are available (*33*). Additional barriers may be other social factors (e.g., risk for personal violence or theft of possessions while accessing bathing or laundry facilities). Combined, those factors result in inadequate personal hygiene practices among PEH, perpetuating disproportionate lice infestation and louseborne disease. One study in San Francisco, California, reported finding body lice infestations in nearly 30% of PEH (*30*). Another study in Marseille, France, found that body lice infestation was associated with 2.75 (95% CI 1.14–6.65) increased odds for *B. quintana* bacteremia (*34*).

B. quintana Epidemiology and Clinical Overview

Molecular evidence indicates that *B. quintana* has infected humans for ≥4,000 years (*35*). First recognized around 1914 during World War I, *B. quintana* infection was primarily known as trench fever or quintan (5-day) fever, an acute syndrome of fever

lasting 1–5 days and recurring at 5-day intervals, accompanied by shin pain, fatigue, headache, and splenomegaly. During World War I, trench fever was estimated to have affected more than 1 million troops (*36*). For most of the 20th century, trench fever was considered a disease of wartime or humanitarian crises, and outbreaks occurred again during World War II (*22,28*). The body louse was identified as the vector of *B. quintana* in the mid-1920s (*22*), but it was not until 1961 that the gram-negative bacterium was successfully isolated in culture (*22,28*). Since its initial recognition, the bacterium has been reclassified several times; initially known as *Rickettsia quintana*, its name was later changed to *Rochalimaea quintana* and then, in 1993, to the current *Bartonella quintana.*

Until the 1980s, *B. quintana* was only known to cause trench fever, the acute symptomatic disease with a relapsing fever pattern, the likely result of an intraerythrocytic phase of infection followed by periodic erythrocyte rupture (*27,37*). In the early years of the HIV/AIDS epidemic, however, *B. quintana* and the closely related species *B. henselae* were identified as the cause of bacillary angiomatosis, causing extremely vascular lesions of the skin. In addition, *B. henselae* was identified as the sole species causing peliosis hepatis, resulting in highly vascular lesions in the liver. Both of those novel vascular proliferative lesions occurred among persons living with advanced immunosuppression caused by AIDS (*38*). In the 1990s, a diverse array of clinical manifestations from *B. quintana* infection were identified, including subacute endocarditis and chronic bacteremia, which disproportionately occurred among PEH who did not have known HIV infection or other immunodeficiency (*39–40*). The prevalence of asymptomatic bacteremia is unknown because of limitations of diagnosis and underreporting, but bacteremia durations of months to years have been described (*26*).

Because *B. quintana* infection is not a nationally reportable condition, most of what is known about its current epidemiology is based on seroprevalence studies. US studies conducted since 1996 have reported *B. quintana* seropositivity rates among PEH of 5%–15% (*1,2,41*). In recent years, outbreaks and *B. quintana* seropositivity have been documented among PEH in geographically diverse urban areas of the United States, including Denver, Colorado (*1,3*); Anchorage, Alaska (*4*); Seattle, Washington (*2*); San Francisco, California (*6*); Baltimore, Maryland (*7*); New York, New York (*42*); and Washington, DC (*5*). Cases have also been reported in Canada (*43*).

Independent risk factors for *B. quintana* seropositivity identified among PEH include duration of homelessness >1 year, age >40 years, and alcohol use disorder (*44*). Intravenous drug use has been identified as another potential risk factor; *B. quintana* seropositivity among persons who use intravenous drugs, irrespective of homelessness, has been reported as 2%–10% in the United States (*7,45*). However, a notable limitation of those serologic studies is the potential for cross-reactivity with antibodies to other bacteria, including other *Bartonella* spp., *Chlamydia* spp., and *Coxiella burnetii* (*46*).

B. quintana is challenging to grow in bacterial culture because it is slow growing (doubling time is ≈21 hours) (*25*) and requires special conditions. When *B. quintana* is suspected, cultures should be held for a minimum of 14 days, much longer than the typical 5-day incubation period for bacterial cultures (*3*). Until recently, serologic assays provided the primary diagnostic approach for detection of *B. quintana* infection, despite challenges with specificity. The most common serologic assay, an indirect immunofluorescent antibody assay, is also limited by low throughput. Although PCR diagnosis was described as early as 1994, molecular diagnosis for detection of *B. quintana* has only recently become more widely available for clinical diagnosis (*39,47*). In a 2023 study describing 430 cases of *Bartonella* spp. infection diagnosed by molecular methods, 15% were positive for *B. quintana*; of those, 82% were in male patients (compared with 18% in female patients), and 83% were in persons 18–65 years of age (*39*). Cell-free DNA testing has also recently emerged as a promising diagnostic tool for detecting *B. quintana* (*48*).

After *B. quintana* infection is known or suspected, treatment typically consists of doxycycline or macrolide antimicrobial therapy for 4–6 weeks, although high-quality evidence for the optimal antimicrobial regimen and duration is still needed. Effective treatment of endocarditis and bacteremia may require months of multiple antimicrobial drugs and should include doxycycline or a macrolide (both bacteriostatic) with the addition of a bactericidal drug such as rifampin (*49,50*). Surgical cardiac valve replacement is often necessary for cases of endocarditis (*51*), which often affects normal valves. Definitive treatment also requires controlling any ongoing body lice infestation to prevent reinfection and further transmission.

B. quintana Prevention, Screening, and Early Treatment

Body lice infestation and *B. quintana* infection and disease can be prevented by promoting universal

housing, increasing access to showers and laundry with hot water, and identifying patients at risk for infection so they can receive early diagnosis and treatment (Figure 2). Public health and clinical professionals have an opportunity to implement those interventions for PEH, the group at highest risk for disease and often from marginalized and minority groups, as well as for organ transplant recipients, who are often uniquely vulnerable to severe disease because of immunosuppressive treatment.

An ethical discussion of whether PEH should be organ donors is ongoing; by current transplant protocols, PEH are usually not considered for receipt of transplanted organs (*11*). Although the proportion of organ donors with a history of homelessness is unknown, PEH currently donate organs for transplantation in the United States; thus, risk for *B. quintana* transmission through organ transplantation should be recognized and mitigated.

With the guiding principles of primary prevention, health equity, and risk mitigation, we make the following calls to action (Figure 3):

Homeless service systems
- Ensure that PEH have consistent, low-barrier access to basic hygiene services, including laundry and showers with hot water. Hygiene services should be offered with dignity and respect while addressing potential challenges of mental health conditions, substance use, risk for sexual violence, and the risk of losing one's belongings or shelter.
- Launder donated clothing and bedding with hot water before distribution to PEH.
- For PEH with body lice infestation, offer a hot shower and a clean change of clothing and bedding. Exercise contact precautions when handling used clothing or bedding to limit infection transmission risk. In general, shelter, resources, and services should not be withheld because of body lice infestation, which is both preventable and treatable.
- Consider referring clients with body louse infestation to health services for *B. quintana* screening and facilitate access to treatment, if possible.

Clinicians
- Ask all patients about current and previous housing status. Housing status should be systematically entered into medical records.
- Evaluate PEH for body lice infestation in a respectful way by asking a screening question about itchy skin and performing a physical examination. If itching is reported or if

excoriations are observed, obtain consent to examine clothing for evidence of body lice. Exercise contact precautions when examining patients with lice infestation to limit infection transmission risk. Treat body lice infestations promptly by coordinating access to a hot shower and a clean change of clothing/bedding.
- Consider testing for *B. quintana* in patients who have evidence of body lice infestation or a history of homelessness and symptoms compatible with *B. quintana* infection. Note: Diagnostic testing for *B. quintana* includes bacterial culture with prolonged incubation time (minimum 14 days), serology, and molecular diagnostic methods (e.g., PCR or microbial cell-free DNA testing).
- Consider empiric treatment or prophylaxis for *B. quintana* for recipients of organs donated by persons with untreated *B. quintana* infection or
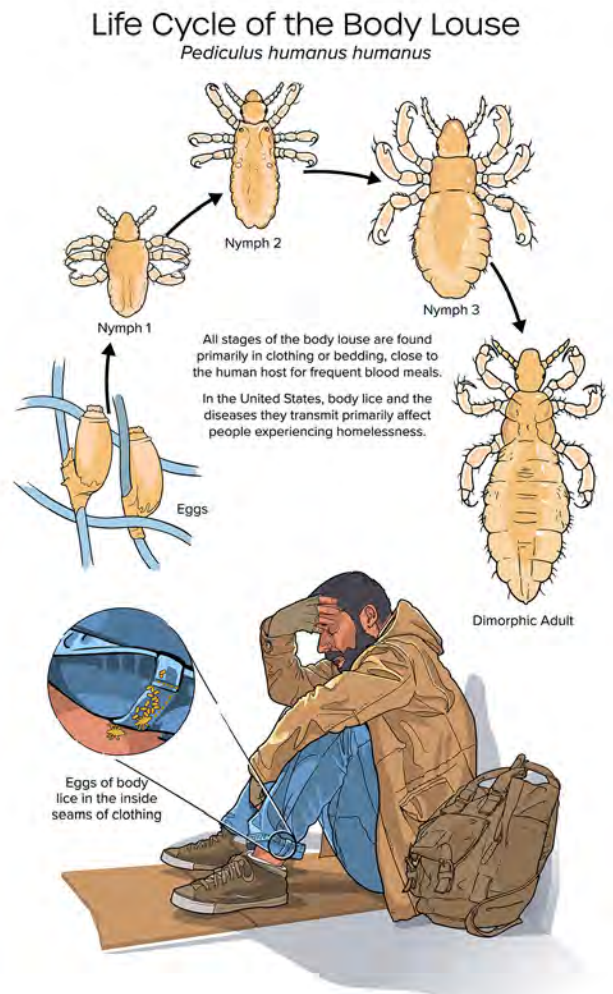
Figure 2. Life cycle of the human body louse (*Pediculus humanus humanus*).

I. Prevent and treat body lice

by persons with a history of homelessness and unknown *B. quintana* infection status.
- Treat all patients with *B. quintana* infection, even if asymptomatic, in consultation with an infectious disease physician.

Organ donor organizations
- Ask all potential organ donors and donor next of kin (for deceased donors) about current and previous housing status in a respectful and dignified way. Housing status should be systematically entered into medical records and reported by regional transplantation organizations.
- Consider screening all organ donors with a known history of homelessness for *B. quintana* and report test result to appropriate public health and medical organizations. Note: Diagnostic testing for *B. quintana* includes bacterial culture with prolonged incubation time (minimum 14 days), serology, and molecular diagnostic methods (e.g., PCR or microbial cell-free DNA testing).

With implementation of the strategies outlined, rates of body lice infestation and bartonellosis from *B. quintana* infection would decrease among PEH and among organ transplant recipients. A future without *B. quintana* infection is achievable if a cohesive, comprehensive approach is adopted that prioritizes universal access to basic hygiene resources.

About the Author

Ms. Henderson is a fourth-year medical student at the University of Colorado School of Medicine. Her primary research focus is on health equity and vectorborne disease prevention among PEH.

Figure 3. Conceptual framework for reducing transmission of *Bartonella quintana* in the United States among PEH and among organ transplant recipients through universal access to hygiene services, prevention and treatment of body lice infestation, and early diagnosis and treatment of *B. quintana* infection. Diagnostic testing for *B. quintana* includes bacterial culture with prolonged incubation time (minimum 14 days), serology, and molecular diagnostic methods (e.g., PCR or microbial cell-free DNA testing). PEH, persons experiencing homelessness.

References
1. McCormick DW, Rowan SE, Pappert R, Yockey B, Dietrich EA, Petersen JM, et al. *Bartonella* seroreactivity among persons experiencing homelessness during an outbreak of *Bartonella quintana* in Denver, Colorado, 2020. Open Forum Infect Dis. 2021;8:ofab230. https://doi.org/10.1093/ofid/ofab230
2. Jackson LA, Spach DH, Kippen DA, Sugg NK, Regnery RL, Sayers MH, et al. Seroprevalence to *Bartonella quintana* among patients at a community clinic in downtown Seattle. J Infect Dis. 1996;173:1023–6. https://doi.org/10.1093/infdis/173.4.1023

3. Shepard Z, Vargas Barahona L, Montalbano G, Rowan SE, Franco-Paredes C, Madinger N. *Bartonella quintana* infection in people experiencing homelessness in the Denver Metropolitan Area. J Infect Dis. 2022;226(Suppl 3):S315–21. https://doi.org/10.1093/infdis/jiac238

4. State of Alaska Epidemiology. *Bartonella quintana* endocarditis following body louse exposure, Anchorage [cited 2024 Jan 12]. https://epi.alaska.gov/bulletins/docs/b2016_11.pdf

5. Ghidey FY, Igbinosa O, Mills K, Lai L, Woods C, Ruiz ME, et al. Case series of *Bartonella quintana* blood culture-negative endocarditis in Washington, DC. JMM Case Rep. 2016;3:e005049. https://doi.org/10.1099/jmmcr.0.005049

6. Bonilla DL, Kabeya H, Henn J, Kramer VL, Kosoy MY. *Bartonella quintana* in body lice and head lice from homeless persons, San Francisco, California, USA. Emerg Infect Dis. 2009;15:912–5. https://doi.org/10.3201/eid1506.090054

7. Comer JA, Flynn C, Regnery RL, Vlahov D, Childs JE. Antibodies to *Bartonella* species in inner-city intravenous drug users in Baltimore, Md. Arch Intern Med. 1996;156:2491–5. https://doi.org/10.1001/archinte.1996.00440200111014

8. Kabbani D, Orenbuch-Harroch E, Boodman C, Broad S, Paz-Infanzon M, Belga S, et al. Donor-derived bartonellosis in solid organ transplant recipients from unhoused donors in Alberta. Am J Transplant. 2024 Sep 24:S1600-6135(24)00595-1 [Epub ahead of print].

9. HUD Exchange. PIT and HIC data since 2007 [cited 2023 Oct 29]. https://www.hudexchange.info/resource/3031/pit-and-hic-data-since-2007

10. de Sousa T, Andrichik A, Cuellar M, Marson J, Prestera E, Rush K. The 2022 Annual Homelessness Assessment Report part 1: point-in-time estimates of homelessness, December 2022. Washington (DC): US Department of Housing and Urban Development; 2022.

11. Warman A, Sparber L, Molmenti AH, Molmenti EP. Homelessness, organ donation, transplantation, and a call for equity in the United States. Lancet Reg Health Am. 2023;22:100523. https://doi.org/10.1016/j.lana.2023.100523

12. Organ Procurement and Transplantation Network Build advanced [cited 2024 Jun 6]. https://optn.transplant.hrsa.gov/data/view-data-reports/build-advanced

13. Roncarati JS, Baggett TP, O'Connell JJ, Hwang SW, Cook EF, Krieger N, et al. Mortality among unsheltered homeless adults in Boston, Massachusetts, 2000–2009. JAMA Intern Med. 2018;178:1242–8. https://doi.org/10.1001/jamainternmed.2018.2924

14. Beeson AM, Rich SN, Russo ME, Bhatnagar J, Kumar RN, Ritter JM, et al. *Bartonella quintana* transmission by kidney transplantation to two recipients from a donor experiencing homelessness. Emerg Infect Dis. 2024;30:2467–2475.

15. DeChants JP, Green AE, Price MN, Davis CK. Homelessness and housing instability among LGBTQ youth [cited 2023 Oct 8]. https://www.thetrevorproject.org/research-briefs/homelessness-and-housing-instability-among-lgbtq-youth-feb-2022

16. Liu M, Koh KA, Hwang SW, Wadhera RK. Mental health and substance use among homeless adolescents in the US. JAMA. 2022;327:1820–2. https://doi.org/10.1001/jama.2022.4422

17. Fine DR, Dickins KA, Adams LD, De Las Nueces D, Weinstock K, Wright J, et al. Drug overdose mortality among people experiencing homelessness, 2003 to 2018. JAMA Netw Open. 2022;5:e2142676. https://doi.org/10.1001/jamanetworkopen.2021.42676

18. Los Angeles County Department of Public Health, Center for Health Impact Evaluation. Mortality rates and causes of death among people experiencing homelessness in Los Angeles County: 2014–2021 [cited 2024 Jan 14]. http://publichealth.lacounty.gov/chie/reports/Homeless_Mortality_Report_2024.pdf

19. Mosites E, Hughes L, Butler JC. Homelessness and infectious diseases: understanding the gaps and defining a public health approach: introduction. J Infect Dis. 2022;226(Suppl 3):S301–3. https://doi.org/10.1093/infdis/jiac352

20. Fazel S, Geddes JR, Kushel M. The health of homeless people in high-income countries: descriptive epidemiology, health consequences, and clinical and policy recommendations. Lancet. 2014;384:1529–40. https://doi.org/10.1016/S0140-6736(14)61132-6

21. Badiaga S, Raoult D, Brouqui P. Preventing and controlling emerging and reemerging transmissible diseases in the homeless. Emerg Infect Dis. 2008;14:1353–9. https://doi.org/10.3201/eid1409.080204

22. Anstead GM. The centenary of the discovery of trench fever, an emerging infectious disease of World War 1. Lancet Infect Dis. 2016;16:e164–72. https://doi.org/10.1016/S1473-3099(16)30003-2

23. Arnaud A, Chosidow O, Détrez M-A, Bitar D, Huber F, Foulet F, et al. Prevalences of scabies and pediculosis corporis among homeless people in the Paris region: results from two randomized cross-sectional surveys (HYTPEAC study). Br J Dermatol. 2016;174:104–12. https://doi.org/10.1111/bjd.14226

24. Fu YT, Yao C, Deng YP, Elsheikha HM, Shao R, Zhu XQ, et al. Human pediculosis, a global public health problem. Infect Dis Poverty. 2022;11:58. https://doi.org/10.1186/s40249-022-00986-w

25. Seki N, Kasai S, Saito N, Komagata O, Mihara M, Sasaki T, et al. Quantitative analysis of proliferation and excretion of *Bartonella quintana* in body lice, *Pediculus humanus* L. Am J Trop Med Hyg. 2007;77:562–6.https://doi.org/10.4269/ajtmh.2007.77.562

26. Kostrzewski J. The epidemiology of trench fever [in undetermined language]. Bull Int Acad Pol Sci Let Cl Med. 1949;7:233–63.

27. Foucault C, Brouqui P, Raoult D. *Bartonella quintana* characteristics and clinical management. Emerg Infect Dis. 2006;12:217–23. https://doi.org/10.3201/eid1202.050874

28. Jacomo V, Kelly PJ, Raoult D. Natural history of *Bartonella* infections (an exception to Koch's postulate). Clin Diagn Lab Immunol. 2002;9:8–18.

29. Rudd N, Zakaria A, Kohn MA, Amerson EH, Fox LP, Linos E, et al. Association of body lice infestation with hemoglobin values in hospitalized dermatology patients. JAMA Dermatol. 2022;158:691–3. https://doi.org/10.1001/jamadermatol.2022.0818

30. Bonilla DL, Cole-Porse C, Kjemtrup A, Osikowicz L, Kosoy M. Risk factors for human lice and bartonellosis among the homeless, San Francisco, California, USA. Emerg Infect Dis. 2014;20:1645–51. https://doi.org/10.3201/eid2010.131655

31. Rich SN, Carpenter A, Dell B, Henderson R, Adams S, Bestul N, et al. Knowledge and practices related to louse- and flea-borne diseases among staff providing services to people experiencing homelessness in the United States. Zoonoses Public Health. 2024;71:642–52. https://doi.org/10.1111/zph.13125

32. Marshall KE, Martinez HE, Woodall T, Guerrero A, Mechtenberg J, Herlihy R, et al. Body lice among people experiencing homelessness and access to hygiene services during the COVID-19 pandemic - preventing trench fever in

Denver, Colorado, 2020. Am J Trop Med Hyg. 2022;107:427–32. https://doi.org/10.4269/ajtmh.22-0118

33. Paudyal V, MacLure K, Forbes-McKay K, McKenzie M, MacLeod J, Smith A, et al. 'If I die, I die, I don't care about my health': perspectives on self-care of people experiencing homelessness. Health Soc Care Community. 2020;28:160–72. https://doi.org/10.1111/hsc.12850

34. Foucault C, Barrau K, Brouqui P, Raoult D. *Bartonella quintana* bacteremia among homeless people. Clin Infect Dis. 2002;35:684–9. https://doi.org/10.1086/342065

35. Fournier PE, Drancourt M, Aboudharam G, Raoult D. Paleomicrobiology of *Bartonella* infections. Microbes Infect. 2015;17:879–83. https://doi.org/10.1016/j.micinf.2015.09.002

36. Byram W, Lloyd LL. Trench fever. In: Lloyd LL, editor. Lice and their Menace to Man. London: Oxford University Press; 1919. p. 120–30.

37. Angelakis E, Raoult D. Pathogenicity and treatment of *Bartonella* infections. Int J Antimicrob Agents. 2014;44:16–25. https://doi.org/10.1016/j.ijantimicag.2014.04.006

38. Koehler JE, Sanchez MA, Garrido CS, Whitfeld MJ, Chen FM, Berger TG, et al. Molecular epidemiology of *Bartonella* infections in patients with bacillary angiomatosis-peliosis. N Engl J Med. 1997;337:1876–83. https://doi.org/10.1056/NEJM199712253372603

39. McCormick DW, Rassoulian-Barrett SL, Hoogestraat DR, Salipante SJ, SenGupta D, Dietrich EA, et al. *Bartonella* spp. infections identified by molecular methods, United States. Emerg Infect Dis. 2023;29:467–76. https://doi.org/10.3201/eid2903.221223

40. Spach DH, Kanter AS, Dougherty MJ, Larson AM, Coyle MB, Brenner DJ, et al. *Bartonella (Rochalimaea) quintana* bacteremia in inner-city patients with chronic alcoholism. N Engl J Med. 1995;332:424–8.https://doi.org/10.1056/NEJM199502163320703

41. Smith HM, Reporter R, Rood MP, Linscott AJ, Mascola LM, Hogrefe W, et al. Prevalence study of antibody to ratborne pathogens and other agents among patients using a free clinic in downtown Los Angeles. J Infect Dis. 2002;186:1673–6. https://doi.org/10.1086/345377

42. Rich SN, Beeson A, Seifu L, Mitchell K, Wroblewski D, Juretschko S, et al. Notes from the field: Severe *Bartonella quintana* infections among persons experiencing unsheltered homelessness—New York City, January 2020–December 2022. MMWR Morb Mortal Wkly Rep. 2023;72:1147–8. https://doi.org/10.15585/mmwr.mm7242a3

43. Boodman C, Wuerz T, Lagacé-Wiens P, Lindsay R, Dibernardo A, Bullard J, et al. Serologic testing for *Bartonella* in Manitoba, Canada, 2010-2020: a retrospective case series. CMAJ Open. 2022;10:E476–82. https://doi.org/10.9778/cmajo.20210180

44. Mai BHA. Seroprevalence of *Bartonella quintana* infection: a systematic review. J Glob Infect Dis. 2022;14:50–6. https://doi.org/10.4103/jgid.jgid_220_21

45. Comer JA, Diaz T, Vlahov D, Monterroso E, Childs JE. Evidence of rodent-associated *Bartonella* and *Rickettsia* infections among intravenous drug users from Central and East Harlem, New York City. Am J Trop Med Hyg. 2001;65:855–60. https://doi.org/10.4269/ajtmh.2001.65.855

46. La Scola B, Raoult D. Serological cross-reactions between *Bartonella quintana*, *Bartonella henselae*, and *Coxiella burnetii*. J Clin Microbiol. 1996;34:2270–4. https://doi.org/10.1128/jcm.34.9.2270-2274.1996

47. Shapira L, Rasis M, Binsky Ehrenreich I, Maor Y, Katchman EA, Treves A, et al. Laboratory diagnosis of 37 cases of *Bartonella* endocarditis based on enzyme immunoassay and real-time PCR. J Clin Microbiol. 2021;59:e02217–20. https://doi.org/10.1128/JCM.02217-20

48. Solanky D, Ahmed AA, Fierer J, Mehta S. 711. Rapid, non-invasive detection and monitoring of *Bartonella quintana* endocarditis by plasma-based next-generation sequencing of microbial cell-free DNA. Open Forum Infect Dis. 2020;7(Suppl_1):S407. https://doi.org/10.1093/ofid/ofaa439.903

49. HIV.gov. Guidelines for the prevention and treatment of opportunistic infections in adults and adolescents with HIV [cited 2024 Feb 7]. https://clinicalinfo.hiv.gov/en/guidelines/hiv-clinical-guidelines-adult-and-adolescent-opportunistic-infections/bartonellosis

50. Rose SR, Koehler J. Mandell, Douglas, and Bennett's Principles and Practice of Infectious Diseases. 9th ed. Philadelphia (PA): Elsevier; 2019.

51. Boodman C, Gupta N, Nelson CA, van Griensven J. *Bartonella quintana* endocarditis: a systematic review of individual cases. Clin Infect Dis. 2024;78:554–61. https://doi.org/10.1093/cid/ciad706

Address for correspondence: Grace Marx, Centers for Disease Control and Prevention, 3156 Rampart Rd, Fort Collins, CO 80521, USA; email: gmarx@cdc.gov

Bartonella quintana Infection in Kidney Transplant Recipients from Donor Experiencing Homelessness, United States, 2022

Amy M. Beeson, Shannan N. Rich, Michael E. Russo, Julu Bhatnagar, Rebecca N. Kumar, Jana M. Ritter, Pallavi Annambhotla, Moe R. Takeda, Kira F. Kuhn, Prishanya Pillai, Marlene DeLeon-Carnes, Rebecca Scobell, Maheswari Ekambaram, Rachel Finkel, Sarah Reagan-Steiner, Roosecelis B. Martines, Rohit S. Satoskar, Gayle M. Vranic, Raji Mohammed, Gloria E. Rivera, Kumarasen Cooper, Heba Abdelal, Marc Roger Couturier, Benjamin T. Bradley, Alison F. Hinckley, Jane E. Koehler, Paul S. Mead, Matthew J. Kuehnert, Joel Ackelsberg, Sridhar V. Basavaraju, Grace E. Marx

Bartonella quintana infection can cause severe disease that includes clinical manifestations such as endocarditis, chronic bacteremia, and vasoproliferative lesions of the skin and viscera. *B. quintana* bacteria is transmitted by the human body louse (*Pediculus humanus corporis*) and is associated with homelessness and limited access to hygienic services. We report *B. quintana* infection in 2 kidney transplant recipients in the United States from an organ donor who was experiencing homelessness. One infection manifested atypically, and the other was minimally symptomatic; with rapid detection, both recipients received timely treatment and recovered. *B. quintana* was identified retrospectively in an archived donor hematoma specimen, confirming the transmission link. Information about the organ donor's housing status was critical to this investigation. Evaluation for *B. quintana* infection should be considered for solid organ transplant recipients who receive organs from donors with a history of homelessness or of body lice infestation.

*B*artonella quintana is a small, facultatively intracellular, gram-negative bacillus that is transmitted to humans through the feces of an infected human body louse (*Pediculus humanus corporis*) (*1*). *B. quintana* infection was first described among soldiers living in poor hygienic conditions during World War I and became known as trench fever (*2*). In the United States and Europe, *B. quintana* infection has become increasingly linked to urban homelessness, a consequence of crowded living conditions and inconsistent access to clean clothes, showers, and laundry facilities (*3,4*).

The clinical manifestations of *B. quintana* infection range from asymptomatic to life-threatening. The most frequently described manifestations are endocarditis, bacteremia, and bacillary angiomatosis, a vasoproliferative disorder that primarily affects the skin but can also affect bones, liver, and spleen (*5,6*). Prolonged *B. quintana* bacteremia may be asymptomatic or pauci-symptomatic over several years (*7*).

Author affiliations: Centers for Disease Control and Prevention, Fort Collins, Colorado, USA (A.M. Beeson, S.N. Rich, A.F. Hinckley, P.S. Mead, G.E. Marx); The Children's Hospital of Philadelphia, Philadelphia, Pennsylvania, USA (M.E. Russo, M.R. Takeda, K.F. Kuhn, R. Scobell, M. Ekambaram, R. Finkel, H. Abdelal); Perelman School of Medicine at University of Pennsylvania, Philadelphia (M.E. Russo, M.R. Takeda, K. Cooper); Centers for Disease Control and Prevention, Atlanta, Georgia, USA (J. Bhatnagar, J.M. Ritter, P. Annambhotla, M. DeLeon-Carnes, R.S. Satoskar, M.J. Kuehnert, S.V. Basavaraju); MedStar Georgetown University Hospital, Washington, DC,

USA (R.N. Kumar, P. Pillai, S. Reagan-Steiner, R.B. Martines, G.M. Vranic); Duke University Medical Center, Durham, NC, USA (G.M. Vranic); Lincoln Medical Center, New York, NY, USA (R. Mohammed); New York City Department of Health and Mental Hygiene, New York (G.E. Rivera, M.J. Kuehnert, J. Ackelsberg); University Hospitals Cleveland Medical Center, Cleveland, Ohio, USA (H. Abdelal); ARUP Laboratories, Salt Lake City, Utah, USA (M.R. Couturier, B.T. Bradley); University of Utah, Salt Lake City (M.R. Couturier, B.T. Bradley); University of California, San Francisco, California, USA (J.E. Koehler).

B. quintana manifestations vary by immune status; bacillary angiomatosis occurs mostly in severely immunocompromised patients (*8*).

B. quintana infection can be identified by serologic testing, culture, or molecular methods (*9*). Current serologic tests do not reliably differentiate *B. quintana* from other *Bartonella* species, including the more common *B. henselae*, which causes cat-scratch fever. *B. quintana* is slow-growing, and culture is aided by prolonged incubation and specialized techniques (*10–12*). Molecular diagnostic tests for *Bartonella* are more sensitive than culture but are currently only available from a few commercial laboratories and vary in their ability to distinguish between *Bartonella* species (*13*).

Bartonella infection has previously been found in solid organ transplant recipients (*14,15*). In most of those cases, *B. henselae* was the suspected or confirmed causative pathogen, and it was presumed the recipient acquired the infection after exposure to household or feral cats (*14,15*). Very rarely, donor-derived *Bartonella* infection has been documented: a *B. henselae* infection (*16*), a renal transplant recipient in the Czech Republic with *B. quintana* infection (*17*), a suspected cluster of *Bartonella* infections in 3 recipients (heart, liver, and kidney) from a donor in the United States (*18*), and a recent cluster among 6 recipients from unhoused seropositive donors in Alberta, Canada (*19*).

In December 2022, a *Bartonella* infection was diagnosed in a kidney transplant recipient in the United States with no identifiable risk factors, spurring a complex investigation to determine the species and source of infection. Molecular testing eventually confirmed *B. quintana* in the recipient. Active screening identified *B. quintana* bacteremia in a second kidney transplant recipient from the same organ donor, and *B. quintana* was detected in an archived, formalin-fixed paraffin-embedded (FFPE) hematoma specimen from the organ donor. We describe the *B. quintana* infections in this organ donor who was experiencing homelessness and the 2 kidney recipients and discuss the diagnostic and treatment considerations among transplant recipients and public health implications.

Methods

Ethics Considerations
This investigation was conducted as part of the Centers for Disease Control and Prevention (CDC) and the New York City (NYC) Department of Health and Mental Hygiene routine public health surveillance and disease investigation activities. The CDC Human Subjects Review committee reviewed this investigation and deemed it to be nonresearch and exempted from full review. Recipient A's guardian and recipient B gave informed consent to include a summary of their cases in this report.

Case Description for Recipient A
In late 2022, a 16-year-old male patient who had received a kidney transplant 3 months before was hospitalized because of progressive abdominal pain over the previous 2 weeks, loose stools, intermittent fevers, and 2 days of cough and posttussive emesis. The patient had chronic kidney disease secondary to atypical hemolytic uremic syndrome as a child and had received his first deceased donor kidney transplant ≥10 years before. After graft failure in 2019 because of antibody-mediated rejection, he received a second deceased donor transplant in 2022 with antithymocyte globulin induction. At the time of admission, 3 months after transplant, the patient's immunosuppressive regimen included tacrolimus, mycophenolate, and prednisone. Since transplantation, he had been receiving prophylactic trimethoprim/sulfamethoxazole and valganciclovir.

Recipient A was febrile and tachycardic on initial examination. We noted right upper quadrant and epigastric tenderness and mild abdominal distension; no hepatosplenomegaly, lymphadenopathy, or skin lesions were observed. Laboratory testing showed creatinine mildly elevated from baseline (from 0.8 to 1.2 mg/dL), low hemoglobin (10.2 g/dL, reference range 13.0–16.0 g/dL), neutropenia (absolute neutrophil count, 950 cells/μL, reference range 1,540–7040 cells/μL), lymphopenia (absolute lymphocyte count, 520 cells/μL, reference range 970–3260 cells/μL), elevated C-reactive protein (5.2 mg/dL, reference range 0.0–0.9 mg/dL), and unremarkable alanine transaminase (19 U/L) and aspartate transaminase (36 U/L) values. His abdominal pain progressively worsened. Signs of peritonitis developed 4 days after admission, and we found an intraperitoneal hemorrhage that required resection. Magnetic resonance imaging revealed multiple T2 hyperintense enhancing lesions in his liver, spleen, and every vertebral body (Figure 1). A ruptured hepatic lesion was believed to be the source of the hemorrhage.

We initiated empiric antimicrobial treatment at admission with cefepime and vancomycin; the patient received multiple β-lactam medications during the first week. An extensive evaluation for infectious etiologies was unremarkable, which included *B. henselae* serologic testing that was negative at admission. Transthoracic echocardiogram revealed no abnormalities. We suspected posttransplant lymphoproliferative
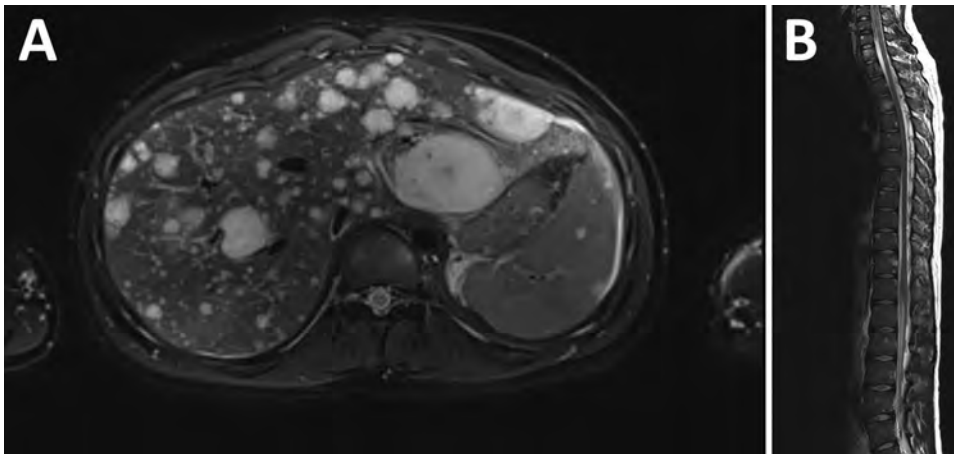
Figure 1. Imaging of a kidney transplant recipient with a *Bartonella quintana* infection linked to a donor who experienced homelessness, United States, 2022. A) Multiple enhancing T2 hyperintense lesions throughout the hepatic parenchyma. B) Numerous enhancing T2 hyperintense lesions affecting cervical, thoracic, and lumbar vertebrae.

disease, but a needle biopsy of recipient A's liver was nondiagnostic. We performed an excisional biopsy of 1 liver lesion (Figure 2) that showed histopathologic findings of a vasoproliferative lesion consistent with bacillary angiomatosis, including clusters of bacteria seen on Warthin-Starry stain, prompting targeted testing for *Bartonella*. Results of *Bartonella* PCR conducted by ARUP Laboratories (Salt Lake City, UT, USA) were positive 30 days after admission (Table 2), and we initiated *Bartonella*–directed therapy. The laboratory-developed test used by ARUP Laboratories is a real-time PCR to detect *Bartonella* species from the liver and blood. The assay uses primers and probes specific for the heat shock protein gene of *Bartonella* species. The assay is validated to detect both *B. henselae* and *B. quintana* with a limit of detection of 643 copies/mL. After nucleic acid extraction, specimens were amplified on the QuantStudio 12k Flex (Thermo Fisher Scientific, https://www.thermofisher.com) instrument using the GoTaq Probe qPCR Master Mix (Promega, https://www.promega.com) with primers and probes manufactured by ELITech (https://www.elitech-group.com). Specimens were considered positive if cycle threshold was ≤36.

Recipient A did not have any known exposures that would confer risk of either *B. henselae* or *B. quintana* infection, such as contact with felines or persons experiencing homelessness or a history of body lice infestation. We filed a report with the Organ Procurement and Transplantation Network for investigation by the ad hoc Disease Transmission Advisory Committee. In addition, we submitted a FFPE liver tissue specimen to CDC for further histopathologic evaluation and laboratory testing (Table 2). Histopathologic features were compatible with bacillary angiomatosis. Results of an immunohistochemical assay for *B. henselae*
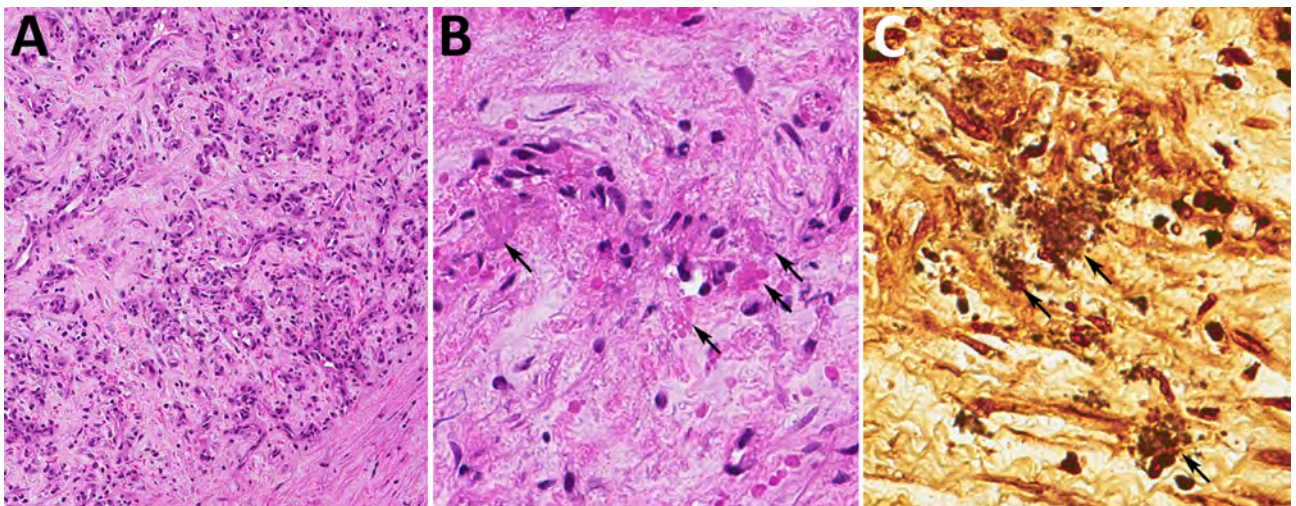
Figure 2. Liver biopsy of a kidney transplant recipient with a *Bartonella quintana* infection linked to a donor who experienced homelessness, United States, 2022. A) Fibrovascular proliferation accompanied by few inflammatory cells. Magnification ×200. B) Myxoid stroma that contains clumps of granular material (arrows). Magnification ×400. C) Warthin-Starry stain highlights clumps of bacilli (arrows). Magnification ×400.

were negative, but results of a conventional *Bartonella* species-specific PCR on DNA extracted from liver tissue were positive, and Sanger sequencing of the PCR products identified *B. quintana*. We conducted a conventional *Bartonella* species-specific heminested PCR targeting the riboflavin synthase-encoding gene on DNA extracted from FFPE tissue (*20*). We confirmed positive results by using sequencing.

The patient's fever and abdominal pain resolved within 1 week of starting *Bartonella*-specific antimicrobial drugs. Results of an eye examination including slit lamp and dilated funduscopic examination were unremarkable. The patient experienced gastrointestinal side effects from the first-line treatment doxycycline, prompting a switch to azithromycin. He then experienced a slight increase in mild preexisting tinnitus that did not progress during the remainder of treatment. He was treated for a total of 23 weeks. Repeat imaging showed nearly complete resolution of liver, spleen, and vertebral lesions with no residual enhancing lesions. *B. henselae* serologic testing was repeated twice, becoming positive on the third test with an IgG titer of 1:512 (Table 1). *B. quintana* serologic testing was not readily available, but the *B. henselae*

assay that was used is known to cross-react with *B. quintana*. The patient remained without symptoms during an 8-month follow-up.

Investigation

Shortly after recipient A began antimicrobial treatment for a *Bartonella* infection, CDC learned of the case through the Emerging Infections Network (*21*) and initiated a collaborative investigation including clinicians and public health authorities in several states, the organ procurement organization, and laboratory partners. The investigation revealed that 2 organs (left and right kidneys) had been recovered from a common donor and transplanted into 2 organ recipients. In addition, bone was recovered from the donor for processing as allograft tissue.

CDC contacted the transplant team caring for the second kidney recipient (recipient B), and the patient was promptly evaluated. In addition, CDC and the NYC Department of Health and Mental Hygiene collaborated to evaluate the possibility of donor-derived *Bartonella* infection through a review of the donor's medical record, phone outreach to the donor's listed contacts, and testing of residual specimens.

Table 1. Serologic test results from kidney transplant recipients and donor with *Bartonella quintana* infection, United States, 2022*

Source	Posttransplant specimen collection, weeks	Test performed	Result
Recipient A	14	*B. henselae* IgG	Negative
		B. henselae IgM	Negative
	19	*B. henselae* IgG	Negative
		B. henselae IgM	Negative
	35	*B. henselae* IgG	1:512
		B. henselae IgM	Negative
Recipient B	26	*B. henselae* IgG	1:16,384
		B. henselae IgM	Negative
	26	*B. quintana* IgG	1:2,048
		B. quintana IgM	1:64
	30	*B. henselae* IgG	1:32,768
		B. henselae IgM	Negative
	30	*B. quintana* IgG	1:4,096
		B. quintana IgM	1:128
	44	*B. henselae* IgG	1:1,024
		B. henselae IgM	Negative
	44	*B. quintana* IgG	1:512
		B. quintana IgM	Negative
	54	*B. henselae* IgG	1:1,024
		B. henselae IgM	Negative
	54	*B. quintana* IgG	1:256
		B. quintana IgM	Negative
	63†	*B. henselae* IgG	1:64
		B. henselae IgM	Negative
	63†	*B. quintana* IgG	Negative
		B. quintana IgM	Negative
Donor	Archived specimen	*B. henselae* IgG	1:256
		B. henselae IgM	Negative
	Archived specimen	*B. quintana* IgG	Negative
		B quintana IgM	Negative

*All serologic testing was performed at ARUP Laboratories (Salt Lake City, Utah, USA).
†Recipient B's 63-week samples were not sent to ARUP Laboratories.
Reference ranges for *B. henselae* and *B quintana* titers: IgG <1:64, negative; 1:64–1:128, equivocal; $\geq$1:256, positive; IgM <1:16, negative; $\geq$1:16, positive.

Table 2. Test results other than serology from kidney transplant recipients and donor with *Bartonella quintana* infection, United States, 2022*

Source	Time posttransplant specimen collection, wk	Specimen type	Test performed (performing laboratory)	Result
Recipient A	16	Liver tissue (FFPE)	*Bartonella* spp. PCR (ARUP Laboratories)	Positive
	16	Liver tissue (FFPE)	*Bartonella* spp. PCR (CDC)	Positive
	16	Liver tissue (FFPE)	*Bartonella* spp. sequencing (CDC)	*B. quintana*
	16	Liver tissue	Fungal, aerobic, and anaerobic tissue culture	No growth
	19	Serum	*Bartonella* spp. PCR (ARUP Laboratories)	Positive
	19	Whole blood	Blood culture	No growth after 5 d
Recipient B	26	Whole blood	*Bartonella* spp. PCR (ARUP Laboratories)	Positive
	54	Serum	*Bartonella* spp. PCR (ARUP Laboratories)	Negative
Donor	Prior to transplant	Whole blood	Blood culture	No growth after 5 d
	Archived specimen	Serum	*Bartonella* spp. PCR (ARUP Laboratories)	Negative
	Archived specimen	Hematoma (FFPE)	*Bartonella* spp. PCR (CDC)	Positive
	Archived specimen	Hematoma (FFPE)	*Bartonella* spp. sequencing (CDC)	*B. quintana*

*CDC, Centers for Disease Control and Prevention; FFPE, formalin-fixed paraffin-embedded.

Case Description for Recipient B

In mid-2022, a 54-year-old male patient underwent a third renal transplant for advanced nephropathy secondary to type 2 diabetes mellitus. Recipient B was evaluated 5 months after transplantation in an infectious disease clinic after the transplant team learned of the infection in recipient A. Recipient B reported feeling well other than bilateral hand and knee arthralgias that had begun shortly after the transplant. His immunosuppressive regimen consisted of tacrolimus, mycophenolate, and prednisone. After the transplant, he received posttransplant prophylaxis with trimethoprim/sulfamethoxazole for 3 months. Recipient B reported 1 pet dog and 3 cats. He reported no history of experiencing homelessness, incarceration, body lice infestation, or contact with persons experiencing homelessness.

Recipient B's physical examination was unremarkable and showed no audible cardiac murmur. We noted hyperpigmented macules on bilateral palms. Laboratory testing showed no acute changes in renal or hepatic function tests, blood chemistry, complete blood count, or C-reactive protein. Serum *Bartonella* PCR results were positive, and the patient was found to have elevated antibody titers (*B. henselae* IgG 1:16,384; *B. henselae* IgM $\leq$1:16; *B. quintana* IgG 1:2,048; *B. quintana* IgM 1:64). *B. henselae* and *B. quintana* IgG were detected at ARUP Laboratories by using the BIOCHIP Mosaic (EuroImmun, https://www.euroimmun.com) indirect immunofluorescence antibody assay (Table 2). Serum specimens were diluted to 1:64 for screening. We serially diluted positive specimens to endpoint reactivity to determine a final titer. Specimens with titers <1:64 were considered

negative. Titers of 1:64–1:128 were considered equivocal and required subsequent convalescent testing for confirmation. Titers $\geq$1:128 were considered positive. We detected *B. henselae* and *B. quintana* IgM by using indirect immunofluorescence antibody assay (DiaSorin, https://int.diasorin.com). We diluted serum specimens to 1:16 and further titrated specimens with reactivity at 1:16 to endpoint reactivity. We reported titers <1:16 as negative and titers $\geq$1:16 as positive. Computed tomography scans without contrast of the abdomen and pelvis showed an edematous, ill-defined transplanted kidney without other acute abnormalities. Dilated eye examination did not reveal retinal abnormalities. Transthoracic and transesophageal echocardiography showed mild thickening of the mitral valve leaflets and moderate thickening of aortic valve leaflets, without definite vegetations. The aortic valve thickening was more prominent compared with a study completed 2 years prior. Recipient B was referred to dermatology for evaluation of palmar lesions, which were not believed to be consistent with Janeway lesions.

Although recipient B did not meet the modified Duke criteria for definite endocarditis, on the basis of the valvular changes, positive *Bartonella* PCR in blood, and potential exposure through transplantation, we initiated treatment for possible *Bartonella* endocarditis with oral doxycycline (100 mg 2×/d) and oral azithromycin (500 mg 1×/d initial dose, then 250 mg 1×/d) (22). Shortly after treatment initiation, the patient's joint pain resolved. After 3 weeks, we stopped the azithromycin. We added rifampin for 6 weeks, during weeks 11–17 of treatment, and then discontinued. Because of the risk for subtherapeutic levels

of tacrolimus with coadministration of rifampin, we tapered and then discontinued the tacrolimus and replaced it with belatacept.

Erythrocyte sedimentation rate and C-reactive protein were unremarkable and repeat antibody titers showed increased *B. henselae* and *B. quintana* titers 1 month after treatment initiation. Approximately 4 months after treatment initiation, the titer values had decreased (Table 1). Recipient B has remained on oral doxycycline (100 mg 2×/d) for maintenance to date. Repeat echocardiography is planned.

Donor Description

Medical records from the organ donor's terminal hospitalization documented a traumatic brain injury that led to brain death despite neurosurgical interventions. A history of alcohol use disorder was noted; the donor had no other known immunocompromising conditions. No concerns for preexisting infection were noted during the terminal hospitalization. The donor underwent 2 surgical evacuations of a subdural hematoma that required multiple blood transfusions. Postoperatively, the donor experienced tachycardia, fever with a temperature ≥106°F, and leukocytosis. Sympathetic nervous system hyperactivity was a suspected cause of the marked hyperthermia. Despite aggressive treatment, the patient was determined to have very limited chance of recovery. The next of kin decided to transition to comfort-focused care, and the patient died shortly afterward.

The donor's hospital record and organ donation records did not explicitly note a history of homelessness or body lice infestation; however, after the recipients became ill, independent interviews with 2 people who knew the donor revealed a history of unsheltered homelessness in the months before the terminal hospitalization. Records at NYC's Department of Homeless Services did not indicate that the donor had ever been registered for services provided by the agency.

We tested a frozen, archived serum sample from the deceased donor for *Bartonella* by using PCR, which was negative. We also tested the donor's serum for antibodies to *B. henselae* and *B. quintana*, which was positive only for *B. henselae* IgG with a titer of 1:256. We located a subdural hematoma specimen from the donor that had been collected during a neurosurgical procedure and preserved. The hematoma showed erythrocytes admixed with fibrin, abundant neutrophils, and cellular debris. We conducted a *Bartonella*-specific PCR on DNA extracts from this FFPE specimen, and results were positive (Table 2). We conducted Sanger sequencing of the PCR products and identified *B. quintana* (Table 2).

The bone that had been recovered from the donor and processed as allograft tissue was quarantined when illness was first identified in recipient A. The bone specimens were not tested because there are few validated tests for this specimen type; the specimens were destroyed at the conclusion of this investigation.

Discussion

Our findings suggest *B. quintana* transmission through solid organ transplantation in 2 recipients from 1 donor, with species-specific confirmation of infection in the donor and recipient A. We suspect the organ donor in this case acquired *B. quintana* from a body lice infestation while experiencing homelessness. In recent decades, numerous cases and clusters of *B. quintana* infection have been described among persons experiencing homelessness in urban areas (4,23–29).

The organ donor in this cluster had slept outdoors in the months before the terminal hospitalization and had a history of alcohol use disorder. Among persons experiencing homelessness, those without consistent access to shower and laundry facilities or clean clothes are at risk for body lice infestation and *B. quintana* systemic infection. In the United States, the prevalence of unsheltered homelessness is increasing, and unsheltered homelessness has been linked to body lice infestation and *B. quintana* in San Francisco and NYC (29,30). Alcohol use disorder has also frequently been associated with *B. quintana* infection (4,27).

The cases in this study came to prompt attention because both recipients were engaged with posttransplant care teams and received a high level of care. However, most patients who have *B. quintana* infections do not receive the same level of attention or prompt treatment. This cluster serves as a reminder that this emerging infection still affects many on the margins of society and that public health measures are needed, including improved hygienic services, healthcare access, substance use treatment programs, and interventions to address the root causes of homelessness.

Limited clinician awareness of the risk factors for *B. quintana* transmission, its variable clinical manifestations, and laboratory diagnostic challenges contribute to the likely underdiagnosis of *B. quintana* infection. Those and other factors might also cause delayed or missed identifications in organ transplant recipients, a population with more consistent healthcare access but at risk for atypical disease manifestations and severe illness or death from *Bartonella* infections because of immunosuppression. Of note, both recipients in this cluster displayed unusual clinical

manifestations of *B. quintana*. Recipient A's case demonstrates the potential for atypical and severe manifestations of *B. quintana* during immunosuppression. Hepatosplenic manifestations of *B. quintana* have rarely been described and are much more characteristic of *B. henselae* infection (*6*); the co-occurrence of osteomyelitis with bacillary angiomatosis of the liver is highly unusual. Recipient B's case demonstrates the potential for indolent, pauci-symptomatic *B. quintana* infection and chronic bacteremia among transplant recipients. Recipient B's infection and probable endocarditis was only found through active screening performed as part of this public health investigation, because he did not report fevers or have symptoms of endocarditis that would typically prompt echocardiography. Of note, *Bartonella* infection occurred despite prolonged use of prophylactic trimethoprim/sulfamethoxazole in both recipients; trimethoprim/sulfamethoxazole is sometimes recommended as treatment for *B. henselae* infection, but treatment failure has been documented in patients with bacillary angiomatosis (*8*). Clinicians caring for transplant recipients should consider *B. quintana* infection in organ transplant recipients with clinical manifestations including prolonged fever, culture-negative endocarditis, or bacillary angiomatosis involving the skin, liver, spleen, or bone.

The cases in this study also underline the diagnostic challenges specific to solid organ transplant recipients. Serologic testing, a mainstay of *Bartonella* diagnosis, may remain negative for a prolonged interval because of immunosuppression. Blood product transfusion during or after transplantation can cloud the interpretation of test results because dilution can cause false negative results, whereas immunoglobulins acquired from donor plasma can result in false-positive results (*31,32*). Serologic tests and many molecular tests for *Bartonella* infections lack species specificity. Identification of specific *Bartonella* species has implications for prevention because those species have distinct transmission pathways and epidemiologic risk factors. In the United States, *B. henselae* is vectored by the cat flea, whereas *B. quintana* is transmitted by the human body louse. Infections with other, less common *Bartonella* species have been associated with other vectors and animals. Because of the unreliability of serologies and the difficulty of isolating *B. quintana* in culture, testing by using molecular diagnostic methods is particularly necessary if *B. quintana* is suspected in solid organ transplant recipients; providers should note that sensitivity may vary according to the specific assay and sample type.

For investigations of suspected transplant-associated transmission, obtaining FFPE tissue specimens when available from the recipient(s) and donor have frequently been used to help establish tissue-based diagnoses that can help guide patient management and inform epidemiologic investigations (*33–35*). Evaluation of such tissue specimens can be especially useful when conventional specimens such as serum and blood are unavailable or when results of testing those specimens are negative or not fully interpretable.

Because laboratory testing for *B. quintana* can be resource-intensive and because of the limitations of existing tests, universal screening of organ and tissue donor specimens for *B. quintana* or *Bartonella* infection before transplantation is neither feasible nor advisable. *B. quintana* is treatable, and positive test results in a prospective donor should not preclude transplantation of a lifesaving organ. As an alternative to universal donor screening, data on the housing status of organ donors (such as a history of homelessness or current homelessness) collected from the donor's next of kin might prove useful to clinicians managing potential donor-derived infections in transplant recipients; unfortunately, those data are not currently collected systematically (*36*). When a history of homelessness or body louse infestation is recognized in a donor, testing donor samples with blood culture, serology, molecular assays, or a combination of those methods should be considered. For recipients from organ donors who test positive, periodic testing, echocardiography, or even preemptive treatment might be relevant to prevent late complications of *B. quintana* infection, even if recipients are asymptomatic.

Although treatment of both organ transplant recipients in this cluster has been successful to date, management of *B. quintana* infection in the setting of transplantation has distinct challenges. Effective antimicrobial drug durations for immunocompromised persons are not clearly established, although the experience with treatment of *Bartonella* infection in severely immunocompromised persons living with HIV has demonstrated that lengthy antimicrobial drug treatment is necessary to prevent relapse. Antimicrobial drugs effective against *B. quintana* include doxycycline, rifampin, aminoglycosides, and macrolides (*37*). After kidney transplantation, rifampin use can be challenging because of interactions with common immunosuppressive medications used to prevent transplant rejection, and aminoglycoside use may be limited by nephrotoxicity.

The first limitation of this report is that, although the NYC Department of Health and Mental Hygiene did not find records to indicate that the donor sought

care for symptoms suggestive of bartonellosis before death, the donor could have sought care at a facility not captured by the regional health information exchange organizations that were queried. Therefore, it remains unknown whether the donor experienced signs or symptoms of *B. quintana* infection before death and whether there might have been missed opportunities for earlier diagnosis. Second, although the donor had epidemiologic risk factors for the acquisition of *B. quintana* through infected body lice, it is also possible that the donor acquired the infection through blood transfusion (*18*) because transmission through blood transfusion has been demonstrated (*38*). Finally, *Bartonella* species confirmation for recipient B and molecular sequencing of donor and recipient specimens could have provided further evidence of donor-to-recipient transmission. We attempted additional 16S sequencing testing on the liver tissue sample from recipient A and the PCR-positive blood sample from recipient B, but results were indeterminate.

In conclusion, this investigation of a donor-derived cluster of *B. quintana* infections in 2 solid organ transplant recipients yields lessons for public health practitioners and clinicians. *B. quintana* is a growing public health problem in the United States, but it is not nationally notifiable and is underrecognized. In this investigation, information sharing and collaboration among clinicians, laboratorians, and public health authorities led to timely testing, treatment, and clinical improvement for both organ recipients. Improving diagnosis, treatment, and prevention of *B. quintana* infections in the United States depends on heightened awareness of this enigmatic pathogen, including its potential to cause illness in solid organ transplant recipients.

Acknowledgments

About the author

Dr. Beeson is a staff physician in Internal Medicine and Pediatrics at Denver Health and Hospital. Her interests include vectorborne and bacterial diseases.

References

1. Karem KL, Paddock CD, Regnery RL. *Bartonella henselae, B. quintana,* and *B. bacilliformis*: historical pathogens of emerging significance. Microbes Infect. 2000;2:1193–205. https://doi.org/10.1016/S1286-4579(00)01273-9

2. Giladi M, Ephros M. *Bartonella* infections, including cat-scratch disease. In: Loscalzo J, Fauci A, Kasper D, Hauser S, Longo D, Jameson JL, editors. Harrison's principles of internal medicine, 21e. New York: McGraw-Hill Education; 2022.

3. Brouqui P, Lascola B, Roux V, Raoult D. Chronic *Bartonella quintana* bacteremia in homeless patients. N Engl J Med. 1999; 340:184–9. https://doi.org/10.1056/NEJM199901213400303

4. Shepard Z, Vargas Barahona L, Montalbano G, Rowan SE, Franco-Paredes C, Madinger N. *Bartonella quintana* infection in people experiencing homelessness in the Denver metropolitan area. J Infect Dis. 2022;226(Suppl 3):S315–21. https://doi.org/10.1093/infdis/jiac238

5. Angelakis E, Raoult D. Pathogenicity and treatment of *Bartonella* infections. Int J Antimicrob Agents. 2014;44:16–25. https://doi.org/10.1016/j.ijantimicag.2014.04.006

6. Koehler JE, Sanchez MA, Garrido CS, Whitfeld MJ, Chen FM, Berger TG, et al. Molecular epidemiology of *Bartonella* infections in patients with bacillary angiomatosis-peliosis. N Engl J Med. 1997;337:1876–83. https://doi.org/10.1056/NEJM199712253372603

7. Foucault C, Barrau K, Brouqui P, Raoult D. *Bartonella quintana* bacteremia among homeless people. Clin Infect Dis. 2002;35:684–9. https://doi.org/10.1086/342065

8. Koehler JE, Tappero JW. Bacillary angiomatosis and bacillary peliosis in patients infected with human immunodeficiency virus. Clin Infect Dis. 1993;17:612–24. https://doi.org/10.1093/clinids/17.4.612

9. Choat J, Yockey B, Sheldon SW, Pappert R, Petersen J, Dietrich EA. Development and validation of a real-time PCR test to detect *Bartonella quintana* in clinical samples. Diagn Microbiol Infect Dis. 2023;106:116000. https://doi.org/10.1016/j.diagmicrobio.2023.116000

10. Battisti JM, Minnick MF. Laboratory maintenance of *Bartonella quintana*: alpha proteobacteria. Curr Protoc Microbiol. 2008;10. https://doi.org/10.1002/9780471729259.mc03c01s10

11. La Scola B, Raoult D. Culture of *Bartonella quintana* and *Bartonella henselae* from human samples: a 5-year experience (1993 to 1998). J Clin Microbiol. 1999;37:1899–905. https://doi.org/10.1128/JCM.37.6.1899-1905.1999

12. Koehler JE, Quinn FD, Berger TG, LeBoit PE, Tappero JW. Isolation of *Rochalimaea* species from cutaneous and osseous lesions of bacillary angiomatosis. N Engl J Med. 1992;327:1625–31. https://doi.org/10.1056/NEJM199212033272303

13. Sander A, Posselt M, Böhm N, Ruess M, Altwegg M. Detection of *Bartonella henselae* DNA by two different PCR assays and determination of the genotypes of strains involved in histologically defined cat scratch disease. J Clin Microbiol. 1999;37:993–7. https://doi.org/10.1128/JCM.37.4.993-997.1999

14. Psarros G, Riddell J IV, Gandhi T, Kauffman CA, Cinti SK. *Bartonella henselae* infections in solid organ transplant recipients: report of 5 cases and review of the literature. Medicine (Baltimore). 2012;91:111–21. https://doi.org/10.1097/MD.0b013e31824dc07a

15. Eid R, Assayag M, Lefevre E, Escaut L, Laifi M, Brodin-Sartorius A, et al. Invasive bacillary angiomatosis in a kidney transplant recipient: a challenging case on belatacept immunosuppression. Int J Infect Dis. 2023;133:43–5. https://doi.org/10.1016/j.ijid.2023.04.404

16. Scolfaro C, Mignone F, Gennari F, Alfarano A, Veltri A, Romagnoli R, et al. Possible donor-recipient bartonellosis transmission in a pediatric liver transplant. Transpl Infect

Dis. 2008;10:431–3. https://doi.org/10.1111/j.1399-3062.2008.00326.x

17. Orsag J, Flodr P, Melter O, Tkadlec J, Sternbersky J, Hruby M, et al. Cutaneous bacillary angiomatosis due to *Bartonella quintana* in a renal transplant recipient. Transpl Int. 2015;28:626–31. https://doi.org/10.1111/tri.12539

18. Morillas JA, Hassanein M, Syed B, Liaqat A, Bergfeld W, Sardiña LA, et al. Early post-transplant cutaneous bacillary angiomatosis in a kidney recipient: case report and review of the literature. Transpl Infect Dis. 2021;23:e13670. https://doi.org/10.1111/tid.13670

19. Kabbani D, Orenbuch-Harroch E, Boodman C, Broad S, Paz-Infanzon M, Belga S, et al. Donor-derived bartonellosis in solid organ transplant recipients from unhoused donors in Alberta. Am J Transplant. 2024;6135:00595–1. https://doi.org/10.1016/j.ajt.2024.09.026

20. Zeaiter Z, Fournier PE, Greub G, Raoult D. Diagnosis of *Bartonella* endocarditis by a real-time nested PCR assay using serum. J Clin Microbiol. 2003;41:919–25. https://doi.org/10.1128/JCM.41.3.919-925.2003

21. Pillai SK, Beekmann SE, Santibanez S, Polgreen PM. The infectious diseases society of America emerging infections network: bridging the gap between clinical infectious diseases and public health. Clin Infect Dis. 2014;58:991–6. https://doi.org/10.1093/cid/cit932

22. Fowler VG Jr, Durack DT, Selton-Suty C, Athan E, Bayer AS, Chamis AL, et al. The 2023 Duke-International Society for Cardiovascular Infectious Diseases criteria for infective endocarditis: updating the modified duke criteria. Clin Infect Dis. 2023;77:518–26. https://doi.org/10.1093/cid/ciad271

23. Ghidey FY, Igbinosa O, Mills K, Lai L, Woods C, Ruiz ME, et al. Case series of *Bartonella quintana* blood culture-negative endocarditis in Washington, DC. JMM Case Rep. 2016;3:e005049. https://doi.org/10.1099/jmmcr.0.005049

24. Raybould JE, Raybould AL, Morales MK, Zaheer M, Lipkowitz MS, Timpone JG, et al. *Bartonella* endocarditis and pauci-immune glomerulonephritis: a case report and review of the literature. Infect Dis Clin Pract. 2016;24:254–60. https://doi.org/10.1097/IPC.0000000000000384

25. Dieringer TD, Huang G, Allyn PR, Klausner J. 696. *Bartonella quintana* endocarditis, a case series. Open Forum Infect Dis. 2020;7(Suppl 1):S400. https://doi.org/10.1093/ofid/ofaa439.888

26. Promer K, Cowell AN, Reed SL, Castellanos LR, Aronoff-Spencer E. *Bartonella quintana* endocarditis in a homeless man with cat exposure in San Diego, California. Vector Borne Zoonotic Dis. 2020;20:468–70. https://doi.org/10.1089/vbz.2019.2556

27. Spach DH, Kanter AS, Dougherty MJ, Larson AM, Coyle MB, Brenner DJ, et al. *Bartonella (Rochalimaea) quintana* bacteremia in inner-city patients with chronic alcoholism. N Engl J Med. 1995;332:424–8. https://doi.org/10.1056/NEJM199502163320703

28. Davidson VJ, Butler JC. *Bartonella quintana* endocarditis following body louse exposure, Anchorage. 2016 Apr 27 [cited 2023 Aug 22]. https://epi.alaska.gov/bulletins/docs/b2016_11.pdf

29. Rich SN, Beeson A, Seifu L, Mitchell K, Wroblewski D, Juretschko S, et al. Notes from the field: severe *Bartonella quintana* infections among persons experiencing unsheltered homelessness–New York City, January 2020–December 2022. MMWR Morb Mortal Wkly Rep. 2023;72:1147–8. https://doi.org/10.15585/mmwr.mm7242a3

30. Bonilla DL, Cole-Porse C, Kjemtrup A, Osikowicz L, Kosoy M. Risk factors for human lice and bartonellosis among the homeless, San Francisco, California, USA. Emerg Infect Dis. 2014;20:1645–51. https://doi.org/10.3201/eid2010.131655

31. Eastlund T. Hemodilution due to blood loss and transfusion and reliability of cadaver tissue donor infectious disease testing. Cell Tissue Bank. 2000;1:121–7. https://doi.org/10.1023/A:1010120115451

32. Blaich A, Manz M, Dumoulin A, Schüttler CG, Hirsch HH, Gerlich WH, et al. Reactivation of hepatitis B virus with mutated hepatitis B surface antigen in a liver transplant recipient receiving a graft from an antibody to hepatitis B surface antigen– and antibody to hepatitis B core antigen–positive donor. Transfusion. 2012;52:1999–2006. https://doi.org/10.1111/j.1537-2995.2011.03537.x

33. Basavaraju SV, Kuehnert MJ, Zaki SR, Sejvar JJ. Encephalitis caused by pathogens transmitted through organ transplants, United States, 2002–2013. Emerg Infect Dis. 2014;20:1443–51. https://doi.org/10.3201/eid2009.131332

34. Gould CV, Free RJ, Bhatnagar J, Soto RA, Royer TL, Maley WR, et al.; Yellow Fever Vaccine Virus Transplant and Transfusion Investigation Team. Transmission of yellow fever vaccine virus through blood transfusion and organ transplantation in the USA in 2021: report of an investigation. Lancet Microbe. 2023;4:e711–21. https://doi.org/10.1016/S2666-5247(23)00170-2

35. Pouch SM, Katugaha SB, Shieh WJ, Annambhotla P, Walker WL, Basavaraju SV, et al.; Eastern Equine Encephalitis Virus Transplant Transmission Investigation Team. Transmission of eastern equine encephalitis virus from an organ donor to 3 transplant recipients. Clin Infect Dis. 2019;69:450–8. https://doi.org/10.1093/cid/ciy923

36. Mosites E, Morris SB, Self J, Butler JC. Data sources that enumerate people experiencing homelessness in the United States: opportunities and challenges for epidemiologic research. Am J Epidemiol. 2021;190:2432–6. https://doi.org/10.1093/aje/kwab051

37. Rolain JM, Brouqui P, Koehler JE, Maguina C, Dolan MJ, Raoult D. Recommendations for treatment of human infections caused by *Bartonella* species. Antimicrob Agents Chemother. 2004;48:1921–33. https://doi.org/10.1128/AAC.48.6.1921-1933.2004

38. Silva MN, Vieira-Damiani G, Ericson ME, Gupta K, Gilioli R, de Almeida AR, et al. *Bartonella henselae* transmission by blood transfusion in mice. Transfusion. 2016;56(6pt2):1556–9. https://doi.org/10.1111/trf.13545

Address for correspondence: Amy M. Beeson, Denver Health and Hospital, 660 Bannock St, Suite 2535, Denver CO 80204 USA; email amy.beeson@dhha.org

Increase in Adult Patients with Varicella Zoster Virus–Related Central Nervous System Infections, Japan

Ayami Yoshikane, Hiroki Miura, Sayuri Shima, Masaaki Matsunaga, Soichiro Ishimaru,
Yuki Higashimoto, Yoshiki Kawamura, Kei Kozawa, Akiko Yoshikawa, Akihiro Ueda,
Atsuhiko Ota, Hirohisa Watanabe, Tatsuro Mutoh, Tetsushi Yoshikawa

An increase in the number of herpes zoster patients has been reported since universal varicella immunization was introduced, perhaps because of reduced opportunities for varicella patients to experience the natural booster effect caused by reexposure. We investigated recent trends of varicella zoster virus (VZV)–related central nervous system (CNS) infections at a university hospital in Japan. We enrolled patients with suspected CNS infection during 2013–2022 and tested cerebrospinal fluid samples by real-time PCR for DNA from 7 human herpesviruses. VZV DNA was the most commonly detected in 62 (10.2%) of 615 patients. Kulldorff's circular spatial scan statistics demonstrated a significant temporal cluster of patients with VZV-related CNS infections during 2019–2022 (p = 0.008). Among persons with such infections, the percentage with aseptic meningitis was significantly higher during 2019–2022 (86.8%), when the temporal cluster of cases occurred, than during 2013–2018 (50.0%) (p = 0.0029).

Primary varicella zoster virus (VZV) infection can cause varicella (chicken pox), which is generally a mild, self-limiting disease; however, VZV infection can also rarely lead to serious complications, such as secondary bacterial superinfection of the skin, pneumonia, encephalitis, and acute cerebellar ataxia. After primary viral infection, VZV establishes latency in sensory neurons and can subsequently reactivate and cause herpes zoster infection (shingles) in elderly and immunosuppressed patients. Because of the major disease burden of varicella, the live attenuated varicella vaccine was developed in 1974 (*1*). This vaccine has been used worldwide for routine childhood immunization, and its high efficacy and safety have been demonstrated (*2,3*). Although the varicella vaccine was developed by researchers in Japan (*1*), for many years it was used as a voluntary base vaccine in Japan, not as a universal vaccine. However, beginning in 2014, two doses of the varicella vaccine were included in the national immunization program in Japan. Consistent with epidemiologic changes observed in other countries that have implemented universal varicella vaccination (*2*), our previous studies showed high efficacy of 2 vaccine doses for preventing VZV infection (*4,5*), as well as a substantial reduction in the number of varicella cases during 2015–2019, after universal immunization was implemented in 2014 (*3*).

The decrease in the number of varicella patients since universal immunization was implemented (*6–8*) has limited the opportunity to induce a natural booster effect in VZV-seropositive persons. The loss of this natural booster effect, which plays a role in preventing viral reactivation (*6*), accelerates the decline in immunity, leading to an increase in the number of herpes zoster infections (*7*). In fact, such increases have been reported in many countries that have initiated universal varicella vaccination (*9–11*), including Japan (*8*). Furthermore, the risk for herpes zoster infection has been suggested to increase with COVID-19 infection (*4*), as well as with COVID-19 mRNA vaccination (*5*). Therefore, the number of herpes zoster infections might have further increased since the onset of the COVID-19 pandemic.

In addition to herpes zoster, VZV reactivation can cause various types of central nervous system (CNS) complications, such as meningitis, meningoencephalitis, myelitis, and cerebral stroke (12). Several cohort studies have suggested that along with the herpes simplex virus, VZV has conferred a substantial disease burden in adult patients with CNS infections (13). In addition, 1 study demonstrated that the detection of VZV DNA in cerebrospinal fluid (CSF) increased the risk for subsequent dementia and epilepsy (14). In our recent cohort study examining the epidemiology of human herpesviruses in adult patients suspected of having CNS infections, ≈10% of those patients were positive for these viruses in the CSF; VZV was the most common (15). That study began in 2013; as previously mentioned, because the number of herpes zoster infections has increased over the years, the number of patients with VZV-related CNS infections might have risen as well. In this study, we sought to analyze the number of patients with VZV-related CNS disease in an adult CNS infection cohort in Japan.

Materials and Methods

Patient and Sample Collection

During January 2013–December 2022, we enrolled patients >15 years of age who were suspected of having CNS infection and from whom CSF was collected in the Department of Neurology of Fujita Health University School of Medicine (Toyoake, Japan). CSF was collected at time of hospital admission, and bacterial CNS infection was ruled out by negative CSF culture. CSF samples were stored at −30°C until examination. This study was approved by the Ethical Review Board of Human Studies at Fujita Health University (accession no. 14-096). Patient consent to participate in this study was obtained through an opt-out method.

Patient Background and Clinical Characteristics

We collected patient background and clinical characteristics (specifically, sex, age, underlying conditions, diagnosis, symptoms, laboratory data, findings of brain magnetic resonance imaging [MRI] and electroencephalography, treatment, and prognosis) retrospectively from medical records. The final diagnosis for each patient was determined by the attending neurologist on the basis of clinical symptoms. Among patients with CSF pleocytosis, patients with impaired consciousness were defined as having encephalitis, whereas patients with clear consciousness were defined as having meningitis. We carried out virologic analysis, as detailed in the next sections. In VZV

DNA–positive patients, we elicited herpes zoster and COVID-19 vaccination status and recent COVID-19 history through telephone interviews.

DNA Extraction and Quantitative PCR

We extracted DNA from 200 μL of CSF using the QIAamp Blood Kit (QIAGEN, https://www.qiagen.com), eluted in 50 μL of elution buffer, then stored at −30°C before assay. We conducted real-time PCR to detect DNA of 7 human herpesviruses: herpes simplex virus (HSV) 1, HSV-2, VZV, cytomegalovirus, Epstein-Barr virus, human herpesvirus (HHV) 6, and HHV-7. The details of those real-time PCR methods for measuring viral DNA loads were described previously (9,10,16). The detection limit of the assays was 10 copies/tube.

Differentiation between Oka VZV Vaccine and Wild-Type Strains

We performed differentiation between the Oka varicella vaccine (BIKEN, https://www.biken.or.jp) and wild-type strains by using a VZV loop-mediated isothermal amplification assay (LAMP) using DNA extracted from VZV-positive CSF samples. To amplify the target sequences, including 2 different single-nucleotide polymorphisms (nucleotides 105,705 and 106,262) located in the ORF62 gene, we designed primers from published sequences (GenBank accession no. NC_001348) using Primer Explorer version 3 software (https://primerexplorer.jp). We used *Sma*I to digest the LAMP products, then subjected them to electrophoresis on 1.5% agarose gels and visualized them under ultraviolet light after ethidium bromide staining (17).

Statistical Analysis

We examined data pertaining to proportions, such as comparisons of patient background and clinical characteristic information, by Fisher exact or χ^2 test. We assessed statistical comparison of numerical differences, such as laboratory findings, by using the Mann-Whitney U test. All reported p values are 2-sided. We used JMP version 12.2 (SAS Institute, https://www.sas.com) for analyses. We used Kulldorff's retrospective space-time scan statistics, calculated using software FleXScan version 3.1 (https://sites.google.com/site/flexscansoftware), to identify temporal clusters of VZV-related CNS infections. We defined statistical significance as $p < 0.05$.

Results

During the observation period, a total of 615 patients (median age 53 years, range 15–91 years) were

enrolled in this study. Herpesvirus DNA was detected in 90 (14.6%) of the 615 patients (Figure 1). The median age of herpesvirus DNA–positive patients was 67 years (interquartile range [IQR] 43–78 years). The most frequently detected herpesvirus was VZV (62 patients), followed by HHV-6 (10 patients), Epstein-Barr virus (10 patients), HSV-1 (7 patients), and HSV-2 (6 patients). Cytomegalovirus and HHV-7 were not detected. The median age of patients who tested positive for VZV DNA in CSF was 70.5 years (IQR 48.5–78 years); 54.8% were male and 45.2% female (Table). In total, meningitis was diagnosed in 45 (72.6%) patients, and encephalitis was diagnosed in 7 (11.3%) patients (Table). Moreover, 49 patients (79.0%) had clinical signs of herpes zoster infection, which most commonly affected the trigeminal nerve area (38.8%). Target sequences in 44 of 62 CSF samples were successfully amplified by LAMP, and all were wild-type strains. The remaining 18 samples could not be analyzed by LAMP, probably because of low copy numbers of VZV DNA.

In Japan, the live-attenuated varicella zoster Oka vaccine (BIKEN) was additionally approved in March 2016, and the recombinant subunit vaccine Shingrix (https://www.shingrix.com) was approved in March 2018 as zoster vaccine for adults >50 years of age. Of 62 patients who had VZV-related CNS infections

Figure 1. Flowchart of virologic examinations of cerebrospinal fluid samples from 615 patients with suspected CNS infection increase in adult patients with VZV-related CNS infections, Japan. Real-time PCR was carried out to detect DNA of 7 human herpesviruses: HSV-1, HSV-2, VZV, CMV, EBV, HHV-6, and HHV-7. Statistical analyses of VZV DNA–positive patients were performed to determine the trends and clinical features of VZV-related CNS infections. CMV, cytomegalovirus; CNS, central nervous system; EBV, Epstein-Barr virus; HHV, human herpesvirus; HSV, herpes simplex virus; VZV, varicella-zoster virus.

develop after 2016, a total of 49 were eligible for zoster vaccination before those CNS infections developed. However, among the 26 patients for whom vaccination status was available, none had received the zoster vaccine. Furthermore, to investigate the relationship between an increase in VZV-related CNS infections and COVID-19 illness or COVID-19 vaccine, we elicited COVID-19 history and COVID-19 vaccination status from patients who had VZV-related CNS infection after 2020. Of the 19 patients for whom COVID-19 history was available, none had COVID-19 before the onset of CNS infection, whereas VZV-related CNS infections developed in 6 patients after they received COVID-19 vaccinations.

The proportion of VZV DNA–positive patients among patients suspected of having CNS infection appeared to be increasing (Figure 2). Kulldorff's circular spatial scan statistics demonstrated a significant temporal cluster of patients with VZV-related CNS infections during 2019–2022 (p = 0.008). This time frame was defined as the late period, in contrast with the early period of 2013–2018. However, the disease trends among hospitalized patients in our institution did not change during the overall study period (2013–2022) (Appendix Figure).

Next, we compared patients' background and clinical characteristics between the early and late periods (2013–2018 vs. 2019–2022) (Table). Background factors (sex, median age, number of underlying conditions, and number receiving prednisolone treatment) did not differ significantly between the 2 periods. However, the percentage of patients with several VZV-related CNS infections differed significantly between the 2 periods. The percentage of patients with aseptic meningitis was significantly higher in the late period (33/38 cases, 86.8%) than in the early period (12/24 cases, 50.0%; p = 0.0029). Meanwhile, the percentage of patients with encephalitis was significantly higher in the early period (6/24 cases, 25.0%) than in the late period (1/38 cases, 2.6%; p = 0.0111). The percentage of patients with herpes zoster infection was higher in the early period (22/24 cases, 91.7%) than in the late period (27/38 cases, 71.1%). We observed no significant difference between the 2 periods either in the percentage of patients with pleocytosis or in the VZV viral load in CSF. The percentage of patients with abnormal brain MRI findings was significantly higher in the early period than in the late period (33.3% vs. 6.9%; p = 0.0253).

Discussion

This cohort study, initiated in 2013, showed that, beginning in 2019, the number of patients with VZV-related

Table. Comparison of background and clinical characteristics of VZV-positive patients during 2013–2018 and 2019–2022 in study of increase in adult patients with VZV-related central nervous system infections, Japan*

Characteristic	Total, N = 62	2013–2018, n = 24	2019–2022, n = 38	p value
Sex				
M	34 (54.8)	13 (54.2)	21 (55.3)	1.0000
F	28 (45.2)	11 (45.8)	17 (44.7)	
Median age (IQR)	70.5 (48.5–78)	69.5 (46.5–78.5)	70.5 (50.3–77.5)	0.9079
Underlying conditions				
Diabetes	13 (21.0)	7 (29.2)	6 (15.8)	0.2217
Hypertension	12 (19.0)	6 (25.0)	6 (15.8)	0.5111
Solid tumor/hematological malignancy	12 (19.0)	5 (20.8)	7 (18.4)	1.0000
Others	48 (77.4)	18 (75.0)	30 (78.9)	0.7617
None	11 (17.7)	4 (16.7)	7 (18.4)	1.0000
Prednisolone treatment	11 (17.7)	2 (8.3)	9 (23.7)	0.1776
Final diagnosis				
Meningitis	45 (72.6)	12 (50.0)	33 (86.8)	0.0029
Encephalitis	7 (11.3)	6 (25.0)	1 (2.6)	0.0111
Myelitis	3 (4.8)	1 (4.2)	2 (5.3)	1.0000
Hunt syndrome	4 (6.5)	2 (8.3)	2 (5.3)	0.6371
Herpes zoster†	2 (3.2)	2 (8.3)	0	0.1460
Peripheral neuritis	1 (1.6)	1 (4.2)	0	0.3871
Clinical symptoms				
Herpes zoster	49 (79.0)	22 (91.7)	27 (71.1)	0.0623
Cervical nerve	11/49 (22.4)	7/22 (31.8)	4/27 (14.8)	0.1854
Trigeminal nerve	19/49 (38.8)	9/22 (40.9)	10/27 (37.0)	1.0000
Thoracic nerve	13/49 (26.5)	6/22 (27.3)	7/27 (25.9)	1.0000
Lumbar nerve	10/49 (20.4)	3/22 (13.6)	7/27 (25.9)	0.4778
Sacral nerve	2/49 (4.1)	0/22 (0.0)	2/27 (7.4)	0.4949
Postherpetic neuralgia	23 (37.1)	10 (41.7)	13 (34.2)	0.7818
Confusion	14 (22.6)	8 (33.3)	6 (15.8)	0.1287
Laboratory data				
Pleocytosis	60 (96.8)	22 (91.7)	38 (100.0)	0.1460
Median VZV DNA copy numbers (IQR)	4.7×10^5 (5.7×10^4–2.3×10^6)	8.2×10^5 (2.8×10^5–5.7×10^6)	4.2×10^5 (5.3×10^4–1.0×10^6)	0.1255
Imaging data				
Abnormal brain MRI finding	9/50‡ (18.0)	7/21 (33.3)	2/29 (6.9)	0.0253
Abnormal EEG finding	7/20§ (35.0)	5/14 (35.7)	2/6 (33.3)	1.0000
Treatment				
Intravenous acyclovir administration	61 (98.4)	24 (100.0)	37 (97.4)	1.0000
Median duration, d (IQR)	14 (10–15)	14 (11.8–15.5)	14 (10–14.6)	0.6480
Adjunctive prednisone	10 (16.1)	2 (8.3)	8 (21.1)	0.0750
Prognosis				
Sequelae	33 (53.2)	14 (50.0)	19 (50.0)	0.4398
Fatal	1 (1.6)	1 (4.2)	0	0.3871

*Values are no. (%) except as indicated. EEG, electroencephalogram; IQR, interquartile range; MRI, magnetic resonance imaging; VZV, varicella zoster virus.
†The classification of herpes zoster as the final diagnosis indicates that those patients were not categorized under any of the other diseases listed in this table; they are classified as having herpes zoster only.
‡Of 62 patients with VZV-related central nervous system infections, 50 underwent brain MRI.
§Of 62 patients with VZV-related central nervous system infections, 20 underwent EEG.

CNS infections increased significantly among patients at our institution in Japan. Furthermore, Kulldorff's circular spatial scan statistics, which are used to elucidate clusters of infectious diseases, including COVID-19, demonstrated a statistically significant temporal cluster of patients with VZV-related CNS infections during 2019–2022 (18,19). Bryant et al. (11) recently performed a molecular epidemiologic study on VZV on the basis of samples collected from patients with CNS infection in New York, USA, and showed a similar increase in patients with VZV-related CNS infection. However, because those study samples were transported to a central laboratory from many hospitals across New York state, whether this trend represents a real increase in disease incidence or an increase in the submission of samples for testing is unclear. Our results of a single-center study clearly demonstrated a recent increase in the number of VZV-related CNS infections, a pattern similar to that recently observed regarding the incidence of herpes zoster infection (20), which strongly supports the findings demonstrated by Bryant et al. (11). On the basis of the Hope-Simpson model, it has been suggested that the greater number of herpes zoster patients may be caused in large part to reduced opportunities for persons previously infected with varicella to experience the natural booster effect caused by reexposure (6). Although the increased incidence of herpes zoster
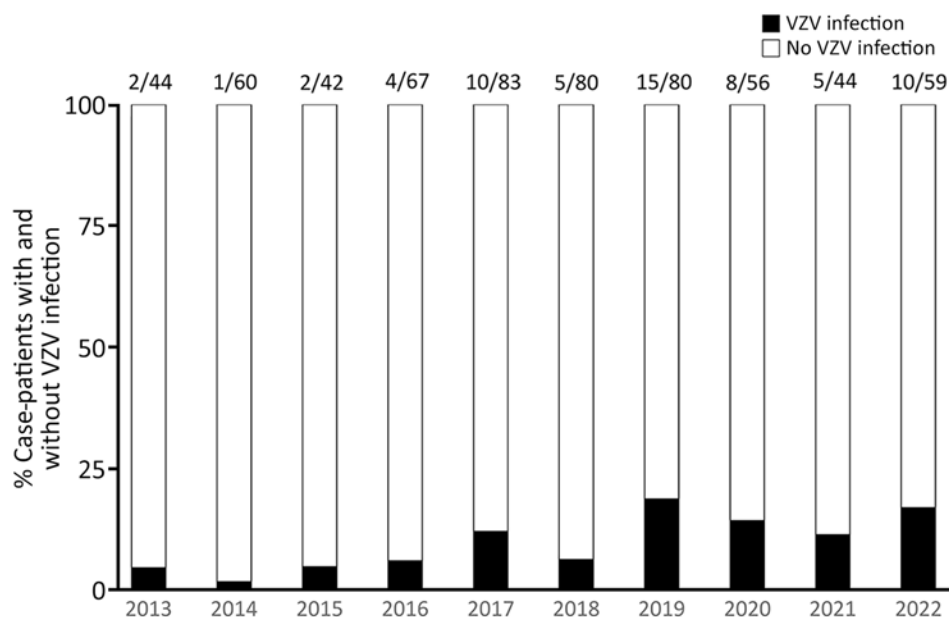
Figure 2. Trends of VZV-related central nervous system infections at Fujita Health University School of Medicine during 2013–2022 in study of increase in adult patients with VZV-related central nervous system infections, Japan. Vertical bars show percentages of patients with (black) and without (white) VZV infection each year. Numbers above bars indicate no. patients positive/no. analyzed. VZV, varicella-zoster virus.

has been demonstrated in many industrial countries with aging populations (*20*), no clear correlation has been demonstrated to date between this increase and the lessened opportunity for the natural booster effect (*21*). The higher incidence of herpes zoster is thought to be associated with increasingly aging populations (*22*) and the growing number of patients at high risk for herpes zoster (*23*), such as immunocompromised persons or persons with diabetes or autoimmune diseases. In any event, data suggest that herpes zoster infection and VZV-related CNS infections should be monitored to accurately assess the disease burden associated with VZV reactivation in adults, especially in aging populations.

Some have suggested that the risk for herpes zoster is increased by COVID-19 (*4*) and COVID-19 mRNA vaccination (*5*), and some case reports have indicated that zoster meningitis developed after COVID-19 mRNA vaccination (*24–26*). Among the patients in our study with an available history of COVID-19 infection and vaccination status, none had COVID-19 before the onset of the VZV-related CNS infection, but VZV-related CNS infections developed in 6 patients after they had COVID-19 vaccinations. Our study is insufficient to elucidate an association between VZV-related CNS infection and COVID-19 or COVID-19 vaccination; further studies are needed to clarify this issue.

Postherpetic neuralgia has been considered to be the greatest contributor to disease burden caused by VZV reactivation, and it has been demonstrated that both live-attenuated and subunit zoster vaccines reduced the risks of herpes zoster infection and postherpetic

neuralgia (*27*). This study shows that in addition to herpes zoster and postherpetic neuralgia, VZV-related CNS infections might be a cause of the disease burden associated with VZV reactivation. The zoster vaccine is expected to reduce the risk for VZV-related CNS infections, as has already been shown for herpes zoster and postherpetic neuralgia (*27*). Recent studies have suggested that VZV reactivation might be associated with the pathogenesis of more severe CNS diseases, such as brain infarction (*28*) and dementia (*29*). Furthermore, large cohort analyses have demonstrated that the zoster vaccine can reduce the risk for brain infarction (*17*) and dementia (*18*). In this study, no patients with VZV-related CNS infection for whom vaccination history was available had received the zoster vaccine. Therefore, determining whether the zoster vaccine can reduce the burden of additional diseases, including VZV-related CNS infection, is key. Such studies will provide information to aid in determining the ability of the zoster vaccine to reduce healthcare costs in aging populations and in evaluating the cost-effectiveness of implementing universal zoster vaccination.

To determine whether the clinical features of VZV-related CNS infections differed at our institution before and after the beginning of the temporal cluster of those diseases in 2019, we compared patients' background and clinical characteristics during 2013–2018 with those during 2019–2022. Of note, most patients (86.8%) in the late period received a diagnosis of aseptic meningitis, compared with only half in the early period (p = 0.0029). Conversely, incidence of encephalitis was significantly higher in the early period (p = 0.014). In addition, a significantly higher percentage of patients had

abnormal brain MRI findings in the early period (p = 0.0253), suggesting a high frequency of encephalitis patients in that period. Although a previous study found that VZV meningitis patients were significantly younger than VZV encephalitis patients (*19*), no statistically significant difference in age was observed between the 2 periods in this study. We did not change the criteria for performing a spinal tap or brain MRI during the study; further research is needed to clarify the reasons for the recent increase in the number of patients with VZV-related aseptic meningitis. Furthermore, most patients with VZV-related CNS infections before 2018 had herpes zoster infection, whereas in the late period, ≈30% of the patients did not have a zosteriform rash (zoster sine herpete); however, no significant difference was observed in frequency. We recently demonstrated that the reactivated Oka vaccine strain caused aseptic meningitis in a child without herpes zoster virus (*30*). Although some physicians might previously not have measured VZV DNA in CSF collected from patients without the typical herpes zoster rash, the recent introduction of comprehensive PCR panel tests, such as FilmArray (bioMérieux, https://www.biomerieux.com), might reveal the precise incidences of VZV-related CNS infections that occur without this rash.

Molecular epidemiologic analysis in this study demonstrated that all evaluated VZV DNA in CSF was derived from wild-type VZV. In Japan, 2 doses of varicella vaccination were introduced as part of the national immunization schedule in 2014. Meanwhile, 2 different zoster vaccines, specifically Shingrix (a recombinant subunit vaccine) and varicella-zoster Oka vaccine (a live-attenuated vaccine), have been licensed and are available in Japan, whereas only Shingrix is currently recommended for herpes zoster vaccination in the United States (*31*). Therefore, some elderly persons have received a live-attenuated zoster Oka vaccine, and the number of recipients of that vaccine is expected to increase dramatically in the future. Although the risk of viral reactivation of the Oka vaccine strain was shown to be lower than that of wild-type VZV on the basis of in vivo (*32*) and in vitro (*33*) studies, the Oka vaccine strain is well known to be capable of reactivating and causing herpes zoster infection (*34*). In addition, a recent study detected Oka vaccine strain DNA in CSF collected from patients with CNS infection, although the number of patients was very small, and all were children and young adults (*11*). Therefore, the reactivated Oka vaccine strain could feasibly cause VZV-related CNS infections, and molecular epidemiologic analysis to distinguish between wild-type and vaccine-type strains will become increasingly key in future.

Conclusions

In this study, we investigated 10-year trends and clinical features of VZV-related CNS infections in adult patients with suspected CNS infection at our university hospital in Japan. Statistical analysis revealed a significant temporal cluster of patients with VZV-associated CNS infections during 2019–2022, as well as an increasing proportion of aseptic meningitis caused by VZV reactivation during that period. Although all detected VZV DNA was the wild-type strain in this study, molecular epidemiologic studies to differentiate between vaccine and wild-type strains will be key in the future.

About the Author

Dr. Yoshikane is a graduate student at Fujita Health University School of Medicine. Her research interest is neurology, with a particular emphasis on analyzing central nervous system infections in adult patients.

References

1. Takahashi M, Otsuka T, Okuno Y, Asano Y, Yazaki T, Isomura S. Live vaccine used to prevent the spread of varicella in children in hospital. Lancet. 1974;2:1288–90. https://doi.org/10.1016/S0140-6736(74)90144-5
2. Seward JF, Watson BM, Peterson CL, Mascola L, Pelosi JW, Zhang JX, et al. Varicella disease after introduction of varicella vaccine in the United States, 1995–2000. JAMA. 2002;287:606–11. https://doi.org/10.1001/jama.287.5.606
3. Hattori F, Kozawa K, Miura H, Kawamura Y, Higashimoto Y, Yoshikawa A, et al.; Nagoya VZV Study Group. Trend in varicella patients 4 years after implementation of universal two-dose varicella vaccination in Japan. Vaccine. 2020;38:7331–6. https://doi.org/10.1016/j.vaccine.2020.09.038
4. Bhavsar A, Lonnet G, Wang C, Chatzikonstantinidou K, Parikh R, Brabant Y, et al. Increased risk of herpes zoster in adults ≥50 years old diagnosed with COVID-19 in the United States. Open Forum Infect Dis. 2022;9:ofac118. https://doi.org/10.1093/ofid/ofac118
5. Wan EYF, Chui CSL, Wang Y, Ng VWS, Yan VKC, Lai FTT, et al. Herpes zoster related hospitalization after inactivated (CoronaVac) and mRNA (BNT162b2) SARS-CoV-2 vaccination: a self-controlled case series and nested case-control study. Lancet Reg Health West Pac. 2022; 21:100393. https://doi.org/10.1016/j.lanwpc.2022.100393
6. Hope-Simpson RE. The nature of herpes zoster: a long-term study and a new hypothesis. Proc R Soc Med. 1965;58:9–20. https://doi.org/10.1177/003591576505800106
7. Brisson M, Gay NJ, Edmunds WJ, Andrews NJ. Exposure to varicella boosts immunity to herpes-zoster: implications for mass vaccination against chickenpox. Vaccine. 2002;20:2500–7. https://doi.org/10.1016/S0264-410X(02)00180-9
8. Toyama N, Shiraki K; Miyazaki Dermatologist Society. Universal varicella vaccination increased the incidence of herpes zoster in the child-rearing generation as its

short-term effect. J Dermatol Sci. 2018;92:89–96. https://doi.org/10.1016/j.jdermsci.2018.07.003

9. Pevenstein SR, Williams RK, McChesney D, Mont EK, Smialek JE, Straus SE. Quantitation of latent varicella-zoster virus and herpes simplex virus genomes in human trigeminal ganglia. J Virol. 1999;73:10514–8. https://doi.org/10.1128/JVI.73.12.10514-10518.1999

10. Tanaka N, Kimura H, Hoshino Y, Kato K, Yoshikawa T, Asano Y, et al. Monitoring four herpesviruses in unrelated cord blood transplantation. Bone Marrow Transplant. 2000;26:1193–7. https://doi.org/10.1038/sj.bmt.1702710

11. Bryant P, Yildirim T, Griesemer SB, Shaw K, Ehrbar D, St George K. Vaccine strain and wild-type clades of varicella-zoster virus in central nervous system and non-CNS disease, New York State, 2004–2019. J Clin Microbiol. 2022;60:e0238121. https://doi.org/10.1128/jcm.02381-21

12. Gershon AA, Breuer J, Cohen JI, Cohrs RJ, Gershon MD, Gilden D, et al. Varicella zoster virus infection. Nat Rev Dis Primers. 2015;1:15016. https://doi.org/10.1038/nrdp.2015.16

13. Persson A, Bergström T, Lindh M, Namvar L, Studahl M. Varicella-zoster virus CNS disease—viral load, clinical manifestations and sequels. J Clin Virol. 2009;46:249–53.

14. Omland LH, Vestergaard HT, Dessau RB, Bodilsen J, Andersen NS, Christiansen CB, et al. Characteristics and long-term prognosis of Danish patients with varicella zoster virus detected in cerebrospinal fluid compared with the background population. J Infect Dis. 2021;224:850–9. https://doi.org/10.1093/infdis/jiab013

15. Ishimaru S, Kawamura Y, Miura H, Shima S, Ueda A, Watanabe H, et al. Detection of human herpesviruses in cerebrospinal fluids collected from patients suspected of neuroinfectious diseases. J Neurovirol. 2022;28:92–8. https://doi.org/10.1007/s13365-021-01040-5

16. Kimura H, Morita M, Yabuta Y, Kuzushima K, Kato K, Kojima S, et al. Quantitative analysis of Epstein-Barr virus load by using a real-time PCR assay. J Clin Microbiol. 1999; 37:132–6. https://doi.org/10.1128/JCM.37.1.132-136.1999

17. Yang Q, Chang A, Tong X, Merritt R. Herpes zoster vaccine live and risk of stroke among Medicare beneficiaries: a population-based cohort study. Stroke. 2021;52:1712–21. https://doi.org/10.1161/STROKEAHA.120.032788

18. Scherrer JF, Salas J, Wiemken TL, Hoft DF, Jacobs C, Morley JE. Impact of herpes zoster vaccination on incident dementia: a retrospective study in two patient cohorts. PLoS One. 2021;16:e0257405. https://doi.org/10.1371/journal.pone.0257405

19. Yan Y, Yuan Y, Wang J, Zhang Y, Liu H, Zhang Z. Meningitis/meningoencephalitis caused by varicella zoster virus reactivation: a retrospective single-center case series study. Am J Transl Res. 2022;14:491–500.

20. Pinchinat S, Cebrián-Cuenca AM, Bricout H, Johnson RW. Similar herpes zoster incidence across Europe: results from a systematic literature review. BMC Infect Dis. 2013;13:170. https://doi.org/10.1186/1471-2334-13-170

21. Carryn S, Cheuvart B, Povey M, Dagnew AF, Harpaz R, van der Most R, et al. No consistent evidence of decreased exposure to varicella-zoster virus among older adults in countries with universal varicella vaccination. J Infect Dis. 2022;225:413–21. https://doi.org/10.1093/infdis/jiab500

22. Varghese L, Standaert B, Olivieri A, Curran D. The temporal impact of aging on the burden of herpes zoster. BMC Geriatr. 2017;17:30. https://doi.org/10.1186/s12877-017-0420-9

23. Marra F, Parhar K, Huang B, Vadlamudi N. Risk factors for herpes zoster infection: a meta-analysis. Open Forum Infect Dis. 2020;7:ofaa005. https://doi.org/10.1093/ofid/ofaa005

24. You IC, Ahn M, Cho NC. A case report of herpes zoster ophthalmicus and meningitis after COVID-19 vaccination. J Korean Med Sci. 2022;37:e165. https://doi.org/10.3346/jkms.2022.37.e165

25. Medhat R, El Lababidi R, Abdelsalam M, Nusair A. Varicella-zoster virus (VZV) meningitis in an immunocompetent adult after BNT162b2 mRNA COVID-19 vaccination: a case report. Int J Infect Dis. 2022;119:184–6.

26. Daouk SK, Kamau E, Adachi K, Aldrovandi GM. Zoster meningitis in an immunocompetent child after COVID-19 vaccination, California, USA. Emerg Infect Dis. 2022;28:1523–4. https://doi.org/10.3201/eid2807.220600

27. Oxman MN, Levin MJ, Johnson GR, Schmader KE, Straus SE, Gelb LD, et al.; Shingles Prevention Study Group. A vaccine to prevent herpes zoster and postherpetic neuralgia in older adults. N Engl J Med. 2005;352:2271–84. https://doi.org/10.1056/NEJMoa051016

28. Lian Y, Zhu Y, Tang F, Yang B, Duan R. Herpes zoster and the risk of ischemic and hemorrhagic stroke: a systematic review and meta-analysis. PLoS One. 2017;12:e0171182. https://doi.org/10.1371/journal.pone.0171182

29. Chen VC, Wu SI, Huang KY, Yang YH, Kuo TY, Liang HY, et al. Herpes zoster and dementia: a nationwide population-based cohort study. J Clin Psychiatry. 2018;79:16m11312. https://doi.org/10.4088/JCP.16m11312

30. Kawamura Y, Suzuki D, Kono T, Miura H, Kozawa K, Mizuno H, et al. A case of aseptic meningitis without skin rash caused by Oka varicella vaccine. Pediatr Infect Dis J. 2022;41:378–9. https://doi.org/10.1097/INF.0000000000003316

31. Boutry C, Hastie A, Diez-Domingo J, Tinoco JC, Yu CJ, Andrews C, et al.; Zoster-049 Study Group. The adjuvanted recombinant zoster vaccine confers long-term protection against herpes zoster: interim results of an extension study of the pivotal phase 3 clinical trials ZOE-50 and ZOE-70. Clin Infect Dis. 2022;74:1459–67. https://doi.org/10.1093/cid/ciab629

32. Weinmann S, Naleway AL, Koppolu P, Baxter R, Belongia EA, Hambidge SJ, et al. Incidence of herpes zoster among children: 2003–2014. Pediatrics. 2019;144:e20182917. https://doi.org/10.1542/peds.2018-2917

33. Sadaoka T, Depledge DP, Rajbhandari L, Venkatesan A, Breuer J, Cohen JI. In vitro system using human neurons demonstrates that varicella-zoster vaccine virus is impaired for reactivation, but not latency. Proc Natl Acad Sci U S A. 2016;113:E2403–12. https://doi.org/10.1073/pnas.1522575113

34. Galea SA, Sweet A, Beninger P, Steinberg SP, Larussa PS, Gershon AA, et al. The safety profile of varicella vaccine: a 10-year review. J Infect Dis. 2008;197(Suppl 2):S165–9. https://doi.org/10.1086/522125

Address for correspondence: Hiroki Miura, Department of Pediatrics, Fujita Health University School of Medicine; 1-98 Dengakugakubo, Kutsukake-cho, Toyoake, Aichi, 470-1192, Japan; email: hiroki-m@fujita-hu.ac.jp

Historical Assessment and Mapping of Human Plague, Kazakhstan, 1926–2003

Nurkuisa Rametov,[1] Ziyat Abdel, Zauresh Zhumadilova, Duman Yessimseit, Beck Abdeliyev, Raikhan Mussagaliyeva, Svetlana Issaeva, Omar F. Althuwaynee, Zhaksybek Baygurin, Kairat Tabynov[1]

Understanding Kazakhstan's plague history is crucial for early warning and effective health disaster management. We used descriptive-analytical methods to analyze spatial data for human cases in natural plague foci in Kazakhstan during 1926–2003. The findings revealed 565 human cases across 82 outbreaks in Almaty (32.22%), Aktobe (1.59%), Atyrau (4.42%), Mangystau (21.24%), and Kyzylorda (40.53%) oblasts. Before antibiotic drugs were introduced in 1947–1948, major plague outbreaks occurred in 1926, 1929, 1945, 1947, and 1948, constituting 80.7% of human transmission. Plague spread through flea bites, camel handling, wild animal contact, aerosol transmissions, and rodent bites. Patients were up to 86 years of age; 49.9% were male and 50.1% female. Pulmonary cases were reported most frequently (72.4%), and person-to-person infection occurred at an incidence rate of 0.29 cases/10,000 population. Risk increased with human expansion into natural plague foci areas. Swift diagnosis and treatment are essential for curbing plague outbreaks in Kazakhstan.

The Soviet plague control system was established in the early 20th Century as a comprehensive strategy to combat plague outbreaks across the vast territories of the former Soviet Union. That system was characterized by its focus on surveillance, prevention, and rapid response to plague epidemics. The approach involved the creation of specialized plague control institutes and stations, which were responsible for monitoring and controlling the spread of plague within designated areas. In Kazakhstan, which has a long history of plague endemicity, the Soviet system was adapted to suit the region's unique geographic and ecologic conditions. Soviet authorities divided plague-endemic territories into natural foci on the basis of ecologic and epidemiologic characteristics. Within those larger foci, the territory was further subdivided into smaller subfoci that represented more specific areas where plague activity was particularly concentrated, often because of specific ecologic conditions, such as soil composition, climate, and particular rodent and flea species.

Plague is an endemic disease of Kazakhstan, and epidemic outbreaks of plague among the population have been known for a long time (*1–3*), which is evidenced by the historical names of geographic areas that include the Kazakh root *oba* (plague), including Karaoba (*kara* [black] plus *oba*); Kosoba (*kos* [both] plus *oba*); Kyzyloba (*kyzyl* [red] plus *oba*), and Besoba (*bes* [five] plus *oba*) (*1,2*). In the late 19th and early 20th Centuries, outbreaks of plague among the population of western Kazakhstan became more frequent and larger. During 1905–1906, an epidemic of the so-called Beketayev plague was registered in the Naryn part of the Volga-Ural sands, where 659 persons fell ill and 621 died (*1–5*). Later, outbreaks of plague among the population of Kazakhstan were also noted in 1907, 1910–1914, 1918, and 1928. However, plague epidemics did not begin to be documented by descriptive epidemiology and microbiology until 1913 (*3–5*). We used historical data on plague recorded in Kazakhstan to describe the epidemiology and spatial characteristics of human plague cases during 1926–2003.

Author affiliations: Institute of Ionosphere, Almaty, Kazakhstan (N. Rametov); M. Aikimbayev National Scientific Center for Especially Dangerous Infections, Almaty (N. Rametov, Z. Abdel, Z. Zhumadilova, D. Yessimseit, B. Abdeliyev, R. Mussagaliyeva, S. Issaeva, K. Tabynov); Kazakh National Research Technical University named after K.I. Satbayev, Almaty (N. Rametov, Z. Baygurin); Institute for Geo-Hydrological Protection of the Italian National Research Council, Perugia, Italy (O.F. Althuwaynee); Kazakh National Agrarian Research University, Almaty (K. Tabynov)

[1]These authors contributed equally to this article.

Methods

Terminology

In the context of plague epidemiology, the term natural plague foci (NPF) refers to relatively limited geographic areas where the plague-causing bacterium, *Yersinia pestis*, circulates persistently among wildlife, particularly rodent populations, over extended periods. Those areas are characterized by specific ecologic conditions that support the continuous presence of the bacterium, its hosts, and vectors, leading to the long-term maintenance of the disease in the environment.

Autonomous plague foci refers to specific geographic areas where *Y. pestis* circulates and persists independently over time without relying on external sources of infection. Those foci are characterized by a stable ecologic and epidemiologic environment that supports *Y. pestis* persistence and transmission among local wildlife, particularly rodent populations and flea vectors. In autonomous plague foci, the disease cycle is self-sustaining, meaning that *Y. pestis* can be maintained within the local ecosystem for extended periods, often decades or even centuries, without the need for reintroduction from other regions. Those foci are essential for understanding the long-term dynamics of plague and are critical targets for surveillance and control efforts to prevent the spread of the disease to surrounding areas.

The term plague carriers refers to persons who were asymptomatic but tested positive for *Y. pestis* through laboratory confirmation. Thus, those persons carried the bacterium without exhibiting typical plague symptoms.

Criteria for Defining Foci and Subfoci

We used the following criteria for defining foci and subfoci. First was, geographic boundaries, the natural boundaries of the landscape, such as mountains, rivers, and deserts, that influenced the distribution of rodent populations. Second was ecologic conditions,
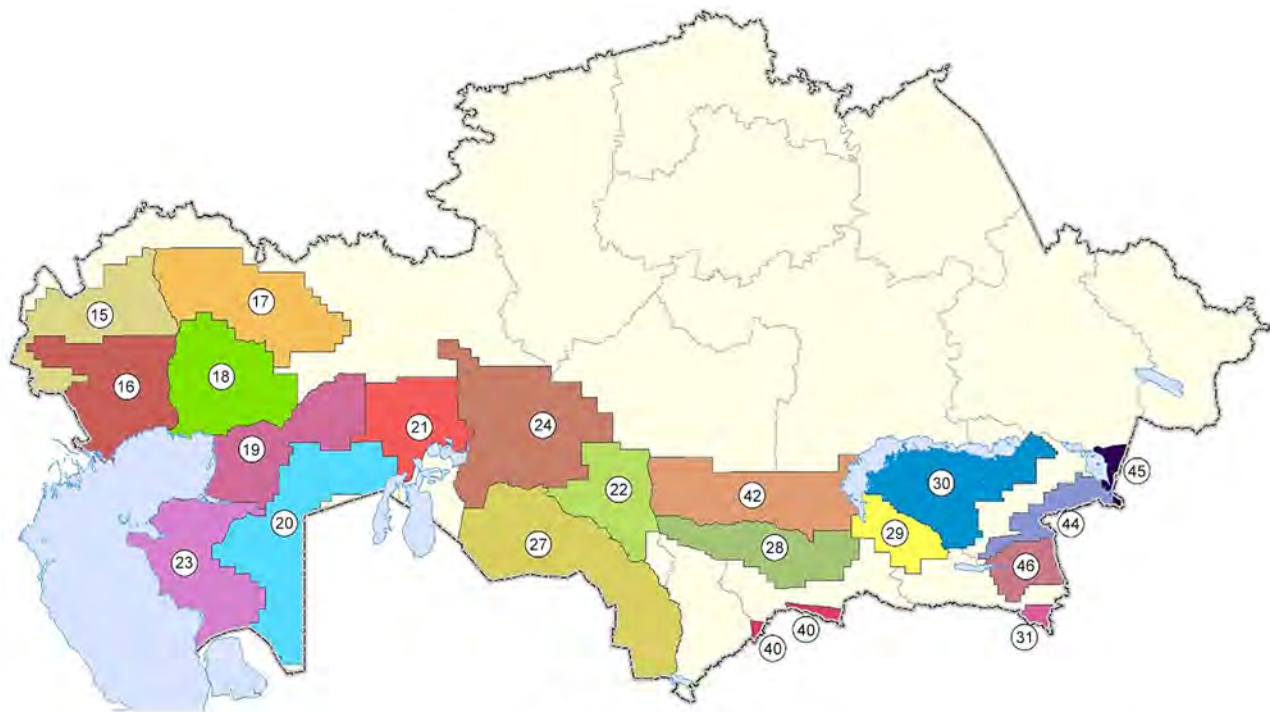
Plague foci

15. Volga-Ural, steppe
16. Volga-Ural, sandy
17. Ural-Uilsky, steppe
18. Ural-Embi, desert
19. Pre-Ustyurt, desert
20. Ustyurt, desert
21. North pre-Aral, desert

22. Aryskum-Daryalyktakyr, desert
23. Mangystau, desert
24. Pre-Aral-Karakum, desert
27. Kyzylkum, desert
28. Muyun-Kum, desert
29. Tau-Kum, desert
20. Pre-Balkhash, desert

42. Betpak-Dala, desert
45. Pre-Alakol, low mountain
46. Ili intermountain;
    Tien Shan high mountain
31. Sarydzhaz high mountain
40. Talas high mountain
44. Dzhungar high mountain

Figure 1. Locations of natural plague foci in a historical assessment and mapping of human plague, Kazakhstan, 1926–2003. Codes according to the unified country certification system, Commonwealth of Independent States. Codes indicate location names and terrain type.
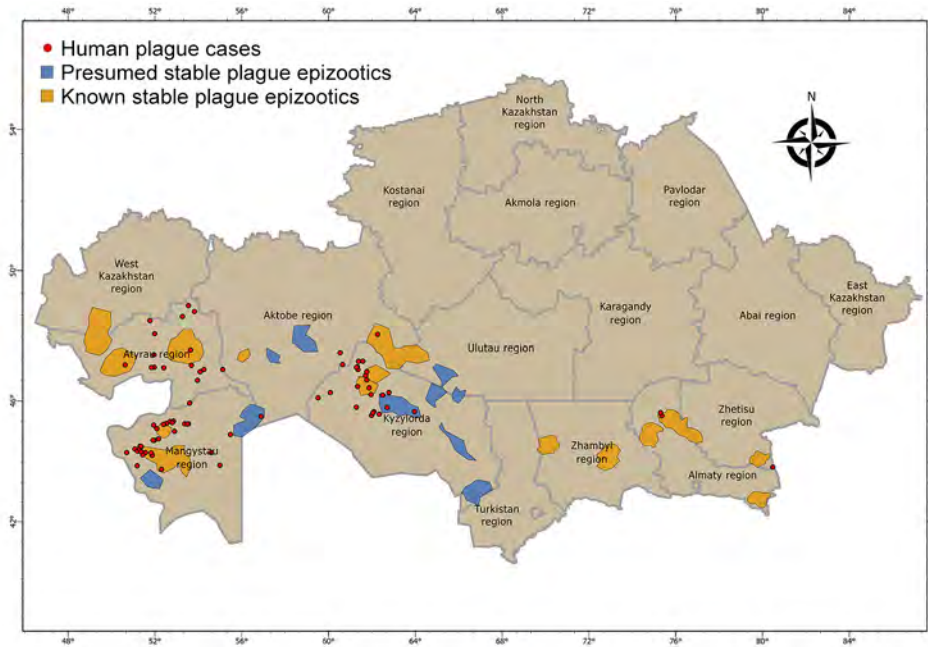
Figure 2. Epizootologic zoning of plague in a historical assessment and mapping of human plague, Kazakhstan, 1926–2003. Human plague cases and known and presumed plague epizootic areas are noted.

which include the type of vegetation, soil characteristics, and climate that affect the habitat suitability for *Y. pestis* reservoirs and vectors. Third was rodent and flea populations and density of specific rodent species known to be primary hosts for *Y. pestis* and the flea species that serve as vectors. Finally was historical data, including records of plague outbreaks and epizootics in the region, which helped identify areas with persistent plague activity.

Adaptation of the Soviet plague control system in Kazakhstan led to the systematic categorization of the region's plague-endemic areas into

foci and subfoci, which were critical for targeted surveillance and control measures. That framework remains a cornerstone of plague management in the region, guiding current efforts to monitor and mitigate risk for outbreaks.

Study Area

The natural plague endemic range in Kazakhstan is located on an area of 1,117,000 km², which is ≈41.0% of the country. The republic includes 6 natural and 15 autonomous plague foci, within which >90 landscape-epizootologic districts are allocated (6,7) (Figure 1).

Table 1. Natural plague foci and years of registration of human plague cases in a historical assessment and mapping of human plague, Kazakhstan, 1926–2003

Region	Natural plague foci	Main rodent host	Main flea vector	Year of human plague cases
Atyrau	Volga-Ural Sand	*Meriones meridianus, M. tamariscinus*	*Xenopsylla conformis, Nosopsyllus laeviceps*	1997
Atyrau	Ural-Emba	*Rhombomys opimus*	*Xenopsylla skrjabini, X. conformis, N. laeviceps, Coptopsylla lamellifer*	1956, 1958, 1964, 1968, 1986, 1988, 1989, 1990, 1992, 1993
Atyrau, Mangystau	Pre-Ustyurt	*R. opimus*	*X. skrjabini, N. laeviceps*	1958, 1959, 1961, 1967, 1975
Mangystau, Aktobe	Ustyurt	*R. opimus*	*X. skrjabini, Xenopsylla nuttalli, Xenopsylla gerbilli*	1926, 1974, 1975, 1999
Aktobe, Kyzylorda	North Pre-Aral	*R. opimus*	*X. skrjabini, N.laeviceps, C. lamellifer*	1945,1993, 1999, 2002
Mangystau	Mangyshlak	*R. opimus*	*X. skrjabini, Xenopsylla nuttalli*	1926, 1927, 1948, 1964, 1973, 1974, 2003
Aktobe, Kyzylorda	Pre–Aral-Karakum	*R. opimus*	*X. skrjabini, N. laeviceps, C. lamellifer*	1947, 1948, 1955, 1959, 1966, 1967, 1969, 1971, 1972, 1979, 1990, 1991, 1999, 2001, 2003
Kyzylorda	Kyzylkum	*R. opimus*	*X. skrjabini, X. gerbilli, Xenopsylla hirtipes*	1966, 1971,1993, 1999
Almaty	Pre-Balkhash	*R. opimus*	*X. skrjabini, X. gerbilli, X. hirtipes*	1947, 1948, 1989
Almaty	Ili Intermountain	*R. opimus*	*X. gerbilli, X. hirtipes*	1929
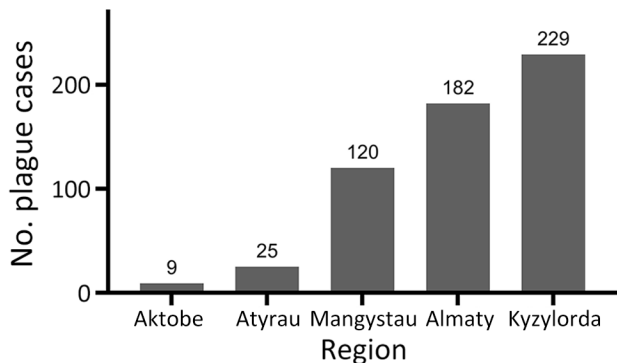
Figure 3. Numbers of human plague cases by region in a historical assessment and mapping of human plague, Kazakhstan, 1926–2003.

The main carriers of plague in the region are gerbils (*Rhombomys opimus*), ground squirrels (*Spermophilus* spp.), and marmots (*Marmota* spp.); the main flea vectors are in the genera *Xenopsylla* and *Nosopsyllus*. In Kazakhstan, plague was found in >40 species of rodents, carnivorous and insectivorous mammals, lagomorphs, ungulates, and 2 species of birds (*5,6,8*).

Human Plague Cases

We collected records of human plague cases in Kazakhstan from 1926 through 2003 from literature sources (*3–6,8–11*). Those sources identified each case by its history, site, disease outcome, suspected source of infection, clinical form, clinical confirmation, and laboratory confirmation through bacteriology or serology. We calculated incidence per 10,000 population. We collected data on the population during 1926–2003 from the archive of demographic documents (*12–14*).

We determined geographic coordinates of human plague sites by using literature sources that included an approximate area of 1,007,350 km² (*3–6,8–10,15*). We used ArcGIS Pro 2.7 software (ESRI, https://www.arcgis.com; *15*) to digitize and map locations of plague cases (Figure 2).

Statistical Analysis

We used GraphPad Prism software version 9.0.0 (GraphPad Software Inc., https://www.graphpad.com) to perform statistical analysis. To analyze age and gender differences between groups, we used 2-way analysis of variance, then the Sidak or Tukey multiple comparisons test. We considered $p<0.05$ statistically significant.

Results

Human Plague Cases

During 1926–2003, a total of 565 plague cases, including 2 cases of plague carriers, were registered in 82 foci (*3–6,8–10,15*). We included those cases in the analysis of epidemiology of plague in Kazakhstan. The last known case occurred in 2003. Plague outbreaks have been registered in 10 of 20 natural plague foci (*3–6,8*) (Table 1).
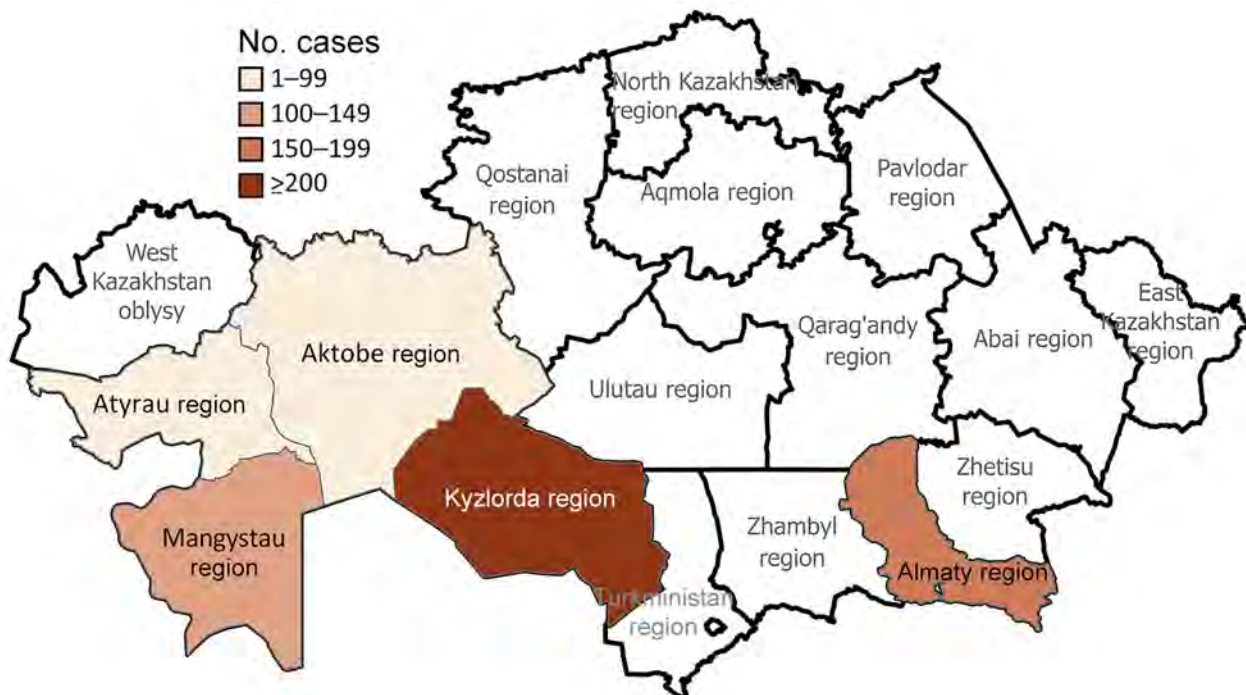
Figure 4. Locations of human plague cases by region in a historical assessment and mapping of human plague, Kazakhstan, 1926–2003.
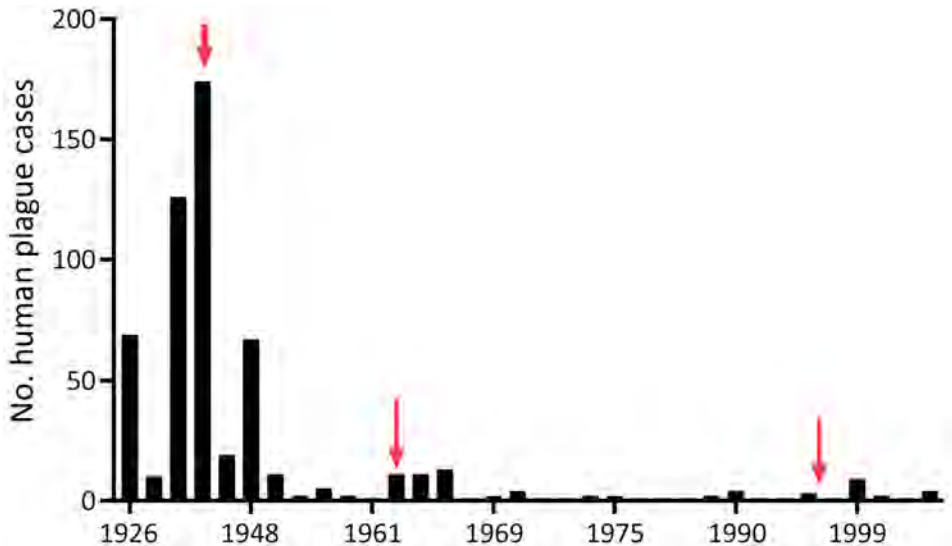
Figure 5. Annual number of cases in a historical assessment and mapping of human plague, Kazakhstan, 1926–2003. Red arrows indicate peaks.

During the 1950s through the 1970s, mass field teams worked in Kazakhstan and identified areas with stable and suspected plague epizootics (*1,2,4*). Almost all studied human plague cases overlapped with areas of stable plague epizootics (*3*) (Figure 2).

During the study period, human plague cases were registered in the regions of Almaty (32.22% of all cases), Aktobe (1.59%), Atyrau (4.42%), Mangystau (21.24%), and Kyzylorda (40.53%). The incidence rate (IR) for all cases registered during the study period was 0.29/10,000 population. The IR per 10,000 population by region was 0.52 in Almaty, 0.05 in Aktobe and Atyrau, 1.11 in Mangystau, and 0.27 in Kyzylorda (Figures 3, 4).

At the beginning of the 20th Century, many plague cases were reported, and then cases decreased. We noted 3 plague peaks during the study period (Figure 5). The first peak occurred during 1926–1948 in the west and south, where 82% of all cases were reported. For example, in 1 outbreak in Kyzylorda oblast in 1945, more than one third (37.4%) of the population became ill with plague. Those epidemics required the organization of scientific and methodology centers in Central Asia. By the Order of the Ministry of Health of the USSR, No. 739, dated December 9, 1948, and January 1, 1949, the Almaty Anti-Plague Station was transformed into the Central Asian Research Anti-Plague Institute of the Ministry of Health of the USSR, later renamed M. Aikimbayev National Scientific Center for Especially Dangerous Infections (NSCEDI) of the Ministry of Health of the Republic of Kazakhstan. NSCEDI conducted research work on plague; produced diagnostic preparations; and provided scientific, methodological, and operational guidance on the organization and implementation of a set of sanitary and prophylactic measures for plague control stations in Kazakhstan and other Central Asia republics. In addition, during 1947–1948, the Public
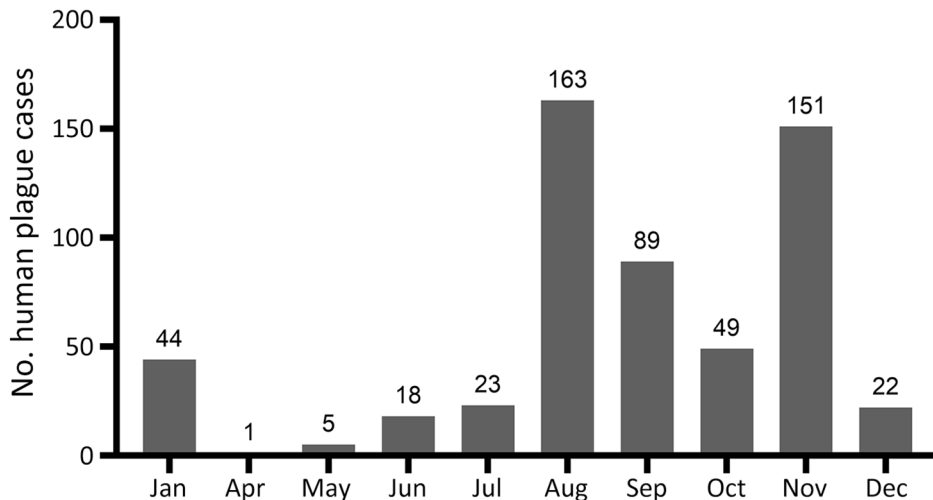
Figure 6. Human plague cases by month in a historical assessment and mapping of human plague, Kazakhstan, 1926–2003.
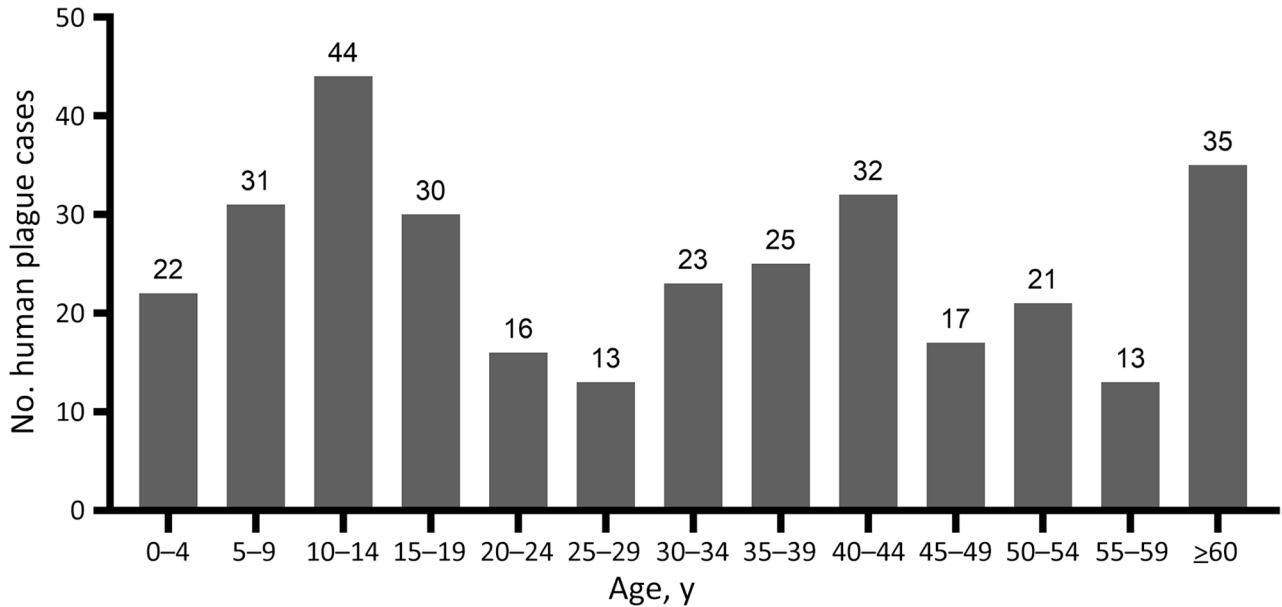
Figure 7. Human plague cases by age group a historical assessment and mapping of human plague, Kazakhstan, 1926–2003.

Health Service of Kazakhstan began to use antibiotic drugs to treat plague, vaccinate the population to prevent the disease, conduct sanitary and preventive work against plague, and conduct epidemiologic field studies. After those measures were applied, plague incidence rapidly decreased.
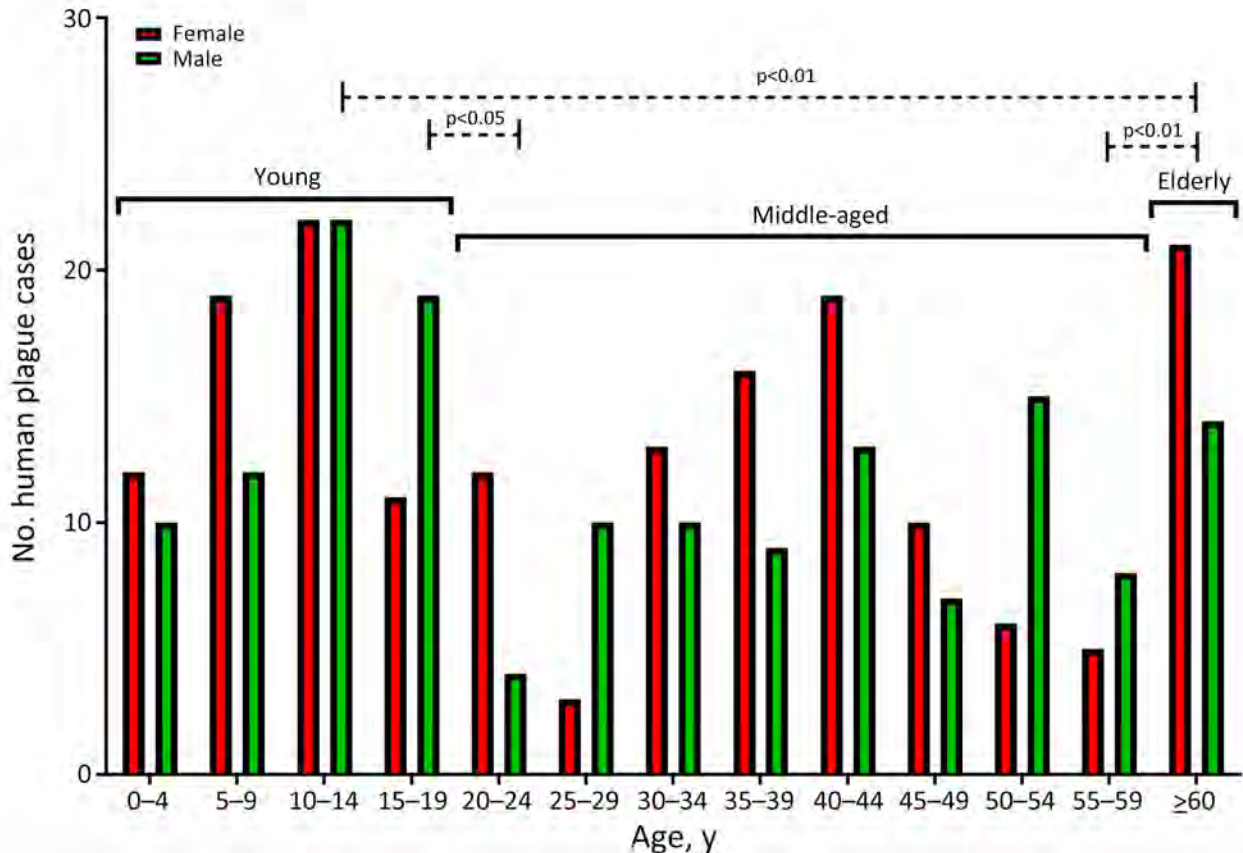
Figure 8. Human plague cases by age group and sex in a historical assessment and mapping of human plague, Kazakhstan, 1926–2003.

Table 2. Percentages of registered human plague cases per year in a historical assessment and mapping of human plague, Kazakhstan, 1926–2003*

Year	% Cases per region					% Total cases	% Confirmed (% not confirmed)	
	Aktobe	Almaty	Atyrau	Kyzylorda	Mangystau		Bacteriology	Serology
1926	0	0	0	0	12.2	12.2	100.0	–
1927	0	0	0	0	1.77	1.77	No data	No data
1929	0	22.3	0	0	0	22.3	100.0	–
1945	0	0	0	30.8	0	30.8	100.0	–
1947	0	2.3	0	1.06	0	3.36	100.0	–
1948	0	7.43	0	0.35	4.07	11.86	92.5 (7.5)‡	–
1955	0	0	0	1.95	0	1.95	100.0	–
1956	0	0	0.35	0	0	0.35	100.0	–
1958	0	0	0.88	0	0	0.88	20.0 (80.0)‡	–
1959	0	0	0.18	0.18	0	0.35	100.0	–
1961	0	0	0.18	0	0	0.18	100.0	–
1964	0	0	0.18	0	1.77	1.95	100.0	–
1966	0.35	0	0	1.59	0	1.95	36.36 (63.64)‡	–
1967	0	0	1.06	1.24	0	2.3	38.46 (46.15)‡	15.38
1968	0	0	0.18	0	0	0.18	100.0	–
1969	0	0	0	0.35	0	0.35	100.0	–
1971	0	0	0	0.71	0	0.71	No data	50.0
1972	0	0	0	0.18	0	0.18	100.0	–
1973	0	0	0	0	0.18	0.18	100.0	–
1974	0	0	0	0	0.35	0.35	100.0	–
1975	0	0	0	0	0.35	0.35	50.0 (50.0)‡	–
1979	0	0	0	0.18	0	0.18	100.0	–
1986	0	0	0.18	0	0	0.18	100.0	–
1988	0	0	0.18	0	0	0.18	100.0	–
1989	0	0.18	0.18	0	0	0.35	100.0	–
1990	0	0	0.35	0.35	0	0.71	75.0	25.0
1991	0	0	0	0.18	0	0.18	100.0	–
1992	0	0	0.18	0	0	0.18	100.0	–
1993	0.18	0	0.18	0.18	0	0.53	100.0	–
1997	0	0	0.18	0	0	0.18	100.0	–
1999	1.06†	0	0	0.53	0	1.59	100.0	–
2001	0	0	0	0.35	0	0.35	50.0	50.0
2002	0	0	0	0.18	0	0.18	0	100.0
2003	0	0	0	0.18	0.53	0.71	75.0	25.0
Total	1.59†	32.21	4.44	40.54	21.22	100.0	92.3	1.41

*–, cases that were not tested
†Cases included 2 plague carrier cases.
‡*Y. pestis* not isolated.

The second plague period occurred during 1955–1989, which accounted for 13.0% of all cases during the analyzed period. Few cases were reported during that time, but a slight increase was noted during 1961–1967 related to the slaughter of plague-affected camels. During those years, 6.37% of the population contracted plague, among whom 75.0% were infected through contact with sick camels. At one time, dozens of persons participated in the slaughter of camels, and all could have contracted plague at the same time. Then, the government issued an order stating that camel owners could receive compensation if their camels were infected with plague and the owners reported infected camels to the authorities. That order contributed to the reduction of cases involving sick camels (*1,3,4*).

A third period of increasing incidence occurred during 1990–2003, which accounted for 5.0% of all cases during the analyzed period. During that time, the Soviet Union collapsed, infrastructure was destroyed,

and the economy in Kazakhstan deteriorated. Epidemiologic surveillance of plague was not fully funded and could not cover all plague endemic areas. After the economic situation of the country improved, plague incidence decreased, and the last case was registered in 2003 (Figure 5).

Most plague cases were reported in the months of January, August, September, October, and November (Figure 6). January, October, November, and December cases occurred during major outbreaks recorded in 1926, 1929, 1945, 1947, and 1948, and plague was spread by humans during those outbreaks (Figure 6).

During the study period, we noted multiple clinical forms of plague. Among reports we found 12.57% bubonic, 5.84% bubonic septicemic, 1.06% bubonic pneumonia, 72.4% pulmonary, 0.35% secondary pneumonia, 2.83% septicemic, 0.18% cutaneous, 0.88% cutaneous bubonic, 0.35% tonsillar, and 0.18% tonsillar bubonic forms; 3.36% of cases had no clinical form data. We also observed that 71.15% of plague
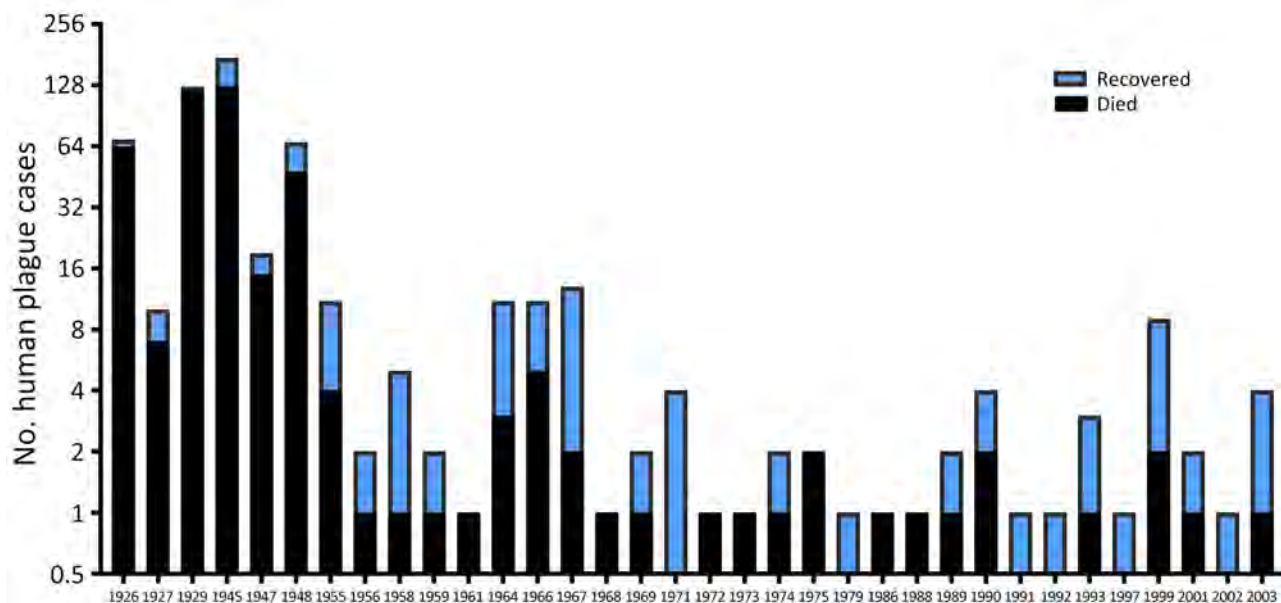
Figure 9. Human plague cases by outcome in a historical assessment and mapping of human plague, Kazakhstan, 1926–2003.

infections occurred from person-to-person transmission. Other infection sources included fleas (12.39%), camels (12.39%), hares (0.88%), aerosols (0.53%), foxes (0.35%), rodent bites (0.18%), saiga antelope (*Saiga tatarica*) (0.18%), and feral cats (0.18%); 1.77% of cases had no available transmission data.

Among case-patients, we noted 3 age subgroups: young (0–19 years of age), middle (20–59 years of age), and older (≥60 years of age) (Figure 7). When we analyzed age and sex distribution, we found that female and male persons were at equal risk for plague infection. However, we found age differences for both sexes in the young, middle, and older age groups (Figure 8). Most cases among female persons were registered in 8 different age groups. The highest number of cases for both sexes was observed in the 10–14-year age group. The highest number of cases in women was observed in the ≥60-year age group and for male persons in the 15–19-year age group. The lowest number of cases among women was observed in the 25–29-year age group and among men in the 20–24-year age group (Figure 8).

In 1913, human plague epidemics began to be documented by using descriptive epidemiology and microbiology (*12*). Cases were confirmed on the basis of epidemiologic, clinical, serologic, and bacteriologic data. Most human plague cases were confirmed by bacteriologic methods and isolation of *Y. pestis* (Table 2).

We noted that higher mortality rates were recorded in 1926, 1927, 1929, 1945, and 1948 (Figure 9). In total, ≈26% of patients recovered from plague. Areas with higher mortality rates included Mangystau

oblast in 1926, 1927, and 1948; Alma-Ata in 1929 and 1948; and Kyzylorda oblast in 1945.

During the study period, the IR was 0.01–56.1/10,000 population, and case-fatality rates (CFRs) ranged up to 100% (Table 3), but CFR was high for most of the study period. IR was high during 1926–1927 but declined after that timeframe (Table 3). The highest observed IR was from the Kul Kara settlement in Mangystau oblast in 1926. During that outbreak in mid-August, the death of a child led to person-to-person spread of infection. By September 20 of that year, 41 of 72 persons living in the village had died of pneumonic plague, and other cases were registered in different villages in Buzachi Peninsula of the oblast. At that time, Mangystau oblast had 12,300 residents (*9,12,13,15,16*).

We analyzed the number of outbreaks and percentage of affected population during the study period. We found that that 31 outbreaks were registered in the Mangyshlak desert NPF, accounting for 13.4% of all plague cases during the study period. In the Priaralie Karakum NPF, 17 foci and 8.8% of plague cases were registered. In the Ural-Emba desert NPF, 11 foci with 2.7% of cases were reported. In the Priustyurt desert NPF, 6 outbreaks occurred and 1.8% of the population was infected. In the Kyzylkum desert NPF, plague infected 1.1% of the population during 5 outbreaks. In the Ustyurt desert NPF, 4 outbreaks occurred, and plague infected 8.1% of the population. In the North-Priaral Desert NPF, 4 outbreaks occurred, and 31.7% of the population was infected. The Volga-Ural sandy NPF only had 1 outbreak, in which 0.2% of the population was infected. One major outbreak

occurred in the Iliysk intermountain NPF, where plague infected 22.3% of the population. Two outbreaks occurred in the Pribalkhash desert NPF, where plague affected 9.9% of the population.

Cases of plague among humans were registered in places with stable epizootic plague activity (Figure 10, panels A, B). Mangystau oblast had the most outbreaks, and Almaty and Aktobe oblasts had the fewest (Figure 10).

Discussion

We analyzed 82 human plague outbreaks that occurred within 10 natural plague foci in Kazakhstan. Although human-to-human plague transmission occurred, we observed that a higher percentage of persons came in contact with *Y. pestis* through flea bites, mainly during summer and fall, and that human cases were associated with local epizootics of plague among wild rodents. Human-to-human transmission has been observed in large and small outbreaks. Other modes of infection were also observed, including cutting or skinning of animals.

We found that camels played a major role as a source of human infections (Table 4). In summer (July and August), camels come in contact with *Y. pestis* during active plague epizootics among rodents. In September and October, camels infected during plague epizootics in summer could transmit *Y. pestis* to humans during butchering. Camels were infected by various flea vectors, depending on the season: *Xenopsylla* spp. fleas during November, December, and January, and fall flea vector fleas *Coptopsylla* spp. and *Ceratophyllus* spp. in September or October (9–11).

We noted persons 0–19 years of age contracted plague while working in the fields, herding livestock, playing in a plague zone, and hunting with falcons and golden eagles. Adults 20–59 years of age were infected with *Y. pestis* while grazing animals, slaughtering camels, hunting, harvesting fox and hare skins, working in the fields, and other outdoor activities. Persons ≥60 years of age mainly were infected while helping in slaughtering animals and working in the fields.

When analyzing cases by age groups and sex, we found that, among age groups 15–19, 25–29, 50–54, and 55–59 years, cases were mostly among men and boys, who were involved in herding animals and slaughtering and skinning sick camels and wild animals. However, we noted more girls and women were infected with plague in other age groups, except in the 10–14-year age group, where the number of cases were equal among girls and boys. More (56%) girls and women were infected with plague during the major epidemics that occurred in 1945, 1947, and 1948; many were infected

while cutting meat from camels or wild animals or during daily work in gardens and fields.

During the analyzed period, 70.1% of plague cases were confirmed by bacteriologic methods, 1.4% by serology after those diagnostic methods were added to surveillance efforts in 1967, and 4.1% by clinical diagnosis; 2.1% of cases had no confirmatory diagnostic data available. According to the records, some patients used antibiotic drugs before samples were collected, and no bacteriologic confirmation was made. Indirect hemagglutination reaction serologic method was used for confirmation in 2% of cases.

The IR for plague was high in the early 20th Century and then decreased, after which the incidence plummeted as a result of plague monitoring and control programs and the use of antimicrobial drugs, insecticides, and vaccine prophylaxis (4,14). During 1926–2003, IR was 0.01–56.1/10,000 population. The mortality rate was high in almost all periods studied. For example, in the 1945 outbreak in Kyzylorda oblast, the mortality rate was 73%. In the 1920s, the mortality rate was high because treatment and

Table 3. Incidence and fatality rates in a historical assessment and mapping of human plague, Kazakhstan, 1926–2003

Year	% Cases*	Incidence rate†	Case-fatality rate, %
1926	12.2	56.1	93.0
1927	1.77	8.13	70.0
1929	22.3	4.56	95.0
1945	30.8	5.3	73.0
1947	3.36	0.17	79.0
1948	11.86	0.58	72.0
1955	1.95	0.34	36.0
1956	0.35	0.08	50.0
1958	0.88	0.20	20.0
1959	0.35	0.03	50.0
1961	0.18	0.04	100.0
1964	1.95	0.34	27.0
1966	1.95	0.15	45.0
1967	2.3	0.22	15.0
1968	0.18	0.04	100.0
1969	0.35	0.06	50.0
1971	0.71	0.08	0.00
1972	0.18	0.02	100.0
1973	0.18	0.05	100.0
1974	0.35	0.10	50.0
1975	0.35	0.09	100.0
1979	0.18	0.02	0.00
1986	0.18	0.03	100.0
1988	0.18	0.03	100.0
1989	0.35	0.01	50.0
1990	0.71	0.04	50.0
1991	0.18	0.02	0.0
1992	0.18	0.02	0.0
1993	0,53	0.02	33.0
1997	0.18	0.02	0.0
1999	1.59	0.07	22.0
2001	0.35	0.03	50.0
2002	0.18	0.02	0.0
2003	0.71	0.04	25.0

*Values indicate percentage of cases recorded during the study period.
†Reported as cases per 10,000 population.
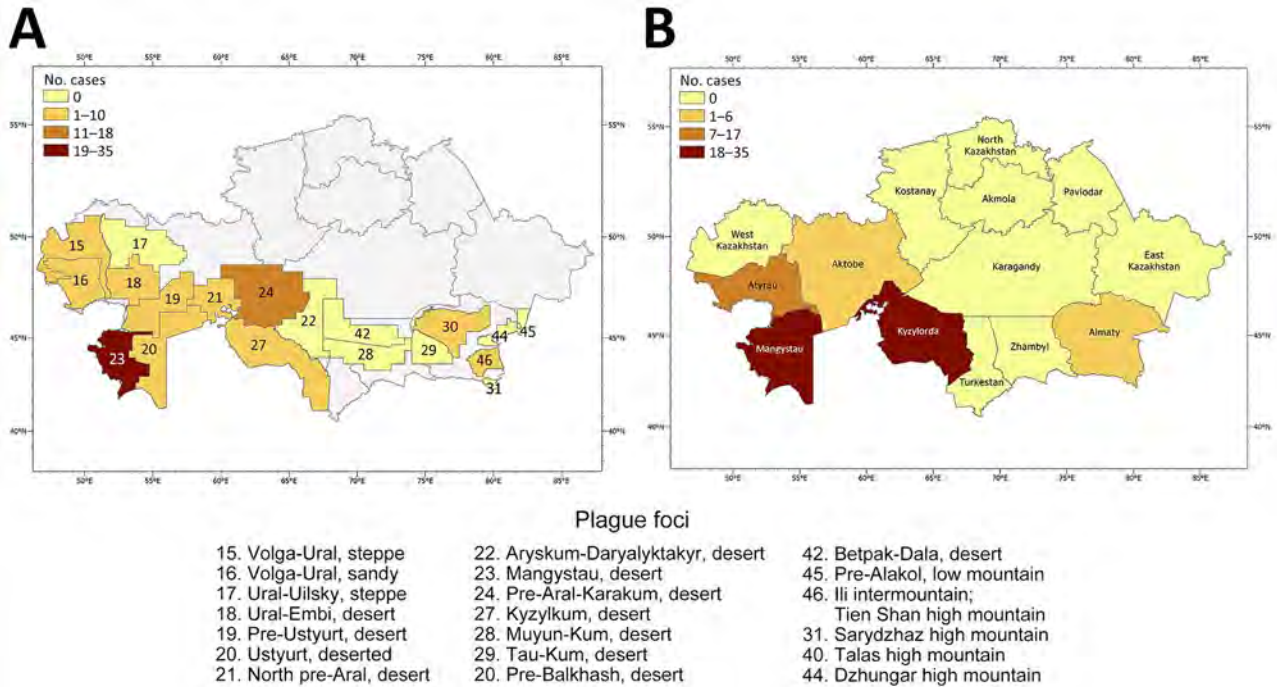
Figure 10. Human plague outbreaks in a historical assessment and mapping of human plague, Kazakhstan, 1926–2003. A) Number of plague outbreaks per natural plague foci; B) number of outbreaks by region.

prophylaxis measures were limited. In subsequent years, high mortality rates were associated with delayed treatment, incorrect and late plague diagnoses, presence of concomitant chronic diseases, late referral of patients to doctors, and remote location of patients.

Of note, study data from 2021 suggest that the area of natural foci with gopher-type *Y. pestis* Medievalis biovar 2.MED strain circulation is 221,347 km² and that the *Y. pestis* sandstone-type has a 1,728,676-km² range (*17*). Thus, *Y. pestis* strains of the phylogenetic branch of the Medievalis biovar 2.MED1 may have been the cause of the 1945 outbreak and 2.MED0 might have been the cause of plague outbreaks in the 1920s.

Natural plague foci in Kazakhstan vary in terms of occupied area, activity of epizootic process manifestation, and studied biocenotic and spatial structure, as well as varying risks for epidemiologic complications. On the basis of our findings, we included 139 sectors in the group with a very high degree of potential epidemic

hazard, 375 sectors with high, 989 sectors with medium, 7,127 sectors with low, and 5,991 sectors with very low degree of potential epidemic hazard (*18*).

Considering the current epizootic plague situation, plague control stations and other medical and prophylactic organizations of Kazakhstan annually carry out the necessary sanitary, and preventive measures. In addition, the country conducts special plague mitigation measures, primarily epizootologic surveillance of focal areas, vaccination of humans and camels, village disinfection and deratization, creation of protective zones by field disinfection around settlements, and sanitary and educational work. The sufficient quantity and timeliness of prophylactic measures in Kazakhstan has reduced the risk for human and camel *Y. pestis* infection and absence of plague since 2003 (*18*).

The study faced difficulties in reconstructing each plague case because the cases were recorded in different sources and some sources did not have complete

Table 4. Month and infection route in a historical assessment and mapping of human plague, Kazakhstan, 1926–2003*

Infection route	Jan	Apr	May	Jun	Jul	Aug	Sep	Oct	Nov	Dec
Human-to-human	7.43	0	0	0.18	0.53	16.81	14.69	6.90	22.30	2.12
Flea bite	0.18	0	0.88	2.65	1.59	2.30	0.53	1.59	2.48	0.35
Animal butchering or skinning	0	0	0	0.35	0	0.53	0	0	0.71	0
Rodent bite	0	0.18	0	0	0	0	0	0	0	0
Camel butchering or skinning	0.18	0	0	0	1.41	7.43	0.53	0.18	1.24	1.41
Aerosol	0	0	0	0	0.53	0	0	0	0	0
Unknown	0	0	0	0	0	1.81	0	0	0	0
Total	7.81	0.18	0.88	3.18	4.07	28.85	15.75	8.67	26.72	3.89

*Values indicate percentage of cases recorded during the study period.

data. In addition, the historical records omitted some data on patients' sex, age, occupation, laboratory data, and clinical confirmation of cases. Those limitations may result in underestimation of incidence and fatality rates and may affect our ability to analyze demographic patterns accurately. Consequently, the study's findings may not fully capture the scope or severity of the epidemic, potentially underrepresenting certain affected groups or trends.

Conclusions

In Kazakhstan, from 1926 through 2003, plague cases were registered for 565 persons in 82 plague foci. Most outbreaks occurred during 1926–1948, before antibiotics and prophylactic measures were introduced in plague-endemic areas, after which the number of cases decreased. All cases were registered in plague areas of a 1,007,350-km^2 area overlapping with stable plague epizootics.

In summary, even though the last case was registered in 2003, plague is still relevant in Kazakhstan; active plague epizootics are observed among wild rodents in plague-endemic areas, and local plague institutions annually isolate *Y. pestis* from animals and flea vectors. Thus, to aid early warning and decision support for adequate treatment, up-to-date descriptive analyses are needed to curb effects of plague on the human population of Kazakhstan.

About the Author

Dr. Rametov is a geographic information system analyst at the M. Aikimbayev National Scientific Center for Especially Dangerous Infections, Almaty, Kazakhstan. His primary research interest is infectious diseases characterization and bioinformatics with the goal of linking outbreak conditions and dynamics to pathogen strain and biology.

References

1. Aikimbayev AM. Plague: manual for practical medical workers [in Russian]. Almaty: Kazinformcenter of Goskomstat RK Publishing House; 1992.
2. Aikimbayev MA, Aubakirov SA, Burdelov AS, Klassovsky LN, Serzhanov OS. Central Asian focus of desert plague [in Russian]. Almaty: Nauka Publishing House; 1987.
3. Rivkus YZ, Blummer AG. Plague epidemic in the deserts of Central Asia and Kazakhstan [in Russian]. Voronezh: Voronezh State University Publishing House; 2016.
4. Kutyrev VV, Popova AY. Cadastre of epidemic and epizootic manifestations of plague in the territory of the Russian Federation and former Soviet Union (1876–2016). Saratov: Amirit, LLC; 2016.
5. Temiraliyeva GA, Lukhnova LY, Arakelyan IS, Martinevsky IL. Historical milestones of formation and development [in Russian]. Almaty: GRDB Publishing House; 1999.
6. Atshabar BB, Burdelov LA, Izbanova UA, Lukhnova LY, Meka-Mechenko TV, Meka-Mechenko VG, et al. Passport of regions of Kazakhstan on especially dangerous infections [in Russian]. Journal of Quarantine and Zoonotic Infections in Kazakhstan. 2015;1:5–177.
7. Kutyrev VV, Popova AY, editors. Atlas of natural plague foci of Russia and foreign countries [in Russian]. Kaliningrad: RA Poligrafych; 2022.
8. Aikimbayev AM, Atshabar BB, Aubakirov SA. Epidemiologic potential of natural plague foci in Kazakhstan [in Russian]. Almaty: DOIVA; 2006.
9. Rivkus YZ, Naumov AV, Khotko NI, Geldiev A. Epidemiology and prevention of plague [in Russian]. Ashgabat: Magarif Publishing House; 1992.
10. Khamzin SH. Prevention of plague in Atyrau region [in Russian]. Almaty: GRDB Publishing House; 1998.
11. Ignatiev AK. Bozache plague outbreak [in Russian]. Bull Microbiol Epidemiol. 1927;6:160–3.
12. Population census of the USSR December 17, 1926: brief summary [in Russian]. Popul USSR. 1927;3:63.
13. Polyakov YA. USSR population census of 1939: main summaries [in Russian]. Moscow: Nauka Publishing House; 1992.
14. Central Statistical Bureau of the USSR. Population of the USSR in 1939 by republics, krays and oblasts [in Russian]. Moscow; The Bureau; 1953.
15. Ormsby T, Napolean EJ, Burke R, Groessl C. Getting to know ArcGIS desktop, second edition, for ArcGIS 10. Redlands (CA): ESRI Press; 2010.
16. Aikimbayev AM, Bekenov JY, Meka-Mechenko TV, Temiraliyeva GA. Epidemiologic surveillance of highly pathogenic diseases in Kazakhstan. In: O'Connell KP, Skowronski EW, Sulakvelidze A, Bakanidze L, editors. Emerging and endemic pathogens: advances in surveillance, detection and identification (NATO science for peace and security series A: chemistry and biology). Tblisi (Georgia): Springer; 2010. p. 15–20.
17. Popov NV, Eroshenko GA, Karnaukhov IG, Kuznetsov AA, Matrosov AN, Ivanova AV, et al. Epidemiological situation of plague in 2020. Forecast of epizootic activity of natural plague foci of the Russian Federation and other CIS countries for 2021 [in Russian]. Problems of Especially Dangerous Infections. 2021;1:52–62. https://doi.org/10.21055/0370-1069-2021-1-52-62
18. Abdel Z, Abdeliyev B, Yessimseit D, Begimbayeva E, Mussagalieva R. Natural foci of plague in Kazakhstan in the space-time continuum. Comp Immunol Microbiol Infect Dis. 2023;100:102025. https://doi.org/10.1016/j.cimid.2023.102025

Address for correspondence: Nurkuisa Rametov or Kairat Tabynov, M. Aikimbayev National Scientific Center for Especially Dangerous Infections, 14 Zhahanger Str, Almaty, 050054, Kazakhstan; email: nurkuisa.rametov@gmail.com or kairat.tabynov@gmail.com

Bartonella quintana Endocarditis in Persons Experiencing Homelessness, New York, New York, USA, 2020–2023

Marina Keller,[1] Mariam Agladze, Tania Kupferman, Shannan N. Rich, Grace E. Marx, Rachel Gnanaprakasam, Rich Kodama, Marta Feldmesser, Kara Mitchell, Danielle Wroblewski, Stefan Juretschko, George M. Kleinman, Matthew J. Kuehnert, Julu Bhatnagar, Marlene Deleon Carnes, Hannah Bullock, Sarah Reagan-Steiner, Gabriella Corvese, Joel Ackelsberg[1]

Bartonella quintana infection can lead to bacillary angiomatosis, peliosis hepatis, chronic bacteremia, and culture-negative endocarditis. Transmitted by the human body louse (*Pediculus humanus humanus*), *B. quintana* infection has become an emerging disease in recent decades among persons experiencing homelessness. By using retrospective laboratory surveillance, we identified 5 cases of left-sided, culture-negative *B. quintana* endocarditis among persons in New York, New York, USA, during January 1, 2020–November 23, 2023. Identifications were made by using molecular assays. All patients experienced unsheltered homelessness in the year before hospitalization. Of those patients, 4 experienced heart failure, 3 renal failure, and 2 embolic strokes; 2 died. Aortic valve replacement occurred in 4 cases. A history of possible body louse infestation was found in 4 cases. Clinicians should consider housing status and history of lice exposure in patients with suspected bartonellosis and have a low threshold for diagnostic testing and empiric treatment in patients experiencing homelessness.

*B*artonella bacteria are fastidious, intracellular gram-negative rods that cause disease in humans, cats, dogs, rodents, and other mammals. Thirteen *Bartonella* species are known to cause human infection (*1*). *B. quintana* infection can cause bacillary angiomatosis, peliosis hepatis, chronic bacteremia (*2–4*), and culture-negative endocarditis (*5,6*). *B. quintana* is transmitted by the human body louse (*Pediculus humanus humanus*) through inoculation of broken skin by contaminated feces. Infection is enabled in settings where personal hygiene is compromised, such as refugee camps (*7*) and wartime environments (*8*). In recent decades, *B. quintana* infection has emerged as a disease primarily affecting persons experiencing homelessness (*3,5,9–20*).

In January 2023, *B. quintana* infection was diagnosed in 2 kidney transplant recipients from 1 donor (*21*). An investigation by the New York City (NYC) Department of Health and Mental Hygiene (New York, NY, USA) determined the donor had experienced unsheltered homelessness and had *B. quintana* bacteremia during their terminal hospitalization in summer 2022. In April 2023, another case of *Bartonella* endocarditis diagnosed in a patient experiencing homelessness was reported to the NYC Department of Health and Mental Hygiene, prompting efforts to identify additional cases to better understand the incidence and severity of *B. quintana* infections in the city (*22*). This article provides information regarding

Author affiliations: Westchester Medical Center, Valhalla, New York, USA (M. Keller, R. Gnanaprakasam, G.M. Kleinman); New York University Grossman School of Medicine, New York, New York, USA (T. Kupferman, M. Agladze); Centers for Disease Control and Prevention, Fort Collins, Colorado, USA (S.N. Rich, G.E. Marx); Memorial Sloan Kettering Cancer Center, New York (R. Kodama); Lenox Hill Hospital, New York (M. Feldmesser); New York State Department of Health, Albany, New York, USA (K. Mitchell, D. Wroblewski); Northwell Health Laboratories, Little Neck, New York, USA (S. Juretschko); Centers for Disease Control and Prevention, Atlanta, Georgia, USA (M.J. Kuehnert, J. Bhatnagar, M.D. Carnes, H. Bullock, S. Reagan-Steiner); New York City Department of Homeless Services, New York (G. Corvese); New York City Department of Health and Mental Hygiene, Long Island City, New York. USA (J. Ackelsberg)

[1]These authors contributed equally to this article.

the clinical manifestations, diagnosis, and treatment of each case and discusses management options for clinicians caring for patients experiencing homelessness who might have bartonellosis.

Methods

The NYC Department of Health and Mental Hygiene conducted retrospective active surveillance for patients with a diagnosed *B. quintana* infection among clinical laboratories of 5 large hospital networks and the Wadsworth Center at the New York State Department of Health. The laboratories identified patients during January 1, 2020–November 23, 2023, who had a *Bartonella* spp. recovered from specimen cultures; who tested positive for *Bartonella* spp. with PCR further confirmed as *B. quintana* by 16S rRNA sequencing; whose plasma yielded $\geq$10 molecules/µL of *B. quintana* cell-free DNA detected with next-generation sequencing (*23*); or whose serum demonstrated *B. quintana* or *B. henselae* IgM or IgG titer results of $\geq$1:128. All serologic testing was conducted at the same commercial clinical laboratory.

We reviewed the electronic medical records of patients identified by the laboratories, accessed by using NYC regional health information organizations for clinical and social history details, which included documentation of housing status. The NYC Department of Homeless Services registration database was queried for evidence that cases received services in the NYC shelter system. The NYC Department of Health and Mental Hygiene's Institutional Review Board determined that the activities described in this article meet the definition of public health surveillance as set forth under 45 CFR§46.102(1)(2).

Results

We identified 5 cases of culture-negative, left-sided *B. quintana* endocarditis. The 5 patients had experienced unsheltered homelessness within 1 year of admission. None were registered in the NYC shelter system. The case descriptions illustrate similarities in clinical manifestations and highlight the concern of delayed diagnosis.

Case 1 Description

In summer 2022, a middle-aged man with schizophrenia and alcohol use disorder was found unresponsive at an assisted living facility where he had lived for ≈1 year for the management of malnutrition and chronic anemia. According to his family, the patient had previously been living unsheltered in NYC and had been treated for body lice. In the emergency department, the patient was unresponsive but had unremarkable vital signs (Table). Laboratory testing revealed severe anemia and renal failure. Computed tomography (CT) scans of the brain revealed a large, acute, right inferior cerebellar intraparenchymal hemorrhage with surrounding edema. Cerebral angiography revealed a 3-mm right posterior inferior cerebellar artery aneurysm that was treated emergently with endovascular coiling.

Transthoracic echocardiogram (TTE) revealed a 2.2 cm vegetation on the noncoronary aortic valve (AV) leaflet and a 2.0 cm vegetation on the anterior mitral valve leaflet, which is associated with severe regurgitation of both valves with preserved left ventricular function and suggestive of bacterial endocarditis. Healthcare providers collected 1 set of blood cultures before antimicrobial administration and 4 sets the first week of hospitalization. Bacterial cultures were held for 5 days, and fungal cultures were held for 30 days. Cultures remained negative. Providers treated the patient empirically for bacterial endocarditis with ceftriaxone and vancomycin for 12 days, then stopped after blood cultures remained negative. Providers did not initially consider bartonellosis.

The patient received anticoagulants and underwent aortic and mitral bioprosthetic valve replacements 38 days after admission and after neurologic recovery. After reassessment of the case by a new consultant 2 days after surgery, doxycycline was started empirically for possible bartonellosis, and serologic testing was conducted. Results of bacterial culture of the explanted valve tissue was negative; fungal and mycobacterial cultures were not performed. *B. henselae* and *B. quintana* IgG titers were $\geq$1:1024; IgM titers were negative.

The patient was discharged and then readmitted 3 weeks later with renal failure. Doxycycline monotherapy was continued for 4 weeks and then switched to azithromycin for an additional 2 weeks because of a drug rash while on doxycycline.

After the second hospital discharge, a nonspecific qualitative PCR at a commercial laboratory detected a *Bartonella* sp. in an explanted AV tissue specimen. The Wadsworth Center conducted *Bartonella* PCR of whole blood that was collected before doxycycline was started, and the PCR was negative. A Warthin-Starry silver stain of the AV tissue revealed small, black, curved organisms that were consistent with *Bartonella* spp. (Figure 1).

The patient's family was contacted after he missed outpatient appointments. They reported that he had left home and was experiencing homelessness. The patient sought treatment at another hospital 2 months after the second discharge. The hospital

clinicians diagnosed *Clostridioides difficile*–associated diarrhea and *Enterococcus faecalis* bacteremia. No additional *Bartonella* testing was conducted. The patient was discharged to hospice and died 10 months after his endocarditis diagnosis.

Several months after the patient's death, formalin-fixed paraffin-embedded explanted AV tissue was submitted to the Centers for Disease Control and Prevention for testing. *B. quintana* was identified by using a *Bartonella*-specific hemi-nested PCR targeting the *ribC* gene (*24*) followed by sequence analysis of 307 bp and 211 bp PCR products.

Electron microscopy revealed *B. quintana* within aortic tissue (Figure 2).

Case 2 Description

In early spring 2022, a middle-aged man with chronic obstructive pulmonary disease who had been experiencing unsheltered homelessness sought care at an emergency department with dyspnea on exertion that progressed to shortness of breath at rest over the previous 2 weeks. He had a history of bipolar disorder, antisocial personality disorder, and alcohol use disorder. Body lice were discovered and treated after admission.

Table. Demographic and clinical features of 5 *Bartonella quintana* endocarditis cases in persons experiencing homelessness, New York, New York, USA, 2020–2023*

Characteristics	Case 1	Case 2	Case 3	Case 4	Case 5
Patient demographics					
Age, y	≈50	≈50	≈70	≈50	≈60
Sex	M	M	F	M	M
Race/ethnicity	Black	Middle Eastern	Unknown	Hispanic	Asian
Admission values					
Temperature at admission, °C	37.0	36.2	36.7	36.4	36.9
Heart rate, beats/min	118	101	46	92	72
Respiratory rate, breaths/min	20	19	9	16	20
Blood pressure, mm Hg	138/108	123/51	82/45	111/66	138/85
Leukocytes, 10^3 cells/mL	8.6	11.1	17	3.1	9.5
Hemoglobin g/dL	6.2	10.3	5.8	8.6	7.8
Platelets, 10^3/mL	233	205	155	123	350
Creatinine, mg/dL	2.8	1.9	1.4	1.3	0.8
Albumin, g/dL	2.9	2.5	2.5	2.7	3.4
Pro-BNP, pg/mL	Not tested	Not tested	2756	40510	Not tested
Diagnoses and course of illness					
Heart failure	Yes	Yes	Yes	Yes	No
Affected heart valve(s)	Aortic, mitral	Aortic	Aortic	Aortic	Aortic, mitral
Valve replacement	Yes	Yes	Yes	Yes	No
Renal failure	Yes	Yes	Yes	No	No
Renal replacement therapy	No	Yes	Yes	No	No
B. quintana IgG titer	≥1:1,024	1:1,280	<1:128	1:640	1:2,560
B. henselae IgG titer	≥1:1,024	1:2,560	>1:1,024	1:2,560	1:2,560
B. quintana IgM titer	Negative	Negative	Negative	Negative	Negative
B. henselae IgM titer	Negative	Negative	Negative	Negative	Negative
Molecular diagnostic assay	HN-PCR valve	PCR/16S rRNA valve	PCR/16S rRNA valve	16S rRNA gene sequencing	cfDNA, 14049 MPM
Molecular diagnosis	*B. quintana*	*B. quintana*	*B. quintana*	*B. quintana*	*B. quintana*
Antimicrobial drugs administered before *B. quintana* treatment started	VAN, CTX	DAP, CTX	VAN, P/T, CTX	VAN, CTX	VAN, CTX
Days before *B. quintana* treatment started	40	4	3	3	8
Hospitalization, d	46	79	34	33	31
Died during hospitalization	No	No	Yes	No	No
Died within 1 year	Yes	No	Yes	No	No
Risk factors					
Alcohol use disorder	Yes	Yes	Unknown	Yes	No
Illicit drug use	No	Yes	Unknown	Yes	No
Schizophrenia	Yes	No	Unknown	No	No
Bipolar disorder	No	Yes	Unknown	Yes	No
Other mental health condition	Unknown	Yes	Unknown	Unknown	No
Unsheltered homelessness at admission	No	Yes	Presumed	Yes	Yes
Unsheltered homelessness within 1 year of admission	Yes	Yes	Presumed	Yes	Yes
Known exposure to body lice	Yes	Yes	bed bugs	Yes	No

*cfDNA, microbial cell-free DNA detection with next-generation sequencing; CTX, ceftriaxone; DAP, daptomycin; HN-PCR, hemi-nested PCR confirmed with sequence analysis; MPM, DNA molecules per microliter (number of DNA fragments present in 1 microliter of plasma); PCR/16S rRNA, real-time PCR of *gltaA* confirmed with full gene sequencing of PCR product; pro-BNP, pro-B-type natriuretic peptide; P/T, piperacillin/tazobactam.

Physical examination revealed bilateral lower extremity and scrotal edema and diffuse pulmonary crackles. The patient was tachycardic (Table). Laboratory testing revealed hematuria, mild neutrophilic leukocytosis, acute kidney injury, and metabolic acidosis. A chest radiograph showed pulmonary congestion and bilateral pleural effusions. TTE revealed severe aortic regurgitation (AR), a 1.7 cm AV vegetation, a small vegetation on the noncoronary aortic leaflet, elevated end diastolic right ventricular pressure, and preserved left ventricular function.

Healthcare providers obtained blood cultures after a single dose of ceftriaxone and before daptomycin was initiated; the cultures remained negative after 5 days. Clinicians became concerned for possible bartonellosis because of the patient's recent homelessness and negative blood cultures. Clinicians changed the patient's antimicrobials to doxycycline and rifampin after serologic testing revealed *B. henselae* titers of IgG >1:2,560 and *B. quintana* titers of IgG >1:1,280; IgM titers were negative.

The patient's renal function continued to decline, likely secondary to glomerulonephritis, and clinicians initiated intermittent dialysis. The patient subsequently refused treatment and laboratory testing but was legally deemed unable to make medical decisions; a court ordered dialysis and cardiothoracic surgery. He underwent bioprosthetic AV replacement and a left atrial appendage ligation on day 29 of hospitalization. The postoperative course was complicated by deterioration of cardiac function and renal failure.

The Wadsworth Center conducted molecular testing of the explanted AV and identified *B. quintana* by using real-time PCR targeting of the *gltA* gene and confirmed the *B. quintana* infection by 16S full gene DNA sequencing of the PCR product. During the hospitalization, the patient completed 10-week courses of doxycycline and rifampin; 6 additional weeks of doxycycline were recommended after hospital discharge. The patient was discharged to a shelter 79 days after admission with hemodialysis scheduled 3 times/week, but he left the facility and did not attend outpatient clinic appointments. He returned to the emergency department 3 months later with volume overload and possible worsening of heart failure (HF), although renal function had recovered. He left against medical advice and was lost to follow-up.

Case 3 Description

An elderly woman with unknown medical history was found disoriented and lying on a subway platform during the winter of 2020. Bed bugs were
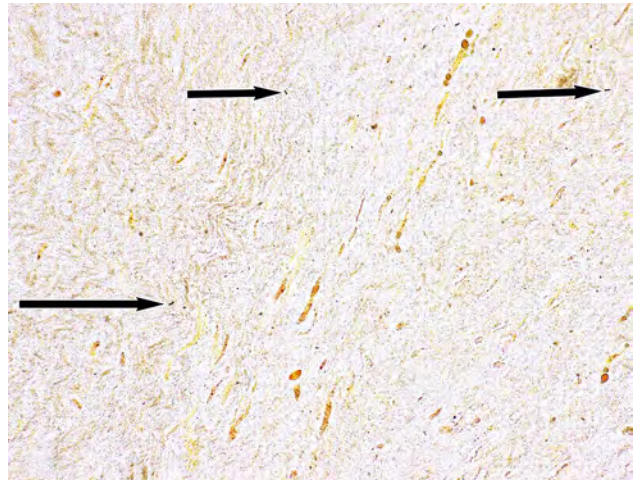
Figure 1. Warthin-Starry staining of aortic valve vegetation from a person experiencing homelessness who had *Bartonella quintana* endocarditis, New York, New York, USA. The presence of argyrophilic microorganisms is consistent with *Bartonella* (arrow). Original magnification ×500.

noted by emergency responders. She was afebrile, bradycardic, and hypotensive, and it was noted she had hyperpigmented lower extremities with 3+ pitting edema (Table). At the hospital, laboratory values revealed moderate leukocytosis, profound anemia, thrombocytopenia, acute kidney injury, elevated pro-B-type natriuretic peptide (pro-BNP), lactic acidosis, and coagulopathy. TTE showed severe AR with large vegetations on the AV noncoronary and right coronary cusps, moderate pulmonary hypertension, moderate tricuspid and severe pulmonic regurgitation, and diastolic dysfunction. Brain magnetic resonance

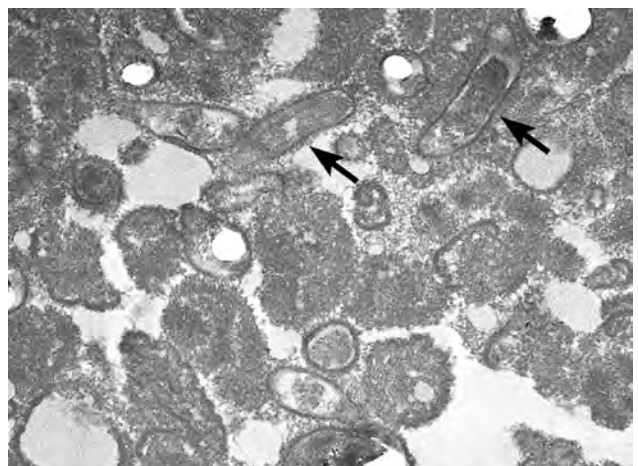**Figure 2.** Transmission electron microscopy image from a person experiencing homelessness who had *Bartonella quintana* endocarditis, New York, New York, USA. Image reveals pleomorphic bacteria from a formalin-fixed paraffin-embedded tissue section. Arrows indicate 2 rod-shaped bacteria present in the aorta of the patient. Scale bar indicates 2 μm.

imaging revealed possible embolic-type infarcts in bilateral cerebral and left cerebellar hemispheres.

Healthcare providers collected blood cultures and then administered ceftriaxone and vancomycin empirically for bacterial endocarditis. Providers started the patient on doxycycline and rifampin 3 days later because the negative blood cultures, homelessness, and the ectoparasitic infestation were suggestive for bartonellosis.

The patient underwent urgent tissue AV replacement and tricuspid valve repair. Warthin-Starry stain was negative. Bacterial cultures held 5 days and fungal cultures held 28 days of the explanted valve were negative. Blood cultures were held for 14 days and remained negative.

The titer for *B. quintana* IgG was <1:128 and the titer for *B. henselae* IgG was >1:1,024; IgM titers were negative. Clinicians changed the patient's antimicrobial drugs to doxycycline and rifampin because of the clinical suspicion of bartonellosis after consideration of the elevated *Bartonella* spp. titers, negative blood cultures, homelessness, and ectoparasitic infestation. The Wadsworth Center conducted molecular testing of the explanted AV and identified *B. quintana*. The patient died from multiorgan failure 3 weeks after surgery.

Case 4 Description

A middle-aged man with a history of asthma, bipolar disorder, alcohol use disorder, hepatitis C infection, pancytopenia, and experiencing unsheltered homelessness sought care at an emergency department in the winter of 2022 with dyspnea and bilateral lower extremity edema over the previous 2 months. He was hospitalized for fluid overload with suspected acute HF. At admission, the patient's vital signs were unremarkable, and no signs or symptoms of systemic infection were noted (Table). Laboratory tests revealed anemia, hypoalbuminemia, and elevated pro-BNP. Chest radiograph showed pulmonary congestion and bilateral pleural effusions.

TTE showed AR, mitral regurgitation, tricuspid regurgitation, mild pulmonary hypertension, and suspected mobile vegetations on the AV. Healthcare providers collected blood cultures before initiating treatment with intravenous vancomycin and ceftriaxone for suspected bacterial endocarditis. Initial and repeated blood cultures remained negative after 21 days. Because of the patient's recent unsheltered homelessness and reported exposure to cats, dogs, and lice, *Bartonella* endocarditis was considered. Clinicians changed the antimicrobial treatment to doxycycline and rifampin. Serologic testing detected

elevated IgG titers to *B. henselae* of 1:2,560 and *B. quintana* of 1:640. *B. henselae* IgM titers were negative.

The patient underwent tissue AV replacement 10 days after admission. Bacterial, fungal, and mycobacterial cultures of the AV tissue were negative. Healthcare providers identified *B. quintana* from the explanted AV by using Sanger sequencing of amplicons obtained from PCR assays targeting 16S rRNA and *ribC* genes. The patient was discharged from the hospital and recommended to complete a 12-week course of doxycycline and 6-week course of rifampin. However, he continued to experience unsheltered homelessness and reported that he was unable to complete the recommended regimen because his medications were stolen.

Case 5 Description

An ≈60-year-old man experiencing unsheltered homelessness was admitted to an emergency department in summer 2023 after being found collapsed on a sidewalk. Physical examination revealed left-sided facial droop and weakness. He was afebrile, and vital signs were unremarkable. Laboratory testing showed severe anemia and normal renal function (Table). CT scans of the patient's head revealed an acute right middle cerebral artery infarct with suspected thrombus. CT angiography showed occlusion of the right M1 segment, which was treated with thrombectomy.

Transesophageal echocardiogram revealed mobile vegetations on each AV leaflet, anterior and posterior mitral valve leaflets, and the tricuspid valve; mild AR; and mild to moderate mitral regurgitation. Digital subtraction angiography revealed a 3 mm distal middle cerebral artery mycotic aneurysm.

Healthcare providers collected blood cultures and initiated vancomycin and ceftriaxone for suspected bacterial endocarditis. Blood cultures were held for 5 days and remained negative.

Clinicians considered the patient at risk for *B. quintana* endocarditis because he experienced recent homelessness. They added doxycycline and rifampin after *B. hensalae* and *B. quintana* IgG titers were both 1:2,560; IgM titers were negative. Clinicians discontinued vancomycin and ceftriaxone when cell-free B. *quintana* DNA was detected in the patient's plasma by using next-generation sequencing.

The patient completed 6 weeks of rifampin and 7 weeks of doxycycline during hospitalization. He did not undergo valve replacement because of stable vegetations and high risk for aneurysm hemorrhage if anticoagulated. He was discharged wheelchair-bound to a shelter. After falling from his wheelchair the next day, he was hospitalized

and completed his doxycycline course during an extended rehabilitation hospitalization.

Discussion

We describe 5 cases of left-sided *B. quintana* endocarditis that occurred during 2020–2023 in persons experiencing unsheltered homelessness in NYC. Most patients had serious complications, including 4 with HF, 3 with renal failure, and 2 with embolic strokes. Renal replacement therapy during hospitalization was required for 2 cases, and 2 patients died.

Echocardiographic findings of AV vegetations prompted evaluations for infective endocarditis. In all cases, negative blood cultures triggered testing for *Bartonella* spp. because clinicians recognized that *B. quintana* infection was a possibility because of the patients' history of experiencing homelessness. Body lice and homelessness have been linked to *B. quintana* infection (*3,9–12,17,19*). In this article, body louse exposure was documented in 3 of 5 endocarditis cases; a fourth patient had what appeared to be bed bugs, which might have been misidentified body lice.

Because of nonspecific clinical manifestations, *B. quintana* endocarditis requires a high index of clinical suspicion to diagnose. Even when clinicians consider bartonellosis, diagnosis can be elusive. The bacterium stains poorly with Gram stain and is visualized better with Giemsa or Warthin-Starry silver stain, although histopathological diagnosis is insensitive and nonspecific (*5*). Diagnosis is commonly made by using serology but can be challenging. Cross-reactivity between different *Bartonella* spp. can affect interpretation (*1,16,25–27*). In the cases reported in this article, titers for *B. henselae* IgG were equal to or higher than for *B. quintana* IgG, and in 1 endocarditis case, *B. quintana* IgG was negative. *B. henselae* and *B. quintana* IgM titers were also negative in all cases, which is expected with prolonged chronic infections.

A standard approach to *B. quintana* diagnosis is lacking. As fastidious organisms, *Bartonella* spp. are difficult to grow by using routine blood culture methods and require up to 3–4 weeks of incubation. *Bartonella* spp. endocarditis blood culture sensitivity can be ≤20% (*1,28*). Periodic subculturing of blood culture broth in shell vials or to solid media with different base formulas has been used, but most clinical laboratories are unable to use these specialized techniques (*1,4,29*). None of the *B. quintana* endocarditis cases in this article were detected by blood culture and in 4/5 cases cultures were only held for 5 days.

Molecular assays, such as PCR amplification of specific gene targets (e.g., the *Bartonella* citrate synthase gene, *gltA*, *ribC*) and 16S rRNA sequencing of PCR products, are the most reliable methods to detect *Bartonella* infection and can be used for blood or fresh tissue specimens (*4,27,30,31*). In addition, molecular assays can be performed on formalin-fixed paraffin-embedded tissues for retrospective analysis. The diagnostic sensitivity of PCR to detect *B. quintana* from cardiac valve tissue in 1 reference center was 81%, compared with 28% for blood to shell vial culture, 44% for valve tissue to shell vial culture, 33% for blood, and 36% for serum (*4,5*). However, molecular diagnosis of *Bartonella* spp. is available in only a limited number of public health and commercial laboratories and tissue is not always available for testing.

In this investigation, molecular testing of excised valve tissue confirmed the detection of *B. quintana* endocarditis in 4 patients, including in 1 patient whose PCR blood test was negative and another with undetectable *B. quintana* IgG. Detection of cell-free *B. quintana* DNA in plasma confirmed the diagnosis in the patient who did not undergo valve replacement.

B. quintana infection results in intraerythrocytic and endothelial propagation with biofilm formation that protects it from the immune response and antimicrobial drugs, which might explain the insidious consequences of prolonged bacteremia, resistance to many antibiotic classes, and propensity for recurrent infection (*1*). Experimental and clinical evidence suggest that aminoglycosides have bactericidal activity against *Bartonella* spp. and should be used for ≥14 days, ideally in combination with a second antimicrobial drug (*32*). Doxycycline plus rifampin has been recommended as an effective alternative regimen (*33*). For *B. quintana* endocarditis, 4–6 weeks of combination therapy is recommended (*1,33,34*), and valve replacement is often necessary.

A low threshold for diagnostic testing and administration of empiric antimicrobial drugs is necessary when *B. quintana* infection is suspected. Because infections can be asymptomatic and prolonged, the diagnosis and treatment of bartonellosis can be challenging, the consequences of untreated infection can be severe, untreated infection poses a risk of subsequent transmission, and the cost for each prolonged hospitalization (mean = 45 days in this article) is great. Persons experiencing homelessness who are unable to maintain regular clothing hygiene are at an increased risk for body louse infestation and *B. quintana* infection. When evaluating patients with vasoproliferative skin lesions, HF, or cardiac valve vegetations, clinicians should routinely ask about housing status and body lice exposure. In this investigation, clinicians started *B. quintana*–directed antimicrobial drugs for 3 patients within 4 days of their

presumptive bacterial endocarditis detection. Those clinicians were in a hospital that frequently treats persons experiencing homelessness.

A history of alcohol use disorder was discovered in 3 of 4 cases with known medical histories, which has been documented previously in patients with *B. quintana* endocarditis (*5,14,16,20*). Those patients also had mental health conditions. Those related conditions may have contributed to delayed detection and poor outcomes.

The burden of *B. quintana* infection in persons experiencing homelessness is unknown. However, we infer from the published literature that this burden might be considerable. In 1999, 25% of clinic patients experiencing homelessness in Seattle, Washington, USA, had elevated antibody titers to *B. quintana*, compared with 1% of blood donor controls (*16*). During 2016–2021, medical centers in Denver, Colorado, USA, reported 12 (85.7%) of 14 patients with *B. quintana* infections were experiencing homelessness (*20*). Over 1-year in Marseille, France, *B. quintana* bacteremia was detected in 10 (14%) of 71 of all patients experiencing homelessness (*3*). With an estimated 653,100 persons experiencing homelessness in the United States (*35*), the potential burden is considerable.

Bartonellosis is not a nationally notifiable disease and is not reportable to the NYC Department of Health and Mental Hygiene. Persons at risk for *B. quintana* infection are also frequently outside the reach of healthcare. Moreover, even if a patient is suspected to have bartonellosis, diagnostic testing is often inconclusive or negative. Therefore, it is likely those cases represent a fraction of all *B. quintana* infections in unsheltered NYC residents during that period.

In conclusion, clinicians who provide clinical services to persons experiencing homelessness should consider *B. quintana* infection when patients have symptoms that may be consistent with bartonellosis, particularly in the setting of prior or current body louse infestation. Available diagnostic testing includes blood and tissue cultures, serologic testing, and molecular assays, which includes cell-free DNA testing; however, negative results do not entirely rule out *B. quintana* infection, and empiric antimicrobial drug treatment should be considered if clinical suspicion for *B. quintana* infection is high.

About the Author
Dr. Keller is an infectious diseases clinician and the associate hospital epidemiologist at Westchester Medical Center in Valhalla, New York. Her research interests include hospital acquired infections, public health, and data analytics.

References
1. Okaro U, Addisu A, Casanas B, Anderson B. *Bartonella* species, an emerging cause of blood-culture-negative endocarditis. Clin Microbiol Rev. 2017;30:709–46. https://doi.org/10.1128/CMR.00013-17
2. Brouqui P, Raoult D. Arthropod-borne diseases in homeless. Ann N Y Acad Sci. 2006;1078:223–35. https://doi.org/10.1196/annals.1374.041
3. Brouqui P, Lascola B, Roux V, Raoult D. Chronic *Bartonella quintana* bacteremia in homeless patients. N Engl J Med. 1999;340:184–9. https://doi.org/10.1056/NEJM199901213400303
4. La Scola B, Raoult D. Culture of *Bartonella quintana* and *Bartonella henselae* from human samples: a 5-year experience (1993 to 1998). J Clin Microbiol. 1999;37:1899–905. https://doi.org/10.1128/JCM.37.6.1899-1905.1999
5. Edouard S, Nabet C, Lepidi H, Fournier PE, Raoult D. *Bartonella*, a common cause of endocarditis: a report on 106 cases and review. J Clin Microbiol. 2015;53:824–9. https://doi.org/10.1128/JCM.02827-14
6. Raoult D, Fournier PE, Vandenesch F, Mainardi JL, Eykyn SJ, Nash J, et al. Outcome and treatment of *Bartonella* endocarditis. Arch Intern Med. 2003;163:226–30. https://doi.org/10.1001/archinte.163.2.226
7. Deng YP, Fu YT, Yao C, Shao R, Zhang XL, Duan DY, et al. Emerging bacterial infectious diseases/pathogens vectored by human lice. Travel Med Infect Dis. 2023;55:102630. https://doi.org/10.1016/j.tmaid.2023.102630
8. Anstead GM. The centenary of the discovery of trench fever, an emerging infectious disease of World War 1. Lancet Infect Dis. 2016;16:e164–72. https://doi.org/10.1016/S1473-3099(16)30003-2
9. Bonilla DL, Kabeya H, Henn J, Kramer VL, Kosoy MY. *Bartonella quintana* in body lice and head lice from homeless persons, San Francisco, California, USA. Emerg Infect Dis. 2009;15:912–5. https://doi.org/10.3201/eid1506.090054
10. Bonilla DL, Cole-Porse C, Kjemtrup A, Osikowicz L, Kosoy M. Risk factors for human lice and bartonellosis among the homeless, San Francisco, California, USA. Emerg Infect Dis. 2014;20:1645–51. https://doi.org/10.3201/eid2010.131655
11. Brouqui P, Stein A, Dupont HT, Gallian P, Badiaga S, Rolain JM, et al. Ectoparasitism and vector-borne diseases in 930 homeless people from Marseilles. Medicine (Baltimore). 2005;84:61–8. https://doi.org/10.1097/01.md.0000152373.07500.6e
12. Brouqui P, Houpikian P, Dupont HT, Toubiana P, Obadia Y, Lafay V, et al. Survey of the seroprevalence of *Bartonella quintana* in homeless people. Clin Infect Dis. 1996;23:756–9. https://doi.org/10.1093/clinids/23.4.756
13. Raoult D, Fournier PE, Drancourt M, Marrie TJ, Etienne J, Cosserat J, et al. Diagnosis of 22 new cases of *Bartonella* endocarditis. Ann Intern Med. 1996;125:646–52. https://doi.org/10.7326/0003-4819-125-8-199610150-00004
14. Spach DH, Kanter AS, Dougherty MJ, Larson AM, Coyle MB, Brenner DJ, et al. *Bartonella (Rochalimaea) quintana*

bacteremia in inner-city patients with chronic alcoholism. N Engl J Med. 1995;332:424–8. https://doi.org/10.1056/NEJM199502163320703

15. Ohl ME, Spach DH. *Bartonella quintana* and urban trench fever. Clin Infect Dis. 2000;31:131–5. https://doi.org/10.1086/313890

16. Jackson LA, Spach DH, Kippen DA, Sugg NK, Regnery RL, Sayers MH, et al. Seroprevalence to *Bartonella quintana* among patients at a community clinic in downtown Seattle. J Infect Dis. 1996;173:1023–6. https://doi.org/10.1093/infdis/173.4.1023

17. Faccini-Martínez AA, Kmetiuk LB, Blanton LS, Felipetto LG, Gravinatti ML, Timenetsky J, et al. *Bartonella* spp. and typhus group rickettsiae among persons experiencing homelessness, São Paulo, Brazil. Emerg Infect Dis. 2023;29:418–21. https://doi.org/10.3201/eid2902.221050

18. Leibler JH, Zakhour CM, Gadhoke P, Gaeta JM. Zoonotic and vector-borne infections among urban homeless and marginalized people in the United States and Europe, 1990–2014. Vector Borne Zoonotic Dis. 2016;16:435–44. https://doi.org/10.1089/vbz.2015.1863

19. Marshall KE, Martinez HE, Woodall T, Guerrero A, Mechtenberg J, Herlihy R, et al. Body lice among people experiencing homelessness and access to hygiene services during the COVID-19 pandemic—preventing trench fever in Denver, Colorado, 2020. Am J Trop Med Hyg. 2022;107:427–32. https://doi.org/10.4269/ajtmh.22-0118

20. Shepard Z, Vargas Barahona L, Montalbano G, Rowan SE, Franco-Paredes C, Madinger N. *Bartonella quintana* infection among people experiencing homelessness in the Denver metropolitan area. J Infect Dis. 2022;226(Suppl 3):S315–21. https://doi.org/10.1093/infdis/jiac238

21. Beeson AM, Rich SN, Russo ME, Bhatnagar J, Kumar RN, Ritter JM, et al. Bartonella quintana infection in kidney transplant recipients from donor experiencing homelessness, United States, 2022. Emerg Infect Dis. 2024;30:2467–2475. https://doi.org/10.3201/eid3012.240310

22. Rich SN, Beeson A, Seifu L, Mitchell K, Wroblewski D, Juretschko S, et al. Severe *Bartonella quintana* infections among persons experiencing unsheltered homelessness—New York City, January 2020–December 2022. MMWR Morb Mortal Wkly Rep. 2023;72:1147–8. https://doi.org/10.15585/mmwr.mm7242a3

23. Park SY, Chang EJ, Ledeboer N, Messacar K, Lindner MS, Venkatasubrahmanyam S, et al. Plasma microbial cell-free DNA sequencing from over 15,000 patients identified a broad spectrum of pathogens. J Clin Microbiol. 2023;61:e0185522. https://doi.org/10.1128/jcm.01855-22

24. Zeaiter Z, Fournier P-E, Greub G, Raoult D. Diagnosis of *Bartonella* endocarditis by a real-time nested PCR assay using serum. J Clin Microbiol. 2003;41:919–25. https://doi.org/10.1128/JCM.41.3.919-925.2003

25. Maurin M, Eb F, Etienne J, Raoult D. Serological cross-reactions between *Bartonella* and *Chlamydia* species:

implications for diagnosis. J Clin Microbiol. 1997;35:2283–7. https://doi.org/10.1128/jcm.35.9.2283-2287.1997

26. Fournier P-E, Mainardi J-L, Raoult D. Value of microimmunofluorescence for diagnosis and follow-up of *Bartonella* endocarditis. Clin Diagn Lab Immunol. 2002; 9:795–801.

27. Rahimian J, Raoult D, Tang YW, Hanna BA. *Bartonella quintana* endocarditis with positive serology for *Coxiella burnetii*. J Infect. 2006;53:e151–3. https://doi.org/10.1016/j.jinf.2005.11.014

28. Houpikian P, Raoult D. Blood culture-negative endocarditis in a reference center: etiologic diagnosis of 348 cases. Medicine (Baltimore). 2005;84:162–73. https://doi.org/10.1097/01.md.0000165658.82869.17

29. Gouriet F, Fenollar F, Patrice J-Y, Drancourt M, Raoult D. Use of shell-vial cell culture assay for isolation of bacteria from clinical specimens: 13 years of experience. J Clin Microbiol. 2005;43:4993–5002. https://doi.org/10.1128/JCM.43.10.4993-5002.2005

30. McCormick DW, Rassoulian-Barrett SL, Hoogestraat DR, Salipante SJ, SenGupta D, Dietrich EA, et al. *Bartonella* spp. infections identified by molecular methods, United States. Emerg Infect Dis. 2023;29:467–76. https://doi.org/10.3201/eid2903.221223

31. Kosoy M, Bai Y, Sheff K, Morway C, Baggett H, Maloney SA, et al. Identification of *Bartonella* infections in febrile human patients from Thailand and their potential animal reservoirs. Am J Trop Med Hyg. 2010;82:1140–5. https://doi.org/10.4269/ajtmh.2010.09-0778

32. Foucault C, Raoult D, Brouqui P. Randomized open trial of gentamicin and doxycycline for eradication of *Bartonella quintana* from blood in patients with chronic bacteremia. Antimicrob Agents Chemother. 2003;47:2204–7. https://doi.org/10.1128/AAC.47.7.2204-2207.2003

33. Rolain J-M, Brouqui P, Koehler JE, Maguina C, Dolan MJ, Raoult D. Recommendations for treatment of human infections caused by *Bartonella* species. Antimicrob Agents Chemother. 2004;48:1921–33. https://doi.org/10.1128/AAC.48.6.1921-1933.2004

34. Rolain J-M, Maurin M, Raoult D. Bactericidal effect of antibiotics on *Bartonella* and *Brucella* spp.: clinical implications. J Antimicrob Chemother. 2000;46:811–4. https://doi.org/10.1093/jac/46.5.811

35. US Department of Housing and Urban Development. The 2023 Annual Homelessness Assessment Report (AHAR) to Congress. Part 1: point-in-time estimates of homelessness. 2023. [cited 2024 Sep 25] https://www.huduser.gov/portal/sites/default/files/pdf/2023-AHAR-Part-1.pdf

Address for correspondence: Joel Ackelsberg, New York City Department of Health and Mental Hygiene, 42-09 28th Street, CN-22, Long Island City, NY 11101, USA; email: jackelsb@health.nyc.gov

Ophthalmic Sequelae of Ebola Virus Disease in Survivors, Sierra Leone

Charlene H. Choo, Laura Ward, Ian Crozier, Tolulope Fashina, Daisy Yan, Brent R. Hayek,
Caleb Hartley, Matthew Vandy, John G. Mattia, Lloyd Harrison-Williams,
Jalikatu Mustapha, Carolyn Drews-Botsch, Steven Yeh,[1] Jessica Shantha[1]

Author affiliations: University of Nebraska Medical Center, Omaha, Nebraska, USA (C.H. Choo, T. Fashina, C. Hartley, S. Yeh); Emory University, Atlanta, Georgia, USA (L. Ward, S. Yeh, J. Shantha); Frederick National Laboratory for Cancer Research, Frederick, Maryland, USA (I. Crozier); University of California, San Francisco, California, USA (D. Yan, J. Shantha); North Georgia Eye Clinic, Gainesville, Georgia, USA (B.R. Hayek); Ministry of Health and Sanitation, Freetown, Sierra Leone (M. Vandy, J.G. Mattia, L. Harrison-Williams, J. Mustapha); George Mason University, Fairfax, Virginia, USA (C. Drews-Botsch)

[1]These authors were co–principal investigators.

The Ebola virus disease (EVD) outbreak of 2013–2016 was large, leaving in its wake an estimated 17,000 survivors in West Africa. Uveitis is one of the most common ophthalmic manifestations of EVD, but long-term follow-up in the at-risk population is lacking. We conducted a retrospective cross-sectional study of 521 EVD survivors from Sierra Leone who underwent comprehensive ophthalmic examination a median of 1,289 days, or ≈3.5 years, after discharge from Ebola treatment units. The most common ophthalmic findings were cataracts (117 eyes, 11.2%), uveitis (86 eyes, 8.3%), dry eyes (81 eyes, 7.8%), and chorioretinal scar (68 eyes, 6.5%). EVD survivors with cataracts, uveitis, optic neuropathy, and corneal scar were more likely to have vision impairment, defined as Snellen visual acuity worse than 20/50. Results of our study highlight the need for ongoing vision care in EVD survivors.

The Ebola virus disease (EVD) outbreak in West Africa during 2013–2016 was large, resulting in 28,652 cases, 11,325 deaths, and ≈17,000 survivors, primarily from Guinea, Liberia, and Sierra Leone (1). Although the epidemic formally ended in 2016, EVD poses an ongoing threat to public health. Another large EVD outbreak occurred in 2018–2019, causing 3,470 cases and 2,287 deaths in Democratic Republic of the Congo (DRC) (1,2), and another in 2022 led to 164 cases and 55 deaths in Uganda (1,3). All EVD outbreaks in West Africa, except for the 1994 outbreak of Taï Forest ebolavirus, have been caused by *Zaire ebolavirus*, the *Ebolavirus* species with the highest fatality rate (40%–90%) (1,4). During a *Zaire ebolavirus* outbreak in DRC in 1995, bilateral conjunctival injection was reported in 48% of hospitalized patients; late ocular findings including uveitis were described in a few surviving patients (5,6). However, the ophthalmic manifestations of EVD were poorly understood before the West Africa EVD outbreak.

Studies on the large number of EVD survivors from the epidemic in 2013 revealed uveitis as the most common ophthalmic sequela. In Liberia, where EVD caused 10,678 cases and 4,810 deaths, uveitis was found in 26% of survivors ≈1 year after symptom onset and in 33% at the 2-year follow-up (7). Another study found that ≈40% of the EVD survivors with uveitis were blind, with visual acuity (VA) of 20/400 or worse (8). In Guinea, where EVD caused 3,814 cases and 2,544 deaths, ocular complications were reported in 18% of survivors and uveitis in 13.5% (9,10). Within Sierra Leone, uveitis was reported in 18%–34% of survivors and was associated with worse VA and higher viral load when they sought care for acute systemic presentation (11,12). Pediatric EVD survivors also experienced uveitis more frequently than close contact controls (10.8% vs. 1.7%; p = 0.03) and had worse vision-related quality of life (13).

In this study, we report the prevalence of long-term ophthalmic findings in the largest long-term cohort of EVD survivors from Sierra Leone who underwent comprehensive ophthalmic examination ≈3.5 years after resolution of their acute illness. We also describe vision impairment associated with uveitis, in addition to the range of ophthalmic manifestations we observed.

Methods

Patient Recruitment and Evaluation

We conducted this study in partnership with the Ministry of Health and Sanitation, Sierra Leone; Emory University (Atlanta, GA, USA); and nongovernmental organizations including Partners in Health, John Snow, Inc., and Central Global Vision Fund. We obtained Institutional Review Board approval for review of retrospective data from Emory University and the Office of Ethics and Scientific Review Committee, Sierra Leone Ministry of Health and Sanitation. We conducted human subject research in accordance with the tenets of the Declaration of Helsinki.

EVD survivors were assessed for ophthalmic complications at the Lowell and Ruth Gess Kissy Eye Hospital (Freetown, Sierra Leone) in June 2018. Patients from outlying districts were examined at the Makeni Government Hospital Eye Clinic (Makeni, Sierra Leone). Full ophthalmic exams were performed and included corrected VA, slit lamp, and dilated funduscopic examination. B-scan ultrasound was performed when clinically indicated due to media opacity (i.e., cataract, vitreous opacity) that precluded a view of the posterior fundus. We confirmed EVD survivor status with survivor certificates or a history of EVD requiring Ebola treatment unit (ETU) admission. We collected demographic information, past medical and ocular history, and current systemic and ocular symptoms during a comprehensive medical interview. We defined active uveitis as the presence of inflammation in the anterior chamber, keratic precipitates, vitreous haze, or retinal or choroidal infiltrates. We graded uveitis according to the Standardization of Uveitis Nomenclature and National Eye Institute guidelines for anterior chamber cell, flare, vitreous cell, and haze (14,15). Data reviewed included past medical and ocular history, ETU admission and discharge dates, and ocular and systemic symptoms during acute EVD.

Statistical Analysis

We analyzed demographic and medical history by patient; we summarized ophthalmic data on a

Table 1. Demographic characteristics of survivors in study of ophthalmic sequelae after Ebola virus disease, Sierra Leone*

Characteristic	Total, N = 521
Age, mean (SD)	31.1 (16.0)
Sex, no.	
F	285 (54.7)
M	236 (45.3)
Ethnicity	n = 485
Temne	297 (61.2)
Limba	64 (13.2)
Mende	44 (9.1)
Fula	18 (3.7)
Other	62 (12.8)
Education level	n = 470
Primary and junior secondary school	177 (37.7)
None or nursery school	175 (37.2)
Higher education	118 (25.1)
Occupation	n = 492
Farmer or trader	213 (43.3)
Student	143 (29.1)
Unemployed or housewife	27 (5.5)
Healthcare or social worker	24 (4.9)
Construction worker	18 (3.7)
Other	67 (13.6)
District of residence	n = 510
Western Area Urban	157 (30.8)
Western Area Rural	141 (27.6)
Bombali or Tonkolili, Northern Province	148 (29.0)
Koidu or Kono, Eastern Province	52 (10.2)
Other	12 (2.4)

*Values are no. (%) except as indicated. ETU, Ebola treatment unit,

per-patient and per-eye basis. For ophthalmic data summarized per-person, if the condition was found in either eye, we counted the patient as having the finding. We summarized descriptive statistics as frequencies for categorical data and mean/SD or median/interquartile range (IQR) for continuous data. We conducted bivariate analysis of factors associated with uveitis using χ^2 test for per-person analysis and unadjusted generalized estimating equations, controlling for the correlation between eyes, for per-eye analysis.

We defined vision impairment as Snellen VA of 20/50 or worse. We converted Snellen VAs to logarithm of the minimum angle of resolution (logMAR) values for all analyses. We calculated mean logMAR VA by eye, as well as by the better-seeing eye and worse-seeing eye. We excluded eyes with no light perception vision (n = 7) from analysis because there is no appropriate logMAR conversion; however, we recognize this exclusion could bias the analyses toward accepting the null hypothesis (16). We created a multivariable model to examine the relationship between vision impairment status and ophthalmic findings of interest and adjusted for cataract, uveitis, corneal scar, and optic neuropathy. We adjusted the correlation between eyes using a compound symmetric correlation structure. We performed all analyses using SAS version 9.4

(SAS Institute Inc., https://www.sas.com); we considered $\alpha \leq 0.05$ statistically significant.

Results

Demographic and Clinical Characteristics
We included 521 EVD survivors from Sierra Leone in this study (Table 1). The cohort had a mean age of 31.1 years (SD 16.0 years); 285 (54.7%) patients were female and 236 (45.3%) male, predominantly of Temne ethnicity (61.2%). Most EVD survivors who were offered eye care services were recruited from the Western Area urban or rural districts (58.4%) or the Northern Province (29.0%).

Patient Medical History and Current Symptoms
The cohort had a median duration of stay in an ETU of 22 (IQR 14–30) days (Table 2). They were examined after a median of 1,289 days (IQR 1,207–1,371), or ≈3.5 years, after ETU discharge. Many survivors reported a history of malaria (47.8%) or typhoid (92.7%) during

Table 2. Medical history and current symptoms of survivors in study of ophthalmic sequelae after Ebola virus disease, Sierra Leone*

Medical history and symptoms	Total, N = 521
Days admitted in ETU, median (IQR)	22 (14–30)
Days from ETU discharge to study enrollment, median (IQR)	1,289 (82)
Had previous eye exam	444 (86.6)
Medical history	n = 510
Malaria	244 (47.8)
Typhoid	473 (92.7)
Lassa fever	7 (1.4)
HIV	3 (0.6)
Other	54 (10.6)
None	10 (2.0)
Ocular history	n = 510
Uveitis	51 (10.0)
Cataract	42 (8.2)
Current systemic symptoms	n = 510
Any systemic symptoms	503 (98.6)
Headache	485 (95.1)
Joint pain	427 (83.7)
Fatigue	369 (72.4)
Chest pain	316 (62.0)
Low mood	305 (59.8)
Abdominal pain	294 (57.6)
Weight loss	276 (54.1)
Joint stiffness and/or swelling	258 (50.6)
Anxiety	235 (46.1)
Current ocular symptoms	n = 510
Any eye symptoms	484 (94.9)
Eye pain	377 (73.9)
Light sensitivity	344 (67.4)
Blurred vision	342 (67.1)
Tearing	298 (58.4)
Eye redness	270 (52.9)
Floaters	152 (29.8)
Vision loss	134 (26.3)

*Values are no. (%) except as indicated. ETU, Ebola treatment unit; IQR, interquartile range.

Table 3. Ophthalmic findings in survivors in study of ophthalmic sequelae after Ebola virus disease, Sierra Leone

Ophthalmic findings	No. (%) patients, N = 521	No. (%) eyes, N = 1,042
Any ophthalmic finding	200 (38.4)	358 (34.4)
Cataract	62 (11.9)	117 (11.2)
Uveitic cataract	10 (16.1)	17 (14.5)
Uveitis	69 (13.2)	86 (8.3)
Anterior uveitis	34 (49.3)	44 (51.2)
Intermediate uveitis	1 (1.4)	1 (1.2)
Anterior/intermediate uveitis	4 (5.8)	5 (5.8)
Posterior uveitis	13 (18.8)	16 (18.6)
Panuveitis	15 (21.7)	17 (19.8)
Unspecified	2 (2.9)	3 (3.5)
Dry eyes	41 (7.9)	81 (7.8)
Chorioretinal scar	56 (10.7)	68 (6.5)
Pterygium	20 (3.8)	43 (4.1)
Drusen	20 (3.8)	36 (3.5)
Refractive error	18 (3.5)	35 (3.4)
Corneal scar	22 (4.2)	28 (2.7)
Vitreous hemorrhage	9 (1.7)	16 (1.6)
Optic neuropathy	6 (1.2)	7 (0.7)

their lifetime. Approximately 87% of the cohort had ≥1 previous eye exam. Fifty-one survivors (10.0%) reported a previous diagnosis of uveitis and 42 survivors (8.2%) a previous diagnosis of cataract.

Most EVD survivors (96.5%) had systemic symptoms, such as headache (95.1%), joint pain (83.7%), fatigue (72.4%), chest pain (62.0%), low mood (59.8%), abdominal pain (57.6%), weight loss (54.1%), joint stiffness/swelling (49.5%), and anxiety (46.1%). Most survivors (92.9%) also had ocular symptoms, such as eye pain (73.9%), light sensitivity (67.4%), blurred vision (67.0%), tearing (58.4%), eye redness (52.9%), floaters (29.8%), and vision loss (26.2%).

Ophthalmic Examination and Diagnosis
A total of 358 eyes (34.4%) had ophthalmic findings (Table 3; Figure 1). The most common diagnoses were

cataract (117 [11.2%]), uveitis (86 [8.3%]), dry eye (81 [7.8%]), chorioretinal scar (68 [6.5%]), and pterygium (43 [4.1%]) (Figures 2, 3). Anterior uveitis was the most common location (44 [51.2%]), followed by panuveitis (17 [19.7%]) and posterior uveitis (16 [18.6%]).

Univariable Analysis in Patients with or without Uveitis
We analyzed demographic and clinical characteristics of the cohort by patients' uveitis status (Tables 4, 5). EVD survivors who were female (p = 0.036) and older (p = 0.048) with a previous history of eye exam (p = 0.006), previous diagnosis of cataracts (p<0.001), previous diagnosis of uveitis (p = 0.030), and symptoms of vision loss (p = 0.026) were more likely to have uveitis. The presence of uveitis was not associated with days spent in the ETU (p = 0.182). Survivors with bullous keratopathy (p<0.001), chorioretinal scar
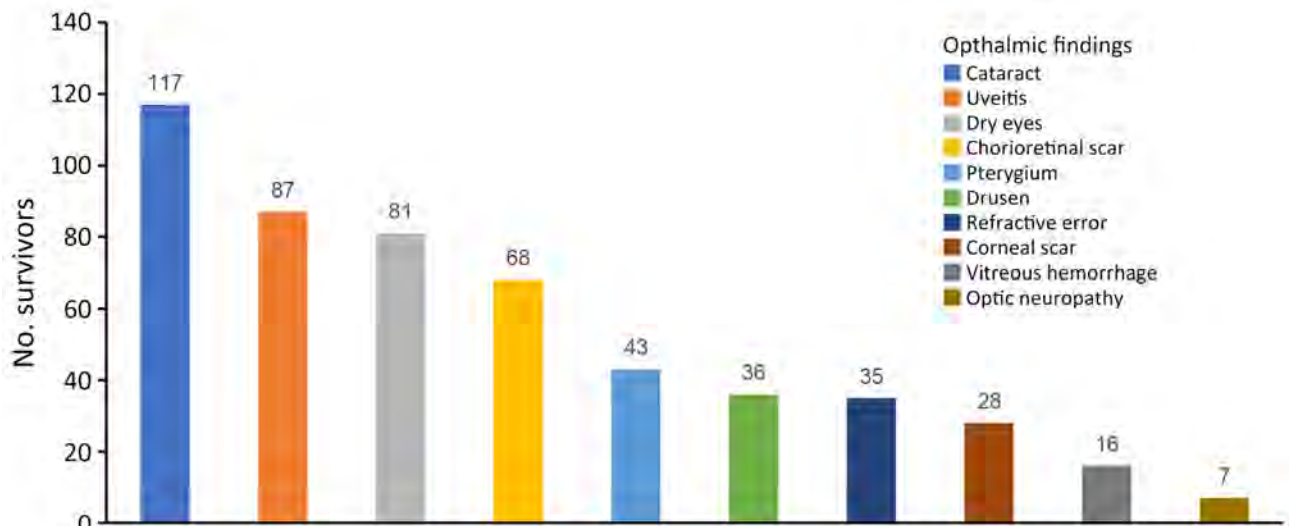

Figure 1. Common ophthalmic findings in Ebola virus disease survivors, Sierra Leone. The most common were cataract (11.2%), uveitis (8.3%), dry eyes (7.8%), chorioretinal scar (6.5%), and pterygium (4.1%).
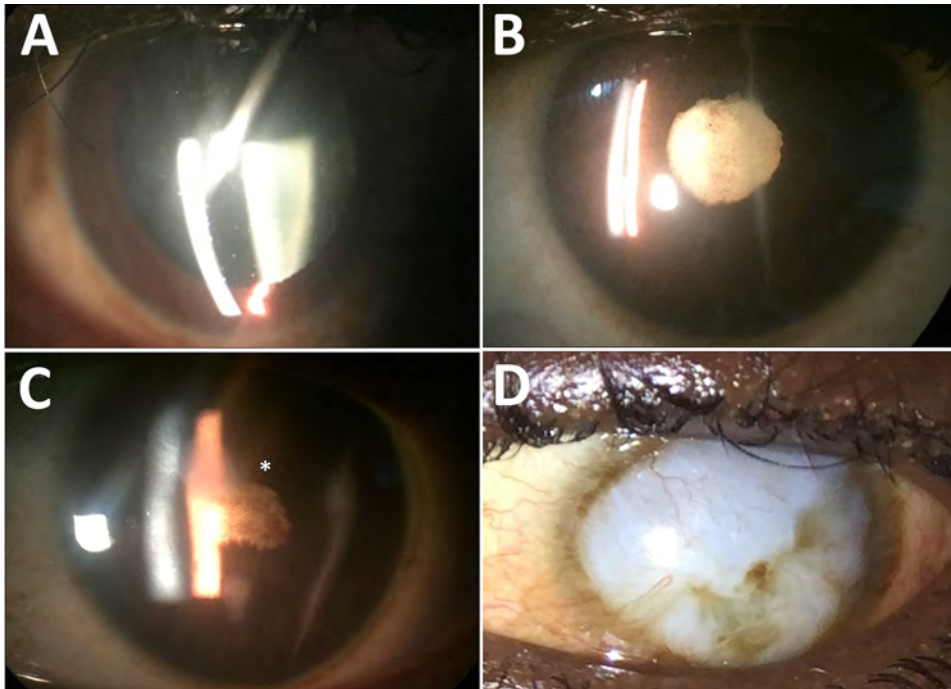
Figure 2. Anterior segment photographs showing the spectrum of ophthalmic sequelae associated with EVD in survivors, Sierra Leone. A) A patient with anterior uveitis has diffuse round keratic precipitates on the corneal endothelium, predominantly within the inferior cornea. B) An EVD survivor with severe, chronic uveitis has posterior synechiae, pigment on the lens capsule, and a dense cataract. C) Another EVD survivor with severe uveitis has dense posterior synechiae overlying a cataract, leading to blindness, and corneal edema involving the superior paracentral cornea (asterisk). D) An external photograph shows a diffuse corneal opacity (leukoma) with superior neovascularization, which was not present before the onset of acute EVD. EVD, Ebola virus disease.

(p = 0.012), posterior synechiae (p = 0.002), retinal detachment (p = 0.012), and vitreous opacity (p = 0.022) were significantly more likely to have uveitis. Cataracts (p = 0.065), corneal scar (p = 0.276), and optic neuropathy (p = 0.790) were not significantly associated with the presence of uveitis. Finally, survivors with vision impairment, defined as Snellen VA worse than 20/50, were significantly more likely to have uveitis (p = 0.004).

Visual Acuity and Multivariable Analysis by Vision Impairment Status

A total of 259 (24.9%) of the 1,042 eyes examined had vision impairment, or Snellen VA worse than 20/50. Vision impairment was found in 18.0% of better-seeing eyes and 32.0% of worse-seeing eyes.

The median logMAR VA was 0.23 (Snellen VA 20/34) in all eyes, 0.19 (Snellen VA 20/30) in the better-seeing eyes, and 0.30 (Snellen VA 20/40) in the worse-seeing eyes. Multivariable analysis revealed that the presence of vision impairment was significantly associated with cataract (odds ratio [OR] = 7.68; p<0.001), uveitis (OR = 2.08; p = 0.007), corneal scar (OR = 4.23; p = 0.001), and optic neuropathy (OR = 6.32; p = 0.034) (Table.

Discussion

This retrospective observational study included a large cohort of 521 EVD survivors who underwent comprehensive ophthalmic examination at long-term follow-up, ≈3.5 years after their initial ETU admission for acute EVD. Results of the study demonstrate a
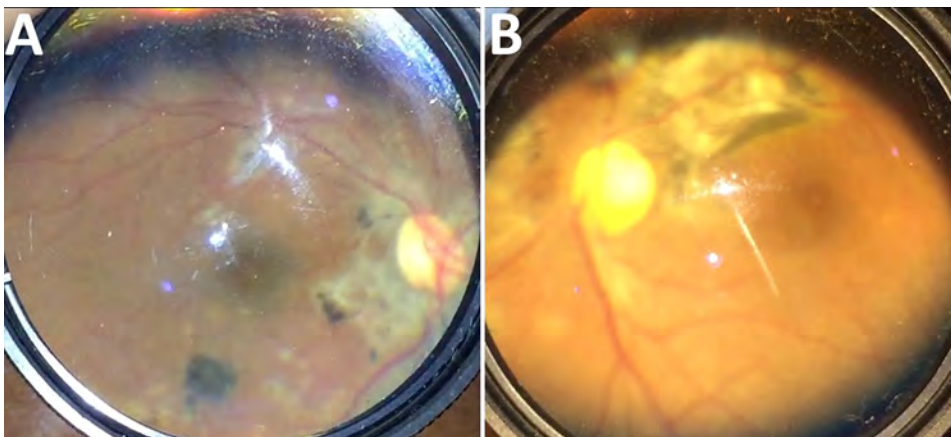
Figure 3. Posterior and fundus photographs showing the spectrum of ophthalmic sequelae associated with EVD in survivors, Sierra Leone. A) Posterior segment photograph of an EVD survivor shows peripapillary chorioretinal scarring and variable pigmentary changes indicative of multifocal choroiditis. B) Fundus photograph of another survivor shows dense chorioretinal scarring along the superotemporal arcade and nasal to the nerve, consistent with inactive posterior uveitis. EVD, Ebola virus disease.

Table 4. Demographic and clinical characteristics associated with uveitis status in survivors in study of ophthalmic sequelae after Ebola virus disease, Sierra Leone*

Characteristics	Total, N = 521	Uveitis, n = 69	No uveitis, n = 452	OR (95% CI)	p value
Age, mean (SD), n = 496	31.1 (16.0)	29.7 (12.7)	31.3 (16.5)	0.97 (0.95–0.99)	0.048
Sex, n = 510				1.78 (1.03–3.05)†	0.036
F	285 (55.9)	46 (16.1)	239 (83.9)		
M	236 (45.3)	13 (9.7)	223 (90.3)		
Days in ETU, mean (SD), n = 184	26.8 (21.4)	22.7 (12.3)	27.4 (22.5)	0.99 (0.97–1.01)	0.182
Previous eye exam, n = 513	444 (86.5)	67 (15.1)	377 (84.9)	5.95 (1.42–24.88)	0.006
History of cataract, n = 510	42 (8.2)	16 (38.1)	26 (61.9)	4.82 (2.43– 9.56)	<0.001
History of uveitis, n = 510	51 (10.0)	12 (17.4)	39 (8.8)	2.17 (1.07–4.39)	0.030
Vision loss symptoms, n = 510	134 (26.3)	26 (19.4)	108 (21.2)	1.86 (1.09–3.18)	0.026

*Values are no. (%) except as indicated. ETU, Ebola treatment unit; OR, odds ratio.
†OR is the odds of uveitis for women vs. men.

broad spectrum of ophthalmic findings that were associated with vision impairment, including cataract, uveitis, corneal scar, and optic neuropathy.

Uveitis remained one of the most common ophthalmic diagnoses found, affecting 8.4% of EVD survivors. The prevalence of uveitis in our study was lower than in other studies from Sierra Leone also conducted during the West Africa EVD outbreak, which reported uveitis in 18%–34% of EVD survivors a few months after ETU discharge (8,11,12). In those studies, EVD survivor status was determined on the basis of EVD survivor certificates, history of ETU admission, and laboratory diagnostics when available. Some EVD survivors in our cohort might have been treated for uveitis in the previous few years; 87% reported having ≥1 previous eye exam, which was also associated with the presence of uveitis (p = 0.05). Another explanation is that EVD-associated uveitis develops shortly after the acute illness; risk declines over time, potentially in relation to the viral load in ocular tissues. One previous study showed that a higher viral load at acute EVD illness was associated with the development of uveitis (11). Viable Ebola virus was detected from the ocular fluid of an EVD survivor at 14 weeks in association with panuveitis but was no longer detected at 27 months, when the uveitis had been inactive for 3 months (17). In the Ebola Virus Persistence in Ocular Tissues and

Fluids (EVICT) study of survivors being evaluated for cataract surgery, 46 survivors with vision-impairing cataract tested negative for Ebola virus RNA in the aqueous humor at 19 months and 34 months after acute EVD (18,19). On the basis of those data, it is possible that EVD survivors have a greater risk for uveitis immediately after acute EVD as a result of viral persistence and that risk for uveitis decreases over time as the virus clears. Further studies will clarify the relationship between viremia, viral persistence in immune-privileged sites such as ocular tissues, and the development and progression of uveitis.

Nearly 20% of EVD survivors in this cohort had moderate vision impairment of 20/50 or worse in their better-seeing eye, which indicated ongoing ophthalmic disease at long-term follow-up. Ophthalmic findings associated with vision impairment in EVD survivors, including uveitis, cataract, corneal scar, and optic neuropathy, indicate a range of ocular disease that may contribute to visual illness and requires ongoing management. The EVICT study reported similar findings that vision-impairing cataract, posterior synechiae, optic neuropathy, and retinal detachment were strongly associated with worse logMAR VA in EVD survivors referred for vision impairment or cataract evaluation (20). In a population-based study conducted in 2021in Sierra Leone, 5.1% of participants were bilaterally blind and ≈16% had varying degrees of vision

Table 5. Ophthalmic examination findings associated with uveitis status in eyes of survivors in study of ophthalmic sequelae after Ebola virus disease, Sierra Leone*

Ophthalmic exam finding	No. (%) eyes			OR (95% CI)	p value
	Total, N = 1,042	Uveitis, n = 86	No uveitis, n = 956		
Bullous keratopathy	2 (0.2)	1 (50.0)	1 (50.0)	11.13 (8.67–14.51)	<0.001
Cataract	117 (11.2)	14 (12.0)	103 (88.0)	1.94 (0.96–3.89)	0.065
Corneal scar	28 (2.7)	5 (17.9)	23 (82.1)	1.94 (0.59–6.37)	0.276
Chorioretinal scar	68 (6.5)	17 (25.0)	51 (75.0)	3.74 (1.84–7.62)	0.012
Optic neuropathy	7 (0.7)	6 (85.6)	1 (14.3)	1.53 (0.07–34.47)	0.790
Posterior synechiae	7 (0.7)	3 (42.9)	4 (57.1)	11.58 (2.23–55.98)	0.002
Retinal detachment	7 (0.7)	3 (42.9)	4 (57.1)	5.64 (1.46–21.67)	0.012
Vitreous opacity	21 (2.0)	8 (38e.1)	13 (61.9)	5.41 (2.04–14.45)	0.022
Visual acuity					
20/40 or better	783 (75.1)	54 (6.9)	729 (93.1)	2.25 (1.32–3.83)	0.004
20/50 or worse	259 (24.9)	32 (12.4)	227 (87.6)	NA	NA

*NA, not applicable; OR, odds ratio.

Table 6. Multivariable model of ophthalmic findings and vision impairment in eyes of survivors in study of ophthalmic sequelae after Ebola virus disease, Sierra Leone*

Ophthalmic finding	No. (%) eyes		OR (95% CI)	p value
	Vision impairment, n = 259	No vision impairment, n = 783		
Cataract	71 (27.4)	46 (5.9)	7.68 (4.32–13.64)	<0.001
Uveitis	32 (12.4)	54 (7.0)	2.08 (1.23–3.52)	0.0065
Corneal scar	12 (4.6)	16 (2.0)	4.23 (1.80–9.95)	0.0010
Optic neuropathy	5 (1.9)	2 (0.3)	6.32 (1.15–34.69)	0.0335
*Vision impairment was defined as visual acuity worse than 20/50 Snellen. OR, odds ratio.				

impairment (21). The most common causes of bilateral blindness in the general population of Sierra Leone were untreated cataracts (59.4%), glaucoma (21.7%), and nontrachomatous corneal opacity (8.4%). Of note, the participants in the population-based study were ≥50 years of age, whereas the median age in our cohort of EVD survivors was 29 years. In addition, uveitis was not reported as a major cause of blindness or vision impairment in the general population.

Cataracts were found in 11.2% of eyes in our cohort and were strongly associated with vision impairment. Our analysis showed that uveitis found in the study exam was associated with a previous diagnosis of cataract (p<0.001); ≈10% of newly diagnosed cataracts were uveitic in nature. Considering the relatively young age of this cohort, a substantial number of the cataracts are likely attributable to previous or ongoing inflammation or treatment with topical corticosteroids. Cataract development related to uveitis was reported in other studies. Tiffany et al. (12) showed that 7 out of 8 EVD survivors with cataracts had concurrent uveitis. Mattia et al. (11) found that 10% of EVD survivors with uveitis had concurrent early cataracts and were relatively young (median age 29 years), suggesting that that the cataracts were not related to age. Thus, early detection and treatment for uveitis in EVD survivors could reduce the frequency of cataract development and improve visual outcomes.

Corneal scar and optic neuropathy were less common in EVD survivors but were also strongly associated with vision impairment status. A post hoc analysis of the EVICT study corroborated findings of worse logMAR VA in survivors with optic nerve disease than those without optic nerve disease (22). However, the presence of ocular surface disease, including dry eye, band keratopathy, and corneal scar, were not strongly associated with worse visual outcomes (23). Further studies will determine whether these ophthalmic manifestations are more common in EVD survivors than control participants and are associated with worse vision. To understand the prevalence of uveitis, visual impairment, and disease pathogenesis of ocular inflammation in EVD survivors compared with close-contact control patients, a longer-term study is currently underway in Sierra Leone (24).

Limitations of our study include the retrospective study design and lack of a control group. Timing or directionality of associations cannot be determined because this was a cross-sectional study. In addition, Ebola serum IgG was not available, so EVD survivor status was determined by survivor certificates and a history of ETU admission. Finally, there is also a potential for selection bias for symptomatic survivors that could skew the results toward a higher prevalence of ophthalmic findings; however, we recruited for examination any EVD survivor in the targeted regions who could be reached.

In summary, this study identified a range of ophthalmic complications that were associated with vision impairment in EVD survivors >3 years after the resolution of their acute illness. Uveitis remained one of the most common ophthalmic findings in EVD survivors, but cataract, corneal scars, and optic neuropathy were also found to be associated with poor visual outcomes. Our findings highlight the need for long-term vision care and follow-up for uveitis as well as a range of ophthalmic conditions in EVD survivors to optimize their visual potential and associated quality of life.

About the Author

Dr. Choo is an ophthalmology resident at the University Nebraska Medical Center. Dr. Choo has published original research articles on corneal dystrophies and ocular inflammatory diseases.

References

1. Centers for Disease Control and Prevention. Ebola outbreak history. 2023 [cited 2023 Jul 10]. https://www.cdc.gov/ebola/outbreaks/index.html
2. Aruna A, Mbala P, Minikulu L, Mukadi D, Bulemfu D, Edidi F, et al. Ebola virus disease outbreak—Democratic Republic of the Congo, August 2018–November 2019. MMWR Morb Mortal Wkly Rep. 2019;68:1162–5.
3. Kiggundu T, Ario AR, Kadobera D, Kwesiga B, Migisha R, Makumbi I, et al.; Uganda Ebola Response Team. Notes from the field: outbreak of Ebola virus disease caused by Sudan ebolavirus—Uganda, August–October 2022. MMWR Morb Mortal Wkly Rep. 2022;71:1457–9. https://doi.org/10.15585/mmwr.mm7145a5
4. Formenty P, Boesch C, Wyers M, Steiner C, Donati F, Dind F, et al. Ebola virus outbreak among wild chimpanzees living in a rain forest of Côte d'Ivoire. J Infect Dis. 1999;179(Suppl 1):S120–6. https://doi.org/10.1086/514296
5. Bwaka MA, Bonnet MJ, Calain P, Colebunders R, De Roo A, Guimard Y, et al. Ebola hemorrhagic fever in Kikwit, Democratic Republic of the Congo: clinical observations in 103 patients. J Infect Dis. 1999;179(Suppl 1):S1–7. https://doi.org/10.1086/514308
6. Kibadi K, Mupapa K, Kuvula K, Massamba M, Ndaberey D, Muyembe-Tamfum JJ, et al. Late ophthalmologic manifestations in survivors of the 1995 Ebola virus epidemic in Kikwit, Democratic Republic of the Congo. J Infect Dis. 1999;179(Suppl 1):S13–4. https://doi.org/10.1086/514288
7. Sneller MC, Reilly C, Badio M, Bishop RJ, Eghrari AO, Moses SJ, et al.; PREVAIL III Study Group. A longitudinal study of Ebola sequelae in Liberia. N Engl J Med. 2019;380:924–34. https://doi.org/10.1056/NEJMoa1805435
8. Shantha JG, Crozier I, Hayek BR, Bruce BB, Gargu C, Brown J, et al. Ophthalmic manifestations and causes of vision impairment in Ebola virus disease survivors in Monrovia, Liberia. Ophthalmology. 2017;124:170–7. https://doi.org/10.1016/j.ophtha.2016.10.011
9. Etard JF, Sow MS, Leroy S, Touré A, Taverne B, Keita AK, et al.; Postebogui Study Group. Multidisciplinary assessment of post-Ebola sequelae in Guinea (Postebogui): an observational cohort study. Lancet Infect Dis. 2017;17:545–52. https://doi.org/10.1016/S1473-3099(16)30516-3
10. Hereth-Hebert E, Bah MO, Etard JF, Sow MS, Resnikoff S, Fardeau C, et al.; Postebogui Study Group. Ocular complications in survivors of the Ebola outbreak in Guinea. Am J Ophthalmol. 2017;175:114–21. https://doi.org/10.1016/j.ajo.2016.12.005
11. Mattia JG, Vandy MJ, Chang JC, Platt DE, Dierberg K, Bausch DG, et al. Early clinical sequelae of Ebola virus disease in Sierra Leone: a cross-sectional study. Lancet Infect Dis. 2016;16:331–8. https://doi.org/10.1016/S1473-3099(15)00489-2
12. Tiffany A, Vetter P, Mattia J, Dayer JA, Bartsch M, Kasztura M, et al. Ebola virus disease complications as experienced by survivors in Sierra Leone. Clin Infect Dis. 2016;62:1360–6. https://doi.org/10.1093/cid/ciw158
13. Shantha JG, Canady D, Hartley C, Cassedy A, Miller C, Angeles-Han ST, et al. Ophthalmic sequelae and psychosocial impact in pediatric Ebola survivors. EClinicalMedicine. 2022;49:101483. https://doi.org/10.1016/j.eclinm.2022.101483
14. Jabs DA, Nussenblatt RB, Rosenbaum JT; Standardization of Uveitis Nomenclature (SUN) Working Group. Standardization of uveitis nomenclature for reporting clinical data. Results of the First International Workshop. Am J Ophthalmol. 2005;140:509–16. https://doi.org/10.1016/j.ajo.2005.03.057
15. Nussenblatt RB, Palestine AG, Chan CC, Roberge F. Standardization of vitreal inflammatory activity in intermediate and posterior uveitis. Ophthalmology. 1985;92:467–71. https://doi.org/10.1016/S0161-6420(85)34001-0
16. Holladay JT. Proper method for calculating average visual acuity. J Refract Surg. 1997;13:388–91.
17. Wells JR, Crozier I, Kraft CS, Sexton ME, Hill CE, Ribner BS, et al. Approach to cataract surgery in an Ebola virus disease survivor with prior ocular viral persistence. Emerg Infect Dis. 2020;26:1553–6. https://doi.org/10.3201/eid2607.191559
18. Varkey JB, Shantha JG, Crozier I, Kraft CS, Lyon GM, Mehta AK, et al. Persistence of Ebola virus in ocular fluid during convalescence. N Engl J Med. 2015;372:2423–7. https://doi.org/10.1056/NEJMoa1500306
19. Shantha JG, Mattia JG, Goba A, Barnes KG, Ebrahim FK, Kraft CS, et al. Ebola Virus Persistence in Ocular Tissues and Fluids (EVICT) study: reverse transcription-polymerase chain reaction and cataract surgery outcomes of Ebola survivors in Sierra Leone. EBioMedicine. 2018;30:217–24. https://doi.org/10.1016/j.ebiom.2018.03.020
20. Berry DE, Bavinger JC, Fernandes A, Mattia JG, Mustapha J, Harrison-Williams L, et al.; Ebola Virus Persistence in Ocular Tissues and Fluids (EVICT) Study Investigators. Posterior segment ophthalmic manifestations in Ebola survivors, Sierra Leone. Ophthalmology. 2021;128:1371–3. https://doi.org/10.1016/j.ophtha.2021.02.001
21. Jolley E, Mustapha J, Smart N, Ibrahim N, Schmidt E. Rapid assessment of avoidable blindness, Sierra Leone. Haywards Heath (UK): Sightsavers; 2022.
22. Nguyen NV, Randleman C, Fashina T, Huang C, Mwanza JC, Shantha J, et al. Neuro-ophthalmology implications in a cohort of Ebola virus disease survivors from the West African Ebola outbreak, Sierra Leone. Invest Ophthalmol Vis Sci. 2023;64:2902.
23. Fashina T, Nguyen NV, Randleman C, Huang C, Mwanza JC, Shantha J, et al. Corneal and conjunctival findings in a cohort of Ebola virus disease survivors from the West African Ebola outbreak. Invest Ophthalmol Vis Sci. 2023;64:2484.
24. Yeh S, Fashina T, Ward L, Hartley C, Nguyen N, Choo C, et al. A study of long-term sequelae in Ebola virus disease survivors, Sierra Leone: baseline characteristics, ophthalmic sequelae, and systemic symptoms. Presented at: American Academy of Ophthalmology Annual Meeting; October 18, 2024; Chicago, Illinois, USA.

Address for correspondence: Jessica Shantha, F.I. Proctor Foundation, University of California San Francisco, 490 Illinois St, San Francisco, CA 94158, USA; email: jessica.shantha@ucsf.edu

Highly Pathogenic Avian Influenza A(H5N1) Virus Infection in Cats, South Korea, 2023

Yong-Myung Kang,[1] Gyeong-Beom Heo,[1] Se-Hee An, Hyunho Lee, Eunhye Park, Ra Mi Cha, Yun Yueng Jang, Mingeun Sagong, Ah-Young Kim, Jongho Kim, Eun-Kyoung Lee, Seong Hee Kim, Kyungki Lee, Bokkyung Ku, Youn-Jeong Lee, Kyunghyun Lee, Kwang-Nyeong Lee

In July 2023, cases of highly pathogenic avian influenza (HPAI) were reported at 2 shelters for stray cats in Seoul, South Korea. The cause of infection was suspected to be improperly sterilized raw food made from domestic duck meat, which was manufactured in South Korea. All viruses isolated from cats at the shelters and from the raw food belonged to HPAI A(H5N1) clade 2.3.4.4b. The gene constellation of all viruses was most similar to that of viruses isolated in Korea in November 2022. Of note, the viruses isolated from infected cats harbored mutations E627K or D701N in polymerase basic 2, which are indicative of adaptation to mammals. Postmortem examination revealed systemic pathologic lesions and the presence of widespread virus in different tissues. Thus, consumption of raw duck meat contaminated with HPAI virus likely caused systemic symptoms and death in cats, indicating the introduction of mammal-adapted mutations of the virus.

Highly pathogenic avian influenza virus (HPAIV) (H5Nx) subtype descendents of the H5N1 Goose-Guangdong (Gs/Gd) lineage emerged in 1996; since then, derivatives of H5Nx have disseminated intercontinentally through wild migratory waterfowl and human activity (1–3). Since 2020, HPAI H5 viruses belonging to the Gs/Gd lineage have become panzootic, demonstrating continual reassortment with low pathogenicity avian influenza viruses (LPAIV). Those viruses have shown unprecedented global spread among poultry and wild birds, even infecting mammals and humans (1,4). In most cases, mammal infection results from direct or indirect contact with infected birds or from consumption of dead birds, suggesting that the avian virus can be transmitted to mammal hosts (5).

Viruses belonging to H5Nx clade 2.3.4.4b caused major outbreaks in wild birds in Asia, Europe, Africa, and America (6,7); infections even extended to both terrestrial and aquatic mammals (8). Wild mammals, such as red foxes, lynxes, and skunks, and domestic mammals, including pet ferrets, domestic mink, raccoon dogs, and arctic foxes, have been infected by H5N1 clade 2.3.4.4b viruses; moreover, the disease has been detected in aquatic mammal species including seals and sea lions in North and South America (6,9,10). In addition, a report from Italy in July 2023 revealed infected cats and dogs living in close proximity to humans (10); studies conducted since June 2023 report that 29 domestic cats in at least 6 regions of Poland were infected with the H5N1 clade 2.3.4.4b virus (10–12).

In South Korea, HPAIV infection of cats and dogs on poultry farms affected by HPAIV were reported in 2015 and 2016. Those infections are thought to have occurred through close contact with, or consumption of, HPAIV-infected birds (13,14). HPAIV was later confirmed in cats at 2 different cat shelters in 2023. In July 2023, cats housed in a cat shelter in Seoul were found dead, leading the owner to request diagnostic tests at a private diagnostic institution. Subsequently, a veterinary laboratory at Seoul National University (SNU) became involved in the diagnosis of those samples. The SNU laboratory contacted the

Author affiliations: Animal and Plant Quarantine Agency, Gimcheon-si, South Korea (Y.-M. Kang, G.-B. Heo, S.-H. An, R.M. Cha, Y.Y. Jang, M. Sagong, A.-Y. Kim, J. Kim, E.-K. Lee, S.H. Kim, Kyungki Lee, B. Ku, Y.-J. Lee, Kyunghyun Lee, K.-N. Lee); Kyungpook National University, Daegu, South Korea (Y.-M. Kang); Seoul National University, Seoul, South Korea (G.-B. Heo); Seoul Metropolitan Government Research Institute of Public Health and Environment, Gwacheon-si, South Korea (H. Lee, E. Park)

[1]These authors contributed equally to this article.

Animal and Plant Quarantine Agency (APQA) in South Korea with the HPAIV-positive test results; the HPAIVs were isolated from dead cats and belonged to H5N1 clade 2.3.4.4b with a D701N mutation in the polymerase basic (PB) 2 gene (*15*). A second shelter in Seoul reported suspected clinical signs of HPAIV infection in cats 5 days later. We obtained additional clinical samples from cats and the environments of the 2 shelters and conducted various tests to identify the source of infection and to characterize the viruses.

In this study, we describe identifying the source of infection through environmental sampling, epidemiologic investigations, and genetic analysis. We also evaluate the risk for human infection and transmission between mammals. Furthermore, we explore disease pathogenesis, focusing on virus replication in tissues and associated pathologic sequelae.

Materials and Methods

Case Description and Sampling

On July 24, 2023, SNU contacted the APQA, the national reference institute headquarters responsible for avian influenza diagnosis in South Korea, to report possible HPAIV infection of cats housed in a shelter located in Yongsan-gu, Seoul (shelter 1). To ensure the results and investigate the case, we collected additional samples from 3 frozen cat carcasses and 2 live cats at the shelter; we also collected blood from 2 live cats, neither of which showed clinical signs for serologic testing. On July 29, 2023, a vet charged with examining hospitalized cats from another cat shelter in Gwanak-gu, Seoul (shelter 2), also reported suspected cases of HPAIV infection. A cat carcass, as well as nasal swab samples from 4 sick cats housed at the animal hospital and from the 122 cats remaining at shelter 2, were collected and tested by the Seoul local veterinary service. The clinical samples and the cat carcasses that tested positive for the H5 gene from shelter 2 were sent to APQA. We performed postmortem examination on all the cat carcasses sent to APQA from the 2 shelters and collected tissue samples from various organs. All those samples and other clinical swab samples were subjected to molecular diagnostic tests for avian influenza or other suspected diseases.

To determine the location and the extent of contamination of the shelters, we conducted environmental sampling (183 swabs) at various locations within 2 shelters within 2–3 days of the report of HPAIV. The swabs were placed in a viral transport medium and delivered to the APQA directly. We categorized environmental samples according to sampling location, type of object sampled, the structures within the shelter itself, whether the items were cat-related (e.g., food), and samples from wildlife residues located outside the shelter.

Furthermore, we conducted epidemiologic environmental sampling at relevant sites associated with contaminated raw food, such as raw duck meat food manufacturers, slaughterhouses, meat storage facilities, suspected duck farms, other cat shelters, and locations associated with feral cats. We collected 214 samples from 9 different locations and tested them at the APQA. In addition, we also sampled and tested all types of raw food for cats or dogs on the market (produced by 10 other manufacturers); in total, we tested 65 raw food products and 24 raw meats of duck or chicken origin.

Molecular Detection, Isolation, and Sequencing

We tested swab samples, tissue samples, and virus isolates by real-time reverse transcription PCR (RT-PCR), as described previously (*16,17*), to detect the matrix (M), H5, or H7 genes of avian influenza (*18*). If a sample tested positive for H5, we amplified the cleavage site within the H5 hemagglutinin (HA) gene by RT-PCR and determined nucleotide sequences using an Applied Biosystems ABI 3500xL Genetic Analyzer (ThermoFisher Scientific, https://ww.thermofisher.com) for pathotyping (*18*).

To isolate and characterize the virus, we inoculated H5-positive samples into 10-day-old embryonated chicken eggs and incubated for 48 hours at 37°C. We extracted viral RNA from the infectious allantoic fluid using an NX-48 Viral NA kit (Genolution, https://genolution.co.kr). We amplified all 8 segments of the isolates by RT-PCR (*19*). We performed complete-genome sequencing using the Illumina Miseq platform with the Nextera DNA Flex Library Prep Kit (https://www.illumina.com) and assembled genomic sequences by using CLC Genomics Workbench version 23 (QIAGEN, https://www.qiagen.com). We deposited the nucleotide sequences of 12 viruses isolated in this study in the GISAID database (https://www.gisaid.org; accession nos. EPI_ISL_18819799–EPI_ISL_18819810). We downloaded the reference datasets for phylogenetic analysis of all the gene segments characterized in this study from GenBank and the GISAID EpiFlu Databases. We aligned those sequences with MAFFT (https://mafft.cbrc.jp/alignment/software) using the default parameters for FASTA alignment. We removed all untranslated regions and retained only the protein-coding sequences of each segment. We constructed maximum-likelihood trees based on the aligned sequences using RAxML on XSEDE version 8.2.12 (*20*). We used bootstrap analysis with 1,000 replicates to assess the reliability

of the trees and generated the tree displays by using the interactive Tree of Life program (*21*).

Pathologic Examination

We conducted necropsy to confirm HPAIV diagnosis and to examine pathologic lesions. We collected tissue samples (brain, heart, lung, spleen, kidney, liver, pancreas, and intestine), fixed for 24 hours in 10% buffered neutral formalin, and then processed for paraffin embedding. We then cut 4-µm sections, mounted, dewaxed, and stained with hematoxylin and eosin. We analyzed duplicate sections by immunohistochemistry to determine the distribution of influenza virus antigens using a monoclonal antibody specific for influenza A virus nucleoprotein (Bio-Rad Laboratories, https://www.bio-rad.com). We used a biotinylated goat anti-mouse IgG and an avidin-biotin complex system, using the RedMap Kit (all Roche, https://www.roche.com) as the chromogenic substrate. We incubated the negative control slide in phosphate-buffered saline instead of the primary antibody.

Serologic Testing

We treated serum samples from 2 surviving cats from shelter 1 with a receptor-destroying enzyme (Denka Seiken, https://www.denka.co.jp), inactivated at 56°C for 30 minutes, and chilled at 10°C. We performed hemagglutination inhibition assays using standard methods and homologous antigens (*22*).

Results

Detecting, Isolating, and Characterizing Viruses from Cats in the Shelters

We detected the H5 gene in nasal swab samples and all tested organs from the 3 carcasses at shelter 1 and 1 cat carcass from the shelter 2–related animal hospital (Table 1). In addition, nasal swab samples as well as from the 3 living cats at the animal hospital and its related shelter 2, were positive for the H5 gene (Table 1). All H5-positive samples had multiple basic amino acid residues at the cleavage site of the HA gene (PLREKRRKR/G), corresponding to the motif that denotes the HPAI virus, was detected. In addition, the analysis of the neuraminidase (NA) sequences assigned all the viruses sequenced to the N1 subtype. As expected, HPAI H5N1 viruses were isolated from the affected cats from the 2 shelters. The 2 surviving cats in shelter 1 had H5-specific antibodies (hemagglutination inhibition titer, 2^5) (Table 1).

The 3 H5N1 viruses isolated from dead cats in shelter 1 were designated A/feline/Korea/M302-5/2023, A/feline/Korea/M302-6/2023, and A/feline/Korea/M302-7/2023, referred to hereafter as M302-5, M302-6, and M302-7. The 4 H5N1 isolates from shelter 2 were named A/feline/Korea/M305-11/2023 (for the dead cat in the hospital), A/feline/Korea/M305-7/2023 (for the sick cat in the hospital), A/feline/Korea/M305-3/2023 and A/feline/Korea/M305-4/2023, referred to hereafter M305-11, M305-7, M305-3, and M305-4.

Table 1. Real-time RT-PCR results for the H5 gene in study of highly pathogenic avian influenza virus A(H5N1) infection in cats, South Korea, 2023*

| Location | ID | Clinical signs | Cycle threshold value | | | | | | | | | | |
			Brain	Feces	Heart	Intestine	Kidney	Liver	Lung	Lymph node	Nasal swab	Spleen	Trachea
Yongsan-gu Shelter 1	Cat carcass no. 1	Death	33	32	32	27	32	27	21	28	35	26	26
	Cat carcass no. 2	Death	20	28	21	27	25	15	18	22	27	21	26
	Cat carcass no. 3	Death	28	31	25	27	27	17	19	24	36	25	23
	Cats nos. 4–5	None	NT	NT	NT	NT	NT	NT	NT	NT	−†	NT	NT
Gwanak-gu Animal hospital	Cat carcass no. 1	Death	22	27	20	19	18	12	15	21	19	17	24
	Cat no. 1	Severe	NT	NT	NT	NT	NT	NT	NT	NT	35	NT	NT
	Cats nos. 2–4	Moderate	NT	NT	NT	NT	NT	NT	NT	NT	−‡	NT	NT
Shelter 2	Cat no. 5	None	NT	NT	NT	NT	NT	NT	NT	NT	29	NT	NT
	Cat no. 6	None	NT	NT	NT	NT	NT	NT	NT	NT	24	NT	NT
	Cats nos. 7–126	None	NT	NT	NT	NT	NT	NT	NT	NT	−§	NT	NT

*ID, identification number; NT, not tested; RT-PCR, reverse transcription PCR; –, negative.
†Two live cats from shelter 1 were negative on H5 real-time RT-PCR but showed seroconversion against H5 antigens.
‡Three cats from the animal hospital were negative on H5 real-time RT-PCR.
§At shelter 2, 120 live cats were negative on H5 real-time RT-PCR.

Pathologic Lesions

We first examined the carcasses (Figure 1) and assigned a body condition score (1–3, poor weight; 4–6, ideal weight; 7–9, overweight) (23); all 3 cat carcasses from shelter 1 (Y cat nos. 1–3) had a score of 7 (Appendix Table 1). Two carcasses (1 from shelter
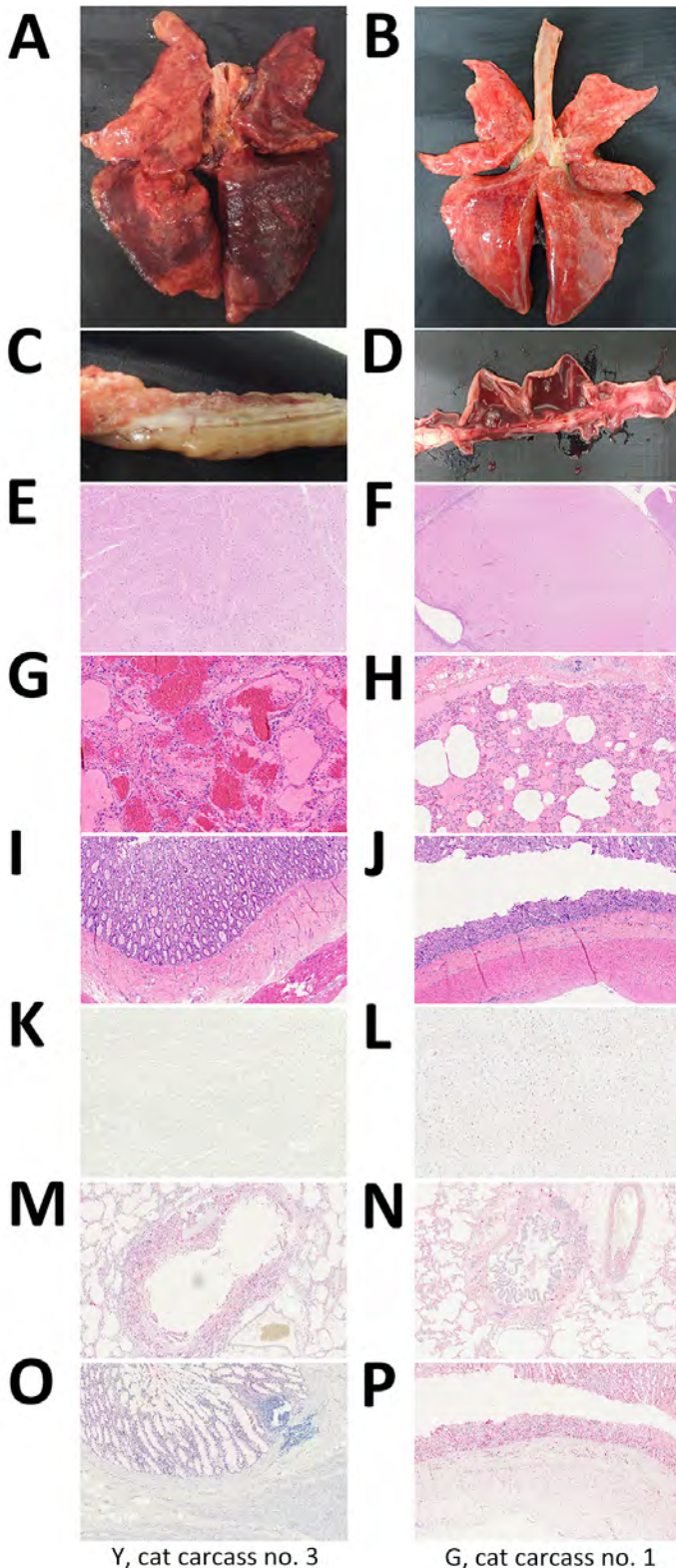

Figure 1. Gross, microscopic, and immunohistochemistry (IHC) findings in cats infected with highly pathogenic avian influenza A(H5N1) virus, South Korea, 2023. Findings are shown for cat carcasses from shelter 1 (Y cat carcass no. 3) and shelter 2 (G cat carcass no. 1). A–D) Gross findings: A) severe congestion and edema in the lungs; B) congestion and edema in the lungs; C) lack of lesions in the small intestine; D) bloody diarrhea in the small intestine (D). E–J) Hemotoxylin and eosin staining: E) brain showing no lesions; F) multifocal gliosis in the brain; G) interstitial pneumonia with focally extensive vascular thrombosis; H) interstitial pneumonia characterized by invasion of the alveolar lumina by mixed neutrophils and macrophages; I) intestine showing no lesions; J) necrotic enteritis with denuded villi. K–P) Immunohistochemical staining: K) brain showing no influenza virus antigens; L) influenza virus antigens in the neurons; M) influenza virus antigens in alveolar macrophages and bronchial epithelial cells; N) influenza virus antigens in alveolar macrophages and bronchial epithelial cells; O) influenza virus antigens in the small intestine; P) influenza virus antigens in the crypt epithelium and blood vessels in the submucosa. Original magnification ×100, except panel F, in which original magnification was ×10.

1 [Y cat no. 3] and 1 from shelter 2 [G cat no. 1]) grossly exhibited diffuse moderate to severe congestion and edema in the lungs (Figure 1, panels A and B), as well as interstitial pneumonia characterized by infiltration of macrophages and degenerated neutrophils into the vascular and alveolar lumina (Figure 1, panels G and H). Y cat no. 3 did not have gross or microscopic lesions in the brain or small intestine (Figure 1, panels C, E, and I); that finding was true for all 3 carcasses from shelter 1. However, the carcass from shelter 2 had multifocal encephalitis, with gliosis and perivascular cuffing in the brain, and bloody diarrhea in the small intestine (Figure 1, panels D, F, and J). Immunohistochemistry revealed influenza virus antigens in alveolar macrophages and bronchial epithelial cells in all 4 cats (Figure 1, panels M, N). The carcass from shelter 2 also had influenza antigens in neurons, glial cells (Figure 1, panel L), and intestinal epithelial cells in the small intestine (Figure 1, panel P). No influenza viral antigens were present in the brains of carcasses from shelter 1, but H5 genes were detected (Table 1; Appendix Table 2).

Environment Sampling

To investigate the source and extent of contamination at the cat shelters, we collected 183 environmental samples from both inside and outside the cat shelters and tested them by real-time RT-PCR. In shelter 1, we detected the M gene in samples taken from staff's shoes and clothing, floors, doors, walls, and refrigerators. In shelter 2, we detected the M gene in vacuum cleaners and in cat feces, whereas we detected the M and H5 gene in the 4 unopened containers of raw cat food manufactured by a company using domestic duck meat as a main ingredient (Appendix Table 3).

Thereafter, we isolated H5N1 virus from the cat raw food, manufactured on July 6; we named the isolte A/environment/Korea/M305E-13/2023(H5N1), referred to hereafter as EV/M305E-13 (Tables 2, 3). Upon

conducting a nationwide recall and investigating the raw food produced by the manufacturer in question, we collected all raw food products of the same brand from customers. Of note, we isolated identical viruses not only from the same brand of food at the manufacturer but also in the food bought by customers, which was manufactured using the same lot of raw duck meat, albeit on different dates (May 26, June 15, and July 6 and 27). The level of viral infectivity in the raw food products was $10^{2.5}$–$10^{3.5}$ 50% egg infectious dose (EID_{50})/g (Table 2). The viruses isolated from them were designated as A/environment/Korea/M305E2-24/2023 (M305E2-24), A/environment/Korea/M305E2-25/2023 (M305E2-25), and A/environment/Korea/M305E3-1/2023 (M305E3-1) (Table 2).

We identified all facilities or companies that had handled the duck meat contained in the infectious raw cat food and tested for the presence of virus; those facilities consisted of suspected duck farms, slaughterhouses, meat processing companies, middlemen, and retailers. No virus could be detected in 214 samples from 9 locations. In addition, all types of raw foods (65 products and 24 meats from 10 manufacturers) for pet cats or dogs on the market were tested and determined to be avian influenza–negative (data not shown).

Genetic Analysis

To identify the source of the H5N1 virus isolated from cats and raw food, we analyzed representative viruses isolated at each location alongside other viruses within H5Nx clade 2.3.4.4b (Figures 2, 3). The 8 genes of the 3 viruses, M302-5, M305-11, and M305E-13, were almost identical among them (99.9% for nucleoprotein, HA, and PB1 and 100% for polymerase acidic [PA], NA, M, and nonstructural [NS]). Phylogenetic analysis revealed that the HA and NA genes of the 3 viruses are most closely related to those of the H5N1 clade 2.3.4.4b identified in 2022–2023 (Figures 2, 3), 1 of which was A/duck/Korea/H537/2022(H5N1); nucleotide identities to them were 99.46%–100%

Table 2. Detection of H5 genes and H5 HPAIV in raw cat food in study of HPAIV A(H5N1) infection in cats, South Korea, 2023*

Sample source	Sample	Manufacturing date	H5 Ct	EID_{50}/g	Strain name
Collected from shelter 2	Raw cat food† (duck meat)	2023 Jul 6	28	$10^{3.5}$	A/environment/Korea/M305E-13/2023(H5N1)
Collected from manufacturer A‡ or the buyer of the foods under tracking investigation†	Raw cat food (duck meat)	2023 May 26	27	$10^{2.5}$	A/environment/Korea/M305E2–24/2023(H5N1)
		2023 Jun 15	28	$10^{3.0}$	A/environment/Korea/M305E2–25/2023(H5N1)
		2023 Jul 27	29	$10^{3.5}$	A/environment/Korea/M305E3–1/2023(H5N1)

*Ct, cycle threshold; EID_{50}, 50% egg infectious dose; HPAIV, highly pathogenic avian influenza virus.
†The same brand of raw cat food products made of raw meat from ducks slaughtered on the same day but on different manufacturing dates were all positive, but the same brand of raw food products made from raw chicken meat was negative (data not shown). Moreover, all kinds of cat food made from raw meat that were recalled nationwide from 10 manufacturers tested negative except for products in Table 2.
‡Manufacturer of avian influenza–positive raw cat food product fed to cats at shelter 2.

across the 8 genes (Appendix Table 4). All the cat viruses isolated from shelter 1, including M302-5, possessed mutation D701N in the PB2 gene, whereas all the cat viruses isolated from shelter 2, including M305-11, possessed mutation E627K in the PB2 gene (Table 3; Appendix Table 4). The D701N and E627K mutations in the PB2 gene are critical markers of virus adaptation to mammals (12).

Discussion

The owner of shelter 1 in Seoul, in which 38 of 40 cats died within a month beginning in late June 2023 (15), had taken sick cats with respiratory and neurologic symptoms to a private animal hospital in early July. Of the 38 cats that died, HPAIV was diagnosed in only 5; the other 33 cat carcasses had been disposed of without diagnosis (15). After the report of the HPAI

Table 3. Amino acid differences identified among highly pathogenic avian influenza A (H5N1) virus detected in domestic ducks, cats, and duck meat–based cat food, South Korea, 2023*

Virus strain		Amino acid differences									
		PB2				HA†				NA‡	
Name	Origin	T271A	K526R	E627K	D701N	S137A	T160A	Q226L	G228S	H274Y	N294S
A/duck/Korea/H537/2022(H5N1)§ (EPI_ISL_18819799)	Poultry in South Korea	T	K	E	D	A	A	Q	G	H	N
A/feline/Korea/M302-5/2023(H5N1) (EPI_ISL_18819808)	Cat carcass in shelter 1	T	K	E	**N**	A	A	Q	G	H	N
A/feline/Korea/M302-6/2023(H5N1) (EPI_ISL_18819809)	Cat carcass in shelter 1	T	K	E	**N**	A	A	Q	G	H	N
A/feline/Korea/M302-7/2023(H5N1) (EPI_ISL_18819810)	Cat carcass in shelter 1	T	K	E	**N**	A	A	Q	G	H	N
A/feline/South_Korea/SNU-01/2023(H5N1) (EPI_ISL_18102700)	Cat carcass in shelter 1	T	K	E	**N**	A	A	Q	G	H	N
A/feline/South_Korea/SNU-02/2023(H5N1) (EPI_ISL_18102701)	Cat carcass in shelter 1	T	K	E	**N**	A	A	Q	G	H	N
A/feline/Korea/M305-3/2023(H5N1) (EPI_ISL_18819805)	Cat in shelter 2¶	T	K	**K**	D	A	A	Q	G	H	N
A/feline/Korea/M305-4/2023(H5N1) (EPI_ISL_18819806)	Cat in shelter 2¶	T	K	**K**	D	A	A	Q	G	H	N
A/feline/Korea/M305-7/2023(H5N1) (EPI_ISL_18819807)	Cat from shelter 2#	T	K	**K**	D	A	A	Q	G	H	N
A/feline/Korea/M305-11/2023(H5N1) (EPI_ISL_18819804)	Cat carcass from shelter 2#	T	K	**K**	D	A	A	Q	G	H	N
A/environment/Korea/M305E2-24/2023(H5N1) (EPI_ISL_18819801)	Raw duck meat food manufactured on May 26	T	K	E	D	A	A	Q	G	H	N
A/environment/Korea/M305E2-25/2023(H5N1) (EPI_ISL_18819802)	Raw duck meat food manufactured on June 15	T	K	E	D	A	A	Q	G	H	N
A/environment/Korea/M305E-13/2023(H5N1) (EPI_ISL_18819800)	Raw duck meat food manufactured on July 6	T	K	E	D	A	A	Q	G	H	N
A/environment/Korea/M305E3-1/2023(H5N1) (EPI_ISL_18819803)	Raw duck meat food manufactured on July 27	T	K	E	D	A	A	Q	G	H	N

*Letters in red denote differences between viruses. HA, hemagglutinin; NA, neuraminidase; PB2, polymerase basic 2.
†H3 numbering.
‡N2 numbering.
§R.M. Cha, unpub. data.
¶Cats living in shelter 2.
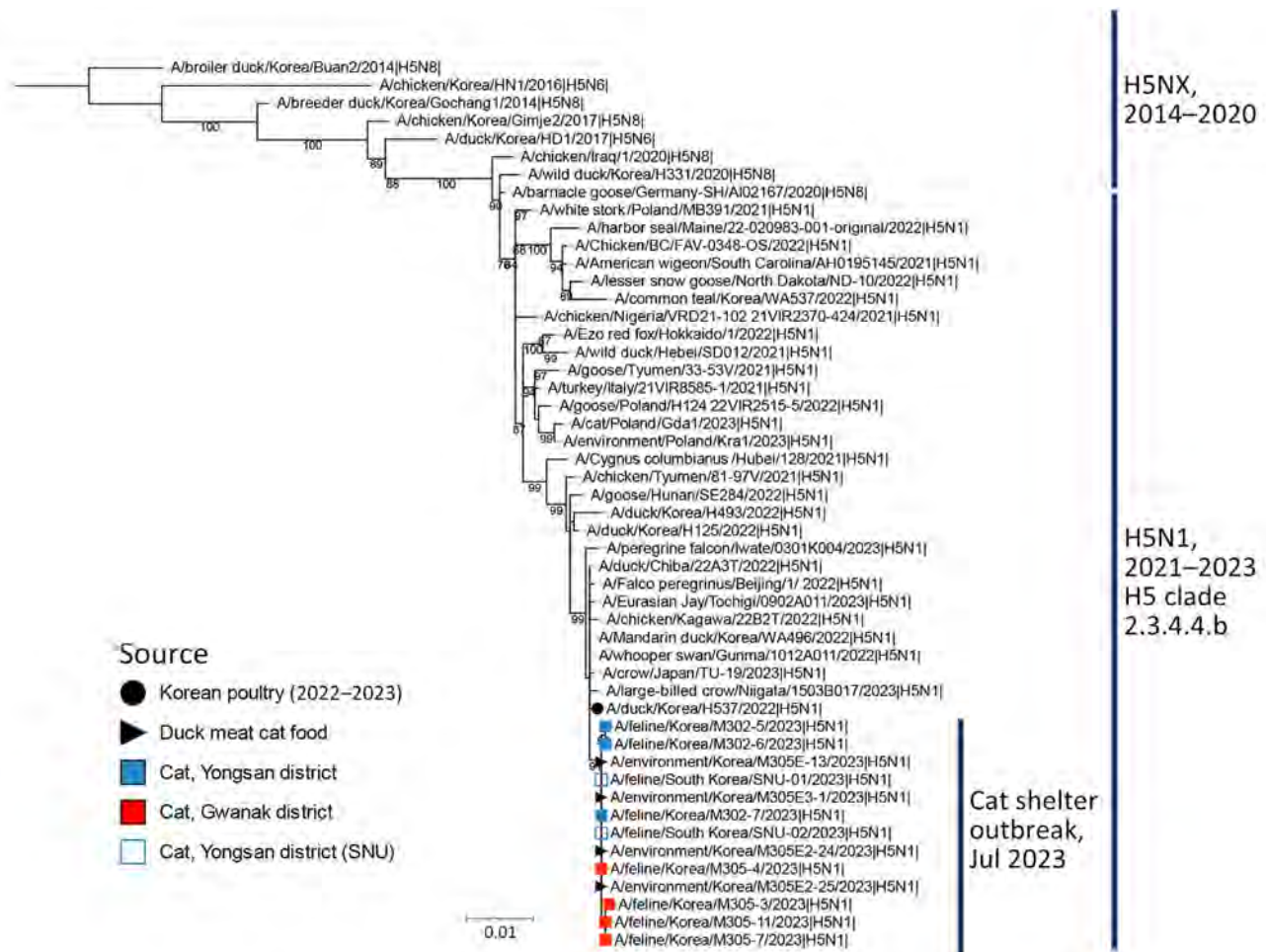#Cats moved from shelter 2 to the animal hospital.

Figure 2. Maximum-likelihood phylogenetic tree for the hemagglutinin (HA) gene in study of highly pathogenic avian influenza virus A(H5N1) infection in cats, South Korea, 2023. The phylogenetic tree is based on H5N1 HA sequences of viruses isolated recently, as well as on the HA gene sequence of other H5Nx viruses. Bootstrap values (1,000 replicates) >70% are displayed at the branch nodes. The black circle denotes virus isolated from poultry in South Korea, 2022–2023, and the black triangle denotes viruses isolated from raw duck meat used for cat food. The blue shaded square denotes viruses isolated from cats in shelter 1, and the red square indicates viruses isolated from cats in shelter 2. The blue outlined square indicates viruses isolated from cats in shelter 1 by SNU. Scale bar indicates number of nucleotide substitutions per site. SNU, Seoul National University.

case in shelter 1, all cat owners, shelters, and veterinarians were urged to report influenza-like illnesses to the government, and another suspicious case in cats originating from shelter 2 was disclosed.

The HPAI infections of dogs (2015) and cats (2016) previously reported in South Korea were related to infected wild birds (*13,14*). However, the infections of cats in 2 shelters located in a metropolitan city in 2023 could not be attributed to direct contact with wild birds or poultry. Therefore, the HPAI-contaminated raw cat food found at shelter 2 was regarded as a critical and direct source of infection. Furthermore, the viruses isolated from the cats (M305-11) and the raw food from shelter 2 (M305E-13) presented a genetic similarity ≥99.9% for all the genes, and that similarity

strongly supports the idea that the raw food was the direct source of infection, particularly in shelter 2. The gene constellation of M302-4, M305-11, and M305E-13 was most similar to that of viruses isolated in Korea in November 2022; 1 of those was A/duck/Korea/H537/2022(H5N1), which had a nucleotide identity of 99.46%–100% across the 8 genes (Appendix Table 4). These viruses possess a gene constellation representing that of a group, including A/duck/Korea/H537/2022(H5N1), dominant in South Korea (R.M. Cha, unpub. data) in the winter of 2022–2023, which was also isolated from birds in Japan during the same period (*15*).

The viral infectivity of the contaminated raw food product ranged from $10^{2.5}$ to $10^{3.5}$ EID_{50}/g,
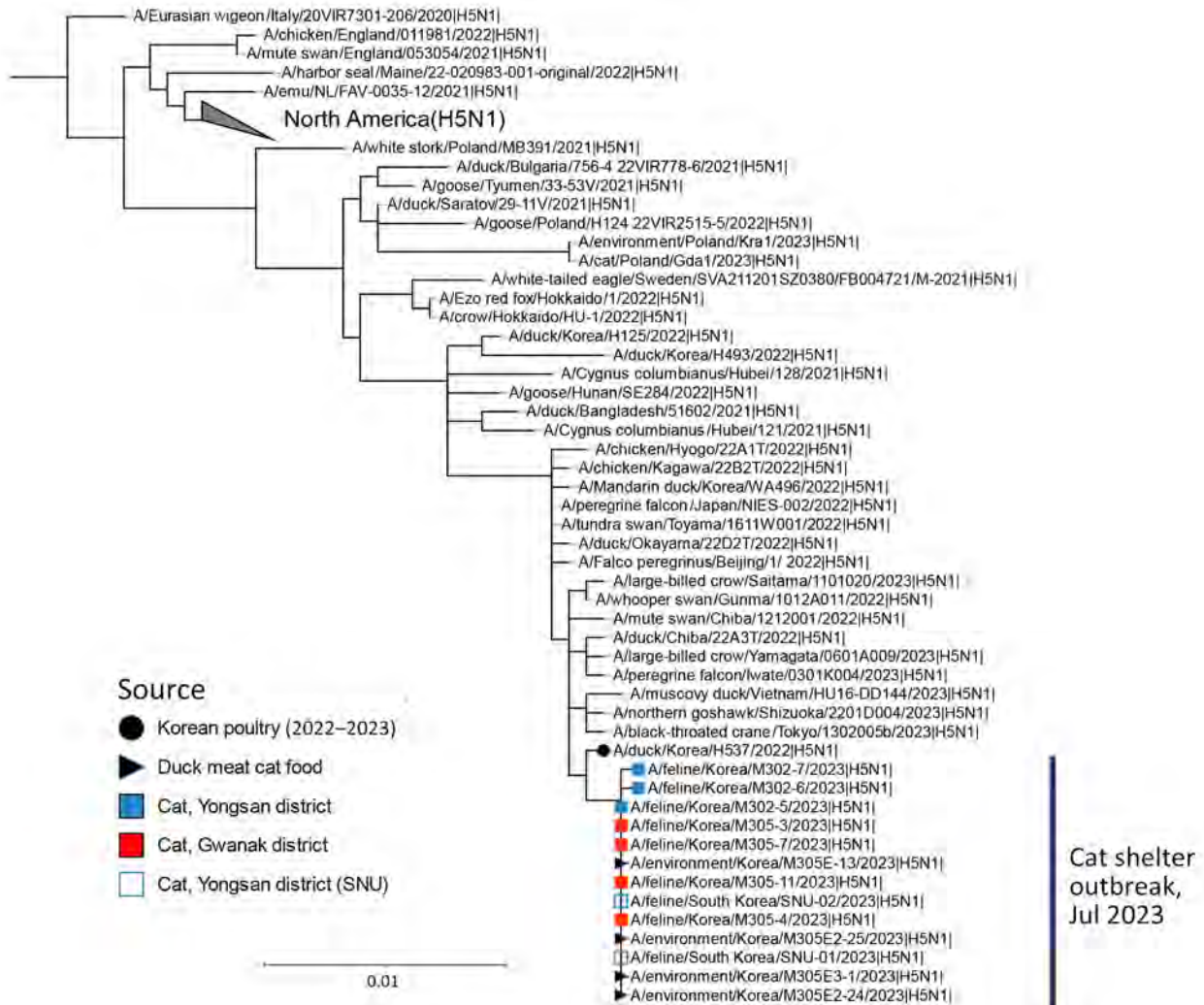
Figure 3. Maximum-likelihood phylogenetic tree for the neuraminidase (NA) gene in study of highly pathogenic avian influenza virus A(H5N1) infection in cats, South Korea, 2023. The phylogenetic tree is based on sequences of H5N1 NA sequences of viruses isolated recently, as well as on the HA gene sequence of other H5Nx viruses. Bootstrap values (1,000 replicates) >70% are displayed at the branch nodes. The black circle denotes virus isolated from poultry in South Korea, 2022–2023, and the black triangle denotes viruses isolated from raw duck meat used for cat food. The blue shaded square denotes viruses isolated from cats in shelter 1, and the red square indicates viruses isolated from cats in shelter 2. The blue outlined square indicates viruses isolated from cats in shelter 1 by SNU. Scale bar indicates number of nucleotide substitutions per site. SNU, Seoul National University.

which is similar to the minimal dose required to infect cats (10^2–10^4 EID_{50}/g) (24). The high viral load in most organs from the dead cats suggests that the virus replicated systemically and affected the host severely, similar to the effects of HPAI in chickens. The pattern of distribution of viral load, virus particles, and lesions observed in the cat carcasses was very similar to that observed in other HPAI H5N1–infected cats (both naturally and experimentally infected cases) (24). Previous studies report that gastrointestinal exposure is sufficient to infect cats with HPAIV; the liver and lungs are the main organs affected (25,26). We also found that the liver, lungs,

and especially the intestines of cats from shelter 2 had the highest viral load among all organs (cycle threshold 12–19), along with clear pathologic lesions (Figure 1). Our results support the fact that oral consumption of contaminated raw food products can induce extensive lesions in the digestive system, along with concurrent infection of the respiratory and digestive systems (Figure 1) (27). The dead cats, and those with clinical signs, at shelter 2 had likely ingested the cat raw food repeatedly, resulting in substantial exposure to the virus. By contrast, the cat carcasses from shelter 1 had been stored in a frozen state, making it difficult to determine the

route of HPAI infection on the basis of pathologic lesions alone. Although no direct evidence of contaminated food was found at shelter 1, the cause of infection is presumed to be the same as at shelter 2; that presumption is based on a statement from the owner of shelter 1 that cats had been fed a variety of types of raw food and the discovery of a receipt for the purchase of the same brand of raw cat food consumed in shelter 2. Of note, the 2 kinds of mutations related to mammalian adaptations, PB2-E627K and PB2-D701N, were observed in the viruses isolated from cats in shelter 1 (PB2-E627K) and shelter 2 (PB2-D701N). However, in the viruses isolated from the raw cat food, none of these point mutations were observed. The mammal-adaptive mutations at the critical genome sites of the HPAI virus are the same as those reported previously (28,29).

In other genomic regions, the viruses isolated from the cats in shelter 2 had amino acid differences in a few locations (Appendix Table 5). Each of those cat viruses in shelter 2, notably, had quasispecies containing minor populations with glutamic acid (E) at 627th in PB2 and major populations with lysine (K) at the same location (data not shown). Therefore, in the case of shelter 2, all the cats were likely infected from the direct ingestion of the contaminated raw foods. For the cat viruses from shelter 1, most of the deceased cats and raw food were disposed of before testing, and feeding records for the infected animals were not maintained, making the route of infection and transmission in that shelter difficult to infer. HPAI infection of cats in Poland during the summer of 2023 was suspected to be caused primarily by cat food made from poultry meat (11,12).

The main ingredient of the raw food collected from shelter 2 was domestic duck meat, and we suspect some infected broiler ducks were slaughtered despite intensive and regular active avian influenza surveillance on broiler duck farms during the HPAI incursion period; broiler duck farms should be tested 3–4 times for avian influenza before ducks are moved to the slaughterhouse (30). Further epidemiologic investigations revealed that the cat food manufacturer had not performed the required electron beam sterilization process during production, and the omission of the sterilization process is considered the most direct cause of cat infection in the shelters (data not shown). Thus, all facilities or companies that handled duck meat were contacted and ordered to clean and disinfect the premises to prevent secondary infections by avian influenza viruses. Promptly identifying the source of infection in shelter 2 led to the recall of all contaminated raw cat food products or products at risk for contamination; all were discarded.

The cases of HPAI infection at 2 cat shelters caring primarily for stray cats located in Seoul, South Korea, were sporadic and irregular. The source of infection at shelters was improperly sterilized raw cat food. We identified systemic virus and pathologic manifestations in the carcasses of cats that had consumed this raw food and confirmed the presence of mammalian-adaptive mutations in the viruses isolated from the cats. From these results, ways to increase disease surveillance sensitivity on poultry farms continue to be sought on the basis of the risk-based surveillance principle (31). In addition, more strict disease monitoring in the slaughterhouse is also necessary, especially for subclinical infection of duck species. As a last resort, the risk for avian influenza virus infection in pets should be mitigated by achieving compliance and enforcing regulations for sterilization of raw food. Moreover, it was also perceived that humans exposed to the risk for HPAI infection must be identified and monitored, and various preventive measures have been implemented by the authorities for human health. In conclusion, strict management and adequate sterilization for raw poultry meat are required, along with active surveillance, to prevent influenza-like illnesses that could become a public health concern.

About the Author

Dr. Kang is a researcher with the Animal and Plant Quarantine Agency and is also a professor at the College of Veterinary Medicine, Kyungpook National University in South Korea. He primary research interest is the diagnosis, vaccine development, and genetic characterization of avian influenza.

References

1. Kalthoff D, Globig A, Beer M. (Highly pathogenic) avian influenza as a zoonotic agent. Vet Microbiol. 2010;140:237–45. https://doi.org/10.1016/j.vetmic.2009.08.022

2. Verhagen JH, Fouchier RAM, Lewis N. Highly pathogenic avian influenza viruses at the wild-domestic bird interface in Europe: future directions for research and surveillance. Viruses. 2021;13:212. https://doi.org/10.3390/v13020212

3. Gauthier-Clerc M, Lebarbenchon C, Thomas F, Thomas F. Recent expansion of highly pathogenic avian influenza H5N1: a critical review. Ibis. 2007;149:202–14. https://doi.org/10.1111/j.1474-919X.2007.00699.x

4. Yamaji R, Saad MD, Davis CT, Swayne DE, Wang D, Wong FYK, et al. Pandemic potential of highly pathogenic avian influenza clade 2.3.4.4 A(H5) viruses. Rev Med Virol. 2020;30:e2099. https://doi.org/10.1002/rmv.2099

5. de Wit E, Kawaoka Y, de Jong MD, Fouchier RA. Pathogenicity of highly pathogenic avian influenza virus in mammals. Vaccine. 2008;26(Suppl 4):D54–8. https://doi.org/10.1016/j.vaccine.2008.07.072

6. Abolnik C, Phiri T, Peyrot B, de Beer R, Snyman A, Roberts D, et al. The molecular epidemiology of clade 2.3.4.4B H5N1 high pathogenicity avian influenza in Southern Africa, 2021–2022. Viruses. 2023;15: 1383. https://doi.org/10.3390/v15061383

7. Jimenez-Bluhm P, Siegers JY, Tan S, Sharp B, Freiden P, Johow M, et al. Detection and phylogenetic analysis of highly pathogenic A/H5N1 avian influenza clade 2.3.4.4b virus in Chile, 2022. Emerg Microbes Infect. 2023;12:2220569. https://doi.org/10.1080/22221751.2023.2220569

8. Lindh E, Lounela H, Ikonen N, Kantala T, Savolainen-Kopra C, Kauppinen A, et al. Highly pathogenic avian influenza A(H5N1) virus infection on multiple fur farms in the South and Central Ostrobothnia regions of Finland, July 2023. Euro Surveill. 2023;28:2300400. https://doi.org/10.2807/1560-7917.ES.2023.28.31.2300400

9. Adlhoch C, Fusaro A, Gonzales JL, Kuiken T, Mirinavičiūtė G, Niqueux É, et al.; European Food Safety Authority; European Centre for Disease Prevention and Control; European Union Reference Laboratory for Avian Influenza. Avian influenza overview June–September 2023. EFSA J. 2023;21:e08328.

10. Moreno A, Bonfante F, Bortolami A, Cassaniti I, Caruana A, Cottini V, et al. Asymptomatic infection with clade 2.3.4.4b highly pathogenic avian influenza A(H5N1) in carnivore pets, Italy, April 2023. Euro Surveill. 2023;28:2300441. https://doi.org/10.2807/1560-7917.ES.2023.28.35.2300441

11. Rabalski L, Milewska A, Pohlmann A, Gackowska K, Lepionka T, Szczepaniak K, et al. Emergence and potential transmission route of avian influenza A (H5N1) virus in domestic cats in Poland, June 2023. Euro Surveill. 2023;28:2300390. https://doi.org/10.2807/1560-7917. ES.2023.28.31.2300390

12. Domańska-Blicharz K, Świętoń E, Świątalska A, Monne I, Fusaro A, Tarasiuk K, et al. Outbreak of highly pathogenic avian influenza A(H5N1) clade 2.3.4.4b virus in cats, Poland, June to July 2023. Euro Surveill. 2023;28:2300366. https://doi.org/10.2807/1560-7917.ES.2023.28.31.2300366

13. Lee K, Lee EK, Lee H, Heo GB, Lee YN, Jung JY, et al. Highly pathogenic avian influenza A(H5N6) in domestic cats, South Korea. Emerg Infect Dis. 2018;24:2343–7. https://doi.org/10.3201/eid2412.180290

14. Animal and Plant Quarantine Agency. 2014–2016 HPAI epidemiological investigation analysis report. Gimcheon-si (South Korea): The Agency; 2016.

15. Lee K, Yeom M, Vu TTH, Do HQ, Na W, Lee M, et al. Characterization of highly pathogenic avian influenza A (H5N1) viruses isolated from cats in South Korea, 2023. Emerg Microbes Infect. 2024;13:2290835. https://doi.org/10.1080/22221751.2023.2290835

16. Sagong M, Lee YN, Song S, Cha RM, Lee EK, Kang YM, et al. Emergence of clade 2.3.4.4b novel reassortant H5N1 high pathogenicity avian influenza virus in South Korea during late 2021. Transbound Emerg Dis. 2022;69:e3255–60. https://doi.org/10.1111/tbed.14551

17. Heo GB, Kye SJ, Sagong M, Lee EK, Lee KN, Lee YN, et al. Genetic characterization of H9N2 avian influenza virus previously unrecognized in Korea. J Vet Sci. 2021;22:e21. https://doi.org/10.4142/jvs.2021.22.e21

18. Slomka MJ, Coward VJ, Banks J, Löndt BZ, Brown IH, Voermans J, et al. Identification of sensitive and specific avian influenza polymerase chain reaction methods through blind ring trials organized in the European Union. Avian Dis. 2007;51(Suppl):227–34. https://doi.org/10.1637/7674-063006R1.1

19. Lee DH. Complete genome sequencing of influenza A viruses using next-generation sequencing. Methods Mol Biol. 2020;2123:69–79. https://doi.org/10.1007/978-1-0716-0346-8_6

20. Miller MA, Pfeiffer W, Schwartz T. Creating the CIPRES Science Gateway for inference of large phylogenetic trees. In: 2010 Gateway Computing Environments Workshop (GCE); New Orleans, LA; 2010 Nov 14. p. 1–8.

21. Letunic I, Bork P. Interactive Tree Of Life (iTOL) v5: an online tool for phylogenetic tree display and annotation. Nucleic Acids Res. 2021;49(W1):W293–6. https://doi.org/10.1093/nar/gkab301

22. World Health Organization. Manual for the laboratory diagnosis and virological surveillance of influenza. Geneva: The Organization; 2011.

23. Teng KT, McGreevy PD, Toribio JALML, Raubenheimer D, Kendall K, Dhand NK. Associations of body condition score with health conditions related to overweight and obesity in cats. J Small Anim Pract. 2018;59:603–15. https://doi.org/10.1111/jsap.12905

24. Vahlenkamp TW, Harder TC, Giese M, Lin F, Teifke JP, Klopfleisch R, et al. Protection of cats against lethal influenza H5N1 challenge infection. J Gen Virol. 2008;89:968–74. https://doi.org/10.1099/vir.0.83552-0

25. Songserm T, Amonsin A, Jam-on R, Sae-Heng N, Meemak N, Pariyothorn N, et al. Avian influenza H5N1 in naturally infected domestic cat. Emerg Infect Dis. 2006;12:681–3. https://doi.org/10.3201/eid1204.051396

26. Vahlenkamp TW, Teifke JP, Harder TC, Beer M, Mettenleiter TC. Systemic influenza virus H5N1 infection in cats after gastrointestinal exposure. Influenza Other Respir Viruses. 2010;4:379–86. https://doi.org/10.1111/j.1750-2659.2010.00173.x

27. Lipatov AS, Kwon YK, Pantin-Jackwood MJ, Swayne DE. Pathogenesis of H5N1 influenza virus infections in mice a nd ferret models differs according to respiratory tract or
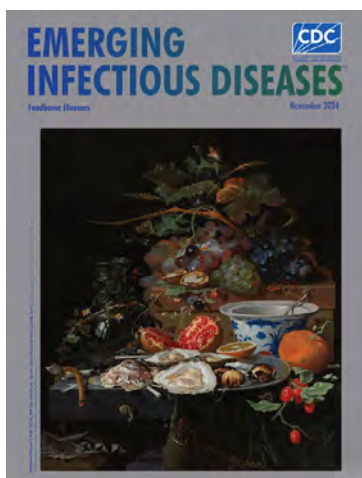
digestive system exposure. J Infect Dis. 2009;199:717–25. https://doi.org/10.1086/596740

28. Alkie TN, Cox S, Embury-Hyatt C, Stevens B, Pople N, Pybus MJ, et al. Characterization of neurotropic HPAI H5N1 viruses with novel genome constellations and mammalian adaptive mutations in free-living mesocarnivores in Canada. Emerg Microbes Infect. 2023;12:2186608. https://doi.org/10.1080/22221751.2023.2186608

29. Gabriel G, Czudai-Matwich V, Klenk HD. Adaptive mutations in the H5N1 polymerase complex. Virus Res. 2013;178:53–62. https://doi.org/10.1016/j.virusres.2013.05.010

30. Kang YM, Heo GB, An SH, Lee YN, Cha RM, Cho HK, et al. Introduction of multiple novel high pathogenicity avian influenza (H5N1) virus of clade 2.3.4.4b into South Korea in 2022. Transbound Emerg Dis. 2023;2023:ID8339427. https://doi.org/10.1155/2023/8339427

31. Kim Y, Fournié G, Métras R, Song D, Donnelly CA, Pfeiffer DU, et al. Lessons for cross-species viral transmission surveillance from highly pathogenic avian influenza Korean cat shelter outbreaks. Nat Commun. 2023;14:6958. https://doi.org/10.1038/s41467-023-42738-w

Address for correspondence: Kwang-Nyeong Lee or Kyunghyun Lee, Avian Influenza Research and Diagnostic Division, Animal and Plant Quarantine Agency, 177, Hyeoksin 8-ro, Gimcheon-si, Gyeongsangbuk-do 39660, South Korea; email: leekwn@korea.kr or mylovehyun@korea.kr

November 2024

Foodborne Illnesses

EMERGING INFECTIOUS DISEASES®

To revisit the November 2024 issue, go to:
https://wwwnc.cdc.gov/eid/articles/issue/30/11/table-of-contents

Human Circovirus in Patients with Hepatitis, Hong Kong

Shusheng Wu,[1] Cyril Chik-Yan Yip,[1] Jianwen Situ,[1] Zhiyu Li, Stanley Siu-Fung Ho,
Jianpiao Cai, Jane Hau-Ching Poon, Nicholas Foo-Siong Chew, Jonathan Daniel Ip,
Tom Wai-Hin Chung, Kelvin Hei-Yeung Chiu, Anna Jinxia Zhang, Estie Hon-Kiu Shun,
James Yiu-Hung Tsoi, Jade Lee-Lee Teng, David Christopher Lung, Kelvin Kai-Wang To
Vincent Chi-Chung Cheng, Irene Oi-Lin Ng, Kwok-Yung Yuen, Siddharth Sridhar

Circovirus human is a new viral species that includes the human circovirus (HCirV), which has been linked to hepatitis in immunocompromised persons. We investigated prevalence of HCirV infection in 278 patients with hepatitis and 184 asymptomatic persons using real-time PCR and sequencing assays. HCirV viremia and sequences were found in 8 (2.9%) hepatitis patients and no asymptomatic patients. Alternate causes of hepatitis (hepatitis E and cholangitis) were clearly identifiable in 2 HCirV-infected patients. HCirV could not be ruled out as a contributor to hepatitis in the remaining 6 patients, 4 of whom were immunocompromised. Persistent infections were documented in 3 patients, but only 1 had relapsing hepatitis. One HCirV patient displayed symptoms of an infectious mononucleosis-like syndrome. Isolates clustered with known HCirV strains from France and China. HCirV-derived virus-like particles bound to PLC/PRF/5 and Hep-G2 human hepatoma cells but not to lung epithelial cells, indicating hepatic tropism.

Hepatitis is a common entity; severity can range from subclinical biochemical transaminitis to acute liver failure. Common etiologies of hepatitis include viral infections, adverse drug reactions, alcohol, autoimmune disorders, metabolic diseases, and biliary pathologies. However, unexplained hepatitis is still frequently encountered in clinical practice. Studies in a variety of practice settings estimate that 11%–35% of acute liver failure cases lack a clear etiology (*1*). This proportion is higher in patients with mild hepatitis, for whom exhaustive laboratory investigations are usually not performed. Therefore, conceivably, some causes of infectious hepatitis remain unknown. A striking example of this possibility was the recent multinational outbreak of pediatric hepatitis for which the best current hypothesis is a co-infection of adeno-associated virus 2 and adenovirus type 41 in children with genetic predispositions (*2*). Another example is rat hepatitis E virus, previously disregarded as a human pathogen but now identified as an endemic hepatitis agent in China and Spain (*3–5*).

Circovirus human is a recently discovered species of the family Circoviridae independently reported in France and China (*6–8*). This species includes human circovirus (HCirV). In China, HCirV was first reported in an intravenous drug user with HIV infection (*6*). A follow-up study identified a second HCirV patient, also an intravenous drug user with HIV and hepatitis C virus (HCV) co-infection (*9*). Sparse clinical details were available for those 2 patients. Around the same time, researchers in France using metagenomic next-generation sequencing identified HCirV infection in a heart–lung transplant recipient with unexplained hepatitis (*7*). HCirV peripheral blood virus loads correlated with derangements in liver function tests (LFTs). Those researchers also demonstrated HCirV mRNA in liver tissue by in situ hybridization indicating virus tropism for hepatocytes (*7*).

In this study, we evaluated the role of HCirV as a cause of viral hepatitis by comparing HCirV infection prevalence in hepatitis cases and asymptomatic controls. We described the clinical profiles and genomic epidemiology of HCirV infection cases. Finally, we

---

[1]These authors contributed equally to this article.

expressed HCirV virus-like particles (VLPs) to probe binding of HCirV to human hepatic cell lines.

Materials and Methods

Study Setting, Patient Specimens, and Animal Samples

This retrospective observational study was conducted at the Queen Mary Hospital (QMH) Department of Microbiology in Hong Kong, China. The study was approved by the Institutional Review Board of the University of Hong Kong, China/Hospital Authority Hong Kong, China West Cluster (UW 23-330). The QMH microbiology laboratory provides viral hepatitis diagnostic services to acute hospitals and transplant services across Hong Kong. We retrieved plasma or serum samples from patients sent to the laboratory for diagnostic evaluation of viral hepatitis (hepatitis cases) during October 1, 2022–November 15, 2023. We assigned patients to the hepatitis cases group if alanine aminotransferase (ALT), aspartate aminotransferase (AST), alkaline phosphatase (ALP), or bilirubin were elevated above respective reference ranges (Appendix Table 1, https://wwwnc.cdc.gov/EID/article/30/12/24-1114-App1.pdf). We excluded persons with isolated elevated ALP if their gamma-glutamyl transpeptidase levels were within reference ranges (indicating extrahepatic source). Similarly, we excluded cases with isolated unconjugated hyper-bilirubinemia. Archived plasma or serum samples from persons with unremarkable LFTs formed a control group; blood samples from those persons were sent to the QMH microbiology laboratory for organ donation evaluation or cytomegalovirus (CMV) reactivation monitoring. We retrieved patient clinical notes, imaging findings, and diagnostic test results from electronic patient records. As described in our previous study (5), we defined patients as immunosuppressed if they met any of the following criteria at time of blood taking: active hematological malignancy, history of solid organ or hematopoietic stem cell transplantation, receiving disease modifying antirheumatic drugs/marrow-suppressive chemotherapy/steroids (>0.5 mg/kg/d prednisolone-equivalent for ≥1 mo), or living with HIV infection with CD4 T-lymphocyte counts <200 cells/mm³.

HCirV PCR screening was conducted by staff blinded to group assignment. Patients were defined as infected with HCirV if they fulfilled both of the following criteria: HCirV PCR positive in serum or plasma with cycle threshold (Ct) <36 and at least a partial HCirV genome fragment sequenced from serum or plasma. The stringent requirement for sequenced isolates eliminated spurious cases of nonspecific PCR positivity because we did not have positive sample controls for PCR reactions at the outset of this study. Clinical records of HCirV-infected persons were assessed for hepatitis at time of blood taking. If hepatitis was present, clinical, imaging, and diagnostic investigation data were independently assessed by 2 experts blinded to study goals to determine the cause of hepatitis.

Real-Time PCR, Sequencing, and Phylogenetic Analysis

The HCirV real-time PCR targets the *rep* gene and was designed based on published genomes of HCirV strains from France (Paris strain) and China (YN09/J030 and YN09/347 strains) (GenBank accession nos. ON677309, ON226770, and OP744467) (Appendix Table 2). We determined performance characteristics including limit-of-detection, linearity, and analytical specificity of the assay as previously described (10,11) and obtained partial HCirV genomes by using Sanger sequencing. If the viral load was sufficiently high by Sanger sequencing, we attempted complete genome sequencing (Appendix Table 3). For phylogenetic analysis, we obtained complete genomes of the 65 exemplar circovirus species as listed by the International Committee on Taxonomy of Viruses as of September 9, 2024, from the National Center for Biotechnology Information (NCBI) GenBank database. We also included an additional 3 complete HCirV genomes (GenBank accession nos. OP744467.1, ON226770.2, and OR905605.1) and those of 4 strains of *Circovirus porcine 3* (PCV3; accession nos. MK095623, MK496297, MH277112, and MK496292). We downloaded 3 complete *Cyclovirus* genomes (accession nos. KT732787, KF031466, GQ404857) for use as an outgroup to root the phylogeny.

We performed multiple sequence alignment of the complete genomes using MAFFT version 7.526 software (–genfapair–maxiterate 1000—adjustdirectionaccurately) (12) and added partial genome sequences to the alignment with MAFFT (–localpair–addfragments–adjustdirectionaccurately) (13). We removed sites with >20% gaps with TrimAl version 1.4.22 (-gt 0.2) (14) and visualized the resulting alignment in JalView (15). We inferred a maximum-likelihood phylogenetic tree using IQ-TREE, using the best-fit substitution model automatically selected by ModelFinder and MixtureFinder (16,17; H. Ren et al., unpub. data, https://www.biorxiv.org/content/10.1101/2024.03.20.586035v2). We assessed branch support using the Shimodaira-Hasegawa–like approximate likelihood ratio test with 10,000 bootstrap replicates. We visualized and annotated the final phylogenetic tree using TreeViewer (18).

HCirV Peptide Expression, Characterization, and Immunoblots

The capsid (Cap) protein encoding the outer capsid of HCirV was expressed in *Escherichia coli*. Proteins were assessed using transmission electron microscopy and sodium dodecyl sulfate polyacrylamide gel electrophoresis (SDS-PAGE). Cap protein was used to raise hyperimmune polyvalent serum samples in mice and IgM/IgG immunoblots of human serum samples as previously described (*19*) (Appendix).

Cell-Binding Assay

We seeded human hepatoma cells (PLC/PRF/5, ATCC CRL-8024; Hep-G2, ATCC CRL-10741) and A549 lung epithelial cells (CCL-185) on glass coverslips in a 24-well plate. When confluence reached 80%, we washed cells with prechilled 1× phosphate-buffered saline (PBS). We incubated Purified Cap protein (10 μg/well) VLPs and control proteins with PLC/PRF/5, Hep-G2, and A549 cells for 1 hour at 4°C. After discarding supernatant, we extensively washed cells with cold PBS 3–4 times to remove unbound VLPs and fixed with 4% paraformaldehyde, then incubated with mouse anti-Cap protein polyvalent immune serum (1:200) diluted in 1% BSA. We used Alexa Fluor 488-conjugated anti-mouse IgG (Thermo Fisher Scientific, https://www.thermofisher.com) as secondary antibody (1:2,000). We counterstained nuclei at AntiFade mounting medium with DAPI (VectorLabs, https://www.vectorlabs.com). We examined slides using a fluorescence microscope and used ImageJ software (https://imagej.net/ij) to measure positive cells.

Testing for Other Causes of Viral Hepatitis

We screened samples positive for HCirV DNA for other viral causes of hepatitis including hepatitis A virus, hepatitis B virus, HCV, hepatitis E virus (HEV), adenovirus, enterovirus, human herpesvirus (HHV) 6, HHV-7, CMV, HIV, and Epstein-Barr virus (EBV) using commercial or in-house–developed serologic and molecular assays (Appendix Table 4). Protocols for molecular assays have been published previously (*10,11,20–23*). We measured Torque teno virus (TTV) DNA using a published protocol (*24*).

Statistical Analysis

We compared proportions of HCirV-positive cases and controls using χ^2 or Fisher exact test, depending on the number of persons. To differentiate cholestatic from hepatocellular liver injury, we calculated the R factor as follows: (ALT value/ALT upper limit of normal) ÷ (ALP value/ALP upper limit of normal). R factor ≤2 corresponds to cholestatic injury, >2 to <5 represents a mixed pattern, and ≥5 corresponds to hepatocellular injury (*25*).

Results

Cases and Controls

We obtained serum or plasma samples from 278 hepatitis patients and 184 controls (Table 1). Immunosuppressed persons were well represented in both groups and accounted for more than half of all controls (Table 1). Degree of hepatitis was typically mild; most patients had anicteric hepatitis. A cause of hepatitis was identified by the clinical team in 123 (44.2%) cases; the remaining 155 (55.8%) were of unspecified etiology. For those with identified etiology, viral hepatitis (18.7%) and drug-induced liver injury (17.9%) were the most commonly diagnosed (Appendix Table 5).

Results of HCirV Screening in Human Samples

The limit-of-detection of the *Rep* gene real-time PCR was 600 copies/mL (Appendix Table 6) with good linearity (Appendix Figure 1). This result was

Table 1. Clinical and demographic characteristics of hepatitis cases and asymptomatic controls in study of human circovirus in patients with hepatitis, Hong Kong

Characteristic	Hepatitis cases, n = 278	Controls, n = 184
Median age, y (IQR)	59 (46–69)	53; 38.8 – 61
Sex		
M	143 (51.4)	96 (52.2)
F	135 (48.6)	88 (47.8)
Immunosuppression	95 (34.2)	117 (63.6)
Hemopoietic stem cell transplant	24	32
Solid organ transplant	43	67
HIV	1	1
Hematological malignancy	14	14
Cancer/chemotherapy	8	0
Other	5	3
Median ALT, U/L (IQR)	126 (66.3–267.3)	NA
Median ALP, U/L (IQR)	142 (97–240)	NA
Median total bilirubin, μmol/L (IQR)	12 (8–30)	NA

*Values are no. (%) except as indicated. ALP, alkaline phosphatase; ALT, alanine aminotransferase; IQR, interquartile range; NA, not applicable because all liver function parameters were below the upper limit of reference ranges (Appendix Table 2, https://wwwnc.cdc.gov/EID/article/30/12/24-1114-App1.pdf).
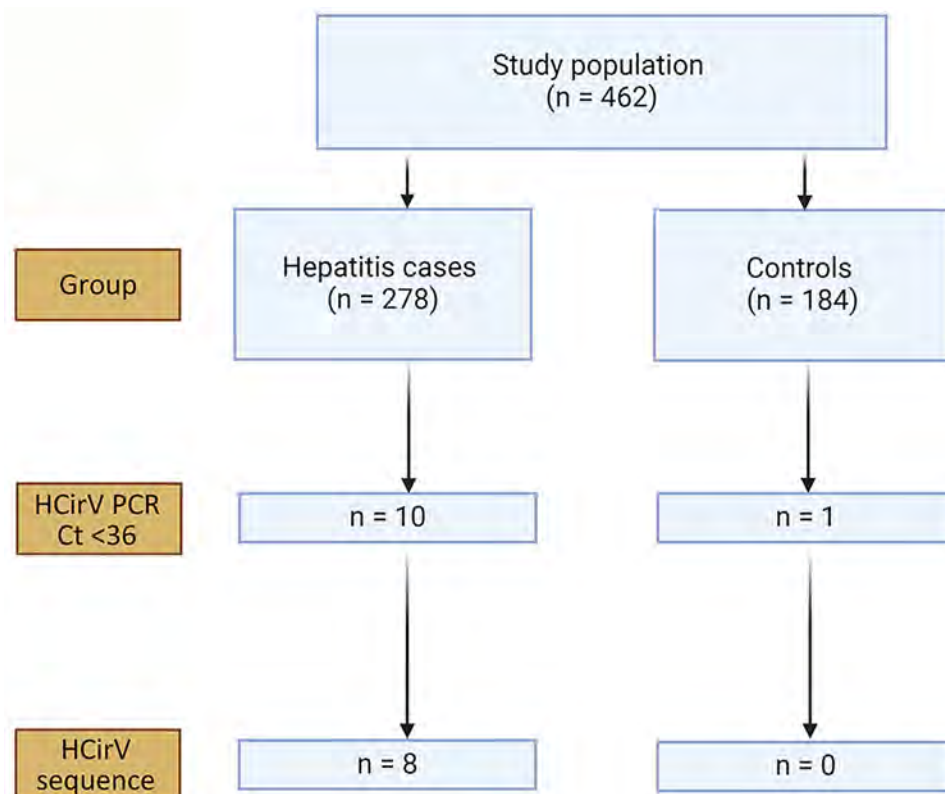
Figure 1. Results of screening in study of human circovirus in patients with hepatitis, Hong Kong. Ct, cycle threshold; HCirV, human circovirus.

comparable to the limit-of-detection in a recent study (26). We screened samples from hepatitis case-patients and from controls for HCirV infection using the *Rep* gene assay, followed by sequencing of positive samples. Of 278 hepatitis patients, 10 (3.6%) tested positive by HCirV PCR, but a sequence could not be obtained from 2 of those. Of the 184 controls, 1 (0.5%) tested positive for HCirV DNA, but a sequence could

not be obtained (Figure 1). The 3 samples that tested positive by PCR without an identifiable sequence had high Ct values at >33. We did not regard those as HCirV infections for the purpose of this study.

HCirV Case Characteristics

The median age of 8 confirmed HCirV-infected persons (PCR-positive with identifiable sequences) was

Table 2. Clinical and demographic characteristics of patients with human circovirus infection, Hong Kong*

Patient no.	1	2	3	4	5	6	7	8
Age	15	59	39	53	67	75	40	42
Sex	M	M	F	F	M	M	M	F
Immunosuppressive condition	Neuroblastoma	None	None	Kidney graft†	Liver graft†	None	None	Liver graft†
Organs / blood products	Y	N	N	Y	Y	N	N	Y
Peak ALT, U/L	672	413	109	96	532	469	401	983
Peak ALP, U/L	2288	139	174	928	601	274	484	168
R factor	0.6	4.7	1.6	0.3	1.4	3.2	1.6	15.2
Peak bilirubin, µmol/L	91	9	23	44	301	28	281	52
Duration of hepatitis	Chronic	Acute	Acute	Acute	Acute, relapse	Acute	Acute	Acute
Outcome	Death	Survived	Death	Survived	Death	Survived	Survived	Survived
Clinician diagnosis	NIC	NIC	NIC	NIC	Chronic rejection	COVID-19	Cholangitis	Anastomotic stricture
Expert 1 diagnosis	Drug-induced hepatitis	NIC	Ischemic hepatitis	Drug-induced cholestasis	NIC	COVID-19	Cholangitis	Rejection
Expert 2 diagnosis	NIC	NIC	NIC	NIC	NIC	Gallstone	Cholangitis	Anastomotic stricture

*ALP, alkaline phosphatase; ALT, alanine aminotransferase; NIC, no identifiable single cause for hepatitis.
†Time from transplantation to hepatitis: patient 4, 1 month; patient 5, 15 years; patient 8, 22 months.
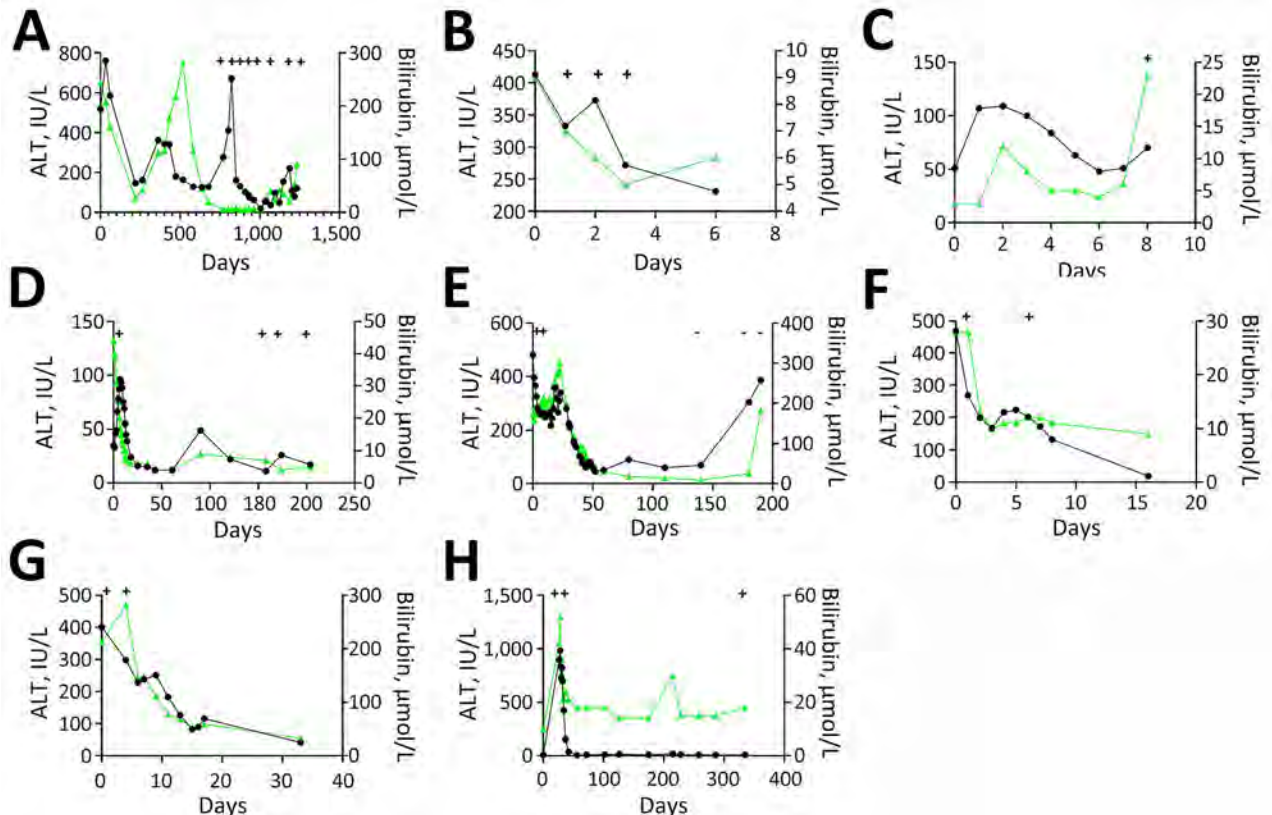
Figure 2. Liver function test kinetics in 8 patients with hepatitis and human circovirus infection, Hong Kong. A) Patient 1; B) patient 2; C) patient 3; D) patient 4; E) patient 5; F) patient 6; G) patient 7; H) patient 8. Black line indicates ALT, and green line indicates bilirubin. Plus signs indicate days when human circovirus DNA was detected in blood, whereas dashes indicate days when human circovirus DNA was not detected in blood. ALT, alanine aminotransferase.

47.5 years; 5 were male and 3 female (Table 2). A total of 4 patients had received an organ graft or blood transfusion within 3 months of hepatitis onset, and 4 persons were immunocompromised. None of the patients were known to be infected with HCV or HIV. R factor indicated cholestatic injury in 5 patients, mixed pattern in 2 persons, and hepatocellular injury in 1 person. Consensus on the cause of hepatitis was only available for 1 patient (patient 7); both experts (who were blinded to study objectives and HCirV screening results) agreed with the clinical team on a diagnosis of cholangitis (Appendix Table 7). Investigations conducted for this study identified HEV viremia in 1 patient (patient 3) who had tested negative for HEV IgM (Appendix Table 7). Consensus on the cause of hepatitis in the other 6 patients was lacking. All but 1 patient had acute hepatitis that resolved within a month. HCirV DNA was detectable in plasma or serum of all patients on >1 day during episodes of hepatitis (except for patient 3, who had only 1 blood sample available for testing) (Figure 2). A total of 3 patients died; cause

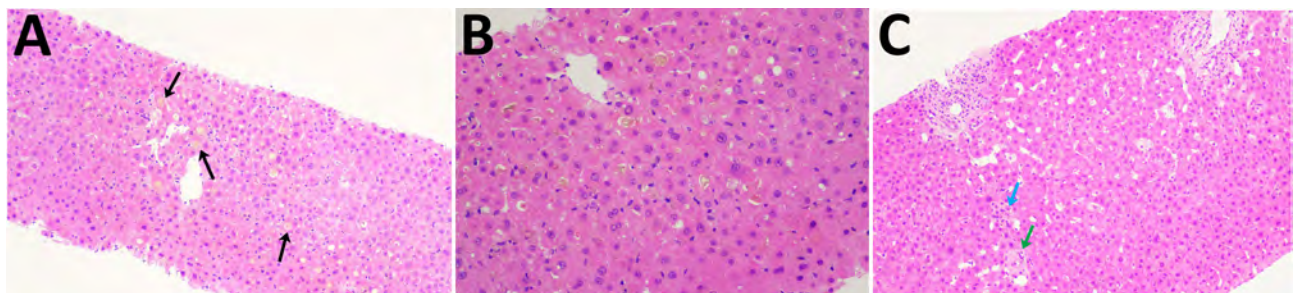**Figure 3.** Hematoxylin and eosin stained liver sections of patients in study of human circovirus in patients with hepatitis, Hong Kong. A, B) Cholestasis with bile pigment in zone 3 canaliculi (arrows) in patient 5 at original magnification ×10 (A) and original magnification ×20 (B). C) Acidophil body (blue arrow) with neutrophils around ducts (green arrow) in patient 8; original magnification ×10.

of death was progression of underlying disease or unexplained cardiac arrest rather than hepatitis.

Of the 4 persons with immunosuppressive conditions, 3 were solid organ transplant recipients and 1 was receiving chemotherapy for neuroblastoma (patient 1). Patient 1 had relapsing hepatitis episodes over 3 years before eventually dying of the underlying disease (Figure 2). HCirV was detected consistently in all plasma samples over a period of 18 months. Virus loads ranged from 5.65×10^3 copies/mL to 1.75×10^6 copies/mL. Patient 4 (kidney graft recipient) and patient 8 (liver graft recipient) also had persistent HCirV viremia over several months despite resolution of the initial hepatitis episode; viremia was highest during hepatitis (10^4–10^5 copies/mL) and declined as LFTs normalized in subsequent months. Archived plasma samples from patient 8 obtained at 1-month and 12-months after transplant tested negative for HCirV DNA, indicating an infection in the second year. Patient 5 (liver graft recipient) had acute hepatitis with transient HCirV DNA detection. Although the hepatitis relapsed around 3 months later, HCirV DNA was no longer detectable in the patient's plasma. The liver histology of patient 5 during the first hepatitis episode was consistent with cholestasis, whereas histology of patient 8 showed neutrophils around biliary ducts and acidophil bodies with no features of acute cellular rejection (Figure 3). Immunohistochemical staining for HCirV capsid protein on a small liver core biopsy from patients 5 and 8 did not show positive signals (Appendix Figure 2).

For some samples with sufficient volume, we also measured concomitant TTV viral load. HCirV was detected in 2 persons with undetectable TTV viremia. In patient 1, who had serial concomitant measures of HCirV and TTV viral loads, viral loads of HCirV tended to fluctuate much less than those of TTV, suggesting that HCirV is not merely an indirect measure of immunosuppression (Appendix Table 8).

The remaining 2 patients (patients 2 and 6) did not have immunosuppressive conditions. Patient 2, a 59-year-old man with good past health, was admitted with fever for 1 week and a maculopapular skin rash. In addition to hepatitis, blood tests revealed a lymphocytosis (3.8×10^9 cells/L) with occasional atypical lymphocytes. Serologic workup for known causes of infectious mononucleosis including EBV, CMV, and HIV yielded negative results (Appendix Table 7). The peripheral blood EBV viral load was detected at <100 IU/mL. Patient 6 was a 75-year-old man admitted for fever. Blood tests showed parenchymal liver dysfunction (Figure 2). Nasopharyngeal swab samples tested positive for SARS-CoV-2 by reverse transcription PCR with a Ct value of 30.4. Chest radiograph did not show lower respiratory tract involvement, and he did not require supplemental oxygen. Ultrasound showed a gallstone but no cholecystitis or cholangitis.

HCirV Genome and Phylogenetic Analysis

Complete HCirV genome was obtained for patient 1 (GenBank accession no. PP968832). Predicted genomic organization of this strain was like other circovirus strains: 2 major open reading frames (ORFs) encoding the *Rep* gene at nucleotide positions (nt) 247–1134 and capsid protein at nt 1368–2012. The *Rep* gene is encoded on the sense strand and the *Cap* gene on the antisense strand. The genome size is 2021 bp, and it is most closely related to the HCirV1 Paris strain (GenBank accession no. ON677309.1), sharing a nucleotide identity of 98.7%. Partial gene sequences were obtained from all the other patients (Appendix Table 9). A phylogenetic tree of complete HCirV genome of patient 1 (HK P1) and partial gene sequences of other isolates showed that strains related to both Paris and Yunnan strains circulate in Hong Kong (Figure 4).

HCirV Immunoassays

HCirV Cap protein was expressed in *E. coli*. This peptide showed a band at 25 kDa on SDS-PAGE (Appendix Figure 3, panel A). The peptides spontaneously assembled into VLPs on transmission electron microscopy (Appendix Figure 3, panel B). Serum samples from 7 HCirV-infected persons were available for antibody immunoassays using HCirV VLP-based immunoblots (Figure 5). All patients were negative on IgM immunoblots. Four patients had discernible bands on IgG immunoblots (patients 1, 4, 7, and 8); of those, 3 patients were immunocompromised. As negative controls, we used 9 HCirV PCR-negative donor samples, as well as a serum pool of 900 healthy donors. None of those samples showed bands in the immunoblot, suggesting reasonable specificity (Appendix Figure 3, panel C).

HCirV Cell-Binding Assay

To further investigate hepatic tropism of HCirV, we tested whether HCirV VLPs could bind to hepatoma cells (PLC/PRF/5). HEV VLPs that are known to bind strongly to PLC/PRF/5 cells served as positive controls. SARS-CoV-2 nucleoprotein served as negative controls. HCirV VLPs were capable of binding to PLC/PRF/5 cells (Figure 6). We found that 27/90 (30%) of cells bound to HCirV VLPs, compared with 30/468 (6.4%) cells that bound to HEV VLPs. We confirmed that HCirV VLPs could bind with Hep-G2, another hepatoma cell line (Appendix Figure 4). Of note, no binding was observed with A549, a lung epithelial cell line (Appendix Figure 4).

Discussion

The association between HCirV and hepatitis requires careful evaluation. Many human DNA viruses have been classified as orphan viruses despite initial discovery in diseased patient cohorts (27–29). Prominent examples include anelloviruses and pegiviruses, which were initially believed to be associated with hepatitis but are now generally considered to be nonpathogenic (30–33).

In this study, we identified HCirV infections in 1.7% of all screened persons using our stringent case
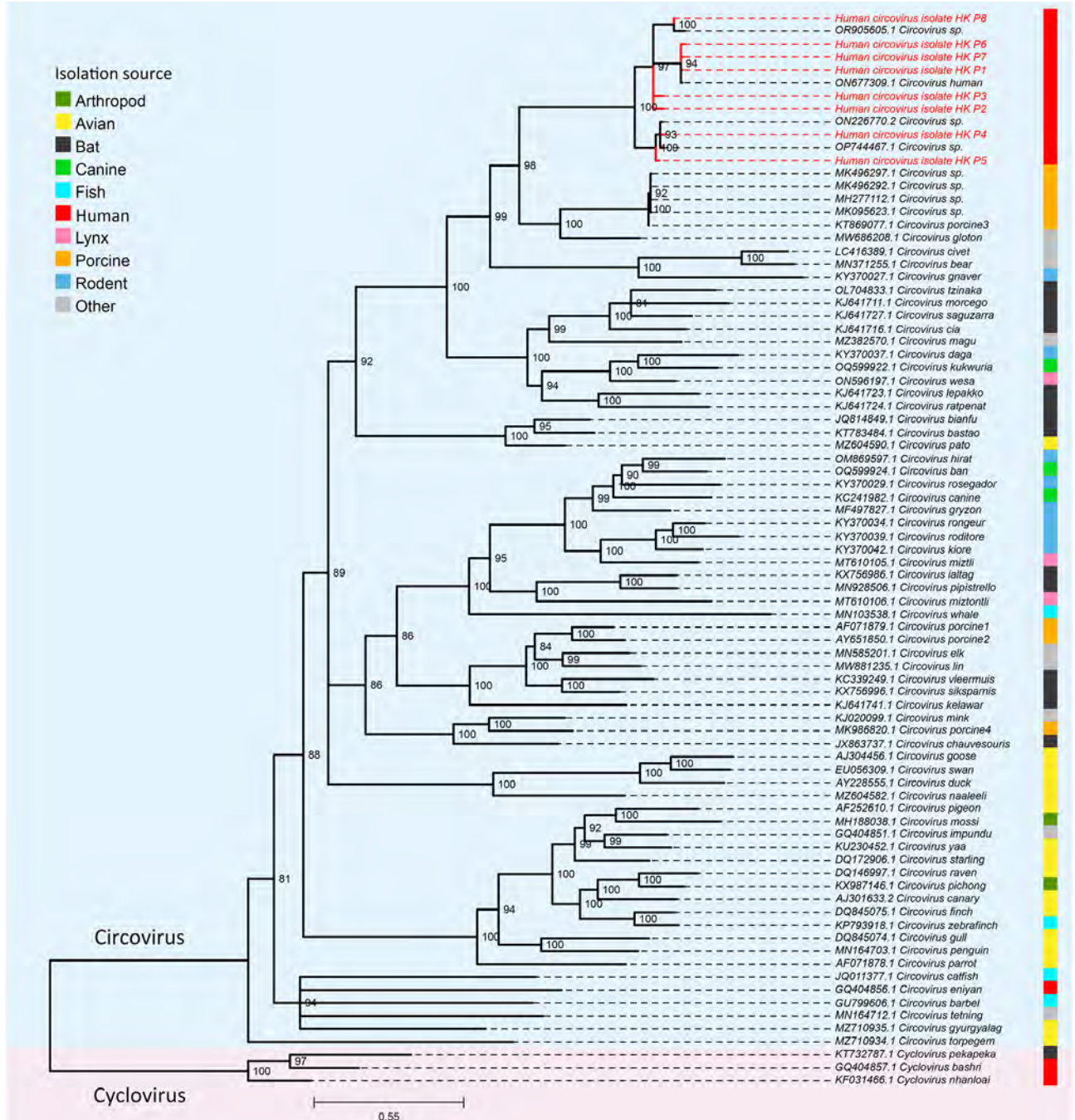
Figure 4. Phylogenetic tree of representative circoviruses and human circoviruses from study of human circovirus in patients with hepatitis, Hong Kong. Maximum-likelihood phylogenetic tree was inferred from a multiple sequence alignment of complete representative *Circovirus* genomes and a mixture of full-length and partial genome sequences from this study (red text) using IQ-TREE (*16*). Three representative species of *Cyclovirus* were used as an outgroup for rooting the tree. Branch supports were assessed using the Shimodaira-Hasegawa–like approximate likelihood ratio test with 10,000 bootstrap replicates. Branches with <80% support were collapsed. Scale bar indicates nucleotide substitutions per site.

definition of PCR positivity with sequenced partial genome. Some persons with high Ct value without identifiable sequences could feasibly have had genuine resolving HCirV infection, in which case the prevalence of HCirV infection in our cohort would be even higher.

Confirming the association between HCirV infection and hepatitis was not straightforward. Alternative explanations for deranged liver function were present in some HCirV patients. However, we could not rule out that HCirV contributed to hepatitis in other cases because of lack of alternate diagnoses, suggestive liver histology, and negative workup for other causes of hepatitis. The case of patient 2, who had an infectious mononucleosis-like syndrome, was particularly striking because of the presence of clinical manifestations that were compatible with acute viral illness. Most infectious mononucleosis-like syndromes are caused by primary/acute EBV, CMV, HIV, and human herpesvirus 6 infections. However, case reports of infectious mononucleosis-like symptoms during noncanonical viral infections such as mpox, parvovirus B19, and human metapneumovirus are also described (34–36). Therefore, we believe that the infectious mononucleosis-like
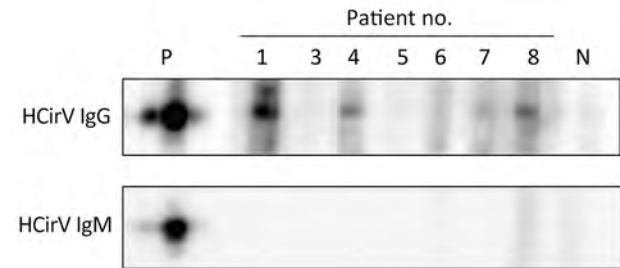
Figure 5. IgM and IgG immunoblots of 7 patients for whom sufficient serum was available from study of HCirV in patients with hepatitis, Hong Kong. P indicates positive control, mouse polyclonal serum raised against HCirV cap protein. N indicates HCirV PCR-negative human donor sample. HCirV, human circovirus.

syndrome in patient 2 was attributable to HCirV. Such clinical manifestations might represent distinctive host responses in a minority of infected patients. We described cholestasis and neutrophil infiltrates in liver tissue of our HCirV-infected patients, which was distinct from the hepatitis with mixed inflammatory infiltrates described by Pérot et al. (7) and Hamelin et al. (37) in HCirV-infected patients. Those results might represent distinct histopathological findings caused by this virus.

Figure 6. Cell-binding assay showing binding of HCirV VLPs to PLC/PRF/5 cells in study of HCirV in patients with hepatitis. HEV VLPs (bHEV p239) is included as a positive control; SARS-CoV-2 NP protein is included as a negative control. Nuclei are counterstained with DAPI. Cap, capsid; HCirV, human circovirus; HEV, hepatitis E virus; NP, nucleoprotein; VLP, virus-like particle.

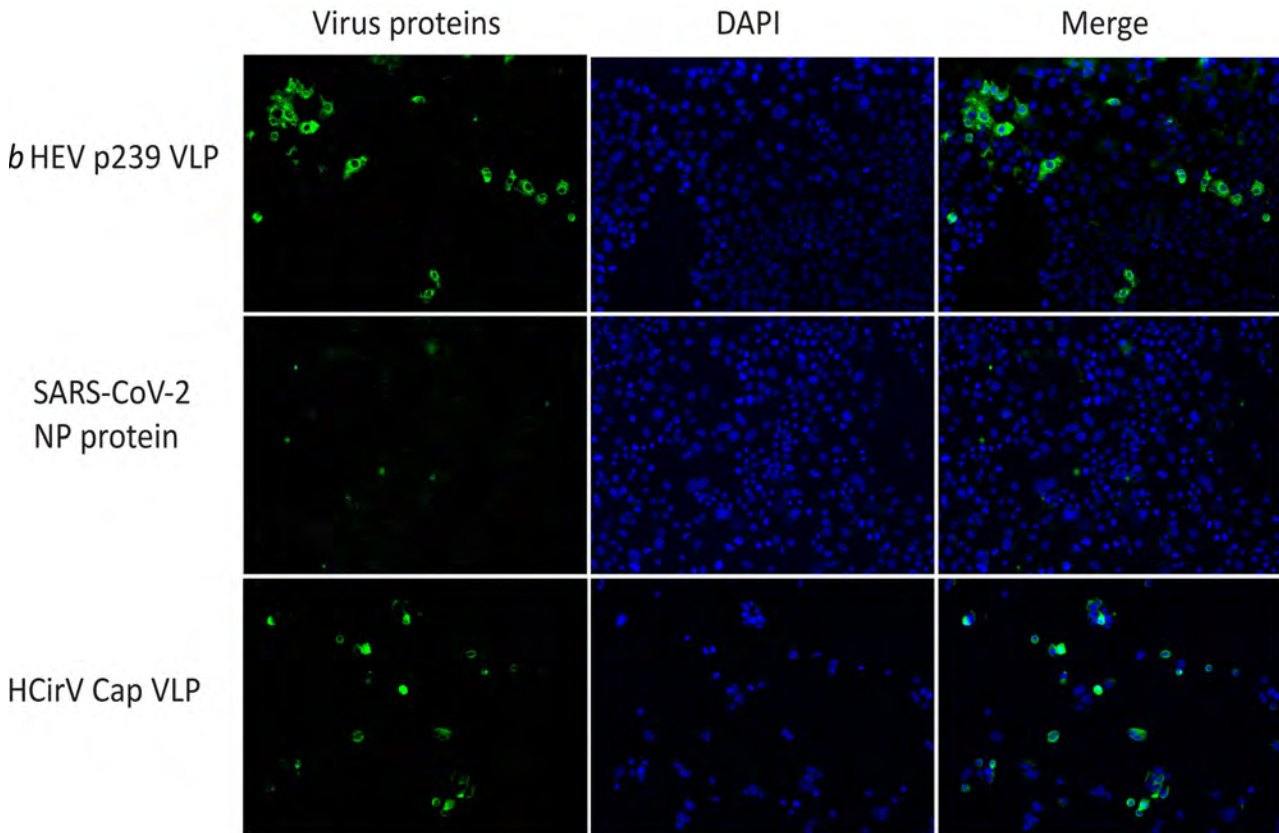On the basis of the pathobiology of other circoviruses, HCirV human infections could run the gamut from silent infection to well-defined clinical syndromes with complex virus-host interactions determining clinical phenotype (38). Detailed surveillance and case descriptions will be required to elucidate the clinical spectrum of this virus. We demonstrate here that HCirV VLPs can bind to liver cells. Tropism for immune cells (like PCV3) could lead to complex virus–host interplay and cytokine dysregulation leading to liver dysfunction (39). The role of co-infections and other inflammatory stimuli in HCirV reactivation cannot be excluded. Of the patients reported in this study, 2 had HEV and COVID-19 concomitantly.

In this study, we confirm that HCirV can cause persistent infection. Of note, LFTs can normalize despite ongoing viremia. Because half the HCirV patients identified in this study were immunocompromised, we speculate that HCirV might establish latency and reactivate during immunosuppression. Another possibility is that those patients acquired HCirV through contaminated blood or organ grafts. We were unable to access blood and organ donor data to evaluate this possibility. Furthermore, a large international study involving >200,000 plasma donations did not find evidence of HCirV contamination (26). However, on the basis of the relatively higher HCirV detection rate in our study, we cannot rule out that prevalence might be higher in our locality. We speculate whether HCirV might be a previously unidentified porcine circovirus capable of zoonotic transmission. PCV3 has been shown to be transmissible to nonhuman primates through xenotransplantation (40).

The first limitation of our study was that we were not able to identify sequences in 3 HCirV PCR-positive samples. Those cases might have been genuine infection cases at early convalescence. The use of rolling circle amplification using a phi29 DNA polymerase would have helped us resolve some of these cases. Other limitations of our study include its retrospective nature; we could not track kinetics of infection in most cases because samples were not available. Liver biopsy was also not available for most cases because of the mild nature of hepatitis. Only small core biopsies of tissue were available from patients 5 and 8, which could explain negative immunohistochemical staining. In situ hybridization would have been a more sensitive approach.

Although not definitive, we believe our findings support further investigation of HCirV as a cause of hepatitis in a proportion of infected human hosts.

Larger case–control studies, liver tissue analysis, and infectious disease models are required to investigate this association further. Clinicians should be aware of this new evidence that HCirV could be a cause of hepatitis in some infected individuals.

About the Author

Mr. Wu is a master of philosophy student at the University of Hong Kong, China. His primary research interest is investigating emerging agents of viral hepatitis from a clinical-translational perspective.

References

1. Bernal W, Auzinger G, Dhawan A, Wendon J. Acute liver failure. Lancet. 2010;376:190–201. https://doi.org/10.1016/S0140-6736(10)60274-7
2. Ho A, Orton R, Tayler R, Asamaphan P, Herder V, Davis C, et al.; DIAMONDS Consortium; ISARIC4C Investigators. Adeno-associated virus 2 infection in children with non-A–E hepatitis. Nature. 2023;617:555–63. https://doi.org/10.1038/s41586-023-05948-2
3. Sridhar S, Yip CCY, Wu S, Cai J, Zhang AJ, Leung KH, et al. Rat hepatitis E virus as cause of persistent hepatitis after liver transplant. Emerg Infect Dis. 2018;24:2241–50. https://doi.org/10.3201/eid2412.180937
4. Rivero-Juarez A, Frias M, Perez AB, Pineda JA, Reina G, Fuentes-Lopez A, et al.; HEPAVIR and GEHEP-014 Study Groups. Orthohepevirus C infection as an emerging cause of acute hepatitis in Spain: first report in Europe. J Hepatol. 2022;77:326–31. https://doi.org/10.1016/j.jhep.2022.01.028
5. Sridhar S, Yip CCY, Lo KHY, Wu S, Situ J, Chew NFS, et al. Hepatitis E virus species C infection in humans, Hong Kong. Clin Infect Dis. 2022;75:288–96. https://doi.org/10.1093/cid/ciab919
6. Li Y, Cao L, Ye M, Xu R, Chen X, Ma Y, et al. Plasma virome reveals blooms and transmission of anellovirus in intravenous drug users with HIV-1, HCV, and/or HBV infections. Microbiol Spectr. 2022;10:e0144722. https://doi.org/10.1128/spectrum.01447-22
7. Pérot P, Fourgeaud J, Rouzaud C, Regnault B, Da Rocha N, Fontaine H, et al. Circovirus hepatitis infection in heart-lung transplant patient, France. Emerg Infect Dis. 2023;29:286–93. https://doi.org/10.3201/eid2902.221468
8. Varsani A, Harrach B, Roumagnac P, Benkő M, Breitbart M, Delwart E, et al. 2024 taxonomy update for the family Circoviridae. Arch Virol. 2024;169:176. https://doi.org/10.1007/s00705-024-06107-2
9. Li Y, Zhang P, Ye M, Tian RR, Li N, Cao L, et al. Novel circovirus in blood from intravenous drug users, Yunnan, China. Emerg Infect Dis. 2023;29:1015–9. https://doi.org/10.3201/eid2905.221617

10. Wong SSY, Yip CCY, Sridhar S, Leung KH, Cheng AKW, Fung AMY, et al. Comparative evaluation of a laboratory-developed real-time PCR assay and RealStar Adenovirus PCR Kit for quantitative detection of human adenovirus. Virol J. 2018;15:149. https://doi.org/10.1186/s12985-018-1059-7

11. Yip CCY, Sridhar S, Cheng AKW, Fung AMY, Cheng VCC, Chan KH, et al. Comparative evaluation of a laboratory developed real-time PCR assay and the RealStar HHV-6 PCR Kit for quantitative detection of human herpesvirus 6. J Virol Methods. 2017;246:112–6. https://doi.org/10.1016/j.jviromet.2017.05.001

12. Katoh K, Standley DM. MAFFT multiple sequence alignment software version 7: improvements in performance and usability. Mol Biol Evol. 2013;30:772–80. https://doi.org/10.1093/molbev/mst010

13. Katoh K, Frith MC. Adding unaligned sequences into an existing alignment using MAFFT and LAST. Bioinformatics. 2012;28:3144–6. https://doi.org/10.1093/bioinformatics/bts578

14. Capella-Gutiérrez S, Silla-Martínez JM, Gabaldón T. trimAl: a tool for automated alignment trimming in large-scale phylogenetic analyses. Bioinformatics. 2009;25:1972–3. https://doi.org/10.1093/bioinformatics/btp348

15. Waterhouse AM, Procter JB, Martin DMA, Clamp M, Barton GJ. Jalview Version 2—a multiple sequence alignment editor and analysis workbench. Bioinformatics. 2009;25:1189–91. https://doi.org/10.1093/bioinformatics/btp033

16. Minh BQ, Schmidt HA, Chernomor O, Schrempf D, Woodhams MD, von Haeseler A, et al. IQ-TREE 2: new models and efficient methods for phylogenetic inference in the genomic era. Mol Biol Evol. 2020;37:1530–4. https://doi.org/10.1093/molbev/msaa015

17. Kalyaanamoorthy S, Minh BQ, Wong TKF, von Haeseler A, Jermiin LS. ModelFinder: fast model selection for accurate phylogenetic estimates. Nat Methods. 2017;14:587–9.

18. Bianchini G, Sánchez-Baracaldo P. TreeViewer: flexible, modular software to visualise and manipulate phylogenetic trees. Ecol Evol. 2024;14:e10873. https://doi.org/10.1002/ece3.10873

19. Sridhar S, Situ J, Cai JP, Yip CC, Wu S, Zhang AJ, et al. Multimodal investigation of rat hepatitis E virus antigenicity: implications for infection, diagnostics, and vaccine efficacy. J Hepatol. 2021;74:1315–24. https://doi.org/10.1016/j.jhep.2020.12.028

20. Sridhar S, Yip CC, Wu S, Chew NF, Leung KH, Chan JF, et al. Transmission of rat hepatitis E virus infection to humans in Hong Kong: a clinical and epidemiological analysis. Hepatology. 2021;73:10–22. https://doi.org/10.1002/hep.31138

21. Yip CCY, Sridhar S, Leung KH, Cheng AKW, Chan KH, Chan JFW, et al. Evaluation of RealStar *Alpha* Herpesvirus PCR Kit for detection of HSV-1, HSV-2, and VZV in clinical specimens. BioMed Res Int. 2019;2019:5715180. https://doi.org/10.1155/2019/5715180

22. Sridhar S, Chung TWH, Chan JFW, Cheng VCC, Lau SKP, Yuen KY, et al. Emergence of cytomegalovirus mononucleosis syndrome among young adults in Hong Kong linked to falling seroprevalence: results of a 14-year seroepidemiological study. Open Forum Infect Dis. 2018;5:ofy262. https://doi.org/10.1093/ofid/ofy262

23. Smith C, Tsang J, Beagley L, Chua D, Lee V, Li V, et al. Effective treatment of metastatic forms of Epstein-Barr virus–associated nasopharyngeal carcinoma with a novel adenovirus-based adoptive immunotherapy. Cancer Res. 2012;72:1116–25. https://doi.org/10.1158/0008-5472.CAN-11-3399

24. Maggi F, Pifferi M, Fornai C, Andreoli E, Tempestini E, Vatteroni M, et al. TT virus in the nasal secretions of children with acute respiratory diseases: relations to viremia and disease severity. J Virol. 2003;77:2418–25. https://doi.org/10.1128/JVI.77.4.2418-2425.2003

25. Kwo PY, Cohen SM, Lim JK. ACG clinical guideline: evaluation of abnormal liver chemistries. Am J Gastroenterol. 2017;112:18–35. https://doi.org/10.1038/ajg.2016.517

26. Pérot P, Da Rocha N, Farcet MR, Kreil TR, Eloit M. Human circovirus is not detected in plasma pools for fractionation. Transfusion. 2024;64:16–8. https://doi.org/10.1111/trf.17604

27. Sridhar S, To KK, Chan JF, Lau SK, Woo PC, Yuen KY. A systematic approach to novel virus discovery in emerging infectious disease outbreaks. J Mol Diagn. 2015;17:230–41. https://doi.org/10.1016/j.jmoldx.2014.12.002

28. Smits SL, Zijlstra EE, van Hellemond JJ, Schapendonk CM, Bodewes R, Schürch AC, et al. Novel cyclovirus in human cerebrospinal fluid, Malawi, 2010–2011. Emerg Infect Dis. 2013;19:1511–3. https://doi.org/10.3201/eid1909.130404

29. Lim ES, Reyes A, Antonio M, Saha D, Ikumapayi UN, Adeyemi M, et al. Discovery of STL polyomavirus, a polyomavirus of ancestral recombinant origin that encodes a unique T antigen by alternative splicing. Virology. 2013;436:295–303. https://doi.org/10.1016/j.virol.2012.12.005

30. Deinhardt F, Holmes AW, Capps RB, Popper H. Studies on the transmission of human viral hepatitis to marmoset monkeys. I. Transmission of disease, serial passages, and description of liver lesions. J Exp Med. 1967;125:673–88. https://doi.org/10.1084/jem.125.4.673

31. Nishizawa T, Okamoto H, Konishi K, Yoshizawa H, Miyakawa Y, Mayumi M. A novel DNA virus (TTV) associated with elevated transaminase levels in posttransfusion hepatitis of unknown etiology. Biochem Biophys Res Commun. 1997;241:92–7. https://doi.org/10.1006/bbrc.1997.7765

32. Sridhar S, Yip CCY, Chew NFS, Wu S, Leung KH, Chan JFW, et al. Epidemiological and clinical characteristics of human hepegivirus 1 infection in patients with hepatitis C. Open Forum Infect Dis. 2019;6:ofz329. https://doi.org/10.1093/ofid/ofz329

33. Berg MG, Lee D, Coller K, Frankel M, Aronsohn A, Cheng K, et al. Discovery of a novel human pegivirus in blood associated with hepatitis C virus co-infection. PLoS Pathog. 2015;11:e1005325. https://doi.org/10.1371/journal.ppat.1005325

34. Li IW, To KK, Tang BS, Chan KH, Hui CK, Cheng VC, et al. Human metapneumovirus infection in an immunocompetent adult presenting as mononucleosis-like illness. J Infect. 2008;56:389–92. https://doi.org/10.1016/j.jinf.2008.03.005

35. Chiu KH, Wong SC, Tam AR, Sridhar S, Yip CC, Chan KH, et al. The first case of monkeypox in Hong Kong presenting as infectious mononucleosis-like syndrome. Emerg Microbes Infect. 2023;12:2146910. https://doi.org/10.1080/22221751.2022.2146910

36. Muñoz-Gómez S, Cunha BA. Parvovirus B19 mimicking Epstein-Barr virus infectious mononucleosis in an adult. Am J Med. 2013;126:e7–8. https://doi.org/10.1016/j.amjmed.2012.12.010

37. Hamelin B, Pérot P, Pichler I, Haslbauer J, Hardy D, Hing D, et al. Circovirus hepatitis in immunocompromised patient, Switzerland. Emer Infect Dis. 2024;30:2140–4.

38. da Silva RR, da Silva DF, da Silva VH, de Castro AMMG. Porcine circovirus 3: a new challenge to explore. Front Vet Sci. 2024;10:1266499. https://doi.org/10.3389/fvets.2023.1266499

39. Chen D, Zhang L, Xu S. Pathogenicity and immune modulation of porcine circovirus 3. Front Vet Sci. 2023; 10:1280177. https://doi.org/10.3389/fvets.2023.1280177

40. Krüger L, Längin M, Reichart B, Fiebig U, Kristiansen Y, Prinz C, et al. Transmission of porcine circovirus 3 (PCV3) by xenotransplantation of pig hearts into baboons. Viruses. 2019;11:650. https://doi.org/10.3390/v11070650

Address for correspondence: Siddharth Sridhar, Department of Microbiology, School of Clinical Medicine, Li Ka Shing Faculty of Medicine, The University of Hong Kong 19-026, Block T, 102 Pokfulam Rd, Hong Kong, China; email: sid8998@hku.hk

—— November 2024 ——

Foodborne Illnesses

EMERGING INFECTIOUS DISEASES®

Rio Mamore Hantavirus Endemicity, Peruvian Amazon, 2020

Marta Piche-Ovares, Maria Paquita García, Andres Moreira-Soto,
Maribel Dana Figueroa-Romero, Nancy Susy Merino-Sarmiento,
Adolfo Ismael Marcelo-Ñique, Edward Málaga-Trillo, Dora Esther Valencia Manosalva,
Miladi Gatty-Nogueira, César Augusto Cabezas Sanchez, Jan Felix Drexler

To explore hantavirus infection patterns in Latin America, we conducted molecular and serologic hantavirus investigations among 3,400 febrile patients from Peru during 2020–2021. Reverse transcription PCR indicated that a patient from Loreto, in the Peruvian Amazon, was positive for Rio Mamore hantavirus (serum, 3.8×10^3 copies/mL). High genomic sequence identity of 87.0%–94.8% and phylogenetic common ancestry with a rodent-associated Rio Mamore hantavirus from Loreto in 1996 indicated endemicity. In 832 samples from Loreto, hantavirus incidence based on IgM ELISA of pooled Sin Nombre (SNV) and Andes virus (ANDV) nucleoproteins and immunofluorescence assay–based end-point titration using SNV/ANDV/Hantaan/Puumala/Saarema/Dobrava/Seoul hantaviruses was 0.5%. Across 3 ecologically distinct departments in Peru, SNV/ANDV IgG ELISA/IFA–based reactivity was 1.7%, suggesting circulation of antigenically distinct New World hantaviruses. Testing for arboviruses, nonendemic pathogens, and antigen-free ELISA corroborated nonspecific reactivity in 2 IgG and several IgM ELISA–positive serum samples. Hantavirus diagnostics and surveillance should be strengthened in Peru and across Latin America..

Acute febrile illness (AFI) is a substantial public health problem in Latin America, exemplified by the almost US $3 billion expended annually for dengue outbreaks (*1*). The main cause of AFI in Latin America is dengue virus (DENV), followed by chikungunya virus, Zika virus, and *Plasmodium* spp. infections (*2*). However, ≈51% of AFI cases remain undiagnosed (*2*). The main reasons for the lack of elucidation of AFI etiology include similar clinical signs/symptoms and lack of robust and accessible diagnostic tools (*3*).

Hantavirus infections in the Americas can cause AFI and severe disease, termed hantavirus pulmonary syndrome (*4*). In South America, at least 12 human pathogenic hantaviruses cause hantavirus pulmonary syndrome, including Andes virus (ANDV), Laguna Negra virus (*5*), and Río Mamore virus (RIOMV). RIOMV has been documented from a single patient in Brazil in 2011, including only partial RIOMV genomic sequence characterization (*6*). RIOMV belongs to the species *Orthohantavirus mamorense,* which also encompasses Maripa and Laguna Negra viruses (family Hantaviridae, subfamily Mammantavirinae, genus *Orthohantavirus*). Human hantavirus infections are rodent-associated zoonoses (*7*). RIOMV in Peru was first described in 1996, isolated from a small-eared rice rat (*Oligoryzomys microtis*) from the department of Loreto in the Peruvian Amazon (*8*).

Hantavirus infection is infrequently diagnosed in humans because lack of testing and short viremia duration hinder direct detection (*7*). During 2011–2013, the Peruvian National Institute of Health (Instituto Nacional de Salud; INS) reported 6 human cases of hantavirus infection, all from Loreto (*7*). Through PCR-based detection and Sanger sequencing, 2 cases were determined by INS to be caused by the ubiquitous rat-associated Seoul virus and 2 by RIOMV;

Author affiliations: Charité-Universitätsmedizin Berlin, Berlin, Germany (M. Piche-Ovares, A. Moreira-Soto, J.F. Drexler); Instituto Nacional de Salud, Lima, Peru (M. Paquita García, M.D. Figueroa-Romero, N.S. Merino-Sarmiento, A.I. Marcelo-Ñique, C.A. Cabezas Sanchez); Universidad Nacional, Heredia, Costa Rica (A. Moreira-Soto); Universidad Peruana Cayetano, Lima (E. Málaga-Trillo); Laboratorio de Referencia Regional de Salud Pública, Lambayeque, Peru (D.E. Valencia Manosalva); Laboratorio de Referencia Regional de Salud Pública, Loreto, Peru (M. Gatty-Nogueira); German Centre for Infection Research, Berlin, Germany (J.F. Drexler)

for 2 cases, the hantavirus could not be identified (*7*). However, the lack of viral genomic sequences in public databases and patient samples hinders confirmation of etiology. To learn more about the epidemiology, distribution, and risk factors of infection with RIOMV and other hantaviruses in Peru, we conducted a hantavirus-specific serologic and molecular investigation among persons with AFI who underwent medical investigation in Peru during 2020.

Material and Methods

Molecular Analyses

We extracted nucleic acids from samples collected during routine AFI surveillance in Peru by using the MagNA Pure 96 DNA and Viral NA Small Volume Kit (Roche, https://www.roche.com). To elucidate potential co-infections, we tested all samples by nested reverse transcription PCR (RT-PCR) for hantavirus RNA and samples from Loreto by quantitative RT-PCR (qRT-PCR) for DENV (*9,10*). We conducted library preparation by using the KAPA RNA HyperPrep Kit (Roche), followed by enrichment via in-solution hybridization capture (Arbor Biosciences, https://arborbiosci.com) as previously described for hantavirus genomic sequencing (*11*). We sequenced the captured library by using an Illumina Miniseq High-Output Reagent Kit 150 cycles paired, and mapped reads against the RIOMV strain HTN-007 by using Geneious 2023.2.1 (https://www.geneious.com) and deposited sequence data in the European Nucleotide Archive (https://www.ebi.ac.uk; accession no. ERR11860590). We attempted to close sequence gaps by using PCR with specific bridging primers (Appendix 1 Table 1, https://wwwnc.cdc.gov/EID/article/30/12/24-0249-App1.pdf) and quantified the viral load by using a set of specific oligonucleotides (Appendix 1 Table 2).

Phylogenetic Analyses

We conducted nucleotide alignments by using MAFFT with an L-INS-I algorithm (https://mafft.cbrc.jp) using Geneious 2023.2.1. We conducted Bayesian phylogenies by using MrBayes 3.2.6 (*12*) with a general time-reversible substitution model with gamma distribution and a complete deletion of all positions containing gaps in the alignment. We retrieved hantavirus reference sequences from GenBank for phylogenetic analysis (Appendix 1 Table 3). We conducted sequence identity plots of partial genomic sequences by using SSE 1.4 (*13*) with a fragment length of 200 and an increment between fragments of 50 nt. We constructed neighbor-joining trees of partial hantaviral genomic sequences in GenBank using 1,000 bootstrap replicates and the pairwise deletion option in MEGA X (*14*) (Appendix 1 Table 4). We determined translated amino acid sequence distances in MEGA X by using a pairwise deletion option (*14*).

Serologic Analyses

We tested serum samples by IgM/IgG ELISA by using a pool of recombinant nucleoproteins from ANDV and Sin Nombre virus (SNV) licensed for diagnostic use in Peru (EUROIMMUN, https://www.euroimmun.com) (Appendix 1). To provide additional validation for the IgM/IgG ELISA-positive samples, we conducted an end-point antibody titration by using an indirect immunofluorescence assay (IFA), as previously reported for hantavirus serologic investigations (*15,16*). For IFA, we tested serum samples at 1:10–1:10,000 dilutions in 10-fold dilution steps. A few samples still yielded weak reactivity at 1:10,000, so we also tested those at 1:12,500. IFA was based on cells infected with ANDV, SNV, Seoul virus, Hantaan virus, Puumala (PUUV), Dobrava (DOBV), and Saaremaa hantaviruses (EUROIMMUN). For IgM-based IFA and ELISA, we pretreated serum samples with the immunoadsorbent Eurosorb (EUROIMMUN) to deplete class IgM rheumatoid factors potentially present in the sample that might react with specifically bound IgG, causing false-positive results and in parallel depleting specific IgG, displacing IgM from the antigen causing false-negative results. IgM and IgG detection relies on specific secondary fluorescein-coupled antibodies for IFA or horseradish peroxidase–coupled antibodies for ELISA.

To test for potential causes of unspecific reactivity in ELISA, we used PCR for pathogens commonly eliciting polyclonal B cell stimulation, including *Plasmodium* spp. (*17*), Epstein-Barr virus (EBV) (*18*), and cytomegalovirus (CMV) (*19*) (TIB Molbiol, https://www.tib-molbiol.de). To assess potentially unspecific reactivity, we used IgM/IgG ELISAs for endemic arboviruses in serum from hantavirus-seropositive patients and controls, including Oropouche virus (OROV) (*20*), Mayaro virus, chikungunya virus (*21*), and nonendemic arbovirus Crimean-Congo hemorrhagic fever virus (CCHFV), and we used IgG ELISAs only for *Plasmodium* spp. (*22,23*), SARS-CoV-2 (nucleoprotein antigen-based) (*24*), and the nonendemic pathogen Middle East respiratory syndrome coronavirus (S1-based; IgM is not commonly tested for respiratory human coronaviruses) (all ELISAs from EUROIMMUN).
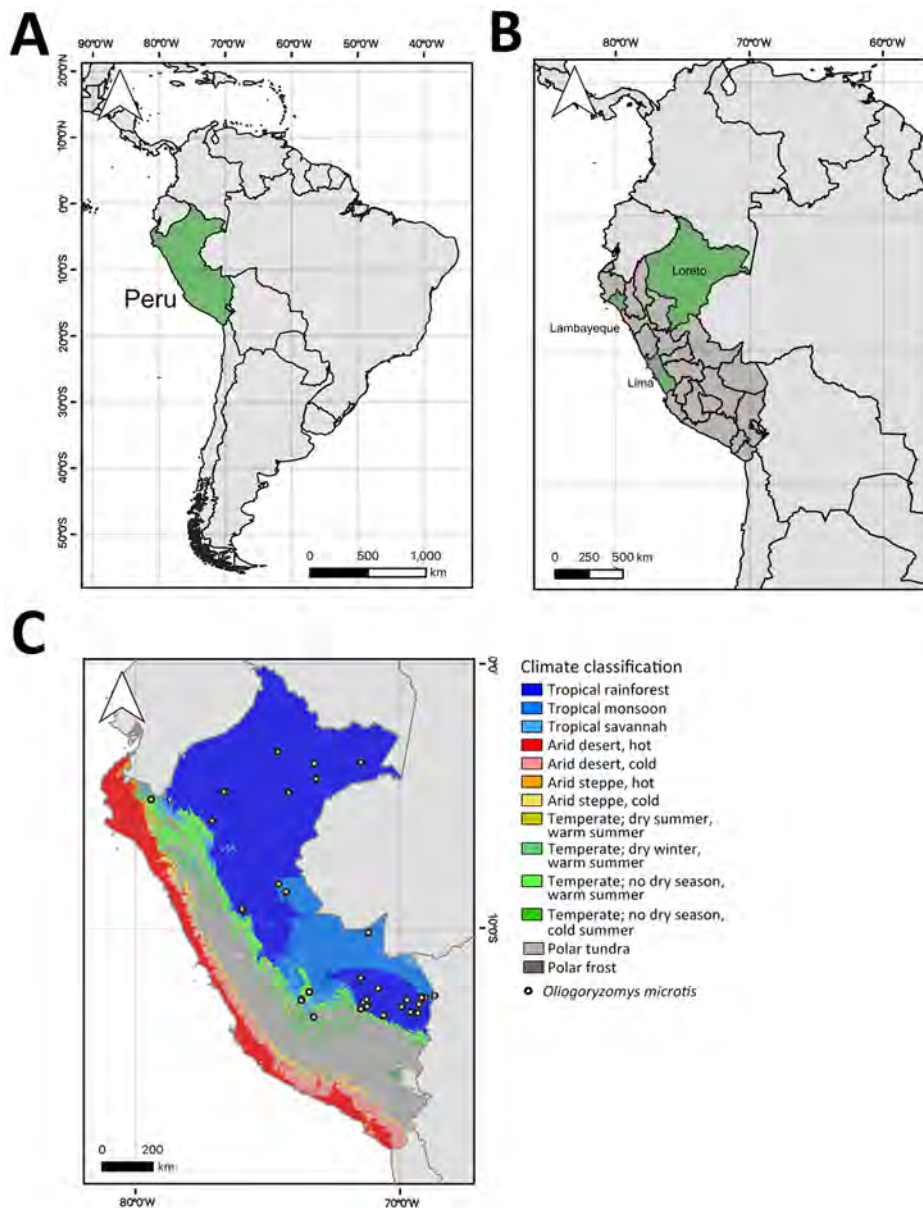
Figure 1. Locations and climate classifications related to study of Rio Mamore hantavirus endemicity in the Peruvian Amazon, 2020. A) Location of Peru (green) in South America. B) Regions in Peru where 3,400 serum samples from febrile patients were collected and stored during a dengue outbreak that overlapped with COVID-19 (*24*) in 3 diverse ecoregions: Loreto (Amazon; n = 1,972 samples), Lambayeque (coastal desert /dry forest; n = 743 samples), and Lima (coastal desert; n = 685 samples) (One Earth, https://www.oneearth.org). C) Climate classification regions of Peru and distribution of *Oligoryzomys microtis* small-eared rice rats (white dots) (https://www.gbif.org) (*26*). All maps were created by using QGIS 3.28.10 (https://hub.arcgis.com) based on freely available maps from Bucknell University.

To exclude a nonspecific reaction to components of the ELISA other than viral antigens, we tested all hantavirus IgM/IgG ELISA–positive samples on non–antigen-coated ELISA plates acquired from the manufacturer, following the same ELISA protocols. We compared serologic reactivity in hantavirus IgM/IgG ELISA-positive serum samples with 38 hantavirus IgM-negative and 38 IgG-negative samples from the same areas and time for which sufficient volumes were available, while ensuring comparable age distribution (hantavirus IgM-negative serum samples, mean patient age 20 years, SD 21.13; hantavirus IgM-positive serum samples, mean patient age 22 years, SD 22.58; *t*-test, *t* = 0.29, p = 0.77; hantavirus IgG-negative serum samples, mean patient age 26 years, SD 17.04; hantavirus IgG-positive serum samples, mean patient age 28 years, SD 24.53; *t*-test, *t* = 0.26, p = 0.80). We considered p<0.05 to indicate statistical significance and conducted all tests by using a 2-tailed approach. We performed statistical analyses by using R software version 2024.04.2 (The R Project for Statistical Computing, https://www.r-project.org).

Virus Isolation

We used Vero E6 and BHK-21 cell lines for virus isolation attempts, as previously described for RIOMV and other hantaviruses (*25*). For both lines, we seeded a monolayer of 1.8×10^5 cells per well
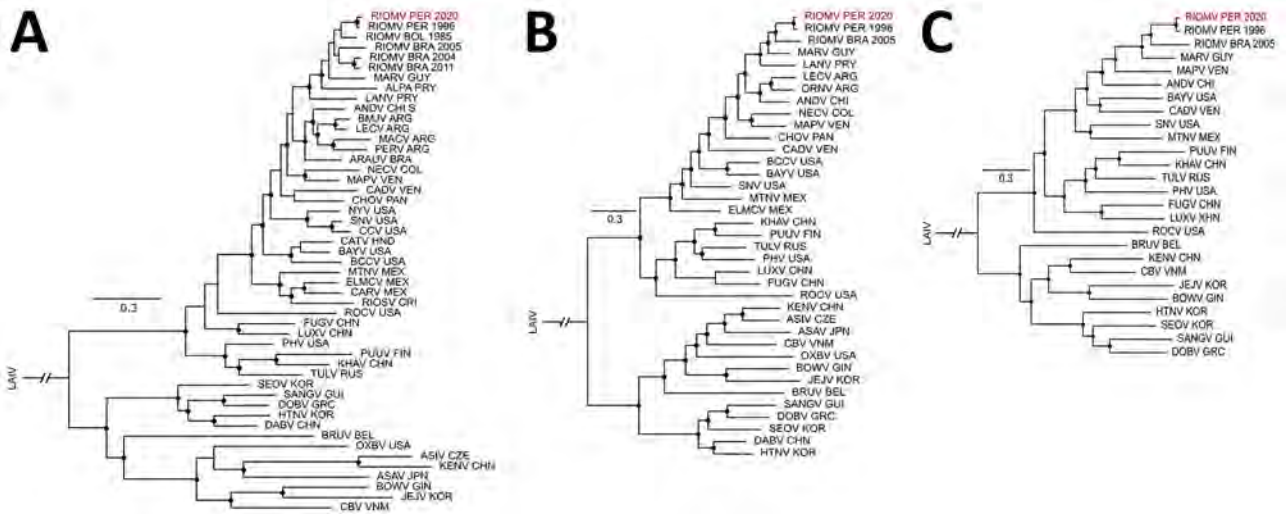
Figure 2. Phylogenetic relationships between partial concatenate sequences of RIOMV from Peru (RIOMV PER 2020, depicted in red) and reference sequences. The phylogenetic trees were constructed by using MrBayes 3.2.6 (http://mrbayes.csit.fsu.edu) and a general time-reversible substitution model with gamma distribution. Black circles at nodes indicate posterior probability ≥0.80. Reference sequences are available in Appendix 1 (https://wwwnc.cdc.gov/EID/article/30/12/24-0249-App1.pdf). A) Partial sequence of the small segment (1,393 nt). B) Partial sequence of the medium segment (1,914 nt). C) Partial sequence of the large segment (1,617 nt). LAIN, Laibin mobatvirus.

in a 12-well dish with Dulbecco Eagle modified medium supplemented with 10% fetal bovine serum and 1% penicillin/streptomycin. We diluted the serum sample 1:25 and inoculated 250 μL onto the cell monolayer. After 1 hour, we removed the inoculum and replaced it with fresh medium. We checked the cells daily to assess the development of cytopathic effects and tested by qRT-PCR. We per-formed 2 blind passages over 1 week each.

Results

Cohort Description

During a 1-year period (January 2020–2021), INS collected and stored 3,400 serum samples from febrile patients for AFI surveillance during a DENV out-
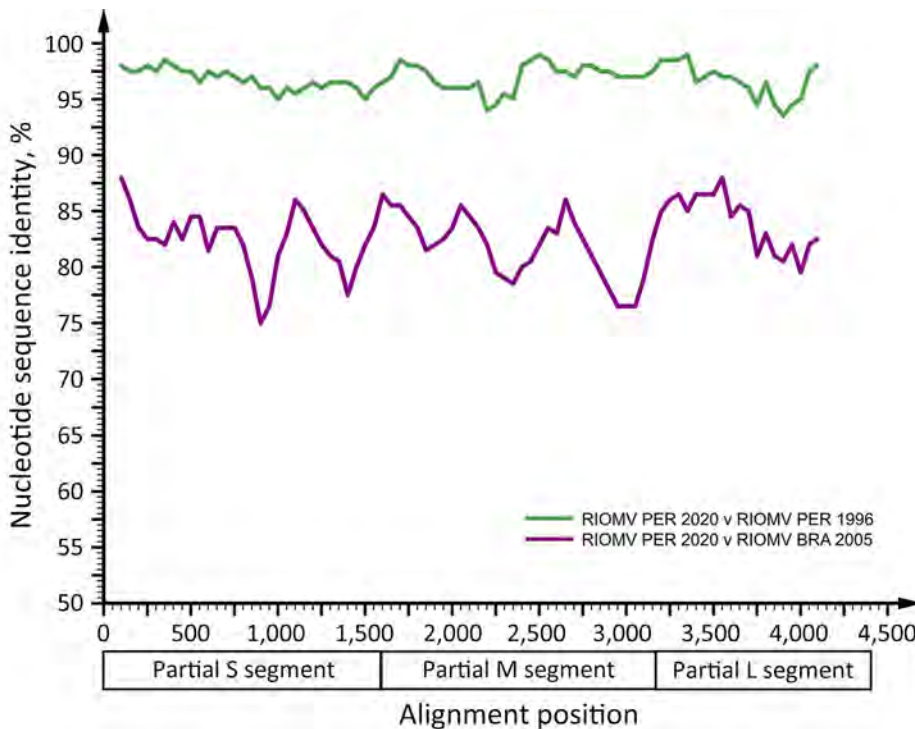
Figure 3. Sequence identity plot comparing RIOMV variants from Peru (RIOMV PER 2020 and RIOMV PER 1996) and Brazil (RIOMV BRA 2005). The identity plot was calculated by using SSE (http://www.virus-evolution.org) with partial concatenate sequences for the alignment of RIOMV (Appendix 1 Figure 2, https://wwwnc.cdc.gov/EID/article/30/12/24-0249-App1.pdf), a fragment length of 200 nt, and an increment between fragments of 50 nt. GenBank accession nos., RIOMV 1996 (FJ532244, FJ608550, FJ809772) and RIOMV Brazil 2005 (JX443679, JX443700, JX443697). L, large; M, medium; RIOMV, Rio Mamore virus; S, small.

Table 1. Hantavirus IgM-positive serum samples from Loreto, Peru*

Sample	IgM ELISA ratio†	Patient age, y/sex	Patient nationality	Date	Hantavirus RT-PCR	IgG ELISA ratio†	IFA result
1395	**1.87**	1/F	Peruvian	2020 Jan	Negative	0.16	SNV-like 1.0×10^1
3260	**5.00**	5/M	Peruvian	2020 Jan	Positive	**1.46**	SNV/ANDV-like 1.0×10^4
3261	**4.00**	3/M	Peruvian	2020 Jan	Negative	0.15	Negative
3265	**1.36**	32/M	Peruvian	2020 Jan	Negative	0.17	Negative
3281	**1.22**	1/M	Peruvian	2020 Jan	Negative	0.57	Negative
3345	**2.96**	<1/M	Peruvian	2020 Jan	Negative	0.27	Negative
3358	**3.73**	45/M	Peruvian	2020 Sep	Negative	0.33	Negative
3376	**1.25**	27/M	Peruvian	2020 Sep	Negative	0.28	SNV-like 1.0×10^1
3630	**2.60**	55/F	Peruvian	2020 May	Negative	0.17	Negative
4242	**2.60**	66/F	Peruvian	2020 Sep	Negative	0.28	SNV/ANDV/PUUV-like 1.0×10^1
4432	**2.03**	27/F	Peruvian	2021 Jan	Negative	0.33	Negative
4605	**1.11**	21/F	Foreign	2020 Dec	Negative	0.29	Negative
4893	**1.13**	2/M	Peruvian	2021 Jan	Negative	0.51	Negative

*ANDV, Andes virus; IFA, immunofluorescence assay; PUUV, Puumala virus; RT-PCR, reverse transcription PCR; SNV, Sin Nombre virus.
†Results with a ratio greater than 1.1 are considered positive and marked in boldface.

break that overlapped with COVID-19 (*24*) in 3 diverse ecoregions: Loreto (Amazon; n = 1,972 samples), Lambayeque (coastal desert /dry forest; n = 743 samples), and Lima (coastal desert; n = 685 samples) (Figure 1). The mean age of patients analyzed was 27 years (SD 18.8); 51.1% (n = 1,735) were female and 48.9% (n = 1,663) male. The overall age and sex distributions were comparable to those of the total population of Peru (mean age 31 years; 50.8% female, 49.2% male) (https://www.inei.gob.pe/media/MenuRecursivo/publicaciones_digitales/Est/Lib1743/Libro.pdf).

Molecular Testing for DENV and Hantaviruses

In January 2020, a serum sample from a 5-year-old boy from Iquitos, Loreto region, was positive for hantavirus RNA by nested RT-PCR (*9*) (Figure 1). Because sampling was conducted during a dengue outbreak and because other viruses may co-occur during dengue outbreaks, as was illustrated by detection of a Fort Sherman orthobunyavirus in a patient from Lambayeque (*27*), DENV infection in Loreto was assessed by qRT-PCR (*10*). The hantavirus-positive serum was negative for DENV, whereas the overall rate of DENV detection in Loreto was 56.8% (95% CI 54.7%–59.0%; n = 1,121/1,972) during 2020–2021. The patient experienced fever, muscle pain, headache, and vomiting for 3 days before sampling; no travel history preceding AFI was reported. No further information about the clinical signs/symptoms and disease outcome of the patient was available. A BLAST (http://blast.ncbi.nlm.nih.gov) comparison of the 347-bp region amplified by hantavirus RT-PCR after the exclusion of primer binding sites showed the highest nucleotide sequence identity (97.1%) to the rodent-associated RIOMV strain from 1996 in Loreto (*8*).

The viral load in the serum sample was low at 3.8 $\times 10^3$ copies/mL, which was consistent with the time since symptom onset, because the viral load is known to decline rapidly from ≈10^5–10^6 copies/mL 3–6 days after symptom onset (*28*). Virus isolation was unsuccessful, most likely because of low viral load and sample degradation under tropical conditions and repeated freeze–thaw cycles.

Genomic Characterization of RIOMV

Using a mixed approach of high-throughput and Sanger sequencing to close multiple gaps after high-throughput sequencing, probably because of low viral load, we reached a genome coverage of 41.4% (4,956 nt; 543,993 reads), of which 1,681 nt were from Sanger sequencing, with coverage of 72.7% for small (S), 52.5% for medium (M), and 24.7% for large (L) segments (GenBank accession nos. OR902838–40) (Appendix 1 Figure 1). Sequence comparisons within a dataset of all hantavirus reference sequences (Appendix 1 Table 3) showed that the 3 segments of the RIOMV strain from our study were most closely related to the rodent-associated RIOMV from 1996 (S segment, 96.8%; M segment, 96.4%; L segment, 97.0%). Separate Bayesian phylogenetic analyses of each segment placed the RIOMV strain consistently in a clade sharing the most recent common ancestry with the rodent-associated RIOMV (Figure 2). The phylogenetic placement of all genomic segments within the same RIOMV clade and similar sequence distance across genomic segments (Figure 3) spoke against reassortment or recombination events in the available dataset (*29*). The clustering of our sequence within the RIOMV clade was also supported by phylogenies relying on all available partial genomic sequences of viruses belonging to the *Orthohantavirus mamorense* species (Appendix 1 Table 4; Figure 2).

Serologic Markers of Acute Hantavirus Infection

To investigate whether the molecular detection of RIOMV was epidemiologically linked to additional hantavirus cases, we selected all AFI samples from Loreto that were negative for DENV during January 2020–2021 (n = 832). We selected DENV-negative serum because acute DENV infection can affect serologic analysis for other pathogens (e.g., SARS-CoV-2) (*30*). Because a RIOMV-specific IgM ELISA was not available, we used a commercially available IgM ELISA licensed for diagnostic use in Peru that relies on pooled ANDV and SNV nucleoproteins, which are suitable for detecting hantavirus-specific immune responses shortly after infection (*31*). The IgM ELISA yielded a detection rate of 1.6% (95% CI 0.9%–2.7%; n = 13/832) averaged over 2020 (Appendix 2, https://wwwnc.cdc.gov/EID/article/30/12/24-0249-App2.xlsx), including detectable IgM in the patient who tested positive by RT-PCR and exhibited high IgM IFA end-point titers of 1.0×10^4 against SNV and ANDV individually (Table 1; Appendix 1 Figure 3, panel A). Among the 13 samples positive for IgM by ELISA, 30.8% (95% CI 12.4%–58.0%; n = 4/13) were positive by IgM IFA (Appendix 1 Figure 3, panel B). The incidence based solely on IFA results was 0.5% (95% CI 0.07%–1.11%; n = 4/832). All IgM-positive samples, except those positive by RT-PCR, were negative for IgG, which may be attributed to the facts that all patients were febrile and that IgG production is expected during the first weeks after symptom onset (Table 1) (*32,33*).

In January 2020, the 2 patients who were positive according to IgM IFA, including the patient who was positive according to RT-PCR, were 1 and 5 years of age. In September 2020, the patients who were IgM positive by IFA were a 27-year-old woman and a 66-year-old man. Beyond the patient positive by PCR, IgM end-point titers were generally low at 1.0×10^1 against SNV and SNV/ANDV/PUUV, suggesting circulation of hantaviruses antigenically related to SNV/ANDV, potentially including RIOMV (Table 1; Appendix 1 Figure 4). Peru is not in the geographic distribution of the primary host of SNV, the North American deer mouse (*Peromyscus maniculatus*) (*34*), and PUUV is not endemic to South America. The reactivity for those viruses is probably explained by cross-reactivity between hantaviral epitopes, as previously described in full virus-based IFA (*35*).

In an IgM ELISA devoid of viral antigen, the optical density (OD) of hantavirus IgM IFA-confirmed serum did not differ significantly from that of IFA IgM-negative serum that had previously tested positive in the hantavirus IgM ELISA (Mann-Whitney *U* test, *U* = 20; p = 0.28) (Figure 4, panel A). We therefore compared reactivity with that of a control group

composed of serum samples negative for hantavirus IgM by ELISA. The OD of serum samples showing reactivity in the hantavirus IgM ELISA was higher (mean 0.61, SD = 0.28) than that of serum samples nonreactive in the hantavirus IgM ELISA (mean 0.07, SD = 0.09; Figure 4, panel A). Among the IgM-positive samples, 83.33% (95% CI 54.0%–96.5%; n = 10/12) also showed reactivity in real-time PCR for CMV, EBV, and *Plasmodium* spp., and in IgM ELISAs for several endemic arboviruses (OROV, chikungunya, and Mayaro virus) and even for the nonendemic
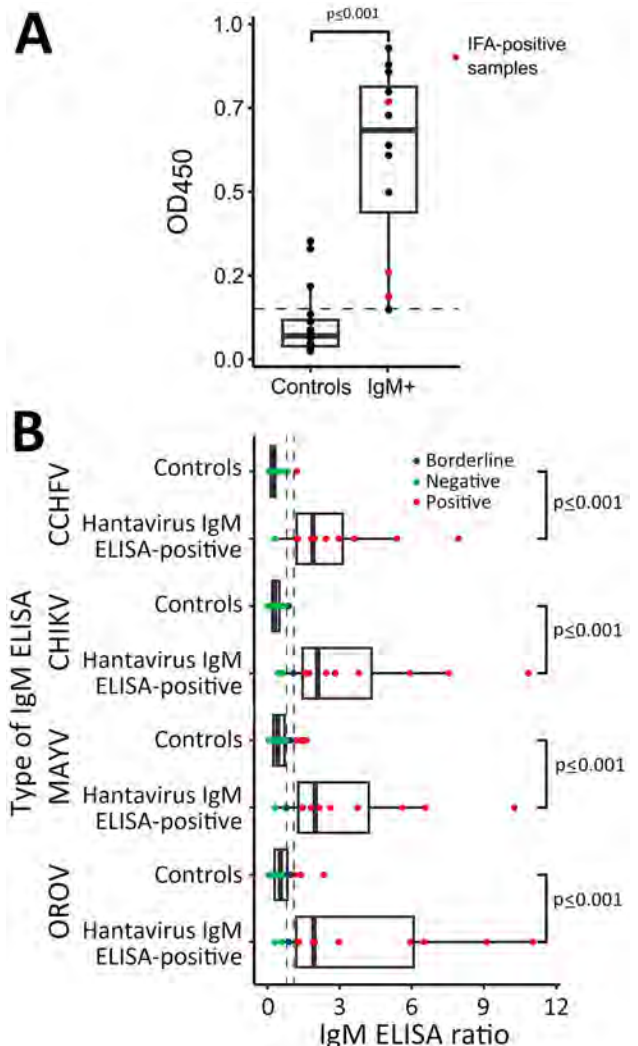
Figure 4. Investigation of unspecific reactivity in serum positive in hantavirus IgM by ELISA, Peru. A) OD$_{450}$ in noncoated ELISA plate. B) Comparison of IgM ELISA reactivity for different arboviruses: Control group, n = 38; hantavirus IgM–positive by ELISA group, n = 12. Tukey-style box plots are given with medians (thick lines within boxes) and interquartile ranges (box top and bottom or left and right edges); whiskers indicate 1.5× interquartile range. CCHFV, Crimean-Congo hemorrhagic fever virus, CHIKV, chikungunya virus, MAYV, Mayaro virus; OD$_{450}$, optical density at 450 nm; OROV, Oropouche virus.

Table 2. Results of complementary ELISA and PCR testing of serum samples positive by hantavirus IgM ELISA, Peru, January 2020–2021*

Sample	IgM ELISA ratio†				PCR copies/mL			Non–antigen coated plate OD
	CCHFV	CHIKV	MAYV	OROV	*Plasmodium* spp.	EBV	CMV	
1395‡	**1.19**	**1.59**	**1.46**	0.89	Negative	Negative	Negative	0.19
3261	**5.38**	**5.91**	**5.61**	**5.94**	Negative	Negative	Negative	0.80
3265	**1.82**	1.10	0.75	**1.30**	**8.4×10^5**	**4.4×10^3**	**1.9×10^3**	0.93
3281	**1.97**	**2.82**	**3.75**	**6.50**	Negative	Negative	Negative	0.73
3345	**2.97**	**7.55**	**6.56**	**2.96**	Negative	Negative	**4.2×10^3**	0.86
3358	**7.95**	**10.86**	**10.25**	**9.11**	**2.8×10^4**	Negative	Negative	0.88
3376	0.34	0.65	0.80	0.60	Negative	Negative	Negative	0.26
3630	**3.61**	**3.80**	**2.17**	**1.30**	Negative	Negative	Negative	0.64
4242‡	**2.43**	**1.74**	**1.47**	**1.97**	Negative	Negative	Negative	0.77
4432	0.32	0.45	0.33	0.31	Negative	Negative	Negative	0.15
4605	**1.28**	**1.74**	**2.63**	**11.04**	Negative	Negative	Negative	0.50
4893	**1.22**	**2.44**	**1.81**	**1.90**	Negative	Negative	Negative	0.61

*Boldface indicates samples that tested positive. CCHFV, Crimean-Congo hemorrhagic fever virus; CHIKV, chikungunya virus; CMV, cytomegalovirus; EBV, Epstein-Barr virus; MAYV, Mayaro virus; OROV, Oropouche virus. The sample that tested positive by reverse transcription PCR was not tested because of limited sample volume after isolation attempts. OD of the negative control for IgM in Sin Nombre virus/Andes virus ELISA on a noncoated plate, 0.15. (Mann-Whitney *U* test, MAYV, *U* = 44; OROV, *U* = 56; CCHFV, *U* = 20, CHIKV, *U* = 15, p<0.001 for all).
†Boldface indicates results with a ratio >1.1 considered positive in all ELISAs.
‡Samples that tested positive by hantavirus IFA.

arbovirus CCHFV (Table 2). Arbovirus IgM ELISA reactivity in hantavirus IgM ELISA-reactive serum samples was consistently higher than that in hantavirus IgM ELISA-nonreactive serum samples (Figure 4, panel B). To avoid false-positive results, when calculating the IgM detection rate, we included only samples that tested positive for IFA.

Serologic Markers of Past Hantavirus Infection
The scarce hantavirus detections in humans and ro-

Table 3. Hantavirus IgG-positive serum samples from Loreto, Lambayeque, and Lima, Peru, 2020*

Sample	Place	Patient age, y/sex	Nationality	Month	IgG ELISA ratio†	IFA result	Interpretation
1788	Lambayeque	13/M	Peruvian	Feb	**1.42**	SNV, 1.0×10^2; ANDV/PUUV, 1.0×10^1	SNV-like
1818	Lambayeque	6/M	Peruvian	Aug	**2.15**	Negative	Negative
1835	Lambayeque	29/F	Peruvian	Nov	**1.15**	Negative	Negative
1866	Lambayeque	60/M	Peruvian	Feb	**1.76**	Negative	Negative
1882	Lambayeque	20/F	Foreign	Mar	**2.24**	SNV 1.0×10^3	SNV-like
1945	Lambayeque	4/F	Foreign	Jan	**1.52**	Negative	Negative
2738	Lambayeque	15/F	Peruvian	Mar	**1.35**	Negative	Negative
2740	Lambayeque	84/M	Peruvian	Mar	**1.77**	Negative	Negative
2003	Lima	48/F	Peruvian	Jan	**1.69**	SNV 1.0×10^1	SNV-like
2069	Lima	19/M	Peruvian	Feb	**1.95**	SNV, 1.0×10^3; ANDV, 1.0×10^2; HTNV/SAAV/DOBV, 1.0×10^1	SNV-like
2139	Lima	2/M	Foreign	Mar	**1.20**	Negative	Negative
2167	Lima	30/M	Peruvian	Jan	**2.80**	ANDV/SNV, 1.0×10^3	ANDV/SNV-like
3136	Loreto	6/F	Peruvian	Jan	**1.64**	ANDV, 1.0×10^1	ANDV-like
3249	Loreto	5/M	Peruvian	Jan	**1.16**	DOBV/SAAV, 1.0×10^1	DOBV/SAAV-like
3260	Loreto	5/M	Peruvian	Jan	**1.46**	ANDV/SNV, 1.0×10^4	ANDV/SNV-like
3317	Loreto	43/M	Peruvian	Jan	**1.17**	HTNV/DOBV, 1.0×10^1	HTNV/DOBV-like
3361	Loreto	22/M	Peruvian	Sep	**2.31**	ANDV/SNV, 1.0×10^2	ANDV/SNV-like
3404	Loreto	16/M	Peruvian	Sep	**1.12**	SNV, 2.5×10^3; ANDV, 1.0×10^2; PUUV, 1.0×10^1	SNV-like
3562	Loreto	<1/F	Peruvian	Mar	**1.96**	Negative	Negative
3615	Loreto	16/M	Peruvian	Apr	**1.67**	SNV, 1.0×10^3; ANDV/HTNV/DOBV, 1.0×10^1	SNV-like
3937	Loreto	<1/M	Peruvian	Mar	**5.30**	Negative	Negative
4524	Loreto	26/F	Peruvian	Dec	**3.16**	ANDV/SNV, 1.0×10^4; HTNV/PUUV/SEOV/DOBV, 1.0×10^1	ANDV/SNV-like
4591	Loreto	71/M	Peruvian	Jan	**1.69**	SNV 2.5×10^3; ANDV 1.0×10^2; PUUV 1.0×10^1	SNV-like

*Boldface indicates positive results (ratio >1.1). ANDV, Andes virus; DOBV, Dobrava virus; HTNV, Hantaan virus; IFA, immunofluorescence assay; PUUV, Puumala virus; SAAV, Saaremaa virus; SEOV, Seoul virus; SNV, Sin Nombre virus.

Table 4. Results for complementary ELISA and PCR testing of serum samples positive by hantavirus IgG ELISA, Peru, January 2020–2021*

Sample	IgG ELISA ratio†							PCR copies/mL			Non–antigen coated plate/OD
	CCHFV	CHIKV	MAYV	OROV	MERS-CoV	SARS-CoV-2	*Plasmodium* spp.	*Plasmodium* spp.	EBV	CMV	
1788‡	0.12	0.11	0.15	0.05	0.06	0.15	2.25	Negative	Negative	Negative	0.04
1818	0.07	0.09	0.03	0.02	0.02	0.79	0.23	Negative	1.2×10^3	Negative	0.03
1835	0.11	0.31	0.04	0.06	0.03	0.18	0.19	Negative	Negative	Negative	0.02
1866	0.15	0.06	0.07	0.06	0.02	0.12	**3.98**	Negative	Negative	Negative	0.02
1882‡	0.05	0.07	0.12	0.04	0.03	0.11	**5.94**	Negative	Negative	Negative	0.01
1945	0.87	0.44	0.21	0.50	0.33	0.32	**7.14**	Negative	Negative	Negative	0.45
2003‡	0.06	0.03	0.03	0.04	0.02	0.11	**3.79**	Negative	Negative	Negative	0.01
2069‡	0.13	0.02	0.07	0.03	0.02	0.15	**1.48**	Negative	Negative	Negative	0.01
2139	0.13	0.10	0.09	0.18	0.04	0.17	0.24	Negative	Negative	Negative	0.05
2167‡	0.17	0.17	0.21	0.34	0.08	0.23	**1.77**	Negative	Negative	Negative	0.05
2216	0.10	0.06	0.06	0.06	0.03	0.17	0.37	Negative	Negative	Negative	0.01
2738	0.08	0.05	0.13	0.06	0.04	0.14	**2.27**	Negative	Negative	Negative	0.02
2740	0.15	0.17	0.09	0.10	0.04	**1.19**	0.43	Negative	Negative	Negative	0.05
3136‡	0.24	0.18	0.08	0.07	0.12	0.22	0.23	Negative	Negative	Negative	0.13
3249‡	0.21	0.17	0.16	0.13	0.04	0.20	0.50	Negative	Negative	Negative	0.04
3317‡	0.08	0.58	**2.43**	0.99	0.02	0.34	0.79	Negative	Negative	Negative	0.02
3361‡	0.06	0.10	0.17	0.08	0.03	0.92	**3.20**	Negative	Negative	Negative	0.02
3404‡	0.08	0.12	0.23	0.06	0.05	0.13	0.99	Negative	Negative	Negative	0.03
3562	**2.71**	**2.02**	**2.30**	**2.97**	0.71	**1.66**	**2.78**	Negative	Negative	1.7×10^3	1.03
3615‡	0.08	0.46	0.49	0.09	0.03	0.30	0.27	Negative	Negative	Negative	0.02
3937	**5.48**	**3.89**	**2.71**	**3.69**	**2.05**	**3.56**	**3.45**	Negative	Negative	2.1×10^3	2.31
4524‡	0.18	**2.70**	**6.54**	0.29	0.04	0.67	**1.79**	Negative	Negative	Negative	0.03
4591‡	0.46	**1.27**	**2.69**	**2.44**	ND	**1.82**	**1.19**	Negative	Negative	Negative	0.02

*The RT-PCR positive sample was not tested because of to limited sample volume after isolation attempts. OD of negative control for IgG in Sin Nombre virus/Andes virus ELISA on a noncoated plate, 0.01. Statistical results comparing the ratios of hantavirus IFA-positive, IFA-negative serum samples, and the control group, Kruskal-Wallis; CCHFV, H = 2.33, p = 0.31; CHIKV, H = 2.0, p = 0.22; MAYV, H = 5.0, p = 0.08; MERS-CoV, H = 0.01, p = 0.99; OROV, H = 8.24, p = 0.02; *Plasmodium* spp., H = 12.21, p = 0.02 and SARS-CoV-2, H = 10.12, p = 0.006. CCHFV, Crimean-Congo hemorrhagic fever virus; CHIKV, chikungunya virus; CMV, cytomegalovirus; EBV, Epstein-Barr virus; IFA, immunofluorescence assay; MAYV, Mayaro virus; MERS-CoV, Middle East respiratory syndrome coronavirus; ND, not done; OD, optical density; OROV, Oropouche virus. Samples that tested positive by hantavirus IFA indicated in bold.
†Results with a ratio >1.1 are considered positive and marked in boldface.
‡Samples that tested positive by hantavirus IFA.

dents in Peru all originated from the Amazon Basin. To compare whether persons living in other ecozones had had previous contact with hantaviruses, we tested 830 samples from Loreto, Lambayeque, and Lima that were DENV-negative by qRT-PCR and were of sufficient serum volume for hantavirus IgG testing by using the same ELISA that we used to detect IgM. The hantavirus IgG ELISA detection rate by region was 4.0% (95% CI 2.1%–7.0%; n = 11/278) in Loreto, 1.4% (95% CI 0.4%–3.8%; n = 4/279) in Lima, and 2.9% (95% CI 1.4%–5.8%; n = 8/273) in Lambayeque (Appendix 1 Figure 5, panel A; Appendix 2). We found no significant difference in hantavirus IgG detection rates by ELISA between sites (χ^2 = 3.32; p = 0.20).

To confirm past hantavirus infections, we again performed IFA-based end-point titration. IgG IFA confirmed 60.9% (95% CI 40.7%–77.9%; n = 14/23) of the IgG ELISA-positive samples IgG positive by ELISA (Appendix 1 Figure 5, panel B). The sample positive by RT-PCR had IgG titers of 1.0×10^4 against SNV and ANDV, a finding consistent with early IgG responses in some hantavirus-infected patients (32). End-point titration suggested 7 past infections with viruses antigenically more related to SNV than to ANDV, according to the highest SNV titers in all 3 ecozones. One serum sample each showed monotypic reactivity with SNV or ANDV (Table 3). Another 6 samples positive by IFA had similar titers against ≥2 hantaviruses, including DOBV/Saaremaa virus, Hantaan virus/DOBV, and SNV/ANDV (Table 3; Appendix 1 Figure 5, panel B). Nine samples positive by IgG ELISA samples were negative by IFA (Table 3).

Complementary testing as before revealed that 2 serum samples (Table 4, samples 3562 and 3937) from children <1 year of age that were positive by the hantavirus IgG ELISA but negative by hantavirus IgG IFA were CMV positive by PCR. In an IgG ELISA plate devoid of viral antigens, the ODs in the 2 CMV-positive serum samples were strikingly higher at 1.03 and 2.31 (mean 1.67, SD = 0.9) compared with the rest of the samples that were hantavirus IgG ELISA-positive (mean 0.05, SD = 0.09). The ODs of samples that were The ODs of samples that were positive by hantavirus IgG ELISA but negative by hantavirus IgG IFA, including those 2 samples, differed significantly from those of the control group (Table 4; Figure 5, panel A). After excluding the 2 CMV-positive samples, we detected no significant differences between the ODs of the
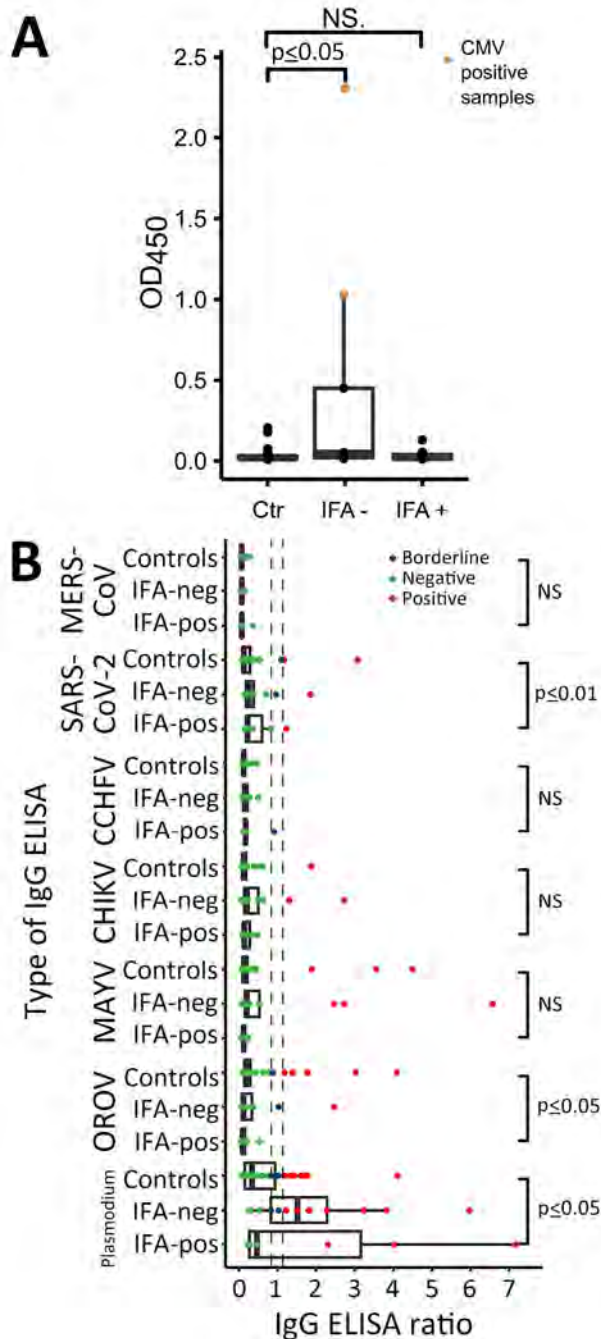
Figure 5. Investigation of unspecific reactivity in serum samples positive in hantavirus in IgG-positive serum by ELISA, Peru. A) OD$_{450}$ in noncoated ELISA plate. B) Comparison of IgG ELISA reactivity for different viruses excluding the CMV-positive samples. Control group, n = 38; ; hantavirus IgG IFA-negative samples, n = 7; hantavirus IgG IFA-positive samples, n = 13. Tukey-style box plots are given with medians (thick lines within boxes) and interquartile ranges (box top and bottom or left and right edges); whiskers indicate 1.5 × interquartile range. CCHFV, Crimean-Congo hemorrhagic fever virus; CHIKV, chikungunya virus; CMV, cytomegalovirus; IFA, immunofluorescence assay; MAYV, Mayaro virus; MERS-CoV, Middle East respiratory syndrome coronavirus; neg, negative; pos, positive; OD$_{450}$, optical density at 450 nm; OROV, Oropouche virus.

3 compared groups. The 2 CMV-positive samples also showed significantly higher reactivity in most complementary ELISAs, including pathogens not found in South America, such as CCHFV and Middle East respiratory syndrome coronavirus (Table 4). After excluding the 2 CMV-positive samples, we found significant differences in ELISA reactivity levels for OROV, SARS-CoV-2, and *Plasmodium* spp. (Figure 5, panel B), whereas the overall number of positive serum samples did not differ among groups (Appendix 1 Table 8). Thus, we calculated the ELISA-based IgG detection rate without the 2 CMV-positive serum samples. The adjusted hantavirus IgG detection rate for Loreto was 3.2% (95% CI 1.6%–6.1%; n = 9/278;); 66.7% (95% CI 45.2%–82.9%; n = 14/21) of the samples also tested positive by IFA, and the overall IgG detection rate was 1.7% (95% CI 1.0%–2.8%; n = 14/830) across the 3 ecozones.

Discussion

We detected and characterized RIOMV and analyzed hantavirus exposure for patients with AFI in Peru. Our serologic results were consistent with those of a previous study conducted in Loreto during 2007–2010 that used an ANDV antigen–based capture ELISA and reported an IgM detection rate of 0.3% (n = 15/5,174) (*36*). Moreover, the high genomic similarity of the RIOMV strain from our study and the rodent-associated RIOMV from 1996 and the geographic distribution of the host in the Amazon suggest endemicity (*37*) (Global Biodiversity Information Facility, https://www.gbif.org). That the only human case described from Brazil also occurred in the Amazon Basin reaffirms the area of RIOMV endemicity and confirms the ability of RIOMV to cause disease in humans (*6*).

The ecology of hantavirus infections is complex and probably varies according to climatic factors, predator/prey relationships, land use changes, host abundance, and virus genetics (*38*). Most cases of infection with ANDV, which is hosted by rodent species of a different genus than those of the genus that hosts RIOMV (*34*), in Argentina and Chile have been reported during spring and summer, when food availability is higher (*39*). In the Amazon region, the relatively constant climatic conditions throughout the year and the continuous harvest of different crops make it challenging to identify risk factors (*40*). However, 2 samples confirmed IgM positive were collected in January and another 2 were collected in September 2020, suggesting the potential for seasonal patterns of hantavirus infection in Loreto.

The lower sensitivity of IFA compared with ELISA may also partly explain the observed difference

between ELISA and IFA reactivity (*41,42*), especially when recombinant nucleoproteins are used rather than full virus-infected cells as antigens (*43,44*) and when RIOMV antigens are not included. Moreover, the nonspecific reactivity in the hantavirus ELISA is compatible with polyclonal B cell activation resulting from CMV, EBV, *Plasmodium* spp., or hantavirus infections (*45*) and emphasizes the value of confirming IgM/IgG ELISA results, ideally by neutralization tests (NTs) for IgG (*15,16*).

Ecologic investigations of hantaviruses in the Peruvian Amazon and their host are thus urgently needed. Further investigation of circulating hantavirus strains in humans in Peru and other regions of South America is also warranted because our serologic findings suggest that antigenically diverse hantaviruses may co-occur.

Among the potential limitations of our study is the use of uneven numbers of samples throughout the year. It is likely that, during the onset of the COVID-19 pandemic, movement restrictions and lack of medical personnel led efforts to be focused on COVID-19, and persons with febrile illness without respiratory signs/symptoms might not have sought medical care (*46,47*). That interpretation is consistent with lower numbers of reported cases of dengue during the onset of the COVID-19 pandemic in Latin America (*47*). In addition, virus NTs might have contributed additional serologic information. However, the cross-reactivity of hantavirus immune responses would probably also have limited unambiguous results in virus NTs, even if we had an RIOMV isolate (*44*). In addition, a comparison of glycoprotein-based IFA- and NT-based serotyping results in a previous study of Old World hantaviruses was consistent in 79.5% of the samples (*42*). Thus, our conclusions, which are based on exhaustive serologic testing, are most likely robust even in the absence of NTs.

The early signs/symptoms of hantavirus infection are nonspecific (*6,7,48*) and resemble those of other AFIs. Therefore, it is necessary to enhance AFI surveillance by incorporating diagnostic protocols for hantavirus in patients in Peru and other ecologically similar regions of Latin America with compatible symptomatology and no evidence of dengue or malaria.

Acknowledgment

About the Author

Mrs. Piche is a PhD student at the Institute of Virology at Charité-Universitätsmedizin, Berlin, and the Institute for the History of Medicine at Justus Liebig University of Giessen. Her research interests include the epidemiology of arthropod-borne viruses from animal reservoirs.

References

1. Laserna A, Barahona-Correa J, Baquero L, Castañeda-Cardona C, Rosselli D. Economic impact of dengue fever in Latin America and the Caribbean: a systematic review. Rev Panam Salud Publica. 2018;42:e111. https://doi.org/10.26633/RPSP.2018.111
2. Moreira J, Bressan CS, Brasil P, Siqueira AM. Epidemiology of acute febrile illness in Latin America. Clin Microbiol Infect. 2018;24:827–35. https://doi.org/10.1016/j.cmi.2018.05.001
3. Moreira J, Barros J, Lapouble O, Lacerda MVG, Felger I, Brasil P, et al. When fever is not malaria in Latin America: a systematic review. BMC Med. 2020;18:294. https://doi.org/10.1186/s12916-020-01746-z
4. Mattar S, Guzmán C, Figueiredo LT. Diagnosis of hantavirus infection in humans. Expert Rev Anti Infect Ther. 2015;13:939–46. https://doi.org/10.1586/14787210.2015.1047825
5. Figueiredo LT, Souza WM, Ferrés M, Enria DA. Hantaviruses and cardiopulmonary syndrome in South America. Virus Res. 2014;187:43–54. https://doi.org/10.1016/j.virusres.2014.01.015
6. de Oliveira RC, Cordeiro-Santos M, Guterres A, Fernandes J, de Melo AX, João GA, et al. Rio Mamoré virus and hantavirus pulmonary syndrome, Brazil. Emerg Infect Dis. 2014;20:1568–70. https://doi.org/10.3201/eid2009.131472
7. Saavedra-Velasco M, Oyarce-Calderón A, Vergas-Herrera N, Pichardo-Rodriguez R, Moreno-Arteaga C. Hantavirus en la selva peruana, una revisión sistemática de series y casos reportados. Revista de la Facultad de Medicina Humana. 2021;21:851–8. https://doi.org/10.25176/RFMH.v21i4.3650
8. Powers AM, Mercer DR, Watts DM, Guzman H, Fulhorst CF, Popov VL, et al. Isolation and genetic characterization of a hantavirus (Bunyaviridae: Hantavirus) from a rodent, *Oligoryzomys microtis* (Muridae), collected in northeastern Peru. Am J Trop Med Hyg. 1999;61:92–8. https://doi.org/10.4269/ajtmh.1999.61.92
9. Klempa B, Fichet-Calvet E, Lecompte E, Auste B, Aniskin V, Meisel H, et al. Hantavirus in African wood mouse, Guinea. Emerg Infect Dis. 2006;12:838–40. https://doi.org/10.3201/eid1205.051487

10. Leparc-Goffart I, Baragatti M, Temmam S, Tuiskunen A, Moureau G, Charrel R, et al. Development and validation of real-time one-step reverse transcription-PCR for the detection and typing of dengue viruses. J Clin Virol. 2009;45:61–6. https://doi.org/10.1016/j.jcv.2009.02.010

11. Weiss S, Sudi LE, Düx A, Mangu CD, Ntinginya NE, Shirima GM, et al. Kiwira virus, a newfound hantavirus discovered in free-tailed bats (Molossidae) in East and Central Africa. Viruses. 2022;14:2368. https://doi.org/10.3390/v14112368

12. Ronquist F, Teslenko M, van der Mark P, Ayres DL, Darling A, Höhna S, et al. MrBayes 3.2: efficient Bayesian phylogenetic inference and model choice across a large model space. Syst Biol. 2012;61:539–42. https://doi.org/10.1093/sysbio/sys029

13. Simmonds P. SSE: a nucleotide and amino acid sequence analysis platform. BMC Res Notes. 2012;5:50. https://doi.org/10.1186/1756-0500-5-50

14. Stecher G, Tamura K, Kumar S. Molecular Evolutionary Genetics Analysis (MEGA) for macOS. Mol Biol Evol. 2020;37:1237–9. https://doi.org/10.1093/molbev/msz312

15. Klempa B, Koivogui L, Sylla O, Koulemou K, Auste B, Krüger DH, et al. Serological evidence of human hantavirus infections in Guinea, West Africa. J Infect Dis. 2010;201:1031–4. https://doi.org/10.1086/651169

16. Landry ML. Immunoglobulin M for acute infection, true or false? Clin Vaccine Immunol. 2016;23:540–5. https://doi.org/10.1128/CVI.00211-16

17. Yadouleton A, Sander AL, Moreira-Soto A, Tchibozo C, Hounkanrin G, Badou Y, et al. Limited specificity of serologic tests for SARS-CoV-2 antibody detection, Benin. Emerg Infect Dis. 2021;27:233–7. https://doi.org/10.3201/eid2701.203281

18. Mrozek-Gorska P, Buschle A, Pich D, Schwarzmayr T, Fechtner R, Scialdone A, et al. Epstein-Barr virus reprograms human B lymphocytes immediately in the prelatent phase of infection. Proc Natl Acad Sci U S A. 2019;116:16046–55. https://doi.org/10.1073/pnas.1901314116

19. Dauby N, Kummert C, Lecomte S, Liesnard C, Delforge ML, Donner C, et al. Primary human cytomegalovirus infection induces the expansion of virus-specific activated and atypical memory B cells. J Infect Dis. 2014;210:1275–85. https://doi.org/10.1093/infdis/jiu255

20. Wesselmann KM, Postigo-Hidalgo I, Pezzi L, de Oliveira-Filho EF, Fischer C, de Lamballerie X, et al. Emergence of Oropouche fever in Latin America: a narrative review. Lancet Infect Dis. 2024;24:e439–52. https://doi.org/10.1016/S1473-3099(23)00740-5

21. Fischer C, Bozza F, Merino Merino XJ, Pedroso C, de Oliveira Filho EF, Moreira-Soto A, et al. Robustness of serologic investigations for chikungunya and Mayaro viruses following coemergence. MSphere. 2020;5:e00915–9. https://doi.org/10.1128/mSphere.00915-19

22. Rosado J, Carrasco-Escobar G, Nolasco O, Garro K, Rodriguez-Ferruci H, Guzman-Guzman M, et al. Malaria transmission structure in the Peruvian Amazon through antibody signatures to *Plasmodium vivax*. PLoS Negl Trop Dis. 2022;16:e0010415. https://doi.org/10.1371/journal.pntd.0010415

23. Lapidus S, Liu F, Casanovas-Massana A, Dai Y, Huck JD, Lucas C, et al. *Plasmodium* infection is associated with cross-reactive antibodies to carbohydrate epitopes on the SARS-CoV-2 spike protein. Sci Rep. 2022;12:22175. https://doi.org/10.1038/s41598-022-26709-7

24. Plasencia-Dueñas R, Failoc-Rojas VE, Rodriguez-Morales AJ. Impact of the COVID-19 pandemic on the incidence of dengue fever in Peru. J Med Virol. 2022;94:393–8. https://doi.org/10.1002/jmv.27298

25. Pádua M, Souza WM, Lauretti F, Figueiredo LT. Development of a novel plaque reduction neutralisation test for hantavirus infection. Mem Inst Oswaldo Cruz. 2015;110:624–8. https://doi.org/10.1590/0074-02760150102

26. Beck HE, Zimmermann NE, McVicar TR, Vergopolan N, Berg A, Wood EF. Present and future Köppen-Geiger climate classification maps at 1-km resolution. Sci Data. 2018;5:180214. https://doi.org/10.1038/sdata.2018.214

27. de Oliveira-Filho EF, Cabezas Sánchez CA, Manosalva DEV, Romero MDF, Sarmiento NSM, Ñique AIM, et al. Fort Sherman virus infection in human, Peru, 2020. Emerg Infect Dis. 2024;30:2211–4. https://doi.org/10.3201/eid3010.240124

28. Bellomo CM, Pires-Marczeski FC, Padula PJ. Viral load of patients with hantavirus pulmonary syndrome in Argentina. J Med Virol. 2015;87:1823–30. https://doi.org/10.1002/jmv.24260

29. Klempa B. Reassortment events in the evolution of hantaviruses. Virus Genes. 2018;54:638–46. https://doi.org/10.1007/s11262-018-1590-z

30. Lustig Y, Mendelson E, Mandelboim M, Biber A, Levin EG, Cohen C, et al. Existence of immunological memory response in true sero-negative individuals post COVID-19 molecular diagnosis. Clin Infect Dis. 2022;10:ciac196. https://doi.org/10.1093/cid/ciac196

31. Vapalahti O, Kallio-Kokko H, Närvänen A, Julkunen I, Lundkvist A, Plyusnin A, et al. Human B-cell epitopes of Puumala virus nucleocapsid protein, the major antigen in early serological response. J Med Virol. 1995;46:293–303. https://doi.org/10.1002/jmv.1890460402

32. MacNeil A, Comer JA, Ksiazek TG, Rollin PE. Sin Nombre virus-specific immunoglobulin M and G kinetics in hantavirus pulmonary syndrome and the role played by serologic responses in predicting disease outcome. J Infect Dis. 2010;202:242–6. https://doi.org/10.1086/653482

33. Padula PJ, Colavecchia SB, Martínez VP, Gonzalez Della Valle MO, Edelstein A, Miguel SD, et al. Genetic diversity, distribution, and serological features of hantavirus infection in five countries in South America. J Clin Microbiol. 2000;38:3029–35. https://doi.org/10.1128/JCM.38.8.3029-3035.2000

34. Milholland MT, Castro-Arellano I, Suzán G, Garcia-Peña GE, Lee TE Jr, Rohde RE, et al. Global diversity and distribution of hantaviruses and their hosts. EcoHealth. 2018;15:163–208. https://doi.org/10.1007/s10393-017-1305-2

35. Lederer S, Lattwein E, Hanke M, Sonnenberg K, Stoecker W, Lundkvist Å, et al. Indirect immunofluorescence assay for the simultaneous detection of antibodies against clinically important old and new world hantaviruses. PLoS Negl Trop Dis. 2013;7:e2157. https://doi.org/10.1371/journal.pntd.0002157

36. Castillo Oré RM, Forshey BM, Huaman A, Villaran MV, Long KC, Kochel TJ, et al. Serologic evidence for human hantavirus infection in Peru. Vector Borne Zoonotic Dis. 2012;12:683–9. https://doi.org/10.1089/vbz.2011.0820

37. Firth C, Tokarz R, Simith DB, Nunes MR, Bhat M, Rosa ES, et al. Diversity and distribution of hantaviruses in South America. J Virol. 2012;86:13756–66. https://doi.org/10.1128/JVI.02341-12

38. Jonsson CB, Figueiredo LT, Vapalahti O. A global perspective on hantavirus ecology, epidemiology, and disease. Clin Microbiol Rev. 2010;23:412–41. https://doi.org/10.1128/CMR.00062-09

39. Astorga F, Escobar LE, Poo-Muñoz D, Escobar-Dodero J, Rojas-Hucks S, Alvarado-Rybak M, et al. Distributional

ecology of Andes hantavirus: a macroecological approach. Int J Health Geogr. 2018;17:22. https://doi.org/10.1186/s12942-018-0142-z

40. Terças-Trettel ACP, Melo AVG, Bonilha SMF, Moraes JM, Oliveira RC, Guterres A, et al. Hantavirus pulmonary syndrome in children: case report and case series from an endemic area of Brazil. Rev Inst Med Trop São Paulo. 2019;61:e65. https://doi.org/10.1590/s1678-9946201961065

41. Elgh F, Lundkvist A, Alexeyev OA, Stenlund H, Avsic-Zupanc T, Hjelle B, et al. Serological diagnosis of hantavirus infections by an enzyme-linked immunosorbent assay based on detection of immunoglobulin G and M responses to recombinant nucleocapsid proteins of five viral serotypes. J Clin Microbiol. 1997;35:1122–30. https://doi.org/10.1128/jcm.35.5.1122-1130.1997

42. Li W, Cao S, Zhang Q, Li J, Zhang S, Wu W, et al. Comparison of serological assays to titrate Hantaan and Seoul hantavirus-specific antibodies. Virol J. 2017;14:133. https://doi.org/10.1186/s12985-017-0799-0

43. Krüger DH, Schönrich G, Klempa B. Human pathogenic hantaviruses and prevention of infection. Hum Vaccin. 2011;7:685–93. https://doi.org/10.4161/hv.7.6.15197

44. Saavedra F, Díaz FE, Retamal-Díaz A, Covián C, González PA, Kalergis AM. Immune response during hantavirus diseases: implications for immunotherapies

and vaccine design. Immunology. 2021;163:262–77. https://doi.org/10.1111/imm.13322

45. Hepojoki J, Cabrera LE, Hepojoki S, Bellomo C, Kareinen L, Andersson LC, et al. Hantavirus infection-induced B cell activation elevates free light chains levels in circulation. PLoS Pathog. 2021;17:e1009843. https://doi.org/10.1371/journal.ppat.1009843

46. Martinez VP, Bellomo CM, Cacace ML, Suarez P, Bogni L, Padula PJ. Hantavirus pulmonary syndrome in Argentina, 1995–2008. Emerg Infect Dis. 2010;16:1853–60. https://doi.org/10.3201/eid1612.091170

47. Chen Y, Li N, Lourenço J, Wang L, Cazelles B, Dong L, et al.; CMMID COVID-19 Working Group. Measuring the effects of COVID-19-related disruption on dengue transmission in southeast Asia and Latin America: a statistical modelling study. Lancet Infect Dis. 2022;22:657–67. https://doi.org/10.1016/S1473-3099(22)00025-1

48. Vial PA, Ferrés M, Vial C, Klingström J, Ahlm C, López R, et al. Hantavirus in humans: a review of clinical aspects and management. Lancet Infect Dis. 2023;23:e371–82. https://doi.org/10.1016/S1473-3099(23)00128-7

Address for correspondence, Jan Felix Drexler, Institute of Virology, Charitéplatz 1, 10117 Berlin, Germany; email: felix.drexler@charite.de

Novel Mastadenovirus Infection as Cause of Pneumonia in Imported Black-and-White Colobuses (*Colobus guereza*), Thailand

Chutchai Piewbang, Sabrina Wahyu Wardhani, Panida Poonsin, Pattiya Lohavicharn,
Ratchanon Tengtawon, Thanakrit Charoenrat, Sitthichok Lacharoje, Sawang Kesdangsakonwut,
Tanit Kasantikul, Nathamon Kosoltanapiwat, Somporn Techangamsuwan

We identified a novel mastadenovirus, herein referred to as colobus adenovirus (CoAdV), as the likely cause of fatal respiratory and enteric diseases in multiple black-and-white colobuses (*Colobus guereza*) imported into Thailand in 2022. Among 9 affected colobuses, 4 died. Viral antigen was abundant in respiratory and enteric tissues, where prominent lesions and clinical signs were observed. We successfully cultivated CoAdV in Vero cells and characterized the complete viral genome, which indicated the virus is genetically distinct from other simian adenoviruses. We also conducted a retrospective study of archival samples from 7 other unrelated colobuses that had respiratory distress or diarrhea and found similar viral strains in 4 of those colobuses. Although we could not determine the potential harm to humans or other nonhuman primates from current information, the zoonotic and spillover potential of this virus to other related hosts should not be neglected. Veterinarians should consider CoAdV when pneumonia is diagnosed in colobuses.

Most adenoviruses that infect mammals belong to the genus *Mastadenovirus*, which is part of the family Adenoviridae and includes a variety of viruses found in humans, nonhuman primates (NHPs), and other mammals (*1,2*). Although many cases of human adenovirus infection are predominantly asymptomatic and infection can be self-limited in immunocompetent hosts, infections in immunosuppressed patients can lead to greater severity and even death (*3–6*).

Of the >50 adenovirus species in the genus *Mastadenovirus*, 9 that infect NHPs, known as simian adenoviruses (SAdVs; SAdV-A–I), and 7 that infect humans, known as human adenoviruses (HAdVs; HAdV-A–G), have been documented (*1*). Although

species domination is considered on the basis of infected hosts, many adenoviruses found in NHPs, have been identified as HAdVs (*7*), and SAdV infections have also been reported in humans who have contact with NHPs (*6*). Because of the phylogenetic proximity between NHPs, and humans, interspecies transmission is highly possible (*8,9*). Although adenoviruses have been considered host-specific and restricted to ≥1 related species (*4*), phylogenetic and evolutionary analyses reveal instances of interspecies transmission that have led to new host-virus adaptations. For example, HAdV-E is believed to have originated from chimpanzee adenoviruses and HAdV-B from gorilla adenoviruses (*10*). In addition, serologic evidence indicates that adenoviruses derived from monkeys can infect humans who have close contact with NHPs (*5,6*). Those findings raise concerns about interspecies transmission and zoonotic potential. Notable examples include canine adenovirus 1, which infects multiple carnivore species, and skunk adenovirus 1, found in marmosets (*Callithrix* spp.), skunks (*Mephitis* spp.), pygmy hedgehogs (*Atelerix albiventris*), and other species, illustrating adenoviruses' ability to cross species

Author affiliations: Chulalongkorn University, Bangkok, Thailand
(C. Piewbang, S.W. Wardhani, P. Poonsin, P. Lohavicharn,
S. Lacharoje, S. Kesdangsakonwut, S. Techangamsuwan);
Goodwill Animal Hospital, Nonthaburi, Thailand (R. Tengtawon,
T. Charoenrat,); Michigan State University, East Lansing, Michigan, USA. (T. Kasantikul); Mahidol University, Bangkok
(N. Kosoltanapiwat)

barriers (*11,12*). Such instances underscore the potential zoonotic threats posed by mastadenoviruses because of their genetic diversity and adaptability (*13*).

Southeast Asia and China are main hubs of the primate trade, both as importers and exporters, for various purposes (*14,15*). Importation of apparently healthy NHPs without specific surveillance for NHP-related adenoviruses may result in the introduction of novel adenoviruses to naive environments or vice versa. We identified a novel adenovirus in colobuses with fatal respiratory distress that were imported into Thailand in 2022.

Materials and Methods

During August–September 2022, nine wild-caught adult black-and-white colobuses (*Colobus guereza*) of unknown specific ages were imported from South Africa and kept as pets in individual stainless-steel cages in Bangkok, Thailand. All animals were shipped together in a single lot and underwent quarantine at customs for several months before all 9 went to a single pet owner. Initially, clinical signs and symptoms began with depression, reduced appetite, and fever, after which coughing, pneumonia, and subsequent respiratory distress developed. Those symptoms were observed shortly (within a few weeks) after the animals arrived at the final destinations with the pet owner. Four of the colobuses (nos. 1–4) succumbed to their illnesses 5–10 days after the onset of clinical symptoms; the other 5 (nos. 5–9) survived after receiving intensive supportive care.

Clinical samples, including oral and rectal swab samples, were collected from all 9 diseased colobuses. Among the 9 colobuses, the 4 that subsequently died (nos. 1–4) were submitted for necropsy at the Department of Pathology, Faculty of Veterinary Science, Chulalongkorn University, Bangkok. We collected vital samples, including brain, trachea, lung, heart, intestine, liver, kidneys, and lymph nodes, and divided samples into 2 cohorts: fresh-frozen tissues and formalin-fixed paraffin-embedded (FFPE) tissues fixed in 10% buffered formalin. This study was approved by Chulalongkorn University Animal Care and Use Committee (approval no. 2431048).

Nucleic Acid Extraction and Routine Diagnostic Panels

We processed collected samples for viral nucleic acid extraction by using QIAamp Viral RNA Mini Kit (QIAGEN, https://www.qiagen.com) according to the manufacturer's guidelines. To elucidate the viral infections in these cases, we subjected the extracted nucleic acid samples to routine virologic testing panels by using pan-family virologic PCRs targeting Herpesviridae (*16*), Paramyxoviridae (*17*), Pneumoviridae (*17*), Parvoviridae (*18*), Orthomyxoviridae (*19*), Retroviridae (*20*), and Adenoviridae (*21*) families. For PCR-positive samples, we sent target amplicons to Celemics, Inc. (https://www.celemics.com) for next-generation sequencing (NGS)–based methods. Furthermore, we submitted fresh lung samples from all investigated colobuses for aerobic bacterial culture.

Detection of Adenovirus DNA and Complete Genome Characterization

For samples that initially tested positive for adenoviruses by pan-Adenoviridae PCR targeting the DNA polymerase (*DNApol*) gene, we reconfirmed results by using a second PCR that targeted the *hexon* gene with established pan-*Mastadenovirus* primers (*22*). We then sequenced the positive amplicons following the protocol described previously. We used nucleic acid extracts obtained from fresh lung tissue of colobus no. 1 for complete adenoviral genome characterization through a de novo–based NGS method (Vishuo Biomedical, https://www.vishuo.com) (Appendix, https://wwwnc.cdc.gov/EID/article/30/12/24-1042-App1.pdf). Subsequently, we aligned the identified sequence with previously described adenovirus sequences found in NHPs, including SAdV-A–I and unclassified SAdVs. We subjected that alignment to maximum-likelihood phylogenetic analysis (Appendix). We also performed recombination analysis by using a recombination detection program (*23*) (Appendix). We refer to this novel virus as colobus adenovirus (CoAdV).

Viral Load Quantification and Localization

To confirm the results from NGS analysis and investigate the genomic distribution of CoAdV in various organs and in other colobuses, we conducted conventional PCR using newly designed primers targeting the *DNApol* gene of CoAdV. In addition, to quantify viral loads in different organs, we performed a SYBR green–based quantitative PCR (qPCR) by using KAPA SYBR Fast qPCR Master Mix (2X) Universal Kit (Sigma-Aldrich, https://www.sigmaaldrich.com) with specific primers designed to target the *DNApol* gene of CoAdV (CoAdV-DpolF-6348, 5′-CAG CTG GTC CTC GTC C-3'; CoAdV-DpolR-6443, 5′-TTG CAG GAC CCC CTG AAG AC-3'). We estimated relative viral loads in each organ on the basis of cycle threshold (Ct) values.

Detection of CoAdV Antigen in FFPE Tissues

To determine the tissue tropism of CoAdV, we subjected FFPE tissues from the 4 necropsied colobuses

that tested positive in both conventional and qPCR to immunohistochemical (IHC) analysis. The examined tissues were brain, lung, liver, lymph node, spleen, heart, kidneys, and intestine. We assessed localization of CoAdV in those tissues by using a horseradish peroxidase polymer-conjugated method with primary antibody against adenovirus clones 2/6 and 20/11 (Chemi-Con, https://chemi-con.com) (Appendix).

Viral Isolation

We conducted virus isolation on Vero cells (ATCC accession no. CCL-81) in 12-well tissue culture plates. We subjected samples to viral isolation, including oral and rectal swab samples from diseased colobus nos. 4–6, 7, and 9 that had been collected in viral transport medium, and supernatants from lung and trachea homogenized in PBS from colobus no. 1 that died (Appendix). We monitored cultures for cytopathic effects (CPE) daily for 5 days (2). We collected supernatants from wells showing CPE and stored at –80°C for subsequent adenovirus-specific PCR confirmation. In addition, we harvested cell pellets and prepared for transmission electron microscopy analysis.

Retrospective Study of CoAdV in Other NHPs

We also used the qPCR described to conduct CoAdV detection on a small sample cohort that underwent postmortem examination at Department of Pathology, Faculty of Veterinary Science, Chulalongkorn University, during 2020–2022. The cohort comprised archival respiratory or rectal swab samples and fresh-frozen lung tissues obtained from 7 other colobuses that died from various causes, plus the fresh-frozen lung or respiratory swab samples from other primates, including 2 Douc monkeys (*Pygathrix* spp.), 1 De Brazza's monkey (*Cercopithecus neglectus*), 6 marmosets, 4 Japanese macaques (*Macaca fuscata*), 2 cotton-top tamarins (*Saguinus oedipus*), and 11 long-tailed macaques (*Macaca fascicularis*).

Results

CoAdV Detection, Genome Characterization, and Phylogenetic Analysis

Apart from negative results of ancillary testing using pan-family virologic PCR panels, the oral swab samples from all 9 colobuses and 5 fecal swab samples obtained from colobuses nos. 1–4 and 7 tested positive by pan-adenovirus PCR. The colobuses that subsequently died (nos. 1–4) predominantly exhibited lower Ct values (Table). Analysis of tissue samples showed that the lung, trachea, and intestines exhibited positive amplification signals for the pan-adenovirus PCR, whereas the other collected tissues had negative results. *Klebsiella* spp. was cultivated from the lung tissue of colobus nos. 1 and 4. We sequenced the positive adenovirus amplicons (460 bp) from all samples, and initial BLASTn (https://blast.ncbi.nlm.nih.gov) results showed 99.9% nucleotide similarities among adenovirus from colobuses and most were closely related to another SAdV (GenBank accession no. JN808448).

NGS results showed a total of 889 sequence reads that mapped to various simian mastadenovirus species. From those sequence reads, we generated a consensus sequence of 33,813 bp, tentatively named CoAdV strain CP001-TH/2023. To confirm the accuracy of the generated CoAdV sequence, we used primers for adenovirus screening as described and submitted the 460-bp PCR products for Sanger sequencing, which showed 100% similarity to the generated sequence. The CoAdV genome comprises 19.85% A, 18.34% T, 30.80% C, and 31.01% G. The CoAdV strain CP001-TH/2023 genome contained 145-bp ends of inverted terminal repeats with a conserved motif CATCATCCAAT, displaying typical mastadenovirus orthologs. The CoAdV CP001-TH/2023 genome possessed 32 predicted proteins and included genus-specific genes encoding proteins V and IX and the early (E) regions E1, E3, and

Table. Immunohistochemistry and quantitative PCR findings in an investigation of novel mastadenovirus infection causing pneumonia in imported black-and-white colobuses (*Colobus guereza*), Thailand*

| Colobus no. | Sample types tested, Ct value/immunohistochemistry findings | | | | | | | | | | |
	Oral swab	Fecal swab	Lung	Trachea	TLN	Intestine	MLN	Liver	Kidney	Heart	Brain
1†	22.5/ND	30.2/ND	18.2/++	20.2/++	30.6/+	29.0/++	–/–	–/–	–/–	–/–	–/–
2†	23.4/ND	32.5)/ND	20.2/++	24.2/+	32.7/–	30.6/+	–/–	–/–	–/–	–/–	–/–
3†	26.9/ND	32.8/ND	22.4/++	23.8/++	30.2/+	30.2/+	–/–	–/–	–/–	–/–	–/–
4†	22.8/ND	29.9)/ND	17.5/++	24.9/++	33.8/–	25.8/+	–/–	–/–	–/–	–/–	–/–
5	29.0/ND	–/ND	NSA	NSA	NSA	NSA	NSA	NSA	NSA	NSA	NSA
6	29.8/ND	–/ND	NSA	NSA	NSA	NSA	NSA	NSA	NSA	NSA	NSA
7	30.5/ND	34.5/ND	NSA	NSA	NSA	NSA	NSA	NSA	NSA	NSA	NSA
8	27.2/ND	–/ND	NSA	NSA	NSA	NSA	NSA	NSA	NSA	NSA	NSA
9	29.3/ND	–/ND	NSA	NSA	NSA	NSA	NSA	NSA	NSA	NSA	NSA

*Staining intensity of immunohistochemistry was semiquantitative. Ct, cycle threshold; MLN, mesenteric lymph node; ND, not determined; NSA, no sample available; TLN, tracheobronchial lymph node; +, positive intensity; ++, strong positive intensity; –, negative.
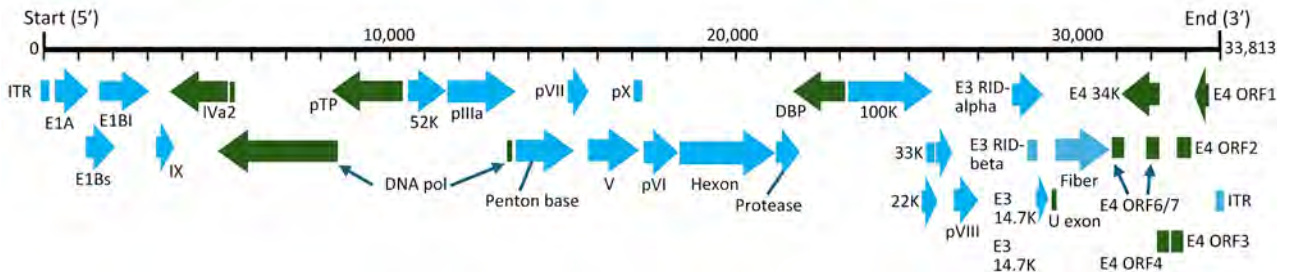†Colobus died.

Figure 1. Genome organization of novel mastadenovirus infection causing pneumonia in imported black-and-white colobuses (*Colobus guereza*), Thailand. Thick black line indicates virus genome; gene length is also indicated. ITR sequences and putative viral genes are represented as rectangles or arrows, corresponding to the transcriptional direction. Within the rectangles or arrows, light blue color indicates 5′ to 3′ translational direction, and dark green indicates complementary translational direction. The virus, tentatively named colobus adenovirus, is available in GenBank (accession no. PP985428). DBP, DNA-binding protein; E, early region; ITR, inverted terminal repeat; ORF, open reading frame; RID, receptor internalization and degradation.

E4. Only one *fiber* gene was observed within the CoAdV CP001-TH/2023 genome (Figure 1). We submitted the CoAdV sequence to GenBank (accession no. PP985428).

The full-length CoAdV strain CP001-TH/2023 exhibited 67.10% nucleotide similarity to the SAdV-6 strain SV-39 (GenBank accession no. JQ776547) from Old World macaque monkeys in the United States. CoAdV CP001-TH/2023 was distinct from other SAdVs, and nucleotide similarities ranged from 66.50% to 50.02%. The human mastadenovirus B isolate KUMC-62 (GenBank accession no. KY320276) was the most distant strain, showing only 50.02% nucleotide similarity to the detected CoAdV. Analysis of *DNApol* gene revealed nucleotide similarities of 62.30%–77.90% and amino acid similarities of 25.40%–57.6% to previously described SAdVs. The SAdV strain ER (GenBank accession no. MZ062897) identified in China was the most genetically similar strain. Phylogenetic analysis of the full-length genome of SAdVs revealed that CoAdV CP001-TH/2023 formed a distinct phylogenetic cluster, and was most closely related to SAdV-A, SAdV-G, and SAdV-I isolated from Old World monkeys (Figure 2) and that SAdV-6 strain SV-39 was the most closely related. The whole-genome phylogenetic tree was consistent with the phylogenetic analysis of amino acid sequences of the *DNApol* and *IVa2* trees (Figures 3, 4).

Because limited information was available on other genes of previously described AdVs identified in colobuses in Germany, we were only able to analyze relatedness in the *fiber* gene (Figure 5). CoAdV CP001-TH/2023 shared 71.75%–80.50% nucleotide similarity with AdVs identified in colobuses in Germany in 2011, and *Colobus guereza* adenovirus 1 (GenBank accession no. JN163994) was the most closely related strain. Although the CoAdV *hexon* gene identified in this study genetically clustered closely with

the *Colobus guereza* adenovirus 1 (GenBank accession no. JN163994) strain, it formed a distant phylogenic topology with 99% bootstrap support (Figure 6). However, CoAdV CP001-TH/2023 had a unique phylogenetic topology and did not cluster with other previously described AdVs identified in colobuses (GenBank accession nos. JN613993 and JN613995). Information for complete genome sequences of SAdV identified in Thailand was limited, and only the *fiber* gene was available. Thus, we also included the *fiber* gene of SAdV-B isolate RBR-7-10 (GenBank accession no. ON072488) to determine the phylogenetic relationship of the detected CoAdV; however, those sequences were distantly related (Figure 5). We did not identify any genetic recombination events within the CoAdV genome.

CoAdV Pathology and Viral Distribution

Overall, histologic findings were consistent across all colobuses and showed varying degrees of severity. The trachea mucosa was extensively replaced by laminated bands of eosinophilic fibrillar material mixed with scant aggregates of karyorrhectic debris. In addition, the tracheal lumen contained a small pool of neutrophils and karyorrhectic debris (Figure 7, panel A). The pulmonary interstitium was diffusely congested, with increased prominence and tortuosity of markedly engorged alveolar capillaries. In colobus no. 1, the pulmonary alveoli were multifocally filled with eosinophilic granular to homogenous material, intermixed with variable numbers of foamy macrophages, and fewer polymorphonuclear cells (Figure 7, panel B). Moreover, alveoli were overlaid by variable flocculent mats of eosinophilic fibrin. Similar mats of eosinophilic fibrin and a few neutrophils were seen in 1 lumen of the large bronchial airways (Figure 7, panel C). In colobus no. 2, we noted similar but milder changes.
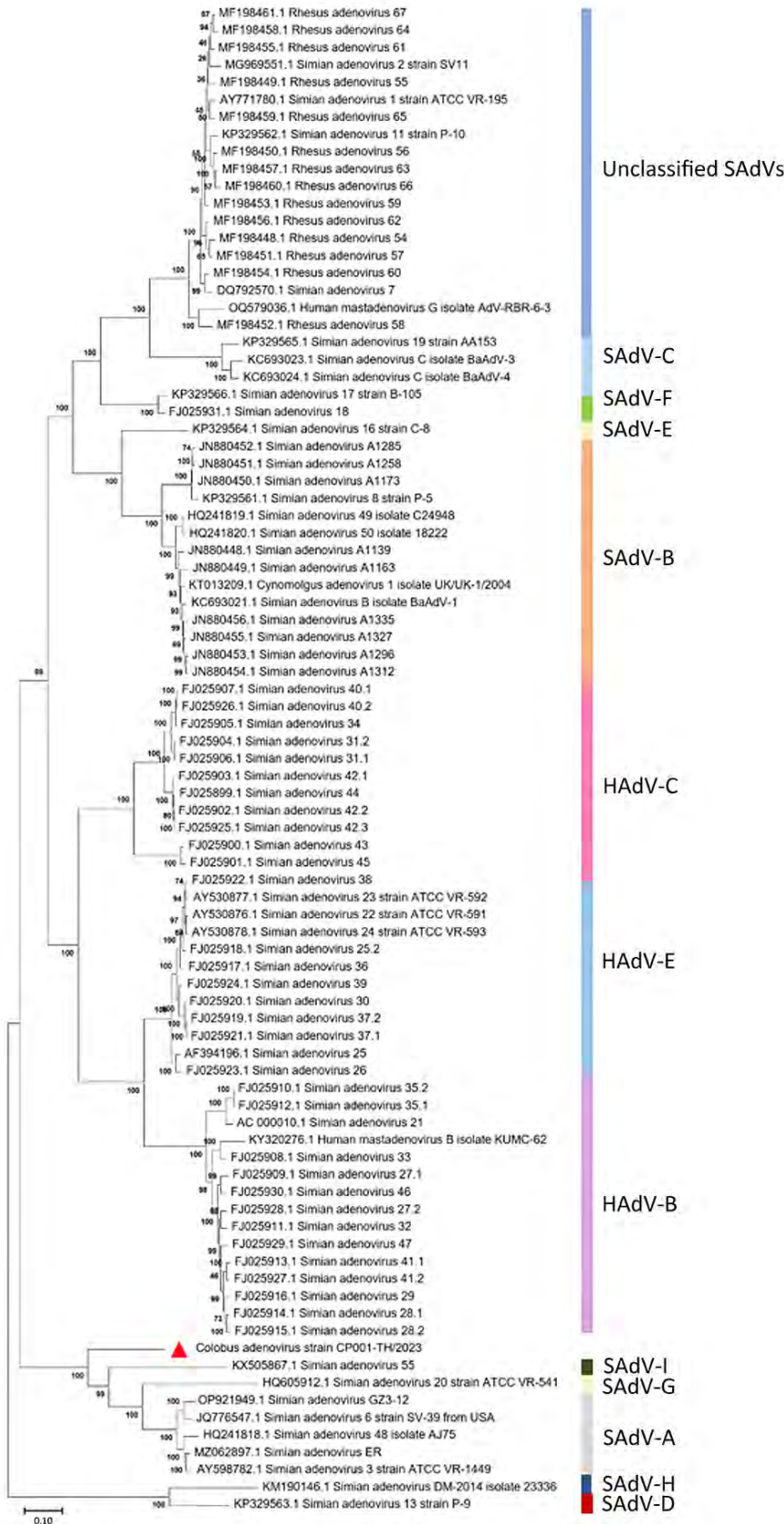
Figure 2. Phylogenetic analysis of complete genome sequence of novel mastadenovirus infection causing pneumonia in imported black-and-white colobuses (*Colobus guereza*), Thailand. Comparative analysis of the genome from this study, tentatively name colobus adenovirus (CoAdV), with various adenoviruses identified in nonhuman primates. Bootstrap values are shown at each node. Red triangle indicates the CoAdV CP001 TH/2023 identified in this study, and phylogenetic reveals this sequence groups with various SAdVs and HAdVs. GenBank accession numbers are provided. Scale bar indicates number of substitutions per site. HAdV, human adenovirus; SAdV, simian adenovirus.

To determine the CoAdV distribution in tissue and localize the virus where lesions were located, we quantified the viral loads by using qPCR (Table). We primarily detected CoAdV in respiratory samples and noted the highest viral loads in the lung but also high loads in trachea tissue and oral and fecal swab samples. We found smaller amounts of the viral genome in the small intestine. We used IHC to determine CoAdV
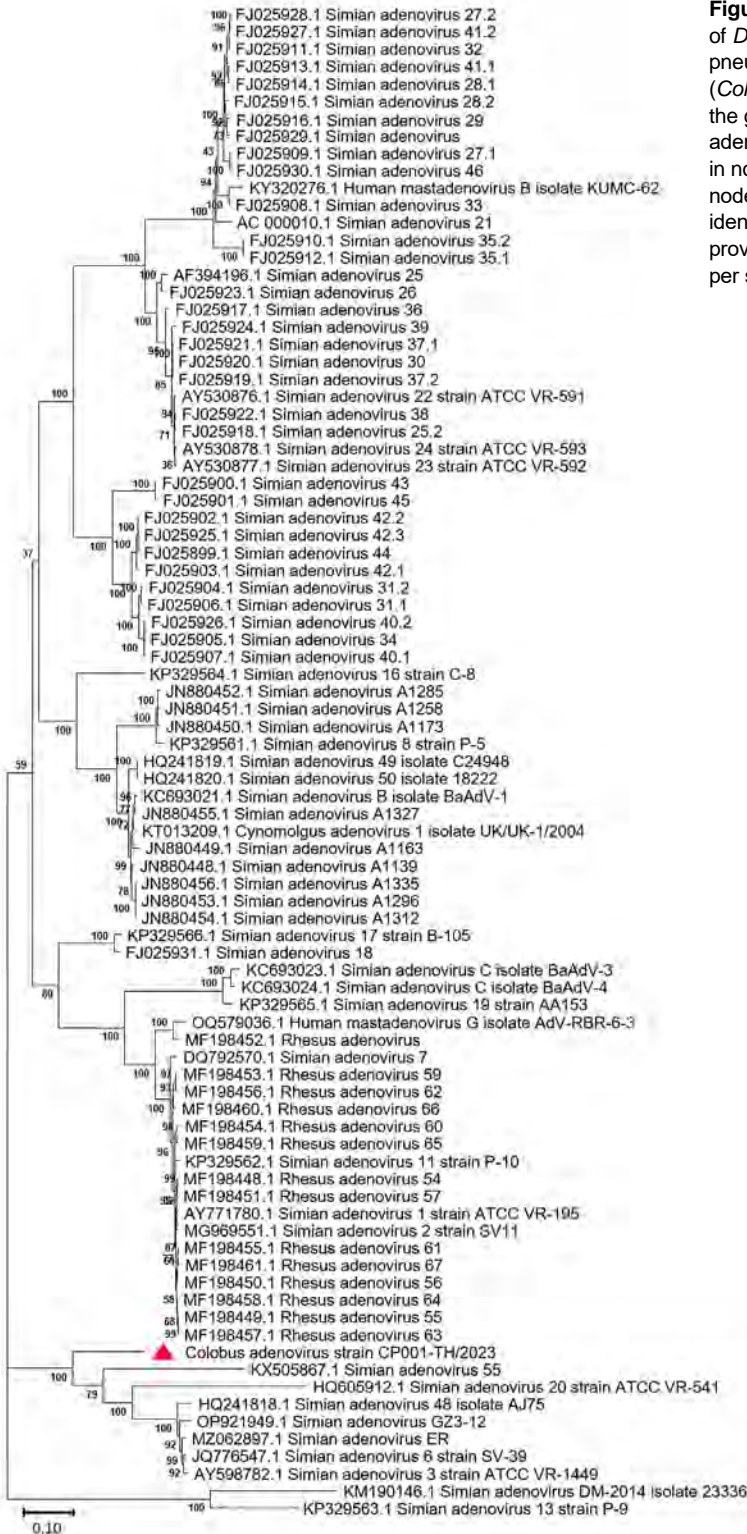
Figure 3. Phylogenetic analysis of amino acid sequences of *DNApol* gene of novel mastadenovirus infection causing pneumonia in imported black-and-white colobuses (*Colobus guereza*), Thailand. Comparative analysis of the genome from this study, tentatively name colobus adenovirus (CoAdV), with various adenoviruses identified in nonhuman primates. Bootstrap values are shown at each node. Red triangle indicates the CoAdV CP001 TH/2023 identified in this study. GenBank accession numbers are provided. Scale bar indicates the number of substitutions per site. AdV, adenovirus; BaAdV, baboon adenovirus.
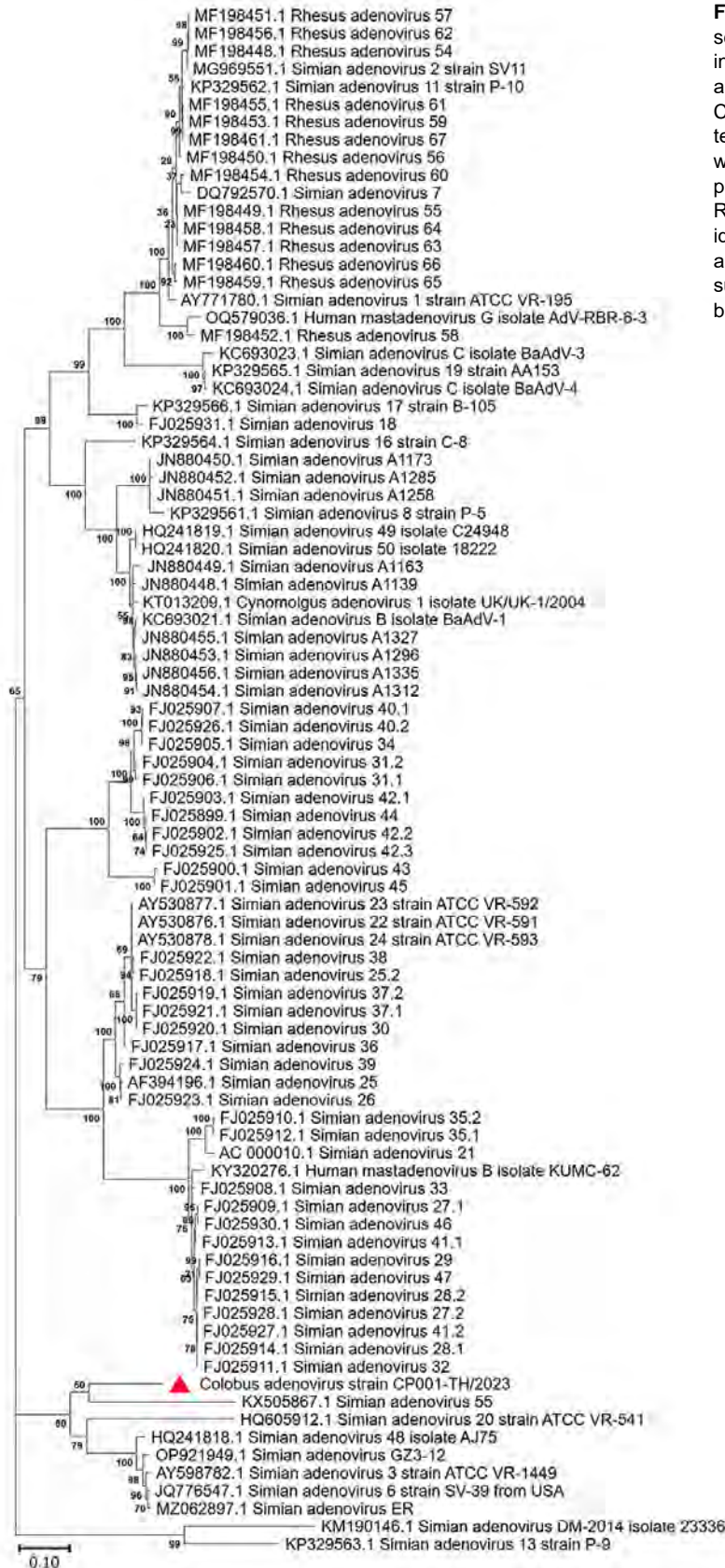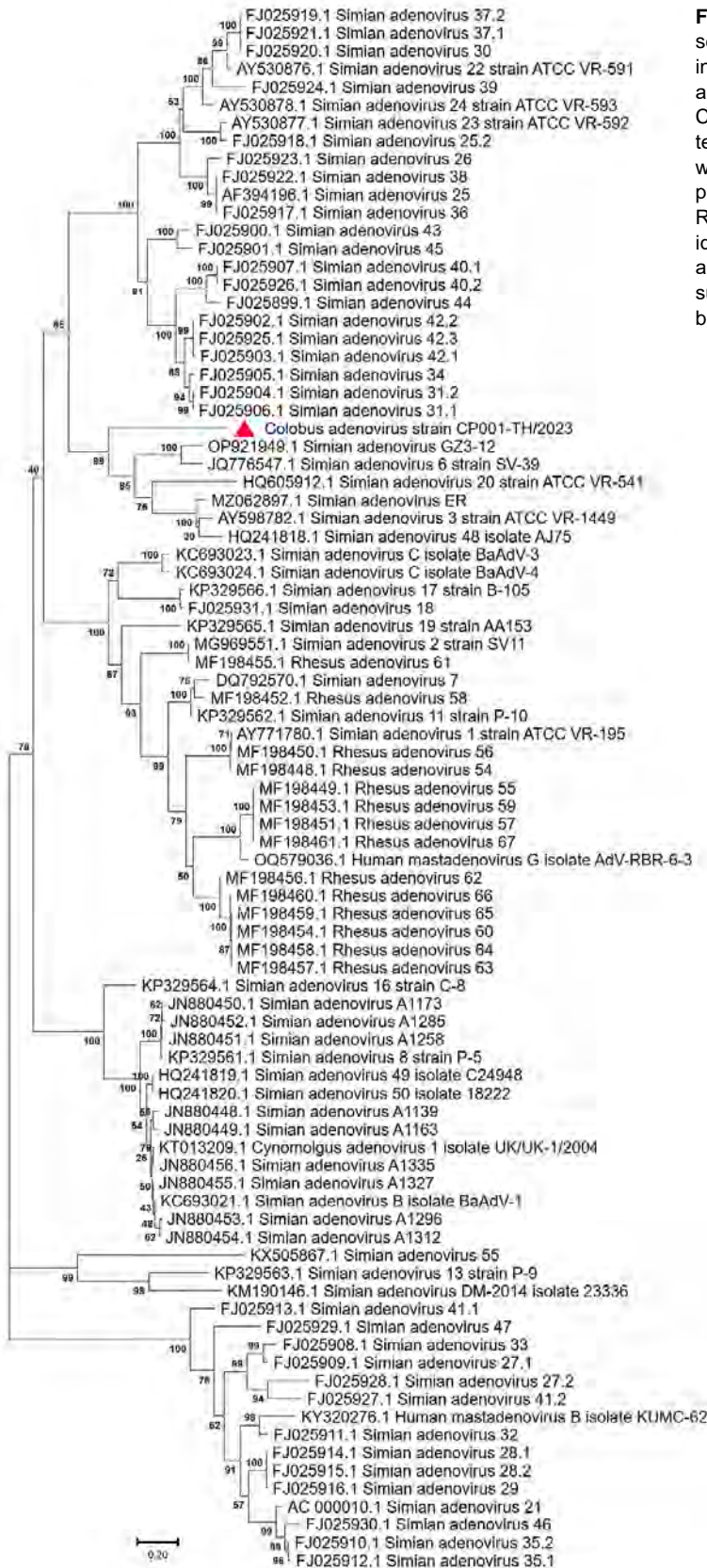
Figure 4. Phylogenetic analysis of amino acid sequences of *IVa2* gene of novel mastadenovirus infection causing pneumonia in imported black-and-white colobuses (*Colobus guereza*), Thailand. Comparative analysis of the genome from this study, tentatively name colobus adenovirus (CoAdV), with various adenoviruses identified in nonhuman primates. Bootstrap values are shown at each node. Red triangle indicates the CoAdV CP001 TH/2023 identified in this study. GenBank accession numbers are provided. Scale bar indicates the number of substitutions per site. AdV, adenovirus; BaAdV, baboon adenovirus.

Figure 5. Phylogenetic analysis of amino acid sequences of *fiber* gene of novel mastadenovirus infection causing pneumonia in imported black-and-white colobuses (*Colobus guereza*), Thailand. Comparative analysis of the genome from this study, tentatively name colobus adenovirus (CoAdV), with various adenoviruses identified in nonhuman primates. Bootstrap values are shown at each node. Red triangle indicates the CoAdV CP001 TH/2023 identified in this study. GenBank accession numbers are provided. Scale bar indicates the number of substitutions per site. AdV, adenovirus; BaAdV, baboon adenovirus.
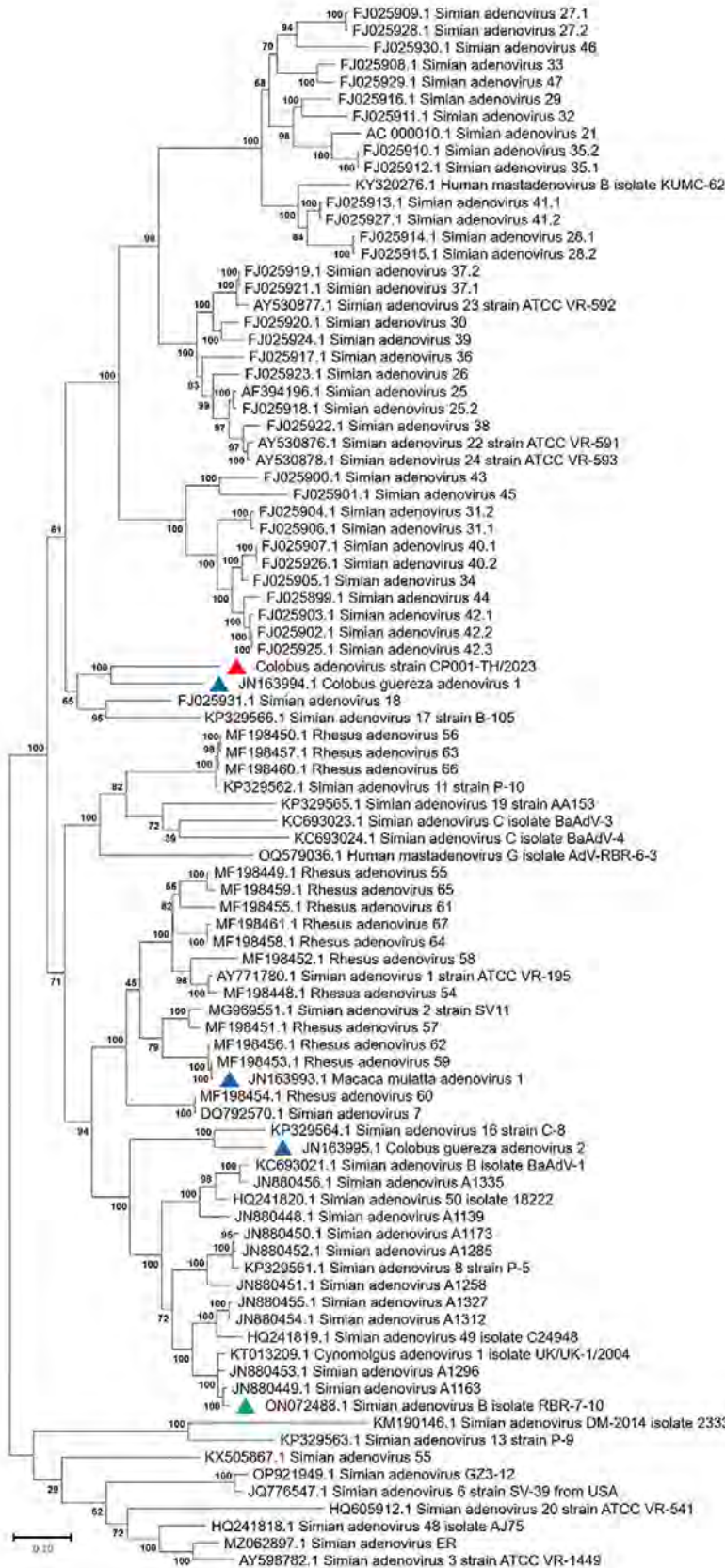
Figure 6. Phylogenetic analysis of amino acid sequences of *hexon* gene of novel mastadenovirus infection causing pneumonia in imported black-and-white colobuses (*Colobus guereza*), Thailand. Comparative analysis of the genome from this study, tentatively name colobus adenovirus (CoAdV), with various adenoviruses identified in nonhuman primates. Bootstrap values are shown at each node. Red triangle indicates the CoAdV CP001 TH/2023 identified in this study; blue triangles indicate AdVs previously identified in colobuses in Germany in 2011; green triangle indicates previously identified adenovirus isolated from macaques in Thailand. GenBank accession numbers are provided. Scale bar indicates the number of substitutions per site. AdV, adenovirus; BaAdV, baboon adenovirus.
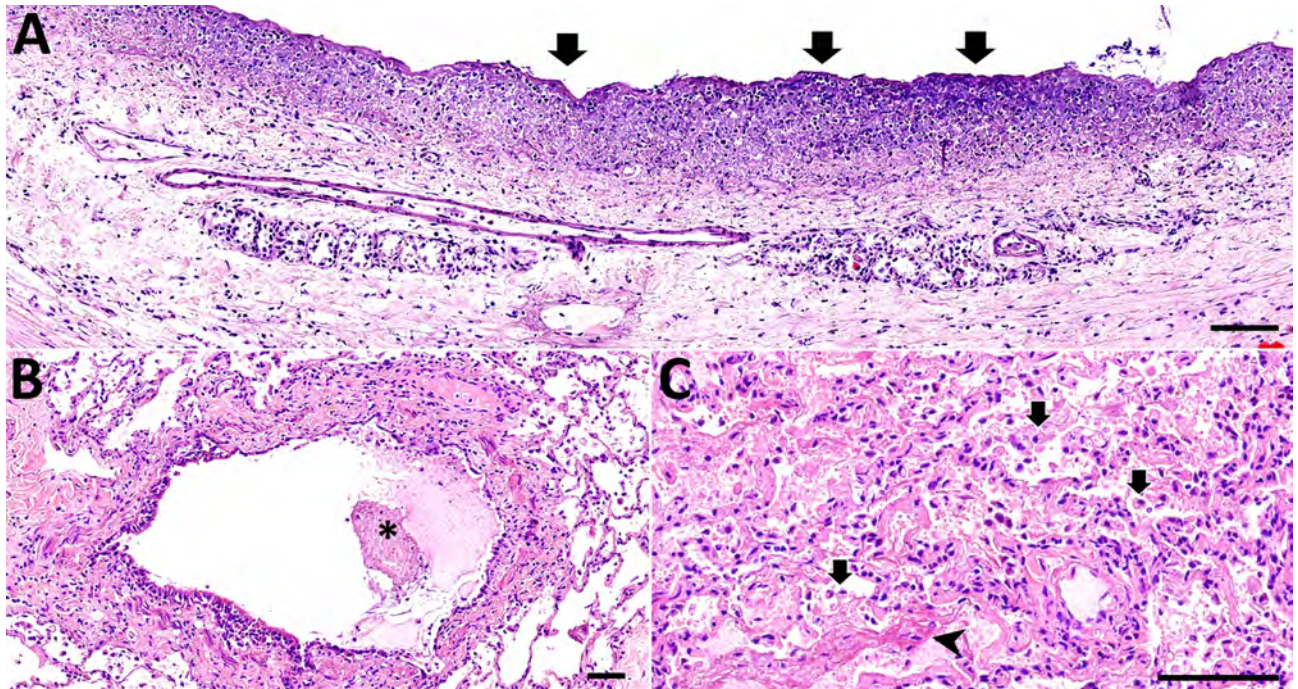
Figure 7. Hematoxylin and eosin–stained tissue samples from colobus 1 in an investigation of novel mastadenovirus infection causing pneumonia in imported black-and-white colobuses (*Colobus guereza*), Thailand. A) Trachea showing mucosa is extensively replaced by laminated bands of fibrillar material (arrows) intermixed with aggregates of karyorrhectic debris and degenerated neutrophils. B) Lung section showing lumen of the bronchial airways; flocculent mats of fibrin (asterisk) and neutrophils can be seen. C) Lung section showing alveoli filled with foamy macrophages (arrows), polymorphonuclear cells and eosinophilic material (arrowhead); alveolar capillaries are markedly engorged. Scale bars indicate 100 µm.

tissue localization, which revealed prominent positive immunoreactivity in the nuclei of bronchial epithelial cells (Figure 8, panel A), pulmonary alveolar macrophages, and endothelial cells of pulmonary capillaries (Figure 8, panel B). We also found local immunolabelling in the mucosal epithelial cells and glands of the trachea, particularly in areas that had pseudodiphtheritic membrane of necrosis (Figure 8, panel C). We identified IHC labeling in the small intestine (Figure 8, panel D) and in single lymphoid cells in mediastinal lymph node and tonsil.

Viral Culture

We successfully isolated CoAdV from fecal and oral swab samples of colobus nos. 6, 7, and 9 and from homogenized trachea and lung tissues of colobus no. 1. However, cell cultures inoculated with samples from colobuses 4 and 5 exhibited severe cytotoxicity, characterized by cell detachment and cell death at the first day postinoculation (dpi), leading us to discard those inoculations. Infected Vero cells revealed nonsyncytia, round-shaped CPE (Figure 9). The CPE first appeared at 3 dpi, characterized by cell rounding and detachment observed by 5 dpi. Subsequent infection of Vero cells with the supernatant from the primary virus

isolation also resulted in similar CPE formation at 3 dpi. Conventional PCR confirmed the presence of CoAdV DNA in the infected cell culture supernatants. Sanger sequencing of the partial *DNApol* gene from cellular supernatant identified partial CoAdV sequences. We did not detect CoAdV DNA in mock-infected cells.

In Situ Ultrastructure of CoAdV

Ultrastructural investigation of CoAdV-infected FFPE sections revealed pulmonary cellular damage by exhibiting rupture of cellular membrane, cytoplasmic vacuolization, and degenerated nuclear compartments. Within intact cells, condensed nuclear membrane contained various sizes of large cytoplasmic vacuolization containing numerous icosahedral electron-dense particles, each ≈80 nm in diameter, characteristic of adenoviruses (Figure 10, panel A). We considered those particles, typically seen attached near ruptured nuclear membranes or distributed randomly within the cytosol (Figure 10, panels B–D), of viral origin. Transmission electron microscopy analysis of CoAdV-infected Vero cells at 1 dpi showed prominent nuclear chromatin with early detection of viral virion within the nucleus (Figure 11, panel A). We also noted vesicles containing 80–90 nm icosahedral
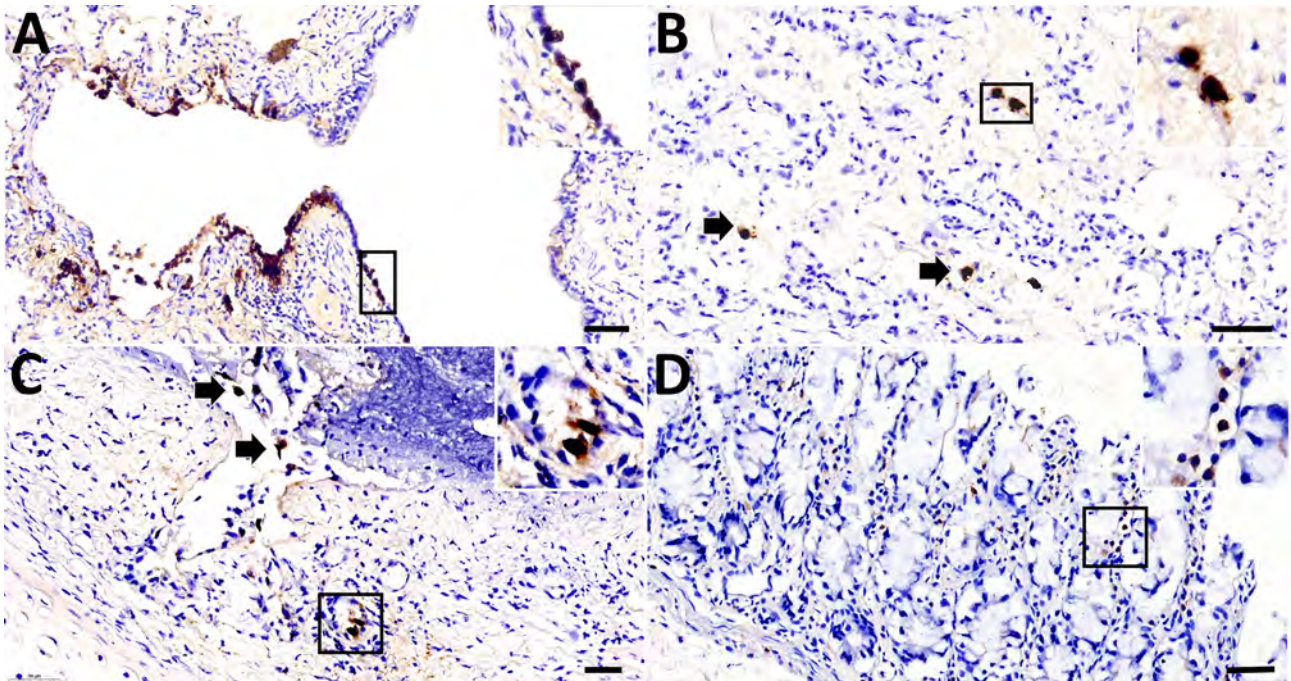
Figure 8. Adenoviral immunohistochemically stained lung and intestine sections from case 1 in an investigation novel mastadenovirus infection causing pneumonia in imported black-and-white colobuses (*Colobus guereza*), Thailand. A–C) Lung sections; D) intestine section. A) Nuclear labeling of adenoviral antigen in the bronchial epithelial lining; inset shows area of interest at 400 × magnification. B) Adenoviral antigen is localized in the nuclei of pulmonary epithelial cells (arrows); inset shows endothelial-like cells from area of interest at 400 × magnification. C) Infiltrated inflammatory cells and bronchial glands of the trachea (arrows); inset shows inflammatory cells at 400 × magnification. D) Adenoviral antigen detected in rare, single inflammatory cells infiltrating the intestinal villi; inset shows area of interest at 400 × magnification. Scale bars indicate 50 μm.

electron-dense or electron-lucent particles. We found cytoplasmic vacuolization and disruption of nuclear membranes in infected Vero cells at 5 dpi. We frequently observed numerous electron-dense particles in the cytosol. Virions were scattered throughout the cytosol and found within the endoplasmic reticulum or Golgi apparatus (Figure 11, panel B). In some infected cells, we observed mature virions fused with the cellular membrane being released into the extra-cellular space or passively through ruptured plasma membranes (Figure 11 panels C, D).

Retrospective Study

We detected CoAdV nucleic acid in 4 oral and 2 rectal swab samples collected and archived from 4 of 7 colobuses that were imported into Thailand, exhibited respiratory distress, and were submitted for postmortem investigation during 2020–2022. Phylogenetic
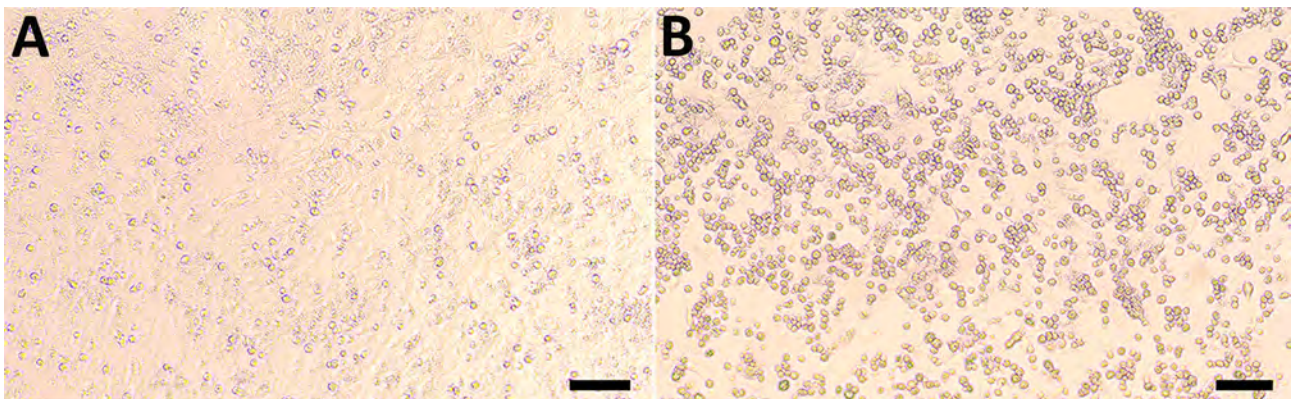

Figure 9. Vero cell isolation of novel mastadenovirus infection causing pneumonia in imported black-and-white colobuses (*Colobus guereza*), Thailand. Over 80% confluence of Vero cells were used for CoAdV isolation. A) Mock-infected cells. B) CoAdV-infected Vero cells at 5 days postinfection; clear cytopathic effects can be seen, characterized by cell rounding and detachment. Scale bars indicate 100 μm.

Figure 10. Transmission electron microscopy of formalin-fixed paraffin embedded lung section of case 1 in an investigation of novel mastadenovirus infection causing pneumonia in imported black-and-white colobuses (*Colobus guereza*), Thailand. A) Destructed bronchial epithelial cell showing degenerated plasma membrane and a large cytoplasmic vacuole containing electron-dense particles (inset area of interest at 100 × magnification). N indicates nuclear membrane. Scale bar indicates 200 nm. B) Random viral particles distributed in cytosol; viral particles are seen near ruptured nuclear (N) membrane (inset area of interest at 100× magnification). Scale bar indicates 100 nm. C) Mature icosahedral electron-dense viral particles in the cytosol. Black arrows indicate plasma membrane. Scale bar indicates 100 nm. D) A vacuole containing electron-lucent particle and a free-living electron-dense particle in the cytosol. Scale bar indicates 100 nm.
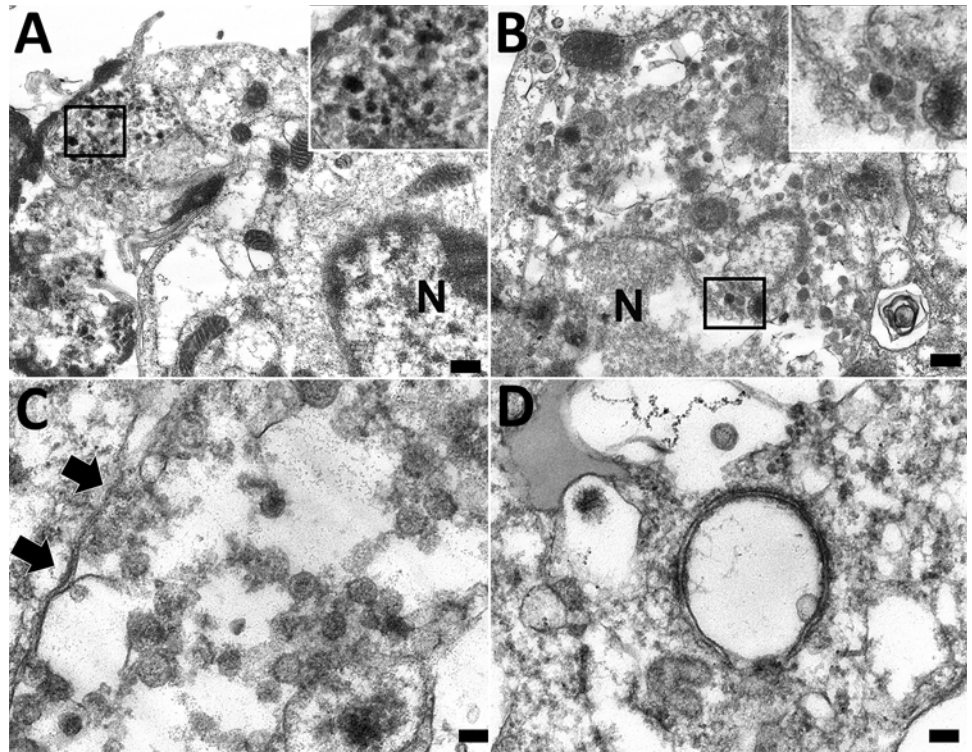
analysis of obtained sequences revealed that the sequences clustered together and were closely related to the CoAdV identified in this study (Appendix Figure). Investigation of archival samples derived from various other simian species were negative.

Discussion

Using conventional PCR targeting the conserved *DNApol* gene of adenoviruses, we identified a novel mastadenovirus, CoAdV, in multiple black-and-white colobuses, a species currently listed as decreasing in population (*24*). Identification of this virus was associated with a fatal outbreak of respiratory disease. We propagated CoAdV in Vero cells and confirmed the virus via PCR and ultrastructural investigation. qPCR quantified viral loads in various organs, and immunohistochemistry and transmission electron microscopy revealed virus localization in tracheal epithelium and pulmonary parenchyma, associated with pneumonia.

We successfully isolated CoAdV and characterized its complete genome sequence. Subsequent tissue analysis revealed that CoAdV infection was linked to respiratory lesions. Detection of CoAdV DNA and its localization in tissues with lesions suggests a major disease burden. Moreover, the identification of CoAdV in colobuses within the same household may indicate the virus' contagious nature. Therefore, CoAdV infection should be considered a concern when pneumonia occurs in this species.

Adenovirus infection in colobuses has been reported previously (*9*), but no information regarding clinical relevance was provided in those cases, and only the partial *hexon* gene was characterized. Although phylogenetic analysis of the *hexon* gene revealed that our CoAdV CP001-TH/2023 is genetically close to *Colobus guereza* adenovirus 1 (GenBank accession no. JN163994), the virus we detected still exhibits diversity and shares less genomic and amino acid similarity with that virus.

Infection associated with fatal outcomes in these colobuses cannot be definitively concluded without conducting animal challenge studies. The clinical severity of adenovirus infection in NHPs varies and often is associated with fatal diseases when infecting immunocompromised subjects (*4*). Although metagenomic studies in the fatal CoAdV cases we report did not indicate other underlying viral infection and results of ancillary testing were negative, the severe clinical outcomes observed suggest a potential role for stress-induced reactivation of a latent virus in the colobuses, exacerbated by transportation stress and possibly inadequate quarantine measures. In addition,

Figure 11. Transmission electron microscopy of Vero cell of case 1 in an investigation of novel mastadenovirus infection causing pneumonia in imported black-and-white colobuses (*Colobus guereza*), Thailand. A) Vero cells 1 day postinfection; B–C) Vero cells at 5 days postinfection A) Cytoplasmic vacuolated Vero cell contains numerous electron-dense particles packed within a destructed nucleus. Inset indicates the overall cellular morphology of an infected cell, and asterisk within indicates the area of higher magnification. Scale bar indicates 400 nm. B) Viral particles arranged within the cytosol as freely-distributed and clustered patterns (black arrows). M indicates mitochondria; N indicates nucleus. Scale bar indicates 300 nm. C) Electron-lucent viral particles within nuclear membrane and fused nuclear membrane (black arrows); electron-dense particles (white arrows) are seen within the endoplasmic reticulum (ER). Scale bar indicates 100 nm. D) A viral particle fused with plasma membrane (black arrow) and the budding virions (white arrow) in extracellular space. Scale bar indicates 100 nm.
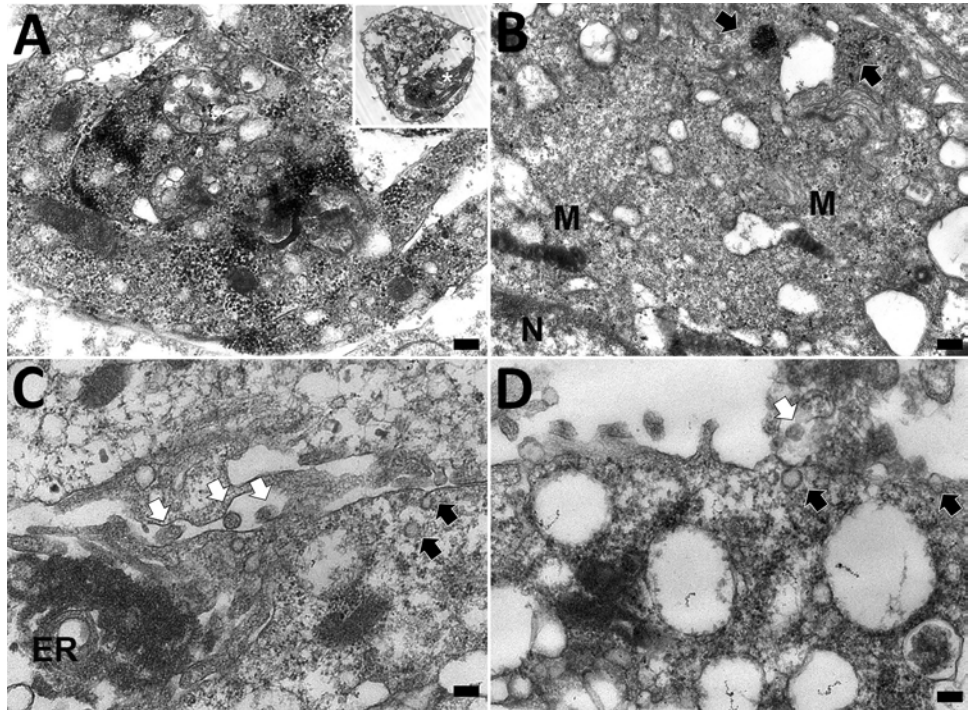
the widespread severity of the illnesses raises the possibility that CoAdV might have originated from another animal source and was not native to this species. Although our phylogenetic analysis did not confirm direct links to viruses in related hosts, the adaptability of adenoviruses across species barriers supports that hypothesis (*6,7,10,11*).

To determine whether CoAdV is circulating or originating in Thailand, we made further attempts to investigate CoAdV infection in other NHPs; however, we could not identify this virus in samples from other NHPs, except in other colobuses that had respiratory problems or diarrhea. Further studies are needed to assess whether CoAdV is host-restricted because the infection appears potentially limited to colobuses. Detection of CoAdV in archival samples suggests the possibility of longstanding circulation within the colobus population. Supporting previous publications (*2,25*), the adenovirus identified in the colobuses was not genetically related to previously described adenoviruses in free-ranging macaques in Thailand. However, because we only investigated a small number of samples, definitive conclusions cannot be drawn. Future investigations incorporating serologic surveys could provide a more comprehensive assessment of the virus' prevalence and transmission patterns. Such studies would be particularly valuable for determin-

ing whether CoAdV is circulating endemically or was recently introduced into Thailand. Because samples from close contact humans have not been investigated, the potential harmful effects of CoAdV infection to humans cannot be extrapolated. Reports of SAdV infection in non–natural hosts and humans, and subsequent transmission to other contracts (*6*), highlight the zoonotic transmission risk. Therefore, the spillover of CoAdV to susceptible hosts, including humans, should not be overlooked.

The CoAdV genome contains 32 putative coding sequences, including unique genes such as *V* and *IX*, and the *E1*, *E3*, and *E4* regions that are specific to the *Mastadenovirus* genus (*1*). CoAdV also has a single *fiber* gene, which is uncommon in related viruses. The <85% amino acid identity to its closest relative, SAdV-6 strain SV-39, and its identification in a new host support classifying CoAdV as a distinct species. Thus, we propose the virus as SAdV-J on the basis of species demarcation.

CoAdV phylogenetically clustered with most mastadenoviruses found in old-world monkeys, confirming unique clusters of adenoviruses within the Cercopithecidae family. Phylogenetic analysis of *DNApol* gene revealed that CoAdV shares genetic similarity with SAdV strain 55, identified in an endangered golden sub-nosed monkey (*Rhinopithecus*

roxellana) in China, suggesting that CoAdV may have co-evolved with that viral SAdV species. Although the partial *hexon* gene of adenoviruses identified in colobuses in Germany was reported (*9*), our phylogenetic analysis of the *hexon* gene indicated that Co-AdV is not related to those former strains. Given the unique phylogenic topology of CoAdV and the fact that interspecies recombination of mastadenoviruses has been previously reported (*8,9*), we investigated the potential recombination events. However, we did not identify any recombination breakpoints within the CoAdV genome. Although we successfully characterized a complete genome sequence of CoAdV, we acknowledge that the genomic analysis was limited to that single sequence. Future studies should aim to include multiple genome sequences to enhance our understanding of the genetic diversity and epidemiology of CoAdV.

Colobuses, native to Africa, are now experiencing a population decline (*24*). Despite extensive efforts to protect this species from becoming endangered, Co-AdV infection causing fatal disease poses a possible threat. The transmission of CoAdV to native monkeys has not been elucidated, and the natural host of this virus remains unidentified, although imported infected reservoirs may spread the infection.

In conclusion, our study demonstrates infection with a novel virus, CoAdV, associated with respiratory disease in imported black-and-white colobuses and describes the isolation and characterization of this virus. CoAdV was identified in all colobus contacts, indicating its transmissibility. Genetic analysis of the isolated virus revealed that CoAdV is distantly related to other previously described SAdVs and appears to be a novel species in the genus *Mastadenovirus.* Although we did not find CoAdV in retrospective samples obtained from other NHPs, the potential for infection in NHPs and humans remains unclear. Further studies are needed to determine the virus' role in disease development and host diversity. Extensive AdV surveillance in various animal species is crucial for elucidating the origins and spread of CoAdV in colobuses.

Acknowledgments

About the Author

Dr. Piewbang is a senior postdoctoral fellow at the Department of Pathology, Faculty of Veterinary Science, Chulalongkorn University, Bangkok, Thailand. His research interests include virus discovery, emerging and re-emerging infections, cross-species transmission, and viral evolution.

References

1. Benkő M, Aoki K, Arnberg N, Davison AJ, Echavarría M, Hess M, et al.; ICTV Report Consortium. ICTV virus taxonomy profile: *Adenoviridae* 2022. J Gen Virol. 2022;103:001721. https://doi.org/10.1099/jgv.0.001721

2. Kosoltanapiwat N, Tongshoob J, Ampawong S, Reamtong O, Prasittichai L, Yindee M, et al. Simian adenoviruses: molecular and serological survey in monkeys and humans in Thailand. One Health. 2022;15:100434. https://doi.org/10.1016/j.onehlt.2022.100434

3. Wachtman LM, Mansfield KG. Opportunistic infections in immunologically compromised nonhuman primates. ILAR J. 2008;49:191–208. https://doi.org/10.1093/ilar.49.2.191

4. Rogers DL, Ruiz JC, Baze WB, McClure GB, Smith C, Urbanowski R, et al. Epidemiological and molecular characterization of a novel adenovirus of squirrel monkeys after fatal infection during immunosuppression. Microb Genom. 2020;6:mgen000395. https://doi.org/10.1099/mgen.0.000395

5. Chiu CY, Yagi S, Lu X, Yu G, Chen EC, Liu M, et al. A novel adenovirus species associated with an acute respiratory outbreak in a baboon colony and evidence of coincident human infection. MBio. 2013;4:e00084-13. https://doi.org/10.1128/mBio.00084-13

6. Chen EC, Yagi S, Kelly KR, Mendoza SP, Maninger N, Rosenthal A, et al. Cross-species transmission of a novel adenovirus associated with a fulminant pneumonia outbreak in a new world monkey colony. PLoS Pathog. 2011; 7:e1002155. https://doi.org/10.1371/journal.ppat.1002155

7. Medkour H, Amona I, Akiana J, Davoust B, Bitam I, Levasseur A, et al. Adenovirus infections in African humans and wild non-human primates: great diversity and cross-species transmission. Viruses. 2020;12:657. https://doi.org/10.3390/v12060657

8. Tan B, Wu LJ, Yang XL, Li B, Zhang W, Lei YS, et al. Isolation and characterization of adenoviruses infecting endangered golden snub-nosed monkeys (*Rhinopithecus roxellana*). Virol J. 2016;13:190. https://doi.org/10.1186/s12985-016-0648-6

9. Wevers D, Metzger S, Babweteera F, Bieberbach M, Boesch C, Cameron K, et al. Novel adenoviruses in wild primates: a high level of genetic diversity and evidence of zoonotic transmissions. J Virol. 2011;85:10774–84. https://doi.org/10.1128/JVI.00810-11

10. Hoppe E, Pauly M, Gillespie TR, Akoua-Koffi C, Hohmann G, Fruth B, et al. Multiple cross-species transmission events of human adenoviruses (HAdV) during hominine evolution. Mol Biol Evol. 2015;32:2072–84. https://doi.org/10.1093/molbev/msv090

11. Needle DB, Selig MK, Jackson KA, Delwart E, Tighe E, Leib SL, et al. Fatal bronchopneumonia caused by skunk adenovirus 1 in an African pygmy hedgehog. J Vet Diagn Invest. 2019;31:103–6. https://doi.org/10.1177/1040638718812123

12. Balboni A, Verin R, Morandi F, Poli A, Prosperi S, Battilani M. Molecular epidemiology of canine adenovirus type 1 and type 2 in free-ranging red foxes (*Vulpes vulpes)* in Italy. Vet Microbiol. 2013;162:551–7. https://doi.org/10.1016/j.vetmic.2012.11.015

13. Borkenhagen LK, Fieldhouse JK, Seto D, Gray GC. Are adenoviruses zoonotic? A systematic review of the evidence. Emerg Microbes Infect. 2019;8:1679–87. https://doi.org/10.1080/22221751.2019.1690953

14. Ni Q, Wang Y, Weldon A, Xie M, Xu H, Yao Y, et al. Conservation implications of primate trade in China over 18 years based on web news reports of confiscations. PeerJ. 2018;6:e6069. https://doi.org/10.7717/peerj.6069

15. Nekaris KAI, Bergin D. Primate trade (Asia). In: Fuentes A, editor. The international encyclopedia of primatology. Hoboken (NJ, USA): John Wiley & Sons; 2017. p. 1–8.

16. VanDevanter DR, Warrener P, Bennett L, Schultz ER, Coulter S, Garber RL, et al. Detection and analysis of diverse herpesviral species by consensus primer PCR. J Clin Microbiol. 1996;34:1666–71. https://doi.org/10.1128/jcm.34.7.1666-1671.1996

17. Tong S, Chern SW, Li Y, Pallansch MA, Anderson LJ. Sensitive and broadly reactive reverse transcription-PCR assays to detect novel paramyxoviruses. J Clin Microbiol. 2008;46:2652–8. https://doi.org/10.1128/JCM.00192-08

18. Mochizuki M, Horiuchi M, Hiragi H, San Gabriel MC, Yasuda N, Uno T. Isolation of canine parvovirus from a cat manifesting clinical signs of feline panleukopenia. J Clin Microbiol. 1996;34:2101–5. https://doi.org/10.1128/jcm.34.9.2101-2105.1996

19. Tong S, Li Y, Rivailler P, Conrardy C, Castillo DA, Chen LM, et al. A distinct lineage of influenza A virus from bats. Proc Natl Acad Sci U S A. 2012;109:4269–74. https://doi.org/10.1073/pnas.1116200109

20. Hwa CZR, Tsai SP, Yee JL, Van Rompay KK, Roberts JA. Evidence of simian retrovirus type D by polymerase chain reaction. J Med Primatol. 2017;46:79–86. https://doi.org/10.1111/jmp.12266

21. Wellehan JF, Johnson AJ, Harrach B, Benkö M, Pessier AP, Johnson CM, et al. Detection and analysis of six lizard adenoviruses by consensus primer PCR provides further evidence of a reptilian origin for the atadenoviruses. J Virol. 2004;78:13366–9. https://doi.org/10.1128/JVI.78.23.13366-13369.2004

22. Crawford-Miksza LK, Nang RN, Schnurr DP. Strain variation in adenovirus serotypes 4 and 7a causing acute respiratory disease. J Clin Microbiol. 1999;37:1107–12. https://doi.org/10.1128/JCM.37.4.1107-1112.1999

23. Poonsin P, Wiwatvisawakorn V, Chansaenroj J, Poovorawan Y, Piewbang C, Techangamsuwan S. Canine respiratory coronavirus in Thailand undergoes mutation and evidences a potential putative parent for genetic recombination. Microbiol Spectr. 2023;11:e0226823. https://doi.org/10.1128/spectrum.02268-23

24. de Jong YA, Butynski TM, Oates JF. *Colobus guereza.* In: International Union for Conservation of Nature and Natural Resources, editor. The IUCN Red List of threatened species 2019 [cited 2024 Jun 16]. https://dx.doi.org/10.2305/IUCN.UK.2019-3.RLTS.T5143A17944705.en

25. Kosoltanapiwat N, van der Hoek L, Kinsella CM, Tongshoob J, Prasittichai L, Klein M, et al. A novel simian adenovirus associating with human adeno-virus species G isolated from long-tailed macaque feces. Viruses. 2023;15:1371. https://doi.org/10.3390/v15061371

Address for correspondence: Somporn Techangamsuwan, Department of Pathology, Faculty of Veterinary Science, Chulalongkorn University, Pathumwan, Bangkok 10330, Thailand; email: somporn62@hotmail.com

Effect of Sexual Partnerships on Zika Virus Transmission in Virus-Endemic Region, Northeast Brazil

Tereza Magalhaes,[1] Flávio Codeço Coelho,[1] Wayner V. Souza, Isabelle F.T. Viana,
Thomas Jaenisch, Ernesto T.A. Marques, Brian D. Foy, Cynthia Braga

The epidemiologic effects of Zika virus (ZIKV) sexual transmission in virus-endemic countries remain unclear. We conducted a 2-level, linear mixed-effects logistic regression analysis by using a recently acquired population-based ZIKV and chikungunya virus (CHIKV) serologic dataset obtained from persons residing in Northeast Brazil (n = 2,070 participants). We adjusted mathematical models for housing type and age of participants; the models indicated a significantly higher likelihood of ZIKV seropositivity among persons engaged in a sexual relationship within the same household (odds ratio 1.25 [95% CI 1.00–1.55]; p = 0.047), regardless of their partner's ZIKV serostatus, and among participants with a ZIKV-seropositive sex partner within the same household (odds ratio 1.54 [95% CI 1.18–2.01]; p = 0.002). CHIKV was also modeled as a control; no sex-associated effects were observed for CHIKV serology. Inclusion of ZIKV sexual transmission in prevention and control strategies is urgently needed, particularly in ZIKV-endemic regions.

In the mid-2010s, Zika virus (ZIKV) emerged as a global health threat despite its discovery in Uganda >6 decades earlier. After spreading across the islands of the South Pacific, the virus reached the Americas in 2013–2014, rapidly infecting >100 million persons during a 2015–2017 pandemic (1). The pandemic was a source for new information on ZIKV pathogenesis, including its potential to induce severe neurologic conditions, such as Guillain-Barré syndrome and congenital Zika syndrome (CZS) (2). It has been hypothesized that the primary mode of ZIKV transmission is through the bite of infected *Aedes* spp. mosquitoes (vector transmission). However, the virus can also be transmitted from mother to fetus through the placenta, potentially leading to CZS, and between persons via sexual intercourse (2,3).

Although ZIKV sexual transmission is recognized by health authorities and the scientific community, determining its epidemiologic relevance and how it contributed to the explosive spread of the virus has proved challenging. The main difficulty lies in distinguishing whether ZIKV infection occurred through mosquito bites or sexual contact, especially in affected persons living in countries with intense mosquito transmission of the virus.

Three field studies have shed light on ZIKV sexual transmission in regions highly affected by the 2015–2017 ZIKV pandemic. The first study was conducted in Puerto Rico and included participants acutely infected with ZIKV and their household members (4). The findings indicated that pairs of persons within the study households engaging in sexual relationships had a higher risk for both persons being ZIKV positive by PCR than other household pairs. The second study, conducted in Northeast Brazil by our group (T.M., T.J., E.T.A.M, and B.D.F.) (5), used a household-based serosurvey and showed that, within households, persons reporting sexual relationships with ZIKV-seropositive index-participants were 3 times more likely to also be ZIKV-seropositive than those without a sexual relationship with the index person. In addition, persons belonging to a sex dyad within households were more likely to be ZIKV seroconcordant than pairs who had no sexual relationship. The same

Author affiliations: Texas A&M University, College Station, Texas, USA (T. Magalhaes); Fundação Getulio Vargas, Rio de Janeiro, Brazil (F.C. Coelho); Instituto Aggeu Magalhães-Fundação Oswaldo Cruz, Recife, Brazil (W.V. Souza, I.F.T. Viana, E.T.A. Marques, C. Braga); Colorado School of Public Health, Aurora, Colorado, USA (T. Jaenisch); Heidelberg University Hospital, Heidelberg, Germany (T. Jaenisch); University of Pittsburgh, Pittsburgh, Pennsylvania, USA (E.T.A. Marques); Colorado State University, Fort Collins, Colorado, USA (B.D. Foy)

[1]These authors contributed equally to this article.

serologic analysis was performed for chikungunya virus (CHIKV) and no associations between paired serologic data and sexual activity among the study participants were observed (*5*). That serosurvey recruited persons who had experienced acute febrile illness caused by arbovirus infection a few months before recruitment (thus, not acutely infected) along with their household members. The third study, also conducted in Northeast Brazil, reported that men residing in a low socioeconomic area and engaging in risky sexual behaviors were more likely to be seropositive for ZIKV than men who did not report risky sexual behaviors (*6*). Those 3 studies provide valuable data supporting sexual activity as a risk factor for ZIKV infection in countries that have intense mosquito transmission; however, factors, such as selection bias (e.g., choosing households on the basis of persons with symptomatic disease) (*5*) and relatively low numbers of participants (*4–6*), limit the generalizability of those findings.

Mathematical models have also been used to estimate the contribution of ZIKV sexual transmission in Zika epidemiology in regions affected by epidemics. In most cases, studies used national datasets of notified ZIKV cases in affected countries, such as Brazil and Colombia. Although some models have indicated minimal contribution of sexual transmission to ZIKV epidemics (*7–9*), the models that considered the synergistic effects of both mosquito and sexual transmission and heterogeneity of sexual relationships have indicated a more substantial role for sex in ZIKV infections overall (*10–13*). However, studies relying on official case notifications might be biased for several reasons. In particular, notified cases do not accurately represent the actual number of affected persons because of underreporting or misdiagnosis. Moreover, biases in gender-based healthcare seeking need to be considered when interpreting data from official notified cases.

We conducted a population- and household-based ZIKV seroprevalence study in an urban center in Northeast Brazil ≈3 years after ZIKV was introduced in the region (*14*); that serosurvey assessed past exposure to ZIKV and other arboviruses among residents of an arbovirus-hyperendemic region, ensuring representative demographic, socioeconomic, and spatial coverage. Using a large dataset obtained from that study (*14*), we performed a secondary analysis of the effect of sexual relationships on ZIKV transmission. The Institutional Review Board of Instituto Aggeu Magalhães approved the original study (protocol/Certificado de Apresentação de Apreciação Ética no. 79605717.9.0000.5190). We used the existing dataset and remained within the scope of the original study aims; thus, no additional approval for the secondary data analysis was required.

Methods

Primary Data Source

We conducted a stratified multistage cluster sampling survey to estimate the seroprevalence of ZIKV, CHIKV, and dengue virus (DENV) in residents of the city of Recife, Brazil, who were 5–65 years of age during August 2018–February 2019 (*14*). Recife, the capital of the state of Pernambuco, has an area of 218.8 km² and a population of ≈1.5 million persons (*15*). Successive arbovirus outbreaks have been registered in the city since the introduction of DENV in the 1980s (*16–18*). After the surge of ZIKV cases in Brazil in 2015, Recife was a hotspot for microcephaly cases in babies associated with ZIKV infection (*19*).

The methods used for the original serosurvey have been previously described (*14*). In brief, we divided the population sample into high, intermediate, and low socioeconomic strata. We used a 2-stage sampling approach involving the random selection of census tracts followed by selection of households. All residents who were within the study age range (5–65 years) in the selected households were eligible to participate in the survey. Of the 2,691 eligible participants, we obtained ZIKV, DENV, and CHIKV serologic data for 2,070 persons; 480 persons were in the high, 815 in the intermediate, and 775 in the low socioeconomic stratum. We included a total of 899 households in the study. We collected individual and household data through interviews performed during home visits by using standardized questionnaires. In addition to collecting sociodemographic data and documenting clinical manifestations of arbovirus infections, we questioned participants about having had a fixed sex partner within the past 4 years. If the response was affirmative, they were then asked whether the sex partner resided in the same household. If the sex partner lived in the same house, study participants were prompted to specify which resident was their partner. After the interview, we collected a venous blood sample from each participant.

We used commercially available or in-house ELISAs to detect ZIKV and CHIKV immunoglobulins (IgG, IgG3, and IgM) in serum samples, as previously described (*14*). Assay sensitivities and specificities and IgG, IgG3, and IgM seroprevalence rates were

determined as previously described (*14*). In addition, a subset of randomly selected serum samples was assayed by using a plaque reduction neutralization assay to further validate ZIKV IgG data.

We used raw serologic data for ZIKV (IgG and IgG3) and CHIKV (IgG and IgM) and the associated variables of interest obtained in the serosurvey (*14*) for the analyses described in this work. Because the DENV seroprevalence rate found in the survey was high, which was expected, we did not include DENV data in the analyses.

Data Analysis

We modeled the odds of testing positive for ZIKV in response to risk factors related to vector and sexual transmission by using a hierarchical 2-level linear mixed effects logistic regression (Appendix Figure, https://wwwnc.cdc.gov/EID/article/30/12/23-1733-App1.pdf). We considered having a sex partner (sexual transmission risk) and living with other ZIKV-seropositive participants (vector transmission risk) in the household as risk factors. Households formed the random intercept. We defined the binomial response variable by combining 2 diagnostic methods for each virus (tests for ZIKV IgG, ZIKV IgG3, CHIKV IgG, and CHIKV IgM) and assigned a positive status to persons who tested positive in ≥1 of the tests. We also investigated the effect of the residence type by adding another binary variable; a value of 1 was given for a person living in ground-

level housing and 0 for a person living in a multistory apartment building. We included a person's age in years in the model as a discrete variable. We calculated the odds ratio (OR) for age, which reflected the change in risk associated with each additional year of age. As a control, we used a model with the same structure to assess the odds of testing positive for CHIKV using the participants' CHIKV serostatus. We reported ORs and 95% CIs for all risk factors included in the model. We interpreted OR values >1 as an increased probability of testing positive for ZIKV or CHIKV for each specific risk factor. We calculated p values according to a null hypothesis of OR = 1 and set the statistical significance threshold at 0.05. We estimated the models by using the lme4 package in R (The R Project for Statistical Computing, https://www.r-project.org).

Results

Among the 2,070 study participants that had ZIKV and CHIKV serologic data, 1,207 (58.3%) were women and 863 (41.7%) men. We determined the frequency distribution of the main characteristics of the study population categorized by sex partner status (Table 1). Of the 2,070 participants, 891 reported having a sex partner within the same household; 873 (98.0%) of those reported being heterosexual, and 18 (2.0%) homosexual (Table 1). Only 7 persons who reported having a sex partner within the household were <18 years of age; each was 17

Table 1. Characteristics of survey participants according to sexual partnership status in study of ZIKV transmission in virus-endemic region, Northeast Brazil*

Characteristics	No. (%) study participants
Participants with a fixed sex partner within the household	891
Housing type†	
Ground-level house	638 (71.6)
Multistory apartment	250 (28.4)
Age group, y	
<18	7 (0.8)
≥18	884 (99.2)
ZIKV serostatus of sex pairs‡	
Both partners positive	245 (27.5)
Discordant, 1 partner positive, 1 negative	256 (28.7)
Both partners negative	179 (20.1)
CHIKV serostatus of sex pairs‡	
Both partners positive	130 (14.6)
Discordant, 1 partner positive, 1 negative	215 (24.1)
Both partners negative	335 (37.6)
Participants with no sex partner within the household	1,179
Housing type	
Ground-level house	886 (75.4)
Multistory apartment	289 (24.6)
Age group, y	
<18	392 (33.4)
≥18	787 (66.6)

*CHIKV, chikungunya virus; ZIKV, Zika virus.
†Housing type was missing for 3 persons.
‡Data on sexual partners was incomplete for 211 persons, leading to their exclusion from the analyses of the effect of sexual partnership when accounting for the partner's ZIKV and CHIKV serostatus.

years of age. ZIKV and CHIKV serostatus data were missing for 211 partners of the 891 participants because of either refusal to have blood drawn or because they were absent during the home visit. As a result, those persons were excluded from the models that accounted for the sex partner's ZIKV and CHIKV serostatus. In the other models, all 2,070 participants were included.

In the ZIKV model, living in the same household with other persons who were ZIKV seropositive, regardless of whether they were sex partners, contributed significantly to the odds of testing positive for ZIKV (OR 1.47 [95% CI 1.17–1.84]; p<0.05) compared with living in a household with only seronegative persons. Having a sex partner within the household, irrespective of the partner's ZIKV serologic status, increased the odds of testing positive for ZIKV by 64% (OR 1.64 [95% CI 1.36–1.99]; p<0.0001) compared with participants who had no sex partner in the household. The odds of testing positive for ZIKV increased by 94% (OR 1.94 [95% CI 1.51–2.5]; p<0.0001) when the sex partner in the household was ZIKV-seropositive compared with participants who did not have a ZIKV-seropositive sex partner. In contrast, the odds of being ZIKV seropositive when the sex partner was seronegative for ZIKV was low, suggesting a potential protective effect, although this effect was not significant (OR 0.79 [95% CI 0.60–1.03]; p = 0.086).

The type of residence was significantly associated with the odds of testing positive for ZIKV; persons living in ground-level housing had ≈3 times higher odds of being seropositive than those living in a multistory apartment building (OR 2.94 [95% CI 2.25–3.84]; p<0.0001). In addition, we previously found that ZIKV seroprevalence differed among age groups, being lower in persons <15 years of age (14); therefore, we fitted a model to assess the effect of age on ZIKV seropositivity. The model showed a positive association between age and ZIKV exposure (OR 1.03 [95% CI 1.02–1.03]; p<0.0001), indicating the odds of testing positive for ZIKV increased by 3% with each additional year of age. Because of the significant effects of both housing type and age on ZIKV serostatus, we adjusted for those variables and reanalyzed the effects of living with other seropositive persons, having a sex partner in the household, or having a ZIKV-seropositive sex partner in the household as risk factors for ZIKV seropositivity. In adjusted models, sex partnerships within the household remained a significant risk factor for ZIKV exposure (Table 2). The heterogeneity of households accounted for 6% variation in the odds of being ZIKV seropositive after controlling for the factors included in the model.

We fitted a separate model using the same structure for CHIKV serologic data to serve as a control. In the CHIKV model, living with other CHIKV-seropositive persons, regardless of whether they were sex partners, contributed significantly to the odds of testing positive for CHIKV (OR 2.59 [95% CI 1.94–3.46]; p<0.0001). Having a sex partner within the household did not contribute significantly to the odds of testing positive for CHIKV (OR 1.13 [95% CI 0.94–1.36]; p = 0.2). Similarly, having a CHIKV-seropositive partner in the household did not significantly contribute to the odds of being CHIKV seropositive (OR 1.29 [95% CI 0.97–1.74]; p = 0.09). Having a CHIKV-seronegative partner decreased the odds of testing positive for CHIKV (OR

Table 2. Associations between sex partnership status within households and ZIKV or CHIKV seropositivity in study of ZIKV transmission in virus-endemic region, Northeast Brazil*

Exposure variables	Odds ratio (95% CI)	p value
ZIKV		
Age†	1.03 (1.02–1.03)	<0.0001
Housing type, ground level versus multistory apartment‡	3.25 (2.54–4.12)	<0.0001
Living with >1 ZIKV-seropositive person§	1.46 (1.13–1.88)	0.003
Sex partner in the household§	1.25 (1.00–1.55)	0.047
ZIKV-seropositive sex partner in the household§	1.54 (1.18–2.01)	0.002
ZIKV-seronegative sex partner in the household§	0.70 (0.52–0.94)	0.018
CHIKV		
Age†	1.01 (1.00–1.01)	0.005
Housing type, ground level versus multistory apartment‡	4.67 (3.28–6.65)	<0.0001
Living with >1 CHIKV-seropositive person§	2.84 (2.24–3.60)	<0.0001
Sex partner in the household§	1.05 (0.80–1.36)	0.739
CHIKV-seropositive sex partner in the household§	1.21 (0.82–1.80)	0.343
CHIKV-seronegative sex partner in the household§	0.71 (0.51–0.98)	0.035

*Mixed-effects hierarchical linear regression model was used to determine associations. Data were from a population-based survey conducted in Northeast Brazil during 2018–2019 (14). Number of study participants was 2,070. CHIKV, chikungunya virus; ZIKV, Zika virus.
†Adjusted for housing type.
‡Adjusted for age.
§Adjusted for age and housing type.

0.69 [95% CI 0.54–0.89]; p = 0.004). The risk factor outcomes remained consistent in the CHIKV models adjusted for housing type and age (Table 2).

Discussion

The role of sexual transmission in ZIKV epidemiology remains poorly understood, especially in virus-endemic countries having high levels of vector transmission. In a previous index- and household-based serosurvey conducted in Recife, Northeast Brazil, we identified sexual relationships within households as a risk factor for ZIKV exposure (5). The most substantial effect of sexual activity in that study was observed when analyzing ZIKV-seropositive index cases, whereby the likelihood of being ZIKV seropositive was 3 times higher for sex partners of ZIKV-seropositive index persons than for non–sex partners of those index persons within a household. That sex effect was not observed for CHIKV, which is transmitted by the same vectors as ZIKV and circulated in the study region around the same time as ZIKV but is not known to be sexually transmitted. That work involved index participants who had experienced symptomatic arboviral disease a few months before enrollment, along with their household members (5). In this study, we assessed whether similar effects would be seen in a dataset from a recent large population-based serologic survey designed to ensure representative demographic, socioeconomic, and spatial coverage across a wider area within the same region (14). Apart from the differences in the datasets (population-based rather than analyzing previously symptomatic index cases), distinct types of models were used.

Residing in a household with a person who was ZIKV or CHIKV seropositive was significantly associated with an increased risk for exposure to the respective virus. This outcome was expected because it is known that populations of *Aedes aegypti* mosquitoes, the vector of ZIKV and CHIKV, tend to establish themselves within domestic and peridomestic environments in residential areas. After a mosquito population is established within those areas and virus circulates, all susceptible residents of a house would have the same risk for vector transmission of the virus, assuming random mosquito biting of the residents. To corroborate this assumption, in the stratified analysis according to housing type, we found that persons residing in ground-level housing were 3 times more likely to be ZIKV or CHIKV seropositive than were persons living in multistory apartments. Efficient household transmission of arboviruses in

areas with ground-level housing has been documented (5,20–24) and points to those houses being more easily infested with *Ae. aegypti* mosquitoes, likely because of mosquito species behavior and their proximity to more open-air water containers that can serve as breeding sites.

A critical finding from this study was that, in the models adjusted for housing type and age, having an active sex partner within a household increased the risk for ZIKV exposure by 25% and having a ZIKV-seropositive sex partner increased risk by 54%. Those findings corroborated our previous data (5) that showed a more robust association between increased risk for ZIKV infection and the sex partner's seropositivity, indicating a higher level of virus exposure through sex corresponds to a greater risk of infection. Because of the low number of homosexual pairs in the study population, we were unable to evaluate potential differential risks between heterosexual and homosexual pairs. The differences in risk factors between those groups should be evaluated in future studies.

Serosurveys are limited in their ability to determine the timing of virus infection because previous exposure (indicated by antibody detection) could have occurred at any timepoint. Moreover, establishing a causal link between ZIKV infection and sexual activity requires assessing the timing of both events. One study conducted in Puerto Rico (4) investigated persons acutely infected with ZIKV and their sexual activity in the days preceding infection; this type of study is less susceptible to timing bias, and, consequently, can indicate a more precise causal link between sexual activity and ZIKV infection, although still indirectly. The population in this study was naive to ZIKV and CHIKV until those viruses were introduced and rapidly spread in the region during 2015–2016. After those initial outbreaks, a sharp decline in ZIKV and CHIKV transmission was observed in the region (25). We conducted the serosurvey (14) when local transmission of both viruses was minimal, meaning the seropositive persons captured in that study were likely infected during the first transmission wave of ZIKV and CHIKV, thus limiting the timeframe of infection occurrence. The underlying assumption in this study was that participants with a fixed sex partner in the household over the 4 years preceding the serosurvey likely maintained regular sexual activity during the period of ZIKV circulation in the region.

Serosurveys can also be biased by cross-reactivity in serologic assays. In this study, cross-reaction between DENV and ZIKV antibodies could have led

to false positives. To minimize this cross-reactivity, we adjusted the cutoff value for the ZIKV ELISA according to well-characterized serum samples; however, some level of cross-reactivity likely still occurred. The residual cross-reactivity between ZIKV and DENV IgG might have slightly diluted the association between sexual partnership and ZIKV exposure, and a more specific test might reveal a stronger association. As previously described (5), the association between sexual partnership within households and ZIKV exposure was stronger when we used serologic data from plaque reduction neutralization tests than when we used IgG data from ELISAs. However, a potential higher-than-expected waning of ZIKV antibodies over time (26–29) could have resulted in some false negatives.

The central message from the population-level data is that sexual activity significantly contributes to ZIKV transmission at a household level in virus-endemic regions. This finding is supported by previous index-case research (5) and 2 other independent studies (4,6), including 1 involving persons acutely infected with ZIKV (4). Our findings also suggest that sexual transmission acts synergistically with vector transmission in ZIKV-endemic regions, but whether household transmission is more often initiated by a vector that then leads to sexual transmission in the household or vice versa remains unknown. Ultimately, the finding that increased risk for ZIKV exposure can be caused by sexual activity challenges the current belief that sexual transmission has minimal effect in ZIKV epidemiology, and transmission models should be recalibrated accordingly. This finding also emphasizes the need for health authorities and the scientific community to recognize ZIKV infection as a potential sexually transmitted disease. We advocate for the urgent inclusion of this transmission mode in ZIKV prevention and control strategies, particularly in virus-endemic countries. Although health authorities such as the World Health Organization and US Centers for Disease Control and Prevention have released official recommendations to prevent ZIKV sexual transmission (30,31), those recommendations have been primarily focused on travel-associated infections and CZS. However, sexual transmission should be considered in the broader context of ZIKV epidemiology because ZIKV infection can lead to different symptoms in an infected person. In addition, symptoms and long-term sequelae related to ZIKV-induced urogenital tract infections are not well understood, nor is the potential relationship between sexual transmission and CZS; both aspects warrant further investigation. For CZS, we strongly suggest including sexual behavior variables in Zika cohort studies, particularly in those studies conducting multivariable regression analyses on risk factors for congenital anomalies.

In conclusion, ZIKV transmission is associated with sexual activity. It is essential to consider gender and socio-economic factors within the context of ZIKV sexual transmission to develop appropriate prevention and control strategies. This need is particularly critical because ≈50% of the global female population have limited autonomy in determining their sexual and reproductive health and rights, as reported by the United Nations Population Fund (32). The involvement of male partners in prevention and control activities, for example, should be highly encouraged. Existing ZIKV control programs in virus-endemic countries, such as Brazil, that only focus on vector transmission are already biased against women, contributing to gender inequalities (33). Special attention should be given to populations at high risk of acquiring sexually transmitted infections, such as sex workers, when designing prevention and control strategies.

About the Author

Dr. Magalhaes is an assistant professor in the Department of Entomology at Texas A&M University. Her research interests focus on factors influencing transmission dynamics of mosquitoborne diseases and integrating laboratory experiments on mosquito-pathogen interactions with studies of human cohorts in disease-endemic regions.

References

1. Zhang Q, Sun K, Chinazzi M, Pastore Y Piontti A, Dean NE, Rojas DP, et al. Spread of Zika virus in the Americas. Proc Natl Acad Sci USA. 2017;114:E4334–43. https://doi.org/10.1073/pnas.1620161114
2. Pierson TC, Diamond MS. The emergence of Zika virus and its new clinical syndromes. Nature. 2018;560:573–81. https://doi.org/10.1038/s41586-018-0446-y
3. Magalhaes T, Foy BD, Marques ETA, Ebel GD, Weger-Lucarelli J. Mosquito-borne and sexual transmission of Zika virus: recent developments and future directions. Virus Res. 2018;254:1–9. https://doi.org/10.1016/j.virusres.2017.07.011
4. Rosenberg ES, Doyle K, Munoz-Jordan JL, Klein L, Adams L, Lozier M, et al. Prevalence and incidence of Zika virus infection among household contacts of patients with Zika virus disease, Puerto Rico, 2016–2017. J Infect Dis. 2019;220:932–9. https://doi.org/10.1093/infdis/jiy689
5. Magalhaes T, Morais CNL, Jacques IJAA, Azevedo EAN, Brito AM, Lima PV, et al. Follow-up household serosurvey in Northeast Brazil for Zika virus: sexual contacts of index patients have the highest risk for seropositivity. J Infect Dis. 2021;223:673–85. https://doi.org/10.1093/infdis/jiaa563
6. Aguilar Ticona JP, Baig H, Nery N, Doss-Gollin S, Sacramento GA, Adhikarla H, et al. Risk of sexually transmitted Zika virus in a cohort of economically disadvantaged urban residents. J Infect Dis. 2021;224:860–4. https://doi.org/10.1093/infdis/jiab001
7. Ferdousi T, Cohnstaedt LW, McVey DS, Scoglio CM. Understanding the survival of Zika virus in a vector interconnected sexual contact network. Sci Rep. 2019;9:7253. https://doi.org/10.1038/s41598-019-43651-3
8. Gao D, Lou Y, He D, Porco TC, Kuang Y, Chowell G, et al. Prevention and control of Zika as a mosquito-borne and sexually transmitted disease: a mathematical modeling analysis. Sci Rep. 2016;6:28070. https://doi.org/10.1038/srep28070
9. Maxian O, Neufeld A, Talis EJ, Childs LM, Blackwood JC. Zika virus dynamics: when does sexual transmission matter? Epidemics. 2017;21:48–55. https://doi.org/10.1016/j.epidem.2017.06.003
10. Cruz-Pacheco G, Esteva L, Ferreira CP. A mathematical analysis of Zika virus epidemic in Rio de Janeiro as a vector-borne and sexually transmitted disease. J Biol Syst. 2019;27:83–105. https://doi.org/10.1142/S0218339019500050
11. de Barros ACWG, Santos KG, Massad E, Coelho FC. Sex-specific asymmetrical attack rates in combined sex-ual-vectorial transmission epidemics. Microorganisms. 2019;7:112. https://doi.org/10.3390/microorganisms7040112
12. Olawoyin O, Kribs C. Effects of multiple transmission pathways on Zika dynamics. Infect Dis Model. 2018;3:331–44. https://doi.org/10.1016/j.idm.2018.11.003
13. Sasmal SK, Ghosh I, Huppert A, Chattopadhyay J. Modeling the spread of Zika virus in a stage-structured population: effect of sexual transmission. Bull Math Biol. 2018;80:3038–67. https://doi.org/10.1007/s11538-018-0510-7
14. Braga C, Martelli CMT, Souza WV, Luna CF, Albuquerque MFPM, Mariz CA, et al. Seroprevalence of dengue, chikungunya and Zika at the epicenter of the congenital microcephaly epidemic in Northeast Brazil: a population-based survey. PLoS Negl Trop Dis. 2023;17:e0011270. PubMed https://doi.org/10.1371/journal.pntd.0011270
15. Government of Brazil, Instituto Brasileiro de Geografia e Estatística. Overview of Recife, Pernambuco, Brazil, 2022 [cited 2023 Dec 6]. https://cidades.ibge.gov.br/brasil/pe/recife/panorama
16. Cordeiro MT, Schatzmayr HG, Nogueira RM, Oliveira VF, Melo WT, Carvalho EF. Dengue and dengue hemorrhagic fever in the state of Pernambuco, 1995–2006. Rev Soc Bras Med Trop. 2007;40:605–11. https://doi.org/10.1590/S0037-86822007000600001
17. Magalhaes T, Braga C, Cordeiro MT, Oliveira ALS, Castanha PMS, Maciel APR, et al. Zika virus displacement by a chikungunya outbreak in Recife, Brazil. PLoS Negl Trop Dis. 2017;11:e0006055. https://doi.org/10.1371/journal.pntd.0006055
18. Pessôa R, Patriota JV, Lourdes de Souza M, Felix AC, Mamede N, Sanabani SS. Investigation into an outbreak of dengue-like illness in Pernambuco, Brazil, revealed a cocirculation of Zika, chikungunya, and dengue virus type 1. Medicine (Baltimore). 2016;95:e3201. https://doi.org/10.1097/MD.0000000000003201
19. de Oliveira WK, de França GVA, Carmo EH, Duncan BB, de Souza Kuchenbecker R, Schmidt MI. Infection-related microcephaly after the 2015 and 2016 Zika virus outbreaks in Brazil: a surveillance-based analysis. Lancet. 2017;390:861–70. https://doi.org/10.1016/S0140-6736(17)31368-5
20. Braga C, Luna CF, Martelli CM, de Souza WV, Cordeiro MT, Alexander N, et al. Seroprevalence and risk factors for dengue infection in socio-economically distinct areas of Recife, Brazil. Acta Trop. 2010;113:234–40. https://doi.org/10.1016/j.actatropica.2009.10.021
21. Harrington LC, Scott TW, Lerdthusnee K, Coleman RC, Costero A, Clark GG, et al. Dispersal of the dengue vector *Aedes aegypti* within and between rural communities. Am J Trop Med Hyg. 2005;72:209–20. https://doi.org/10.4269/ajtmh.2005.72.209
22. Mammen MP, Pimgate C, Koenraadt CJM, Rothman AL, Aldstadt J, Nisalak A, et al. Spatial and temporal clustering of dengue virus transmission in Thai villages. PLoS Med. 2008;5:e205. https://doi.org/10.1371/journal.pmed.0050205
23. Stoddard ST, Forshey BM, Morrison AC, Paz-Soldan VA, Vazquez-Prokopec GM, Astete H, et al. House-to-house human movement drives dengue virus transmission. Proc Natl Acad Sci USA. 2013;110:994–9. https://doi.org/10.1073/pnas.1213349110
24. Yoon IK, Getis A, Aldstadt J, Rothman AL, Tannitisupawong D, Koenraadt CJM, et al. Fine scale spatiotemporal clustering of dengue virus transmission in children and *Aedes aegypti* in rural Thai villages. PLoS Negl Trop Dis. 2012;6:e1730. https://doi.org/10.1371/journal.pntd.0001730
25. Gardini Sanches Palasio R, Marques Moralejo Bermudi P, Luiz de Lima Macedo F, Reis Santana LM, Chiaravalloti-Neto F. Zika, chikungunya and co-occurrence in Brazil: space-time clusters and associated environmental-socioeconomic factors. Sci Rep. 2023;13:18026. https://doi.org/10.1038/s41598-023-42930-4

26. Magalhaes T, Morais CNL, Azevedo EAN, Jacques IJAA, Castanha PMS, Cordeiro MT, et al. Two-year decay of Zika virus neutralizing antibodies in people living in an endemic region in Brazil. Am J Trop Med Hyg. 2022;107:186–9. https://doi.org/10.4269/ajtmh.21-1279

27. Aubry M, Teissier A, Huart M, Merceron S, Vanhomwegen J, Roche C, et al. Zika virus seroprevalence, French Polynesia, 2014–2015. Emerg Infect Dis. 2017;23:669–72. https://doi.org/10.3201/eid2304.161549

28. Henderson AD, Aubry M, Kama M, Vanhomwegen J, Teissier A, Mariteragi-Helle T, et al. Zika seroprevalence declines and neutralizing antibodies wane in adults following outbreaks in French Polynesia and Fiji. ELife. 2020;9:e48460. https://doi.org/10.7554/eLife.48460

29. Langerak T, Kasbergen LMR, Chandler F, Brinkman T, Faerber Z, Phalai K, et al. Zika virus antibody titers three years after confirmed infection. Viruses. 2021;13:1345. https://doi.org/10.3390/v13071345

30. Polen KD, Gilboa SM, Hills S, Oduyebo T, Kohl KS, Brooks JT, et al. Update: interim guidance for preconception counseling and prevention of sexual transmission of Zika virus for men with possible Zika virus exposure—United States, August 2018. MMWR Morb Mortal Wkly Rep. 2018;67:868–71. https://doi.org/10.15585/mmwr.mm6731e2

31. World Health Organization. WHO guidelines for the prevention of sexual transmission of Zika virus. 2020 [cited 2023 Dec 27]. https://www.who.int/publications/i/item/9789241550482

32. United Nations Population Fund. My body is my own: claiming the right to autonomy and self-determination. 2021 [cited 2023 Dec 12]. https://algeria.unfpa.org/sites/default/files/pub-pdf/sowp2021_report_-_en_web_23.3.21_10_0.pdf

33. Coutinho RZ, Villanueva A, Weitzman A, Marteleto LJ. Zika virus public health crisis and the perpetuation of gender inequality in Brazil. Reprod Health. 2021;18:40. https://doi.org/10.1186/s12978-021-01067-1

Address for correspondence: Tereza Magalhaes, Texas A&M University, Department of Entomology, TAMU 2475, College Station, TX 77843, USA; email: tereza.magalhaes@ag.tamu.edu

etymologia revisited

Coronavirus
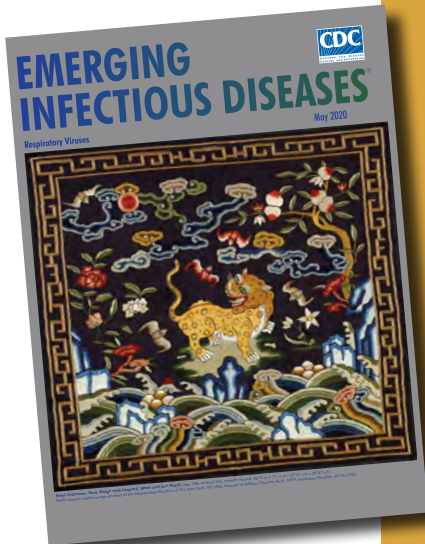
Originally published in May 2020

The first coronavirus, avian infectious bronchitis virus, was discovered in 1937 by Fred Beaudette and Charles Hudson. In 1967, June Almeida and David Tyrrell performed electron microscopy on specimens from cultures of viruses known to cause colds in humans and identified particles that resembled avian infectious bronchitis virus. Almeida coined the term "coronavirus," from the Latin *corona* ("crown"), because the glycoprotein spikes of these viruses created an image similar to a solar corona. Strains that infect humans generally cause mild symptoms. However, more recently, animal coronaviruses have caused outbreaks of severe respiratory disease in humans, including severe acute respiratory syndrome (SARS), Middle East respiratory syndrome (MERS), and 2019 novel coronavirus disease (COVID-19).

References:

1. Almeida JD, Tyrrell DA. The morphology of three previously uncharacterized human respiratory viruses that grow in organ culture. J Gen Virol. 1967;1:175–8. https://doi.org/10.1099/0022-1317-1-2-175
2. Beaudette FR, Hudson CB. Cultivation of the virus of infectious bronchitis. J Am Vet Med Assoc. 1937;90:51–8.
3. Estola T. Coronaviruses, a new group of animal RNA viruses. Avian Dis. 1970;14:330–6. https://doi.org/10.2307/1588476
4. Groupe V. Demonstration of an interference phenomenon associated with infectious bronchitis virus of chickens. J Bacteriol. 1949;58:23–32. https://doi.org/10.1128/JB.58.1.23-32.1949

https://wwwnc.cdc.gov/eid/article/26/5/et-2605_article

Concurrent Rabies and Canine Distemper Outbreaks and Infection in Endangered Ethiopian Wolves

Jorgelina Marino,[1] Elizabeth F.R. Preston,[1] Muktar Abute, Alo Hussein, Fekede Regassa,
Asefa Deressa, Eric Bedin, Ashley C. Banyard, Anthony R. Fooks, Claudio Sillero-Zubiri

Intensive disease surveillance in an endangered population of Ethiopian wolves provided evidence of concurrent outbreaks of rabies and canine distemper viruses in 2019, including co-infection in an individual animal. Disease surveillance and intensive monitoring of wolf packs in Ethiopia were essential in detecting the concurrent outbreaks and enabled accurate assessment of disease from both pathogens. The study highlights the risk posed to endangered populations that are susceptible to, or live in areas with, reservoir hosts for canine distemper and rabies viruses. Instances of concurrent distemper and rabies outbreaks appear unusual in the existing literature; modeling for one disease might underestimate the risk for extinction. Concurrent outbreaks may have a larger effect than single-disease outbreaks, even in a population that has partial vaccination coverage. Researchers studying wildlife populations from a conservation perspective should be aware that both diseases can strike at once where susceptible populations exist.

Infectious diseases are an increasing threat to wildlife, domestic species, and humans around the world (*1,2*). Although the recent SARS-CoV-2 pandemic has demonstrated the effects of zoonotic transmission of viral diseases from wildlife to the human population, the dynamics of pathogen transmission between domesticated animal populations and sylvatic populations can drive the emergence of infectious diseases in wildlife species, with potentially catastrophic outcomes (*2*). The risk from disease is greatest for small populations that live in close proximity to humans and their livestock and companion animals; small populations face a greater likelihood of stochastic population change caused by disease spillover that can further reduce population size or even lead to extinction (*1,2*). Domestic dogs are a particular danger to wild carnivores and are linked to many incidences of pathogen transmission that cause conservation issues (*3–7*), because increasing populations of free-ranging dogs in rural and wild areas lead to frequent spillovers of disease into wildlife (*3,4*).

Rabies affects many mammal species, including humans and livestock. When the virus persists within domestic dog populations, it is often a public health and conservation threat (*8*). Rabies virus is a particular concern for several threatened carnivores (*9*) including endangered African wild dogs (*Lycaon pictus*) (*10–12*) and Ethiopian wolves (*Canis simensis*) (*13–16*). Rabies virus is one of the few viral pathogens that almost always causes a fatal clinical disease from a productive infection. Other diseases of domestic and wild animals are emerging as threats to endangered species worldwide, including canine distemper virus (CDV). CDV is a highly infectious virus that causes a profound immunosuppression after infection, often leading to secondary opportunistic infections driving high rates of illness and death (*17*). In contrast to rabies virus, CDV can circulate in a mild state; disease outcomes are dependent on viral and host genetics, immunostatus, nutritional status, and species susceptibility (*18*). In recent years, spillovers of CDV from domestic dogs have been associated with severe declines in wild carnivore populations worldwide. Outbreaks have been recorded in African wild dogs (*5,6,19,20*), lions (*Panthera leo*) (*19,21*), black-footed ferrets (*Mustela nigripes*) (*22*), Ethiopian wolves (*16,23*), Santa Catalina island foxes (*Urocyon littoralis*)

Author affiliations: University of Oxford and Ethiopian Wolf Conservation Programme, Tubney, UK (J. Marino, E.F.R. Preston, C. Sillero-Zubiri); University of Oxford and Ethiopian Wolf Conservation Programme, Robe-Bale, Ethiopia (M. Abute, A. Hussein, E. Bedin); Ethiopian Wildlife Conservation Authority, Addis Ababa, Ethiopia (F. Regassa); Ethiopian Public Health Institute, Addis Ababa (A. Deressa); Animal and Plant Health Agency, Weybridge, UK (A.C. Banyard, A.R. Fooks)

[1]These first authors contributed equally to this article.

(24), Caspian seals (*Pusa caspica*) (25), spotted hyenas (*Crocuta crocuta*) (26), Amur tigers (*Panthera tigris altaica*) (27), and gray wolves (*Canis lupus*) (28).

Across rural Africa, the interface between domestic and wild animals provides many opportunities for transmission of infectious viral diseases; Ethiopia experiences some of the highest incidences of rabies in the world (29). In this context, there is an unexplored risk for population decline or extinction from concurrent disease outbreaks in wildlife. Several case studies have investigated the effect of disease on population extinction risk and management strategies to reduce this (30–32), but they tend to focus on a single disease in the system or the presence of a single disease at a time. Diseases, however, can function differently in the same population; for example, CDV and rabies differ in their reservoir species and dynamics in African wild dogs (6,7). Carnivore species have experienced outbreaks of each of these diseases on separate occasions or in different populations (5,6,10–12,16,19–21,23), yet concurrent infections have only been recorded in northern raccoons (*Procyon lotor*), red foxes (*Vulpes vulpes*), and striped skunks (*Mephitis mephitis*), in the United States (33–35). There is a critical knowledge gap on the demographic outcomes of multiple viral infections in wildlife, in the face of increasing frequency of CDV and resulting illness in wild carnivores (36,37). Studies that report co-infection rarely address demographic outcomes and are often limited to either individual deaths (38) or report co-infections not linked to disease outbreaks (39).

The risk for concomitant outbreaks should be considered and explored further in vulnerable populations, particularly those of conservation concern (16,40). Concurrent outbreaks, like single outbreaks, can easily be unnoticed unless disease monitoring and diagnoses are sustained throughout an outbreak, and testing is performed for multiple pathogens. Here, we report concurrent outbreaks of rabies and distemper among Ethiopian wolves, describing the spatial and temporal spread of deaths and the overall impacts on the host population. Individually, those diseases have had a substantial impact upon the Ethiopian wolf population in the Bale Mountains of Ethiopia (the largest population, with more than half the surviving 500 wolves), and consecutive outbreaks have led to extinction of one of the smallest populations (16).

Materials and Methods

Wildlife Population
Monitoring of the Ethiopian wolves in the Bale Mountains has been continuous since 1997, with a long-term focus on 2 core subpopulations, Sanetti Plateau and Web Valley; the neighboring subpopulations of Morebawa (connected to the Web Valley by the Genale Corridor) and Chafadalacha were also monitored. Subpopulations are groups of neighboring wolf packs separated from others by geographic barriers or habitat bottlenecks. A team of 6–8 experienced monitors routinely observe Ethiopian wolf packs on foot or horseback, during the daytime, following standard protocols (15,41). Disease surveillance is also part of the routine field monitoring; carcasses are found opportunistically or in response to reports by park rangers and members of the local community, and searches intensify afterward. Well-established disease alert networks, involving local communities, animal health offices and park staff, also contribute to detection of diseases among local dog populations. We implemented oral rabies vaccination campaigns in 2018 and 2019, concentrated in Morebawa (10 packs) and the Web Valley (2 packs); no packs in the Sanetti Plateau were vaccinated before the outbreak (Ethiopian Wolf Conservation Programme, unpub. data). A limited trial of a CDV vaccine targeting packs in Chafadalacha (2 packs) and Morebawa (1 pack) was also performed.

Observations and Data Collection
In March 2019, an Ethiopian wolf carcass was found in the Bale Mountains, and an infectious disease was suspected as the cause of death; subsequently, monitoring for carcasses increased across the area. We conducted detailed necropsy examinations of carcasses whenever possible and collected tissue samples, including lymph node, lungs, spleen, and brain. We targeted tissue collection to ensure that organs assessed for infection were appropriate for each pathogen tested. The estimated time of death was assigned into categories according to the level of decomposition: within 1 day, 1–2 days, within 1 week, within 1 month, and >1 month.

Laboratory Procedures
We tested samples for both rabies and CDV viral nucleic acids because these diseases have previously been detected in the population and caused outbreaks of disease in this area. For evaluation of viral nucleic acid within samples, we extracted total RNA as described previously (42); all suspect material was handled within a Biosafety Level 3 facility at the Animal and Plant Health Agency (Weybridge, UK). To detect rabies virus nucleic acid, we used a pan-lyssavirus SYBR green reverse transcription PCR as described previously (43). We detected canine distemper virus using an in-house real-time reverse transcription PCR (42).

Disease Mapping and Population Assessment

We mapped the spread of diseases across the Bale Mountains wolf population from the global positioning satellite locations of carcasses and adjusted by the estimated time of death. We derived complementary data on population change from intensive monitoring of packs in the 2 core areas, Web Valley and Sanetti Plateau, including the complete set of neighboring packs (8 in Web Valley and 5 in Sanetti Plateau). Those social groups and their territories were typically stable, which aided us in total counts; sightings of large and complete groups were common, particularly during early morning and evening communal greetings, during pack territorial patrols, and around dens during the breeding season. We followed standard protocols for close observations of focal packs throughout the year to obtain accurate information on their size, composition, and reproductive success; observation enabled us to perform complete enumerations of wolves into age and sex classes and to note individuals recognized by ear marks or morphologic clues (41). We assessed population change as a result of the outbreaks by comparing the total number of wolves and the number of wolves of different age and sex categories, compared before and after the outbreaks, based on the estimated time of death of the first and the last carcass found.

Results

Deaths

During March 2019–November 2019, we found 57 carcasses and observed another 5 wolves with advanced clinical signs consistent with an infectious agent (Table 1; Appendix Table 1, https://wwwnc.cdc.gov/EID/article/30/12/24-0432-App1.pdf). Wolves died in at least 19 packs in 4 subpopulations: Sanetti Plateau, Chafadalacha, Web Valley, and Morebawa. We extracted samples for laboratory analyses from 19 of those carcasses; other carcasses were in an advanced state of decomposition or severely scavenged. Seven animals tested positive for rabies virus and 13 tested positive for CDV, 1 individual tested positive for both pathogens. In the animals with confirmed diagnoses, death caused by distemper was higher than death apportioned to rabies. However, we were unable to extrapolate those findings to populations because less than half of the carcasses detected could be tested for diseases, but the number tested is still significant in comparison with data from other studies.

Figure 1. Characteristics of Ethiopian wolf carcasses found in the Bale Mountains in a study of concurrent outbreaks of rabies and canine distemper, Ethiopia, 2019*

Pack	Carcasses found	Known sex		Known age†			Carcasses tested	Rabies positive	CDV positive
		M	F	Adult	Subadult	Juvenile			
Sanetti Plateau subpopulation									
Badagasa	8	0	3	1	1	2	2	1	1‡
Batu	3	0	0	2	0	0	0	0	0
BBC	4		3	2	0	1	2	0	2
Bilisa	1	1	0	1	0	0	1	0	1
Buyamo	1	0	0	0	0	0	0	0	0
Garba Gurracha	1	0	0	0	1	0	0	0	0
Chafadalacha subpopulation									
Chafadalacha	1	0	0	0	0	0	0	0	0
Konteh	2	0	0	0	1	0	0	0	0
Web Valley subpopulation									
Alandu	1	0	1	0	0	1	1§	1§	1§
Bowman	4	2	1	1	1	2	2	1‡	1
Gata	1	1	0	0	1	0	0	0	0
Habale	1	0	0	1	0	0	0	0	0
Hangafo	2	1	1	1	0	1	1	1	0
Mckenna	1	0	0	1	0	0	0	0	0
Megity	10	5	1	3	2	1	4	1	3
Megity3	9	4	1	4	2	1	4	1	3
Tarura	2	2	0	2	0	0	1	1	0
Unknown	1	1	0	0	0	1	0	0	0
Genale Corridor subpopulation									
Genale	3	0	0	1	2	0	0	0	0
Morebawa subpopulation									
Gurati	1	0	1	0	1	0	1	1	1
Totals	57	17	12	20	12	10	19	7	13

*CDV, canine distemper virus,
†Adult, >2 y; subadult, 1 to <2 y; juvenile, <1 y.
‡Indicates the first confirmed case of each disease.
§Indicates case of co-infection.

Patterns of Disease Spread

The timing and location of carcasses encountered suggest pathways of disease dispersion across subpopulations (Figures 1–3). The center of infection was in the Sanetti Plateau, where the first 2 carcasses were found in March and April 2019, but CDV was first confirmed from a carcass sampled in May 2019. Overall mortality rate peaked in July 2019, five months after the onset of the outbreak, by which time disease had spread southwards to Chafadalacha and to the more distant Web Valley (Figures 2 and 3). At the peak of the outbreak, both CDV and rabies were common in Web Valley, whereas rabies virus was not detected in Sanetti Plateau until a month later (Figure 3). The spread of rabies and distemper appeared to occur in both directions, indicating different origins for the initial infections (Figure 2).

During August–October 2019, disease spread along the Genale habitat corridor connecting Web Valley with the Morabawa subpopulation; at least 1 death from distemper was confirmed toward the end of the outbreak (Figures 1, 2). Monitoring effort in Morabawa was relatively low in comparison with that in Web Valley and Sanetti Plateau.

Population Effects

The number of carcasses encountered (n = 57) provided an indirect and partial measure of overall mortality during the outbreaks (Table 1). We assessed local population effect from total counts of Ethiopian wolves in 2 core monitoring areas by comparing pack compositions before and after the outbreaks in the Sanetti Plateau (5 packs) and Web Valley (8 packs) subpopulations (Table 2). We noted a total of 64 animals unaccounted for in the 2 subpopulations, where 50 carcasses had been found: 17 × in the Sanetti Plateau, representing 60% decline, and 47 × unaccounted for in the Web Valley, representing 53% decline.

We assessed mortality patterns in 29 carcasses that could be classified by age and 42 by sex (Table 1). More carcasses were from adult wolves (>2 years of age), followed by subadults (1–2 years of age) and then juveniles (<1 year of age) (Table 1), and appeared to be split unevenly between the sexes (17 male animals, 11 female, and 29 unknown). Of the 13 carcasses tested positively for CDV, 6 were adults, 4 subadults, and 3 juveniles; 6 were female and 7 male). We confirmed rabies in samples from 3 adults and 4 juveniles but no subadults, albeit on a small sample (n = 7). The animal that tested positive for both diseases was a juvenile female.

Mortality inferred by changes in pack composition (Table 2) was consistent with the age distribution of carcasses: of the wolves missing in the population, 54 were adults, 40 subadults and 16 juveniles. In the Web Valley subpopulation, death rates were 53% among adults and 73% among subadults. In the Sanetti Plateau subpopulation, death rates were 41% among adults and 80% among subadults. More female wolves were missing than males (38 females vs. males).

Discussion

Intensive monitoring of an Ethiopian wolf population provided confirmation of concurrent outbreaks and
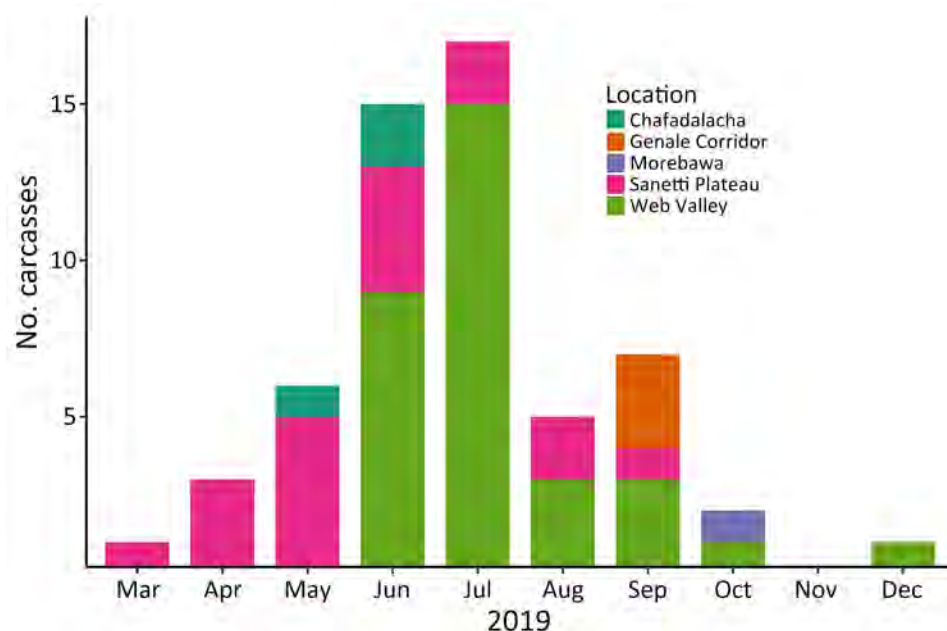

Figure 1. Carcasses of Ethiopian wolves retrieved in the Bale Mountains, by month and subpopulation, in a study of concurrent rabies and canine distemper outbreaks, Ethiopia, 2019. Estimated time of death determined from postmortem observations.
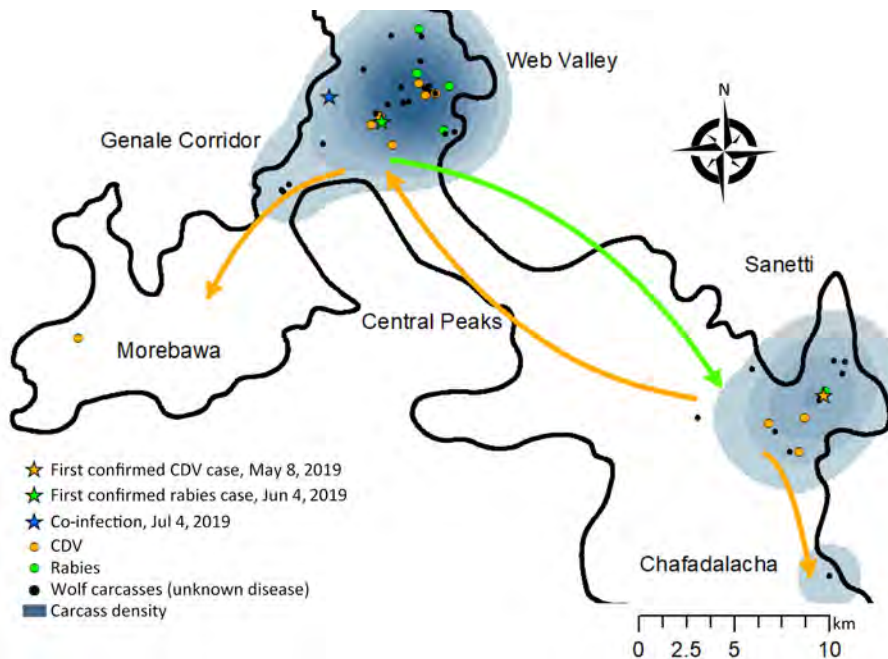
Figure 2. Location of Ethiopian wolf carcass found in the Bale Mountains in a study of concurrent rabies and canine distemper outbreaks, Ethiopia, 2019. Shades of blue represent the kernel density distribution of all observed carcasses. Arrows indicate the direction of spread of infections as revealed by positive cases of each disease through time and across subpopulations. CDV, canine distemper virus.

co-infection with rabies virus and CDV in an endangered mammalian species, and new information on population-level impact. Our findings support expectations that concurrent outbreaks can be more damaging to the survival of the Ethiopian wolf than single disease outbreaks (*16,40*); that expectation may also apply to other species that can contract both of these diseases, including African wild dogs, lions, and other carnivores. Studies of viral infections in wildlife are rare for several reasons, and therefore the knowledge gleaned from the concurrent outbreaks has important implications for disease surveillance and control, as well as some limitations.

Spreading monitoring effort across the extent of a population and over time enabled detection of multiple pathogens which could otherwise be missed, and we found only 1 other incidence of co-infection in an individual *33*). Indeed, because rabies and CDV are not uncommon diseases among wild carnivores and affect many of the same species, a likely reason that concurrent outbreaks are rarely reported is that they go unmonitored, which can happen if monitoring is concentrated in 1 subpopulation and misses 1 disease initially, or if all deaths are assumed to be attributable to a single disease. In our study, sustained and intensive monitoring maximized detection of deaths across the landscape, enabling us to recover 57 wolf carcasses; we found no evidence of deaths in other species. More often, most carcasses go undetected or the identification of the sex or age of a carcasses is impaired because of late detection. Time periods leading

to death from rabies virus infection for canine species is typically within 2 weeks of infection. In contrast, CDV infection can cause clinical disease within a few days of infection and either results in clearance and survival from infection or progresses to a severe disease characterized by an acute leukopenia that may lead to secondary infections and death. Timelines for infection for CDV can vary, but in cases in which the disease leads to death, the timeline will often be in a similar time period to that observed with rabies virus infection. Carcass detection is inherently imperfect and depends on the monitoring effort.

The risks posed by concomitant outbreaks include wolf deaths lasting over a longer period and spreading further geographically than previously known. The carcasses detected in the Bale Mountains showed that this combined outbreak lasted ≥220 days and affected 4 subpopulations, compared with previous records of single-pathogen outbreaks among Ethiopian wolves shown to last for 3 months (*14,15,42,44*) and affecting 1 (*44*), 2 (*14,15,42*) or 3 (*42*) subpopulations. The unprecedented duration of the event was likely because of the overlapping outbreaks starting at slightly different times, as indicated by the timing and location of carcasses and adjusted by estimations of time since death from postmortems or body remains. The reconstructed pathways of disease spread indicated 2 different geographic origins and directions of spread for the rabies and CDV outbreak. Those chains of transmission between subpopulations coincide with those observed in previous outbreaks, involving an initially quick

transmission within packs because of social bonds and shared space within pack territories, followed by transmission to neighboring packs. The absence of observations or reports of CDV or rabies cases among domestic dogs or other carnivore species living within or in close vicinity of Ethiopia wolf territories supports the wolf-to-wolf transmission pathway and coincides with descriptions of previous outbreaks. Although whole-genome sequencing and phylogenetic analysis will ultimately infer transmission dynamics, our findings were supported by a rate of carcass detection and diagnoses that we had not previously found in any wild population affected by these viruses.

Despite the large number of Ethiopian wolf deaths and disappearances during the concurrent outbreaks, declines of 53% and 60% in the 2 core subpopulations were comparable to death rates recorded during previous CDV outbreaks (43%–68% decline) (42) and slightly lower than most rabies outbreaks (49%–77% decline) (14,15,44). The implication that a combined outbreak might not be necessarily worse than a single-disease outbreak, however, is misleading; a degree of herd immunity existed in the population at the time of the outbreaks. Individually identifiable wolf carcasses that were tested for either disease (n = 6) had not been vaccinated against the
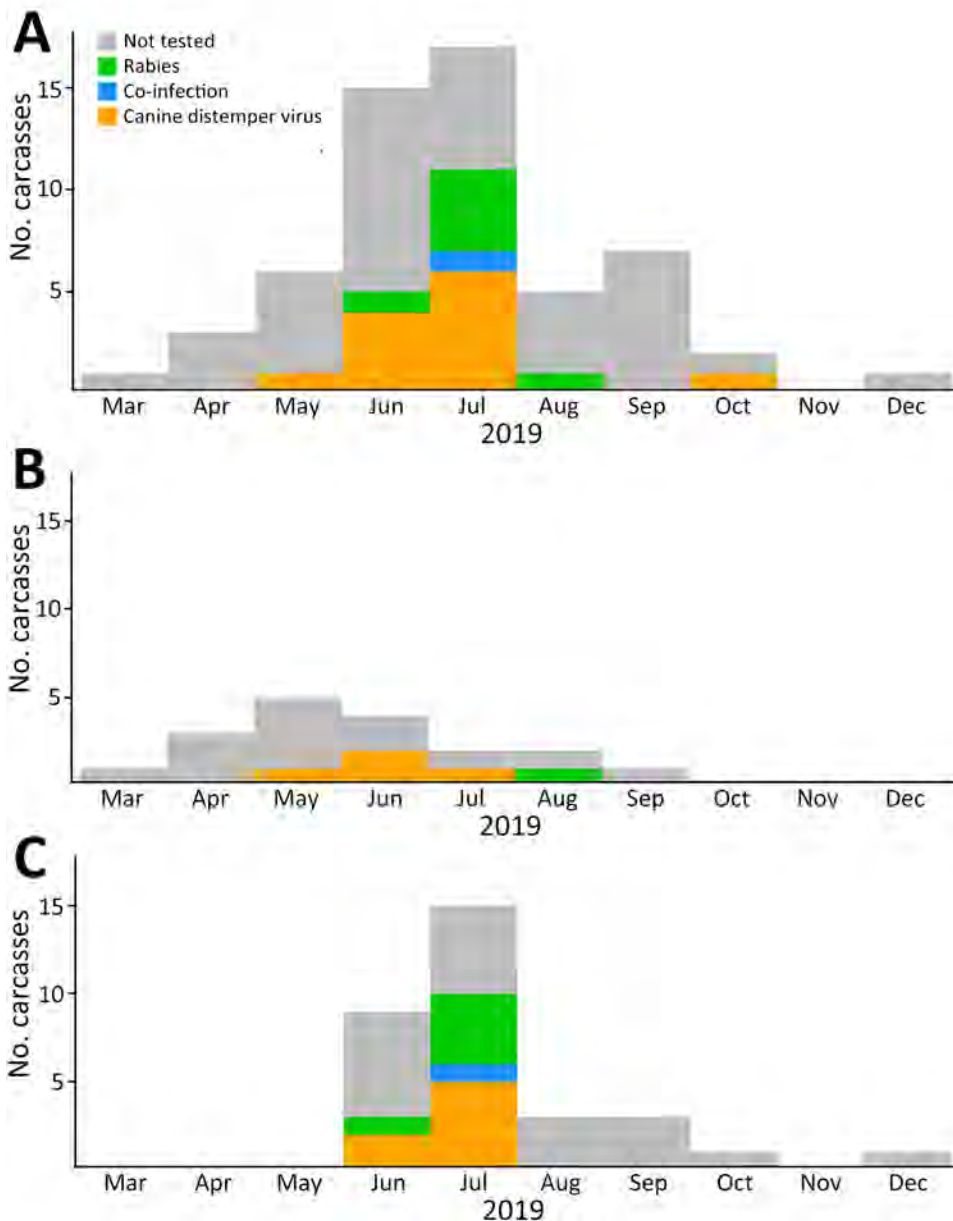
Figure 3. Number of carcasses retrieved per month in a study of concurrent rabies and canine distemper outbreaks in Ethiopian wolves, Ethiopia, 2019. Estimated time of death determined from postmortem observations. A) Full wolf population in the Bale Mountains. B) Sanetti Plateau subpopulation. C) Web Valley subpopulation.

Table 2. Changes in composition of wolf packs in Ethiopian wolves before and after concurrent outbreaks of rabies and canine distemper, Ethiopia, 2019*

Pack	Before outbreaks						After outbreaks			
	Adult		Subadult				Adult/subadult			
	M	F	M	F	Juveniles	Sex ratio	M	F	Subadults†	Sex ratio
Sanetti Plateau subpopulation										
Bagadasa	3	2	2	2	4	1.25	1	1	1	1
Garba Gurracha	2	1	0	1	0	1	2	1	0	2
Batu	2	2	1	1	0	1	2	1	0	2
BBC	3	2	1	2	0	1	2	1	0	2
BBC2	3	2	0	0	5	1.5	1	1	1	1
Total	22		10		9		13		2	
Web Valley subpopulation										
Alando	2	2	0	0	4	1	2	1	1	2
Bowman	4	7	2	2	5	0.666667	1	1	0	1
Habale	4	3	2	2	4	1.2	2	1	2	2
Hangafo	2	1	2	2	3	1.333333	2	1	0	2
Mckenna	3	2	1	1	0	1.333333	2	1	0	2
Megity	3	3	2	2	3	1	2	1	0	2
Megity 3	3	2	2	2	5	1.25	0	0	0	
Tarura	6	5	2	2	5	1.142857	3	4	4	0.75
Total	52		26		29		24		7	

*Sex ratio calculated as the ratio between male and female wolves ≥1 y of age. It excludes juveniles at the time of the outbreaks because they are difficult to sex when young,
†These subadults were juveniles before the outbreak.

disease for which they tested positive but had often been vaccinated against the other disease. More in-depth analyses would be needed to ascertain the effect of the previous vaccinations in the study population. Whereas rabies often causes overt clinical disease with an inherent zoonotic risk, the dynamics of CDV can be difficult to understand without serosurveillance because the virus can circulate in wild populations subclinically.

Population declines of the severity reported here highlight concern for any threatened species that exists in small populations such as the Ethiopian wolf. In the past, consecutive outbreaks of distemper and rabies led to the smallest population of this species becoming functionally extinct in Delanta (*16*). Ongoing oral vaccination of Ethiopian wolves against rabies have the potential to reduce risks of populations going extinct; it is a crucial intervention where rabies remains endemic in terrestrial carnivores in vast areas (*45*). Approaches to control rabies are relatively advanced and accessible because of the virus's relevance to human and livestock health (*46*). Tools to control distemper in wildlife are less developed, because it generally does not infect humans and is therefore considered to be of lesser importance. Canine distemper vaccines have been available for decades but are rarely used in wildlife, and their efficacy is not well known, in part due to the complexity of CDV dynamics in natural ecosystems (*18*). A CDV vaccine is currently under trial (Ethiopian Wolf Conservation Programme, unpub. data).

Knowledge of the age and sex composition in disease-related deaths can also help deduce disease dynamics and immunity (*47*) to investigate relative risks and fitness costs of infection in social species (*26*). By combining information from carcasses with our knowledge of Ethiopian wolf packs' demography, this study provides insights into the effects of CDV in wildlife populations, a neglected area of research. Statistical analyses by the age and sex of carcasses would be questionable because a large proportion of the deceased animals were of unknown age or sex; however, assessing such data is valuable because we know of no comparable level of disease surveillance and carcass recovery in other wildlife populations. Positivity for CDV spanned across age classes and was highest among adults, in itself not an indication of age-biased transmission or mortality because adults make a large proportion of the Ethiopian wolf population (*48*). When compared with single CDV outbreaks in Ethiopian wolves, these concurrent outbreaks were still unusual in the proportion of adult deaths recorded (47% adult mortality averaged across 2 subpopulations, compared with 34% during a CDV outbreak in 2006 and 39% in 2010). Subadult mortality rate was comparatively lower, 77% average, compared with 83% in the 2006 CDV outbreak and 87% in 2010. Although fatalities could not always be assigned to infections by rabies virus or CDV, high adult mortality is ultimately expected to reduce the capacity for recovery of this population (*48*) because it is more likely to lead to the extinction of a pack (*48*). The mortality rate among female wolves is higher than expected, given that there are more males in the populations

we studied, which can also slow down population growth by limiting the effective population size.

In conclusion, this study highlights the risk to susceptible populations of threatened carnivores from concurrent infection from multiple pathogens. CDV and rabies viruses can strike at the same time and have a large effect even in a population that has partial vaccination coverage. Vaccination strategies using multivalent rabies/CDV vaccines should be favored when possible, in light of the possibility of concurrent outbreaks; the simultaneous impact of both diseases should be included in future models of vaccination programs and extinction risk of susceptible endangered populations. Existing models applied to Ethiopian wolf populations should be updated to integrate more and new information on potential multiple hosts of CDV, acquired immunity (*49*) and effectiveness of ongoing oral rabies vaccinations (*50*). The case of the Ethiopian wolf highlights the need for effective monitoring of endangered wildlife populations at risk for co-infections so that concurrent outbreaks are detected and their true impacts assessed accurately and incorporated into models to avoid underestimating the risk for extinction from disease.

About the Author

Dr. Marino is the science director of the Ethiopian Wolf Conservation Programme and a research fellow at the Wildlife Conservation Research Unit, University of Oxford. She has worked with Ethiopian wolves since 1999 and recorded and monitored several disease outbreaks in the population during this time. Dr. Preston is a lecturer in Wildlife Ecology at the Royal Veterinary College. She worked with the Ethiopian Wolf Conservation Programme during the concurrent outbreaks.

References

1. Daszak P, Cunningham AA, Hyatt AD. Emerging infectious diseases of wildlife—threats to biodiversity and human health. Science. 2000;287:443–9. https://doi.org/10.1126/science.287.5452.443
2. Cunningham AA, Daszak P, Wood JLN. One Health, emerging infectious diseases and wildlife: two decades of progress? Philos Trans R Soc Lond B Biol Sci. 2017; 372:20160167.
3. Doherty TS, Dickman CR, Glen AS, Newsome TM, Nimmo DG, Ritchie EG, et al. The global impacts of domestic dogs on threatened vertebrates. Biol Conserv. 2017;210:56–9.
4. Knobel D, Butler JRA, Lembo T, Critchlow R, Gompper ME. Dogs, disease, and wildlife. In: Gompper ME, editor. Free-ranging dogs and wildlife conservation. Oxford: Oxford University Publishing; 2013. p. 144–69.
5. Flacke G, Becker P, Cooper D, Szykman Gunther M, Robertson I, Holyoake C, et al. An infectious disease and mortality survey in a population of free-ranging African wild dogs and sympatric domestic dogs. Int J Biodivers. 2013;2013:497623. https://doi.org/10.1155/2013/497623
6. Woodroffe R, Prager KC, Munson L, Conrad PA, Dubovi EJ, Mazet JAK. Contact with domestic dogs increases pathogen exposure in endangered African wild dogs (*Lycaon pictus*). PLoS One. 2012;7:e30099. https://doi.org/10.1371/journal.pone.0030099
7. Prager KC, Mazet JAK, Dubovi EJ, Frank LG, Munson L, Wagner AP, et al. Rabies virus and canine distemper virus in wild and domestic carnivores in northern Kenya: are domestic dogs the reservoir? EcoHealth. 2012;9:483–98.
8. Fooks A, Cliquet F, Finke S, Freuling C, Hemachudha T, Mani R., et al. Rabies. Nat Rev Dis Primers. 2017;3:17091.
9. Stuchin M, Machalaba C, Olival K, Artois M, Bengis R, Diaz F, et al. Rabies as a threat to wildlife. Revue Scientifique et Technique (International Office of Epizootics). 2018;37:341–57.
10. Gascoyne SC, Laurenson MK, Lelo S, Borner M. Rabies in African wild dogs (*Lycaon pictus*) in the Serengueti Region, Tanzania. J Wildl Dis. 1993;29:396–402.
11. Hofmeyr M, Hofmeyr D, Nel L, Bingham J. A second outbreak of rabies in African wild dogs (*Lycaon pictus*) in Madikwe Game Reserve, South Africa, demonstrating the efficacy of vaccination against natural rabies challenge. Anim Conserv. 2004;7:193–8. https://doi.org/10.1017/S1367943004001234
12. Kat PW, Alexander KA, Smith JS, Munson L. Rabies and African wild dogs in Kenya. Proc Biol Sci. 1995;262:229–33. https://doi.org/10.1098/rspb.1995.0200
13. Randall DA, Marino J, Haydon DT, Sillero-Zubiri C, Knobel DL, Tallents LA, et al. An integrated disease

management strategy for the control of rabies in Ethiopian wolves. Biol Conserv. 2006;131:151–62. https://doi.org/10.1016/j.biocon.2006.04.004

14. Johnson N, Mansfield KL, Marston DA, Wilson C, Goddard T, Selden D, et al. A new outbreak of rabies in rare Ethiopian wolves (*Canis simensis*). Arch Virol. 2010;155:1175–7. https://doi.org/10.1007/s00705-010-0689-x

15. Sillero-Zubiri C, King AA, Macdonald DW. Rabies and mortality in Ethiopian wolves (*Canis simensis*). J Wildl Dis. 1996;32:80–6. https://doi.org/10.7589/0090-3558-32.1.80

16. Marino J, Sillero-Zubiri C, Deressa A, Bedin E, Bitewa A, Lema F, et al. Rabies and distemper outbreaks in smallest Ethiopian wolf population. Emerg Infect Dis. 2017;23:2102–4. https://doi.org/10.3201/eid2312.170893

17. Sykes JE. Immunodeficiencies caused by infectious diseases. Vet Clin North Am Small Anim Pract. 2010;40:409–23. https://doi.org/10.1016/j.cvsm.2010.01.006

18. Wilkes RP. Canine distemper virus in endangered species: species jump, clinical variations, and vaccination. Pathogens. 2022;12:57. https://doi.org/10.3390/pathogens12010057

19. Cleaveland S, Mlengeya T, Kaare M, Haydon D, Lembo T, Laurenson MK, et al. The conservation relevance of epidemiological research into carnivore viral diseases in the Serengeti. Conserv Biol. 2007;21:612–22. https://doi.org/10.1111/j.1523-1739.2007.00701.x

20. Ginsberg JR, Mace GM, Albon S. Local extinction in a small and declining population: wild dogs in the Serengeti. Proc Biol Sci. 1995;262:221–8. https://doi.org/10.1098/rspb.1995.0199

21. Roelke-Parker ME, Munson L, Packer C, Kock R, Cleaveland S, Carpenter M, et al. A canine distemper virus epidemic in Serengeti lions (*Panthera leo*). Nature. 1996;379:441–5. https://doi.org/10.1038/379441a0

22. Thorne ET, Williams ES. Disease and endangered species: the black-footed ferret as a recent example. Conserv Biol. 1988;2:66–74. https://doi.org/10.1111/j.1523-1739.1988.tb00336.x

23. Laurenson K, Sillero-Zubiri C, Thompson H, Shiferaw F, Thirgood S, Malcolm J. Disease as a threat to endangered species: Ethiopian wolves, domestic dogs, and canine pathogens. Anim Conserv. 1998;1:273–80

24. Timm SF, Munson L, Summers BA, Terio KA, Dubovi EJ, Rupprecht CE, et al. A suspected canine distemper epidemic as the cause of a catastrophic decline in Santa Catalina Island foxes (*Urocyon littoralis catalinae*). J Wildl Dis. 2009;45:333–43. https://doi.org/10.7589/0090-3558-45.2.333

25. Kuiken T, Kennedy S, Barrett T, Van de Bildt MWG, Borgsteede FH, Brew SD, et al. The 2000 canine distemper epidemic in Caspian seals (*Phoca caspica*): pathology and analysis of contributory factors. Vet Pathol. 2006;43:321–38. https://doi.org/10.1354/vp.43-3-321

26. Marescot L, Benhaiem S, Gimenez O, Hofer H, Lebreton J-D, Olarte-Castillo XA, et al. Social status mediates the fitness costs of infection with canine distemper virus in Serengeti spotted hyenas. Funct Ecol. 2018;32:1237–50. https://doi.org/10.1111/1365-2435.13059

27. Seimon TA, Miquelle DG, Chang TY, Newton AL, Korotkova I, Ivanchuk G, et al. Canine distemper virus: an emerging disease in wild endangered Amur tigers (*Panthera tigris altaica*). mBio. 2013;4:e00410–13.

28. Johnson MR, Boyd DK, Pletscher DH. Serologic investigations of canine parvovirus and canine distemper in relation to wolf (*Canis lupus*) pup mortalities. J Wildl Dis. 1994;30:270–3. https://doi.org/10.7589/0090-3558-30.2.270

29. Yizengaw E, Getahun T, Mulu W, Ashagrie M, Abdela I, Geta M. Incidence of human rabies virus exposure in

northwestern Amhara, Ethiopia. BMC Infect Dis. 2018 2018;18:597.

30. Vucetich JA, Creel S. Ecological interactions, social organization, and extinction risk in African wild dogs. Conserv Biol. 1999;13:1172–82. https://doi.org/10.1046/j.1523-1739.1999.98366.x

31. McCallum H, Jones M, Hawkins C, Hamede R, Lachish S, Sinn DL, et al. Transmission dynamics of Tasmanian devil facial tumor disease may lead to disease-induced extinction. Ecology. 2009;90:3379–92.

32. Maslo B, Stringham OC, Bevan AJ, Brumbaugh A, Sanders C, Hall M, et al. High annual survival in infected wildlife populations may veil a persistent extinction risk from disease. Ecosphere. 2017;8:e02001.

33. Jardine CM, Buchanan T, Ojkic D, Campbell GD, Bowman J. Frequency of virus co-infection in raccoons (*Procyon lotor*) and striped skunks (*Mephitis mephitis*) during a concurrent rabies and canine distemper outbreak. J Wildl Dis. 2018;54:622–5. https://doi.org/10.7589/2017-04-072

34. Hamir AN, Summers BA, Rupprecht CE. Concurrent rabies and canine distemper encephalitis in a raccoon (*Procyon lotor*). J Vet Diagn Invest. 1998;10:194–6. https://doi.org/10.1177/104063879801000218

35. Moessner H, Brunt S, Diaz A, Davis A. Co-infection of canine distemper virus and rabies virus in wildlife samples submitted for routine rabies testing. J Wildl Dis. 2023;59:310–4, 5.

36. Di Blasio A, Irico L, Caruso C, Miceli I, Robetto S, Peletto S, et al. Canine distemper virus as an emerging multihost pathogen in wild carnivores in northwest Italy. J Wildl Dis. 2019;55:844–56. https://doi.org/10.7589/2018-09-226

37. Terio KA, Craft ME. Canine distemper virus (CDV) in another big cat: should CDV be renamed carnivore distemper virus? MBio. 2013;4:e00702–13. https://doi.org/10.1128/mBio.00702-13

38. Needle DB, Marr JL, Park CJ, Andam CP, Wise AG, Maes RK, et al. Concurrent infection of skunk adenovirus-1, *Listeria monocytogenes*, and a regionally specific clade of canine distemper virus in one gray fox (*Urocyon cinereoargenteus*) and concurrent listeriosis and canine distemper in a second gray fox. Pathogens. 2020;9:591. https://doi.org/10.3390/pathogens9070591

39. Hoarau AOG, Mavingui P, Lebarbenchon C. Co-infections in wildlife: focus on a neglected aspect of infectious disease epidemiology. PLoS Pathog. 2020;16:e1008790. https://doi.org/10.1371/journal.ppat.1008790

40. Haydon DT, Laurenson MK, Sillero-Zubiri C. Integrating epidemiology into population viability analysis: managing the risk posed by rabies and canine distemper to the Ethiopian wolf. Conserv Biol. 2002;16:1372 85.

41. Zubiri CS, Gottelli D. Spatial organization in the Ethiopian wolf *Canis simensis*: large packs and small stable home ranges. J Zool (Lond). 1995;237:65–81. https://doi.org/10.1111/j.1469-7998.1995.tb02747.x

42. Gordon CH, Banyard AC, Hussein A, Laurenson MK, Malcolm JR, Marino J, et al. Canine distemper in endangered Ethiopian wolves. Emerg Infect Dis. 2015;21:824–32. https://doi.org/10.3201/eid2105.141920

43. Marston DA, Jennings DL, MacLaren NC, Dorey-Robinson D, Fooks AR, Banyard AC, et al. Pan-lyssavirus real time RT-PCR for rabies diagnosis. J Vis Exp. 2019;149:e59709.

44. Randall DA, Williams SD, Kuzmin IV, Rupprecht CE, Tallents LA, Tefera Z, et al. Rabies in endangered Ethiopian wolves. Emerg Infect Dis. 2004;10:2214–7. https://doi.org/10.3201/eid1012.040080

45. Taylor LH, Nel LH. Global epidemiology of canine rabies: past, present, and future prospects. Vet Med

(Auckl). 2015;6:361–71. https://doi.org/10.2147/VMRR.S51147
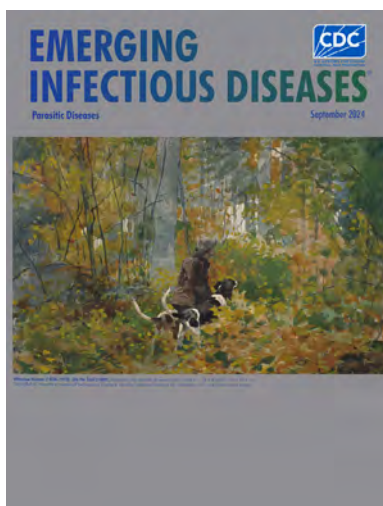
46. Viana M, Cleaveland S, Matthiopoulos J, Halliday J, Packer C, Craft ME, et al. Dynamics of a morbillivirus at the domestic-wildlife interface: canine distemper virus in domestic dogs and lions. Proc Natl Acad Sci U S A. 2015;112:1464–9. https://doi.org/10.1073/pnas.1411623112

47. Härkönen T, Harding K, Rasmussen TD, Teilmann J, Dietz R. Age- and sex-specific mortality patterns in an emerging wildlife epidemic: the phocine distemper in European harbour seals. PLoS One. 2007;2:e887. https://doi.org/10.1371/journal.pone.0000887

48. Marino J, Sillero-Zubiri C, Macdonald DW. Trends, dynamics and resilience of an Ethiopian wolf population. Anim Conserv. 2006;9:49–58. https://doi.org/10.1111/j.1469-1795.2005.00011.x

49. Kennedy LJ, Randall DA, Knobel D, Brown JJ, Fooks AR, Argaw K, et al. Major histocompatibility complex diversity in the endangered Ethiopian wolf (*Canis simensis*). Tissue Antigens. 2011;77:118–25. https://doi.org/10.1111/j.1399-0039.2010.01591.x

50. Sillero-Zubiri C, Marino J, Gordon CH, Bedin E, Hussein A, Regassa F, et al. Feasibility and efficacy of oral rabies vaccine SAG2 in endangered Ethiopian wolves. Vaccine. 2016;34:4792–8. https://doi.org/10.1016/j.vaccine.2016.08.021

Address for correspondence: Jorgelina Marino, University of Oxford and Ethiopian Wolf Conservation Programm, The Recanati-Kaplan Centre, Tubney House, Tubney OX13 5QL, UK; email: jorgelina.marino@biology.ox.ac.uk

September 2024
Parasitic Diseases

EMERGING INFECTIOUS DISEASES®

Autochthonous *Blastomyces dermatitidis*, India

Anuradha Chowdhary, Gaston I. Jofre, Ashutosh Singh, Andrius J. Dagilis,
Victoria E. Sepúlveda, Allison T. McClure, Daniel R. Matute

Blastomyces spp. fungi, the causal agent of blastomycosis, are common in North America but do occur in other areas of the world. The most prevalent pathogen in the genus is *B. dermatitidis*. Most *B. dermatitidis* isolates originate from North America, but there are sporadic reports of *B. dermatitidis* recovery from Africa and Asia. High-quality reports that incorporate genetic information about the fungus outside North America have been rare. Genome sequencing of 3 fungal isolates from patients in India with chronic respiratory diseases revealed that the isolates belong to a genetically differentiated lineage of *B. dermatitidis*. Because the patients had no history of traveling outside of Asia, blastomycosis was most likely autochthonously acquired, which suggests a local population of *B. dermatitidis*. Our results suggest the endemic range of *B. dermatitidis* is larger than previously thought, calling for a reassessment of the geographic range of different agents of endemic mycoses.

Blastomycosis is a fungal disease prevalent among immunosuppressed patients (*1–5*) that can develop as a progressive disease with either pulmonary or extrapulmonary involvement (*1–3,6–10*). Blastomycosis is caused by *Blastomyces* spp., which are thermal dimorphic fungi with a saprophytic mycelial form in the soil and a pathogenic yeast form in hosts (*2,3,6,11,12*). The transition between those 2 forms is mediated by temperature; at ≈37°C, the mycelial (or conidia) form transforms into a yeast (*13–15*). Most often, human infections occur after breathing in fungal spores from the environment (*16*), but a very small fraction of cases have demonstrated sexual transmission from patient to patient (*17,18*).

B. dermatitidis is the most heavily studied species of *Blastomyces* (*4,5,19–21*) and is considered endemic to North America. Some reports have suggested the range of *B. dermatitidis* might extend outside North America (*22,22–25*), but the actual range of the species is debated (*23,26*). Reports of blastomycosis in Asia have been considered either of poor-quality diagnosis or imported (*25,26*). In addition, the identity of the causative agent of blastomycosis in those locales remains largely unknown. PCR-based assays suggest some of the isolates recovered from patients in India could be *B. dermatitidis* (*27*), but those reports predate the acknowledgment of the existence of multiple species of *Blastomyces*.

In this article, we report a cluster of cases of blastomycosis from India. By using genomewide sequencing and phylogenetic reconstruction, we determined the etiologic agent of blastomycosis in the 3 cases is *B. dermatitidis*. The *B. dermatitidis* isolates form a differentiated lineage from the isolates in North America. The 3 cases reported in this article have no patient history of travel outside of India, which suggest either secondary infections from a traveler (unlikely given the known mode of transmission of *Blastomyces*) or locally acquired infections.

Methods

Blastomyces-Like Isolates from India

Isolate Collection and Morphology

We obtained isolates from 3 patients who had chronic respiratory disease during 2006–2010 and were referred to the Medical Mycology laboratory, Vallabhbhai Patel Chest Institute, at the University of Delhi (Delhi, India) for identification of mycotic etiology. The 3 patients' infections were unresponsive to antitubercular therapy. A detailed assessment of the patients' travel history was taken; none reported any travel outside of India. No follow-up record is available for the patients.

Figure 1. Autochthonous *Blastomyces dermatitidis* biopsy and culture findings from a patient in India. Microscopic characteristics are consistent with *Blastomyces dermatitidis*. A) Gomori's methenamine silver–stained section of a subcutaneous nodule biopsy obtained from sternum region showing a large, thick-walled broad-based budding yeast cell (white arrows) typical of *Blastomyces*. B) Lactophenol cotton blue mount of the 6-day-old yeast form on pea seed agar at 37°C, showing numerous large thick-walled and broad-based budding yeast cells (white arrow). Original magnification is ×100.
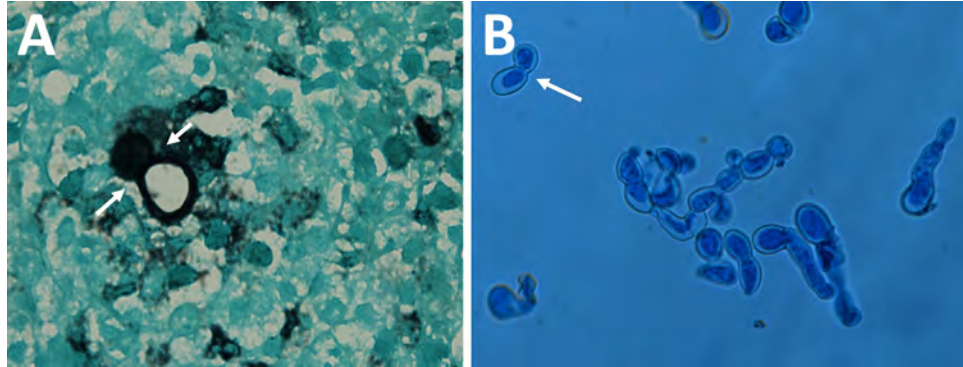
We processed the samples by using standard protocols; they were anonymized before they were received. The isolates were cultured from lung aspirate, lymph node biopsy, and discharging sinus of the sternum (Appendix Table 1, https://wwwnc.cdc.gov/EID/article/30/12/24-0830-App1.pdf). We subcultured the isolates on Sabouraud dextrose agar (SDA) at 25°C to induce mycelial growth. To assess whether the isolates showed transition to a yeast form when exposed to 37°C, we inoculated conidia on
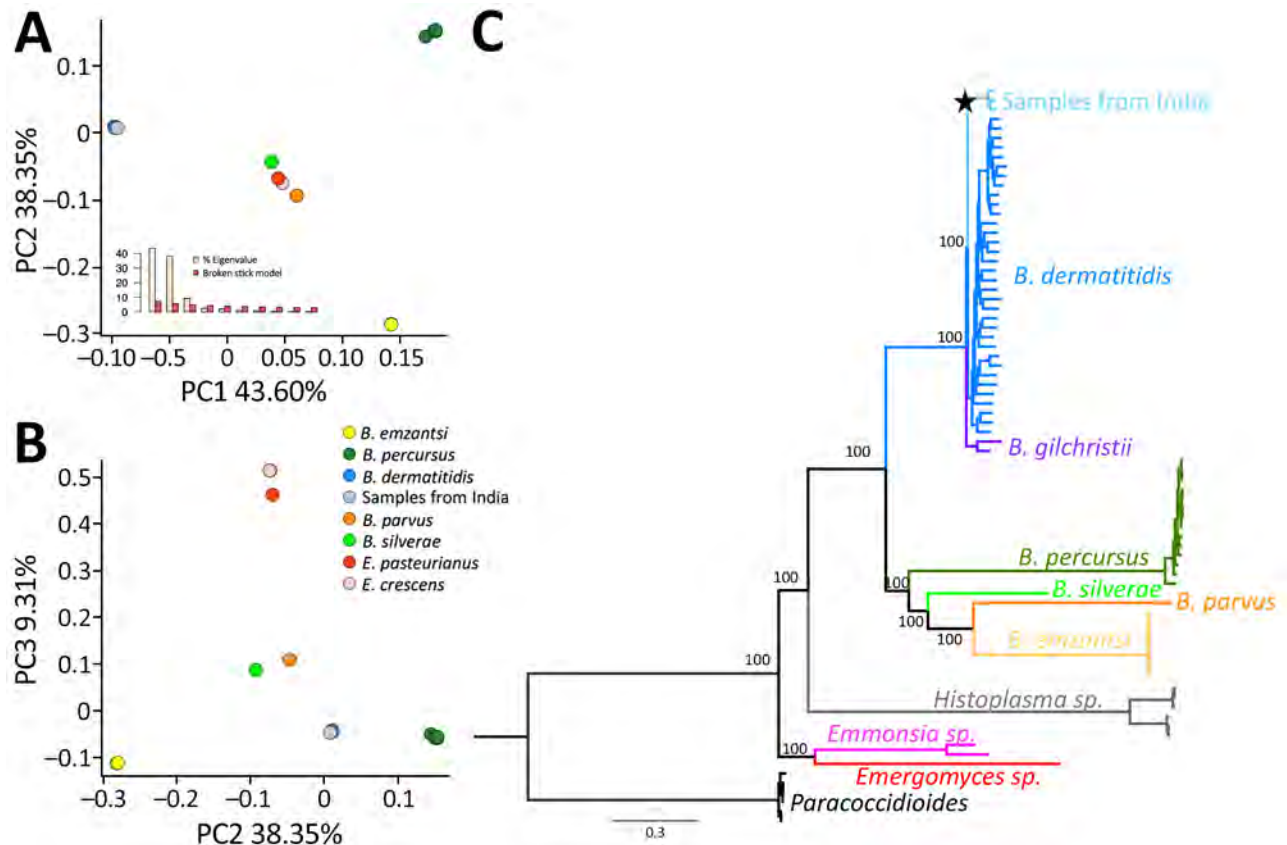

Figure 2. Genetic differentiation between 3 *Blastomyces dermatitidis* from India and other dimorphic fungi. A) PC analyses showing the 3 isolates from India (light blue) clustering with *B. dermatitidis* (dark blue) in PC 1 and PC2. The broken stick model (inset) demonstrates the first 3 PCs are significant. B) PC analyses showing the 3 isolates from India (light blue) clustering with *B. dermatitidis* (dark blue) in PC 32 and PC 3. C) Rooted phylogram for autochthonous *B. dermatitidis* isolates from India and the genetic relationships with other *Blastomyces* fungi. A maximum-likelihood tree derived from genomewide concatenated markers using the *B. dermatitidis* reference genome suggests a close phylogenetic relationship between *B. dermatitidis* and the 3 isolates from India. The star shows the node leading to the *B. dermatitidis* lineage from India. Scale bar represents the number of substitutions per site. PC, principal component.

Table 1. Approximative 2-sample Fisher-Pitman permutation tests comparing π and DXY values between different lineages of *Blastomyces dermatitidis* from India and North America*

Clade 1	Clade 2	π Clade 1	π Clade 2	D_{XY}	Z-score	p value
India	*B. dermatitidis*	0.0003	0.0037	0.0098	21.6158	<0.0001
India	*B. gilchristii*	0.0003	0.002	0.0111	2.9833	0.0046
India	*B. emzantsi*	0.0003	0.0003	0.1920	7.3485	<0.0001
India	*B. parvus*	0.0003	0.2167	0.1908	2.1673	0.0250
India	*B. percursus*	0.0003	0.0056	0.1916	11.6084	<0.001
B. dermatitidis	*B. gilchristii*	0.0037	0.0022	0.0127	21.7077	<0.001
B. dermatitidis	*B. emzantsi*	0.0037	0.0003	0.1935	29.3221	<0.001
B. dermatitidis	*B. parvus*	0.0037	0.2167	0.1926	24.4538	<0.001
B. dermatitidis	*B. percursus*	0.0037	0.0056	0.1935	33.565	<0.001

*The pairwise comparison between intraclade variation and the pairwise differentiation suggests divergence between the India clade and the North America clade of *B. dermatitidis*. The nonsignificant value between India and *B. parvus* is an artifact of the paraphyletic nature of *B. parvus*, which has an extremely high π value (Figure). DXY, extent of divergence between clades

pea seed agar and incubated the isolates for 7 days. We microscopically examined the isolates after mounting them with lactophenol cotton blue.

Genome Sequencing

Next, we used the cultures to extract DNA from each isolate as previously described (*28,29*). We pooled the resulting genomic libraries sequenced in a single S4 flow cell (2 × 150 bp read length) by using the NovaSeq 6000 (Illumina, https://www.illumina.com). The target sequencing depth was 40 (Appendix Table 2). This sequencing process was done to obtain whole genome sequences of each isolate, which enabled us to differentiate the isolates from India in comparison with isolates from North America. We have described all variant calling protocols, phylogenetic, and population genetic approaches in detail in the appendix (Appendix). We deposited all analytical code related to this study into GitHub (https://github.com/gjofre/BlastomycesIndia).

Results

A histological section of 1 of the samples (subcutaneous, nodule sternum) revealed the presence of a large thick-walled broad-based budding yeast with a double refractile wall (Figure 1, panel A). This cell yeast morphology is typical of *Blastomyces*. The macroscopic mycelial colony morphologies were also consistent with that of *Blastomyces*. When grown on SDA at 25°C, all 3 isolates grew white downy colonies. We conducted microscopic examination of lactophenol cotton blue mounts from SDA slide cultures of each strain that revealed thin septate hyphae, bearing spherical to pyriform smooth-walled microconidia. Subcultured colonies on pea seed agar incubated at 37°C showed conversion from a mold to a yeast form.

Finally, microscopic yeast morphology in culture was also consistent with that of *Blastomyces*. Similar to the yeast cells observed in the biopsy (Figure 1, panel A), microscopic examination of the growth of yeast revealed numerous thick-walled and broad-based budding yeast cells (Figure 1, panel B), which are typical of the genus (*30*).

Next, we obtained whole genome sequences for the 3 putative isolates of *Blastomyces* (mean coverage 20.47) (Appendix Table 1). A principal component analysis that included 2 genera from the dimorphic fungi strongly suggested the 3 isolates from India belonged to *Blastomyces* (Figure 2, panel A). Phylogenetic analyses confirmed that the 3 *Blastomyces* isolates from India are closely related to other isolates of *B. dermatitidis* and form a monophyletic group. This group is sister to the North America samples of *B. dermatitidis*. We recovered this topology regardless of the approach to generate the phylogenetic tree (Appendix Figure 1). In all cases, the branch is well supported (ultrafast bootstrap on 1,000 replicates = 100%). Assuming a mutation rate similar to that of other Ascomycetes (*31,32*), we found that the origin of the India clade of *B. dermatitidis* is not recent (divergence point estimate ≈0.8 million years, SE 0.12 million years) and might precede the settlement of modern humans in the Indian subcontinent (*33,34*).

Finally, we tested whether the monophyletic group of *Blastomyces* isolates from India were differentiated from the other isolates of *B. dermatitidis*. The India group showed the lowest level of diversity of any *Blastomyces* species, lower than that of the North American clade of *B. dermatitidis* and *B. gilchristii* (Table 2). The diversity values are similar in scale to the amount of variability in other fungal species (*35*). The extent of divergence between clades is much higher

Table 2. Test results on the basis of Patterson's D statistic showing extensive introgression between the Indian lineage of *Blastomyces dermatitidis* from India and other *Blastomyces* species*

P1	P2	P3	D-statistic	F_d	F4-ratio	Z-score	p value
India	*B. dermatitidis*	*B. gilchristii*	0.0422	0.0515	0.1011	7.1146	5.61×10^{-13}

*Additional D-statistics values are available in the Appendix Table (https://wwwnc.cdc.gov/EID/article/30/12/24-0830-App1.pdf).

than π, a proxy of intraclade variability, for both the *B. dermatitidis* and *B. gilchristii* and for the *B. dermatitis* from India versus the rest of *B. dermatitidis* comparisons, suggesting genetic differentiation between the lineage from India and the other lineages of *Blastomyces* (Table 1) (*36,37*). Nonetheless, divergent statistics show there is a substantial level of admixture between *B. dermatitidis* from North America and India (Table 2; Appendix Table 3). Those results suggest that, despite the monophyly of this India *Blastomyces* group, the triad of isolates from India still exchanges genetic material with the North America lineage of *B. dermatitidis*.

Discussion

In this article, we report a small cluster of cases of blastomycosis in patients from India with no travel history outside the country. By using genomewide sequencing, we determined that the 3 isolates are *B. dermatitidis*. To date, most cases of *B. dermatitidis*–caused blastomycosis outside of North America have had travel history to that continent (*25*). Because of the lack of evidence of person-to-person transmission in blastomycosis, the most likely explanation is that those cases were acquired from the environment. This hypothesis is consistent with environmental collections of *B. dermatitidis* from bat specimens in India (*38,39*).

Previous efforts have reported the occurrence of clinical cases of blastomycosis in India, and in all cases, the fungus was assumed to be *B. dermatitidis*; however, those reports preceded the description of other *Blastomyces* species and thus should be revisited. The first report of *Blastomyces* in a patient from India (*40,41*) revealed that 3 of 4 suspected cases had a positive immunodiffusion response against anti–*B. dermatitidis* serum precipitins. The efficacy of immunodiffusion to differentiate among *Blastomyces* species is unknown. Because the first report of *Blastomyces* in a patient from India predates DNA sequencing (*40,41*), it is unclear whether the samples included isolates from *Blastomyces* species other than *B. dermatitidis*. Previous reports from India have documented isolation of *B. dermatitidis* from insectivorous bats (*38,39,41–43*), and dogs (*44*), suggesting that the disease has an endemic niche in India. A second effort to characterize the global diversity of *Blastomyces* used restriction fragment-length polymorphisms to typify 52 isolates, including 3 isolates from India (*45*). That survey found 2 isolates from India (1 from a patient and 1 from a bat) were genetically similar to each other but were dissimilar from all other isolates included (*45*). Our phylogenetic reconstruction reveals a similar result in that the isolates from India reported in this article form a distinct genetic group within *B. dermatitidis*.

India has reported cases of blastomycosis imported from the United States (*22,41*). In those instances, the fungus was confirmed to be *B. dermatitidis* by DNA sequencing of 2 loci. Our phylogenetic analyses suggest that the lineage of *B. dermatitidis* we sampled in India diverged long ago from the North America lineage. Our results indicate that systematic collections of environmental and patient samples of *Blastomyces*, along with the use of genomics and phylogenetics, are needed to elucidate the natural occurrence and epidemiology of the etiologic agents of blastomycosis. Clinicians should be aware of the possibility of autochthonous blastomycosis in India, particularly among patients with chronic respiratory diseases.

About the Author

Dr. Chowdhary is a medical mycologist and a physician scientist with the national reference laboratory for antimicrobial resistance in fungal pathogens. Her interests include human fungal infections and antimicrobial resistance.

References

1. Castillo CG, Kauffman CA, Miceli MH. Blastomycosis. Infect Dis Clin North Am. 2016;30:247–64. https://doi.org/ 10.1016/j.idc.2015.10.002
2. Klein BS, Vergeront JM, Davis JP. Epidemiologic aspects of blastomycosis, the enigmatic systemic mycosis. Semin Respir Infect. 1986;1:29–39.
3. Mazi PB, Rauseo AM, Spec A. Blastomycosis. Infect Dis Clin North Am. 2021;35:515–30. https://doi.org/10.1016/ j.idc.2021.03.013
4. Schwartz IS, Wiederhold NP, Hanson KE, Patterson TF, Sigler L. *Blastomyces helicus*, a new dimorphic fungus causing fatal pulmonary and systemic disease in humans and animals in Western Canada and the United States. Clin Infect Dis. 2019;68:188–95. https://doi.org/10.1093/cid/ciy483
5. Maphanga TG, Birkhead M, Muñoz JF, Allam M, Zulu TG, Cuomo CA, et al. Human blastomycosis in South Africa caused by *Blastomyces percursus* and *Blastomyces emzantsi* sp. nov., 1967–2014. J Clin Microbiol. 2020;58:e01661–19. https://doi.org/10.1128/JCM.01661-19

6. Gilchrist TC. A case of blastomycetic dermatitis in man. Johns Hopkins Hosp Rep. 1896;1(269–298):70.

7. Gonyea EF. The spectrum of primary blastomycotic meningitis: a review of central nervous system blastomycosis. Ann Neurol. 1978;3:26–39. https://doi.org/10.1002/ana.410030106

8. Bariola JR, Perry P, Pappas PG, Proia L, Shealey W, Wright PW, et al. Blastomycosis of the central nervous system: a multicenter review of diagnosis and treatment in the modern era. Clin Infect Dis. 2010;50:797–804. https://doi.org/10.1086/650579

9. Martin DS, Smith DT. Blastomycosis, American blastomycosis, Gilchrist's disease: I. A review of the literature. Am Rev Tuberc. 1939;39:275–304.

10. Martin DS, Smith DT. Blastomycosis, American blastomycosis, Gilchrist's disease: II. A report of thirteen new cases. Am Rev Tuberc. 1939;39:488–515.

11. Klein BS, Vergeront JM, Weeks RJ, Kumar UN, Mathai G, Varkey B, et al. Isolation of *Blastomyces dermatitidis* in soil associated with a large outbreak of blastomycosis in Wisconsin. N Engl J Med. 1986;314:529–34. https://doi.org/10.1056/NEJM198602273140901

12. Gilchrist TC, Stokes WR. A case of pseudo-lupus vulgaris caused by a *Blastomyces*. J Exp Med. 1898;3:53–78. https://doi.org/10.1084/jem.3.1.53

13. Fierer J. Invasive endemic fungi of the Western Hemisphere. Virulence. 2019;10:832–4. https://doi.org/10.1080/21505594.2019.1664719

14. Levine S, Ordal ZJ. Factors influencing the morphology of *Blastomyces dermatitidis*. J Bacteriol. 1946;52:687–94. https://doi.org/10.1128/jb.52.6.687-694.1946

15. McBride JA, Gauthier GM, Klein BS. Turning on virulence: mechanisms that underpin the morphologic transition and pathogenicity of *Blastomyces*. Virulence. 2019;10:801–9. https://doi.org/10.1080/21505594.2018.1449506

16. Saccente M, Woods GL. Clinical and laboratory update on blastomycosis. Clin Microbiol Rev. 2010;23:367–81. https://doi.org/10.1128/CMR.00056-09

17. Farber ER, Leahy MS, Meadows TR. Endometrial blastomycosis acquired by sexual contact. Obstet Gynecol. 1968;32:195–9.

18. Craig MW, Davey WN, Green RA. Conjugal blastomycosis. Am Rev Respir Dis. 1970;102:86–90.

19. Jiang Y, Dukik K, Muñoz JF, Sigler L, Schwartz IS, Govender NP, et al. Phylogeny, ecology and taxonomy of systemic pathogens and their relatives in Ajellomycetaceae (Onygenales): *Blastomyces*, *Emergomyces*, *Emmonsia*, *Emmonsiellopsis*. Fungal Divers. 2018;90:245–91. https://doi.org/10.1007/s13225-018-0403-y

20. Brown EM, McTaggart LR, Zhang SX, Low DE, Stevens DA, Richardson SE. Phylogenetic analysis reveals a cryptic species *Blastomyces gilchristii*, sp. nov. within the human pathogenic fungus *Blastomyces dermatitidis*. PLoS One. 2013;8:e59237. https://doi.org/10.1371/journal.pone.0059237

21. Schwartz IS, Wiederhold NP, Patterson TF, Sigler L. *Blastomyces helicus*, an emerging dimorphic fungal pathogen causing fatal pulmonary and disseminated disease in humans and animals in western Canada and United States. Open Forum Infect Dis. 2017;4(Suppl 1):S83–S84. https://doi.org/10.1093/ofid/ofx163.030

22. Kumar A, Kunoor A, Eapen M, Singh PK, Chowdhary A. Blastomycosis misdiagnosed as tuberculosis, India. Emerg Infect Dis. 2019;25:1776–7. https://doi.org/10.3201/eid2509.190587

23. Chakrabarti A, Slavin MA. Endemic fungal infections in the Asia-Pacific region. Med Mycol. 2011;49:337–44. https://doi.org/10.3109/13693786.2010.551426

24. Salzer HJ, Stoney RJ, Angelo KM, Rolling T, Grobusch MP, Libman M, et al. Epidemiological aspects of travel-related systemic endemic mycoses: a GeoSentinel analysis, 1997–2017. J Travel Med. 2018;25(1):10.1093/jtm/tay055. https://doi.org/10.1093/jtm/tay055

25. Gugnani HC, Sharma A, Sood N. A review of blastomycosis in Indian subcontinent. Eur J Med Health Sci. 2022;4:01–7. https://doi.org/10.34104/ejmhs.022.01007

26. Ashraf N, Kubat RC, Poplin V, Adenis AA, Denning DW, Wright L, et al. Re-drawing the maps for endemic mycoses. Mycopathologia. 2020;185:843–65. https://doi.org/10.1007/s11046-020-00431-2

27. Yates-Siilata KE, Sander DM, Keath EJ. Genetic diversity in clinical isolates of the dimorphic fungus *Blastomyces dermatitidis* detected by a PCR-based random amplified polymorphic DNA assay. J Clin Microbiol. 1995;33:2171–5. https://doi.org/10.1128/jcm.33.8.2171-2175.1995

28. Jofre GI, Singh A, Mavengere H, Sundar G, D'Agostino E, Chowdhary A, et al. An Indian lineage of *Histoplasma* with strong signatures of differentiation and selection. Fungal Genet Biol. 2022;158:103654. https://doi.org/10.1016/j.fgb.2021.103654

29. Sepúlveda VE, Márquez R, Turissini DA, Goldman WE, Matute DR. Genome sequences reveal cryptic speciation in the human pathogen *Histoplasma capsulatum*. MBio. 2017;8:e01339–17. https://doi.org/10.1128/mBio.01339-17

30. Linder KA, Kauffman CA, Miceli MH. Blastomycosis: a review of mycological and clinical aspects. J Fungi (Basel). 2023;9:117. https://doi.org/10.3390/jof9010117

31. Lynch M, Sung W, Morris K, Coffey N, Landry CR, Dopman EB, et al. A genome-wide view of the spectrum of spontaneous mutations in yeast. Proc Natl Acad Sci U S A. 2008;105:9272–7. https://doi.org/10.1073/pnas.0803466105

32. Farlow A, Long H, Arnoux S, Sung W, Doak TG, Nordborg M, et al. The spontaneous mutation rate in the fission yeast *Schizosaccharomyces pombe*. Genetics. 2015;201:737–44. https://doi.org/10.1534/genetics.115.177329

33. Thangaraj K, Chaubey G, Kivisild T, Reddy AG, Singh VK, Rasalkar AA, et al. Reconstructing the origin of Andaman Islanders. Science. 2005;308:996–996. https://doi.org/10.1126/science.1109987

34. Tamang R, Thangaraj K. Genomic view on the peopling of India. Investig Genet. 2012;3:20. https://doi.org/10.1186/2041-2223-3-20

35. Leffler EM, Bullaughey K, Matute DR, Meyer WK, Ségurel L, Venkat A, et al. Revisiting an old riddle: what determines genetic diversity levels within species? PLoS Biol. 2012;10:e1001388. https://doi.org/10.1371/journal.pbio.1001388

36. Matute DR, Sepúlveda VE. Fungal species boundaries in the genomics era. Fungal Genet Biol. 2019;131:103249. https://doi.org/10.1016/j.fgb.2019.103249

37. Cai L, Giraud T, Zhang N, Begerow D, Cai G, Shivas RG. The evolution of species concepts and species recognition criteria in plant pathogenic fungi. Fungal Divers. 2011;50:121–33. https://doi.org/10.1007/s13225-011-0127-8

38. Khan ZU, Randhawa HS, Lulla M. Isolation of *Blastomyces dermatitidis* from the lungs of a bat, *Rhinopoma hardwickei hardwickei* Gray, in Delhi. Sabouraudia. 1982;20:137–44. https://doi.org/10.1080/00362178285380211

39. Randhawa HS, Chaturvedi VP, Kini S, Khan ZU. *Blastomyces dermatitidis* in bats: first report of its isolation from the liver of *Rhinopoma hardwickei hardwickei* Gray. Sabouraudia. 1985;23:69–76. https://doi.org/10.1080/00362178585380111
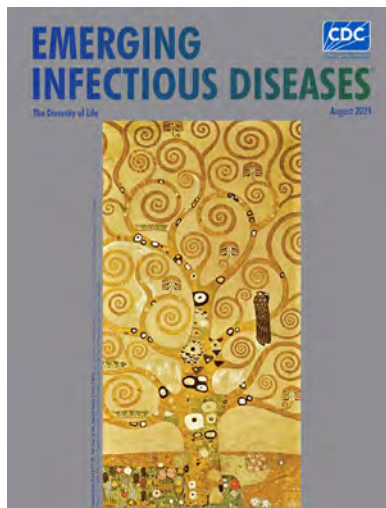
40. Randhawa HS, Khan ZU, Gaur SN. *Blastomyces dermatitidis* in India: first report of its isolation from clinical material. Sabouraudia. 1983;21:215–21. https://doi.org/10.1080/00362178385380331

41. Randhawa HS, Chowdhary A, Kathuria S, Roy P, Misra DS, Jain S, et al. Blastomycosis in India: report of an imported case and current status. Med Mycol. 2013;51:185–92. https://doi.org/10.3109/13693786.2012.685960

42. Chaturvedi VP, Randhawa HS, Kini S, Khan ZU. Survival of *Blastomyces dermatitidis* in the gastrointestinal tract of an orally infected insectivorous bat, *Rhinopoma hardwickei hardwickei* Gray. J Med Vet Mycol. 1986;24:349–52. https://doi.org/10.1080/02681218680000521

43. Raymond JT, White MR, Kilbane TP, Janovitz EB. Pulmonary blastomycosis in an Indian fruit bat (*Pteropus giganteus*). J Vet Diagn Invest. 1997;9:85–7. https://doi.org/10.1177/104063879700900117

44. Sestero CM, Scalarone GM. Detection of IgG and IgM in sera from canines with blastomycosis using eight *Blastomyces dermatitidis* yeast phase lysate antigens. Mycopathologia. 2006;162:33–7. https://doi.org/10.1007/s11046-006-0028-7

45. McCullough MJ, DiSalvo AF, Clemons KV, Park P, Stevens DA. Molecular epidemiology of *Blastomyces dermatitidis*. Clin Infect Dis. 2000;30:328–35. https://doi.org/10.1086/313649

Address for correspondence: Daniel R. Matute, Department of Biology, University of North Carolina, 3161 Genome Sciences building, CB 3280, Chapel Hill, NC 27599, USA; email: dmatute@email.unc.edu

To revisit the August 2024 issue, go to:
https://wwwnc.cdc.gov/eid/articles/issue/30/8/table-of-contents

Clinical Manifestations, Antifungal Drug Susceptibility, and Treatment Outcomes for Emerging Zoonotic Cutaneous Sporotrichosis, Thailand

Pattriya Jirawattanadon, Sumanas Bunyaratavej, Charussri Leeyaphan,
Piriyaporn Chongtrakool, Panitta Sitthinamsuwan, Waratchaya Panjapakkul,
Suthasanee Prasertsook, Phuwakorn Saengthong-aram,
Nicha Wareesawetsuwan, Julaluck Posri, Penvadee Pattanaprichakul

We analyzed clinical manifestations, antifungal susceptibility, and treatment outcomes of cutaneous sporotrichosis in Thailand during 2018–2022. The study included 49 patients whose mean age was 58.7 (SD 16.9) years; 65.3% were female and 34.7% male. A history of cat exposure was reported in 32 (65.3%) patients who had a significantly higher prevalence of upper extremity lesions than did those without cat contact (90.6% vs. 41.7%; adjusted odds ratio 18.9 [95% CI 3.2–92.9]). Among patients >60 years of age, lesions were more likely to be nonpustular than for patients <60 years of age (82.1% vs. 52.4%; p = 0.033). All 9 isolates tested for antifungal drug susceptibility exhibited an itraconazole MIC of ≤1 μg/mL. Oral itraconazole monotherapy was effective; the median time-to-cure was 180 days (interquartile range 141–240 days). Physicians should heighten their awareness of potential sporotrichosis causes, particularly when a history of animal contact exists.

Sporotrichosis is a chronic infection caused by *Sporothrix* spp., dimorphic fungi that exist in a hyphal form at low temperatures or as budding yeast at high temperatures. This pathogen is found in soil, plants, and organic matter and gives rise to an anthropozoonotic disease primarily affecting the skin and subcutaneous tissues after traumatic inoculation by contaminated materials (*1–3*). *Sporothrix* spp. have been previously classified under the *S. schenckii* complex, which comprise *S. schenckii* sensu stricto, *S. brasiliensis*, *S. globosa*, *S. luriei*, *S. pallida*, *S. mexicana*, and *S. chilensis*. The classification system has been updated to include a clinical clade consisting of *S. schenckii*,

S. globosa, *S. brasiliensis*, and *S. luriei*. Species from the environmental clade, including *S. pallida*, *S. mexicana*, and *S. chilensis*, rarely cause human infection (*4*).

Although sporotrichosis has a global distribution, clinical and epidemiologic features vary. It is endemic in regions that have tropical and subtropical climates and maintain high humidity and 25°C–28°C temperatures (*2,5,6*). Several reports have cited case series or outbreak instances among occupational groups prone to minor soil- and plant-inflicted injuries, such as florists, miners, foresters, and gardeners (*7–12*). Furthermore, since the 1980s, owning cats has emerged as a risk factor for zoonotic transmission of sporotrichosis (*13,14*). Human sporotrichosis outbreaks have been linked to scratches or bites from infected cats. Domestic cats, because of their pathogen-rich lesions and intimate interactions with humans, serve as *Sporothrix* spp. vectors (*15–20*).

The disease has an incubation period ranging from a few days to several months (*21*) and can manifest in cutaneous, pulmonary, and disseminated forms. Cutaneous manifestation is the most common, typically occurring as erythematous papules or pustules that form ulcerated nodules involving local lymphatic channels, which cause lymphangitis and lymphadenopathy (*2,22*). Sporotrichosis can also be categorized into fixed cutaneous, lymphocutaneous, and disseminated cutaneous forms. Although the fixed and lymphocutaneous forms are commonly observed, disseminated cutaneous sporotrichosis is rarely reported except in immunosuppressed patients (*23*). Fungi isolation is the standard for diagnosis; the first-line treatment is itraconazole (*24*). For antifungal susceptibility testing of *Sporothrix* spp., broth microdilution, as recommended by the Clinical and

Laboratory Standards Institute (https://clsi.org/standards/products/microbiology/documents/m38), is the primary protocol used to determine in vitro MICs for drugs used in sporotrichosis treatment. Itraconazole is the most effective drug for treating sporotrichosis. A cutoff point of 1 µg/mL is used according to a previous study correlating the itraconazole MIC with clinical outcomes (25). Terbinafine has demonstrated the lowest geometric mean MIC, followed by ketoconazole (26). No associations have been found between higher amphotericin B or itraconazole MIC values and unfavorable outcomes (25).

Sporotrichosis is a relatively rare disease in Thailand. However, since 2018, a substantial increase in the number of sporotrichosis patients has been observed at the outpatient dermatology clinic at Siriraj Hospital in Bangkok, Thailand. This surge parallels the growing evidence of feline sporotrichosis observed in Thailand since 2018 (27). We investigated the clinical manifestations and treatment outcomes for a recent emerging outbreak of cutaneous sporotrichosis in Thailand.

Methods

We conducted a retrospective study of patients who had a cutaneous sporotrichosis diagnosis at the dermatology clinic of Siriraj Hospital during January 1, 2018–August 27, 2022. The Siriraj Hospital Institutional Review Board authorized the study protocol (approval nos. Si 979/2020 and Si 671/2021). We enrolled patients in the study if the diagnosis was confirmed by positive isolation of *S. schenckii* complex in culture. We extracted patient sex, age, duration of symptoms, underlying medical conditions, occupation, exposure history (animal contact, injury history, and contamination with soil), clinical manifestations, histopathology, laboratory culture, susceptibility testing of the causative fungus, treatment options, and treatment outcomes from medical records. We considered patients to be immunocompromised if they exhibited specific conditions that can cause host defense defects, such as cirrhosis, diabetes mellitus, or recent chemotherapy (28).

Hospital staff collected specimens for histopathologic examination and laboratory culture; specimens were collected from tissue biopsies or pus from cutaneous lesions. Fungi were identified by phenotypic characteristics, including colony morphology, conidial arrangement, and physiologic traits (carbohydrate assimilation of dextrose, sucrose, and raffinose), as well as temperature tolerance at 37°C and 40°C. Antifungal susceptibility testing was undertaken in some cases on the basis of convenience selection by using the Clinical and Laboratory Standards Institute broth dilution method, as noted . Testing was performed for 5-flucytosine, amphotericin B, anidulafungin, caspofungin, micafungin, fluconazole, itraconazole, posaconazole, and voriconazole.

We defined an improved lesion as a lesion that had become smaller or drier without cutaneous extension and a cure as a complete healing of lesions with or without scarring or hyperpigmentation. We conducted telephone interviews to assess patients who had incomplete data because of loss to follow-up during the treatment course.

Statistical Analysis

We used descriptive statistics for demographic data, clinical manifestations, histopathologic examinations, laboratory findings, antifungal susceptibility, treatments, and treatment outcomes. We calculated means and SDs for normally distributed continuous data, medians and interquartile ranges (IQRs) for non–normally distributed continuous data, and numbers and percentages for categorical data. We used χ^2 and Fisher exact tests to compare clinical characteristics between patients who had or did not have exposure to cats. We used a binary logistic regression model and forward stepwise selection method to estimate the odds ratio (OR) of a binary response. We constructed a Cox proportional hazards model to determine the hazard ratio for each factor and to measure time-to-improve and time-to-cure. We adjusted for patient sex and age in the multivariable analysis of both binary logistic regression and Cox proportional hazards models. In addition, we calculated the OR, hazard ratio, and 95% CI for each pertinent variable. We analyzed data by using PASW Statistics 18.0 (SPSS, https://www.sbas.com.hk). A p value of <0.05 indicated statistical significance.

Results

We included 49 patients who had cutaneous sporotrichosis during 2018–2022 and summarized their clinical characteristics (Table 1). We observed a marked increase in cases each year during this period, escalating from 1 case to 3 cases, then to 6 cases, 14 cases, and finally 25 cases (Figure 1). The mean age of patients was 58.7 (SD 16.9) years; 32 (65.3%) were female and 17 (34.7%) male. Only 9 patients were immunocompromised, having diabetes mellitus or sigmoid colon cancer with recent chemotherapy. The median duration from lesion onset to diagnosis was 30 (range 7–180) days. Before sporotrichosis diagnosis, 15 (30.6%) patients had undergone treatment regimens for nontuberculous mycobacterial infections but had no observed improvement.

Thirty-five (71.4%) patients reported a history of animal exposure; 32 had been exposed to cats and 3 to insects. Of the 3 patients with insect bites, 2 had bites from mosquitoes and 1 had an unidentified insect bite. For all 3 patients, lesions developed later on the lower extremities at the sites of those insect bites. Among the patients exposed to cats, 23 had direct contact, and 22 (95.7%) of those 23 reported scratches

Table 1. Patient demographics in study of clinical manifestations, antifungal drug susceptibility, and treatment outcomes for emerging zoonotic cutaneous sporotrichosis, Thailand*

Demographic data	Sporotrichosis cases, n = 49
Patient sex	
F	32 (65.3)
M	17 (34.7)
Mean age, y (±SD)	58.7 (±16.9)
Median symptom duration, d (IQR)	30 (21–60)
Immune status	
Immunocompetent host	40 (81.6)
Immunocompromised host	9 (18.4)
Diabetes mellitus	8/9 (88.9)
Sigmoid carcinoma and recent chemotherapy	1/9 (11.1)
Occupation	
Retired/unemployed	15 (30.6)
Officer	10 (20.4)
Merchant/business owner	8 (16.3)
Veterinarian/veterinary assistants	4 (8.2)
Student	4 (8.2)
Housekeeper/cleaner	4 (8.2)
Other†	4 (8.2)
Exposure history	
Zoonosis	35 (71.4)
Cats	32/35 (91.4)
Insect bite	3/35 (8.6)
Wound contact with soil	1 (2.0)
Unknown	13 (26.5)
Family history of cutaneous sporotrichosis	5 (10.2)
Clinical symptoms	
Painless	24 (49.0)
Painful	19 (38.8)
Itching	6 (12.2)
Lesions	
Median no. lesions (IQR)	2.0 (1.0–3.0)
Single	20 (40.8)
Multiple	29 (59.2)
Unilateral	25/29 (86.2)
Bilateral	4/29 (13.8)
Morphology	
Nonpurulent, nonulcerative papule, plaque, or nodule	34 (69.4)
Purulent, ulcerative pustule, ulcer, abscess	15 (30.6)
Arrangement	
Satellite nodules around the ulcer rim	27 (55.1)
Lymphocutaneous pattern	22 (44.9)
Lesion site	
Head and neck	3 (6.1)
Trunk	1 (2.0)
Upper extremities	36 (73.5)
Lower extremities	11 (22.4)
Lymphadenopathy, n = 44	6/44 (13.6)
Histopathology, n = 44	
Mixed cell, suppurative granuloma	36/44 (81.8)
Nonspecific granulomatous inflammation	3/44 (6.8)
Evidence of fungus observed	0/44 (0.0)
Outcome	
Completely cured	41 (83.7)
Lost to follow-up	8 (16.3)
Treatment duration	
Median duration until improved, d (IQR)	46 (30–90)
Mean duration until cured, d (IQR), n = 41	180 (141–240)

*Values are no. patients/total no. patients (%) except as indicated. IQR, interquartile range.
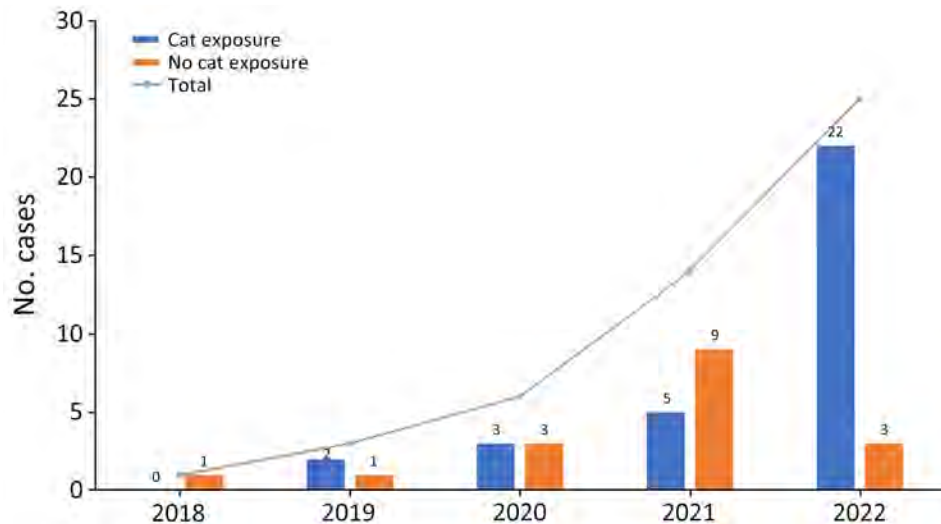†Other occupations included teacher, monk, and boat driver.

Figure 1. Numbers of sporotrichosis cases during 2018–2022 in study of clinical manifestations, antifungal drug susceptibility, and treatment outcomes for emerging zoonotic cutaneous sporotrichosis, Thailand. Line indicates the total number of cases each year. Numbers above each bar indicate the number of patients exposed or not exposed to cats.

or bites (Table 2). Most (27/32) patients exposed to cats had contact with their own cats, and all let their cats roam outdoors. In addition, 21 (65%) patients had been in direct contact with cats that had sporotrichosis diagnosed by a veterinarian. Although 15 (30.6%) patients were retired or unemployed, 4 (8.2%) patients were employed in veterinary professions; 2 were veterinarians and 2 veterinary assistants. All 4 of those patients were scratched or bitten by cats that had sporotrichosis. Only 2/49 (4.1%) patients had a history of gardening, and none reported exposure to rose thorns. One patient reported falling from a bicycle onto soil causing an abrasion wound on his left leg, which later developed into lymphocutaneous lesions. Sporotrichosis developed in 13/49 (26.5%) patients who had no recognized risk factors.

No pain was experienced in 49.0% of patients. Multiple lesions were observed in 59.2% of cases manifesting a lymphocutaneous pattern (44.9%; Figure 2, panel A). Fifteen (30.6%) patients had purulent

discharge and ulceration. Single lesions, which mostly had satellite nodules around the ulcer rim, were found in 40.8% of patients (Figure 2, panel B). Three (6.1%) patients had solitary or multiple verrucous plaques (Figure 2, panel C). Most (73.5%) lesions were located on the upper extremities, and only 13.6% of patients manifested lymphadenopathy. Patients >60 years of age also had significantly more nonpustular lesions than younger patients (23/28 [82.1%] vs. 11/21 [52.4%]; p = 0.033).

Patients with a history of cat contact exhibited higher levels of immunocompetence (90.6% vs. 64.7%; adjusted OR 5.2 [95% CI 1.1–24.8]), and lesions were more frequently located on the upper extremities (90.6% vs. 41.7%; adjusted OR 18.9 [95% CI 3.2–92.9]) than in those who had no cat exposure (Table 3). The difference in lesion frequency was also statistically significant in multivariate analysis. In addition, lesions tended to be multiple and arranged in a lymphocutaneous pattern in patients who had cat contact.

Histopathologic analysis was conducted for 44 of 49 patients and revealed mixed cell or suppurative granuloma in 81.8% of lesions and nonspecific granulomatous inflammation in 6.8% of lesions. Periodic acid Schiff and Gomori methenamine silver stains were performed in all cases. No evidence of fungi was detected. Only 1 patient did not undergo a skin biopsy; their sporotrichosis diagnosis was confirmed through a positive pus culture result. Antifungal susceptibility testing for 9 patients was reported, and all 9 isolates exhibited an itraconazole MIC of ≤1 µg/mL (Table 4).

Of the 49 patients, 41 received itraconazole and 5 terbinafine as first-line treatment. The remaining 3 patients were lost to follow-up before beginning

Table 2. Patient exposure to cats in study of clinical manifestation antifungal drug susceptibility, and treatment outcomes for emergir zoonotic cutaneous sporotrichosis, Thailand*

Patient exposures to cats	No. sporotrichosi cases/total (%)
Direct contact	23/32 (71.9)
Being scratched or bitten	22/23 (95.7)
Feeding	16/23 (69.6)
Attending to cat wound	4/23 (17.4)
Indirect contact†	9/32 (28.1)
Types of cat socialization	
Owned, outdoor cat‡	27/32 (84.4)
Stray cat	5/32 (15.6)
Exposed to cat with sporotrichosis diagnosis	21/32 (65.6)

*Patients could have >1 contact history.
†Patients reported stray cats in the vicinity of their homes but indicated r direct contact.
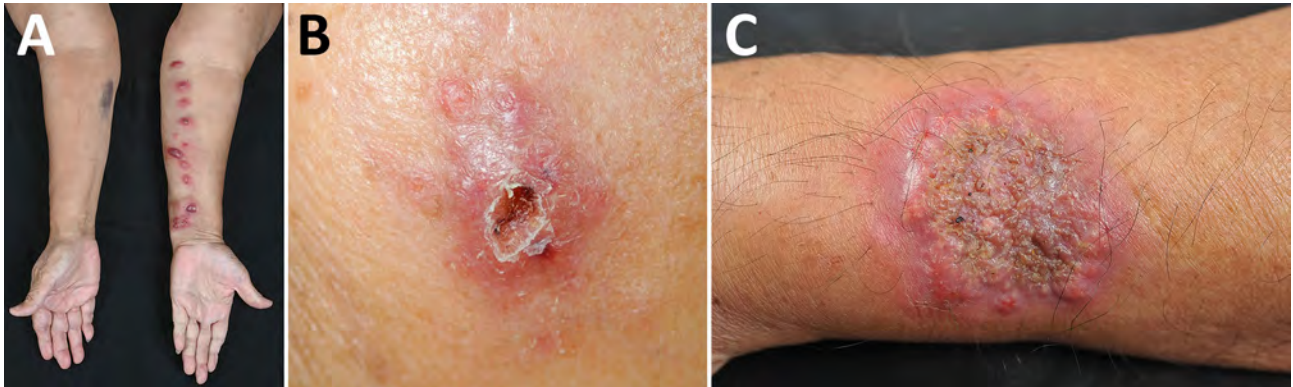‡Cats that have homes but can go outside.

Figure 2. Clinical disease manifestations in study of antifungal drug susceptibility and treatment outcomes for emerging zoonotic cutaneous sporotrichosis, Thailand. A) Lymphocutaneous pattern on a patient's left forearm; B) satellite nodules encircling ulcer rim on a patient's left cheek; C) verrucous plaque on a patient's left forearm.

treatment. Treatment outcomes could only be observed in 41 patients; the remaining 8 were lost to follow-up. All itraconazole-treated patients received an initial dose of 200 mg/day. After ≈2 months of treatment, the itraconazole dose was increased to 400 mg/day in 11 (26.8%) patients because of worsening lesions. All 11 patients entered remission within a

median of 127 (IQR 60–203) days after the dose increase. Antifungal susceptibility testing had been performed for 2 of those 11 patients (patients 2 and 7; Table 4), 1 of whom failed to improve after 4 months of increased itraconazole dose and was, therefore, treated by excision, followed by another 7 weeks of itraconazole and remission. We did not observe a significant

Table 3. Clinical manifestation comparisons between patients with and without cat exposure in study of clinical manifestations, antifungal drug susceptibility, and treatment outcomes for emerging zoonotic cutaneous sporotrichosis, Thailand*

| | | | Univariate analysis | | Multivariate analysis† | |
Demographic data	Cat exposure, n = 32	No cat exposure, n = 17	Crude OR (95% CI)	p value	Adjusted OR‡ (95% CI)	p value
Patient sex						
M	9 (28.1)	8 (47.1)	2.3 (0.7–7.7)	0.189	NA	
F	23 (71.9)	9 (52.9)	Referent			
Mean age, y (±SD)	55.0 (±16.4)	65.5 (±16.1)	0.9 (0.9–1.0)	0.084	1.0 (0.9–1.0)	0.095
Median symptom duration, d (IQR)	30.0 (21.0–83.0)	30.0 (22.0–60.0)	1.0 (0.9–1.0)	0.916	NA	
Immunologic status						
Immunocompromised	3 (9.4)	6 (35.3)	5.3 (1.1–24.8)	**0.036**	5.2 (1.1–24.8)	**0.036**
Immunocompetent	29 (90.6)	11 (64.7)	Referent		Referent	
Sporotrichosis in family member, n = 47	5/32 (15.6)	0/15 (0.0)	NA	0.162	NA	
Lesions						
Single	9 (28.1)	11 (64.7)	Referent	**0.016**	Referent	0.100
Multiple	23 (71.9)	6 (35.3)	4.7 (1.3–16.5)		6.1 (0.9–24.4)	
Lesions site						
Head and neck	0 (0)	3 (17.6)	NA	0.073	NA	
Trunk	0 (0.0)	1 (5.9)	NA	0.347	NA	
Upper extremities	29 (90.6)	7 (41.2)	13.8 (3.0–63.9)	**0.001**	18.9 (3.2–92.9)	**0.001**
Lower extremities	5 (15.6)	6 (35.3)	0.3 (0.1–1.4)	0.125	NA	
Morphology						
Nonpustular	23 (71.9)	11 (64.7)	Referent	0.605	NA	
Pustular	9 (28.1)	6 (35.3)	0.7 (0.2–2.5)			
Arrangement						
Lymphocutaneous pattern	18 (56.3)	4 (23.5)	4.2 (1.1–15.7)	**0.034**	3.7 (0.8–16.7)	0.093
Lymphadenopathy, n = 44	3/28 (10.7)	3/16 (18.8)	0.5 (0.1–3.0)	0.460		
Median treatment duration, d (IQR)						
Until improvement	46.0 (30.0–107.0)	53.0 (30.0–90.0)	1.0 (0.9–1.0)	0.625	NA	
Until cured	183.0 (135.0–246.0)	165.0 (136.0–206.0)	1.0 (0.9–1.0)	0.495	NA	

*Values are no. patients/total no. patients (%) except as indicated. Bolded numbers are significant p values <0.05. IQR, interquartile range; NA, not applicable; OR, odds ratio.
Multivariate analysis was conducted by using multiple binary logistic regression.

Table 4. Antifungal susceptibility test results for 9 patients in study of clinical manifestations, antifungal drug susceptibility, and treatment outcomes for emerging zoonotic cutaneous sporotrichosis, Thailand*

Antifungal drug	MIC, μg/mL								
	Patient 1	Patient 2	Patient 3	Patient 4	Patient 5	Patient 6	Patient 7	Patient 8	Patient 9
5-Flucytosine	0.5	32	1	32	2	2	2	2	2
Amphotericin B	2	2	4	1	4	4	4	2	2
Anidulafungin	4	>8	>8	1	>8	0.5	1	>8	0.5
Caspofungin	>8	>8	>8	>8	>8	4	>8	>8	1
Fluconazole	>256	256	32	256	256	256	>256	256	>256
Itraconazole	1	0.25	0.5	0.5	0.25	1	1	0.5	0.25
Micafungin	>8	>8	>8	>8	>8	>8	>8	>8	>8
Posaconazole	0.5	0.5	0.5	1	0.25	0.25	0.25	0.25	0.25
Voriconazole	0.12	0.25	0.06	1	0.03	0.06	0.5	0.25	0.06

*Sporothrix schenckii complex fungi isolated from patient specimens were tested for susceptibility to antifungal drugs.

difference in itraconazole MICs between patients who had treatment failure and those who had successful treatment at the dose of 200 mg/day (median MIC 1.0 [IQR 0.25–1.0] μg/mL vs. 0.5 [IQR 0.25–0.625] μg/mL; p = 0.414). No patients reported serious side effects from itraconazole.

The median time-to-improvement was ≈46 (IQR 30–90) days, and the median time-to-cure was 180 (IQR 141–240) days. According to the Cox proportional hazards model, no variable was significantly associated with improvement or cure rates (Table 5). By 6 months after treatment, remission had been achieved in 50% of patients, and by 8 months, ≈75% of patients had entered remission (Figure 3).

Discussion

Four human cases of sporotrichosis have previously been reported in Thailand (29–31). This study documents a high number of patients with sporotrichosis reported in the country during 2018–2022. The historically low reported incidence might have been from underreporting or underdiagnosis, possibly because of limited laboratory capabilities in Thailand (29).

Sporotrichosis is endemic in various regions worldwide (32), including Latin America, South

Table 5. Comparison of hazard ratios for time-to-improvement and time-to-cure among patients in study of clinical manifestations, antifungal drug susceptibility, and treatment outcomes for emerging zoonotic cutaneous sporotrichosis, Thailand*

Variables	Time-to-improvement†		Time-to-cure			
	Univariate analysis		Univariate analysis		Multivariate analysis	
	Crude HR (95% CI)	p value	Crude HR (95% CI)	p value	Adjusted HR‡ (95% CI)	p value
Patient sex						
M	Referent	0.452	Referent	0.102	Referent	0.620
F	1.3 (0.7–2.5)		1.8 (0.9–3.7)		1.9 (0.9–4.1)	
Patient age at diagnosis, y						
≤60	Referent	0.587	Referent	0.176	Referent	0.109
>60	1.2 (0.7–2.1)		1.5 (0.8–2.9)		1.7 (0.9–3.1)	
Immunologic status						
Immunocompromised	1.5 (0.7–3.4)	0.299	0.8 (0.4–2.0)	0.686	NA	
Immunocompetent	Referent		Referent		NA	
Cat exposure						
Yes	0.9 (0.5–1.7)	0.648	0.7 (0.4–1.4)	0.349	NA	
No	Referent		Referent		NA	
Lesions						
Single	Referent	0.253	Referent	0.761	NA	
Multiple	0.7 (0.4–1.3)		1.1 (0.6–2.1)		NA	
Morphology						
Nonpustular	Referent	0.445	Referent	0.448	NA	
Pustular	0.8 (0.4–1.5)		1.3 (0.7–2.5)		NA	
Arrangement						
Lymphocutaneous pattern	0.9 (0.5–1.8)	0.773	1.2 (0.6–2.3)	0.559	NA	
Lymphadenopathy	0.9 (0.6–2.4)	0.895	2.6 (0.9–7.1)	0.086	2.7 (1.0–7.5)	0.106
Itraconazole susceptibility§						
MIC <1 μg/mL	Referent	0.735	Referent	0.998	NA	
MIC = 1 μg/mL	1.3 (0.3–5.9)		1.1 (0.2–4.3)		NA	

*HRs were calculated by using the Cox proportional hazard model. HR, hazard ratio; NA, not applicable.
†Multivariate analysis was not performed for time-to-improvement variables.
‡Adjusted for patient age and sex.
§Itraconazole susceptibility tests were performed for specimens from 9 patients. A cutoff point of 1 μg/mL was used according to a previous study relating the itraconazole MIC to clinical outcomes (26).
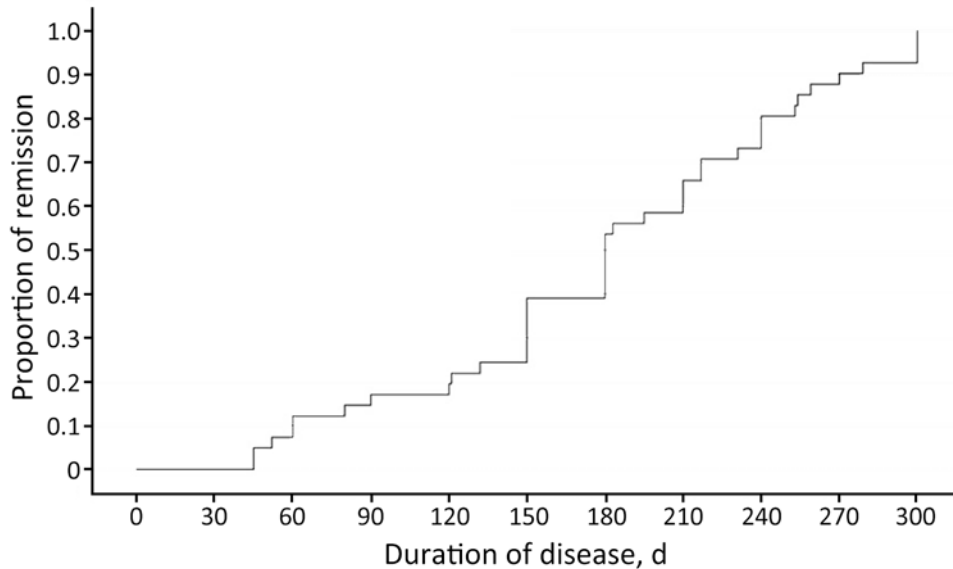
Figure 3. Proportion of patients in remission over time in study of clinical manifestations, antifungal drug susceptibility, and treatment outcomes for emerging zoonotic cutaneous sporotrichosis, Thailand. Kaplan–Meier survival analysis was used to determine the duration of cutaneous sporotrichosis in patients.

Africa, Australia, and several countries in Asia, such as India, China, Japan, and Malaysia (*33*). The largest known zoonotic outbreak since the 20th Century was reported in Brazil (*32*). In Thailand, sporotrichosis cases have rarely been documented before 2018; our hospital typically encountered an average of only 1 case per year, initially linked to a case series reported in another hospital (*29*). However, since 2018, sporotrichosis has been increasingly reported in stray cats in Thailand (*34*), accompanied by a corresponding rise in human disease diagnosed at our hospital. Laboratory detection methods have remained consistent; conventional fungal detection techniques have been used routinely at our facility because of their cost-effectiveness for clinical services, whereas molecular techniques are primarily reserved for research purposes. Therefore, the increase in case numbers is more likely attributable to a true outbreak.

More women were enrolled in this study, ≈2 times more women than men. This ratio aligns with most other sporotrichosis outbreak reports, which have indicated similar percentages of women in study populations, ranging from 53% to 72% (*35–38*). The most commonly reported mean or median age has been 40–50 years (*35–38*), which is younger than that found in this study. Most patients were immunocompetent hosts, suggesting that immune status is not a determining factor for susceptibility to sporotrichosis.

A history of direct contact with cats that had current sporotrichosis diagnoses was reported by 21 (42.8%) of the 49 patients, suggesting that zoonotic transmission from cats was likely for those particular cases. Cats are the principal transmission vector leading to sporotrichosis outbreaks in many countries, particularly in South America and some countries in Asia (*16,33,39*). Claws, skin lesions, nasal and oral cavities, and feces of infected cats contain a considerably higher number of fungi than environmental sources, suggesting that *Sporothrix* spp. transmission more likely occurs from infected cats than from environmental sources (*40*). The rising incidence of the disease in humans aligns with the previously reported outbreak of feline sporotrichosis in Thailand (*27*). Although insects are known to be carriers of *Sporothrix* spp. fungi (*41*), a history of insect bites in patients with sporotrichosis has rarely been reported. In this study, 3 patients had lesions located in the area of previous insect bites. Sapronosis is another commonly cited primary mode of transmission in sporotrichosis outbreak studies (*35*). However, only 1 patient in this study reported possible sapronotic transmission from contact with contaminated soil after a bicycle fall.

The upper extremities have been ranked first and lower extremities ranked second as the most common sites for *Sporothrix* lesions (*29,35,36*). Moreover, lesions in the upper extremities are more likely to be reported in patients exposed to cats. Most sporotrichosis manifestations were lymphocutaneous or fixed cutaneous forms and occurred in similar proportions, aligning with our results. Disseminated sporotrichosis has rarely been reported globally (*29,38,37*) and has not been reported in Thailand (*29*).

Patients >60 years of age tended to have nonpustular lesions more frequently than did younger persons. This age-related pattern could be caused by immunosenescence, which is characterized by alterations in innate and adaptive immunity (*42,43*). As a person ages, their immunologic functions gradually decline,

contributing to poor responses and diminished levels of inflammation after new infections (*42,43*).

Different *Sporothrix* species are predominant in various regions worldwide. *S. schenckii* is the primary species causing sporotrichosis in Australia, America, and South Africa, whereas *S. globosa* is the etiologic agent in most patients in China (*4,24*). *S. brasiliensis* is the main organism causing feline and human sporotrichosis in Brazil (*4,44*). Feline sporotrichosis caused by *S. schenckii* s.s. has been reported in southern Thailand, which suggests species transmission to humans (*27*). In Thailand, further studies and molecular identification of species causing human sporotrichosis are needed to explain the epidemiology and association with feline sporotrichosis. This study only reported the *S. schenckii* complex by using fungal culture and colony morphologic identification during routine laboratory investigations in clinical practice.

No evidence of fungal forms was seen in our cases during histopathologic examination; the absence of fungi in histopathologic sections remains unclear. However, on the basis of previous research, several factors might influence pathogen load in tissue biopsies. One factor is the onset or duration of the disease before the biopsy is obtained. A study of liver granuloma formation after *Histoplasma* sp. infection reported the highest fungal load in tissue at 7 days postinfection; substantial infection control was observed by 50 days (*45*). That finding suggests that early biopsy within the first week of symptoms might increase the likelihood of detecting the pathogen. Conversely, over time, granulomas might undergo structural changes that reduce their capacity to contain the infection (*46*). Another factor is the virulence of the pathogen; some fungi possess virulence factors that enable them to overcome host defenses (*47*). For example, *S. brasiliensis* has structural features that potentially inhibit and evade phagocytosis, contributing to its higher virulence than that for *S. schenckii* (*48*). Those factors might explain why our findings align with a study in Malaysia that reported low evidence of fungal organisms in tissues, rather than with higher detection rates observed in Brazil (*38,39*). Further studies involving larger populations are needed to explore those hypotheses.

Numerous treatments for cutaneous sporotrichosis are available. For example, oral antifungal agents, a saturated oral solution of potassium iodide, and excision can be used as standalone or combination therapies. However, oral itraconazole remains the treatment of choice, and the length of treatment is dependent upon lesion recovery (*4,24,36*). Despite the lack of a defined cutoff value for antifungal susceptibility among *Sporothrix* spp., our study found that all 9

isolates subjected to susceptibility testing exhibited an itraconazole MIC of ≤ 1 μg/mL. However, no significant difference was observed for itraconazole MICs between patients with and without treatment failure at a dose of 200 mg/day. Time-to-event analysis also showed no significant difference in time-to-improvement or time-to-cure between patients with a 1 μg/mL MIC and <1 μg/mL MIC, consistent with the study from Brazil (*25*). This study's median duration until cure was 180 days, aligning with the findings from a 19-case review in Southeast Asia (*29*) and other studies (*49,50*). This study did not identify any clinical factors that influenced the duration until cure.

In conclusion, cutaneous sporotrichosis is a rare disease in Thailand. However, the number of cases has escalated dramatically since 2018, and ≈65% of patients have reported a history of cat exposure. Consequently, taking a thorough risk-factor history, especially regarding cat exposure, is crucial for guiding early clinical suspicion of disease and diagnosis. The standard for diagnosis is fungus isolation; the *S. schenckii* complex is suspected to be the primary sporotrichosis-causing species in Thailand. Itraconazole is the first-line treatment, and resistance to this drug has not been reported. Physicians and veterinary personnel should heighten their awareness of the sporotrichosis outbreak in Thailand to enable more effective disease control. In addition, early recognition of suspected sporotrichosis cases in cats, appropriate antifungal treatment, and education on how persons can avoid zoonotic transmission and manage owned or infected cats are all recommended to potentially minimize zoonotic transmission of sporotrichosis.

About the Author

Dr. Jirawattanadon is a staff member in the Department of Dermatology, Faculty of Medicine Siriraj Hospital, Mahidol University, Thailand. Her research interests focus on dermatology and infectious diseases.

References

1. Lopes-Bezerra LM, Schubach A, Costa RO. *Sporothrix schenckii* and sporotrichosis. An Acad Bras Cienc. 2006;78:293–308. https://doi.org/10.1590/S0001-37652006000200009
2. Mahajan VK. Sporotrichosis: an overview and therapeutic options. Dermatol Res Pract. 2014;2014:272376. https://doi.org/10.1155/2014/272376
3. Rodrigues AM, Bagagli E, de Camargo ZP, Bosco Sde M. *Sporothrix schenckii* sensu stricto isolated from soil in an armadillo's burrow. Mycopathologia. 2014;177:199–206. https://doi.org/10.1007/s11046-014-9734-8
4. Orofino-Costa R, Macedo PM, Rodrigues AM, Bernardes-Engemann AR. Sporotrichosis: an update on epidemiology, etiopathogenesis, laboratory and clinical therapeutics. An Bras Dermatol. 2017;92:606–20. https://doi.org/10.1590/abd1806-4841.2017279
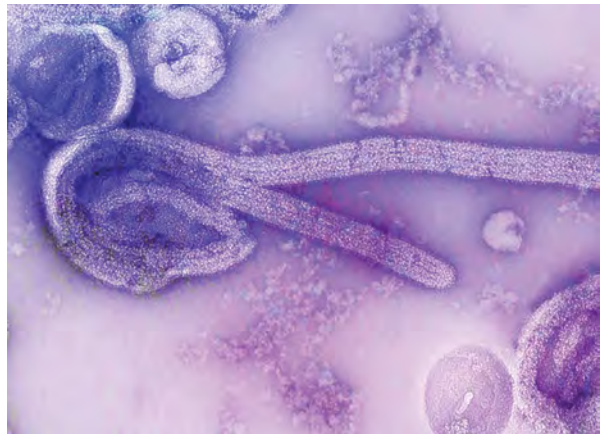
5. Bonifaz A, Saúl A, Paredes-Solis V, Fierro L, Rosales A, Palacios C, et al. Sporotrichosis in childhood: clinical and therapeutic experience in 25 patients. Pediatr Dermatol. 2007;24:369–72. https://doi.org/10.1111/j.1525-1470.2007.00452.x

6. Paixão AG, Galhardo MCG, Almeida-Paes R, Nunes EP, Gonçalves MLC, Chequer GL, et al. The difficult management of disseminated Sporothrix brasiliensis in a patient with advanced AIDS. AIDS Res Ther. 2015;12:16. https://doi.org/10.1186/s12981-015-0051-1

7. Werner AH, Werner BE. Sporotrichosis in man and animal. Int J Dermatol. 1994;33:692–700. https://doi.org/10.1111/j.1365-4362.1994.tb01512.x

8. Quintal D. Sporotrichosis infection on mines of the Witwatersrand. J Cutan Med Surg. 2000;4:51–4. https://doi.org/10.1177/120347540000400113

9. Centers for Disease Control. Multistate outbreak of sporotrichosis in seedling handlers, 1988. MMWR Morb Mortal Wkly Rep. 1988;37:652–3.

10. Anderson PC. Cutaneous sporotrichosis. Am Fam Physician. 1983;27:201–4.

11. Mahmoudi S, Zaini F. Sporotrichosis in Iran: a mini review of reported cases in patients suspected to cutaneous leishmaniasis. Curr Med Mycol. 2015;1:39–45.

12. Kazemi A, Razi A. Sporotrichosis in Iran. Rev Iberoam Micol. 2007;24:38–40. https://doi.org/10.1016/S1130-1406(07)70009-8

13. Gremião IDF, Miranda LHM, Reis EG, Rodrigues AM, Pereira SA. Zoonotic epidemic of sporotrichosis: cat to human transmission. PLoS Pathog. 2017;13:e1006077. https://doi.org/10.1371/journal.ppat.1006077

14. Lyon GM, Zurita S, Casquero J, Holgado W, Guevara J, Brandt ME, et al.; Sporotrichosis in Peru Investigation Team. Population-based surveillance and a case-control study of risk factors for endemic lymphocutaneous sporotrichosis in Peru. Clin Infect Dis. 2003;36:34–9. https://doi.org/10.1086/345437

15. de Lima Barros MB, de Oliveira Schubach A, Galhardo MC, Schubach TM, dos Reis RS, Conceição MJ, et al. Sporotrichosis with widespread cutaneous lesions: report of 24 cases related to transmission by domestic cats in Rio de Janeiro, Brazil. Int J Dermatol. 2003;42:677–81. https://doi.org/10.1046/j.1365-4362.2003.01813.x

16. Barros MB, Schubach AO, do Valle AC, Gutierrez Galhardo MC, Conceição-Silva F, Schubach TM, et al. Cat-transmitted sporotrichosis epidemic in Rio de Janeiro, Brazil: description of a series of cases. Clin Infect Dis. 2004;38:529–35. https://doi.org/10.1086/381200

17. Fleury RN, Taborda PR, Gupta AK, Fujita MS, Rosa PS, Weckwerth AC, et al. Zoonotic sporotrichosis. Transmission to humans by infected domestic cat scratching: report of four cases in São Paulo, Brazil. Int J Dermatol. 2001;40:318–22.

18. Kovarik CL, Neyra E, Bustamante B. Evaluation of cats as the source of endemic sporotrichosis in Peru. Med Mycol. 2008;46:53–6. https://doi.org/10.1080/13693780701567481

19. Schubach AO, Schubach TM, Barros MB. Epidemic cat-transmitted sporotrichosis. N Engl J Med. 2005;353:1185–6. https://doi.org/10.1056/NEJMc051680

20. Reis RS, Almeida-Paes R, Muniz MM, Tavares PM, Monteiro PC, Schubach TM, et al. Molecular characterisation of Sporothrix schenckii isolates from humans and cats involved in the sporotrichosis epidemic in Rio de Janeiro, Brazil. Mem Inst Oswaldo Cruz. 2009;104:769–74. https://doi.org/10.1590/S0074-02762009000500018

21. Mercurio MG, Elewski BE. Therapy of sporotrichosis. Semin Dermatol. 1993;12:285–9.

22. Barros MB, de Almeida Paes R, Schubach AO. Sporothrix schenckii and sporotrichosis. Clin Microbiol Rev. 2011;24:633–54. https://doi.org/10.1128/CMR.00007-11

23. Freitas DFS, de Siqueira Hoagland B, do Valle ACF, Fraga BB, de Barros MB, de Oliveira Schubach A, et al. Sporotrichosis in HIV-infected patients: report of 21 cases of endemic sporotrichosis in Rio de Janeiro, Brazil. Med Mycol. 2012;50:170–8. https://doi.org/10.3109/13693786.2011.596288

24. Sizar O, Talati R. Sporotrichosis. In: StatPearls. Treasure Island (FL): StatPearls Publishing; 2023

25. Fichman V, Almeida-Silva F, Francis Saraiva Freitas D, Zancopé-Oliveira RM, Gutierrez-Galhardo MC, Almeida-Paes R. Severe sporotrichosis caused by Sporothrix brasiliensis: antifungal susceptibility and clinical outcomes. J Fungi (Basel). 2022;9:49. https://doi.org/10.3390/jof9010049

26. Marimon R, Serena C, Gené J, Cano J, Guarro J. In vitro antifungal susceptibilities of five species of Sporothrix. Antimicrob Agents Chemother. 2008;52:732–4. https://doi.org/10.1128/AAC.01012-07

27. Indoung S, Chanchayanon B, Chaisut M, Buapeth KO, Morteh R, Jantrakajorn S. Feline sporotrichosis caused by Sporothrix schenckii sensu stricto in southern Thailand: phenotypic characterization, molecular identification, and antifungal susceptibility. Med Mycol. 2022;60:myac075. https://doi.org/10.1093/mmy/myac075

28. Dropulic LK, Lederman HM. Overview of infections in the immunocompromised host. Microbiol Spectr. 2016;4:10.1128/microbiolspec.DMIH2-0026-2016. https://doi.org/10.1128/microbiolspec.DMIH2-0026-2016

29. Tovikkai D, Maitrisathit W, Srisuttiyakorn C, Vanichanan J, Thammahong A, Suankratay C. Sporotrichosis: the case series in Thailand and literature review in Southeast Asia. Med Mycol Case Rep. 2020;27:59–63. https://doi.org/10.1016/j.mmcr.2020.01.002

30. Kwangsukstith C, Vanittanakom N, Khanjanasthiti P, Uthammachai C. Cutaneous sporotrichosis in Thailand: first reported case. Mycoses. 1990;33:513–7. https://doi.org/10.1111/myc.1990.33.11-12.513

31. Taninratapat N, Srisuttiyakorn C. Localized cutaneous sporotrichosis on face in healthy Thai female. Mycopathologia. 2019;184:539–42. https://doi.org/10.1007/s11046-019-00354-7

32. Queiroz-Telles F, Bonifaz A, Rossow J, Chindamporn A. Sporothrix and sporotrichosis. Encyclopedia Infect Immun. 2022;2:376–96. https://doi.org/10.1016/B978-0-12-818731-9.00046-X

33. Kamal Azam NK, Selvarajah GT, Santhanam J, Abdul Razak MF, Ginsapu SJ, James JE, et al. Molecular epidemiology of Sporothrix schenkii isolates in Malaysia. Med Mycol. 2020;58:617–25. https://doi.org/10.1093/mmy/myz106

34. Yingchanakiat K, Limsivilai O, Sunpongsri S, Niyomtham W, Lugsomya K, Yurayart C. Phenotypic and genotypic characterization and antifungal susceptibility of Sporothrix schenckii sensu stricto isolated from a feline sporotrichosis outbreak in Bangkok, Thailand. J Fungi (Basel). 2023;9:590. https://doi.org/10.3390/jof9050590

35. Sharma R, Mahajan VK, Singh Chauhan P, Mehta KS, Sharma A, Sharma J. The clinico-epidemiological characteristics and therapeutic experience of 152 patients with cutaneous sporotrichosis: a 10-year retrospective study from India. Int J Dermatol. 2021;60:99–106. https://doi.org/10.1111/ijd.15299

36. de Lima Barros MB, Schubach AO, de Vasconcellos Carvalhaes de Oliveira R, Martins EB, Teixeira JL, Wanke B. Treatment of cutaneous sporotrichosis with itraconazole—study of 645 patients. Clin Infect Dis. 2011;52:e200–6. https://doi.org/10.1093/cid/cir245

37. Brandolt TM, Madrid IM, Poester VR, Sanchotene KO, Basso RP, Klafke GB, et al. Human sporotrichosis: a zoonotic outbreak in southern Brazil, 2012–2017. Med Mycol. 2019;57:527–33. https://doi.org/10.1093/mmy/myy082

38. Quintella LP, Passos SR, do Vale AC, Galhardo MC, Barros MB, Cuzzi T, et al. Histopathology of cutaneous sporotrichosis in Rio de Janeiro: a series of 119 consecutive cases. J Cutan Pathol. 2011;38:25–32. https://doi.org/10.1111/j.1600-0560.2010.01626.x

39. Tang MM, Tang JJ, Gill P, Chang CC, Baba R. Cutaneous sporotrichosis: a six-year review of 19 cases in a tertiary referral center in Malaysia. Int J Dermatol. 2012;51:702–8. https://doi.org/10.1111/j.1365-4632.2011.05229.x

40. Lloret A, Hartmann K, Pennisi MG, Ferrer L, Addie D, Belák S, et al. Sporotrichosis in cats: ABCD guidelines on prevention and management. J Feline Med Surg. 2013;15:619–23. https://doi.org/10.1177/1098612X13489225

41. Carrada-Bravo T, Olvera-Macías MI. New observations on the ecology and epidemiology of *Sporothrix schenckii* and sporotrichosis 2. Ecological niches of *S. schenckii* and zoonotic outbreaks. Rev Mex Patol Clin Med Lab. 2013;60:5–24.

42. Accardi G, Caruso C. Immune-inflammatory responses in the elderly: an update. Immun Ageing. 2018;15:11. https://doi.org/10.1186/s12979-018-0117-8

43. Fuentes E, Fuentes M, Alarcón M, Palomo I. Immune system dysfunction in the elderly. An Acad Bras Cienc. 2017;89:285–99. https://doi.org/10.1590/0001-3765201720160487

44. Rodrigues AM, de Melo Teixeira M, de Hoog GS, Schubach TM, Pereira SA, Fernandes GF, et al. Phylogenetic analysis reveals a high prevalence of *Sporothrix brasiliensis* in feline sporotrichosis outbreaks. PLoS Negl Trop Dis. 2013;7:e2281. https://doi.org/10.1371/journal.pntd.0002281

45. Heninger E, Hogan LH, Karman J, Macvilay S, Hill B, Woods JP, et al. Characterization of the *Histoplasma capsulatum*-induced granuloma. J Immunol. 2006;177:3303–13. https://doi.org/10.4049/jimmunol.177.5.3303

46. Collette JR, Lorenz MC. Mechanisms of immune evasion in fungal pathogens. Curr Opin Microbiol. 2011;14:668–75. https://doi.org/10.1016/j.mib.2011.09.007

47. Romani L. Immunity to fungal infections. Nat Rev Immunol. 2004;4:1–23. https://doi.org/10.1038/nri1255

48. Etchecopaz A, Toscanini MA, Gisbert A, Mas J, Scarpa M, Iovannitti CA, et al. *Sporothrix brasiliensis*: a review of an emerging South American fungal pathogen, its related disease, presentation and spread in Argentina. J Fungi (Basel). 2021;7:170. https://doi.org/10.3390/jof7030170

49. Restrepo A, Robledo J, Gómez I, Tabares AM, Gutiérrez R. Itraconazole therapy in lymphangitic and cutaneous sporotrichosis. Arch Dermatol. 1986;122:413–7. https://doi.org/10.1001/archderm.1986.01660160069021

50. Sharkey-Mathis PK, Kauffman CA, Graybill JR, Stevens DA, Hostetler JS, Cloud G, et al.; NIAID Mycoses Study Group. Treatment of sporotrichosis with itraconazole. Am J Med. 1993;95:279–85. https://doi.org/10.1016/0002-9343(93)90280-3

Address for correspondence: Penvadee Pattanaprichakul, Department of Dermatology, Faculty of Medicine Siriraj Hospital, Mahidol University, 2 Wang Lang Rd, Bangkok Noi, Bangkok 10700, Thailand; email: penvadee.pat@gmail.com

Cost-effectiveness Analysis of Japanese Encephalitis Vaccination for Children <15 Years of Age, Bangladesh

An Nguyen,[1] Rebeca Sultana,[1] Elisabeth Vodicka, Zareen Tasnim, Kamran Mehedi, Md. Monjurul Islam, S.M. Abdullah Al Murad, Md. Redowan Ullah, Sharmin Sultana, Tahmina Shirin, Clint Pecenka

Japanese encephalitis (JE) is preventable using the affordable, effective, and safe live attenuated SA 14-14-2 JE vaccine (CD-JEV). We used a Markov model to evaluate the cost-effectiveness of 1 dose of CD-JEV compared with no vaccination in 3 vaccination strategies in Bangladesh: subnational campaign and routine immunization, subnational campaign and national routine immunization, and national routine immunization alone. For input parameters, we gathered information from a cost-of-illness study, medical literature, government documents, and expert opinions. The base-case analysis estimated that a subnational campaign for children <15 years of age and routine immunization over 20 birth cohorts in Rajshahi, Rangpur, and Chattogram yielded (in 2021 US dollars) a cost of $82.2 million, $981/disability-adjusted life years averted, $9,964/case averted, and $49,819/death averted (societal perspective). We projected CD-JEV vaccination would be cost-effective across cost perspectives and vaccination strategies in Bangladesh, yielding an incremental cost-effectiveness ratio of approximately one third of per capita national gross domestic product.

Japanese encephalitis (JE) is a leading cause of viral encephalitis, particularly in endemic regions of the world; Asia bears a disproportionately high burden (1,2). JE virus is a mosquitoborne flavivirus that leads to acute encephalitis syndrome in an estimated 67,900 new clinical cases annually, mostly among children

and young adults (1). JE virus kills ≈30% of those infected (1,3). Among survivors, ≈70% have long-term sequelae with possible motor, cognitive, and language impairments, as well as convulsions, behavioral problems, and mental disorders (1,3). No treatment for JE exists, but the disease can be effectively prevented with vaccines.

Since the first JE vaccine was developed in the 1930s, ≈15 additional vaccines with different technology platforms, presentations, and formulations have been added. Among them, the single-dose live attenuated SA14-14-2 JE vaccine (CD-JEV) has been the most widely used in JE-endemic countries; CD-JEV is affordable, effective, and safe (4,5). Over the past 3 decades, ≈350,000 children have been vaccinated with CD-JEV in 14 clinical safety trials, and 400 million doses have been administered (6). The seroprotection rates of CD-JEV in children vary from 80.2% to 99.1% in clinical trials (7–9). Vaccine effectiveness in endemic settings ranges from 80% to 99.3% at 6–15 months to 71% at 6 years after vaccination (10–14).

In Bangladesh, the first JE outbreak was in 1977, but systematic assessment of disease occurrence was not conducted until hospital-based surveillance programs were implemented in 2003–2005 and 2007–2016 (15–17). Bangladesh has an annual incidence of 2.5 JE cases/100,000 persons <15 years of age, lower than in China (12.7), Korea (12.6), and Cambodia (10.6) (1). However, a recent cost-of-illness study in Bangladesh found that, despite the low incidence, JE remains a devastating disease because of its substantial economic burden (US$929/acute episode) and detrimental toll on the physical and psychosocial health of patients and their families (18).

[1]These first authors contributed equally to this article.

Over the past several decades, Bangladesh has made substantial progress in controlling vaccine-preventable diseases with high routine immunization coverage and introduction of new vaccines such as *Hemophilus influenzae* type B, rubella, pneumococcal conjugate vaccine, and inactivated polio vaccine (*19*). JE vaccine, however, has yet to be introduced into Bangladesh. In a multicriteria decision analysis by the World Health Organization (WHO), JE vaccine was ranked among the most highly recommended for introduction into Bangladesh (*20*), and several efforts have been made, including through advocacy workshops with decision-makers, to prioritize JE vaccine introduction in Bangladesh (*21–25*). A mass vaccination campaign including JE vaccine in the routine immunization program could have a profound effect on health outcomes. However, JE vaccine introduction may also create budget challenges for the government. Cost-effectiveness of and cost savings from JE vaccination has been demonstrated in many countries (*26–31*), but no such data exists for Bangladesh. We conducted this analysis to assess the effect and cost-effectiveness of CD-JEV vaccination compared with no vaccination among children in Bangladesh. We evaluated various vaccination strategies to inform the strategic decision-making of the government and international partners as they consider JE vaccine introduction and budgetary resources in the country. We obtained informed consent from the participants of this study. We conducted the study according to the guidelines of the institutional review board of icddr,b (Dhaka, Bangladesh), which approved the study protocol.

Materials and Methods

Modeled Vaccination Strategies and Target Population
We met with policy makers, Expanded Program on Immunization (EPI) officers, international partners, and JE experts to identify vaccination strategies of interest. From this meeting, we identified 3 vaccination strategies to model. Strategy 1 (S1) is a subnational 1-time immunization campaign for children <15 years of age and subnational routine immunization for 9-month-old children. The subnational approach focused on 3 divisions with a high number of JE cases: Rangpur, Rajshahi, and Chattogram. Strategy 2 (S2) is a subnational 1-time immunization campaign and national routine immunization. Strategy 3 (S3) is national routine immunization only.

To have adequate time to observe immunization effectiveness on the population and explore changes in costs of the vaccination program, for each analysis

strategy, we examined 10- and 20-year time horizons corresponding to consecutive 10 and 20 annual birth cohorts receiving vaccination. We adopted both governmental and societal cost perspectives. The societal cost perspective includes costs to the government, patients, and households to provide a complete picture of cost-effectiveness for healthcare payers in Bangladesh. The base case was the S1 strategy from a societal perspective for a 20-year time horizon.

The target population for a JE vaccination campaign is children <15 years of age. On the basis of expert opinion, we assumed an average 5 years of age for children vaccinated during a JE campaign and a vaccination coverage rate of 88.6% on the basis of measles and rubella vaccine coverage rates in the EPI Coverage Evaluation Survey (*32*). The population for routine immunization is 9-month-old infants across 10 or 20 cohorts with an average annual birth rate of 1.81% as reported by the Bangladesh Bureau of Statistics. We sourced population sizes by divisions and age groups from Bangladesh 2022 census data. We used Bangladesh Bureau of Statistics life tables for background mortality rates in each age group to calculate non-JE deaths across participant life-cycles (*33,34*).

For the campaign strategy, we summed outputs from the population of children 0–14 years of age. For the routine immunization strategy, we aggregated outputs of vaccinating 10 or 20 birth cohorts on the basis of current birth rates. We divided incremental costs for the vaccination compared with no-vaccination groups by incremental disability-adjusted life years (DALYs) to obtain the incremental cost-effectiveness ratio (ICER). We compared ICERs from different scenarios and presented findings as percentages of Bangladesh gross domestic product (GDP) per capita to evaluate the cost-effectiveness of CD-JEV in different vaccination strategies.

Model Framework
For the analysis, we used a previously developed cost-effectiveness model and input parameters gathered from global, regional, and Bangladesh national literature; published and unpublished government documents; and expert opinions from in-country public health leaders, immunization programs officers, and JE experts. We used the Microsoft Excel-based model (https://www.microsoft.com) that PATH developed and used in JE cost-effectiveness analyses for Indonesia and the Philippines (*26,30*). PATH developed a Markov model simulating costs and outcomes for children from time of vaccination or no vaccination until death or until reaching the time horizon of 100

years of age. Each child entered the model at a state of no JE and could remain in that state until death or transition to JE states, which included asymptomatic or acute JE (Figure 1). The probability of transition to acute JE was incidence in the no-vaccination group (comparator) and incidence multiplied by vaccine ineffectiveness rate in the vaccinated group (Table 1). Asymptomatic JE case-patients remained in this state, without any JE-associated costs or DALYs, until death. We assumed patients to have lifelong immunity because they did not transition to acute JE and could not return to the no-JE state. Acute JE case-patients accrued costs of care and quality of life decrements associated with an acute JE episode, then progressed to a postacute JE state with no, mild, moderate, or severe sequelae (on the basis of JE-associated chronic condition rates) or to death (on the basis of mortality rates) (Table 1). Case-patients in the postacute JE state remain in that state, with or without sequelae, until death. We modeled 1-year cycles as the time of transition between health states and distributed costs for sequelae care and DALYs by sequelae presence and severity (Table 1).

Among those progressing to JE, we assumed vaccination affected the probability of transition from the no-JE state to acute or asymptomatic JE but not duration or severity of JE and sequelae. We assumed no serious adverse event associated with JE vaccination but incorporated per-person costs associated with minor adverse events (Table 2). Main outputs included the number of JE cases averted, deaths averted, DALYs averted, costs of the vaccination program, total healthcare costs, and ICERs, calculated by dividing incremental costs by incremental DALY averted. We discounted costs and health outcomes by 3%/year using the common discount rate for lower-middle income countries and adjusted all monetary units amounts to 2021 US dollars (US $) (35).

Sensitivity Analyses

To consider the uncertainty of model parameters, we conducted 1-way and probabilistic sensitivity analyses.
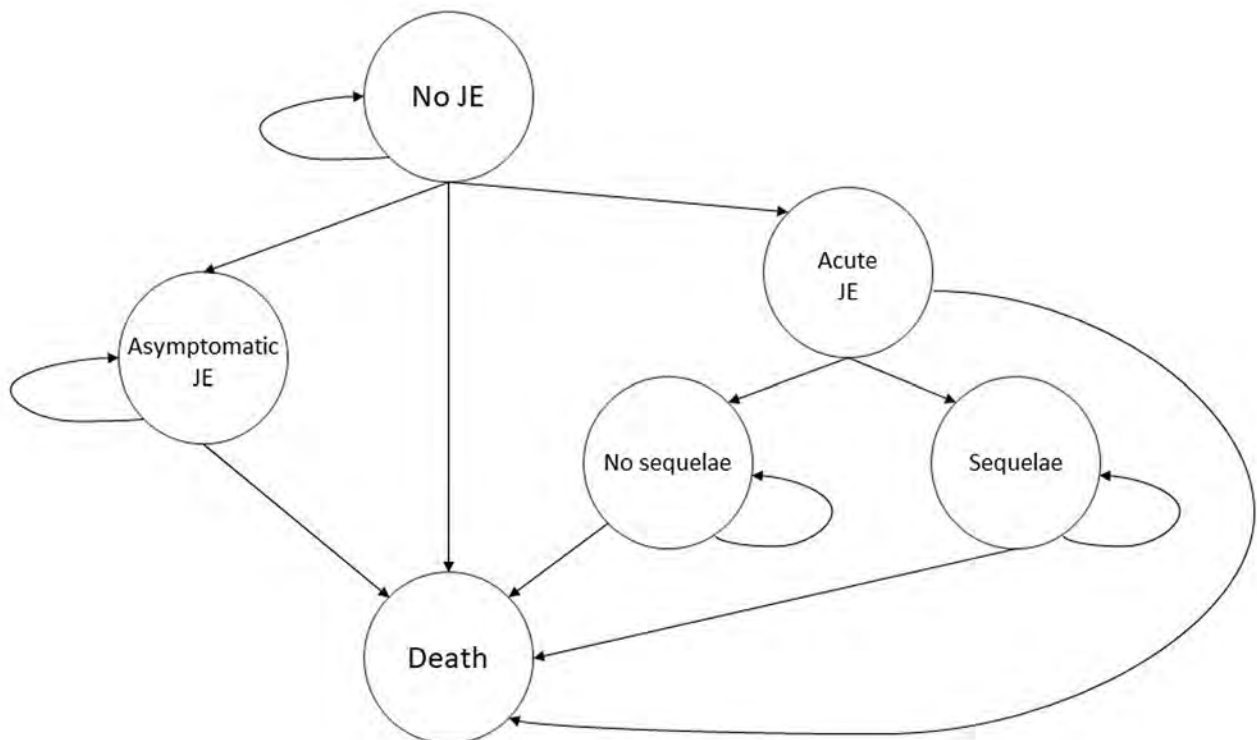

Figure 1. Markov model simulating costs and outcomes in cost-effectiveness analysis of JE vaccination for children <15 years of age, Bangladesh. All persons enter the model with no JE. Acute JE implies symptomatic JE and is a tunnel state, meaning any person in that state stays there for exactly 1 cycle. Those who had acute JE do have a higher mortality rate but must accrue the costs and disability-adjusted life years (DALYs) of the acute event before transitioning to death. Asymptomatic JE is not associated with higher mortality, costs, or DALYs; rather it eliminates any transition to acute JE. Costs and DALYs for acute and postacute JE are distributed by sequelae presence and severity. Vaccination changes the probability of transitioning from no JE to acute or asymptomatic JE. No other probabilities are changed by presence or absence of vaccination. Each state is associated with an annual cost and disability weight where applicable. This figure was remade from the Markov model in the study conducted in Philippines by the same research group from PATH (31). JE, Japanese encephalitis virus.

Table 1. Summary of model parameters for Japanese encephalitis vaccination and epidemiology in Bangladesh, 2023*

Parameter	Base case estimate	Range	Source
Average age of vaccinated child in campaign, y	5	4–6	In-country expert opinion
Acute/symptomatic JE incidence, per 100,000 population	2.5	1.75–5.89	(1,36)
Asymptomatic-to-acute JE, ratio	300:1	25–1000:1	(39)
Case fatality/acute JE, %	20	10–30	(Institute of Epidemiology, unpub. data, email, 2023 Oct 03)
Duration of acute JE event	2.8 wks	2.2–3.3 wks	(46)
Sequelae incidence, %	58	46–70	(Institute of Epidemiology, unpub. data, email, 2023 Oct 03)
Sequelae severity, %			
Mild	16	13–19	(18)
Moderate	37	29–44	(18)
Severe	47	38–57	(18)
Probability of treatment by sequelae severity, %			
Mild	84	67–100	(18)
Moderate	89	72–100	(18)
Severe	96	77–100	(18)
Vaccine efficacy, %	86.3	69–98	(9,12)
Vaccine coverage, %	88.6	70.9–100	(32)
Discount rate for costs and health outcomes	3	NA	Assumption
Disability weight for acute JE, per event	0.133	0.088–0.190	Infectious disease acute episode–severe (38)
Disability weights for long-term sequelae, annual			
Mild	0.031	0.018–0.050	Motor/cognitive impairments–mild (38)
Moderate	0.203	0.134–0.290	Motor/cognitive impairments–moderate (38)
Severe	0.542	0.374–0.702	Motor/cognitive impairments–severe (38)

*JE, Japanese encephalitis; NA, not applicable.

In the 1-way sensitivity analysis, we varied each model parameter across a range of 95% CIs, or ±20% mean value, to observe how variation of each model input (e.g., sequelae incidence or vaccine efficacy) changed the ICER. To allow for exploring a wide range of JE incidence, we used 1.75–5.89 cases/100,000 persons <15 years of age on the basis of modeling estimates across divisions in Bangladesh (36). Using those variables, we defined key drivers of model outcomes as the parameters that had the largest effect on ICER.

In the probabilistic sensitivity analysis, we explored the effect on model outcomes when jointly varying all model parameters over 10,000 Monte Carlo simulations. In each simulation, we randomly selected a value in every parameter's distribution and used randomly selected values of all parameters to calculate model outputs. After conducting 10,000 simulations, we obtained the distribution of the mean and 95% CIs of model output values. We used a normal distribution for population size, age, duration of the acute JE event, and asymptomatic JE; γ distribution for costs; and β distribution for disability weights and percentages. We plotted results on a cost-effectiveness acceptability curve and evaluated them against willingness-to-pay thresholds to evaluate the likelihood that projected ICERs would be considered cost-effective in Bangladesh where no formal cost-effectiveness threshold has been established.

Model Outcomes and Costs

Health Outcomes

The health outcomes we calculated were JE cases, deaths, expected life-years, and DALYs associated with acute JE episodes and different levels of sequelae. We calculated the number of JE cases based on JE incidence in children <15 years of age (2.5 cases/100,000 children) in low-incidence JE-endemic areas without a vaccination program, including Bangladesh (1). The vaccination group had fewer cases than the no-vaccination group because of the protective effect from CD-JEV calculated in the base case using a vaccine efficacy of 86.3% sourced from a clinical trial in Bangladesh (9). For sensitivity analysis, we used a 69%–98% efficacy range, the 95% CI for the pooled efficacy estimate from a systematic review of clinical trials (12). The mortality rate among symptomatic acute JE cases was 20% (S. Sultana, unpub. data, email, 2023 Oct 03). Among survivors, 58% had sequelae, among which 16% were mild, 37% moderate, and 47% severe, according to an unpublished estimation of 10 years of JE surveillance from the Institute of Epidemiology Diseases Control and Research (IEDCR) and a JE cost-of-illness study in Bangladesh (18,37). For DALYs associated with acute JE, we used disability weights for severe infectious disease acute episodes and for sequelae, and motor and cognitive

impairments at mild, moderate, and severe levels from the literature (*38*). Those disability weights were used by WHO for the Global Burden of Disease study 2016, 2019, and 2021 editions and are the DALY weight descriptions that best match the symptoms of JE. For asymptomatic JE cases, which accrued no cost or disability weight, we used 300:1 for the rate of asymptomatic to symptomatic JE cases, as reported in the literature (*39*).

Costs of Vaccination and Healthcare

We sourced costs of acute JE episodes and sequelae care from a JE cost-of-illness study that analyzed 10-year data from Bangladesh (*18*). We explored costs from governmental and societal perspectives. The governmental perspective considers direct medical costs (including for medicines, diagnostic tests, procedures, services, and facility fees) paid by the healthcare system to provide care for acute JE patients and those with sequelae. The societal perspective considers direct medical costs paid by the healthcare system and costs for the households including out-of-pocket medical costs, nonmedical costs (e.g., transportation, meals, and accommodations), and indirect costs for patients and caregivers, including income lost while caring for ill friends or family members (*18*).

Expenses for the vaccination program were cost of the vaccine, including vaccine delivery during campaigns and routine immunization, supplies, and adverse events (Table 2). We used an assumed cost/CD-JEV dose in Bangladesh of US $0.44 on the basis of a reported 2023 price for Gavi-eligible countries (*37*). Supplies included unit costs of US $0.042/syringe and US $0.0056/syringe safety box (Najibullah S, unpub. data, internal report, 2023 Sep 16). According to WHO information, adverse events for CD-JEV vaccine include injection site reaction, fever, vomiting, abnormal crying, drowsiness, appetite loss, and irritability (*40*). There was no report on hypersensitivity reactions. We included an EPI-estimated adverse event cost of US $0.0081/dose for JE vaccine in the vaccination cost/dose (Government of Bangladesh, unpub. data, internal report, 2024 Aug 12). We estimated CD-JEV delivery costs in Bangladesh as US $1.71/dose for routine immunization (*40*) and US $1.10/dose during a vaccination campaign (*41*). We used rates of 10% for wastage and buffer and 5% for annual increases in vaccine cost based on expert opinion from the meeting with experts (policy makers, EPI officers, international partners, and JE experts).

Results

For base analysis S1 (subnational campaign and subnational routine immunization in Rangpur, Rajshahi, and Chattogram divisions), we estimated that the discounted vaccine program costs borne by the government would be US $82.2 million for 20 years but would save households and the government of Bangladesh US $75.1 million in healthcare costs. We calculated the S1 vaccination strategy would prevent 7,544 JE cases and 1,509 deaths (Table 3) and yield ICERs of US $94/DALY averted, $958/case averted, and $4,790/death

Table 2. Summary of model parameters for costs of Japanese encephalitis vaccine delivery and Japanese encephalitis treatment, Bangladesh, 2023*

Parameter	Base case estimate	Range	Source
Japanese encephalitis treatment costs, US $			
Japanese encephalitis-related hospitalization costs per event			
Direct medical cost to health system	106	77–135	(*18*)
Medical and non-medical cost to household	487	415–559	(*18*)
Indirect cost to household	351	254–448	(*18*)
Annual sequelae costs to health system			
Mild	6	0–14	(*18*)
Moderate	84	0–201	(*18*)
Severe	83	15–150	(*18*)
Annual sequelae costs to household			
Mild	213	71–355	(*18*)
Moderate	705	458–952	(*18*)
Severe	846	552–1,140	(*18*)
Vaccine-related costs			
Vaccine, adverse events, and supplies cost to government, per dose, US $	0.50	0.40–0.59	(*37*; S. Najibullah, unpub. data, internal report, 2023 Sep 16)
Annual increase in vaccine cost, %	5	4–6	Assumption
Vaccine delivery cost per dose for routine immunization, US $	1.71	1.37–2.05	(S. Najibullah, unpub. data, internal report, 2023 Sep 16)
Vaccine delivery cost per dose for campaign-based delivery, US $	1.10	0.88–1.32	(*41*)
Wastage, %	10	8–12	In-country expert opinion
Buffer, %	10	8–12	In-country expert opinion

*Costs are given in 2001 US dollars (US $).

Table 3. Discounted incremental outcomes and program costs of different Japanese encephalitis vaccination strategies as compared with no vaccination from the governmental payer and societal perspectives in Bangladesh

Discounted incremental outcomes	Routine immunization birth cohorts	Strategy 1, subnational campaign + subnational routine*	Strategy 2, subnational campaign + national routine†	Strategy 3, national routine‡
Cases averted	10	5,733	8,962	5,663
	20	7,544	13,176	9,876
DALYs averted	10	58,130	91,104	57,829
	20	76,624	134,134	100,859
Deaths averted	10	1,147	1,792	1,133
	20	1,509	2,635	1,975
Total vaccinated	10	30,337,406	45,866,646	27,234,783
	20	42,042,950	73,101,429	54,469,566
Discounted vaccine program costs, $§	10	57.1M	95.5M	67.3M
	20	82.2M	154.0M	125.8M

*Subnational 1-time immunization campaign for children <15 years of age and subnational routine immunization for 9-month-old children. The subnational approach focuses on 3 divisions with a high number of JE cases: Rangpur, Rajshahi, and Chattogram.
†Subnational 1-time immunization campaign and national routine immunization.
‡S3, national routine immunization only.
§US dollars.

averted from the societal perspective and $981/DALY averted, $9,964/case averted, and $49,819/death averted from the governmental perspective (Table 4). The costs/DALY averted correspond to 3.5%–36.6% of Bangladesh 2021 GDP per capita. Estimating results from S1 with a shorter time horizon, 1-time campaign, and 10 years of routine immunization led to lower costs but fewer health outcomes averted because fewer children (≈12 million) would be vaccinated (Tables 3, 4). The cost/DALY averted varied within 0.8%–33.3% of Bangladesh GDP per capita, depending on societal or governmental perspective.

For S2, with CD-JEV included as part of the routine immunization program implemented nationwide instead of only subnationally in 3 divisions with high endemicity, as was the plan in S1, vaccine program costs increased to US $154 million over 20 years. However, S2 would save society US $134.8 million in downstream healthcare and household costs from 13,176 JE cases and 2,635 deaths averted. S2 strategy had ICERs of US $143/DALY averted, $1,458/case averted, and $7,290/death averted from a societal perspective and $1,053/DALY averted, $10,720/case averted, and $53,601/death averted from a governmental perspective (Table 4). With a higher overall ICER than S1, the S2 vaccination strategy was less cost-effective.

S3 (standalone national routine immunization) resulted in fewer vaccinated children than in S1, the base case scenario, over a 10-year period but more children over a 20-year period (Table 3). The S3 strategy had higher program costs than S1, regardless of the time horizon. It also had the highest ICER among the 3 vaccination strategies, with US $208/DALY averted, $2,128/case averted, and $10,640/death averted from a societal perspective and $1,149/DALY averted,

Table 4. Discounted incremental costs of different Japanese encephalitis vaccination strategies as compared with no vaccination from the governmental payer and societal perspectives in Bangladesh*

Discounted incremental outcomes	Routine immunization birth cohorts	Strategy 1, subnational campaign + subnational routine†		Strategy 2, subnational campaign + national routine‡		Strategy 3, national routine§	
		Govt	Soc	Govt	Soc	Govt	Soc
Discounted healthcare costs averted through vaccination	10	5.3M	55.8M	8.5M	90.1M	5.7M	60.1M
	20	7.1M	75.1M	12.7M	134.8M	9.9M	104.8M
Deterministic ICER: cost per DALY averted	10	892	23	955	60	1,066	126
	20	981	94	1,053	143	1,149	208
Deterministic ICER: cost per case averted	10	9,046	230	9,710	609	10,888	1,283
	20	9,964	958	10,720	1,458	11,733	2,128
Deterministic ICER: cost per death averted	10	45,230	1,148	48,549	3,045	54,441	6,413
	20	49,819	4,790	53,601	7,290	58,667	10,640
Probabilistic ICER: cost per DALY averted, mean (95% CI)	10	991 (358–2,272)	173 (−632 to 1,719)	1,351 (453–3,469)	196 (−501 to 2,614)	1,374 (439–3,557)	445 (−644 to 2,430)
	20	1,198 (444 to 2,807)	307 (−538 to 1,971)	1,249 (352 to 2,684)	377 (−593 to 2,520)	1,394 (559 to 2,834)	560 (−475 to 2,879)

*Values are in US dollars. DALY, disability-adjusted life year; ICER, incremental cost-effectiveness ratio; govt, governmental costs; soc, societal costs.
†Subnational 1-time immunization campaign for children <15 years of age and subnational routine immunization for 9-month-old children. The subnational approach focuses on 3 divisions with a high number of JE cases: Rangpur, Rajshahi, and Chattogram.
‡Subnational 1-time immunization campaign and national routine immunization.
§National routine immunization only.

$11,733/case averted, and $58,667/death averted from a governmental perspective (Table 4). Thus, S3 was the least cost-effective among the 3 vaccination strategies (Appendix Table, https://wwwnc.cdc.gov/EID/article/30/12/23-1657-App1.pdf).

One-way sensitivity analysis results (shown as tornado plots) identified the parameters most influencing cost/DALY averted (Figures 2, 3). The strongest cost drivers from the societal perspective were symptomatic JE incidence, vaccine efficacy, sequelae incidence, and sequelae costs. From the governmental perspective, the strongest cost drivers were case-fatality rate, symptomatic JE incidence, vaccine efficacy, and sequelae incidence. When these key cost drivers were adjusted higher or lower, ICERs varied from negative (cost saving) values to the highest value of US $1,420/DALY for S1, $1,521/DALY for S2, and $1,655/DALY for S3 from the governmental perspective; social perspectives produce lower ICERs. Maximum ICERs corresponded to 53% of the Bangladesh GDP per capita for S1, 57% for S2, and 62% for S3.

When we varied all parameters in their distribution for the probabilistic sensitivity analysis, our results were robust. Probabilistic ICERs were close to deterministic ICERs (Table 4). We performed 10,000 simulations to calculate incremental costs and DALYs averted in which we randomly selected all model parameters from their distribution (Figure 4). In many simulations, the subnational campaign (S1) and national routine immunization (S2) were cost-saving from the societal perspective through 20 birth cohorts. When we compared ICER results with potential willingness-to-pay thresholds in Bangladesh, we projected that the S1 vaccination strategy of subnational campaign plus subnational routine immunization from the societal perspective over 20 birth cohorts would be considered cost-effective in 99% of simulations at a willingness-to-pay threshold of US $2,400/DALY averted, which is <1 times GDP per capita (Figure 5).

Discussion

Our findings show that introducing CD-JEV vaccination could avert JE cases and deaths and improve the quality of life for the at-risk population in Bangladesh. In addition, we show that vaccine program costs are offset by large cost savings from healthcare services and costs to families. CD-JEV appears to be cost-effective because ICERs were approximately one third GDP per capita, regardless of vaccination strategy or cost perspective.

Our projection was robust in deterministic and probabilistic analyses in which we varied model parameters to account for uncertainties. We applied a
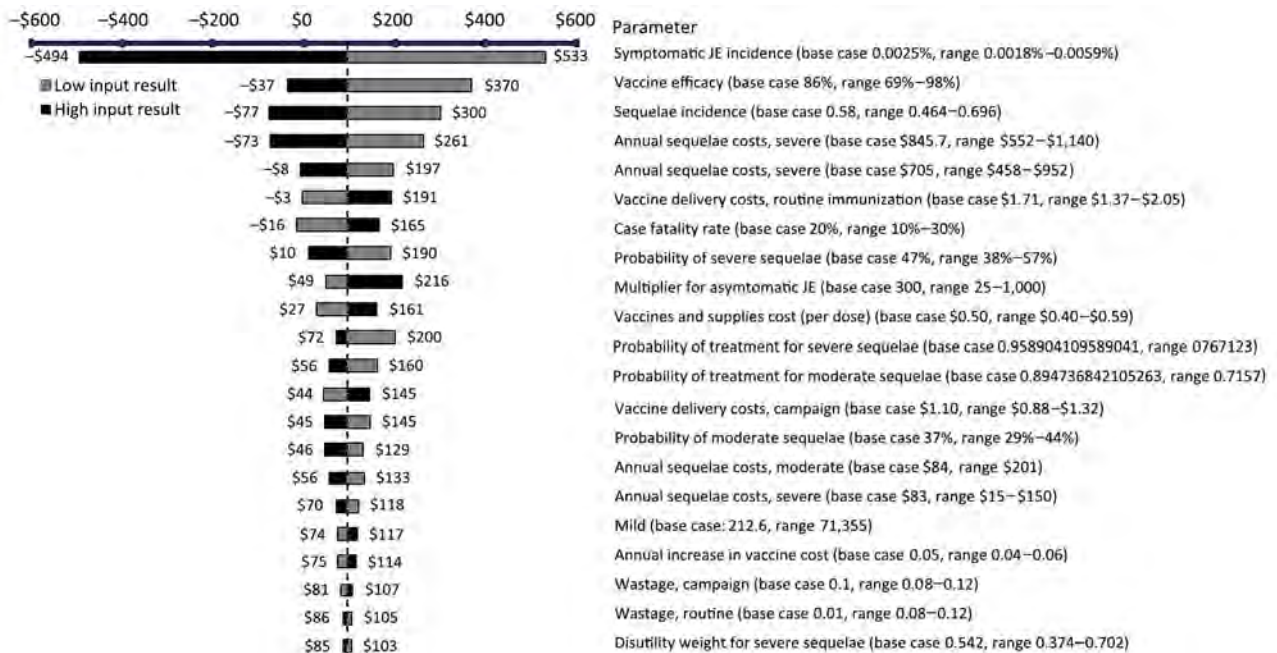

Figure 2. Societal perspective for 1-way sensitivity analysis of key cost drivers for cost per DALY averted with strategy 1 in cost-effectiveness analysis of JE vaccination for children <15 years of age, Bangladesh. Strategy 1 consisted of a subnational 1-time immunization campaign for children <15 years of age and subnational routine immunization for 9-month-old children over 20 birth cohorts. The subnational approach focuses on 3 divisions with a high number of JE cases: Rangpur, Rajshahi, and Chattogram. Values are US dollars. JE, Japanese encephalitis virus.

Figure 3. Governmental perspective for 1-way sensitivity analysis of key cost drivers for cost per DALY averted with strategy 1 in cost-effectiveness analysis of JE vaccination for children <15 years of age, Bangladesh. Strategy 1 consisted of a subnational 1-time immunization campaign for children <15 years of age and subnational routine immunization for 9-month-old children over 20 birth cohorts. The subnational approach focuses on 3 divisions with a high number of JE cases: Rangpur, Rajshahi, and Chattogram. Values are US dollars. JE, Japanese encephalitis virus.

relatively conservative estimate of vaccine efficacy (86.3%), one of the key drivers of cost/DALY averted. Estimates in the literature report a higher vaccine efficacy of 93% based on pooled odds ratios from 5 case–control studies evaluating the effectiveness of a live attenuated SA14-14-2 JE vaccine (10). We evaluated the potential impact of higher vaccine efficacy (up to 98%) through sensitivity analysis with ICER results ranging from cost saving to US $1,260/DALY averted. Varying input parameters across their uncertainty ranges still showed robust evidence of cost-effectiveness with the maximum ICERs corresponding to 52%–62% GDP per capita. Without an established

cost-effectiveness threshold in Bangladesh, CD-JEV vaccination is projected to be 99% cost-effective at a willingness-to-pay level of <US $2,676 or 1 GDP per capita and is projected to be 100% cost-effective at 1–3 times GDP per capita willingness-to-pay.

The large difference between governmental- and societal-perspective ICERs (US $892–$981 vs. $23–$94/ DALY averted) in our analysis reflects that the cost of JE illness in Bangladesh is borne largely by patients and their families (18). Our findings on the cost-effectiveness of CD-JEV immunization is similar to other studies (26,29–31,42). However, the burden of disease borne by families, reflected by differences in governmental
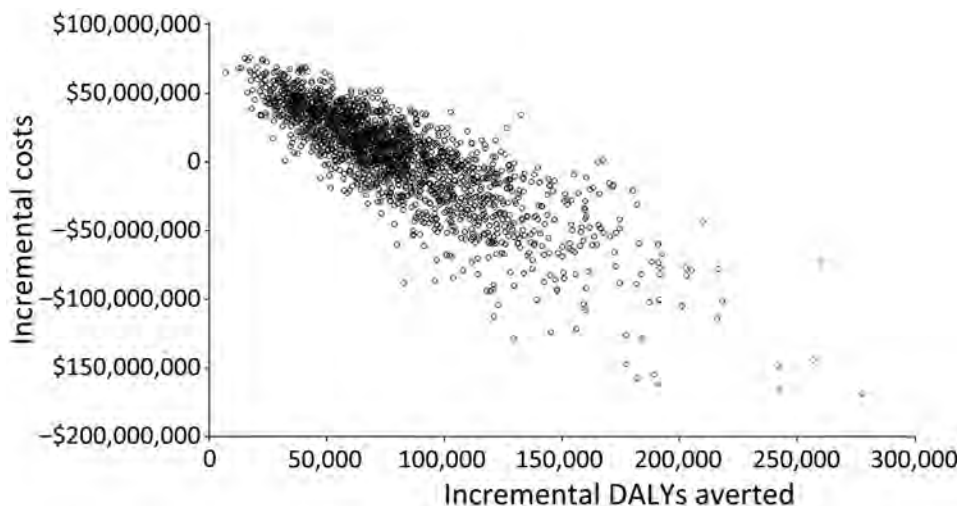
Figure 4. Societal perspective for probabilistic results of key cost drivers for cost per DALY averted with strategy 1 in cost-effectiveness analysis of JE vaccination for children <15 years of age, Bangladesh. Strategy 1 consisted of a subnational 1-time immunization campaign for children <15 years of age and subnational routine immunization for 9-month-old children over 20 birth cohorts. The subnational approach focuses on 3 divisions with a high number of JE cases: Rangpur, Rajshahi, and Chattogram. Values are US dollars. JE, Japanese encephalitis virus.

Figure 5. Cost-effectiveness of strategy 1 in cost-effectiveness analysis of JE vaccination for children <15 years of age, Bangladesh. Strategy 1 consisted of a subnational 1-time immunization campaign for children <15 years of age and subnational routine immunization for 9-month-old children over 20 birth cohorts. The subnational approach focuses on 3 divisions with a high number of JE cases: Rangpur, Rajshahi, and Chattogram. This strategy would be considered cost-effective in 99% of simulations at a willingness-to-pay threshold of US $2,400/DALY averted, which is <1 times gross domestic product per capita. DALY, disability-adjusted life year; JE, Japanese encephalitis virus.
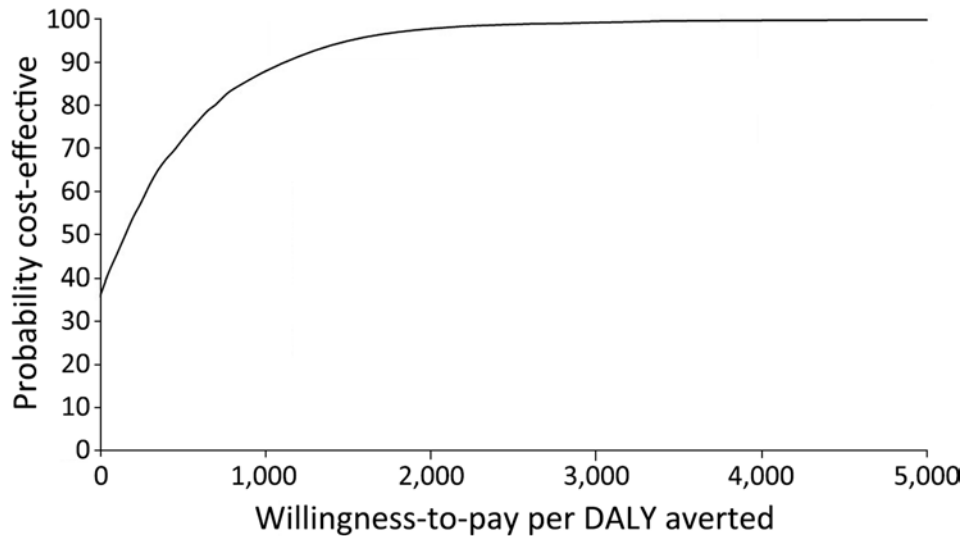
and societal ICERs, is more substantial in Bangladesh, where governmental:societal ICER ratio is >10:1, than in Indonesia, where the ratio is ≈2:1 (*27*), or the Philippines, where the ratio varies from 4:1 to 9:1 (*30*).

A limitation of our study was lack of epidemiologic evidence for JE incidence in Bangladesh. We used the symptomatic JE incidence of 2.5 cases/100,000 persons <15 years of age sourced from a systematic review of studies from many countries, including Bangladesh (*31*). However, the data are from 2011 and might not reflect the most current JE status in the country. In the sensitivity analysis, we used a different source of incidence, taken from a modeling study in 2014 based on a range of incidence across divisions in Bangladesh (1.75–5.89/100,000 persons <15 years of age) (*36*). Our analysis might have underestimated the true number of JE cases, because numerous encephalitis patients never participated in the hospital-based surveillance program because of long distance (*43*), limited access to healthcare services in rural Bangladesh (*44*), or unwillingness to receive care from hospitals (*45*). Furthermore, we depended on expert guidance for our vaccine coverage rate in the absence of available evidence. Nevertheless, in a country like Bangladesh, where there is scant evidence available on incidence, outcomes, and costs associated with JE, our study can contribute to introducing and expanding the JE vaccine program.

Our study provided evidence of CD-JEV cost-effectiveness for different vaccination strategies and supports value-based decision-making for JE vaccine introduction in Bangladesh. We project that subnational or national routine immunization, combined with a one-time subnational introductory campaign, would be more cost-effective than national routine immunization alone. That projection aligns with the WHO position that the most effective JE vaccine introduction strategy is a one-time campaign followed by adding JE vaccination to routine immunization practices (*4*). Both S1 and S2 vaccination strategies were cost-effective with maximum ICERs at the WTP level of ≈50% of GDP per capita. A 10-year vaccination program using the S2 strategy could, at a cost of an additional US $38 million, immunize >15 million more children than the S1 strategy.

Our study adds more evidence on the cost-effectiveness of CD-JEV in general and provides cost-effectiveness data on the various vaccination strategies. These findings have strong policy implications in Bangladesh, where policymakers are considering JE-vaccine introduction, and will help determine resource availability and introduction strategies to maximize public health impact from and cost-effectiveness of CD-JEV.

core/unrestricted support.

About the Author

Dr. Sultana is a cultural epidemiologist with academic training in medical anthropology and health economics. She specializes in infectious disease research on emerging and reemerging infectious diseases, particularly Nipah, avian influenza, COVID-19, and Japanese encephalitis, in Bangladesh. Dr. Nguyen is a senior health economist in the Center for Vaccine Innovation and Access at PATH. Her expertise includes economic evaluations of medicines, medical devices, and healthcare programs.

References

1. Campbell GL, Hills SL, Fischer M, Jacobson JA, Hoke CH, Hombach JM, et al. Estimated global incidence of Japanese encephalitis: a systematic review. Bull World Health Organ. 2011;89:766–74, 74A–74E.
2. Solomon T, Dung NM, Kneen R, Gainsborough M, Vaughn DW, Khanh VT. Japanese encephalitis. J Neurol Neurosurg Psychiatry. 2000;68:405–15. https://doi.org/10.1136/jnnp.68.4.405
3. Kumar R, Mathur A, Singh KB, Sitholey P, Prasad M, Shukla R, et al. Clinical sequelae of Japanese encephalitis in children. Indian J Med Res. 1993;97:9–13.
4. World Health Organization. WHO position paper, February 2015—recommendations. Vaccine. 2016;34:302–3. https://doi.org/10.1016/j.vaccine.2015.07.057
5. UNICEF. Japanese encephalitis vaccine: market and supply update [cited 2023 Apr 14]. https://www.unicef.org/supply/reports/japanese-encephalitis-vaccine-market-and-supply-update
6. PATH. Safety of CD-JEV: a proven tool for JE prevention [cited 2023 Sep 4]. https://media.path.org/documents/CVIA_Safety_CD_JEV_fs.pdf
7. Feroldi E, Pancharoen C, Kosalaraksa P, Chokephaibulkit K, Boaz M, Meric C, et al. Primary immunization of infants and toddlers in Thailand with Japanese encephalitis chimeric virus vaccine in comparison with SA14-14-2: a randomized study of immunogenicity and safety. Pediatr Infect Dis J. 2014;33:643–9. https://doi.org/10.1097/INF.0000000000000276
8. Kim DS, Houillon G, Jang GC, Cha SH, Choi SH, Lee J, et al. A randomized study of the immunogenicity and safety of Japanese encephalitis chimeric virus vaccine (JE-CV) in comparison with SA14-14-2 vaccine in children in the Republic of Korea. Hum Vaccin Immunother. 2014;10:2656–63. https://doi.org/10.4161/hv.29743
9. Ahaduzzaman M, Hassan M, Alam M, Islam SKM, Uddin I. Antimicrobial resistance pattern against *Staphylococcus aureus* in environmental effluents. Res J Vet Pract. 2014;2:13–6. https://dx.doi.org/10.14737/journal.rjvp/2014/2.1.13.16
10. Bista MB, Banerjee MK, Shin SH, Tandan JB, Kim MH, Sohn YM, et al. Efficacy of single-dose SA 14-14-2 vaccine against Japanese encephalitis: a case control study. Lancet. 2001;358:791–5. https://doi.org/10.1016/S0140-6736(01)05967-0
11. Khan SA, Choudhury P, Kakati S, Doley R, Barman MP, Murhekar MV, et al. Effectiveness of a single dose of Japanese encephalitis vaccine among adults, Assam, India, 2012–2018. Vaccine. 2021;39:4973–8. https://doi.org/10.1016/j.vaccine.2021.07.041
12. Kumar R, Tripathi P, Rizvi A. Effectiveness of one dose of SA 14-14-2 vaccine against Japanese encephalitis. N Engl J Med. 2009;360:1465–6. https://doi.org/10.1056/NEJMc0808664
13. Li X, Ma SJ, Liu X, Jiang LN, Zhou JH, Xiong YQ, et al. Immunogenicity and safety of currently available Japanese encephalitis vaccines: a systematic review. Hum Vaccin Immunother. 2014;10:3579–93. https://doi.org/10.4161/21645515.2014.980197
14. Ohrr H, Tandan JB, Sohn YM, Shin SH, Pradhan DP, Halstead SB. Effect of single dose of SA 14-14-2 vaccine 1 year after immunisation in Nepalese children with Japanese encephalitis: a case-control study. Lancet. 2005;366:1375–8. https://doi.org/10.1016/S0140-6736(05)67567-8
15. Hossain MJ, Gurley ES, Montgomery S, Petersen L, Sejvar J, Fischer M, et al. Hospital-based surveillance for Japanese encephalitis at four sites in Bangladesh, 2003–2005. Am J Trop Med Hyg. 2010;82:344–9. https://doi.org/10.4269/ajtmh.2010.09-0125
16. Khan AM, Khan AQ, Dobrzynski L, Joshi GP, Myat A. A Japanese encephalitis focus in Bangladesh. J Trop Med Hyg. 1981;84:41–4.
17. Paul KK, Sazzad HMS, Rahman M, Sultana S, Hossain MJ, Ledermann JP, et al. Hospital-based surveillance for Japanese encephalitis in Bangladesh, 2007–2016: implications for introduction of immunization. Int J Infect Dis. 2020;99:69–74. https://doi.org/10.1016/j.ijid.2020.07.026
18. Sultana R, Slavkovsky R, Ullah MR, Tasnim Z, Sultana S, Khan S, et al. Cost of acute and sequelae care for Japanese encephalitis patients, Bangladesh, 2011–2021. Emerg Infect Dis. 2023;29:2488–97. https://doi.org/10.3201/eid2912.230594
19. World Health Organization. Immunization in Bangladesh [cited 2024 May 14]. https://www.who.int/bangladesh/health-topics/immunization
20. Vannice KS, Hills SL, Schwartz LM, Barrett AD, Heffelfinger J, Hombach J, et al.; Japanese encephalitis vaccination experts panel. The future of Japanese encephalitis vaccination: expert recommendations for achieving and maintaining optimal JE control. NPJ Vaccines. 2021;6:82. https://doi.org/10.1038/s41541-021-00338-z
21. Integrated efforts crucial to prevent JE disease [cited 2023 Aug 1]. https://www.bssnews.net/news/104208
22. Akram A. Japanese encephalitis—emerging disease in Bangladesh. Bangladesh J Med Microbiol. 2018;12:21–3. https://doi.org/10.3329/bjmm.v12i2.51694
23. Haider MS, Youngkong S, Thavorncharoensap M, Thokala P. Priority setting of vaccine introduction in Bangladesh: a multicriteria decision analysis study. BMJ Open. 2022; 12:e054219. https://doi.org/10.1136/bmjopen-2021-054219
24. Paul RC, Rahman M, Gurley ES, Hossain MJ, Diorditsa S, Hasan AM, et al. A novel low-cost approach to estimate the incidence of Japanese encephalitis in the catchment area of three hospitals in Bangladesh. Am J Trop Med Hyg. 2011;85:379–85. https://doi.org/10.4269/ajtmh.2011.10-0706
25. Zahid SH. Thrust on joint efforts to contain JE. The Financial Express [cited 2023 Apr 14]. https://today.thefinancialexpress.com.bd/country/thrust-on-joint-efforts-to-contain-je-1673277777
26. Kosen S, Khoe LC, Indriasih E, Tarigan I, Iriawan RW, Agustiya RI, et al. Expanding Japanese encephalitis vaccination to selected endemic Indonesia provinces: a cost-effectiveness analysis. Vaccine X. 2022;11:100179. https://doi.org/10.1016/j.jvacx.2022.100179
27. Siraprapasiri T, Sawaddiwudhipong W, Rojanasuphot S.

Cost benefit analysis of Japanese encephalitis vaccination program in Thailand. Southeast Asian J Trop Med Public Health. 1997;28:143–8.

28. Suraratdecha C. A cost-effectiveness analysis of strategies for controlling Japanese encephalitis in Andhra Pradesh, India. J Pharm Finance Econ Policy. 2006;15:21–40.

29. Touch S, Suraratdecha C, Samnang C, Heng S, Gazley L, Huch C, et al. A cost-effectiveness analysis of Japanese encephalitis vaccine in Cambodia. Vaccine. 2010;28:4593–9. https://doi.org/10.1016/j.vaccine.2010.04.086

30. Vodicka E, Zimmermann M, Lopez AL, Silva MW, Gorgolon L, Kohei T, et al. Japanese encephalitis vaccination in the Philippines: a cost-effectiveness analysis comparing alternative delivery strategies. Vaccine. 2020;38:2833–40. https://doi.org/10.1016/j.vaccine.2020.02.018

31. Yin Z, Beeler Asay GR, Zhang L, Li Y, Zuo S, Hutin YJ, et al.; Guizhou JE Study Group. An economic evaluation of the use of Japanese encephalitis vaccine in the expanded program of immunization of Guizhou province, China. Vaccine. 2012;30:5569–77. https://doi.org/10.1016/j.vaccine.2012.05.068

32. Bangladesh Directorate General of Health Services. EPI Coverage Evaluation Survey 2019 [cited 2023 Apr 20]. https://dghs.gov.bd/images/docs/vpr/Coverage_Evaluation_Survey_2019.pdf

33. Bangladesh Bureau of Statistics. Population and housing census 2022: preliminary report [cited 2023 Sep 15]. https://sid.portal.gov.bd/sites/default/files/files/sid.portal.gov.bd/publications/01ad1ffe_cfef_4811_af97_594b6c64d7c3/PHC_Preliminary_Report_(English)_August_2022.pdf

34. Bangladesh Bureau of Statistics. Report on Bangladesh sample vital statistics 2018 [cited 2023 Sep 15]. https://bbs.portal.gov.bd/sites/default/files/files/bbs.portal.gov.bd/page/b343a8b4_956b_45ca_872f_4cf9b2f1a6e0/2021-06-28-07-11-c1784c6fe700cf52ff934e8d-d7cf9147.pdf

35. World Bank. Official exchange rate (LCU per US$, period average)—Bangladesh [cited 2022 Oct 5]. https://data.worldbank.org/indicator/PA.NUS.FCRF

36. Rothenberg CM. Estimating the incidence of Japanese encephalitis in divisions of Bangladesh [cited 2024 May 9]. https://elischolar.library.yale.edu/ysphtdl/1251

37. Institute of Epidemiology, Disease Control and Research. Disease surveillance systems of Bangladesh: acute meningo-encephalitis surveillance (AMES) [cited 2023 Sep 15]. https://www.iedcr.org/Default.aspx

38. Salomon JA, Haagsma JA, Davis A, de Noordhout CM, Polinder S, Havelaar AH, et al. Disability weights for the Global Burden of Disease 2013 study. Lancet Glob Health. 2015;3:e712–23. https://doi.org/10.1016/S2214-109X(15)00069-8

39. Misra UK, Kalita J. Overview: Japanese encephalitis. Prog Neurobiol. 2010;91:108–20. https://doi.org/10.1016/j.pneurobio.2010.01.008

40. World Health Organization. WHO vaccine reaction rates information sheets: Japanese encephalitis vaccine information sheet [cited 2024 Aug 20]. https://www.who.int/publications/m/item/je-vaccine-information-sheet

41. Sarker AR, Khan AI, Islam MT, Chowdhury F, Khanam F, Kang S, et al. Cost of oral cholera vaccine delivery in a mass immunization program for children in urban Bangladesh. Vaccine X. 2022;12:100247. https://doi.org/10.1016/j.jvacx.2022.100247

42. Ding D, Kilgore PE, Clemens JD, Wei L, Zhi-Yi X. Cost-effectiveness of routine immunization to control Japanese encephalitis in Shanghai, China. Bull World Health Organ. 2003;81:334–42.

43. Hegde ST, Salje H, Sazzad HMS, Hossain MJ, Rahman M, Daszak P, et al. Using healthcare-seeking behaviour to estimate the number of Nipah outbreaks missed by hospital-based surveillance in Bangladesh. Int J Epidemiol. 2019;48:1219–27. https://doi.org/10.1093/ije/dyz057

44. Akter M, Kabir H. Health inequalities in rural and urban Bangladesh: the implications of digital health. Mayo Clin Proc Digit Health. 2023;1:201–2. https://doi.org/10.1016/j.mcpdig.2023.04.003

45. Institute of Epidemiology, Disease Control and Research. Estimation from IEDCR 10-year JE surveillance.

46. Alera MT, Velasco JM, Ypil-Cardenas CA, Jarman RG, Nisalak AN, Thaisomboonsuk B, et al. Hospital-based surveillance of Japanese encephalitis at a tertiary hospital in Manila. Southeast Asian J Trop Med Public Health. 2013;44:791–8.

Address for correspondence: Rebeca Sultana, icddr,b, Shaheed Tajuddin Ahmed Ave, Dhaka 1213 Bangladesh; email: rebeca@icddrb.org

Dogs as Reservoirs for *Leishmania donovani*, Bihar, India, 2018–2022

Anurag Kumar Kushwaha,[1] Ashish Shukla,[1] Breanna M. Scorza, Rahul Chaubey,
Dharmendra Kumar Maurya, Tulika Kumari Rai, Shyamali Yaduvanshi, Shweta Srivastava,
Gaetano Oliva, Epke A. Le Rutte, Rajiv Kumar, Om Prakash Singh, Puja Tiwary, Shakti Kumar Singh,
Scott A. Bernhardt, Phillip Lawyer, Edgar Rowton, Christine A. Petersen,[1] Shyam Sundar[1]

Visceral leishmaniasis derived from *Leishmania donovani* is transmitted by sand flies (*Phlebotomus argentipes*) throughout the Indian subcontinent. Although considered anthroponotic, *L. donovani* infects other mammals susceptible to sand fly bites, including dogs. Aggressive strategies to reduce sand fly populations in India have led to flies seeking nonhuman hosts, so understanding the role of dogs in *L. donovani* transmission has become critical. Our study investigated *L. donovani* infection in dogs and the potential for such infections to be transmitted back to sand flies. We performed xenodiagnosis by using *P. argentipes* on dogs (n = 73) with quantitative PCR–detectible parasitemia in both endemic and outbreak villages. We found that 12% (9/73) of dogs were infectious to sand flies during winter and rainy seasons. Patients with visceral leishmaniasis remain primary sources of *L. donovani* transmission, but our findings suggest a possible link between canine infection and human exposure.

Visceral leishmaniasis (VL), caused by *Leishmania donovani*, is transmitted by *Phlebotomus argentipes* on the Indian subcontinent. Depending on the geographic region of India, 2 different epidemiologic cycles sustain VL: a zoonotic cycle (*Leishmania infantum*), in which dogs are the primary reservoir, and an anthroponotic cycle (*L. donovani*). Active case detection and indoor residual spraying programs have reduced phlebotomine sand fly populations and have been linked to substantial declines in VL incidence across India (*1*). Although indoor residual spraying campaigns have made considerable progress in reducing VL in India, Nepal, and Bangladesh, and elimination was validated in Nepal and Bangladesh in 2020, India remains endemic and has persistent areas of infection in Uttar Pradesh and Bihar districts. The World Health Organization is formulating 2030 targets to identify knowledge gaps and sustain elimination of the disease, simulating interventional impact—including early outbreak identification—to impede or avoid VL spread (*2,3*). Both elimination goals and maintenance of validated elimination would be at risk if nonhuman sources of infection were found. Current elimination strategies in India do not target nonhuman sources of VL.

We theorized that indoor residual spraying might have altered *P. argentipes* behavior from endophilic to exophilic patterns. In fact, some reports have shown *P. argentipes* to feed indiscriminately on multiple mammalian hosts, particularly cattle and dogs (*4,5*). However, cattle, goats, and buffalo were not hosts for *L. donovani* (*6*). Although the role of dogs in *L. donovani* transmission remains unclear, canine reservoirs are well accepted as a major source of zoonotic transmission to maintain periurban and rural *L. infantum* infection (*7*). On the Indian subcontinent, health officials reconsidered nonhuman transmission of *Leishmania* spp. parasites after detection of *Leishmania* antibodies and *Leishmania*-specific DNA was demonstrated from livestock (*8,9*). *L. donovani* DNA

was detected in the blood of village dogs, goats, and cows from India and Bangladesh, suggesting *L. donovani* infection (*8–11*). We investigated the potential role of dogs in the ecology of *L. donovani* on the Indian subcontinent, particularly whether dogs were capable hosts for transmission of *L. donovani* parasites to *P. argentipes* sand flies.

Materials and Methods

Selection of Study Area and Epidemiologic Database
This study included 15 villages in the Muzaffarpur district (26.07°N, 85.45°E) of the state of Bihar, India, with endemic VL (*12*). Sampled villages had active *Leishmania* transmission during 2017–2022. Temperatures in Muzaffarpur range from 14°C during December–January to 32°C during April–

May, and the average annual precipitation is ≈1,300 mm during the monsoon season during late June–September. We selected villages with active transmission based on VL history determined by the Health and Demographic Surveillance System (*13*) and Kala-azar Management Information System (*14*) (Figure 1).

Sampling Procedures
We found that in endemic villages, dogs roamed near households without shelter, exposing them to harsh weather, and dogs often were malnourished. We surveilled the canine population and captured 10% of dogs across seasons. We captured mixed-breed male and female dogs, typically 1–4 years of age, based on physical appearance of illness and requested recruiters to seek out "sick" dogs for the study. We
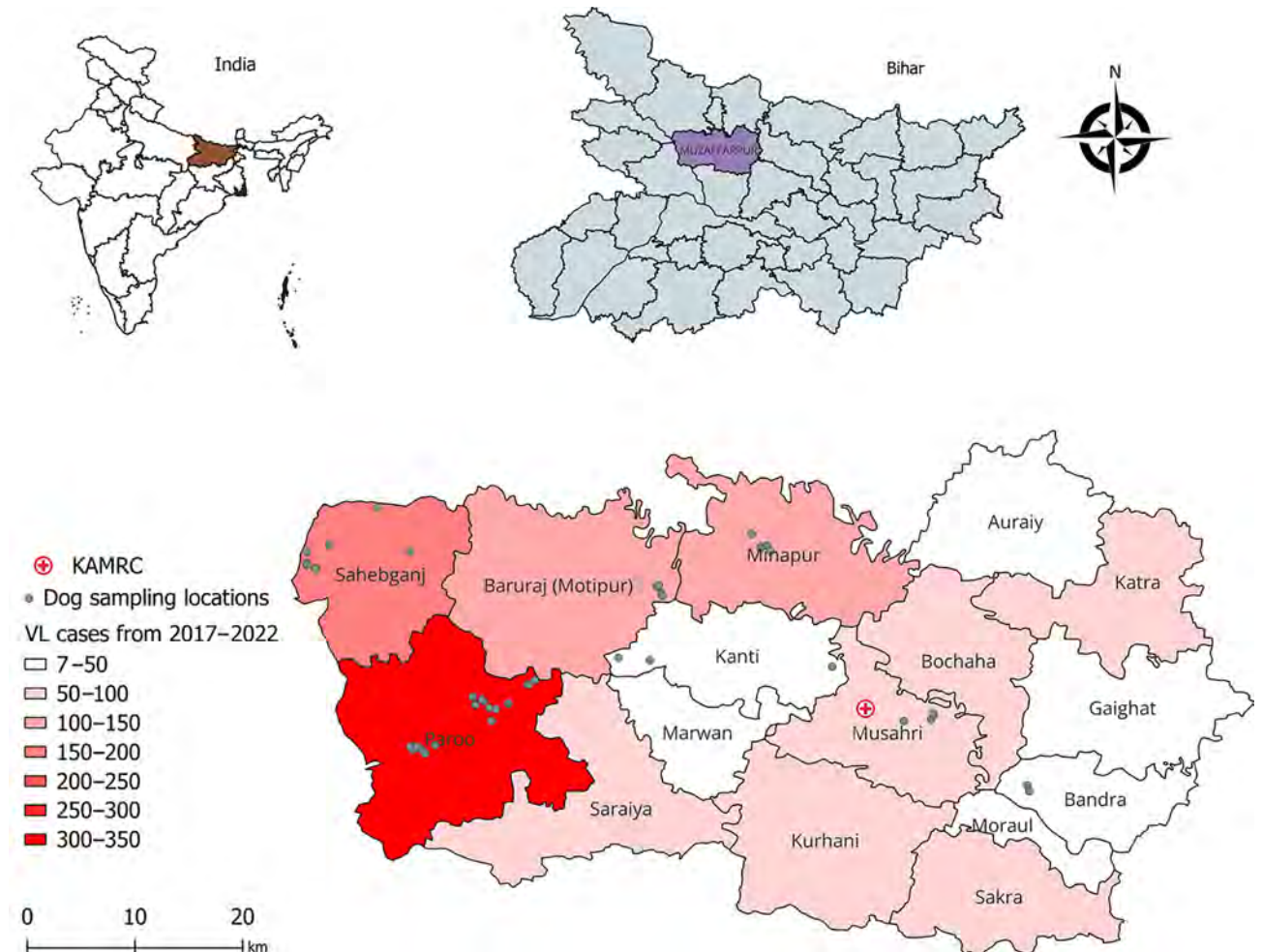
Figure 1. Locations of study villages and 5-year incidence of VL in a study of dogs as reservoirs for *Leishmania donovani*, Bihar, India, 2018–2022. A) Map of India showing Bihar; B) Bihar detail showing Muzaffarpur district study area; C) detail of sampling locations and VL cases, Muzaffarpur district. Geographic information system locations of study sampling sites calculated from a latitude-longitude application. Map produced using QGIS software version 3.30.3 (https://qgis.org) with open-access shapefile (https://onlinemaps.surveyofindia.gov.in). KAMRC, Kala-Azar Medical Research Center.

anesthetized dogs intravenously with Dexdomitor (Zoetis Inc., https://www.zoetisus.com) and reversed anesthetic effects with Antesedan (Zoetis Inc.), according to estimated bodyweight. We obtained physical exams and history, when available. We assessed disease state based on physical signs of canine leishmaniasis (CanL), including lymphadenopathy, anemia, dermatitis, and rough hair coat (15), and scored each dog on a 5-scale basis (i.e., number of clinical signs). We administered rabies vaccine to all dogs sampled. We collected blood samples in ethylenediaminetetraacetic acid vials and m-tube vials, transported samples on ice packs, and then aliquoted and stored samples at −20°C for serologic and molecular assays (Appendix Figure 1, https://wwwnc.cdc.gov/EID/article/30/12/24-0649-App1.pdf). We performed xenodiagnosis by using laboratory-reared *P. argentipes* sand flies on 73 dogs from 15 villages in the Muzaffarpur district.

Preparation of Sand Flies for Xenodiagnosis

We used *P. argentipes* sand flies from a closed, certified, pathogen-free colony for xenodiagnoses, as previously described (16,17). We loaded 30–35 mature (3- to 5-days-old), 12-hours-starved *P. argentipes* female flies plus 10 males into feeding cups.

Xenodiagnosis on Dogs

We assessed infectiousness of dogs in endemic villages by direct feeding of *P. argentipes* on the animals (xenodiagnosis) (6,7). We placed feeding cups on the ears and inguinal areas of sedated dogs for 30 minutes. We performed xenodiagnosis under local environmental conditions. We transferred blood-engorged females to 1-pint cups and kept them in an environmental chamber at 27°C and 80% humidity for 48 hours with access to a 30% sugar solution. We stored flies in 70% ethanol for processing.

DNA Extraction from Whole Blood and Blood-Fed Sand Flies

We extracted DNA from whole blood by using QIAamp DNA Blood Mini Kit (QIAGEN, http://www.qiagen.com), according to manufacturer's instructions. We extracted DNA from individual blood-fed sand flies by using Gentra Puregene Tissue DNA Extraction Kit (QIAGEN), optimized for individual sand flies (7) and endemic site (6). We assessed DNA quality by using Nanodrop Spectrophotometer (Thermo Scientific, https://www.thermofisher.com). We used DNA samples with 260/280 ratio 1.8–2.0 and 260/230 ratio >1.5 for real-time quantitative PCR (qPCR).

qPCR

We performed quantification of parasites in whole blood and blood-fed flies by qPCR. We ran TaqMan-based qPCR on each DNA sample in duplicate on an Applied Biosystems 7500 Real-Time PCR system (Thermo Fisher Scientific) to amplify an *L. donovani* kinetoplast minicircle kDNA4 target with forward primer (4GGGTGCAGAAATCCCGTTCA), reverse primer (4 CCCGGCCCTATTTTACACCA), and probe (ACCCCCAGTTTCCCGCCCCG) (6,17). We used nuclease-free water (Thermo Fisher Scientific) and blood DNA from nonendemic healthy control dogs and DNA from pooled uninfected laboratory-reared *P. argentipes* as negative controls. We calculated quantification of parasite equivalents in test samples by using a standard curve generated from DNA from healthy human blood and uninfected sand flies spiked with a serial dilution of cultured *Leishmania* spp. parasites run in parallel to each set of test samples, as previously described (18). We considered PCR cycle threshold cutoff to be >35 for negative for blood and tissue. For sand flies, we considered a stringent cycle threshold >30 to be xenodiagnosis negative (6,7).

Recombinant K39 Antigen ELISA

To measure antibodies in dog serum against recombinant K-39 (rK39) antigen, we coated 25 ng/well of rK39 antigen to 96-well, flat-bottom microtiter plates in coating buffer (0.1 mol carbonate-bicarbonate buffer, pH 9.6) and incubated samples overnight at 4°C. We blocked the plates with blocking buffer (1% bovine serum albumin in 0.05 mol phosphate buffer) at 25°C for 2 hours. We then added 100 µL of serum samples (1:200 dilution) to the plates and incubated plates at 25°C for 30 minutes. We assayed each sample in duplicate. We washed the plates with phosphate-buffered saline (pH 7.4) containing 0.1% Tween 20 (Sigma-Aldrich, https://www.sigmaaldrich.com). We used rabbit anti-dog IgG peroxidase conjugated secondary antibody (1:4,000 dilution, Sigma-Aldrich) with o-phenylenediamine dihydrochloride for 15 minutes and measured optical density at 490 nm (7). We used serum from infected dogs with CanL as assay-positive controls (C.A. Petersen, unpub. data).

Statistical Analyses

We determined cutoff values for positive serology by adding 2 standard deviations to the mean optical density of canine-negative control sera (C.A. Petersen, unpub. data). We determined *Leishmania* spp. exposure prevalence based on rK39 ELISA. We assessed normality of data by using the D'Agostino-Pearson test. For comparisons between subjects or groups,

we performed Mann-Whitney test or Fisher exact test. When appropriate, we used Kruskal-Wallis with Dunn's posttest for multiple comparisons.

Results

In *L. infantum*–endemic areas with vector transmission, 67%–80% of dogs had *Leishmania* antibodies or were positive for *Leishmania* DNA by qPCR, but characteristic of the ratio of asymptomatic to symptomatic disease, some dogs that had no outward clinical signs of CanL were infectious to sand flies (*19*). As we reported in a prior study, domestic cattle, goats, buffalo, and rodents were exposed to *L. donovani* parasites as evidenced by seropositivity on rK39 ELISA but did not show evidence of clinical infection and were not infectious to sand flies (*6*). To establish whether dogs had active infection or disease after exposure to *L. donovani*, we used physical and clinicopathologic examination, reinforced by diagnostic parameters, to evaluate dogs for their clinical status in an *L. donovani*–endemic area in Bihar, India. We analyzed parasitemia by qPCR and *Leishmania* serology by using blood from village dogs. We included 73 dogs in this study (Table).

Despite asking for "sick dogs," we classified 60% (44/73) of the dogs as subclinical and the other 40% (29/73) as clinical (i.e., >2 physical signs of CanL). Among subclinical dogs, 9% (4/44) were *Leishmania*-positive by blood qPCR (Figure 2, panel A). We determined that 21% (6/29) of clinically affected dogs had detectable parasitemia (Figure 2, panel B) (Fisher exact test p = 0.18). Thirty percent (13/44) of subclinical dogs had *Leishmania* antibodies via rK39 ELISA (Figure 2, panel C), and 76% (22/29) of dogs with clinical signs consistent with CanL were seropositive for *Leishmania* antibodies (Figure 2, panel D) (Fisher exact test p = 0.0001). Only 5% (2/44) of subclinical dogs were qPCR and ELISA positive (Figure 2, panel E); 14% (4/29) of clinical dogs were positive by both qPCR and rK39 ELISA (Figure 2, panel F) (Fisher exact test p = 0.21). Dogs from VL-endemic villages in Bihar with clinical signs consistent with CanL were >2 times more likely to have been exposed to *Leishmania* parasites as demonstrated by rK39 ELISA and 3 times more likely to have either been exposed or demonstrated parasitemia with *L. donovani* than other dogs from the same villages.

Temperature and rainfall (humidity) can play a crucial role in vector emergence and survival, directly affecting transmission of *Leishmania* spp. (*15*). Bihar has 3 distinct seasons with different temperatures and humidity. Research has documented seasonal differences in human VL incidence, and most transmission occurs in the rainy season (*20*). To better understand the timing of *L. donovani* parasite transmission to and from dogs, we assessed both parasitemia level and rK39 antibody production in dogs across seasons: summer (n = 16), rainy (n = 47), and winter (n = 10) (Table). We found qPCR-confirmed *L. donovani*–positive dogs during only the rainy season. The difference between the rainy season and winter was not statistically significant (Fisher exact test p = 0.18), but the difference between the rainy season and summer was significant (Fisher exact test p = 0.05) (Figure 3). By comparison, we found no seasonal pattern for *Leishmania* rK39 antibody levels in endemic-village dogs.

L. infantum–infected dogs transmit parasites from skin to naive sand flies, and some evidence shows that clinically apparent dogs with anemia can be infectious (*7,19,21*). Popular understanding of *L. donovani* qualifies the species as anthroponotic and no previous evidence indicates dogs as a parasite source to *P. argentipes* sand flies. In performing xenodiagnosis on 73 dogs across villages endemic for VL (Figure 1), we found positive results from dogs with clinical signs consistent with leishmaniosis. Dogs with clinically observed signs of disease (CanL) provided a significantly higher average number of *Leishmania*-positive sand flies per dog than from dogs with <2 clinical signs of disease (p = 0.02) (Figure 4, panel A,B). A significantly higher percentage of sand flies fed on dogs with clinical signs consistent with CanL took up

Table. Canine diagnostic test outcomes and sand fly qPCR positivity after xenodiagnosis in a study of dogs as reservoirs for *Leishmania donovani*, Bihar, India, 2018–2022*

Clinical signs	Diagnostic test results	No. CanL-positive dogs/no. dogs			No. qPCR-positive fed sand flies/no. dogs		
		Summer	Rainy	Winter	Summer	Rainy	Winter
Total no. (%), n = 73	NA	16 (22)	47 (64)	10 (14)	16 (22)	47 (64)	10 (14)
No CanL clinical signs, n = 44	qPCR–, ELISA–	7/9	17/30	5/5	0	5/2	1/1
	qPCR+, ELISA–	0	2/30	0	0	0	0
	qPCR–, ELISA+	2/9	9/30	0	0	0	0
	qPCR+, ELISA+	0	2/30	0	0	0	0
CanL clinical signs, n = 29	qPCR–, ELISA–	2/7	0	3/5	0	0	9/2
	qPCR+, ELISA–	0	2/17	0	0	0	0
	qPCR–, ELISA+	5/7	11/17	2/5	0	9/2	8/2
	qPCR+, ELISA+	0	4/17	0	0	0	0

*CanL, canine leishmaniosis; NA, not applicable; qPCR, quantitative PCR; +, positive; –, negative.

parasites (mean ≈3% of all fed sand flies) compared with those fed on subclinical dogs (mean ≈0.3% of fed sand flies, p = 0.02) (Figure 4, panel B,C). The average parasite burden among flies containing a blood-meal after feeding on dogs with clinical signs of CanL was significantly higher than the comparative average burden of parasites from blood-fed flies after xenodiagnosis on dogs without physical abnormalities
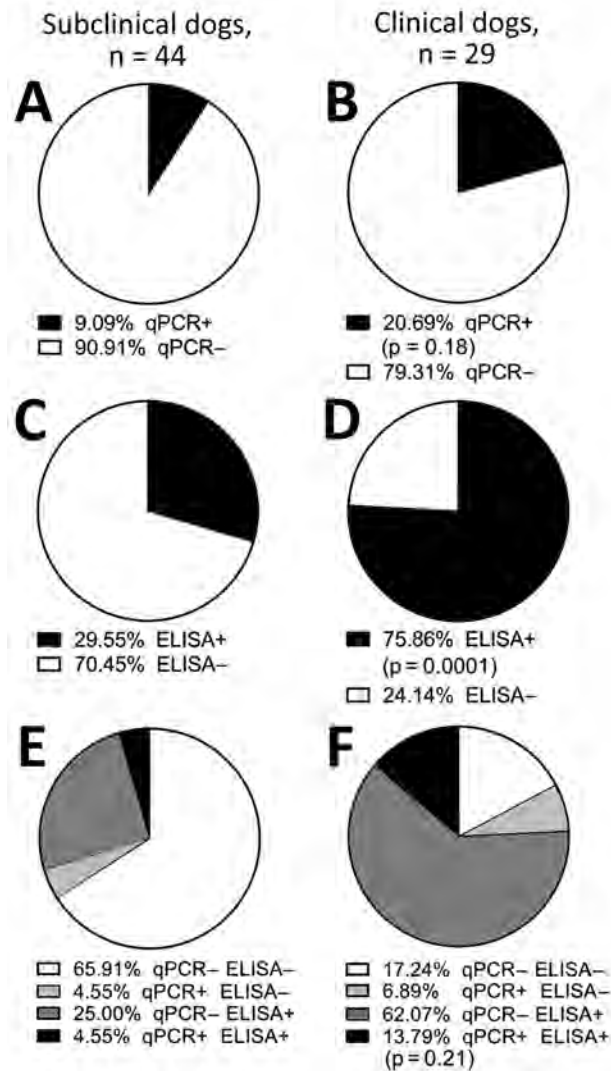
(p = 0.03) (Figure 4, panel D). That finding is within the range of findings from patients with VL in previous studies (22,23).

We found that dogs showing signs of CanL had a higher rate of seroreactivity to *Leishmania* rK39 antigen, indicating previous exposure to the parasite. Dogs with signs of disease were better able to transmit parasites to sand flies. Pathogenesis of CanL and VL is widely believed to be secondary to antigen or antibody complexes and can be correlated with *Leishmania* antibody serologic levels (24). On the basis of this assumed correlation, we evaluated whether transmission from Bihar village dogs to sand flies would correlate with the presence of positive rK39 ELISA. We found that seropositive and seronegative dogs were similarly infectious to sand flies (Appendix Figure 2, panel A). We observed no significant difference in parasite uptake, percent positivity of sand flies, or average parasite burden within sand flies fed on rK39-seropositive versus rK39-seronegative dogs, indicating that parasite exposure (i.e., rK39 seropositivity) did not predict infectiousness to sand flies.

Sand flies emerge during the rainy season, after the dry, hot summer, hungry and looking for blood meals (20). We found that dogs had higher parasitemia during the rainy season. Therefore, we wanted to test whether canine infectiousness was influenced by season. Sand flies that fed on dogs during rainy and winter seasons were positive for *L. donovani* kDNA as confirmed by qPCR (Figure 5). No dogs were infectious to sand flies via xenodiagnosis during summer (Figure 5, panel A). The percentage of sand flies positive for *Leishmania* DNA was highest during winter (Figure 5, panel B). Per dog, the average parasite burden in fed sand flies was higher in winter than in the rainy season (Figure 5, panel D). We noted that 50% (5/10) of parasite-positive sand flies were fed during winter, a rate higher than that for sand flies fed on dogs in the rainy season, 13% (4/30). Across both the rainy and winter seasons, 46% (6/13) of dogs with clinical signs were infectious to sand flies and only 11% (3/37) of subclinical dogs were infectious to sand flies (Figure 5, panel E). Our data revealed that canine infectiousness was associated with clinical disease, regardless of clinical classification or how infection was detected.

Figure 2. Seropositivity among endemic dogs with clinical signs consistent with CanL from the Muzaffarpur district in a study of dogs as reservoirs for *Leishmania donovani*, Bihar, India, 2018–2022. A,C,E) Results from subclinical (healthy) dogs; B,D,F) results from dogs with ≥2 clinical signs of CanL. Percentage of positive (black) versus negative (white) results by kinetoplastid-targeted qPCR or by rK39 ELISA are shown. E,F) Percentage of dogs with single-positive or double-positive diagnostic status among subclinical dogs (E) and clinical dogs (F). Statistical significance between subclinical and clinical groups measured by Fisher exact test. CanL, canine leishmaniosis; qPCR, quantitative PCR; +, positive; −, negative.

Discussion

We investigated canine exposure to *L. donovani* parasites in Bihar, India, and performed xenodiagnosis to explore the role of dogs in transmitting parasites to sand flies. Published literature regarding *L. donovani*
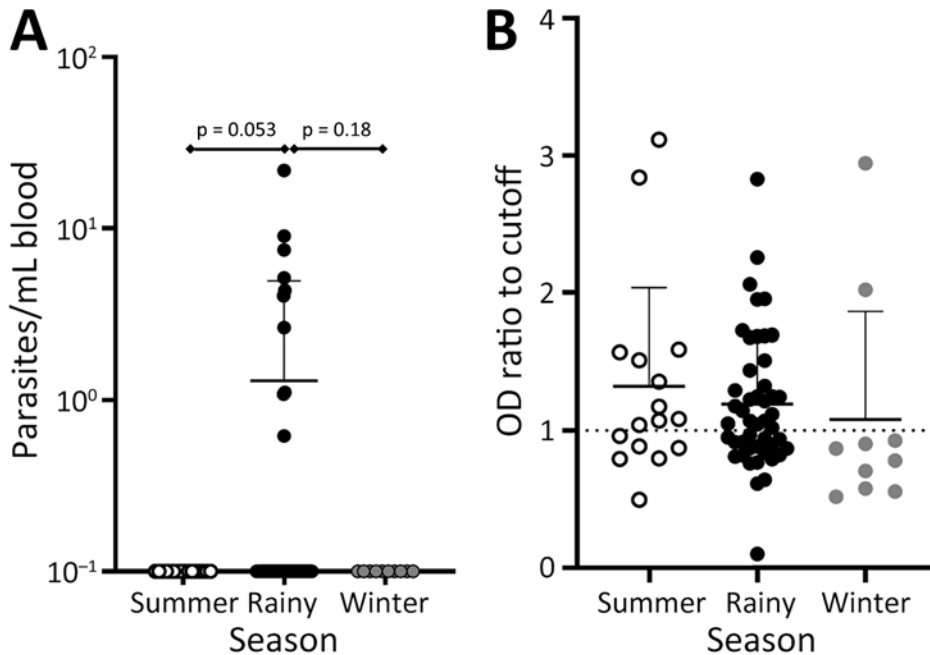
Figure 3. Plot of dogs with detectable parasitemia during the rainy season from villages in the Muzaffarpur district in a study of dogs as reservoirs for *Leishmania donovani*, Bihar, India, 2018–2022. Lower level of whiskers indicate mean, upper level indicates standard deviation. A) Parasitemia measured by quantitative PCR of whole blood DNA. Statistical significance between different seasons (shown above diamond bars) measured by Fisher exact test. B) *Leishmania* rK39 ELISA absorbance ratio detected from canine serum. Dotted line indicates OD cutoff. Kruskal-Wallis with Dunn's posttest was performed, but no statistically significant differences were found for B. OD, optical density.

parasites suggests that the species is strictly anthroponotic on the Indian subcontinent, but studies have reported seropositivity in nonhuman mammals (*6*). *Leishmania* spp. are a parasite of sand flies, which serve as vessels where parasite meiosis occurs (*25*). Sand fly blood meal analyses in Bihar and elsewhere revealed that 10%–25% of sand flies took blood from dogs (*5*). Although controversial, the fact that dogs can be infected by and be a source of *L. donovani* parasites may not be surprising based on the ecology of *L. donovani*–complex parasites globally.

In our study, prevalence of *L. donovani* parasite exposure was high (45%, 35/73) in endemic dogs, consistent with other serologic studies of dogs (*9,11*). Sand fly abundance is highly influenced by seasonality. Previous studies showed that sand flies emerge and are most abundant during the rainy season (*20*), and that the highest proportion of gravid females and highest parasitic loads were found in summer (*20,26*). We found the highest canine seropositivity in summer, perhaps due to significantly more parasitized sand flies and gravid females feeding in preparation of egg laying.

Quantitative serology is a sensitive tool for CanL surveillance and positive serology has previously been correlated with presence of clinical signs (*27*). We found that 76% (22/29) of dogs with signs consistent with CanL were seropositive for *L. donovani* antibodies. Our analyses revealed that 55% (5/9) of seronegative dogs were infectious to *P. argentipes* sand flies, a finding consistent with previous study

results showing that 27.4% of seronegative dogs had *L. infantum* infection (*28*). We did not observe a correlation between the serostatus of dogs and their relative infectiousness to *P. argentipes* sand flies. Dogs with subclinical infections typically remain healthy for many years due to effective cell-mediated immunity (*7*). We performed molecular diagnostic tests to detect *Leishmania* DNA in dog blood. We detected low parasitemia from dogs during the rainy season. Conversely, we could not detect *Leishmania* DNA in dog blood from summer or winter. *L. infantum* DNA has been shown to rise over time in dogs, depending on disease presentation, bone marrow parasite load, and renal disease severity, often impacted by other comorbid diseases (*7,21*). Only after parasite burden increases in the bone marrow or dogs have advanced renal disease do they become consistently parasitemic. (*7,21*) Previous studies have revealed that after peak *Leishmania* parasite transmission season, because of the presence of many infectious sand flies, parasite DNA could be present in domestic mammals in proximity to humans (*6*).

Detection of PCR positivity does not dictate that dogs are critical for the life cycle of *L. donovani* parasites in India. Sand flies are telmophages that feed after skin laceration, so dermal parasite burden might be an important factor. Xenodiagnosis studies on patients with post-kala-azar dermal leishmaniasis (PKDL, a dermal leishmaniasis that manifests after VL as macular, papular, or nodular rash that usually appears on face, upper arms,

and trunk [2]) revealed that parasitemia was very low, and no significant correlation was observed between dermal parasitic load and parasitemia. (*17*) Despite low parasitemia, 88% (23/26) of patients with PKDL transmitted parasites to at least 1 sand fly (*17*). Parasitemia, therefore, is not always the best predictor of a host's outward transmission (*29*). Research has demonstrated *L. infantum* parasites to be especially dermotrophic, and skin-parasite burden is highly correlated with parasite transmission to sand flies (*19*).

In our study, the proportion of dogs that transmitted *L. donovani* parasites to at least 1 sand fly was 12% (9/73), much lower than transmitted by dogs with active CanL due to *L. infantum* (58%, 15/26) (*30*). Our 12% finding is also lower than

results from more recent xenodiagnosis studies in patients with nodular (67%, 18/27) and macular (35%, 9/27) PKDL and in patients with VL (67%, 10/15) in Bangladesh (*22*). In contrast, none of the 184 asymptomatic enrolled participants in a study population in Bihar, India were infectious to sand flies (*17*). Our data revealed sand flies were positive for kDNA qPCR after being fed on subclinical dogs (n = 3), but with a low resultant sand fly parasite load. Despite that finding, we theorize that low infectiousness of multiple village dogs could affect *L. donovani* parasite transmission and potentially be an outbreak source, particularly if canine parasitologic status remains stable and the number of individual infected dogs accumulates over time.

Our xenodiagnosis investigation showed that most fed sand flies acquired <100 parasites. Another study showed that a subsequent blood meal greatly augmented sand fly infectiousness (*31*), observing that sand flies acquired a larger burden (>100) of *Leishmania* amastigotes from a second feeding. In our experiments, we assessed only the presence of *L. donovani* parasites during the early stages of development in the vector 48 hours after 1 experimental blood meal. A relatively small number of parasites acquired by sand flies after feeding on infected dogs might be able to survive and replicate in the gut of the vector after a second blood meal. The *Leishmania* life cycle within the sand fly takes ≈8–10 days to reach stationary phase growth. Extending the post-xenodiagnosis time for parasite replication to the metacyclic stage would verify whether parasites can then be transmitted to humans. Such verification requires additional studies to understand outgoing sand fly infectiousness and the effect of >1 blood meal on infectious dogs.

Xenodiagnosis on livestock and rodents in endemic villages of Bihar indicated that those animals were exposed to *Leishmania* parasites but had a limited or no role in the spread of infection (*6*). Presence of rK39 antibodies with supporting *Leishmania* DNA–specific PCR from blood and blood-fed sand flies suggests that even though multiple domestic animal species are exposed to *L. donovani* after infectious sand fly bites, only dogs, known to be noteworthy reservoir species for other *L. donovani* complex spp., were infectious to sand flies. Our data suggest that, unlike livestock or rodents, dogs are infectious to sand flies and present a risk for outbreak infections in areas where human disease elimination has been established in India. Dogs have been implicated as a bridge between the sylvatic cycle of *Leishmania* to persons. A study of the emergence of *L. infantum*–
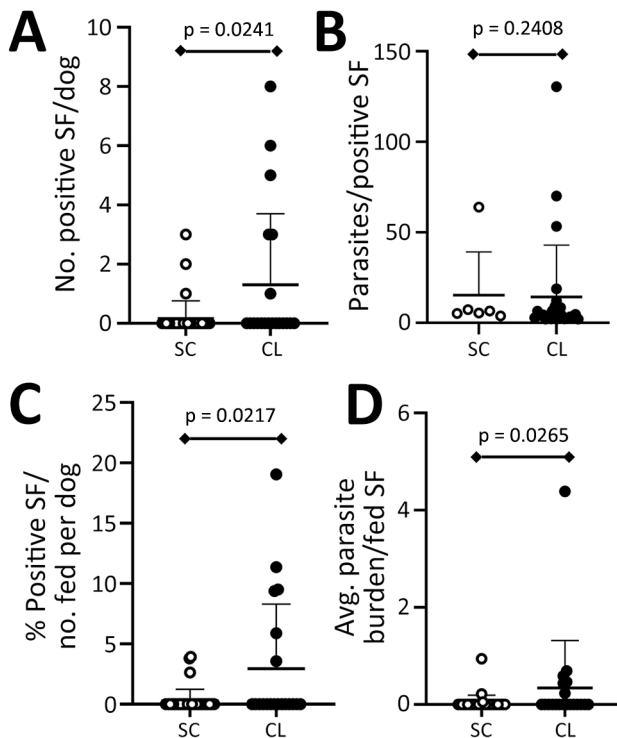

Figure 4. Plot of parasite load in sand flies in a study of dogs as reservoirs for *Leishmania donovani*, Bihar, India, 2018–2022. Plots show higher transmission and parasite load in sand flies fed on dogs with signs consistent with CanL in the Muzaffarpur district. A) Number of parasite DNA–positive sand flies obtained from each dog undergoing xenodiagnosis by qPCR. B) Parasite load calculated within individual *L. donovani* qPCR-positive sand flies. C) Percent positive sand flies out of total number of sand flies fed per dog. D) Average parasite burden of blood-fed sand flies per canine subject. Data for healthy, subclinical dogs depicted with white dots. Data for dogs with CanL clinical signs depicted with black dots. Lower lever of whiskers indicate mean, upper level indicates standard deviation. Statistical results by Mann-Whitney test shown above diamond bars. CanL, canine leishmaniosis; CL, CanL clinical signs; SC, subclinical (i.e., healthy) dogs; SF, sand fly.
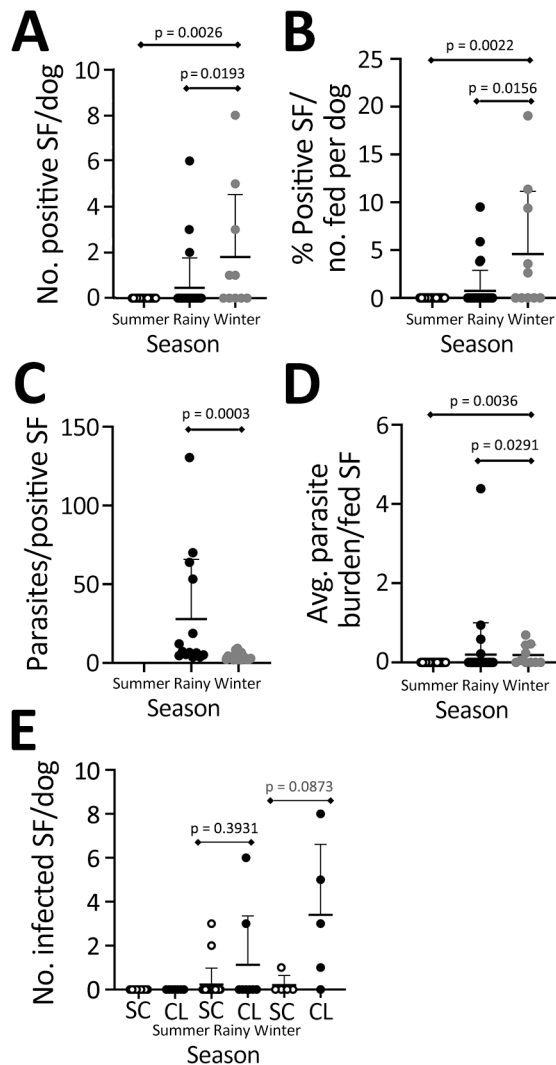
Figure 5. Results of xenodiagnoses in a study of dogs as reservoirs for *Leishmania donovani*, Bihar, India, 2018–2022. Plots show dogs infect more sand flies in winter and transmit more parasites per sand fly during the rainy season. A) Number of positive sand flies; B) parasite load in xenodiagnosis-positive sand flies; C) percent positive sand flies fed on dogs; D) average parasite burden of fed sand flies; E) evaluation of infectiousness of dogs to sand flies by clinical classification and seasonal variation. Lower lever of whiskers indicate mean, upper level indicates standard deviation. Kruskal-Wallis test with Dunn's post-test used to calculate statistical significance between groups (shown above diamond bars). CanL, canine leishmaniosis; CL, CanL clinical signs; SC, subclinical (i.e., healthy) dogs; SF, sand fly.

based CanL in Israel indicated a high prevalence of infected dogs, in the presence of a competent vector species, which led to the onset of parasite transmission to humans in the area (*1*).

In conclusion, identifying and establishing the role of dogs in the ecology of *L. donovani* by investigating the extent to which they contribute to

disease transmission is critical. Increased understanding of a causal link between infected dogs and humans—or vice versa (reverse zoonoses)—can be garnered through additional epidemiologic studies. Research has shown effective prevention of parasite transmission from dogs to sand flies through application of topical insecticides or insecticide-impregnated collars (*32*). Outbreak villages serve as ideal settings for natural experiments to assess topical insecticide interventions focused on preventing transmission from infected dogs and sustaining the elimination efforts in India and wherever *L. donovani* is endemic. Health officials should consider topical or oral insecticidal interventions that prevent sand fly feeding on dogs in epidemic villages to maintain elimination.

About the Author
Dr. Kushwaha is a Raja Jwala Prasad postdoctoral research fellow at the Department of Biochemistry, Institute of Science, Banaras Hindu University, Varanasi, India. His research interest focuses on understanding the transmission mechanisms of vectorborne pathogens in their reservoir animals, informing the reservoir targeted prevention, as well as immunotherapies to those diseases using in vitro and in vivo models. Mr. Shukla is a PhD candidate at the

Department of Medicine, Institute of Medical Sciences, Banaras Hindu University, Varanasi, India. His research focuses on transmission dynamics of leishmaniasis and elucidating mechanisms contributing to sand fly resistance to insecticides.

References

1. Rijal S, Sundar S, Mondal D, Das P, Alvar J, Boelaert M. Eliminating visceral leishmaniasis in South Asia: the road ahead. BMJ. 2019;364:k5224. https://doi.org/10.1136/bmj.k5224
2. World Health Organization. Leishmaniasis, key facts [cited 2022 Mar 20]. https://www.who.int/news-room/fact-sheets/detail/leishmaniasis
3. Cameron MM, Acosta-Serrano A, Bern C, Boelaert M, den Boer M, Burza S, et al. Understanding the transmission dynamics of *Leishmania donovani* to provide robust evidence for interventions to eliminate visceral leishmaniasis in Bihar, India. Parasit Vectors. 2016;9:25. https://doi.org/10.1186/s13071-016-1309-8
4. Garlapati RB, Abbasi I, Warburg A, Poché D, Poché R. Identification of bloodmeals in wild caught blood fed *Phlebotomus argentipes* (Diptera: Psychodidae) using cytochrome b PCR and reverse line blotting in Bihar, India. J Med Entomol. 2012;49:515–21. https://doi.org/10.1603/ME11115
5. Kushwaha AK, Tiwary P, Sundar S. Blood meal identification in wild-caught sand flies from the endemic region of visceral leishmaniasis in India. Int J Infect Dis. 2018;73:296. https://doi.org/10.1016/j.ijid.2018.04.4089
6. Kushwaha AK, Shukla A, Scorza BM, Kumari Rai T, Chaubey R, Kumar Maurya D, et al. Livestock and rodents within an endemic focus of visceral leishmaniasis are not reservoir hosts for *Leishmania donovani.* PLoS Negl Trop Dis. 2022;16:e0010347. https://doi.org/10.1371/journal.pntd.0010347
7. Scorza BM, Mahachi KG, Cox AC, Toepp AJ, Leal-Lima A, Kumar Kushwaha A, et al. *Leishmania infantum* xenodiagnosis from vertically infected dogs reveals significant skin tropism. PLoS Negl Trop Dis. 2021;15:e0009366. https://doi.org/10.1371/journal.pntd.0009366
8. Singh N, Mishra J, Singh R, Singh S. Animal reservoirs of visceral leishmaniasis in India. J Parasitol. 2013;99:64–7. https://doi.org/10.1645/GE-3085.1
9. Sharma NL, Mahajan VK, Negi AK, Verma GK. The rK39 immunochromatic dipstick testing: a study for K39 seroprevalence in dogs and human leishmaniasis patients for possible animal reservoir of cutaneous and visceral leishmaniasis in endemic focus of Satluj River Valley of Himachal Pradesh (India). Indian J Dermatol Venereol Leprol. 2009;75:52–5. https://doi.org/10.4103/0378-6323.45221
10. Rohousova I, Talmi-Frank D, Kostalova T, Polanska N, Lestinova T, Kassahun A, et al. Exposure to *Leishmania* spp. and sand flies in domestic animals in northwestern Ethiopia. Parasit Vectors. 2015;8:360. https://doi.org/10.1186/s13071-015-0976-1
11. Akter S, Alam MZ, Nakao R, Yasin G, Kato H, Katakura K. Molecular and serological evidence of *Leishmania* infection in stray dogs from visceral leishmaniasis–endemic areas of Bangladesh. Am J Trop Med Hyg. 2016;95:795–9. https://doi.org/10.4269/ajtmh.16-0151
12. Kumar V, Mandal R, Das S, Kesari S, Dinesh DS, Pandey K, et al. Kala-azar elimination in a highly-endemic district of Bihar, India: a success story. PLoS Negl Trop Dis. 2020;14:e0008254. https://doi.org/10.1371/journal.pntd.0008254
13. Malaviya P, Picado A, Hasker E, Ostyn B, Kansal S, Singh RP, et al. Health & demographic surveillance system profile: the Muzaffarpur-TMRC health and demographic surveillance system. Int J Epidemiol. 2014;43:1450–7. https://doi.org/10.1093/ije/dyu178
14. Bindroo J, Priyamvada K, Chapman LAC, Mahapatra T, Sinha B, Banerjee I, et al. Optimizing village-level targeting of active case detection to support visceral leishmaniasis elimination in India. Front Cell Infect Microbiol. 2021;11:648847. https://doi.org/10.3389/fcimb.2021.648847
15. Solano-Gallego L, Miró G, Koutinas A, Cardoso L, Pennisi MG, Ferrer L, et al.; The LeishVet Group. LeishVet guidelines for the practical management of canine leishmaniosis. Parasit Vectors. 2011;4:86. https://doi.org/10.1186/1756-3305-4-86
16. Tiwary P, Singh SK, Kushwaha AK, Rowton E, Sacks D, Singh OP, et al. Establishing, expanding, and certifying a closed colony of *Phlebotomus argentipes* (Diptera: Psychodidae) for xenodiagnostic studies at the Kala Azar Medical Research Center, Muzaffarpur, Bihar, India. J Med Entomol. 2017;54:1129–39. https://doi.org/10.1093/jme/tjx099
17. Singh OP, Tiwary P, Kushwaha AK, Singh SK, Singh DK, Lawyer P, et al. Xenodiagnosis to evaluate the infectiousness of humans to sandflies in an area endemic for visceral leishmaniasis in Bihar, India: a transmission-dynamics study. Lancet Microbe. 2021;2:e23–31. https://doi.org/10.1016/S2666-5247(20)30166-X
18. Sudarshan M, Singh T, Singh AK, Chourasia A, Singh B, Wilson ME, et al. Quantitative PCR in epidemiology for early detection of visceral leishmaniasis cases in India. PLoS Negl Trop Dis. 2014;8:e3366. https://doi.org/10.1371/journal.pntd.0003366
19. Courtenay O, Carson C, Calvo-Bado L, Garcez LM, Quinnell RJ. Heterogeneities in *Leishmania infantum* infection: using skin parasite burdens to identify highly infectious dogs. PLoS Negl Trop Dis. 2014;8:e2583. https://doi.org/10.1371/journal.pntd.0002583
20. Tiwary P, Kumar D, Mishra M, Singh RP, Rai M, Sundar S. Seasonal variation in the prevalence of sand flies infected with *Leishmania donovani.* PLoS One. 2013;8:e61370. https://doi.org/10.1371/journal.pone.0061370
21. Waugh MC, Cyndari K, Lynch T, Koh S, Henao-Ceballos F, Oleson JJ, et al. Clinical anemia predicts dermal parasitism and reservoir infectiousness during progressive visceral leishmaniosis. PLoS Negl Trop Dis. 2024;18:e0012363. https://doi.org/10.1371/journal.pntd.0012363
22. Mondal D, Bern C, Ghosh D, Rashid M, Molina R, Chowdhury R, et al. Quantifying the infectiousness of post-kala-azar dermal leishmaniasis toward sand flies. Clin Infect Dis. 2019;69:251–8. https://doi.org/10.1093/cid/ciy891
23. Mukhopadhyay AK, Mishra RN. Development of *Leishmania donovani* in *Phlebotomus argentipes* & *Ph. papatasi* fed on kala-azar patients in Bihar. Indian J Med Res. 1991;93:152–4.
24. Gupta AK, Das S, Kamran M, Ejazi SA, Ali N. The pathogenicity and virulence of *Leishmania* – interplay of virulence factors with host defenses. Virulence. 2022;13:903–35. https://doi.org/10.1080/21505594.2022.2074130
25. Franssen SU, Durrant C, Stark O, Moser B, Downing T, Imamura H, et al. Global genome diversity of the *Leishmania donovani* complex. eLife. 2020;9:e51243. https://doi.org/10.7554/eLife.51243
26. Poché D, Garlapati R, Ingenloff K, Remmers J, Poché R. Bionomics of phlebotomine sand flies from three villages in Bihar, India. J Vector Ecol. 2011;36:S106–17. https://doi.org/10.1111/j.1948-7134.2011.00119.x
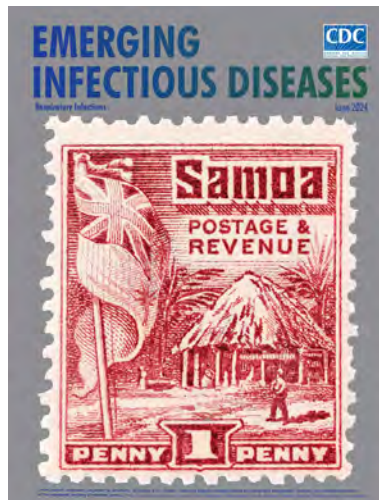
27. Esch KJ, Schaut RG, Lamb IM, Clay G, Morais Lima AL, do Nascimento PR, et al. Activation of autophagy and nucleotide-binding domain leucine-rich repeat-containing-like receptor family, pyrin domain-containing 3 inflammasome during *Leishmania infantum*-associated glomerulonephritis. Am J Pathol. 2015;185:2105–17. https://doi.org/10.1016/j.ajpath.2015.04.017

28. Gondim CN, Ferreira SA, Vasconcelos BKS, Wouters F, Fujiwara RT, de Castro JC, et al. Visceral leishmaniasis in a recent transmission region: 27.4% infectivity rate among seronegative dogs. Parasitology. 2022;149:1–6. https://doi.org/10.1017/S0031182022000063

29. Prina E, Roux E, Mattei D, Milon G. *Leishmania* DNA is rapidly degraded following parasite death: an analysis by microscopy and real-time PCR. Microbes Infect. 2007;9:1307–15. https://doi.org/10.1016/j.micinf.2007.06.005

30. Magalhães-Junior JT, Mota TF, Porfirio-Passos G, Larangeira DF, Franke CR, Barrouin-Melo SM. Xenodiagnosis on dogs with visceral leishmaniasis: canine and sand fly aspects related to the parasite transmission. Vet Parasitol. 2016;223:120–6. https://doi.org/10.1016/j.vetpar.2016.04.031

31. Serafim TD, Coutinho-Abreu IV, Oliveira F, Meneses C, Kamhawi S, Valenzuela JG. Sequential blood meals promote *Leishmania* replication and reverse metacyclogenesis augmenting vector infectivity. Nat Microbiol. 2018;3:548–55. https://doi.org/10.1038/s41564-018-0125-7

32. Courtenay O, Bazmani A, Parvizi P, Ready PD, Cameron MM. Insecticide-impregnated dog collars reduce infantile clinical visceral leishmaniasis under operational conditions in NW Iran: a community-wide cluster randomised trial. PLoS Negl Trop Dis. 2019; 13:e0007193. https://doi.org/10.1371/journal.pntd.0007193

Address for correspondence: Christine A. Petersen, College of Veterinary Medicine, Ohio State University, Columbus, OH 43210, USA; email: petersen.307@osu.edu

June 2024

Respiratory Infections

EMERGING INFECTIOUS DISEASES®

To revisit the June 2024 issue, go to:
https://wwwnc.cdc.gov/eid/articles/issue/30/6/table-of-contents

Mpox Vaccine Acceptance, Democratic Republic of the Congo

Skylar Petrichko,[1] Jason Kindrachuk,[1] Dalau Nkamba, Megan Halbrook, Sydney Merritt, Handdy Kalengi, Leonard Kamba, Michael Beya, Nicole A. Hoff, Christophe Luhata, Didine K. Kaba,[2] Anne W. Rimoin[2]

We report general acceptance (61.0%) of an mpox vaccine in the Democratic Republic of the Congo among 5,226 survey respondents. Healthcare workers and respondents in historic mpox-endemic regions had higher acceptance rates. These data highlight the need for increased community engagement and sensitization before widespread deployment of mpox vaccines.

Mpox, caused by monkeypox virus (MPXV), is a zoonotic infectious disease endemic to the Democratic Republic of the Congo (DRC) (*1–3*). In 2022, rapid worldwide spread of MPXV clade IIb resulted in >91,000 confirmed infections and prompted the World Health Organization to declare a public health emergency of international concern (*4*). In DRC, incident cases quadrupled from 2021 to 2023; during January 2023–July 2024, >28,000 suspected cases were reported, and new introductions were recorded in neighboring Burundi, Rwanda, Kenya, and Uganda (*5*). In August 2024, a travel-associated clade Ib case was reported in Sweden (*6*). In response to the expanding burden of mpox in 2024, the Africa Centres for Disease Control and Prevention declared a public health emergency of continental security (*7*) and the World Health Organization declared a public health emergency of international concern (*4*).

Despite deployment of a modified vaccinia Ankara-Bavarian Nordic vaccine (https://www.bavarian-nordic.com) to many high- and middle-income countries, access mpox vaccine is not currently available for the general population in Africa. One vaccination model suggests that vaccination of 80% of children <15 years of age in DRC would result in robust reductions in illness, death, and MPXV circulation (*8*). We conducted a survey to determine population attitudes towards and willingness to receive mpox vaccination in DRC.

The Study

For our cross-sectional analysis, we used data from a larger longitudinal telephone survey on COVID-19–related topics and vaccine hesitancy that began in 2022. The survey included participants from all 26 provinces in DRC and primarily targeted healthcare workers (HCWs). Participants were selected from historical telephone survey records of >10,000 persons. During December 2023–February 2024, trained interviewers contacted 5,226 adult participants and administered surveys in Swahili, French, Lingala, Kikongo, or Tshiluba. Survey questions addressed behavioral and social drivers of vaccination and attitudes toward introduction of new vaccines, including for mpox. Mpox vaccine acceptance was measured by asking participants about their interest in inclusion of an mpox vaccine in the national vaccination schedule. Response choices were yes, for adults, children, or both; no; and I do not know this disease (Appendix Table 1, https://wwwnc.cdc.gov/EID/article/30/12/24-1226-App1.xlsx). We collapsed all yes responses for analysis. We assessed attitudes, vaccine acceptance by province, and sociodemographic characteristics via 5- or 3-level Likert scale questions and used a χ^2 test for significance (α = 0.05).

Among respondents, 79.2% were male, 20.8% were female, and most (12.6%) were from Kwilu Province. Participant representation from urban or

[1]These first authors contributed equally to this article.

[2]These last authors contributed equally to this article..

rural settings was roughly equivalent. Most (41.2%) respondents reported some college or university education, and 55.5% identified as HCWs (Table).

Participants generally disagreed with the statement that new vaccines carry more risks than older vaccines. However, in 4 provinces, Sud Kivu, Nord Ubangi, Nord Kivu, and Lualaba, >50% of respondents agreed with or felt that greater risks exist with newer vaccines. Respondents generally agreed with the statement that information received from the vaccination program was reliable and trustworthy. In Sankuru Province, 29.5% of respondents felt neutral about the reliability of vaccine program information; the highest percentage of vaccine information distrust and disagreement with the statement were in Haut Katanga (7.6%) and Lomami (6.8%) Provinces (Figure 1; Appendix Table 2).

Nationally, 61.0% (95% CI 59.6%–62.4%) of respondents expressed acceptance of an mpox vaccination, 21.7% had no interest, and 17.3% reported no knowledge of mpox. At the province level, >80% of respondents from Kwango, Tshuapa, Nord Ubangi, Tanganyika, and Maniema reported vaccine acceptance. Sankuru had the lowest acceptance rates (19.9%; 95% CI 14.3%–26.6%) and highest percentage (57.4%; 95% CI 49.7%–64.8%) of participants reporting no mpox knowledge. In general, rates of mpox vaccine acceptance and mpox disease knowledge were not influenced by the history of mpox cases within the province (Figure 2).

Interest in an mpox vaccine varied significantly by province (p<0.0001). When stratified by educational attainment, respondents with a high school diploma had much lower (49.8%; 95% CI 47.3%–52.3%) acceptance of the mpox vaccine than other groups. Among reported occupations, HCWs had the highest acceptance rates (69.4%; 95% CI 67.6%–71.1%). Respondents from rural locations indicated greater mpox vaccine acceptance than their urban counterparts (64.4% vs. 57.7%; p<0.0001). Among 4,396 respondents who reported receiving a COVID-19 vaccine, 63.2% indicated mpox vaccine acceptance. In addition, persons without chronic conditions reported higher rates of mpox vaccine acceptance than persons with chronic conditions (62.2% vs. 51.0%) (Figure 3).

Conclusions

Given the ongoing mpox clade Ia and clade Ib outbreaks in the DRC and identification of cases in adjacent countries in Central Africa, introduction of a vaccine is increasingly needed. However, a paucity of information has been available regarding mpox knowledge and vaccine acceptance across DRC. We observed greater interest in mpox vaccine deployment among respondents from rural than urban locations. That finding could be explained by the historic mpox burden in DRC, where mpox cases

Table. Characteristics of participants in a telephone phone survey about mpox vaccine acceptance conducted during December 2023–February 2024, Democratic Republic of the Congo*	
Characteristics	Value, n = 5,226
Median age (IQR)	42 (26–58)
Sex	
M	4,138 (79.2)
F	1,088 (20.8)
Education level	
Less than high school	359 (6.9)
Graduated high school	1,589 (30.4)
Some college	2,158 (41.3)
Bachelor or advanced degree	1,120 (21.4)
Province	
Maindombe	134 (2.6)
Kwango	183 (3.5)
Kwilu	657 (12.6)
Kongo Central	312 (6.0)
Equateur	162 (3.1)
Mongala	238 (4.6)
Tshuapa	63 (1.2)
Nord Ubangi	113 (2.2)
Sud Ubangi	91 (1.7)
Kasai Oriental	597 (11.4)
Sankuru	176 (3.4)
Lomami	192 (3.7)
Kasai	118 (2.3)
Kasai Central	87 (1.7)
Haut Katanga	331 (6.3)
Tanganyika	151 (2.9)
Haut Lomami	50 (1.0)
Lualaba	168 (3.2)
Kinshasa	251 (4.8)
Maniema	98 (1.9)
North Kivu	140 (2.7)
Bas Uele	246 (4.7)
Haut Uele	137 (2.6)
Ituri	239 (4.6)
Tshopo	144 (2.8)
Sud Kivu	148 (2.8)
Geographic area	
Urban	2,659 (50.9)
Rural	2,567 (49.1)
Occupation	
Healthcare worker	2,899 (55.5)
Religious leader	89 (1.7)
Community or essential services leader	768 (14.7)
Public service sector or educator	670 (12.8)
Other worker	513 (9.8)
Not working	287 (5.5)
Health conditions	
Chronic lung disease	32 (0.6)
Diabetes	209 (4.0)
Cardiovascular disease	254 (4.9)
Chronic renal disease	12 (0.2)
Chronic liver disease	9 (0.2)
Immunocompromised	10 (0.2)
No conditions	4,700 (89.9)

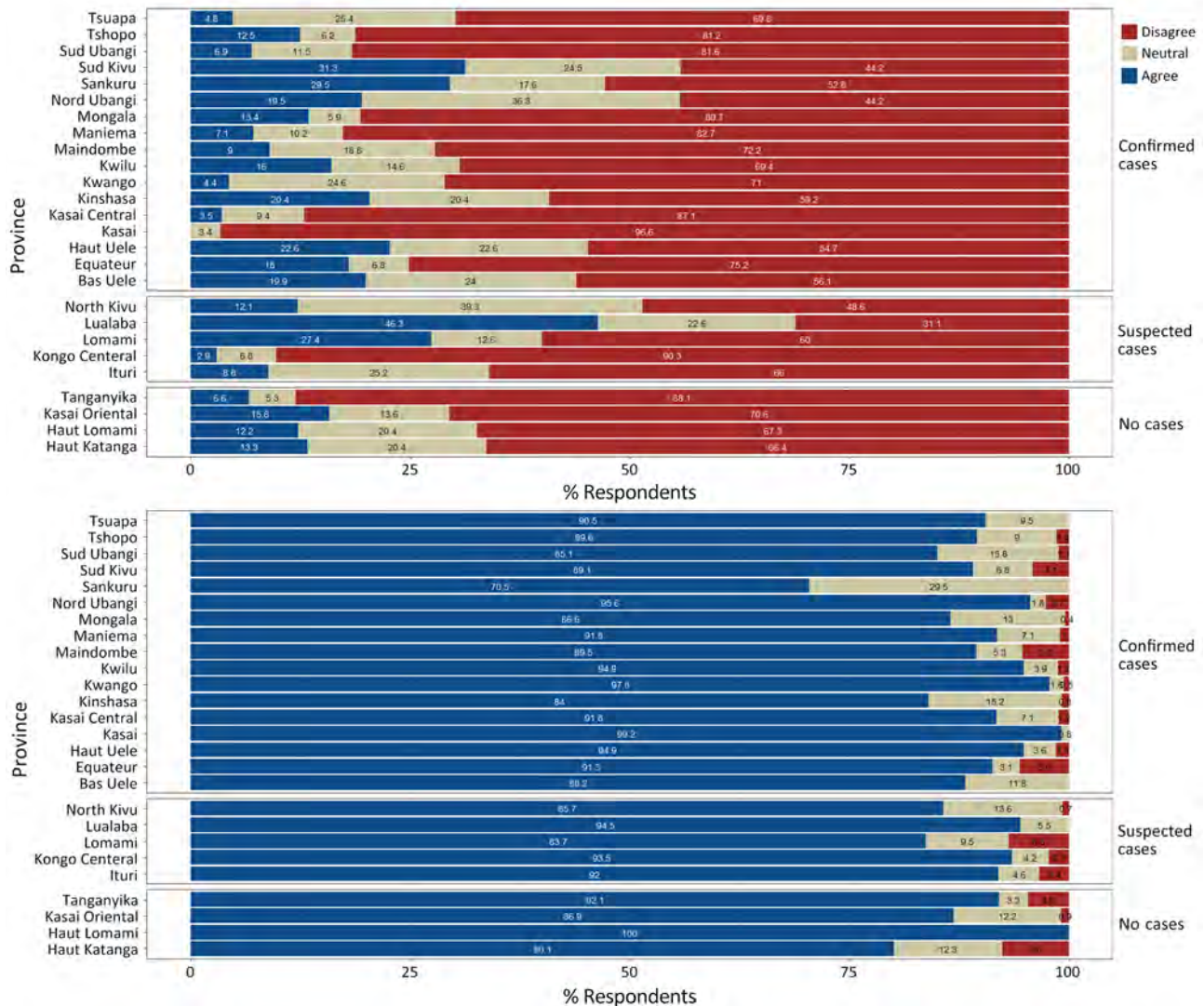*Values are no. (%) except as indicated. IQR, interquartile range.

Figure 1. General mpox vaccine attitudes and perceptions from a telephone phone survey about mpox vaccine acceptance conducted during December 2023–February 2024, by province, Democratic Republic of the Congo. A) Reported responses to the statement: new vaccines carry more risks than older vaccines; B) reported responses to the statement: information I receive about vaccines from the vaccine program is reliable and trustworthy. Provinces are listed by whether they had confirmed, suspected, or no mpox cases detected. The 3-level responses were collapsed from a 5-point Likert scale.

primarily were among children in rural regions. Currently, reported mpox cases are rising in urban centers, further challenging response and vaccine planning efforts.

Assessing mpox vaccine trust and acceptance across provinces that have and have not experienced mpox cases and across demographic variables did not yield clear or neatly described trends. Instead, we observed several outliers that may reflect the diversity of DRC. For example, differing vaccine acceptance rates between persons with and without chronic health conditions may indicate underlying health anxieties among persons with persistent health problems;

further investigation is needed to clarify that relationship. In addition, Sankuru Province was consistently a vaccine-hesitant outlier in this survey. Sankuru had the lowest percentage of respondents who trust information received from national vaccine programs and the lowest mpox vaccine acceptance, primarily because 57.4% of respondents stated no knowledge of mpox. In DRC, most mpox-endemic provinces consist of rainforest or forest-savanna mosaic geographies; the southeast provinces are primarily savanna and grassland and have no history of reported mpox cases. However, in June 2024, Lualaba Province in the southeast reported its first mpox case. Of note, that province
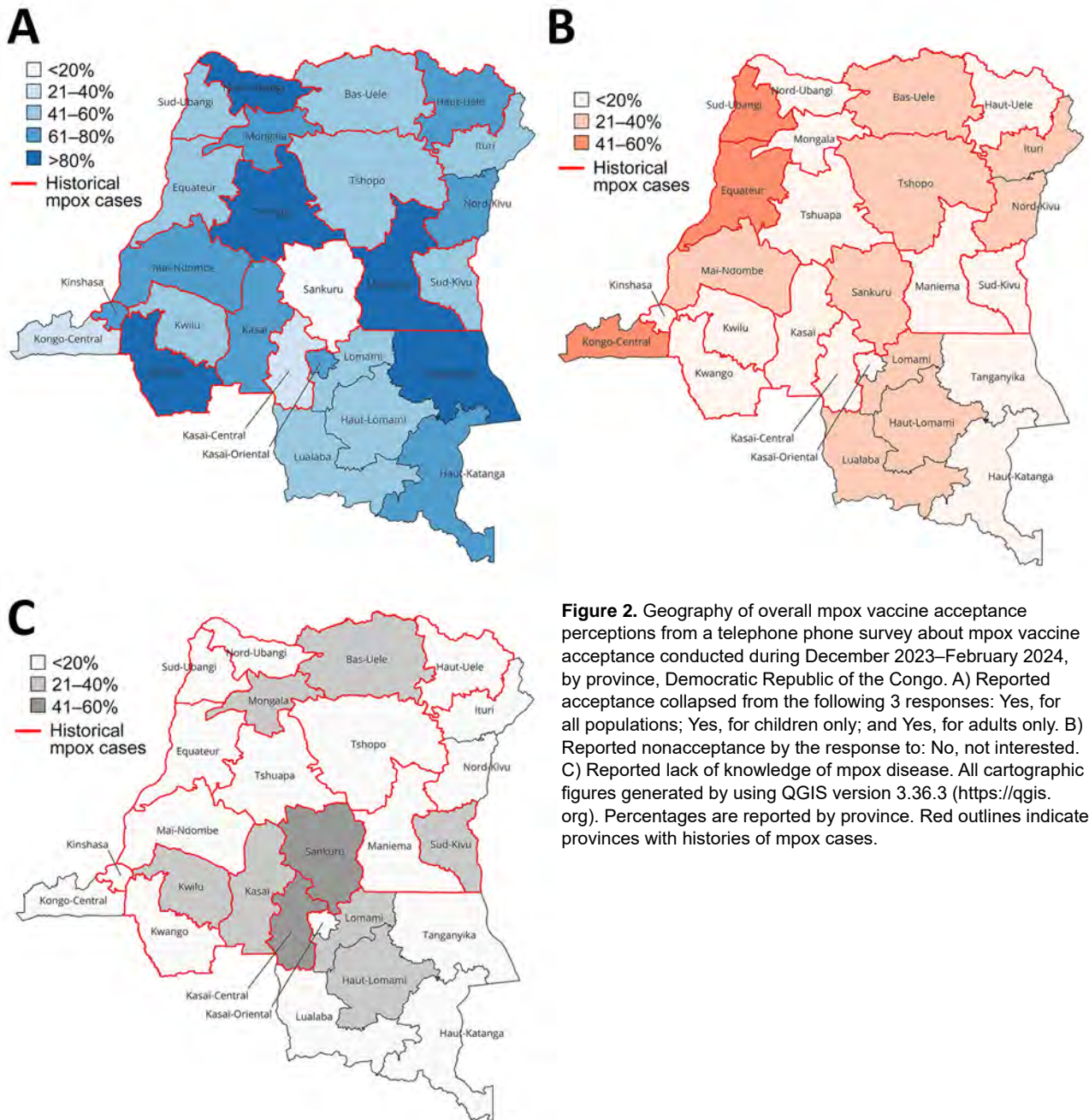
Figure 2. Geography of overall mpox vaccine acceptance perceptions from a telephone phone survey about mpox vaccine acceptance conducted during December 2023–February 2024, by province, Democratic Republic of the Congo. A) Reported acceptance collapsed from the following 3 responses: Yes, for all populations; Yes, for children only; and Yes, for adults only. B) Reported nonacceptance by the response to: No, not interested. C) Reported lack of knowledge of mpox disease. All cartographic figures generated by using QGIS version 3.36.3 (https://qgis.org). Percentages are reported by province. Red outlines indicate provinces with histories of mpox cases.

had the highest percentage of respondents believing that new vaccines have greater risks than older vaccines, although overall trust in national vaccine programs was high.

Although our results report an overall trend of vaccine trust and acceptance nationwide, they also indicate the need for a multifaceted approach to vaccine education and rollout. Strategies should be tailored to historically endemic regions and areas with lower vaccine acceptance, such as Sankuru or Kasai

Central, and consider how personal experiences and cultural considerations intersect with mpox outbreaks. Of note, Haut Lomami Province has been the setting of long-standing routine immunization revitalization efforts (*9,10*), and 100% of respondents from that province reported that they feel information from the national vaccine program is reliable. That highly positive response is perhaps reflective of the many years of vaccine campaigns and education efforts in the region.
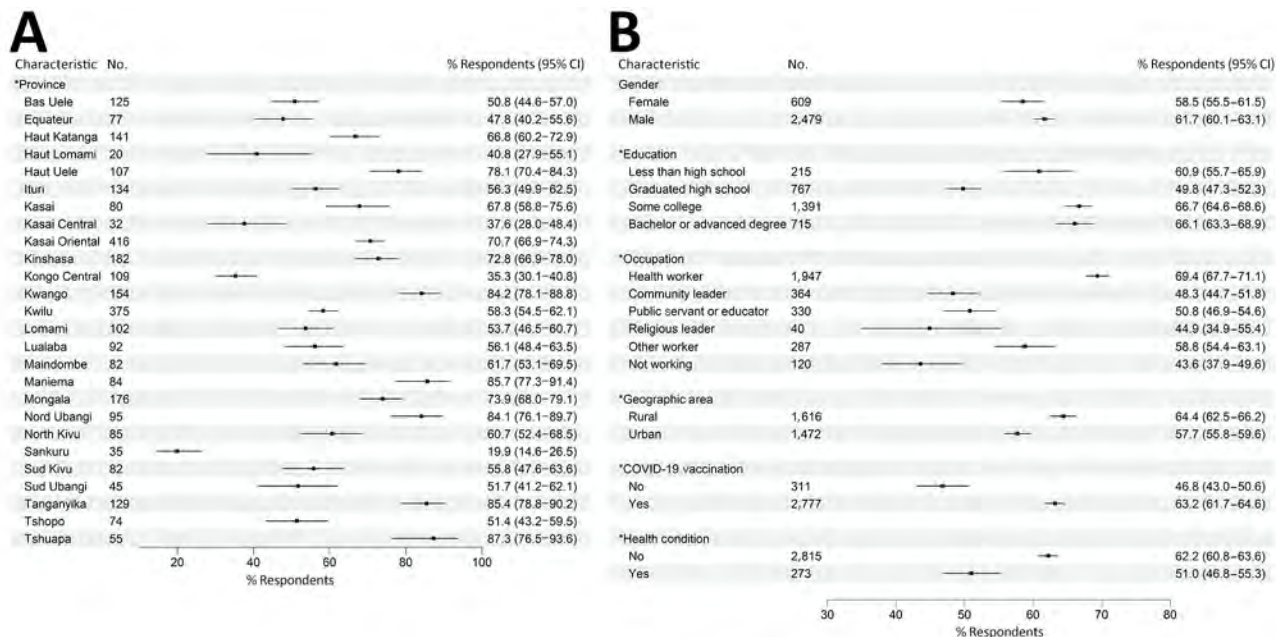
A

Characteristic	No.		% Respondents (95% CI)
*Province			
Bas Uele	125		50.8 (44.6–57.0)
Equateur	77		47.8 (40.2–55.6)
Haut Katanga	141		66.8 (60.2–72.9)
Haut Lomami	20		40.8 (27.9–55.1)
Haut Uele	107		78.1 (70.4–84.3)
Ituri	134		56.3 (49.9–62.5)
Kasai	80		67.8 (58.8–75.6)
Kasai Central	32		37.6 (28.0–48.4)
Kasai Oriental	416		70.7 (66.9–74.3)
Kinshasa	182		72.8 (66.9–78.0)
Kongo Central	109		35.3 (30.1–40.8)
Kwango	154		84.2 (78.1–88.8)
Kwilu	375		58.3 (54.5–62.1)
Lomami	102		53.7 (46.5–60.7)
Lualaba	92		56.1 (48.4–63.5)
Maindombe	82		61.7 (53.1–69.5)
Maniema	84		85.7 (77.3–91.4)
Mongala	176		73.9 (68.0–79.1)
Nord Ubangi	95		84.1 (76.1–89.7)
North Kivu	85		60.7 (52.4–68.5)
Sankuru	35		19.9 (14.6–26.5)
Sud Kivu	82		55.8 (47.6–63.6)
Sud Ubangi	45		51.7 (41.2–62.1)
Tanganyika	129		85.4 (78.8–90.2)
Tshopo	74		51.4 (43.2–59.5)
Tshuapa	55		87.3 (76.5–93.6)

% Respondents (20 40 60 80 100)

B

Characteristic	No.		% Respondents (95% CI)
Gender			
Female	609		58.5 (55.5–61.5)
Male	2,479		61.7 (60.1–63.1)
*Education			
Less than high school	215		60.9 (55.7–65.9)
Graduated high school	767		49.8 (47.3–52.3)
Some college	1,391		66.7 (64.6–68.6)
Bachelor or advanced degree	715		66.1 (63.3–68.9)
*Occupation			
Health worker	1,947		69.4 (67.7–71.1)
Community leader	364		48.3 (44.7–51.8)
Public servant or educator	330		50.8 (46.9–54.6)
Religious leader	40		44.9 (34.9–55.4)
Other worker	287		58.8 (54.4–63.1)
Not working	120		43.6 (37.9–49.6)
*Geographic area			
Rural	1,616		64.4 (62.5–66.2)
Urban	1,472		57.7 (55.8–59.6)
*COVID-19 vaccination			
No	311		46.8 (43.0–50.6)
Yes	2,777		63.2 (61.7–64.6)
*Health condition			
No	2,815		62.2 (60.8–63.6)
Yes	273		51.0 (46.8–55.3)

% Respondents (30 40 50 60 70 80)

Figure 3. Percentage of mpox vaccine acceptance and demographic characteristic perceptions from a telephone phone survey about mpox vaccine acceptance conducted during December 2023–February 2024, by province, the Democratic Republic of the Congo. Responses were stratified by sociodemographic characteristics and known mpox risk factors; COVID-19 vaccination was dichotomized by whether the respondent received the COVID-19 vaccine. Health conditions were dichotomized on the basis of whether the respondent stated they had a chronic disease or were immunocompromised. Asterisks (*) indicate $p<0.05$ by χ^2 test. Error bars indicate 95% CIs.

This survey was limited to persons with access to telephones; persons with a lower socioeconomic status, including those in largely rural regions, may have been inadvertently excluded. This study included respondents from all provinces in DRC and targeted HCWs. Past studies in DRC have demonstrated 54% acceptance toward outbreak-related vaccines, and HCWs continually express the highest acceptance among respondents (11). Because this study sought to enroll HCWs and community and religious leaders, we observed an overrepresentation of men because men primarily hold leadership roles in the country. Because HCWs and religious leaders serve as health recommenders for their communities, however, identifying and addressing vaccine acceptance among those groups is critical.

In conclusion, our findings provide insights regarding mpox vaccine acceptance within DRC. Our data highlight the need for increased community engagement and sensitization before widespread mpox vaccine deployment.

This article was preprinted at https://www.medrxiv.org/content/10.1101/2024.08.15.24311971v2.

About the Authors

Ms. Petrichko is a master of public health student in the Department of Epidemiology at the Fielding School of Public Health, University of California, Los Angeles, Los Angeles, California, USA. Her research interests focus on infectious disease surveillance. Dr. Kindrachuk is an associate professor and Canada Research Chair at the University of Manitoba, Winnipeg, Manitoba, Canada. His research interests focus on the investigation of emerging and re-emerging viruses.

References

1. Bremen JG, Kalisa-Ruti, Steniowski MV, Zanotto E, Gromyko AI, Arita I. Human monkeypox, 1970–79. Bull World Health Organ. 1980;58:165–82.

2. Foster SO, Brink EW, Hutchins DL, Pifer JM, Lourie B, Moser CR, et al. Human monkeypox. Bull World Health Organ. 1972;46:569–76.

3. Ladnyj ID, Ziegler P, Kima E. A human infection caused by monkeypox virus in Basankusu Territory, Democratic Republic of the Congo. Bull World Health Organ. 1972;46:593–7.

4. World Health Organization. Emergencies: mpox (monkeypox) outbreak [cited 2024 Aug 8]. https://www.who.int/europe/emergencies/situations/monkeypox

5. World Health Organization, Regional Office for Africa. Mpox epidemic: Situation Report (SITREP) N°8 of 6 June 2024 [in French]. Kinshasa, DRC: Institut National de Sante Publique; 2024.

6. European Center for Disease Prevention and Control. Mpox due to monkeypox virus clade I: epidemiological update. Geneva: The Center; 2024.

7. Africa Centres for Disease Control and Prevention. Mpox outbreaks in Africa constitute a public health emergency of continental security [cited 2024 Aug 08]. https://africacdc.org/news-item/mpox-outbreaks-in-africa-constitute-a-public-health-emergency-of-continental-security

8. Savinkina A, Kindrachuk J, Bogoch I, Rimoin AW, Hoff NA, Shaw SY, et al. Modelling vaccination approaches for mpox containment and mitigation in the Democratic Republic of the Congo. Lancet Glob Health. 2024 Oct 9 [Epub ahead of print]. https://doi.org/10.1016/S2214-109X(24)00384-X

9. Lame P, Milabyo A, Tangney S, Mbaka GO, Luhata C, Gargasson JL, et al. A successful national and multipartner approach to increase immunization coverage: the Democratic Republic of Congo Mashako Plan 2018–2020. Glob Health Sci Pract. 2023;11: e2200326. https://doi.org/10.9745/GHSP-D-22-00326

10. Banza Mpiongo P, Kibanza J, Kambol Yav F, Nyombo D, Mwepu L, Basame D, et al. Strengthening immunization programs through innovative sub-national public-private partnerships in selected provinces in the Democratic Republic of the Congo. Vaccine. 2023;41:7598–607. https://doi.org/10.1016/j.vaccine.2023.11.029

11. Peckeu-Abboud L, Mangoni P, Chammam K, Kwete P, Mutombo Lupola P, Vanlerberghe V, et al. Drivers of routine and outbreak vaccination uptake in the western Democratic Republic of Congo: an exploratory study in ten health zones. Vaccines (Basel). 2022;10:1066. https://doi.org/10.3390/vaccines10071066

Address for correspondence: Anne W. Rimoin, Department of Epidemiology, Gordon-Levin Endowed Chair in Infectious Diseases and Public Health, Jonathan and Karin Fielding School of Public Health, University of California, Los Angeles, 650 Charles E. Young Dr, CHS 41-275, Los Angeles, CA 90095, USA; email: arimoin@ucla.edu
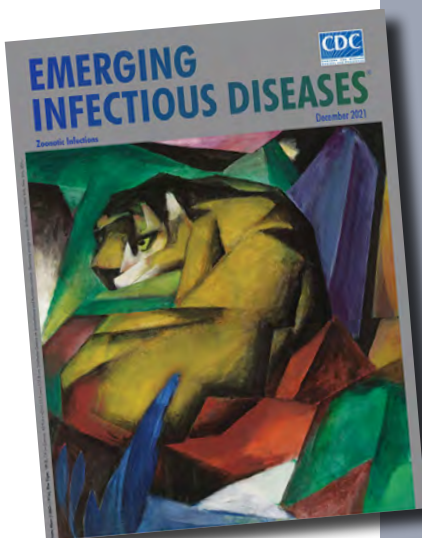
etymologia revisited

Trichinella spiralis

[tri·kuh·neh'·luh spr·a'·luhs]

*T*richinella is derived from the Greek words *trichos* (hair) and *ella* (diminutive); *spiralis* means spiral. In 1835, Richard Owen (1804–1892) and James Paget (1814–1899) described a spiral worm (*Trichina spiralis*)–lined sandy diaphragm of a cadaver. In 1895, Alcide Raillet (1852–1930) renamed it as *Trichinella spiralis* because *Trichina* was attributed to an insect in 1830. In 1859, Rudolf Virchow (1821–1902) described the life cycle. The genus includes many distinct species, several genotypes, and encapsulated and nonencapsulated clades based on the presence/absence of a collagen capsule.

Originally published in December 2021

References

1. Campbell WC. History of trichinosis: Paget, Owens and the discovery of *Trichinella spiralis*. Bull Hist Med. 1979;53:520–52.
2. Centers for Disease Control and Prevention. Trichinellosis: general information [cited 2021 May 11]. https://www.cdc.gov/parasites/trichinellosis/ gen_info/faqs.html
3. Gottstein B, Pozio E, Nöckler K. Epidemiology, diagnosis, treatment, and control of trichinellosis. Clin Microbiol Rev. 2009;22:127–45. https://doi.org/10.1128/CMR.00026-08
4. Observations on *Trichina spiralis*. Boston Med Surg J. 1860; 63:294–8. https://doi.org/10.1056/NEJM186011080631504
5. Zarlenga D, Thompson P, Pozio E. *Trichinella* species and genotypes. Res Vet Sci. 2020;133:289–96. https://doi.org/10.1016/j.rvsc.2020.08.012

Incursion of Novel Eurasian Low Pathogenicity Avian Influenza H5 Virus, Australia, 2023

Michelle Wille, Victoria Grillo, Silvia Ban de Gouvea Pedroso, Natasha D. Brohier, Ivano Broz,
Charlotte Burgoyne, Allison Crawley, Kelly Davies, Mark Ford, Joanne Grimsey,
Nina Y.H. Kung, Jasmina M. Luczo, Cornelius Matereke, Peter T. Mee,
Patrick Mileto, Matthew J. Neave, Megan Poon, Vittoria Stevens, Guy Weerasinghe,
Sara Zufan, Ian G. Barr, Marcel Klaassen, Andrew C. Breed, Frank Y.K. Wong

Australia is a sink for low pathogenicity avian influenza viruses, with isolated circulation occurring on the continent. We report the incursion of a Eurasian low pathogenicity avian influenza H5 virus into Australia. This report benefits surveillance and diagnostic work because of the risk and current absence of highly pathogenic avian influenza A(H5N1).

Australia is a sink for the diversity of avian influenza viruses, wherein viruses circulating in Eurasia and North America are occasionally introduced to the continent, followed by long-term, isolated circulation (1). Whereas a diversity of low pathogenicity avian influenza (LPAI) viruses exist, Oceania is the only continent where the goose/Guangdong lineage of highly pathogenic avian influenza (HPAI) A(H5N1) is absent (2). An HPAI incursion has never been detected in Oceania, although several HPAI outbreaks have occurred in poultry, all following evolution of endemic Australian lineage LPAI H7 viruses from the wild bird reservoir (3). Because of the risk to poultry and wild birds in Australia, a key aim of the National Avian Influenza in Wild Birds (NAIWB) surveillance program is the detection and characterization of circulating H5 and H7 viruses (4).

The Study

In 2023, through both the NAIWB targeted surveillance (4) and passive surveillance, we detected 17 LPAI H5 viruses by quantitative PCR (qPCR) and recovered 8 genomes. The genomes comprised 7 complete or near-complete genomes and 1 partial genome, which included hemagglutinin (HA), nucleoprotein, neuraminidase (NA), matrix, and nonstructural protein (NS) segments. We recovered viral HA fragments from 2 additional detections that identified lineage only (Table). We collected, screened, and sequenced samples as described in previous publications (1). We deposited the sequences into GenBank (GenBank accession nos. PP947529–52 and PP922943–79).

The HA segments of LPAI H5 viruses we sequenced were unrelated to LPAI H5 viruses previously characterized in Australia. The HA sequences had a PQRETR/GLF cleavage site, which contrasts with the PQKATR/GLF cleavage site found in all LPAI H5 viruses reported in Australia since 2005 (1). The detections we found all belonged to a single Eurasian-lineage LPAI H5 that was detected in 4 Australia jurisdictions over a 7-month period. We detected the first occurrence of the LPAI H5 in April 2023 (Figure

Author affiliations: Centre for Pathogen Genomics, The University of Melbourne, Melbourne, Victoria, Australia (M. Wille, S. Zufan); Peter Doherty Institute for Infection and Immunity, Melbourne (M. Wille, I.G. Barr); Wildlife Health Australia, Canberra, Australian Capital Territory, Australia (V. Grillo, S.B. de Grouvea Pedroso); Department of Energy, Environment, and Climate Action, Bundoora, Victoria, Australia (N.D. Brohier, P.T. Mee); Australian Centre for Disease Preparedness, Geelong, Victoria, Australia (I. Broz, K. Davies, M. Ford, J. Grimsey, J.M. Luczo, P. Mileto, M.J. Neave, M. Poon, V. Stevens, F.Y.K. Wong); Northern Australia Quarantine

Strategy, Department of Agriculture, Fisheries, and Forestry, Darwin, Northern Territory, Australia (C. Burgoyne, G. Weerasinghe); Department of Primary Industries and Regions, Glenside, South Australia, Australia (A. Crawley, C. Matereke); Department of Agriculture and Fisheries Coopers Plains, Queensland, Australia (N.Y.H. Kung); Deakin University, Geelong (M. Klassen); University of Queensland, Brisbane, Australia (A.C. Breed); Department of Agriculture, Fisheries, and Forestry, Canberra (A.C. Breed)

Table. Genome constellations for each virus sequenced in the study of an incursion of novel Eurasian low pathogenicity avian influenza H5 virus, Australia, 2023*

Virus designation	Date	PB2	PB1	PA	HA	NP	NA	M	NS
A/chestnut teal/Victoria/23-01686-0034/2023 (H5N3)	2023 Apr 26	Aus	Aus (B)	Aus	H5–EUR-novel	Aus	N3–Aus	Aus (A)	A–Aus
A/Pacific black duck/Victoria/23-01686-0039/2023 (H5N3)	2023 Apr 26	Aus	Aus (A)	Aus	H5–EUR-novel	Aus	N3–Aus	Aus (A)	B–Aus
A/gray teal/Victoria/23-01688-0045/2023 (mixed)†	2023 Apr 26	Aus	Aus (A)	Aus	H5–EUR-novel	Aus	N3–Aus/ N7–Aus	Aus (A)	B–Aus
A/Pacific Black Duck/Victoria/17363/2023 (H5N3)	2023 Jun 22	Aus	Aus (A)	Aus	H5–EUR-novel	Aus‡	N3–Aus	Aus (A)	A–Aus
A/wild waterbird/Queensland/ P23–02457–48/2023 (H5N3)	2023 Jun 23	Aus	Aus (C)	Aus	H5–EUR-novel	Aus	N3–Aus	Aus (B)	A–Aus
A/wild waterbird/Queensland/ P23–02457–51/2023 (H5N3)	2023 Jun 23	Aus	Aus (C)	Aus	H5–EUR-novel	Aus	N3–Aus	Aus (B)	A–Aus
A/wild waterbird/South Australia/23–80999145–13/2023 (H5N9)	2023 Jul 31	Aus	Aus (C)	Aus	H5–EUR-novel	Aus‡	N9–Aus	Aus (A)	B–Aus
A/Radjah Shelduck/Northern Territory/ 20231282–03/2023 (H5N1)	2023 Oct 30	ND	ND	ND	H5–EUR-novel	Aus‡	N1–Aus	Aus (A)	A–Aus

*In cases where viruses fell into different Australian lineages we added an indicatory letter in parentheses to show the different lineages. In the case of NS, whether the virus fell into the A or B allele is indicated before the lineage name. (e.g., B–Aus for an Australian lineage in the B allele). Similarly, for the neuraminidase subtype information is incorporated (e.g., N1–Aus for an Australian lineage in the N1). Aus, established Australian clade; EUR-novel, novel incursion from Eurasian lineage; HA, hemagglutinin; M, matrix protein; ND, no sequence data available; NA, neuraminidase; NP, nucleoprotein; NS, nonstructural protein; PA, polymerase acidic; PB, polymerase basic.
†A/gray teal/Victoria/23-01688-0045/2023 comprised H5 and H10, and N3 and N7.
‡Cases where viruses fell into the same Australian lineage but were not sister to each other.

1) in Victoria from 3 hunter shot waterfowl: 1 Pacific black duck (*Anas superciliosa*), 1 gray teal (*Anas gracilis*), and 1 chestnut teal (*Anas castanea*). In June 2023, we detected another LPAI H5 occurrence in Victoria in a live-captured Pacific black duck and 2 LPAI H5 occurrences in Queensland from wild waterbird fecal environmental samples. We detected another LPAI H5 occurrence in July 2023 from wild waterbird fecal samples in South Australia. Finally, we detected 1 LPAI H5 virus in a wild duck in October 2023 through passive surveillance in the Northern Territory.

Samples collected from live birds were done in accordance with Deakin University Animal Ethics (ethics approval no. B39-2019). Ethics approvals were not required for fecal environmental samples, samples collected from hunter-shot birds, or samples collected for disease investigations.

We conducted BLASTn analysis (https://blast.ncbi.nlm.nih.gov) by using the National Center for Biotechnology Information nucleotide database. We conducted phylogenetic analysis of the HA sequences and found the sequenced viruses
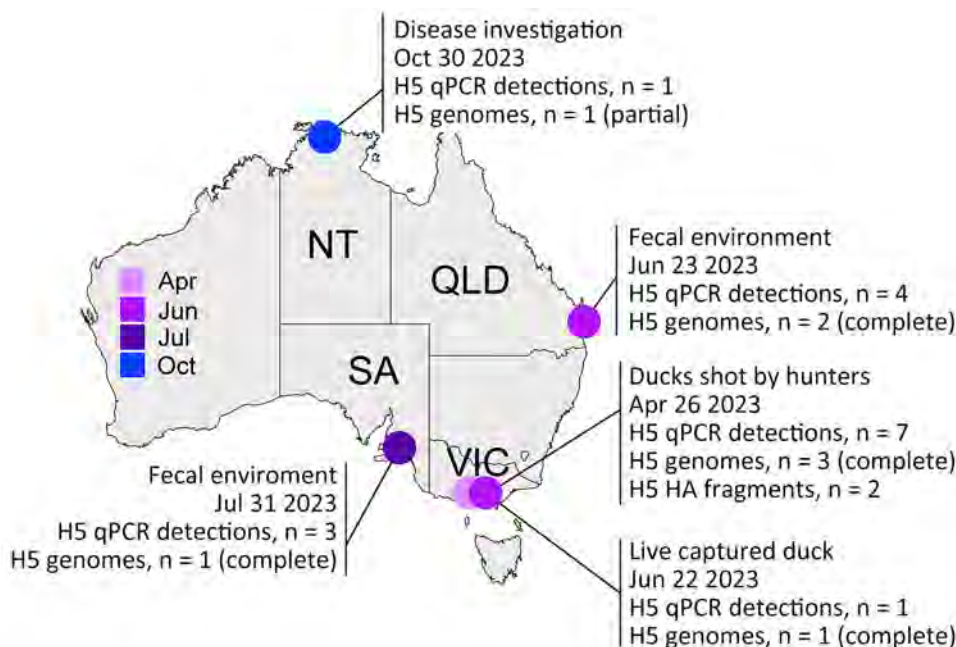

Figure 1. Locations of Eurasian lineage low pathogenic avian influenza H5 virus detections in Australia, 2023. Information is provided about the location, sample type, and date of H5 detections. NT, Northern Territory; QLD, Queensland; SA, South Australia; VIC, Victoria.
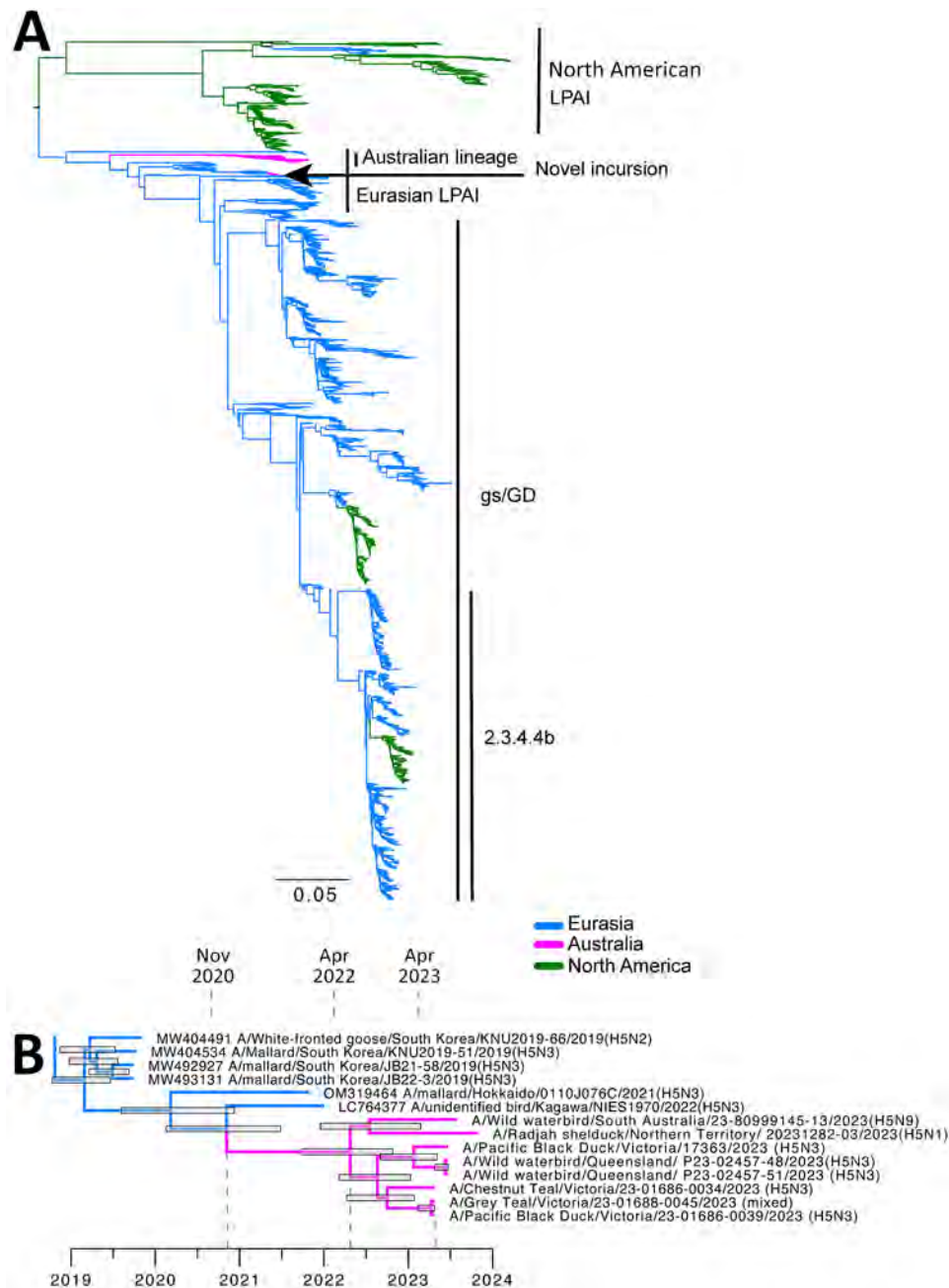
Figure 2. Phylogenetic analysis of Eurasian lineage LPAI H5 virus detected in Australia, 2023. A) Maximum-likelihood phylogenetic tree of all H5 sequences from Asia, North America, and Oceania since 2010. Major clades have been highlighted. The arrow indicates the novel lineage detection in Australia. The tree has been rooted between the North American and Eurasian lineages. Scale bar indicates number of substitutions per site. B) Cropped time-structured phylogenetic tree. Dashed lines indicate the date of divergence from GenBank reference sequences, the most recent common ancestor of all Australian sequences, and the date of first detection. Node bars comprise the 95% highest posterior density. Scale bar is time in years. gs/GD, goose/Guangdong lineage of highly pathogenic avian influenza A(H5N1); LPAI, low pathogenicity avian influenza.

were most closely related (≤98%) to LPAI H5 viruses detected during 2019–2022 in Japan and South Korea (Figures 1, 2). Those countries contribute most influenza genomes recovered from the East Asian–Australasian databases. Alignments and .xml files for all trees are available at https://github.com/michellewille2/Eurasian-LPAI-H5-incursion-to-Australia. We investigated the potential temporal incursion window in Australia by using time-structured phylogenetic analysis, as outlined in previous publications (*1*). The most recent common ancestor of the 8 complete HA sequences was from April 2022 (95% highest posterior density [HPD] September 2021–October 2022), almost a year before the first detection, but with a large HPD (Figure 1). To examine H5 activity in the previous year, we queried all H5 detections for 2022 reported to the NAIWB surveillance program and found 12 LPAI H5 viruses were detected by qPCR in wild bird samples (New South Wales, n = 3; Tasmania, n = 1; Victoria, n = 5; Western Australia, n = 3) (*5*). Of the viruses sequenced, all HA sequences fell into the previously described

Australian LPAI H5 lineage that has been circulating since 2007, although it was likely present since the 1990s (*1*). Hence, cryptic circulation of the novel Eurasian lineage LPAI H5 in Australia may have occurred in locations or in avian hosts that are not included in NAIWB surveillance and therefore were not detected in 2022. Alternatively, incursion might have only occurred in early 2023, but rather than a single viral introduction, multiple viruses with closely related HA sequences were separately introduced. Unfortunately, the scarcity of available HA reference sequences from 2022 and 2023 from Asia because of limitations in wild bird surveillance or sequence deposition into GenBank hinders understanding of introduction dynamics.

We investigated the reassortment patterns in the segments to gain additional insight. All other gene segments fall into viral lineages already present in Australia (Table; Appendix Figure, Tables 1, 2, http://wwwnc.cdc.gov/EID/article/30/12/24-0919-App1.pdf). Genome constellations were partially conserved, and all viruses shared the same polymerase basic (PB) 1, polymerase acidic, nucleoprotein, and matrix segment lineages, although within-clade segments were not always 100% identical (Appendix Figure). We detected 3 different PB1 lineages and 2 different NS lineages (both the A and B alleles). We obtained full genomes of 4 viruses from wild birds in Victoria, 3 from the same sampling event. Of the full genomes obtained, 2 had identical genome constellations, although A/gray teal/Victoria/23-01688-0045/2023 was a mixed infection with H5, H10, N3 and N7 segments recovered. Co-sampled A/chestnut Teal/Victoria/23–01686-0034/2023(H5N3) was different in both the PB1 and NS sequence compared with the other 2 viruses. A/Pacific black duck/Victoria/17363/2023(H5N3), which was detected 2 months after the initial detections in Victoria, had a similar genome constellation to the other sequences from Victoria, despite having an HA sequence sister to those from Queensland (detected June 2023), rather than those from Victoria. A/wild waterbird/South Australia/23–80999145–13/2023(H5N9) had a different PB1 and NA sequence, and A/radjah shelduck/Northern Territory/20231282–03/2023(H5N1) also had a different NA subtype. The 2 genomes from Queensland shared the same PB1 sequence as A/wild waterbird/South Australia/23-80999145-13/2023(H5N9) but had unique M segments. A reasonable explanation for those results is a single introduction followed by a reassortment event incorporating 7 Australian-lineage segments. As the virus spread across Australia, additional reassortment events contributed to the genome constellation diversity (i.e., diversity in the PB1, NA, and NS segments).

Conclusions

There are 3 implications of this viral incursion. First, the delayed detection highlights limitations in the national targeted surveillance program that, in combination with investigation of consequential wild bird illness and death events, is necessary to rapidly detect and respond to an incursion of goose/Guangdong HPAI H5N1 into Australia. Second, while the KATR cleavage site found in Australian-lineage viruses has not yet been associated with evolution of LPAI to HPAI, the RETR cleavage site in the novel Eurasian lineage incursion has been identified as a precursor to HPAI H5 viruses (*6*). This incursion may increase the risk for evolution of HPAI H5 in Australia. Finally, as part of the surveillance and diagnostic processes, H5 qPCRs are designed to rapidly differentiate LPAI H5 of Australian lineage from Eurasian lineage LPAI and HPAI. The presence of a novel LPAI lineage requires a diagnostic update. Understanding viral incursions is a global concern, as demonstrated by the numerous incursions and intercontinental spread of HPAI H5N1 clade 2.3.4.4b. Determining the patterns of viral incursion and spread and identifying the hosts involved is necessary for effective disease risk management and communication that supports disease preparedness and response.

About the author

Dr. Wille is a senior research fellow at the Centre for Pathogen Genomics, University of Melbourne. Her interests include viruses of birds, ecology and evolution of avian influenza, and ecology of bird viral communities.

References

1. Wille M, Grillo V, Ban de Gouvea Pedroso S, Burgess GW, Crawley A, Dickason C, et al. Australia as a global sink for the genetic diversity of avian influenza A virus. PLoS Pathog. 2022;18:e1010150. https://doi.org/10.1371/journal.ppat.1010150
2. Wille M, Atkinson R, Barr IG, Burgoyne C, Bond AL, Boyle D, et al. Long-distance avian migrants fail to bring 2.3.4.4b HPAI H5N1 into Australia for a second year in a
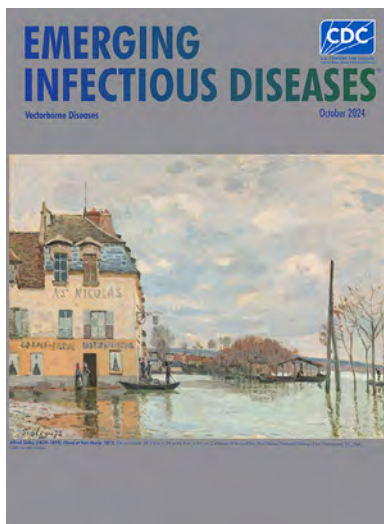
row. Influenza Other Respir Viruses. 2024;18:e13281. https://doi.org/10.1111/irv.13281

3. Scott A, Hernandez-Jover M, Groves P, Toribio JA. An overview of avian influenza in the context of the Australian commercial poultry industry. One Health. 2020;10:100139. https://doi.org/10.1016/j.onehlt.2020.100139

4. Grillo VL, Arzey KE, Hansbro PM, Hurt AC, Warner S, Bergfeld J, et al. Avian influenza in Australia: a summary of 5 years of wild bird surveillance. Aust Vet J. 2015;93:387–93. https://doi.org/10.1111/avj.12379

5. National Avian Influenza Wild Bird Program. Wild bird news, issue 9. 2023 [cited 2024 Sep 12].

https://wildlifehealthaustralia.com.au/Resource-Centre/Surveillance-Reports

6. Luczo JM, Stambas J, Durr PA, Michalski WP, Bingham J. Molecular pathogenesis of H5 highly pathogenic avian influenza: the role of the haemagglutinin cleavage site motif. Rev Med Virol. 2015;25:406–30. https://doi.org/10.1002/rmv.1846

Address for correspondence: Michelle Wille, University of Melbourne,792 Elizabeth St, Melbourne, VIC 3000, Australia; email: michelle.wille@unimelb.edu.au

October 2024

Vectorborne Diseases

EMERGING INFECTIOUS DISEASES®

Heartland Virus Infection in Elderly Patient Initially Suspected of Having Ehrlichiosis, North Carolina, USA

Alexis M. Barbarin, Teresa G. Fisher, Michael H. Reiskind, Carl Williams,
Bryan N. Ayres, Kristen L. Burkhalter, William L. Nicholson

We report a patient in North Carolina, USA, with Heartland virus infection whose diagnosis was complicated by previous *Ehrlichia chaffeensis* infection. We identified *E. ewingii*–infected and Bourbon virus–infected tick pools at the patient's residence. Healthcare providers should consider testing for tickborne viruses if ehrlichiosis is suspected.

*E*hrlichia chaffeensis* and *E. ewingii* are tickborne intracellular bacteria that cause human ehrlichiosis (*1*). In the United States, ehrlichiosis occurs primarily in south-central, southeastern, and mid-Atlantic states. In 2019, nearly half of *E. chaffeensis* ehrlichiosis cases occurred in 4 US states: Arkansas, Missouri, New York, and North Carolina (*2*). Heartland virus (HRTV), another tickborne pathogen, is an emerging zoonotic virus and has been reported in 14 states, including North Carolina, since its initial discovery in 2009 in Missouri. (*3*). We report a case of HRTV infection in a patient in North Carolina who was initially suspected of having ehrlichiosis.

The Study

In March 2022, a North Carolina resident sought care at an emergency room and was subsequently admitted to the hospital because of a suspected case of ehrlichiosis. The patient sought care after experiencing 48 hours of fever, chills, shortness of breath, and diarrhea. Upon admission, the patient had acute leukopenia, thrombocytopenia, anemia, acute kidney

Author affiliations: North Carolina Division of Public Health, Raleigh, North Carolina, USA (A.M. Barbarin, T.G. Fisher, C. Williams); North Carolina State University, Raleigh (M.H. Reiskind); Centers for Disease Control and Prevention, Atlanta, Georgia, USA (B.N. Ayres, W.L. Nicholson); Centers for Disease Control and Prevention, Fort Collins, Colorado, USA (K.L. Burkhalter)

injury, transaminitis, abdominal distension with splenomegaly, and meningoencephalitis. Hospital staff discovered 2 ticks attached to the patient and identified them as lone star ticks (*Amblyomma americanum*). Identification by a North Carolina Division of Public Health (NCDPH) entomologist (A.M.B.) subsequently confirmed the ticks as male and nymphal lone star ticks; the ticks collected from the patient were not tested for pathogens. Although no history of travel was reported, the patient practiced multiple daily walks to the edge of their 5.6-acre property, located in rural North Carolina.

The patient was initially treated for tickborne pathogen infections and meningitis by using broad spectrum antimicrobial drugs, including doxycycline, on day 2 after admission. On day 3, the patient required increased support because of progressive encephalopathy, hypotension, lactate elevation, and concerns of gastrointestinal bleeding, along with thrombocytopenia and was transferred to the medical intensive care unit. The patient experienced continued fevers and altered mental status. Results of differential testing for other infectious etiologies were negative (Table 1). Laboratory results indicated secondary hemophagocytic lymphohistiocytosis (Appendix Table, https://wwwnc.cdc.gov/EID/article/30/12/24-0646-App1.pdf), an increasingly recognized complication of rickettsial diseases (*4,5*). The patient was placed on anakinra on day 8 after hospital admission to address the hemophagocytic lymphohistiocytosis, and mental status slowly improved. Although the patient experienced mild improvement after treatment with anakinra and doxycycline, it was decided that the patient should transition to home hospice care after 18 days in the hospital. The patient recovered after 4 weeks at home and was removed from hospice care.

Indirect fluorescence antibody testing of serum revealed the patient was positive for *E. chaffeensis*

IgG on day 4 after symptom onset, indicating a history of *Ehrlichia* infection (Table 1). Because of limited improvement after doxycycline administration and concerns about possible arbovirus infection, staff (T.G.F.) at NCDPH coordinated specimen collection with the local county health department to send a

Table 1. Vectorborne disease testing in case study of Heartland virus infection in elderly patient initially suspected of having ehrlichiosis, North Carolina, USA*

Test, specimen source	Specimen collection date	Result	Reference values
Vectorborne and zoonotic organisms			
Ehrlichia chaffeensis **IgG, serum**	2022 Mar 29	**1:512 titer**	<1:64 titer
Heartland virus real-time RT-PCR, serum	2022 Apr 5	**Positive**	Negative
Bourbon virus real-time RT-PCR, serum	2022 Apr 5	Negative	Negative
Bourbon PRNT, serum	2022 Apr 5	<1:10 titer, negative	<1:10 titer
Heartland PRNT, serum	2022 Apr 5	<1:10 titer, negative	<1:10 titer
Rickettsia rickettsii IgG, serum	2022 Apr 5	1:64 titer	<1:128 titer
E. chaffeensis **IgG, serum**	2022 Apr 5	**1:1,024 titer**	<1:64 titer
R. rickettsii IgG, serum	2022 May 11	1:64 titer	<1:128 titer
E. chaffeensis **IgG, serum**	2022 May 11	**1:512 titer**	<1:64 titer
E. chaffeensis PCR, serum	2022 Mar 29	Negative	Negative
Eastern equine encephalitis virus IgM, serum	2022 Apr 2	Negative	Negative
Viruses			
Hepatitis A virus IgG, serum	2022 Mar 28	Positive	Negative
Hepatitis A virus IgM, serum	2022 Mar 28	Negative	Negative
Hepatitis B surface antibody, serum	2022 Mar 28	Negative	Negative
Hepatitis B core antibody, serum	2022 Mar 28	Negative	Negative
Hepatitis C virus antibody, serum	2022 Mar 28	Negative	Negative
Cytomegalovirus IgG, serum	2022 Mar 28	Positive	Negative
Cytomegalovirus IgM, serum	2022 Mar 28	Negative	Negative
Cytomegalovirus PCR, blood	2022 Apr 1	Negative	Negative
Herpes simplex virus 1/2 PCR, serum	2022 Apr 2	Negative	Negative
Herpes simplex virus 1 IgG, serum	2022 Apr 2	Positive	Negative
Herpes simplex virus 2 IgG, serum	2022 Apr 2	Negative	Negative
Epstein-Barr virus PCR, serum	2022 Mar 31	Negative	Negative
HIV-1/2 antibody, serum	2022 Mar 29	Negative	Negative
HIV-1 p24 antigen, serum	2022 Mar 29	Negative	Negative
Sapovirus PCR, feces	2022 Mar 29	Negative	Negative
Adenovirus F40/41 PCR, feces	2022 Mar 29	Negative	Negative
Astrovirus PCR, feces	2022 Mar 29	Negative	Negative
Norovirus PCR, feces	2022 Mar 29	Negative	Negative
Rotavirus A PCR, feces	2022 Mar 29	Negative	Negative
Respiratory syncytial virus PCR, nasopharyngeal swab	2022 Mar 27	Negative	Negative
Influenza A/B PCR, nasopharyngeal swab	2022 Mar 27	Negative	Negative
SARS-CoV-2 PCR, nasopharyngeal swab	2022 Mar 27	Negative	Negative
Parvovirus IgM, serum	2022 Mar 29	Negative	Negative
Bacteria			
Streptococcus pneumoniae antigen, urine	2022 Apr 2	Negative	Negative
Legionella pneumophila antigen, urine	2022 Mar 31	Negative	Negative
Coxiella burnetii PCR, serum	2022 Apr 2	Negative	Negative
Campylobacter PCR, feces	2022 Mar 29	Negative	Negative
Plesiomonas shigelloides PCR, feces	2022 Mar 29	Negative	Negative
Salmonella PCR, feces	2022 Mar 29	Negative	Negative
Vibrio cholerae PCR, feces	2022 Mar 29	Negative	Negative
Vibrio PCR, feces	2022 Mar 29	Negative	Negative
Yersinia enterocolitica PCR, feces	2022 Mar 29	Negative	Negative
Enteroaggregative *Escherichia coli* PCR, feces	2022 Mar 29	Negative	Negative
Enteropathogenic *E. coli* PCR, feces	2022 Mar 29	Negative	Negative
Enterotoxigenic *E. coli* PCR, feces	2022 Mar 29	Negative	Negative
Enteroinvasive *E. coli* PCR, feces	2022 Mar 29	Negative	Negative
Shiga-toxin producing *E. coli* PCR, feces	2022 Mar 29	Negative	Negative
Clostridioides difficile PCR, feces	2022 Mar 29	Negative	Negative
Francisella tularensis, serum	2022 Apr 2	Negative	Negative
Culture, blood	2022 Apr 5	No growth	No growth
Parasites			
Cryptosporidium PCR, feces	2022 Mar 29	Negative	Negative
Cryptosporidium cayetanensis PCR, feces	2022 Mar 29	Negative	Negative
Entamoeba histolytica PCR, feces	2022 Mar 29	Negative	Negative
Giardia lamblia PCR, feces	2022 Mar 29	Negative	Negative
Parasite smear, feces	2022 Mar 31	Negative	Negative
Toxoplasma IgM/IgG, serum	2022 Apr 2	Negative	Negative

*Bold text indicates positive acute test result. PRNT, plaque reduction neutralization test; RT-PCR, reverse transcription PCR.

serum sample to the Centers for Disease Control and Prevention (CDC) in Fort Collins, Colorado, USA, for testing. Quantitative reverse transcription PCR (RT-PCR) was positive for HRTV RNA (6).

In conjunction with university partners, NCDPH conducted environmental sampling. In May and June 2022, we conducted standard tick drags at the patient's home. The habitat surrounding the home was primarily deciduous, hardwood forest that had some understory growth and heavy leaf litter. We collected ticks by passing a 1-m² cotton drag cloth over ground level vegetation. We checked the cloth every 10 m² and collected ticks for pathogen testing (7). We collected 608 ticks in May and 656 ticks in June 2022 after 5 hours of total collection time (Table 2). We sent *A. americanum* tick specimens collected in May 2022 to CDC in Atlanta, Georgia, USA, and in Fort Collins to test for Bourbon virus (BRBV), HRTV, *E. chaffeensis*, and *E. ewingii*. We sent *A. americanum* ticks collected in June 2022 to CDC in Fort Collins for BRBV and HRTV testing. *E. chaffeensis* and *E. ewingii* DNA testing consisted of real-time PCR that amplified an 82-bp fragment of the 16S rRNA gene for both species and used 2 probes specific for either *E. chaffeensis* or *E. ewingii* detection (8). CDC tested ticks for HRTV and BRBV by using real-time RT-PCR primers and probes specific for each virus, as described previously (9,10). Pathogen testing of *A. americanum* ticks did not detect HRTV but did detect 2 *E. ewingii*–positive tick pools (1 pool = 25 nymphs; 1 pool = 5 adult ticks) out of a total of 43 pools (587 total ticks), indicating a minimum infection rate (MIR) of 0.34% (2 pools/587 ticks). In addition, BRBV was also detected in 1 tick pool (n = 25 ticks), indicating an MIR of 0.08% (1 pool/1,264 total ticks).

Conclusions

This patient had a substantially elevated antibody titers against *E. chaffeensis* antigen at the time of symptom manifestation, suggesting a previous infection at some undetermined time; the lack of a rise in titer during hospitalization and the ineffectiveness of doxycycline argued against a current *Ehrlichia* infection. Therefore, other tickborne illnesses were considered for testing. The patient's laboratory and clinical history were consistent with both HRTV and *Ehrlichia* spp. infections, but serologic and molecular testing are needed to distinguish between the 2 infections. The patient was negative for BRBV RNA by RT-PCR and negative for both HRTV and BRBV antibodies by using plaque reduction neutralization tests. However, additional testing for HRTV RNA revealed a positive RT-PCR result, indicating the patient had an active HRTV infection.

First identified in 2 farmers in Missouri, USA, in 2009, HRTV has been identified in >60 patients across the United States (11–13), including 1 previous case in North Carolina. In North Carolina, co-infection with *Ehrlichia* spp. and HRTV is possible because those pathogens are naturally maintained in a common tick vector. Although no evidence of co-infection existed in this case, the patient was likely exposed to both pathogens on their property. The additional findings of BRBV and *E. ewingii* in the collected tick pools indicate a further environmental risk for tickborne diseases at that residential site.

The MIR for *E. ewingii* in the collected ticks from this study is not uncommon for this region; prevalence rates for *Ehrlichia* spp. have been documented across the mid-Atlantic region. *E. chaffeensis* was detected in 2.6% and *E. ewingii* in 0.8% of *A. americanum* ticks in Tennessee (14). Virginia reported infection rates of 0%–5.08% for *E. chaffeensis* and 0%–8.20% for *E. ewingii* in *A. americanum* ticks (15). BRBV was identified in 1 pool of ticks collected in a North Carolina location where no BRBV in ticks has been previously reported. The presence of BRBV in *A. americanum* ticks indicates that citizens are at risk, albeit low, of contracting BRBV in North Carolina if bitten by lone star ticks.

Table 2. Entomologic surveillance at patient's residence in case study of Heartland virus infection in elderly patient initially suspected of having ehrlichiosis, North Carolina, USA

Surveillance data	May 2022	June 2022
Collection time	11 AM–2 PM	11 AM–1 PM
Mean air temperature, °F/°C	69/21	87/31
Area covered, m²	3,760	3,250
No. ticks collected, by species		
Amblyomma americanum, male	58	43
A. americanum, female	49	64
A. americanum, nymph	480	549
A. maculatum, nymph	1	0
Dermacentor variabilis, male	4	0
D. variabilis, female	2	0
Ixodes scapularis, male	9	0
I. scapularis, female	5	0
Total no. ticks collected	608	656

Initial acute clinical features of ehrlichiosis and tickborne virus infections are similar. Therefore, healthcare providers should also consider testing patients for tickborne viruses if ehrlichiosis is suspected, especially when the infection is not responsive to doxycycline treatment. Furthermore, persons at risk for tick bites should use tick exposure prevention methods, such as applying N,N-diethyl-meta-toluamide and other US Environmental Protection Agency–approved repellants; wearing permethrin-treated clothing, long pants, and long sleeves; and performing tick checks after spending time in wooded areas.

Acknowledgments

About the Author

Dr. Barbarin served as an entomologist in the Epidemiology Section, Communicable Disease Branch at NDCPH and is currently a field services unit program manager. Her interests include ticks and tickborne diseases.

References

1. Dawson JE, Anderson BE, Fishbein DB, Sanchez JL, Goldsmith CS, Wilson KH, et al. Isolation and characterization of an *Ehrlichia* sp. from a patient diagnosed with human ehrlichiosis. J Clin Microbiol. 1991;29:2741–5. https://doi.org/10.1128/jcm.29.12.2741-2745.1991
2. Centers for Disease Control and Prevention. Tickborne diseases of the United States [cited 2024 May 1]. https://www.cdc.gov/ticks/hcp/data-research/tickborne-disease-reference-guide
3. Centers for Disease Control and Prevention. Data and maps for Heartland [cited 2024 May 1]. https://www.cdc.gov/heartland-virus/data-maps
4. Cascio A, Giordano S, Dones P, Venezia S, Iaria C, Ziino O. Haemophagocytic syndrome and rickettsial diseases. J Med Microbiol. 2011;60:537–42. https://doi.org/10.1099/jmm.0.025833-0
5. Liu S, Kannan S, Meeks M, Sanchez S, Girone KW, Broyhill JC, et al. Fatal case of Heartland virus disease acquired in the mid-Atlantic region, United States. Emerg Infect Dis. 2023;29:992–6. https://doi.org/10.3201/eid2905.221488
6. Lindsey HS, Calisher CH, Matthews JH. Serum dilution neutralization test for California group virus identification and serology. J Clin Microbiol. 1976;4:503–10. https://doi.org/10.1128/jcm.4.6.503-510.1976
7. Falco RC, Fish D. A comparison of methods for sampling the deer tick, *Ixodes dammini*, in a Lyme disease endemic area. Exp Appl Acarol. 1992;14:165–73. https://doi.org/10.1007/BF01219108
8. Killmaster LF, Loftis AD, Zemtsova GE, Levin ML. Detection of bacterial agents in *Amblyomma americanum* (Acari: Ixodidae) from Georgia, USA, and the use of a multiplex assay to differentiate *Ehrlichia chaffeensis* and *Ehrlichia ewingii*. J Med Entomol. 2014;51:868–72. https://doi.org/10.1603/ME13225
9. Savage HM, Godsey MS, Lambert A, Panella NA, Burkhalter KL, Harmon JR, et al. First detection of Heartland virus (Bunyaviridae: Phlebovirus) from field collected arthropods. Am J Trop Med Hyg. 2013;89:445–52. https://doi.org/10.4269/ajtmh.13-0209
10. Lambert AJ, Velez JO, Brault AC, Calvert AE, Bell-Sakyi L, Bosco-Lauth AM, et al. Molecular, serological and *in vitro* culture-based characterization of Bourbon virus, a newly described human pathogen of the genus *Thogotovirus*. J Clin Virol. 2015;73:127–32. https://doi.org/10.1016/j.jcv.2015.10.021
11. Staples JE, Pastula DM, Panella AJ, Rabe IB, Kosoy OI, Walker WL, et al. Investigation of Heartland virus disease throughout the United States, 2013–2017. Open Forum Infect Dis. 2020;7:ofaa125. https://doi.org/10.1093/ofid/ofaa125
12. Brault AC, Savage HM, Duggal NK, Eisen RJ, Staples JE. Heartland virus epidemiology, vector association, and disease potential. Viruses. 2018;10:498. https://doi.org/10.3390/v10090498
13. McMullan LK, Folk SM, Kelly AJ, MacNeil A, Goldsmith CS, Metcalfe G, et al. A new phlebovirus associated with severe febrile illness in Missouri. N Engl J Med. 2012;367:834–41. PubMed https://doi.org/10.1056/NEJMoa1203378
14. Cohen SB, Yabsley MJ, Freye JD, Dunlap BG, Rowland ME, Huang J, et al. Prevalence of *Ehrlichia chaffeensis* and *Ehrlichia ewingii* in ticks from Tennessee. Vector Borne Zoonotic Dis. 2010;10:435–40. https://doi.org/10.1089/vbz.2009.0058
15. Wright CL, Gaff HD, Hynes WL. Prevalence of *Ehrlichia chaffeensis* and *Ehrlichia ewingii* in *Amblyomma americanum* and *Dermacentor variabilis* collected from southeastern Virginia, 2010–2011. Ticks Tick Borne Dis. 2014;5:978–82. PubMed https://doi.org/10.1016/j.ttbdis.2014.07.023

Address for correspondence: Alexis M. Barbarin, North Carolina Division of Public Health, 1902 Mail Service Center, Raleigh, NC 27699-1902, USA; email: alexis.barbarin@dhhs.nc.gov

Mycobacterium leprae in Nine-Banded Armadillos (*Dasypus novemcinctus*), Ecuador

Daniel Romero-Alvarez, Manuel Calvopiña, Emily Cisneros-Vásquez, Daniel Garzon-Chavez, Alaine K. Warren, Lauren S. Bennett, Ritika R. Janapati, Carlos Bastidas-Caldes, Melanie Cabezas-Moreno, Jacobus H. de Waard, Daniela Silva-Martinod, Roxane Schaub, Mary Jackson, A. Townsend Peterson, Charlotte Avanzi

We found *Mycobacterium leprae*, the most common etiologic agent of Hansen disease or leprosy, in tissues from 9 (18.75%) of 48 nine-banded armadillos (*Dasypus novemcinctus*) collected across continental Ecuador. Finding evidence of a wildlife reservoir is the first step to recognizing leprosy zoonotic transmission pathway in Ecuador or elsewhere.

The World Health Organization Global Leprosy Strategy targets the long-term goal of leprosy elimination through interruption of disease transmission (*1*). One factor that can impair that goal is environmental or animal reservoirs that contribute to persistence of the *Mycobacterium leprae* bacteria and potential spillover into the human population. The Strategy acknowledges that *M. leprae* zoonotic transmission exists but with a lower risk and highly localized in North America (*1*), possibly because of a lack of research on new and existing animal reservoirs in other locations.

M. leprae, the main causative agent of leprosy, has a broad range of animal hosts, including wild armadillos (*Dasypus* spp.) in the Americas, red squirrels (*Sciurus vulgaris*) in the British Isles. and nonhuman primates in the Philippines and Africa (*2*). Armadillos are a family of medium-sized mammals, belonging to the Xenarthrans, which also includes sloths and anteaters (*3*). At least 20 armadillo species have been recognized (*3*). The Cingulata order encompasses >9 *Dasypus* species, including the nine-banded armadillo (*D. novemcinctus*), considered the main *M. leprae* reservoir in the Americas (*2*).

Ecuador, located in northwestern South America, is a medium-income economy nation with ≈18 million inhabitants (*4*). Officially, Ecuador eliminated leprosy as a public health threat, which means incidence is <1 new case/10,000 inhabitants; only 41 new leprosy cases were registered in 2022 (*5*). Scientific literature on leprosy in Ecuador is scarce; nonetheless, the Ministry of Public Health suggests a higher disease incidence across the country (*6*). Armadillos are found throughout Ecuador and are valued as a protein source and a cultural item in many rural settings (*7*). In view of the uncertain epidemiologic landscape of leprosy in Ecuador and the occurrence of a possible animal reservoir in the country, we investigated *M. leprae* infection in armadillos in Ecuador.

The Study

We gathered tissue samples from 45 armadillos via local hunters who use the mammal as a protein source for their families and communities. The Instituto Nacional de Biodiversidad (Quito, Ecuador) also donated 3 additional samples stored in 70% ethanol, for a total of 48 armadillos. We performed tissue collection according to a protocol approved by the Ministerio del Ambiente, Agua y Transición Ecológica, as part

Author affiliations: Universidad Internacional SEK, Quito, Ecuador (D. Romero-Alvarez); University of Kansas, Lawrence, Kansas, USA (D. Romero-Alvarez, A.T. Peterson); Universidad de las Américas, Quito (M. Calvopiña, E. Cisneros-Vásquez, C. Bastidas-Caldes, J.H. de Waard, D. Silva-Martinod); Universidad San Francisco de Quito, Quito (D. Garzon-Chavez); Colorado State University, Fort Collins, Colorado, USA (A.K. Warren, L.S. Bennett, R.R. Janapati, M. Jackson, C. Avanzi); Agrocalidad, Quito (M. Cabezas-Moreno); Centre Hospitalier de Cayenne, Cayenne, French Guiana (R. Schaub)

Table. Characteristics of animals and samples tested in a study of *Mycobacterium leprae* in nine-banded armadillos (*Dasypus novemcinctus*), Ecuador*

Categories	No. (%)	*M. leprae*–positive, no. (%)
Tissue samples		
Liver	38 (45.24)	8 (21.05)
Spleen	26 (30.95)	4 (15.38)
Muscle	10 (11.90)	1 (10)
Heart	3 (3.57)	0 (0)
Kidney	3 (3.57)	0 (0)
Lung	3 (3.57)	0 (0)
Ear	1 (1.19)	0 (0)
Total	84 (100)	13 (15.48)
Armadillo species		
Dasypus novemcinctus	40 (83.33)	9 (22.50)
Dasypus spp.	6 (12.5)	0 (0)
D. pastasae	1 (2.08)	0 (0)
Cabassous centralis	1 (2.08)	0 (0)
Total	48 (100)	9 (18.75)
Provinces		
Esmeraldas	10 (20.83)	1 (10)
Sucumbíos	9 (18.75)	1 (11.11)
Guayas	7 (14.58)	0 (0)
Santo Domingo de los Tsáchilas	7 (14.58)	3 (42.86)
Morona Santiago	4 (8.3)	0 (0)
Pastaza	3 (6.25)	1 (33.33)
Imbabura	2 (4.17)	1 (50)
Manabí	2 (4.17)	1 (50)
Cañar	1 (2.08)	1 (100)
Cotopaxi	1 (2.08)	0 (0)
Los Ríos	1 (2.08)	0 (0)
No information	1 (2.08)	0 (0)
Total	48 (100)	9 (18.75)

*A total of 84 tissue samples corresponding to 48 individual armadillos from 4 species were tested for *Mycobacterium leprae*. Percentage of *M. leprae* positives is calculated with the total sampling of each row. No samples were positive for *M. lepromatosis*.

of the Genetic Resources Access Framework contract (contract no. MAATE-DBI-CM-2021-0172). We established definitive armadillo species identification by morphological features, known geographic distributions, and molecular diagnosis (Appendix 1, https://wwwnc.cdc.gov/EID/article/30/12/23-1143-App1.pdf). We processed ≥2 tissues from 36 armadillos and only 1 tissue for the other 12; we examined each tissue ≥2 times (Appendix 1). We performed DNA extraction and pathogen identification via real-time quantitative PCR (qPCR) using previously well-established primers and protocols (8,9) (Appendix 1). We considered a sample positive for *M. leprae* or *M. lepromatosis* only if 2 independent qPCR runs yielded a cycle threshold (Ct) <35 (9,10).

We processed a total of 84 armadillo tissue samples (Appendix 2, https://wwwnc.cdc.gov/EID/article/30/12/23-1143-App2.xlsx), including 38 (45.24%) liver, 26 (30.95%) spleen, and 10 (11.9%) muscle samples (Table). We identified *M. leprae* DNA in 13 (15.48%) samples, mostly from liver (n = 8/38 [21.05%]) and spleen (n = 4/26 [15.38%]) (Table). For 3 armadillos with varying

results between tissues, the liver was the source of positivity (Appendix 2). All 84 tissue samples were negative for *M. lepromatosis* according to our protocols.

The 48 individual armadillos belonged to 4 different species: 40 (83.33%) were *D. novemcinctus*, 6 (12.5%) *Dasypus* spp. (not identified to species), 1 (2.08%) *D. pastasae*, and 1 (2.08%) *Cabassous centralis* (Table; Figure). We detected *M. leprae* in 9 *D. novemcinctus* armadillos, for an overall prevalence of 18.75%. Ct values were 26.01–33.66 (Table, Figure; Appendix 2). Most (20.83%, 10/48) armadillos were collected in the Esmeraldas province along the coast, among which only 1 (10%) *D. novemcinctus* armadillo was *M. leprae*–positive (Figure, Table). We observed the highest prevalence (42.86%) of infected armadillos in Santo Domingo de los Tsáchilas, in the northwest, where 3 of 7 animals were *M. leprae*–positive (Figure).

To characterize potential clusters of infected *D. novemcinctus* armadillos in Ecuador, we used the localities of the 9 *M. leprae*–positive armadillos to develop a species distribution model based on 1-class support vector machine hypervolumes (11) and 20 environmental predictors (Figure, panel C; Appendix 1 Figure 1). The subtropical region of Ecuador, west of the Andes mountains, had the highest concentration of environments like those with *M. leprae*–positive detections (Figure, panel D). Specifically, Esmeraldas, Los Ríos, Santo Domingo de los Tsáchilas, Santa Elena, northern Bolívar and Guayas, and southern Manabí are regions with environmental similarities to locales where infected *D. novemcinctus* armadillo were found (Figure).

Conclusions

The canon of leprosy transmission has been actively rewritten in the past 2 decades (2). Confirmation of zoonotic *M. leprae* transmission in the United States (7) prompted a series of studies to evaluate the spread of leprosy bacilli in the *D. novemcinctus* armadillo across its range in the Americas (Appendix 1 Figure 2). Our research demonstrated that nine-banded armadillos from the 3 continental regions of Ecuador host *M. leprae* with an 18.75% prevalence (Table; Figure). Detection of bacilli in wild armadillos is the first step in evaluating leprosy as a zoonotic pathogen in Ecuador. All 84 tissues examined were negative for *M. lepromatosis*, in agreement with previous results for other mammals in Europe and Mexico (12,13) and for armadillo specimens from across the Americas (8).

One limitation of our study was that our sampling scheme depended on local hunters who collect armadillos; thus, systematic sampling representing specific
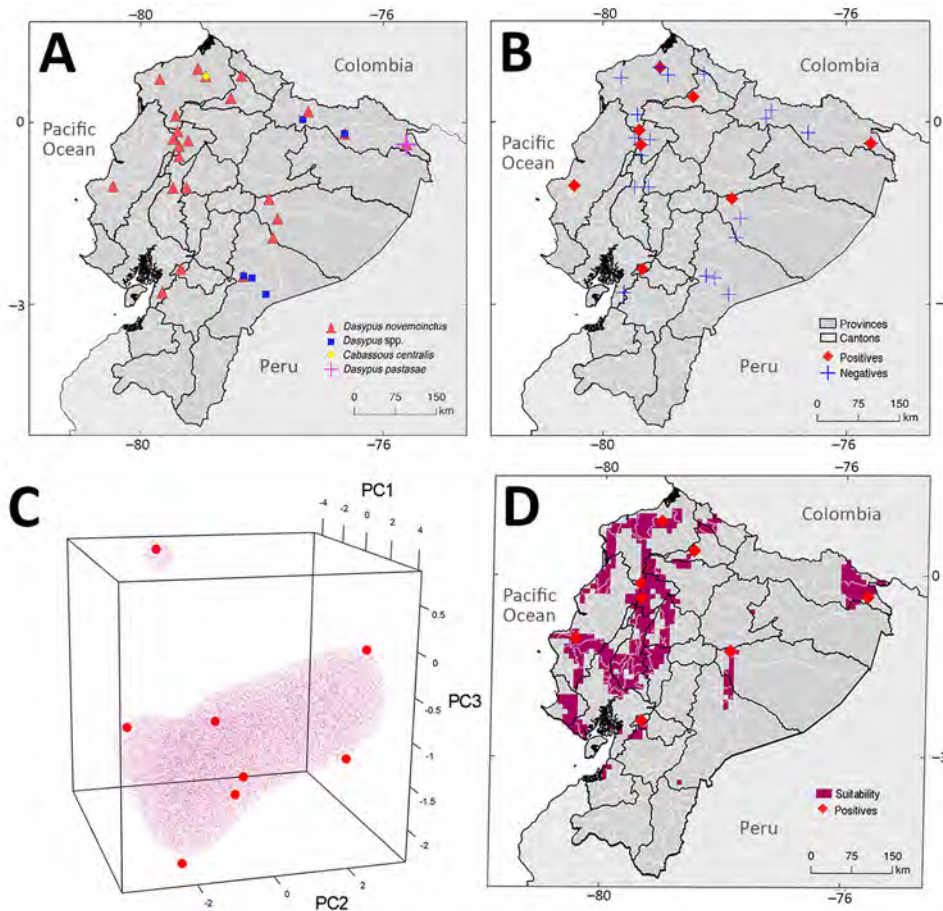
Figure. Locations of and geographic range *Mycobacterium leprae* detections in a study of *M. leprae* in nine-banded armadillos (*Dasypus novemcinctus*), Ecuador. A) Locations of armadillo collections and species identified. B) Locations from which *M. leprae*–positive armadillos samples collected. In southern Santo Domingo de los Tsáchilas, >1 armadillo was collected (Appendix 2, https://wwwnc.cdc.gov/EID/articles/30/12/23-1143-App2.xlsx). No samples were positive for *M. lepromatosis*. C, D) Vector machine hypervolume and its projected geography. C) One-class support vector machine hypervolume with enclosed regions of environmental similarity to areas with *M. leprae* detections (red points); D) map with projected geography for *M. leprae* detections. Latitude and longitude are shown at edges. Mapping developed with the information available in Appendix 2. PC, principal component (see Appendix 1, https://wwwnc.cdc.gov/EID/articles/30/12/23-1143-App1.pdf).

ecologic regions was unfeasible. Moreover, sampling scope was initially limited to tissues in ethanol, preventing serology and histopathology investigations. Nevertheless, we were able to collect tissues from across the country and observed consistency in the molecular detection of *M. leprae* with multiple rounds of qPCR in DNA extracted from various tissues from the same armadillo (Table; Appendix 2). Of note, a Ct value <35 in 2 independent qPCR rounds per tissue as criteria for *M. leprae* positivity is conservative, yet informative of the pathogen in nine-banded armadillos in the country.

Ecuador hosts at least 5 armadillo species: *Cabassous centralis*, *C. unicinctus*, *Priodontes maximus*, *D. pastasae*, and *D. novemcintus* (*14*). *D. novemcintus* was the most common (83.33%) armadillo species in our sampling and the only *M. leprae*–positive species (Table). We identified 3 other armadillo species, but all were *M. leprae*–negative (Figure, Table). Apart from *D. novemcintus*, armadillo species in which *M. leprae* has been identified beyond Ecuador include *Euphractus sexcinctus, Dasypus* spp. nov., and *D. sabanicola*. Moreover, *D. septemcinctus* armadillos have been shown to be susceptible to *M. leprae* laboratory infections (*15*).

Species distribution models have seldom been used to characterize leprosy geographic range. Given the epidemiologic tenets of *M. leprae*, including long incubation period and human-to-human transmission, data for those models is difficult to obtain. Moreover, information on *M. leprae* prevalence in armadillos is either overrepresented as in the southern United States, or scant and dispersed as in the rest of the Americas (*2*) (Appendix 1 Figure 4). Thus, by leveraging our *M. leprae*–positive armadillo detections across the landscape of Ecuador, our model depicted clusters of environmental similarity. Considering the inherent challenges to collecting and studying armadillos (*3*), our model could be used to optimize future expedition sampling.

In conclusion, presence of a nonhuman *M. leprae* host carrier, the nine-banded armadillo, is likely to contribute directly or indirectly to the human leprosy incidence in Ecuador and other countries and will likely impair long-term goals of disease elimination. However, the detection of *M. leprae* in armadillos from Ecuador should exemplify how continued sampling and surveillance in wildlife can avert future zoonotic infections.

About the Author

Dr. Romero-Alvarez is an infectious disease eco-epidemiologist from Ecuador working as an associate professor in the Research Group of Emerging and Neglected Diseases, Ecoepidemiology and Biodiversity, in the Faculty of Health Science at the Universidad Internacional SEK (UISEK), Quito, Ecuador. His research interests include ecology of infectious diseases, zoonotic surveillance, and spatial epidemiology.

References

1. World Health Organization. Towards zero leprosy: global leprosy (Hansen's disease) strategy 2021–2030 [cited 2024 May 21]. https://apps.who.int/iris/handle/10665/340774
2. Ploemacher T, Faber WR, Menke H, Rutten V, Pieters T. Reservoirs and transmission routes of leprosy: a systematic review. PLoS Negl Trop Dis. 2020;14:e0008276. https://doi.org/10.1371/journal.pntd.0008276
3. Feijó A, Vilela JF, Cheng J, Schetino MAA, Coimbra RTF, Bonvicino CR, et al. Phylogeny and molecular species delimitation of long-nosed armadillos (*Dasypus*: Cingulata) supports morphology-based taxonomy. Zool J Linn Soc. 2019;186:813–25. https://doi.org/10.1093/zoolinnean/zly091
4. World Bank. Ecuador data 2023 [cited 2024 May 21]. https://data.worldbank.org/country/EC
5. World health Organization. Global leprosy (Hansen disease) update, 2022: new paradigm—control to elimination [cited 2024 May 21]. https://www.who.int/publications/i/item/who-wer9837-409-430
6. Ministerio de Salud Pública del Ecuador. Health implements prevention and control actions against leprosy in Ecuador [in Spanish] [cited 2024 May 21]. https://www.salud.gob.ec/salud-implementa-acciones-de-prevencion-y-control-contra-la-lepra-en-el-ecuador
7. Romero V. *Dasypus novemcinctus*. In: Brito J, Camacho MA, Romero V, Vallejo AF, editors. Mammals of Ecuador, version 2018.0 [in Spanish]. Museo de Zoología, Pontificia Universidad Católica del Ecuador (PUCE); 2021. [cited 2024 May 21]. https://bioweb.bio/faunaweb/mammaliaweb/FichaEspecie/Dasypus novemcinctus
8. Romero-Alvarez D, Garzon-Chavez D, Jackson M, Avanzi C, Peterson AT. *Mycobacterium leprae* in armadillo tissues from museum collections, United States. Emerg Infect Dis. 2023;29:622–6. https://doi.org/10.3201/eid2903.221636
9. Truman RW, Andrews PK, Robbins NY, Adams LB, Krahenbuhl JL, Gillis TP. Enumeration of *Mycobacterium leprae* using real-time PCR. PLoS Negl Trop Dis. 2008;2:e328. https://doi.org/10.1371/journal.pntd.0000328
10. Collins JH, Lenz SM, Ray NA, Balagon MF, Hagge DA, Lahiri R, et al. A sensitive and quantitative assay to e numerate and measure *Mycobacterium leprae* viability in clinical and experimental specimens. Curr Protoc. 2022;2:e359. https://doi.org/10.1002/cpz1.359
11. Blonder B, Morrow CB, Maitner B, Harris DJ, Lamanna C, Violle C, et al. New approaches for delineating n-d imensional hypervolumes. Methods Ecol Evol. 2018;9:305–19. https://doi.org/10.1111/2041-210X.12865
12. Avanzi C, Del-Pozo J, Benjak A, Stevenson K, Simpson VR, Busso P, et al. Red squirrels in the British Isles are infected with leprosy bacilli. Science. 2016;354:744–7. https://doi.org/10.1126/science.aah3783
13. Schilling AK, Avanzi C, Ulrich RG, Busso P, Pisanu B, Ferrari N, et al. British red squirrels remain the only known wild rodent host for leprosy bacilli. Front Vet Sci. 2019;6:8. https://doi.org/10.3389/fvets.2019.00008
14. Museo de Biología, Pontificia Universidad Católica del Ecuador. Order Cingulata [in Spanish] [cited 2024 May 21]. https://bioweb.bio/faunaweb/mammaliaweb/BusquedaSencilla/Cingulata
15. Schaub R, Avanzi C, Singh P, Paniz-Mondolfi A, Cardona-Castro N, Legua P, et al. Leprosy transmission in Amazonian countries: current status and future trends. Curr Trop Med Rep. 2020;7:79–91. https://doi.org/10.1007/s40475-020-00206-1

Address for correspondence: Daniel Romero-Alvarez, Universidad Internacional SEK, Alberto Einstein S/N y 5ta transveral, Quito, Ecuador; email: daromero88@gmail.com or daniel.romero@uisek.edu.ec

Human and Canine Blastomycosis Cases Associated with Riverside Neighborhood, Wisconsin, USA, December 2021–March 2022[1]

Hannah E. Segaloff, Karen Wu, Samantha L. Williams, Summer Shaw, Shanna Miko, Lindsay A. Parnell, Andrew S. Hanzlicek, Kendra M. Carlson, Mark Lindsley, Ryan P. Westergaard, Mitsuru Toda,[2] Suzanne N. Gibbons-Burgener[2]

We investigated a blastomycosis cluster among humans and canines in a neighborhood in Wisconsin, United States. We conducted interviews and collected serum specimens for *Blastomyces* antibody testing by enzyme immunoassay. Although no definitive exposure was identified, evidence supports potential exposures from the riverbank, riverside trails or yards, or construction dust.

Blastomycosis, caused by the dimorphic fungus *Blastomyces*, is a potentially severe disease of humans and animals. *Blastomyces* favors moist and organically rich soil, and soil disruption can lead to aerosolization and inhalation of infectious *Blastomyces* conidia (*1,2*). Most blastomycosis cases in the United States are sporadic and occur in the midwestern, south-central, and southeastern states. Infrequently, clusters of blastomycosis are reported because of common occupational and recreational activities near waterways (*3*).

In January 2022, St. Croix County Public Health, the Wisconsin Department of Health Services, and the Centers for Disease Control and Prevention (CDC) were notified of a cluster of human and canine blastomycosis cases near the Willow River in St. Croix County, Wisconsin (*4*). A clinical veterinarian reported 4 canine cases living within a radius of a few miles; 2 cases among persons living in the same area were reported to public health. The multiagency team investigated this cluster to identify risk factors for blastomycosis and to encourage persons in blastomycosis-endemic areas with consistent symptoms to seek healthcare.

The population at risk was defined as persons living within a 1.5-mile diameter of where the human and canine cases occurred. Members of the investigation team administered questionnaires to consenting households (Appendix 1, https://wwwnc.cdc.gov/EID/article/30/12/24-0390-App1.pdf), and collected information on exposures, symptoms, and risk factors for blastomycosis occurring during September 2021–March 2022.

Respondents were eligible to participate in serologic testing; pet owners were offered serologic testing for their dogs. We collected 5–10 mL of venous blood; serum samples were sent to MiraVista Diagnostics (Indianapolis, IN, USA) for *Blastomyces* spp. IgG testing by enzyme immunoassays (EIA) for human and canine serum samples and by immunodiffusion assay for human serum samples (*5*). This activity was reviewed by CDC and was conducted consistent with applicable federal law and CDC policy.

We defined human cases of blastomycosis among neighborhood residents who had illness onset during September 2021–March 2022. Included residents met clinical case criteria according to the Council of State and Territorial Epidemiologists case definition and met either confirmatory laboratory criteria or

---

[1]The results of this investigation were presented at the Council for State and Territorial Annual Conference, June 25–29, 2023; Salt Lake City, Utah, USA.

[2]These senior authors contributed equally to this article.

presumptive laboratory criteria, including a positive *Blastomyces* antigen test or a detection of serum antibody through immunodiffusion or EIA (*6*). Canine cases were dogs that exhibited clinical signs and either had received a diagnosis of blastomycosis from a veterinarian during September 2021–March 2022 or had detectable *Blastomyces* spp. antibodies.

We described the demographics, recreational exposure history, symptoms, and any symptom-related healthcare visits of persons by clinical case status. We compared recreational exposures between those with antibodies detected (positive or intermediate results) with exposures of those without antibodies detected. Prevalence ratios (PRs) and 95% CIs were calculated using robust Poisson models. All analyses were completed using R version 4.1.3 (The R Project for Statistical Computing, https://www.r-project.org).

We interviewed members of 60 households, 46 (77%) of whom participated in serologic testing (Figure). The median length of time lived in the neighborhood at time of interview was 4.9 years (range 1 month–56.5 years) (Table 1). The median distance to the in-neighborhood river was 342 (range 1.7–791.0) meters.

During our investigation, 3 previously unreported human cases and 2 additional canine cases of blastomycosis were identified clinically after public health

notification to local veterinarians, clinicians, and residents. A total of 5 human and 6 canine cases were included in this investigation (Appendix 2 Tables 1, 2, https://wwwnc.cdc.gov/EID/article/30/12/24-0390-App2.pdf).

The median age among human case-patients was 54 years, and most (60%, n = 3) had ≥1 comorbidity. All persons reported cough, fever, and fatigue associated with their illness. The initial 2 reported patients were hospitalized, and 1 died (*4*) (Appendix 2 Table 1). Isolates from the 2 initial cases were sent to the CDC Mycotic Diseases Branch laboratory for species identification, which determined the species to be *Blastomyces gilchristii*. In the canine cases, 5 of 6 (83%) were in sporting breeds; less than half of participating dogs were sporting breeds (n = 26, 42%). All dogs with a blastomycosis diagnosis were lethargic and anorexic; most had difficulty breathing (83%, n = 5) and cough and fever (67%, n = 4) (Appendix 2 Table 2). Human and canine case exposures varied.

We performed serologic testing on 89 (61%) of 147 human participants and 51 (79%) of 65 dogs (by EIA for dogs and immunodiffusion for humans). A total of 87 persons consented to further testing; their serum samples were later tested by a newly approved EIA. Among persons tested for antibodies, 1 person had detectable *Blastomyces* antibod-
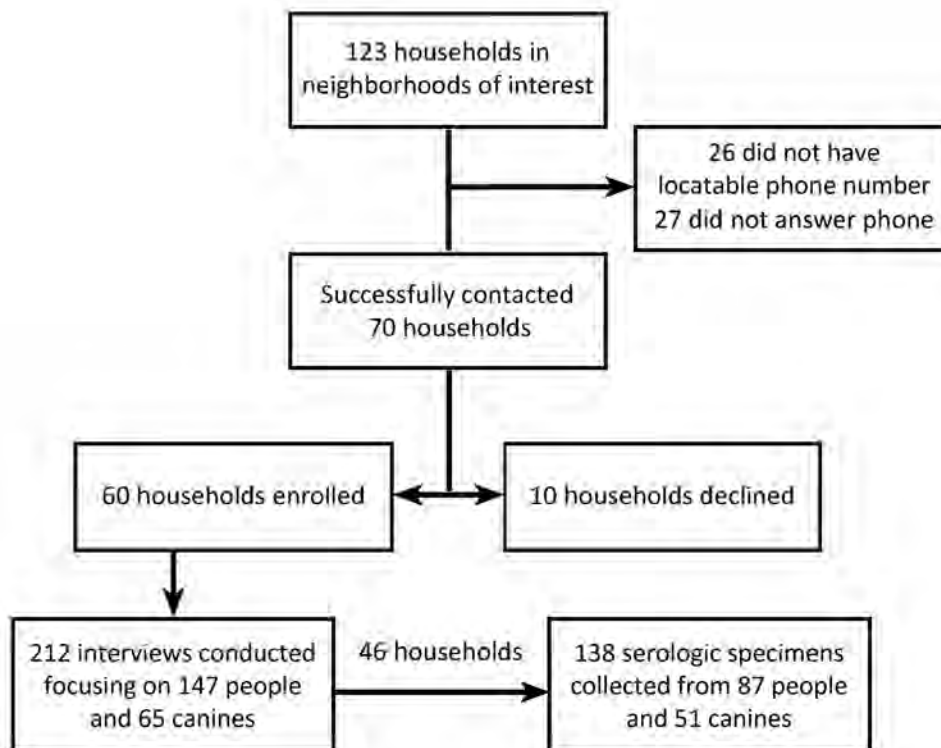

Figure. Flowchart of enrollment of households into investigation of human and canine blastomycosis cases associated with riverside neighborhood, Wisconsin, USA, December 2021–March 2022. Enrolled refers to a household in which ≥1 family member participated in the interview.

Table 1. Characteristics of 60 enrolled households during investigation of human and canine blastomycosis cases associated with riverside neighborhood, Wisconsin, USA, December 2021–March 2022*

Characteristic	Values
No. humans in household	2 (1–7) [2.0–3.0]
No. humans tested for antibodies in household	2 (0–4) [0.8–2.0]
No. humans with antibodies detected in household†	1 (0–3) [0–1.0]
No. dogs in household	1 (0–4) [0–1.3]
No. dogs tested for antibodies in household‡	1 (0–4) [0–1.0]
No. dogs with antibodies detected in household	0 (0–2) [0]
Length of time living in neighborhood	4.9 y (1 mo–56.5 y) [3.2 y–15.5 y]
Distance of house from construction, m	144 (0–814.8) [92.7–219.4]
Distance of house from river, m	341.7 (1.7–791.0) [231.1–463.2]
No. (%) households in neighborhood	
Neighborhood 1	20 (33.3)
Neighborhood 2	29 (48.3)
Neighborhood 3	11 (18.3)
No. (%) households with a clinically diagnosed case	
Human case	5 (8.3)
Canine case	6 (10.0)
Both human and canine cases	0 (0.0)
No. (%) households with any antibodies detected, n = 46	34 (73.9)
Humans with detected antibodies†	31 (67.4)
Canines with detected antibodies	7 (15.2)
Both humans and canines with detected antibodies‡	4 (6.7)
No. (%) household members (human or canine) with antibodies detected, n = 46	
0	12 (26.1)
1	22 (47.8)
2	7 (15.2)
3	4 (8.7)
4	1 (2.2)
No. (%) households with a clinically diagnosed case, n = 11	
Neighborhood 1, n = 20	2 (10.0)
Neighborhood 2, n = 29	8 (27.6)
Neighborhood 3, n = 11	1 (9.1)
No. (%) households that participated in the serosurvey, n = 46	
Neighborhood 1, n = 20	15 (75.0)
Neighborhood 2, n = 29	24 (82.8)
Neighborhood 3, n = 11	7 (63.6)
No. (%) households with antibodies detected, n = 46	
Neighborhood 1, n = 15	11 (73.3)
Neighborhood 2, n = 24	18 (75.0)
Neighborhood 3, n = 7	5 (71.4)

*Values are median (range) [IQR] except as indicated. IQR, interquartile range.
†For humans, antibodies were considered detected in those returning a positive or intermediate result.
‡Antibody testing was completed by MiraVista Diagnostics for *Blastomyces* human and canine enzyme immunoassay.

ies detected by immunodiffusion (also detected by EIA), and 44 (51%) persons had IgG detected by EIA (Table 2). Demographics and recreational exposures did not vary by antibody status, but male participants had 1.5 (95% CI 1.0–2.3) times the prevalence of antibodies than did female participants. Persons who reported a recreational activity involving the in-neighborhood river had 1.5 (95% CI 0.9–2.4) times greater prevalence of detectable antibodies, but was not statistically significant.

Among the 51 dogs tested, 8 (16%) had detectable antibodies, of which 6 (75%) had a clinical diagnosis. Higher number of years lived in the neighborhood was associated with decreased antibody prevalence (PR 0.32; 95% CI 0.1–0.9). Dogs that walked on the trails (PR 10.0; 95% CI 1.3–75.4), specifically those that walked off-leash (PR 6.8; 95% CI 2.0–23.9) had a

higher prevalence of antibodies compared with dogs who did not (Table 3). Dogs who lived farther from the river had lower prevalence of antibodies (PR 0.98; 95% CI 0.97–0.99).

We investigated a Wisconsin cluster of blastomycosis in which 5 human cases, resulting in 2 hospitalizations and 1 death, and 6 canine cases were identified. Using a multidisciplinary One Health approach to trigger notification and investigation of this cluster expanded both the investigative team and the outreach and effects among residents, pet owners, veterinarians, construction workers, and healthcare providers. The elevated awareness likely led to additional residents and dogs identified with blastomycosis illness and exposures.

The serological survey revealed nearly half of residents had *Blastomyces* antibodies detected by

EIA. Although this result suggests widespread exposure, the length of time that *Blastomyces* antibodies remain detectable in the blood and the baseline antibody prevalence in the community are unknown (*5,7*). Although low sensitivity of immunodiffusion limits its use for detecting antibodies (*8*), this study used an EIA targeting the BAD-1 antigen with increased sensitivity.

Although we were unable to identify a definitive exposure as the likely cause of this cluster, several sites such as the riverbank, riverside trails or yards, or construction dust, could have plausibly been sources of *Blastomyces* spores. Although not statistically significant, antibody prevalence was increased in persons who reported participating in activities along the river, as did dogs who walked on in-neighborhood trails (Appendix 2, Table 3, Figure). Extensive neighborhood construction and excavation during the exposure period might have increased risk for exposure because most recent home construction occurred close to the river. Construction and excavation have been implicated in previous clusters of blastomycosis (*9–11*).

Conclusion

Prevention of blastomycosis is challenging. Recommendations for persons in blastomycosis-endemic areas include avoiding activities that disrupt dirt and leaf litter and wearing a well-fitted, high-quality facemask during those activities. Immunocompromised persons are at higher risk for severe blastomycosis and should avoid those activities.

Table 2. Characteristics by antibody detection among humans during investigation of human and canine blastomycosis cases associated with riverside neighborhood, Wisconsin, USA, December 2021–March 2022*

Characteristic	Total, N = 87	Antibodies detected, n = 44	Antibodies not detected, n = 43	Prevalence ratio (95% CI)	p value
Median time lived in neighborhood, y (IQR)	5.0 (3.1–13.5)	5.0 (3.5–14.0)	5.2 (2.8–13.5)	1.00 (0.99–1.00)	0.98
Median distance from construction, m (IQR)†	138 (92–191)	136 (102–213)	139 (92–179)	1.00 (0.99–1.00)	0.98
Median distance from river, m (IQR)	338 (247–483)	313 (193–437)	350 (286–513)	0.99 (0.99–1.00)	0.08
Neighborhood of residence					
Neighborhood 1	31 (35.6)	16 (36.4)	15 (34.9)	1.1 (0.7–1.7)	0.81
Neighborhood 2	43 (49.4)	21 (47.7)	22 (51.2)	Referent	
Neighborhood 3	13 (14.9)	7 (15.9)	6 (14.0)	1.1 (0.6–2.0)	0.74
Age group, y					
<18	7 (8.0)	5 (11.4)	2 (4.7)	1.4 (0.7–2.8)	0.30
18–64	64 (73.6)	31 (70.5)	33 (76.7)	1.0 (0.6–1.7)	0.91
>64	16 (18.4)	8 (18.2)	8 (18.6)	Referent	
Sex					
M	38 (43.7)	24 (54.5)	14 (32.6)	1.5 (1.0–2.3)	0.04
F	49 (56.3)	20 (45.5)	29 (67.4)	Referent	
Race/ethnicity					
White, non-Hispanic	84 (96.6)	42 (95.5)	42 (97.7)	0.8 (0.3–1.7)	0.50
Other	3 (3.4)	2 (4.5)	1 (2.3)	Referent	
Immunosuppressive chronic conditions‡					
Any	20 (23.0)	8 (18.2)	12 (27.9)	0.7 (0.4–1.3)	0.32
Diabetes	3 (3.4)	0 (0.0)	3 (7.0)	NA	
Asthma	5 (5.7)	2 (4.5)	3 (7.0)	0.8 (0.3–2.3)	0.66
Other	12 (13.8)	6 (13.6)	6 (14.0)	1.0 (0.5–1.8)	0.97
Smoking history					
Current	3 (3.4)	2 (3.4)	1 (2.3)	Referent	
Former	16 (18.4)	8 (18.2)	8 (18.6)	0.8 (0.3–1.9)	0.55
Never	68 (78.2)	34 (77.3)	34 (79.1)	0.8 (0.3–1.7)	0.50
Any recreational activity§	74 (85.1)	37 (84.1)	37 (86.0)	0.9 (0.5–1.6)	0.79
Any recreational activity in neighborhood	44 (50.6)	20 (45.5)	24 (55.8)	0.8 (0.5–1.2)	0.34
Any recreational activity in river	10 (11.5)	7 (15.9)	3 (7.0)	1.5 (0.9–2.4)	0.10
Any soil-disturbing activity¶	81 (93.1)	42 (95.5)	39 (90.7)	1.6 (0.5–4.9)	0.45
Any soil-disturbing activity in neighborhood	76 (87.4)	38 (87.4)	38 (88.4)	0.9 (0.5–1.6)	0.77
Used walking trails	43 (49.4)	21 (47.7)	22 (51.2)	0.9 (0.6–1.4)	0.75

*Values are no. (%) except as indicated. Antibody testing was completed by MiraVista Diagnostics for *Blastomyces* human and canine enzyme immunoassay. IQR, interquartile range; NA, not applicable because model does not provide meaningful value.
†Distance to construction is measured as the distance in meters from the house to the nearest lot with a construction permit in 2021.
‡Chronic and immunosuppressive conditions consisted of chronic obstructive pulmonary disease, diabetes, cancer, arthritis, organ transplant, long-term steroid treatment, asthma, and asplenia.
§Recreational activities consisted of hunting, fishing, visiting a cabin, camping, hiking, biking, using an ATV, going to a park, and kayaking
¶Soil disturbing activities consisted of chopping wood, excavation, gardening, mulching, exposure through one's occupation, exposure to construction, lawn care, and composting.

Table 3. Characteristics by antibody detection among canines in investigation of human and canine blastomycosis cases associated with riverside neighborhood, Wisconsin, USA, December 2021–March 2022*

Characteristic	Total, N = 51	Antibodies detected, N = 8	Antibodies not detected, N = 43	Prevalence ratio (95% CI)	p value
Median time lived in the neighborhood, y (IQR)	3.5 (2.0–5.6)	3.0 (1.8–3.2)	4.0 (2.0–5.6)	0.32 (0.1–0.9)	0.03
Median distance lived from construction, m (IQR)†	150 (92–214)	170 (121–183)	139 (92–257)	0.99 (0.98–1.00)	0.13
Median distance lived from river, m (IQR)	349 (271–555)	293 (256–341)	364 (286–578)	0.98 (0.97–0.99)	0.02
Neighborhood of residence					
Neighborhood 1	24 (47.1)	2 (25.0)	22 (51.2)	0.3 (0.1–1.2)	0.08
Neighborhood 2	19 (37.3)	6 (75.0)	13 (30.2)	Referent	
Neighborhood 3	8 (15.7)	0 (0.0)	8 (18.6)	0.0 (0.0–0.0)	<0.0001
Age group, y‡					
<2	12 (24.5)	3 (37.5)	9 (22.0)	1.5 (0.4–6.2)	0.58
2–8	19 (38.8)	2 (25.0)	17 (41.5)	0.6 (0.1–3.4)	0.59
>8 y	18 (36.7)	3 (37.5)	15 (36.6)	Referent	
Sex					
M neutered	23 (45.1)	3 (37.5)	20 (46.5)	0.7 (0.2–2.4)	0.52
M intact	3 (5.9)	0 (0.0)	3 (7.0)	0.0 (0.0–0.0)	<0.001
F spayed	25 (49.0)	5 (62.5)	20 (46.5)	Referent	
F intact	0 (0.0)	0 (0.0)	0 (0.0)	NA	
Breed§					
Sporting breed pedigree¶	21 (32.0)	6 (75.0)	15 (35.7)	4.1 (0.9–18.5)	0.06
Other	29 (58.0)	2 (25.0)	27 (64.3)	Referent	
Weight, pounds				1.2 (0.7–2.0)	0.44
Small (<25)	8 (15.7)	0 (0.0)	8 (18.6)		
Medium (25–49)	14 (27.5)	3 (37.5)	11 (25.6)		
Large (≥50)	29 (56.9)	5 (62.5)	24 (55.8)		
Any recreational activity#					
Yes	32 (62.7)	4 (50.0)	28 (65.1)	0.6 (0.2–2.1)	0.41
No	19 (37.3)	4 (50.0)	15 (34.9)		
Any recreation in neighborhood					
Yes	13 (25.5)	3 (37.5)	10 (23.3)	1.8 (0.5–6.3)	0.39
No	38 (74.5)	5 (62.5)	33 (76.7)		
Any soil-disturbing activity**					
Yes	46 (90.2)	4 (50.0)	42 (97.7)	0.1 (0.0–0.3)	<0.001
No	5 (9.8)	4 (50.0)	1 (2.3)		
Any soil-disturbing activity in neighborhood					
Yes	40 (78.4)	4 (50.0)	36 (83.7)	0.3 (0.1–0.9)	0.04
No	11 (21.6)	4 (50.0)	7 (16.3)		
Used trails	21 (41.2)	7 (87.5)	14 (32.6)	10.0 (1.3–75.4)	0.03
Off-leash on trail	10 (19.6)	5 (62.5)	5 (11.6)	6.8 (2.0–23.9)	0.003
Off-leash out of yard††	20 (39.2)	6 (75.0)	14 (32.6)	1.1 (0.9–1.4)	0.50
Recreation in river	10 (19.6)	2 (25.0)	8 (18.6)	1.4 (0.3–5.8)	0.67
Frequent digger	24 (47.1)	5 (62.5)	19 (44.2)	1.9 (0.5–7.0)	0.35

*Values are no. (%) except as indicated. Antibody testing was completed by MiraVista Diagnostics for *Blastomyces* human and canine enzyme immunoassay (EIA). NA, not applicable because model does not provide meaningful value.
†Distance to construction is measured as the distance in meters from the house to the nearest lot with a construction permit in 2021.
‡Information on age was missing for 2 dogs.
§Breed information was missing for 1 dog.
¶Sporting breed category includes mixed-breed dogs.
#Recreational activities consisted of hunting, fishing, visiting a cabin, camping, hiking, visiting parks, visiting a dog park, and kayaking.
**Soil-disturbing activities consisted of exposure to lawn care, excavation, or gardening.
††Information about time spent off-leash out of the yard was missing for 1 dog.

Risk for blastomycosis cannot be eliminated, and symptoms of blastomycosis can be indistinguishable from other illnesses. Increasing disease awareness is critical to improve early identification and treatment of patients.

those who supplemented our field team, including Lynn Roberts from Wisconsin Department of Health Services, Meredith Smith from Countryside Veterinary Clinic, Bethany Allen from the University of Minnesota, and Martha Pott from Magnusson Veterinary Clinic. We thank Anastasia Livintseva and Joe Sexton for technical assistance and expertise, Andrew Wiese and Andrea Goeldner for their assistance in the initial stages of the investigation, and the GIS Team for their assistance with the spatial analyses.

About the Author

Dr. Segaloff is a Career Epidemiology Field Officer with the Centers for Disease Control and Prevention assigned to the Wisconsin Department of Health Services, Madison, Wisconsin. Her research interests include respiratory and emerging infectious diseases surveillance and response.

References

1. Sarosi GA, Hammerman KJ, Tosh FE, Kronenberg RS. Clinical features of acute pulmonary blastomycosis. N Engl J Med. 1974;290:540–3. https://doi.org/10.1056/NEJM197403072901004
2. Klein BS, Vergeront JM, Weeks RJ, Kumar UN, Mathai G, Varkey B, et al. Isolation of Blastomyces dermatitidis in soil associated with a large outbreak of blastomycosis in Wisconsin. N Engl J Med. 1986;314:529–34. https://doi.org/10.1056/NEJM198602273140901
3. Benedict K, Gibbons-Burgener S, Kocharian A, Ireland M, Rothfeldt L, Christophe N, et al. Blastomycosis surveillance in 5 states, United States, 1987–2018. Emerg Infect Dis. 2021;27:999–1006. https://doi.org/10.3201/eid2704.204078
4. Segaloff HE, Wu K, Shaw S, Klasen EM, Peterson L, Lindberg S, et al. Notes from the field: cluster of blastomycosis among neighborhood residents—St. Croix County, Wisconsin, 2022. MMWR Morb Mortal Wkly Rep. 2023;72:348–9. https://doi.org/10.15585/mmwr.mm7213a5
5. Mourning AC, Patterson EE, Kirsch EJ, Renschler JS, Wolf LA, Paris JK, et al. Evaluation of an enzyme immunoassay for antibodies to a recombinant Blastomyces adhesin-1 repeat antigen as an aid in the diagnosis of blastomycosis in dogs. J Am Vet Med Assoc. 2015;247:1133–8. https://doi.org/10.2460/javma.247.10.1133
6. Centers for Disease Control and Prevention. Blastomycosis 2020 case definition [cited 2024 Feb 5]. https://ndc.services.cdc.gov/case-definitions/blastomycosis-2020
7. Spector D, Legendre AM, Wheat J, Bemis D, Rohrbach B, Taboada J, et al. Antigen and antibody testing for the diagnosis of blastomycosis in dogs. J Vet Intern Med. 2008;22:839–43. https://doi.org/10.1111/j.1939-1676.2008.0107.x
8. Klein BS, Vergeront JM, DiSalvo AF, Kaufman L, Davis JP. Two outbreaks of blastomycosis along rivers in Wisconsin. Isolation of Blastomyces dermatitidis from riverbank soil and evidence of its transmission along waterways. Am Rev Respir Dis. 1987;136:1333–8. https://doi.org/10.1164/ajrccm/136.6.1333
9. Frye MD, Seifer FD. An outbreak of blastomycosis in eastern Tennessee. Mycopathologia. 1991;116:15–21. https://doi.org/10.1007/BF00436085
10. Kitchen MS, Reiber CD, Eastin GB. An urban epidemic of North American blastomycosis. Am Rev Respir Dis. 1977;115:1063–6.
11. Tosh FE, Hammerman KJ, Weeks RJ, Sarosi GA. A common source epidemic of North American blastomycosis. Am Rev Respir Dis. 1974;109:525–9.

Address for correspondence: Suzanne Gibbons-Burgener, 1 West Wilson St, Rm 272, Madison, WI 53703, USA; email: Suzanne.gibbonsburgener@dhs.wi.gov

Lack of Lloviu Virus Disease Development in Ferret Model

Paige Fletcher, Kyle L. O'Donnell, Joseph F. Rhoderick, Corey W. Henderson, Atsushi Okumura, Trenton Bushmaker, Ayato Takada, Chad S. Clancy, Gábor Kemenesi, Andrea Marzi

The first isolate of the emerging filovirus Lloviu virus (LLOV) was obtained in 2022. No animal disease models have been established. We assessed the pathogenic potential of LLOV in ferrets after intranasal, intramuscular, or aerosol exposure. The lack of disease development shows ferrets are not a disease model for LLOV.

Members of the *Filoviridae* family are negative-sense, nonsegmented, single-stranded RNA viruses with the potential to cause hemorrhagic disease in humans and nonhuman primates. Lloviu virus (LLOV) is an emerging filovirus that is currently the only virus within the *Cuevavirus* genus (*1*). LLOV was first identified in Schreiber's bats (*Miniopterus schreibersii*) in 2002 in Cueva del Lloviu, Spain (*2*), but no other reports were published until 2016, when it was identified in Schreiber's bats in Hungary (*3*). LLOV has also been identified in Bosnia-Herzegovina and Italy (*4,5*). The first infectious LLOV isolate was obtained in 2022 (*6*). The human pathogenic potential is currently unknown, although LLOV can infect human cells, which suggests a potential for zoonotic spillover (*6*). No animal disease models have been established to assess LLOV pathogenicity and to better understand this novel filovirus.

Because the ferret model has recently been used to assess wild-type filovirus pathogenesis (*7*), we chose domestic ferrets to investigate the pathogenic potential of LLOV. Mucosal inoculation was of interest because LLOV RNA has been detected in lung samples of infected Schreiber's bats (*6*). Intranasal (IN), intramuscular (IM), and aerosol inoculations were evaluated to compare different LLOV exposure routes.

Author affiliations: National Institute of Allergy and Infectious Diseases, Hamilton, Montana, USA (P. Fletcher, K.L. O'Donnell, J.F. Rhoderick, C.W. Henderson, A. Okumura, T. Bushmaker, C.S. Clancy, A. Marzi); Hokkaido University, Sapporo, Japan (A. Takada); University of Pécs, Pécs, Hungary (G. Kemenesi)

The Study

We used 18 domestic ferrets (*Mustela putorius furo*) that were 19 weeks old and 0.52–0.97 kg in weight. On 0 days postinfection (dpi), we inoculated the ferrets by either IM (0.4 mL/ferret; 4 female and 2 male), IN (0.3 mL/ferret; 2 female and 4 male), or aerosol (4 female and 2 male) routes of exposure with 1,000 focus-forming units (FFU) of wild-type LLOV (GenBank accession no. OQ630505), as previously described (*8*). We conducted examinations and sample collections on 0, 2, 4, 6, 8, 10, 14, and 21 dpi. At 21 dpi, we humanely euthanized 6 of 18 surviving ferrets (n = 2/exposure group) and repurposed the remaining 12 ferrets to a different study. We conducted analysis by using GraphPad Prism software v. 9.3.1 (GraphPad, https://www.graphpad.com).

We conducted all infectious work with LLOV following standard operating procedures approved by the Rocky Mountain Laboratories (RML) Institutional Biosafety Committee in the maximum containment laboratory at RML, National Institute of Allergy and Infectious Diseases, National Institutes of Health. We conducted animal work in accordance with recommendations described in the Guide for the Care and Use of Laboratory Animals of the National Institutes of Health, the Office of Animal Welfare, and the United States Department of Agriculture. Animal work was approved by the RML Animal Care and Use Committee. Procedures were conducted in animals anesthetized by trained personnel under the supervision of veterinary staff. Ferrets were monitored ≥1 time/day for clinical signs of disease, including appearance, level of activity, body temperature, and bodyweight determination. Endpoint criteria were used as specified by RML Animal Care and Use Committee approved clinical score parameters.

We achieved the LLOV target dose for each route of exposure as indicated by LLOV inoculum RNA (Appendix Figure 1, panel A, https://wwwnc.cdc.gov/EID/article/30/12/24-0818-App1.pdf). We

determined RNA levels by using a LLOV-specific primer-probe set with extractions and real-time reverse transcription PCR methods as previously described (8). All ferrets survived LLOV inoculation (Figure 1, panel A) with no signs of disease regardless of exposure route throughout the study (Figure 1, panel B). Slight fluctuations of temperature levels were detected by transponders that we inserted on 0 dpi (Figure 1, panel C). We detected sporadic LLOV RNA at low levels in the blood, swab, urine, or tissue samples collected throughout the study (Appendix Figure 1, panels B–F). We detected limited titers of LLOV glycoprotein (GP)-specific IgG on 21 dpi in the aerosol-exposed group (8) but only negligible amounts in the IM- and IN-exposed ferrets (Figure 1, panel D).

We next investigated the hematology and serum biochemistry of LLOV-exposed ferrets, as previously described (9). Platelet and lymphocyte (Appendix Figure 2, panels A, B) cell counts remained at normal levels throughout the study regardless of exposure route.

Similarly, liver and kidney (Appendix Figure 2, panels C–F) enzyme levels remained normal throughout the study regardless of exposure route, which indicated no clinically relevant organ damage. Those findings were confirmed by histopathologic analysis with hematoxylin and eosin staining, as previously described (9). No inflammation or classic filovirus lesions were observed on 21 dpi for any exposure route in the lung, liver, or spleen tissues of the 6 ferrets assessed (Figure 2).

There are no established animal disease models to assess LLOV pathogenicity because it is a novel filovirus. Immunodeficient mice, especially type I interferon receptor knockout (IFNAR$^{-/-}$) mice, have been shown to be susceptible to wildtype filovirus infection (10), but a recent study showed that disease did not develop in IFNAR$^{-/-}$ mice after LLOV inoculation regardless of dose and route of exposure (8). Domestic ferrets have previously been shown to be susceptible to filovirus infection, and disease developed after IM or IN inoculation with Ebola virus, Bundibugyo virus, Sudan virus,
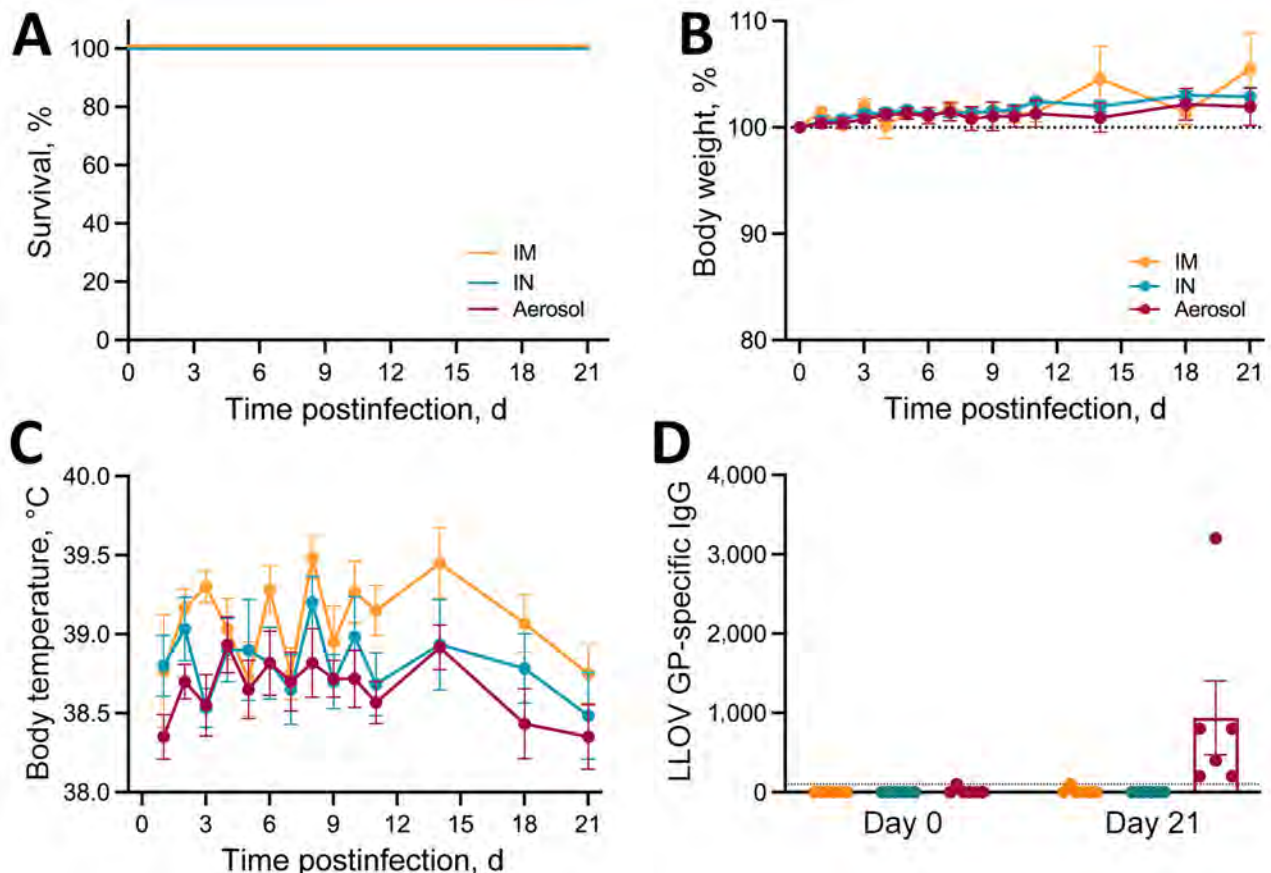
Figure 1. Clinical findings after experimental LLOV exposure in ferrets. Ferrets were inoculated through IM, IN, or aerosol (n = 6/group) routes with 1,000 focus-forming units of LLOV. A) Survival curve. B) Bodyweight percentage; dotted line is normalized to day of infection; error bars indicate standard error of the mean. C) Transponder temperature beginning at 1 day postinfection; error bars indicate standard error of the mean. D) LLOV glycoprotein-specific IgG titers in serum measured by ELISA. Dotted line indicates the limit of detection; error bars indicate standard error of the mean. IM, intramuscular; IN, intranasal; LLOV, Lloviu virus.
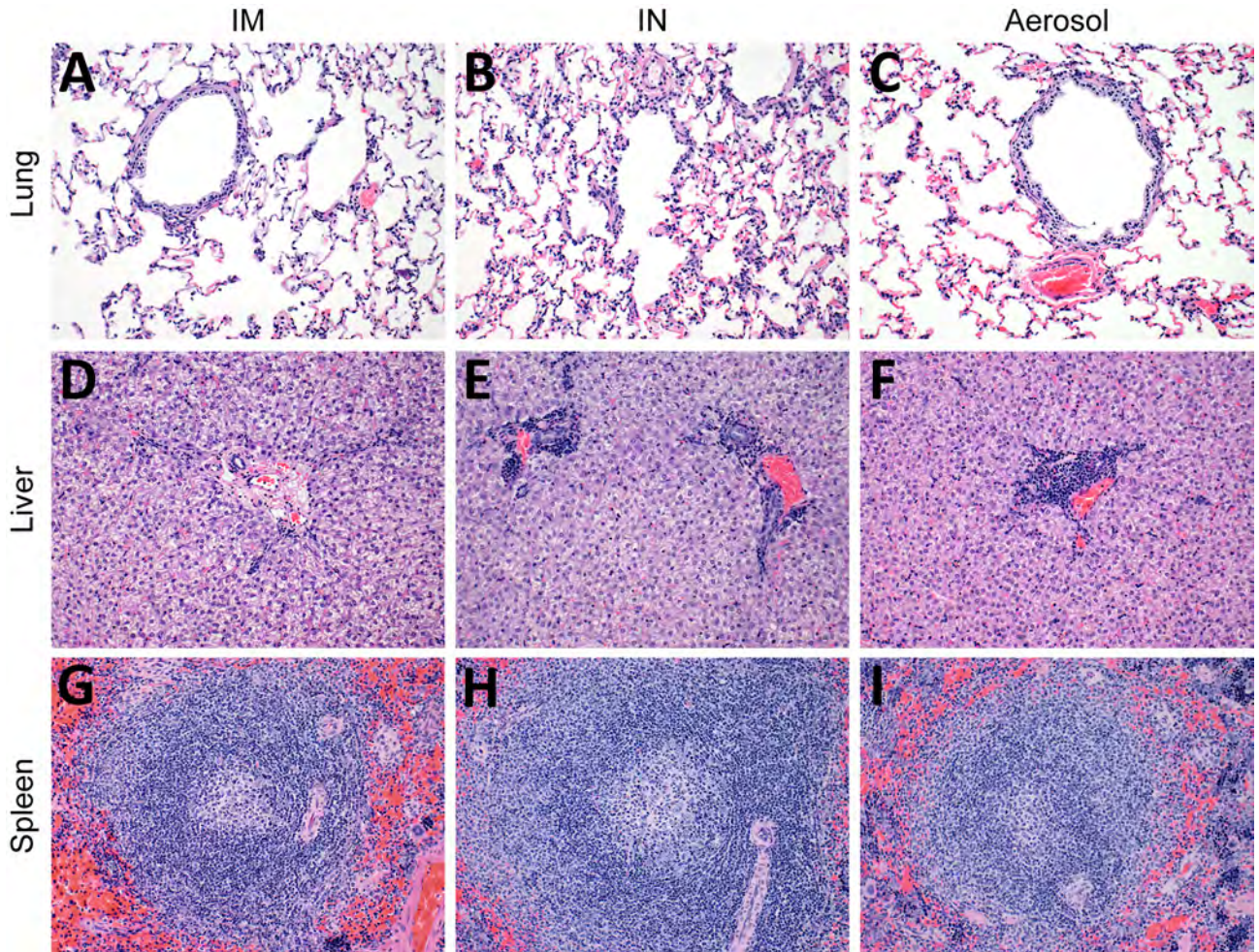
Figure 2. Histopathologic findings after experimental LLOV exposure in ferrets. Ferret tissues showed no abnormalities after LLOV exposure at 21 days postinfection. A–C) Lung tissue; D–F) liver tissue; G–I) spleen tissue. Hematoxylin and eosin staining; original magnification ×200. Ferrets were inoculated through IM, IN, or aerosol (n = 6/group) routes with 1,000 focus-forming units of LLOV. IM, intramuscular; IN, intranasal; LLOV, Lloviu virus.

or Reston virus (7). Therefore, we assessed LLOV inoculation either by IM, IN, or aerosol routes of exposure in the ferret model.

Our results show the LLOV-exposed ferrets did not develop any signs of disease and survived after exposure, regardless of route, and miniscule amounts of LLOV RNA were detected. Animals maintained normal levels of clinical and hematology parameters throughout the study, and histopathologic assessments indicated no lesions or inflammation. The aerosol group demonstrated the most evidence of LLOV replication and as a result recorded the highest LLOV GP-specific IgG titers. This route of infection was specifically included to deposit the virus directly in the lungs because LLOV was isolated from bat lung samples (6). Of note, those results mimic previously published results in the ferret model for IM, IN, or intraperitoneal inoculation of Marburg virus (MARV) and IM or IN inoculation of Ravn virus (11,12). The differences between filovirus infectivity in ferrets could be related to innate immune evasion in this model. A previous LLOV in vitro study investigated the effect of plasmid-expressed viral proteins (VP) VP24, VP35, and VP40 as innate immune antagonists and found LLOV VP24 and VP35 inhibited interferon responses whereas VP40 did not; although testing was performed in human and bat cells (*Epomops buettikoferi*) and not ferret cells (13). That result is of interest because LLOV VP40 is similar to MARV VP40 (2); however, MARV VP40 is an interferon antagonist in a species-specific manner (14). Further research is needed to assess potential species-specific differences with filovirus infections and their invasion of the innate immune response.

Conclusions

In this study, all LLOV-exposed ferrets showed no signs of disease, and survival was 100% regardless of exposure route. Our results indicate a limited value for investigation of LLOV pathogenicity and disease development in this model. Our data potentially indicates that LLOV may be less infectious or pathogenic than other previously characterized filoviruses. Those viruses include MARV and Ravn virus, which cause disease in IFNAR$^{-/-}$ mice but not in ferrets, and Ebola virus, Sudan virus, Reston virus, and Bundibugyo virus, which cause lethal disease in ferrets. This result may be because the LLOV isolate used is closely related to the isolate from Hungary. However, LLOV could be less capable of infecting certain animal species, or LLOV infection might occur by specific exposure routes only, in this case by aerosol exposure. Further studies might reveal if LLOV is pathogenic in any animal species other than bats and determine if the virus poses a zoonotic threat.

About the Author

Dr. Fletcher performed this work as a postdoctoral fellow at the Rocky Mountain Laboratories, National Institute of Allergy and Infectious Diseases, National Institutes of Health. Her research interests include investigating the pathogenicity of lesser-known filoviruses and the preclinical development of filovirus vaccines.

References

1. Burk R, Bollinger L, Johnson JC, Wada J, Radoshitzky SR, Palacios G, et al. Neglected filoviruses. FEMS Microbiol Rev. 2016;40:494–519. https://doi.org/10.1093/femsre/fuw010
2. Negredo A, Palacios G, Vázquez-Morón S, González F, Dopazo H, Molero F, et al. Discovery of an ebolavirus-like filovirus in Europe. PLoS Pathog. 2011;7:e1002304. https://doi.org/10.1371/journal.ppat.1002304
3. Kemenesi G, Kurucz K, Dallos B, Zana B, Földes F, Boldogh S, et al. Re-emergence of Lloviu virus in *Miniopterus schreibersii* bats, Hungary, 2016. Emerg Microbes Infect. 2018;7:66. https://doi.org/10.1038/s41426-018-0067-4
4. Goletic S, Goletic T, Omeragic J, Supic J, Kapo N, Nicevic M, et al. Metagenomic sequencing of Lloviu virus from dead Schreiber's bats in Bosnia and Herzegovina. Microorganisms. 2023;11:2892. https://doi.org/10.3390/microorganisms11122892
5. Tóth GE, Hume AJ, Suder EL, Zeghbib S, Ábrahám Á, Lanszki Z, et al. Isolation and genome characterization of Lloviu virus from Italian Schreiber's bats. Sci Rep. 2023;13:11310. https://doi.org/10.1038/s41598-023-38364-7
6. Kemenesi G, Toth GE, Mayora-Neto M, Scott S, Temperton N, Wright E, et al. Isolation of infectious Lloviu virus from Schreiber's bats in Hungary. Nat Commun. 2022;13:1706.
7. Schiffman Z, Liu G, Cao W, Zhu W, Emeterio K, Qiu X, et al. The ferret as a model for filovirus pathogenesis and countermeasure evaluation. ILAR J. 2022;61:62–71. https://doi.org/10.1093/ilar/ilab011
8. Fletcher P, Feldmann F, Takada A, Crossland NA, Hume AJ, Albariño C, et al. Pathogenicity of Lloviu and Bombali viruses in type I interferon receptor knockout mice. J Infect Dis. 2023;228(Suppl 7):S548–53. https://doi.org/10.1093/infdis/jiad226
9. Fletcher P, O'Donnell KL, Doratt BM, Malherbe DC, Clancy CS, Rhoderick JF, et al. Single-dose VSV-based vaccine protects cynomolgus macaques from disease after Taï Forest virus infection. Emerg Microbes Infect. 2023;12:2239950. https://doi.org/10.1080/22221751.2023.2239950
10. Wong G, Qiu XG. Type I interferon receptor knockout mice as models for infection of highly pathogenic viruses with outbreak potential. Zool Res. 2018;39:3–14.
11. Wong G, Zhang Z, He S, de La Vega MA, Tierney K, Soule G, et al. Marburg and ravn virus infections do not cause observable disease in ferrets. J Infect Dis. 2018;218(suppl_5):S471–4. https://doi.org/10.1093/infdis/jiy245
12. Cross RW, Mire CE, Agans KN, Borisevich V, Fenton KA, Geisbert TW. Marburg and ravn viruses fail to cause disease in the domestic ferret (*Mustela putorius furo*). J Infect Dis. 2018;218(suppl_5):S448–52. https://doi.org/10.1093/infdis/jiy268
13. Feagins AR, Basler CF. Lloviu virus VP24 and VP35 proteins function as innate immune antagonists in human and bat cells. Virology. 2015;485:145–52. https://doi.org/10.1016/j.virol.2015.07.010
14. Valmas C, Basler CF. Marburg virus VP40 antagonizes interferon signaling in a species-specific manner. J Virol. 2011;85:4309–17. https://doi.org/10.1128/JVI.02575-10

Address for correspondence: Andrea Marzi, National Institute of Allergy and Infectious Diseases, 903 South 4th St, Hamilton, MT 59840, USA; email: marzia@niaid.nih.gov.

Umatilla Virus in Zoo-Dwelling Cape Penguins with Hepatitis, Germany

Monica Mirolo,[1] Madeleine de le Roi,[1] Katja von Dörnberg, Franziska Kaiser, Adnan Fayyad, Christina Puff, Ulrich Voigt, Ursula Siebert, Martin Ludlow, Wolfgang Baumgärtner, Albert Osterhaus

Analysis of liver tissue from a Cape penguin that died with hepatitis at a zoo in Germany revealed Umatilla virus. Testing uncovered Umatilla virus RNA in samples from 2 other deceased Cape penguins at the zoo. Our results expand knowledge of the prevalence of this virus in bird species across Germany.

Researchers first isolated Umatilla virus (UMAV) from wild birds in the United States in the 1960s, also identifying the virus in several species of *Culex* mosquitoes in Australia, Japan, China, and the United States (*1–5*). The low pathogenicity of UMAV has contributed to the incidental detection of the virus in wild birds. In Germany, investigators identified 3 UMAV strains (ED-I-93/19, ED-I-87/19, and ED-I-205/19) in wild bird species in 2022 (*6*).

UMAV is a mosquitoborne arbovirus (genus *Orbivirus,* family Sedoreoviridae) with a 10-segment, double-stranded RNA genome and 7 structural proteins forming the inner and outer core. The structural RNA-dependent RNA polymerase viral protein (VP) 1 and inner-core protein VP3 are the most conserved proteins among orbiviruses. In contrast, the outer-capsid protein VP2 and, to a lesser extent, VP5 are more variable among orbivirus species and distinguish virus serotypes (*7–9*). The UMAV life cycle is sustained between UMAV-competent *Culicinae* mosquitoes and wild birds, the primary virus hosts. Limited studies on the UMAV sylvatic life cycle in wild birds and the respective vector species has created a paucity of knowledge regarding the diversity of susceptible hosts, the pathogenicity of the virus, and the genetic diversity of circulating strains.

The Study

A Cape penguin (*Spheniscus demersus*) died without overt clinical signs in August 2019 at Hannover Adventure Zoo, Hannover, Germany. Histopathologic examination revealed mild-to-moderate, periportal, lymphocytic hepatitis with hepatocellular necrosis (Figure, panel A) indicative of a viral infection. Routine immunohistochemical tests for influenza virus yielded negative results (data not shown). Virus isolation from homogenized liver tissue in a chicken liver–derived (leghorn male hepatocellular [LMH]) cell line showed a cytopathic effect at 3 days postinoculation (Appendix 1 Figure 1, https://wwwnc.cdc.gov/EID/article/30/12/24-0498-App1.pdf). We extracted RNA from clarified supernatant of inoculated LMH cells and conducted next-generation sequencing according to methods previously described (*10*). We conducted bioinformatic analyses of raw next-generation sequence reads by using the CZ-ID bioinformatic pipeline (*11*), which showed 304,052 reads aligning to orbiviruses, with UMAV demonstrating the highest percent homology. We then performed nucleotide sequence analyses on the isolated UMAV strain (Umatilla virus isolate DE/Penguin/2019) and found it to be homologous (94%–99% identical) to ED-87-19, ED-93-19, and ED-205-19 (*6*) in all genome regions except for segment 3, where a nucleotide sequence identity ≤72% was observed with other UMAV strains from Germany (GenBank accession nos. PP669535–44) (Appendix 2 Table 1, https://wwwnc.cdc.gov/EID/article/30/12/24-0498-App2.xlsx). The sequence variation of the outer capsid protein has been previously observed for UMAV in Germany (*6*), and we could not rule out that it might result from a reassortment with other circulating but not yet sequenced UMAVs.

Amino acid sequences generated from each UMAV genomic segment showed alignment with multiple orbiviruses (Appendix 2 Table 2). We constructed maximum-likelihood consensus trees with

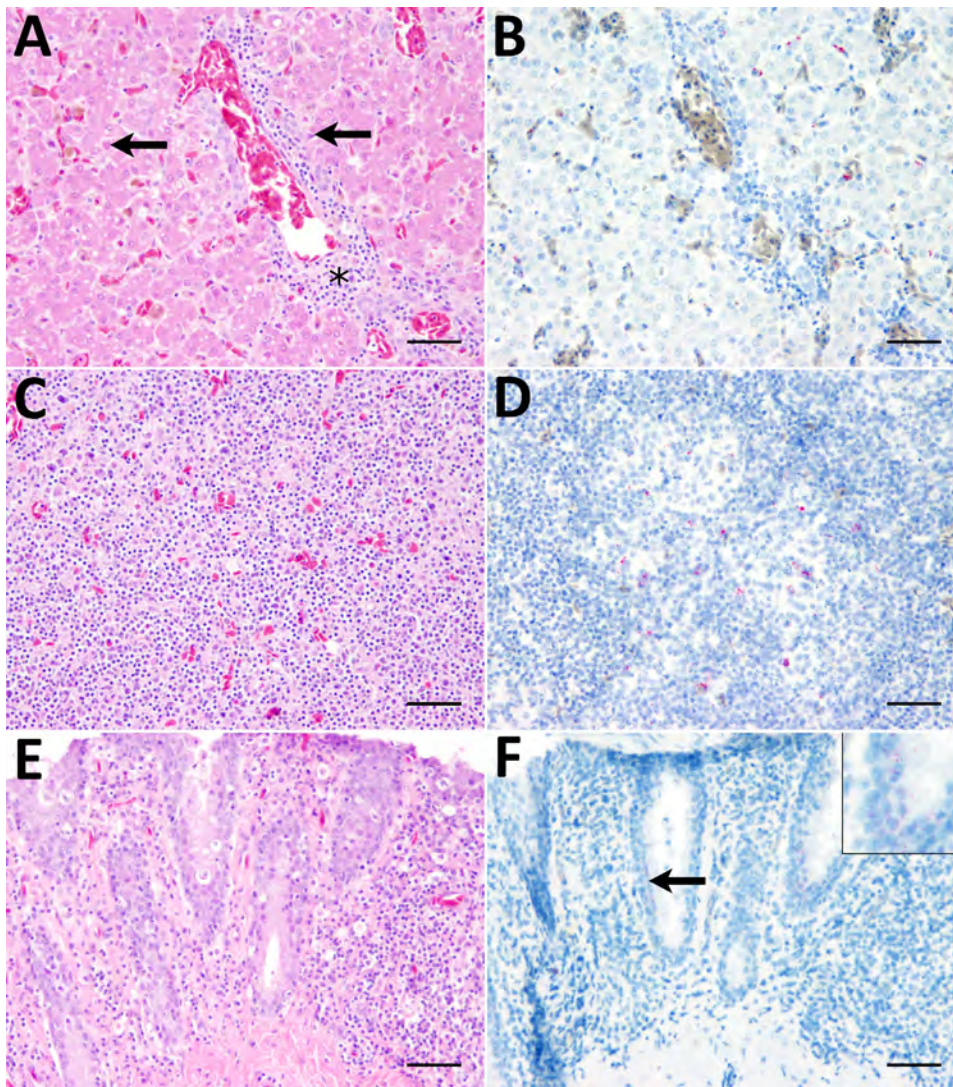[1]These authors contributed equally to this article.

Figure. Histopathologic findings and fluorescence in situ hybridization (FISH) results in a deceased zoo-dwelling, Umatilla virus (UMAV)–infected penguin, Germany, 2019. A) Hematoxylin and eosin (H&E) stain of liver tissue shows mild, multifocal, randomly distributed, coagulative necrosis of hepatocytes (arrows) and mild-to-moderate, periportal, lymphocytic hepatitis (asterisk). B) FISH of liver tissue shows intracytoplasmically UMAV RNA-positive hepatocytes. C) H&E stain of spleen tissue shows no significant histopathologic alterations. D) FISH of spleen tissue shows multifocal cells within follicle centers, most likely macrophages, tested cytoplasmatically positive for UMAV RNA. E) H&E stain of small intestine tissue shows mild, multifocal necrosis of epithelial cells of the small intestine. () FISH of small intestine tissue shows positive UMAV RNA signal within enterocytes. Inset: Multifocal, granular red signal within cytoplasm of enterocytes. Scale bars indicate 50 μm.

1,000 bootstraps in accordance with the best-fit model calculated by using MEGA 11 software (12). Phylogenetic trees based upon amino acid sequences of UMAV proteins exhibited analogous topology (Appendix 1 Figure 2). We used the nucleotide sequence of UMAV segment 2 to design a quantitative reverse transcription PCR (qRT-PCR) and a fluorescence in situ hybridization (FISH) probe to evaluate UMAV tissue tropism. We detected UMAV RNA in hematopoietic cells, most likely macrophages, within hepatic sinusoids and in hepatocytes (Figure, panel B). We detected no marked histopathologic changes in the spleen (Figure, panel C), but macrophage-like cells in the follicle centers tested positive for UMAV by FISH (Figure, panel D). Enterocytes of the small intestine displayed mild multifocal necrosis (Figure, panel E) and were positive for UMAV by FISH (Figure, panel F); other organs were negative by nucleic acid detection methods. We noted high quantification cycle values (30–33.2) in lung, small and large intestine, and brain, and spleen, kidney, and liver showed the lowest UMAV quantification cycle values (25.5–27.2) (Table 1). In contrast to the qRT-PCR results, kidneys tested negative by FISH. Those apparently conflicting data are consistent with the lower sensitivity of FISH for formalin-fixed, paraffin-embedded (FFPE) tissues (13).

Table 1. Comparison of qRT-PCR and FISH results for a UMAV-infected zoo-dwelling penguin, Germany, 2019*

Sample name and source	qRT-PCR, C_q	FISH
S849/19 liver	27.24	Positive
S849/19 kidney	26.37	Negative
S849/19 lung	30.37	Negative
S849/19 duodenum	30.04	Positive
S849/19 brain	33.22	Negative
S849/19 colon	32.69	Negative
S849/19 spleen	25.71	Positive

*C_q, quantification cycle; FISH, fluorescence in situ hybridization; qRT-PCR, quantitative reverse transcription PCR; UMAV, Umatilla virus.

We investigated whether additional UMAV infections had occurred in other penguins from the same zoo in Germany by performing FISH on FFPE liver samples from 15 penguins that died without overt clinical signs during 2005–2021. Histologically, 9 of those penguins displayed hepatitis. UMAV RNA was detected by FISH in 2 Cape penguins, 1 dying in 2005 and 1 in 2011 (Appendix 1 Figure 3). However, we could not confirm those data by qRT-qPCR performed on RNA extracted from the same FFPE material, possibly because of poor RNA quality and fragmentation (14). We also screened for UMAV neutralizing antibodies in 7 serum samples from penguins and in IgY extracted from egg yolks from 9 penguins and 1 red cardinal (*Cardinalis cardinalis*) from the same zoo. We mixed serial serum sample dilutions (1:10) and IgY sample dilutions (1:20–80) and added 600 $TCID_{50}$ (50% tissue culture infectious dose) per well of isolated UMAV, before applying the solution onto LMH cells. Positive results relied on 100% virus neutralization, determined by immunofluorescence staining of intracellular UMAV double-stranded RNA (dsRNA) by using mouse monoclonal antibody J2 (15). The analysis revealed no UMAV antibodies in the samples. We applied the same analysis to 94 serum samples collected from wild pheasants captured in northwestern Germany during 2011–2017. We noted an overall seroprevalence of ≤37%, the highest in 2011 (Table 2).

Conclusion

We isolated and molecularly characterized UMAV from the liver of a deceased Cape penguin in a zoo in Germany. This penguin had lymphocytic hepatitis and UMAV RNA in hepatocytes. qRT-PCR revealed a systemic infection with high viral loads in spleen and kidney. Phylogenetic analyses indicated that the UMAV strain involved is closely related to UMAVs isolated from wild birds in Germany. The virus caused systemic infection consistent with published findings (6). Two other penguins with hepatitis that died in the same zoo, 1 in 2005 and 1 in 2011, tested positive for UMAV by FISH. The use of dsRNA antibodies as an alternative virus detection method should be interpreted with caution because, as revealed in this investigation, different cell types tested UMAV-positive as determined by dsRNA in liver tissue compared with positive cell types detected by FISH.

Serologic analysis showed evidence of UMAV transmission among free-living pheasants in northwestern Germany in 2011–2017. UMAV infections among wild birds increases the likelihood of virus transmission to additional susceptible hosts. We theorized that the carrier mosquitoes transmitted the virus from free-living wild birds to the penguins in the affected zoo.

Table 2. UMAV neutralization test results for serum samples from wild-caught pheasants in northern Germany*

Year	Animal ID	Collection date	UMAV antibody titer†
2011	11005	Mar 3	1:20
	11014	Apr 4	1:20
	11019	Apr 7	1:20
	11024	Apr 7	1:40
2012	12056	Mar 21	1:40
2014	14103	Mar 11	1:40
	14108	Mar 11	>1:80

*UMAV, Umatilla virus.
†The antibody titers were measured in semiquantitative scale: <1:20 serum dilution was considered as negative, and then 1:20, 1:40, 1:80, or >1:80.

This case study of penguins in Germany expands the collective knowledge regarding the susceptible host range for UMAV, as well as aspects of the pathogenesis and the epidemiology of UMAV infections in birds with the specific clade of virus previously identified in Germany. Our seroprevalence data indicate the need for further investigation into the susceptibility of domesticated birds, such as poultry, to UMAV infection. Controlled, in vivo infection studies of UMAV in domestic and wild bird species would be useful in better defining the virulence of this virus. Coupled with reported serologic evidence of UMAV infection in goats, horses, and donkeys in Australia (2), our findings suggest the need for more in-depth exploration into the potential for UMAV infection in mammal species, including humans.

About the Author

Ms. Mirolo is a PhD student at the University of Veterinary Medicine, Hannover, Germany. Her research interests are virus discovery and virus cross-species transmission.

References

1. Belaganahalli MN, Maan S, Maan NS, Tesh R, Attoui H, Mertens PP. Umatilla virus genome sequencing and phylogenetic analysis: identification of Stretch Lagoon orbivirus as a new member of the Umatilla virus species. PLoS One. 2011;6:e23605. https://doi.org/10.1371/journal.pone.0023605
2. Cowled C, Palacios G, Melville L, Weir R, Walsh S, Davis S, et al. Genetic and epidemiological characterization of Stretch

Lagoon orbivirus, a novel orbivirus isolated from *Culex* and *Aedes* mosquitoes in northern Australia. J Gen Virol. 2009;90:1433–9. https://doi.org/10.1099/vir.0.010074-0

3. Tangudu CS, Charles J, Hurt SL, Dunphy BM, Smith RC, Bartholomay LC, et al. Skunk River virus, a novel orbivirus isolated from *Aedes trivittatus* in the United States. J Gen Virol. 2019;100:295–300. https://doi.org/10.1099/jgv.0.001219

4. Ejiri H, Kuwata R, Tsuda Y, Sasaki T, Kobayashi M, Sato Y, et al. First isolation and characterization of a mosquito-borne orbivirus belonging to the species Umatilla virus in East Asia. Arch Virol. 2014;159:2675–85. https://doi.org/10.1007/s00705-014-2117-0

5. Yang Z, Li N, He Y, Meng J, Wang J. Genetic characterization of DH13M98, *Umatilla Virus*, isolated from *Culex tritaeniorhynchus Giles* in Yunnan Province, China. Vector Borne Zoonotic Dis. 2023;23:35–43. https://doi.org/10.1089/vbz.2022.0031

6. Santos PD, Ziegler U, Szillat KP, Szentiks CA, Strobel B, Skuballa J, et al. In action—an early warning system for the detection of unexpected or novel pathogens. Virus Evol. 2021;7:veab085. https://doi.org/10.1093/ve/veab085

7. Maan S, Maan NS, Samuel AR, Rao S, Attoui H, Mertens PPC. Analysis and phylogenetic comparisons of full-length VP2 genes of the 24 bluetongue virus serotypes. J Gen Virol. 2007;88:621–30. https://doi.org/10.1099/vir.0.82456-0

8. Huismans H, Erasmus BJ. Identification of the serotype-specific and group-specific antigens of bluetongue virus. Onderstepoort J Vet Res. 1981;48:51–8. PMID: 6273773

9. Mertens PP, Pedley S, Cowley J, Burroughs JN, Corteyn AH, Jeggo MH, et al. Analysis of the roles of bluetongue virus outer capsid proteins VP2 and VP5 in determination of virus serotype. Virology. 1989;170:561–5. https://doi.org/10.1016/0042-6822(89)90447-9

10. Jesse ST, Ciurkiewicz M, Siesenop U, Spitzbarth I, Osterhaus ADME, Baumgärtner W, et al. Molecular characterization of a bovine adenovirus type 7 (Bovine Atadenovirus F) strain isolated from a systemically infected calf in Germany. Virol J. 2022;19:89. https://doi.org/10.1186/s12985-022-01817-y

11. Kalantar KL, Carvalho T, de Bourcy CFA, Dimitrov B, Dingle G, Egger R, et al. IDseq—an open source cloud-based pipeline and analysis service for metagenomic pathogen detection and monitoring. Gigascience. 2020;9:giaa111. https://doi.org/10.1093/gigascience/giaa111

12. Tamura K, Stecher G, Kumar S. MEGA11: Molecular Evolutionary Genetics Analysis Version 11. Mol Biol Evol. 2021;38:3022–7. https://doi.org/10.1093/molbev/msab120

13. Polampalli S, Choughule A, Prabhash K, Amare P, Baisane C, Kabre S, et al. Role of RT-PCR and FISH in diagnosis and monitoring of acute promyelocytic leukemia. Indian J Cancer. 2011;48:60–7. https://doi.org/10.4103/0019-509X.75831

14. Vermeulen J, De Preter K, Lefever S, Nuytens J, De Vloed F, Derveaux S, et al. Measurable impact of RNA quality on gene expression results from quantitative PCR. Nucleic Acids Res. 2011;39:e63. https://doi.org/10.1093/nar/gkr065

15. Weber F, Wagner V, Rasmussen SB, Hartmann R, Paludan SR. Double-stranded RNA is produced by positive-strand RNA viruses and DNA viruses but not in detectable amounts by negative-strand RNA viruses. J Virol. 2006;80:5059–64. https://doi.org/10.1128/JVI.80.10.5059-5064.2006

Address for correspondence: Albert Osterhaus, Research Center for Emerging Infections and Zoonoses (RIZ), University of Veterinary Medicine, Hannover D-30559, Germany; email: albert.osterhaus@tiho-hannover.de

Influenza A Virus Antibodies in Ducks and Introduction of Highly Pathogenic Influenza A(H5N1) Virus, Tennessee, USA

David E. Stallknecht, Deborah L. Carter, Abigail G. Blake-Bradshaw, Nicholas M. Masto, Cory J. Highway, Jamie C. Feddersen, Richard Webby, Bradley Cohen, Jeffery D. Sullivan, Rebecca L. Poulson

Testing of ducks in Tennessee, United States, before introduction of highly pathogenic influenza A(H5N1) virus demonstrated a high prevalence of antibodies to influenza A virus but very low prevalence of antibodies to H5 (25%) or H5 and N1 (13%) subtypes. Antibody prevalence increased after H5N1 introduction.

Highly pathogenic (HP) influenza A virus (IAV), subtype H5N1, clade 2.3.4.4b was detected in North America in November 2021; many infections and mass deaths were subsequently reported in wild birds from North America to Antarctica (1–3). The IAV immunologic status in waterfowl before the HP H5N1 introduction are largely unknown; however, infections with endemic low pathogenicity (LP) IAV occur in ducks every year and peak during fall migration (4,5). Prevalence of IAV antibodies in waterfowl also increases during migration; reported estimates in mallard ducks (*Anas platyrhynchos*) were 51%–75% for hatch year and 86%–93% for *A. platyrhynchos* sampled in September after hatch year (6). In contrast, prevalence of infection and antibodies to specific IAV hemagglutinin (HA) and neuraminidase (NA) subtypes, such as H5 and N1, can vary annually and often are low (4,6). How immunity from previous LP IAV exposure, especially with LP H5 and N1 IAV subtypes, affects duck susceptibility to HP H5N1 infection, illness, and death, or transmission and maintenance of new IAV in the system, have not been adequately explored. Data from field studies and experimental infections of waterfowl supported the need for further study and demonstrated that previous infections with LP IAV can reduce infection, death, and viral shedding during subsequent infections with both LP and HP IAV and increase the infective dose required for infection (7–9). Those effects are more pronounced with genetically similar or matched HA subtypes and repeated LP IAV infections (10,11). NA is associated with susceptibility of mice and humans to IAV infection (12), but less is known about potential protective effects of immunity to NA in ducks. We sampled ducks to investigate IAV immunity in waterfowl before and after HP H5N1 was detected in Tennessee, USA.

The Study

We tested cloacal and oropharyngeal swab samples from ducks sampled in western Tennessee, United States, during November 7, 2021–January 31, 2022 for IAV infection before and after detection of HP H5N1 at the study site on January 24, 2022. A telemetry study conducted on a subsample of those birds showed no effect of HP H5N1 infection on survival or movement of mallard ducks (13). We collected serum samples (not included in the telemetry study) that enabled us to estimate prevalence of antibodies to IAV nucleoprotein (NP), to IAV HA subtype H5, and to NA subtype N1 before identification of HP H5N1 introduction into the population; document short-term antibody responses in the population after HP H5N1 introduction; examine antibody levels in individual ducks infected with HP H5N1; and address the need

Author affiliations: University of Georgia, Athens, Georgia, USA (D.E. Stallknecht, D.L. Carter, R.L. Poulson); Tennessee Technical University, Cookeville, Tennessee, USA (A.G. Blake-Bradshaw, C.J. Highway, B. Cohen); Cornell University, Ithaca, New York, USA (N.M. Masto); Tennessee Wildlife Resources Agency, Nashville, Tennessee, USA (J.C. Feddersen); St. Jude Children's Research Hospital, Memphis, Tennessee, USA (R. Webby); US Geological Survey, Laurel, Maryland, USA (J.D. Sullivan)

to consider population immunity when evaluating effects of HP H5N1 infection on wild avian species. Duck capture and handling procedures in this study were conducted in accordance with Tennessee Technological University's Institutional Animal Care and Use Committee (IACUC protocol no. 19-20-002) and authorized under Federal Banding Permit nos. 05796 and 24239.

We tested combined cloacal and oropharyngeal swab samples for IAV, including H5 clade 2.3.4.4b, by virus isolation in embryonating chicken eggs and by real-time reverse transcription PCR, as previously described (13). We submitted all H5 nonnegative isolates to the US Department of Agriculture National Veterinary Services Laboratory (Ames, Iowa) for confirmation of subtype and pathogenicity. Duck species tested included mallard (n = 236), northern pintail (*A. acuta*, n = 19), gadwall (*Mareca strepera*, n = 4), and American wigeon (*M. americana*, n = 3). We did not detect HP H5N1 or LP IAV in any samples collected before January 24, 2022 (n = 220). During January 24–31, 2022, the laboratory detected and confirmed HP H5N1 in samples collected from 12/38 (32%) mallards, 3/4 (75%) gadwalls, and 2/2 (100%) American wigeon. Phylogenetic analyses of sequences from a subset of isolated IAV indicated that sequences belonged to genotype A1 of clade 2.3.4.4b viruses, the same genotype as the virus clade first detected in North America in Canada (3).

We tested serum samples for antibodies to IAV NP using a commercial bELISA (IDEXX AI MultiScreen AB test; IDEXX Laboratories, https://www.idexx.com). We further tested samples testing positive (sample to negative absorbance ratio <0.7) for antibodies against H5 and N1 by using hemagglutination inhibition (HI), virus neutralization (VN), and enzyme linked lectin assay (ELLA), as described previously (6,14). We further tested only a subset of samples from the pre–H5N1 detection period. We used 2 attenuated viruses produced by reverse genetics as antigens for HI and VN: reverse genetics BWT, containing HA and NA from the LP A/Blue-winged teal/AI12–4150/Texas/2012 (H5N2), and reverse genetics AST IDCDC-RG71A (H5N8), containing a modified HA and NA from HP 2.3.4.4b A/Astrakhan/3212/2020 (H5N8); remaining gene segments from both viruses were from A/Puerto Rico/8/34. For ELLA, we used A/ruddy turnstone/New Jersey/AI13–2948/2013 (H10N1) as an antigen. We considered samples that tested positive for either antigen at a titer of 32 for HI or 20 for VN positive for H5 antibodies. For ELLA we considered a titer of 80 positive.

IAV NP antibodies were prevalent (79%) in ducks at the study site before introduction of HP H5N1 virus; antibody prevalence increased to 100% after H5N1 was detected (Table 1). Antibody prevalence for H5, based on reactivity to reverse genetics BWT or reverse genetics AST, however, was low before HP H5N1 introduction, as determined by both HI (8%) and VN (25%). By the postdetection sample period, January 30–31, 2022, antibody prevalence increased, as determined by HI (27%) and VN (53%) (Table 1). Antibody prevalence to N1 subtype also increased from 40% before HP H5N1 detection to 86% after detection (Table 1). We observed an increase in the percentage of ducks testing seropositive for H5 after HP H5N1 detection by both HI and

Table 1. Antibodies detected in wintering ducks in study of influenza A virus antibodies in ducks and introduction of highly pathogenic influenza A(H5N1) virus, Tennessee, USA*

Time sampled	Total	HI H5†	VN H5†	ELLA N1‡	Antibodies to H5 and N1§	
					Total	Prevalence, %¶
Pre–H5N1 detection, Nov 7, 2021–Jan 5, 2022						
Total	0/218 (0)	6/63 (10)	21/65 (32)	33/65 (51)	11/65 (17)	13
bELISA-positive	173/218 (79)					
% Testing positive		8	25	40		
H5N1 detection, Jan 24–25, 2022						
Total	14/29 (48)	1/26 (4)	3/26 (12)	15/24 (63)	3/24 (13)	12
bELISA-positive	26/29 (90)					
% Testing positive		4	10	57		
Post–H5N1 detection, Jan 30–31, 2022						
Total	3/15 (20)	4/15 (27)	8/15 (53)	11/13 (85)	8/13 (62)	62
bELISA-positive	15/15 (100)					
% Testing positive		27	53	85		

*Values are no. positive/no. tested (%) except as indicated. For HI, VN, and ELLA, testing was limited to bELISA-positive serum. bELISA, blocking enzyme-linked immunosorbent assay; ELLA, enzyme-linked lectin assay; HI, hemagglutination inhibition; VN, virus neutralization.
†Tests completed with 2 antigens: reverse genetics BWT, HA and NA from A/Blue-winged teal/AI12–4150/Texas/2012 (H5N2) on PR8 backbone; and reverse genetics AST antigen, IDCDC-RG71A (H5N8) with modified HA and NA from A/Astrakhan/3212/2020 (H5N8) on PR8 backbone.
‡Test used A/ruddy turnstone/New Jersey/AI13–2948/2013(H10N1) as antigen.
§Ducks tested positive for antibodies against H5 and N1 as determined by HI, VN, or both, and ELLA.
¶Apparent prevalence in sampled population, adjusted for bELISA results.

Table 2. Antibodies to H5 detected in wintering ducks in a study of influenza A virus antibodies in ducks and introduction of highly pathogenic influenza A(H5N1) virus, Tennessee, USA*

	Hemagglutination inhibition H5†		Virus neutralization H5†	
Time sampled	rg BWT	rg AST	rg BWT	rg AST
Pre–H5N1 detection, Nov 7, 2021–Jan 5, 2022	6/63 (10)	1/63 (2)	21/65 (32)	2/65 (3)
H5N1 detection, Jan 24–25, 2022	1/26 (4)	0/26 (0)	3/24 (13)	1/26 (4)
Post–H5N1 detection, Jan 30–31, 2022	4/15 (27)	3/15 (20)	7/12 (58)	3/12 (25)

*Values are no. positive/no. tested (%). As determined by hemagglutination inhibition and virus neutralization using 2 H5 antigens of North American low pathogenicity IAV (reverse genetics BWT) and goose/Guangdong clade 2.3.4.4b H5 lineage of highly pathogenic IAV (reverse genetics AST). AST, IDCDC-RG71A (H5N8) with modified HA and NA from A/Astrakhan/3212/2020 (H5N8) on PR8 backbone; BWT, HA and NA from A/Blue-winged teal/AI12–4150/Texas/2012 (H5N2) on PR8 backbone; HA, hemagglutinin; HI, hemagglutination inhibition; IAV, influenza A virus; NA, neuraminidase; rg, reverse genetics; VN, virus neutralization.
†Both tests completed with 2 antigens. Reverse genetics BWT antigen: HA and NA from A/Blue-winged teal/AI12–4150/Texas/2012 (H5N2) on PR8 backbone; and reverse genetics AST antigen: IDCDC-RG71A (H5N8). Modified HA and NA from A/Astrakhan/3212/2020 (H5N8) on PR8 backbone.

VN (Table 2). For H5N1-infected ducks, 15/17 (88%) tested seropositive for NP, 1 (6%) tested seropositive for H5 by HI, 2 (12%) were seropositive for H5 by VN, and 12/16 (75%) tested seropositive for N1. Some of those antibody-positive results, especially in postdetection sampling, could have resulted from seroconversion, but still reflect a very low prevalence of antibodies to H5 at time of infection.

Conclusions

Although antibody prevalence to NP was high in ducks before HP H5N1 virus introduction at the site, likely reflecting previous infections with LP IAV, the prevalence of antibodies to H5 and N1 subtypes was low; few (11 [17%]) ducks tested seropositive for both (Table 1). The lack of immunity to H5 and N1 possibly enabled the successful introduction of HP H5N1 into this population and into North America. That pattern was also apparent in individual ducks that were infected with HP H5N1 at the time we collected serum samples. We detected an increase in antibody prevalence with all serologic tests after HP H5N1 introduction; 62% of birds sampled in the postdetection sample period tested seropositive for both H5 and N1. Whether the developing immunity affected subsequent HP H5N1 transmission as birds migrated from this site is unknown, but many (38%) departing birds apparently remained unexposed. The population was not immunologically naive to IAV at the time of HP H5N1 introduction and could have been partially protected from clinical effects caused by existing heterosubtypic immunity; however, that did not prevent infection or rapid transmission through the population. After HP H5N1 introduction, substantial immunity to H5 and N1 was present. Future studies should address whether existing heterosubtypic or developing homosubtypic immunity affected survival or migration of this duck population; such studies could apply to other wild bird species that may be more vulnerable than ducks to HP H5N1. Monitoring IAV in wild migratory populations can inform influenza spillover risks to domestic animals and humans.

About the Author

Dr. Stallknecht is a professor emeritus in the department of population health in the College of Veterinary Medicine at the University of Georgia, Athens, GA. His research focuses on the epidemiology of viral and vectorborne diseases.

References

1. Banyard AC, Bennison A, Byrne AMP, Reid SM, Lynton-Jenkins JG, Mollett B, et al. Detection and spread of high pathogenicity avian influenza virus H5N1 in the Antarctic Region. Nat Commun. 2024;15:7433. https://doi.org/10.1038/s41467-024-51490-8
2. Leguia M, Garcia-Glaessner A, Muñoz-Saavedra B, Juarez D, Barrera P, Calvo-Mac C, et al. Highly pathogenic avian influenza A (H5N1) in marine mammals and seabirds in Peru. Nat Commun. 2023;14:5489. https://doi.org/10.1038/s41467-023-41182-0
3. Youk S, Torchetti MK, Lantz K, Lenoch JB, Killian ML, Leyson C, et al. H5N1 highly pathogenic avian influenza clade 2.3.4.4b in wild and domestic birds: introductions into the United States and reassortments, December 2021–April 2022. Virology. 2023;587:109860. https://doi.org/10.1016/j.virol.2023.109860
4. Diskin ER, Friedman K, Krauss S, Nolting JM, Poulson RL, Slemons RD, et al. Subtype diversity of influenza A

virus in North American waterfowl: a multidecade study. J Virol. 2020;94:e02022–19. https://doi.org/10.1128/JVI.02022-19

5. Kent CM, Ramey AM, Ackerman JT, Bahl J, Bevins SN, Bowman AS, et al. Spatiotemporal changes in influenza A virus prevalence among wild waterfowl inhabiting the continental United States throughout the annual cycle. Sci Rep. 2022;12:13083. https://doi.org/10.1038/s41598-022-17396-5

6. Stallknecht DE, Fojtik A, Carter DL, Crum-Bradley JA, Perez DR, Poulson RL. Naturally acquired antibodies to influenza A virus in fall-migrating North American mallards. Vet Sci. 2022;9:214. https://doi.org/10.3390/vetsci9050214

7. Latorre-Margalef N, Grosbois V, Wahlgren J, Munster VJ, Tolf C, Fouchier RA, et al. Heterosubtypic immunity to influenza A virus infections in mallards may explain existence of multiple virus subtypes. PLoS Pathog. 2013;9:e1003443. https://doi.org/10.1371/journal.ppat.1003443

8. Segovia KM, França MS, Leyson CL, Kapczynski DR, Chrzastek K, Bahnson CS, et al. Heterosubtypic immunity increases infectious dose required to infect mallard ducks with influenza A virus. PLoS One. 2018;13:e0196394. https://doi.org/10.1371/journal.pone.0196394

9. Tarasiuk K, Kycko A, Świętoń E, Bocian Ł, Wyrostek K, Śmietanka K. Homo- and heterosubtypic immunity to low pathogenic avian influenza virus mitigates the clinical outcome of infection with highly pathogenic avian influenza H5N8 clade 2.3.4.4.b in captive mallards (*Anas platyrhynchos*). Pathogens. 2023;12:217. https://doi.org/10.3390/pathogens12020217

10. Latorre-Margalef N, Brown JD, Fojtik A, Poulson RL, Carter D, Franca M, et al. Competition between influenza A virus subtypes through heterosubtypic immunity modulates re-infection and antibody dynamics in the mallard duck. PLoS Pathog. 2017;13:e1006419. https://doi.org/10.1371/journal.ppat.1006419

11. Segovia KM, Stallknecht DE, Kapczynski DR, Stabler L, Berghaus RD, Fotjik A, et al. Adaptive heterosubtypic immunity to low pathogenic avian influenza viruses in experimentally infected mallards. PLoS One. 2017;12:e0170335. https://doi.org/10.1371/journal.pone.0170335

12. Chen YQ, Wohlbold TJ, Zheng NY, Huang M, Huang Y, Neu KE, et al. Influenza infection in humans induces broadly cross-reactive and protective neuraminidase-reactive antibodies. Cell. 2018;173:417–429.e10. https://doi.org/10.1016/j.cell.2018.03.030

13. Teitelbaum CS, Masto NM, Sullivan JD, Keever AC, Poulson RL, Carter DL, et al. North American wintering mallards infected with highly pathogenic avian influenza show few signs of altered local or migratory movements. Sci Rep. 2023;13:14473. PubMed https://doi.org/10.1038/s41598-023-40921-z

14. Stallknecht DE, Kienzle-Dean C, Davis-Fields N, Jennelle CS, Bowman AS, Nolting JM, et al. Limited detection of antibodies to clade 2.3.4.4 A/goose Guandong/1/1996 lineage highly pathogenic H5 avian influenza virus in North American waterfowl. J Wildl Dis. 2020;56:47–57. https://doi.org/10.7589/2019-01-003

Address for correspondence: Rebecca Poulson, 103 Wildlife Health, Department of Population Health, College of Veterinary Medicine, The University of Georgia, Athens, GA 30602, USA; email: rpoulson@uga.edu

Ehrlichia canis in Human and Tick, Italy, 2023

Giovanni Sgroi, Nicola D'Alessio, Vincenzo Veneziano, Giuseppe Rofrano, Giovanna Fusco, Mariaelisa Carbonara, Filipe Dantas-Torres, Domenico Otranto, Roberta Iatta

In August 2023, ehrlichiosis was confirmed in a patient in Italy with a *Haemaphysalis punctata* tick attached to his neck. Gene sequences of *Ehrlichia canis* from the tick and the patient were identical, indicating a potential risk for this uncommon infection for persons participating in outdoor activities.

*E*hrlichia canis (order Rickettsiales, family Anaplasmataceae) is the causative agent of canine monocytic ehrlichiosis and may be incidentally transmitted by brown dog ticks (*Rhipicephalus sanguineus* sensu lato) to a plethora of mammalian hosts, including cats and humans (*1*). In humans, asymptomatic or paucisymptomatic infections have been occasionally reported from the United States (*2*,*3*), Venezuela (*4*,*5*), and Costa Rica (*6*). Despite the risk being relatively uncommon, persons living or visiting environments where ticks and *E. canis* are prevalent in dogs may potentially be at risk for infection (*7*). We report a case of human ehrlichiosis caused by *E. canis* in a patient from Italy, indicating the risk for unconventional tickborne infection in humans participating in outdoor activities in rural areas in Italy.

The Study

In August 2023, a 42-year-old male patient was referred to the Experimental Zooprophylactic Institute of Southern Italy with a tick attached to his neck. The patient had noticed the tick 48 hours after a hike in a rural

Author affiliations: Experimental Zooprophylactic Institute of Southern Italy, Portici, Italy (G. Sgroi, N. D'Alessio, G. Rofrano, "G. Fusco), University of Naples Federico II, Naples, Italy (V. Veneziano), University of Bari Aldo Moro, Bari, Italy (M. Carbonara, D. Otranto, R. Iatta), Aggeu Magalhães Institute, Recife, Brazil (F. Dantas-Torres); City University of Hong Kong, Hong Kong Special Administrative Region, People's Republic of China (D. Otranto)

area of Salerno Province, Campania region, southern Italy. After obtaining the patient's signed informed consent, we removed the tick with fine-tipped tweezers, checked the patient's skin for other ticks, and collected a 7-mL blood sample from his cephalic vein. We used a 2-mL aliquot placed in a Vacutainer (https://www.bd.com) K3-EDTA tube for complete blood count on a CELL-DYN 3700 Hematology Analyzer (Abbott, https://www.abbott.com). We added the remaining 5 mL to a Vacutainer clot activator serum tube for biochemical analysis on a SAT 450 Random Access Analyzer (KPM Analytics, https://www.kpm-analytics.com) after centrifugation for 15 min at 1,500 *g* at room temperature. We classified the tick with regard to developmental stage (larva, nymph, or adult), sex (male or female), and feeding status (engorged or not engorged) by using a Leica MS5 stereomicroscope (https://www.leica-microsystems.com). Then we taxonomically identified the tick by using morphological keys. In addition, we looked for pathogenic microorganisms by performing Romanowsky staining using Diff Stain Quick Kit (ProEko, https://www.proekosrl.com) on smears of the gut, hemolymph, and salivary glands of the tick and peripheral blood of the patient.

We extracted DNA from the tick and the patient's blood by using QIAamp DNA Blood and Tissue kit (QIAGEN, https://www.qiagen.com) and molecularly tested it for tickborne pathogens (*8*,*9*) (Table 1). The tick was also molecularly identified at species level by the amplification of a 248-bp partial fragment of the 16S rRNA gene, with forward (5′-CTGCTCAATGATTTTTTAAATTGCTGT-3′) and reverse (5′-TTACGCTGTTATCCCTAGAG-3′) primers, by using the following thermocycling conditions: 95°C for 10 minutes of initial denaturation followed by 35 cycles of 94°C for 45 seconds, 58°C for 60 seconds, 72°C for 60 seconds, and 72°C for 7 minutes of final extension. We ran all PCRs in a final volume of 50 μL including 5 μL of 10× PCR

Table 1. Targeted pathogens and related PCR protocols used in study of *Ehrlichia canis* in human and tick, Italy, 2023

Pathogen	Target gene	Primer name	Primer sequence, 5′→3′	Amplicon length, bp	Reference
Anaplasma, *Ehrlichia*, *Candidatus* Neoehrlichia spp.	16S rRNA	EHR16-SD EHR16-SR	GGTACCYACAGAAGAAGTCC TAGCACTCATCGTTTACAGC	345	(8)
Ehrlichia canis	*groEL*	Ehr-groel-F Ehr-groel-R	GTTGAAAARACTGATGGTATGCA ACACGRTCTTTACGYTCYTTAAC	590	(9)
Babesia, *Theileria* spp.	18S rRNA	RLB-F RLB-R	GAGGTAGTGACAAGAAATAACAATA TCTTCGATCCCCTAACTTTC	460–520	(8)
Borrelia burgdorferi sensu lato complex	*Flagellin*	FLA1 FLA2	AGAGCAACTTACAGACGAAATTAAT CAAGTCTATTTTGGAAAGCACCTAA	482	(8)
Coxiella burnetii	IS1111a	Trans-1 Trans-2	TATGTATCCACCGTAGCCAGT CCCAACAACACCTCCTTATTC	687	(8)
Rickettsia spp.	*gltA*	CS-78F CS-323R	GCAAGTATCGGTGAGGATGTAAT GCTTCCTTAAAATTCAATAAATCAGGAT	401	(8)

buffer II, 6 µL of 25 mmol MgCl$_2$, 5 µL of 1.25 mmol of dNTPs, 0.5 µL of 100 pmol/µL of each primer, and 1.25 U of AmpliTaq Gold (Applied Biosystems, https://www.thermofisher.com). We sequenced the purified amplicons in both directions by using a BigDye Terminator v3.1 Cycle Sequencing Kit in a 3130 Genetic Analyzer (Applied Biosystems), then used Geneious version 9.0 (https://www.geneious.com) for editing and analysis. We compared the resulting sequences with those available in the GenBank database by using Nucleotide BLAST (https://blast.ncbi.nlm.nih.gov/Blast.cgi) and performed the phylogenetic analysis by using the maximum-likelihood method based on the

general time reversible model with gamma distribution to assess evolutionary differences among sites (+G) selected by best-fit model (10) with MEGA X software (11). Our study was approved by the Experimental Zooprophylactic Institute of Southern Italy within the framework of a memorandum of agreement (authorization no. IZSM-DIMBA/23) with the Interdisciplinary Department of Medicine, University of Bari Aldo Moro, according to national regulations.

We identified the tick removed from the patient as an engorged female *Haemaphysalis punctata* (GenBank accession no. PP419005). According to PCR testing, the tick and the patient's blood scored
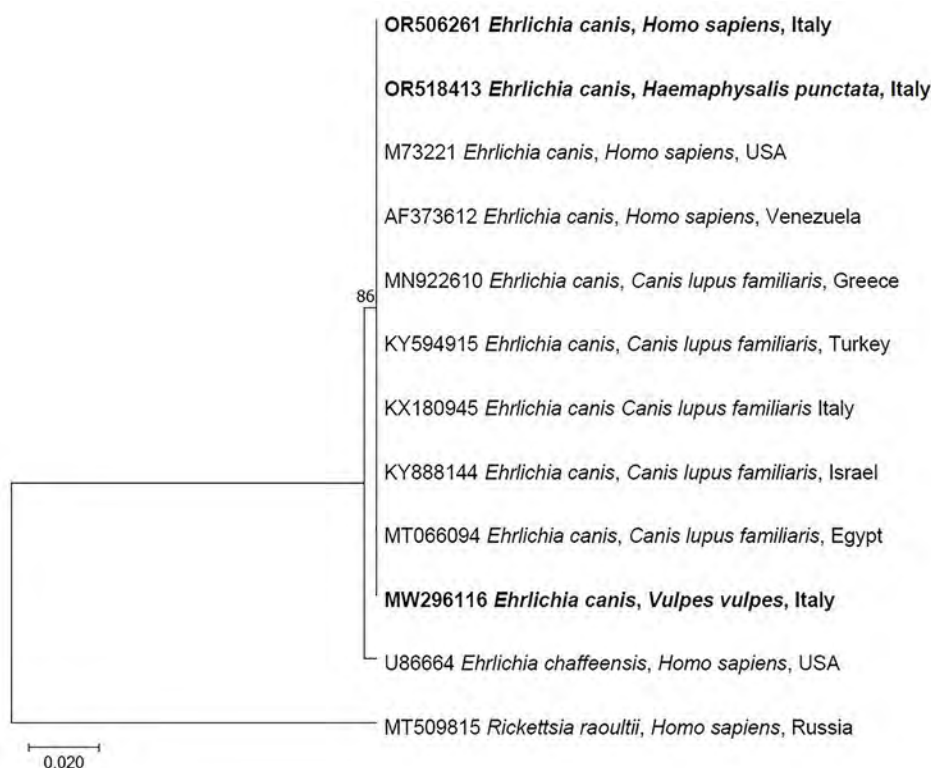
Figure. Maximum-likelihood phylogenetic tree of *Ehrlichia canis* 16S rRNA sequences detected in a patient's blood and in a *Haemaphysalis punctata* tick removed from the patient in Italy, 2023. Boldface indicates sequences amplified in the study area. The tree was inferred including 12 partial sequences (281 bp) under the maximum-likelihood method based on the general time reversible model (10) and a discrete gamma distribution was used to model evolutionary rate differences among sites (5 categories) (+*G*, parameter = 0.3727). The percentage of trees in which the associated taxa clustered together is shown next to the branches. A consensus sequence of *Rickettsia raoultii* (MT509815) in a human from Russia was used as outgroup. The tree with the highest log likelihood (−559.69) is shown, obtained from 1,000 bootstrap replications with MEGA X software (11). Scale bar indicates nucleotide substitutions per site.

positive for a fragment of the *E. canis* 16S rRNA gene. The sequences we obtained (GenBank accession nos. OR518413 and OR506261) were identical to each other (100% query cover) and to those of *E. canis* obtained from a red fox (*Vulpes vulpes*) in the same study area, humans from United States and Venezuela, and dogs from Mediterranean Basin countries (Italy, Greece, Israel, Egypt, and Turkey) (Figure). We confirmed the molecular identification of *E. canis* from the tick and the patient's blood by amplifying the *groEL* gene. The sequences obtained were identical to each other (GenBank accession no. PP839296). Other pathogens were not detected by PCR or cytologic examination of stained smears. No major clinicopathologic abnormalities were detected in the patient, except severely increased alanine aminotransferase and mildly decreased total leukocyte count and aspartate aminotransferase (Table 2). Three days after the first visit, the patient complained of mild symptoms (i.e., fever of 38°C, headache, muscle pain, and malaise) which spontaneously healed within a week, without antimicrobial drug treatment.

Conclusions

Data suggest that *E. canis* may infect persons bitten by *H. punctata* ticks in Europe, which may represent a potential risk for persons participating in outdoor activities (e.g., hiking), where those ticks are commonly found on vegetation from spring to autumn in southern Italy (*12*). The finding of *E. canis* DNA in the tick removed from the *E. canis*–positive patient indicates the potential involvement of *H. punctata* ticks in transmission of the pathogen. Although no experimental evidence of the competence of this tick species for transmitting *E. canis* is available, circumstantial evidence suggests its participation as a vector. For instance, in southern Italy, *H. punctata* ticks parasitize humans (*7*) and harbor *E. canis* DNA (*13*).

The similarity of *E. canis* sequences from the tick and patient with those of foxes from the same study area (GenBank accession no. MW296116) suggests circulation of the same *E. canis* genotype among dogs, humans, and wildlife. A previous analysis of the *E. canis* TRP36 gene sequences from different countries revealed the occurrence of the US genogroup in foxes from southern Italy (*14*). The US genogroup is the most common genotype found in dogs and ticks in Eurasia (*14*). The role of foxes as wild reservoirs of *E. canis* needs to be interpreted with caution, especially considering that dogs are the principal reservoirs of this bacterium. The absence of *E. canis* inclusions in the stained smears from the tick and the patient

Table 2. Complete blood count and serum chemistry for patient positive for *Ehrlichia canis* infection, Italy, 2023*

Parameter	Value (reference range)
Hemoglobin, g/dL	15.0 (13.5–18.0)
Platelets, 10³/μL	247.0 (150.0–400.0)
Mean platelet volume, fL	7.8 (6.0–11.5)
Leukocytes, 10³/μL	**3.7 (4.0–10.0)**
Erythrocytes, 10⁶ μL	4.9 (4.5–5.9)
Hematocrit, %	46.8 (41.0–53.0)
Mean corpuscular volume, fL	94.6 (80.0–100.0)
Mean corpuscular hemoglobin, pg/dL	30.3 (26.0–34.0)
Mean corpuscular hemoglobin concentration, g/dL	32.0 (31.0–37.0)
Red cell distribution width, %	13.7 (11.5–14.5)
Hemoglobin distribution width, %	2.6 (2.0–3.2)
Neutrophils, %	43.1 (40.0–74.0)
Lymphocytes, %	48.0 (19.0–48.0)
Monocytes, %	5.7 (3.4–9.0)
Eosinophils, %	1.2 (0–8.0)
Basophils, %	1.0 (0–1.5)
Urea, mg/dL	33.0 (20.0–50.0)
Creatinine, mg/dL	1.2 (0.7–1.3)
Cholesterol, mg/dL	198.0 (<200)
High-density lipoprotein-cholesterol, mg/dL	70.0 (40.0–150.0)
Triglycerides, mg/dL	86.0 (<150)
Aspartate aminotransferase, UI/L	**36.0 (<34)**
Alanine aminotransferase, UI/L	**122.0 (10.0–49.0)**

*Boldface indicates out of reference range. fL,femtoliter.

was somewhat expected considering the low sensitivity of the method, even for detecting morulae of other ehrlichial species that are more frequently found in human patients (*15*). The patient's clinicopathological abnormalities (i.e., decreased leukocytes and aspartate transaminase and increased alanine transaminase) and clinical signs and symptoms (i.e., fever of 38°C, headache, muscle pain, and malaise) are in accordance with previous data (*2,5*). Future molecular surveys assessing the circulation of *E. canis* in persons, dogs, and wildlife exposed to ticks should ultimately increase awareness about this zoonosis and be used to establish proper strategies to mitigate the risk for transmission.

About the Author

Dr. Sgroi is an associate and researcher at the Experimental Zooprophylactic Institute of Southern Italy.

His main research activity is focused on biology, epidemiology, and control of vectorborne pathogens of zoonotic concern in wildlife and humans.

References

1. Mylonakis ME, Harrus S, Breitschwerdt EB. An update on the treatment of canine monocytic ehrlichiosis (*Ehrlichia canis*). Vet J. 2019;246:45–53. https://doi.org/10.1016/j.tvjl.2019.01.015
2. Maeda K, Markowitz N, Hawley RC, Ristic M, Cox D, McDade JE. Human infection with *Ehrlichia canis*, a leukocytic rickettsia. N Engl J Med. 1987;316:853–6. https://doi.org/10.1056/NEJM198704023161406
3. Ewing SA, Johnson EM, Kocan KM. Human infection with *Ehrlichia canis*. N Engl J Med. 1987;317:899–900. https://doi.org/10.1056/NEJM198710013171412
4. Perez M, Rikihisa Y, Wen B. *Ehrlichia canis*-like agent isolated from a man in Venezuela: antigenic and genetic characterization. J Clin Microbiol. 1996;34:2133–9. https://doi.org/10.1128/jcm.34.9.2133-2139.1996
5. Perez M, Bodor M, Zhang C, Xiong Q, Rikihisa Y. Human infection with *Ehrlichia canis* accompanied by clinical signs in Venezuela. Ann N Y Acad Sci. 2006;1078:110–7. https://doi.org/10.1196/annals.1374.016
6. Bouza-Mora L, Dolz G, Solórzano-Morales A, Romero-Zuñiga JJ, Salazar-Sánchez L, Labruna MB, et al. Novel genotype of *Ehrlichia canis* detected in samples of human blood bank donors in Costa Rica. Ticks Tick Borne Dis. 2017;8:36–40. https://doi.org/10.1016/j.ttbdis.2016.09.012
7. Otranto D, Dantas-Torres F, Giannelli A, Latrofa MS, Cascio A, Cazzin S, et al. Ticks infesting humans in Italy and associated pathogens. Parasit Vectors. 2014;7:328. https://doi.org/10.1186/1756-3305-7-328
8. Sgroi G, Iatta R, Lia RP, D'Alessio N, Manoj RRS, Veneziano V, et al. Spotted fever group rickettsiae in *Dermacentor marginatus* from wild boars in Italy. Transbound Emerg Dis. 2021;68:2111–20. https://doi.org/10.1111/tbed.13859
9. Cicculli V, Masse S, Capai L, de Lamballerie X, Charrel R, Falchi A. First detection of *Ehrlichia minasensis* in *Hyalomma marginatum* ticks collected from cattle in Corsica, France. Vet Med Sci. 2019;5:243–8. https://doi.org/10.1002/vms3.140
10. Nei M, Kumar S. Molecular evolution and phylogenetics. New York: Oxford University Press; 2000.
11. Kumar S, Stecher G, Li M, Knyaz C, Tamura K. MEGA X: Molecular Evolutionary Genetics Analysis across computing platforms. Mol Biol Evol. 2018;35:1547–9. https://doi.org/10.1093/molbev/msy096
12. Dantas-Torres F, Otranto D. Species diversity and abundance of ticks in three habitats in southern Italy. Ticks Tick Borne Dis. 2013;4:251–5. https://doi.org/10.1016/j.ttbdis.2012.11.004
13. Chisu V, Foxi C, Mannu R, Satta G, Masala G. A five-year survey of tick species and identification of tick-borne bacteria in Sardinia, Italy. Ticks Tick Borne Dis. 2018;9:678–81. https://doi.org/10.1016/j.ttbdis.2018.02.008
14. Bezerra-Santos MA, Nguyen VL, Iatta R, Manoj RRS, Latrofa MS, Hodžić A, et al. Genetic variability of *Ehrlichia canis* TRP36 in ticks, dogs, and red foxes from Eurasia. Vet Microbiol. 2021;255:109037. https://doi.org/10.1016/j.vetmic.2021.109037
15. Centers for Disease Control and Prevention. Tickborne diseases of the US: a reference manual for health care providers, 6th edition. Colorado (CO); The Centers; 2022.

Address for correspondence: Giovanni Sgroi, Experimental Zooprophylactic Institute of Southern Italy, 2 Via Salute, 80055 Portici, Naples, Italy; email: giovanni.sgroi@izsmportici.it

Feline Panleukopenia Virus in a Marsican Brown Bear and Crested Porcupine, Italy, 2022–2023

Georgia Diakoudi, Gianvito Lanave, Shadia Berjaoui, Costantina Desario,
Giovanni Di Teodoro, Violetta Iris Vasinioti, Francesco Pellegrini, Sabrina V.P. Defourny,
Stefania Salucci, Antonio Cocco, Alessio Lorusso, Vito Martella, Nicola Decaro

The virus species *Protoparvovirus carnivoran 1* encompasses pathogens that infect both domestic and wild carnivores, including feline panleukopenia virus. We identified and characterized feline panleukopenia virus strains in a Marsican brown bear (*Ursus arctos marsicanus*) and a crested porcupine (*Hystrix cristata*) in Italy, extending the known host range of this virus.

Parvoviruses (genus *Protoparvovirus*, family Parvoviridae) are small, nonenveloped, single-stranded DNA viruses ≈4.5–5.5-kb long. Their linear DNA genome contains 2 major open reading frames encoding for 2 nonstructural proteins (1 and 2) and 2 capsid proteins (VP1 and VP2). Feline panleukopenia virus (FPV) and the closely related canine parvovirus (CPV or CPV-2), included in the species *Protoparvovirus carnivoran 1*, are highly contagious pathogens that cause acute and often fatal diseases in domestic and wild felids and canids (*1*).

FPV and CPV are closely related genetically and antigenically but differ in their host range and pathogenicity. The biological differences are determined by a few amino acid mutations in the VP2 capsid protein that modulate the ability to bind to cellular transferrin receptor type 1 (*2*). Parvoviruses have long been considered to be species specific; however, FPV and CPV-2 variants (i.e., 2a, 2b, and 2c) have been reported in a wide variety of wild carnivores. Of note, some species (e.g., cats, foxes, badgers, and giant pandas)

Author affiliations: University of Bari Aldo Moro, Bari, Italy
G. Diakoudi, G. Lanave, C. Desario, V.I. Vasinioti, F. Pellegrini,
V. Martella, N. Decaro); Istituto Zooprofilattico Sperimentale di
Abruzzo e Molise 'Giuseppe Caporale,' Teramo, Italy (S. Berjaoui,
G. Di Teodoro, S.V.P. Defourny, S. Salucci, A. Cocco, A. Lorusso);
University of Veterinary Medicine, Budapest, Hungary (V. Martella)

may be infected by both FPV and CPV strains (*3*). We conducted a molecular investigation for *Protoparvovirus carnivoran 1* viruses in wildlife in Italy.

The Study

During January 2022–May 2023, we collected tissue samples by convenience sampling from 89 animals: 44 wolves (*Canis lupus*), 26 red foxes (*Vulpes vulpes*), 15 European badgers (*Meles meles*), 2 stone martes (*Martes foina*), 1 Marsican brown bear (*Ursus arctos marsicanus*), and 1 crested porcupine (*Hystrix cristata*). All animals were found already dead in the regions of Abruzzo and Molise, Italy, and sample collection was conducted during routine necropsy procedures at Istituto Zooprofilattico Sperimentale of Abruzzo and Molise 'Giuseppe Caporale.' All tissues were temporarily stored at −20°C before being transported by cold chain to the Infectious Diseases Unit of the Department of Veterinary Medicine, University of Bari, Bari, Italy.

We homogenized the tissues (10% wt/vol) in Dulbecco's modified Eagle medium and extracted viral DNA from the supernatant of the homogenates of all samples by using the IndiSpin Pathogen Kit (Indical Bioscience GmbH, https://www.indical.com), according to the manufacturer's instructions. We used quantitative PCR (qPCR) to screen DNA extracts for the presence of CPV/FPV DNA (*4*) and further characterized positive samples by qPCR based on minor groove binder able to differentiate CPV types 2a/2b and 2b/2c and CPV/FPV, as described previously (*4*).

Overall, 52 (58.4%) of 89 samples tested positive in the qPCR screening for CPV/FPV DNA (Table 1) with a geometric mean value of 8.91×10^3 copies of parvovirus DNA/10 μL of template (range 8.48×10^0 to 5.71×10^6 DNA copies/10 μL of template), including the samples from the Marsican brown bear and

Table 1. Results of testing for *Protoparvovirus carnivoran 1* viruses in wild animals, Abruzzo and Molise regions, Italy, January 2022–May 2023*

Animal species	No. animals tested	No. animals positive				Total no. (%) samples positive, tissue type
		FPV	CPV-2a	CPV-2b	CPV-2c	
Wolf (*Canis lupus*)	44	7	4	11	8	30 (68.2), I = 27, S = 3
Red fox (*Vulpes vulpes*)	26	3	7	0	2	12 (46.2), I = 12
European badger (*Meles meles*)	15	5	0	2	0	7 (46.7), I = 6, MLN = 1
Stone martens (*Martes foina*)	2	1	0	0	0	1 (50), I = 1
Marsican brown bear (*Ursus arctos marsicanus*)	1	1	0	0	0	1 (100), I = 1
Crested porcupine (*Hystrix cristata*)	1	1	0	0	0	1 (100), MLN = 1
Total	89	18	11	13	10	52 (58.4), I = 47, S = 3, MLN = 2

*CPV, canine parvovirus; FPV, feline panleukopenia virus; I, intestine; MLN, mesenteric lymph node; S, spleen.

the crested porcupine. We characterized the bear and porcupine viruses as FPV by using the minor groove binder qPCR with viral loads of 8.40×10^5 (bear) and 4.43×10^5 (porcupine) DNA copies/10 µL of template.

To acquire the complete viral genome sequence of the FPV strains from the 2 animals, we designed 2 multiplex PCR protocols amplifying 15 PCR-tiling amplicons of 388–511 bp (Table 2), following an ARTIC-like strategy (*5*). We designed primer pairs based on the consensus sequence of *Protoparvovirus carnivoran1* genomes recovered from GenBank. We performed PCR by using TaKaRa La Taq polymerase (Takara Bio Europe, https://www.takarabio.com). We used 500 ng of equimolar pooled PCR products for each FPV-positive sample as the input to the libraries prepared by using Ligation Sequencing Kit (SQK-LSK110; Oxford Nanopore Technologies, https://nanoporetech.com), according to the manufacturer's guidelines. We sequenced the libraries independently by using flongle flowcell FLO-FLG001, R9.4.1, adapted in a MinION Mk1C platform (Oxford Nanopore Technologies) for 24 hours each. We subjected FastQ MinION files to quality control, trimming, and reference assembly by using Minimap2 plugin implemented in Geneious Prime software v.2021.2.2 (Biomatters Ltd., https://www.geneious.com).

We generated the complete coding regions of the genomes for FPV strains ITA/2023/bear/74 (submitted to GenBank under accession no. OR602717) and ITA/2023/hystrix/213 (submitted to GenBank

Table 2. Oligonucleotides used for the multiplex PCR protocols based on ARTIC-like strategy used in study of feline panleukopenia virus in wild animals, Abruzzo and Molise, Italy, January 2022–May 2023*

Primer	Sequence, 5′ → 3′	Amplicon size, bp
CPV1_left	AATGATAGGCGGTTTGTGTGTTT	396
CPV1_right	CAACTTCCGATTCCCAGTCCAT	396
CPV2_left	CCAATTCAAAATGAAGAGCTAACATCTT	410
CPV2_right	GTCACCCATTCACTATCTTCTGCA	410
CPV3_left	TGGAGTAGATGGTTGGTGACTCT	416
CPV3_right	ACCAAGTCCCGCAAAGTACATT	416
CPV4_left	AGCACACTTTACACTGAACAAATGA	401
CPV4_right	GCTATAGCGTGACAAACTTTAATCCA	401
CPV5_left	AGCAAGAACAAAAACAGCATTTGAA	402
CPV5_right	TGATCAATTCTAATTGTTTGTCCAGAACA	402
CPV6_left	AAAAATTTAATTTGGATTGAAGAAGCTGGT	407
CPV6_right	CCTTCTTGTATTTTAGGCTCCGC	407
CPV7_left	TGAATCAACCATGGCTAACTATACACA	393
CPV7_right	GGAGGTGCCATCGTACCTTAATC	393
CPV8_left	TGGTCCGAAATAGAGGCAGACC	393
CPV8_right	CCCCCAATCTTTAGCGTCCTTA	393
CPV9_left	GCTGCTTATCTTCGCTCTGGTA	412
CPV9_right	AAATCCCCACACCCCCAGAA	412
CPV10_left	GCACCAATGAGTGATGGAGCA	410
CPV10_right	TCACTCATAGTATTAACAATTAGTTGCCA	410
CPV11_left	TGCACAAATTGTAACACCTTGGT	388
CPV11_right	ATTTGTTGGTGTGCCACTAGTTC	388
CPV12_left	ACCAACCATACCAACTCCATGG	411
CPV12_right	TAACCAACCTCAGCTGGTCTCA	411
CPV13_left	GGAGTTCAACAAGATAAAAGACGTGG	396
CPV13_right	ACCTCCAATTGGATCTGTTGGT	396
CPV14_left	TCCAGAAGGAGATTGGATTCAAAATATT	411
CPV14_right	TTCCAAGTATGAGAGGCTCTTAGTT	411
CPV15_left	TTGATACTGACTTAAAACCAAGACTTCA	511
CPV15_right	ACAGTTATTGTATACCATATAACAAACCTTCT	511

*ARTIC-like strategy as shown in (*5*). CPV, canine parvovirus.
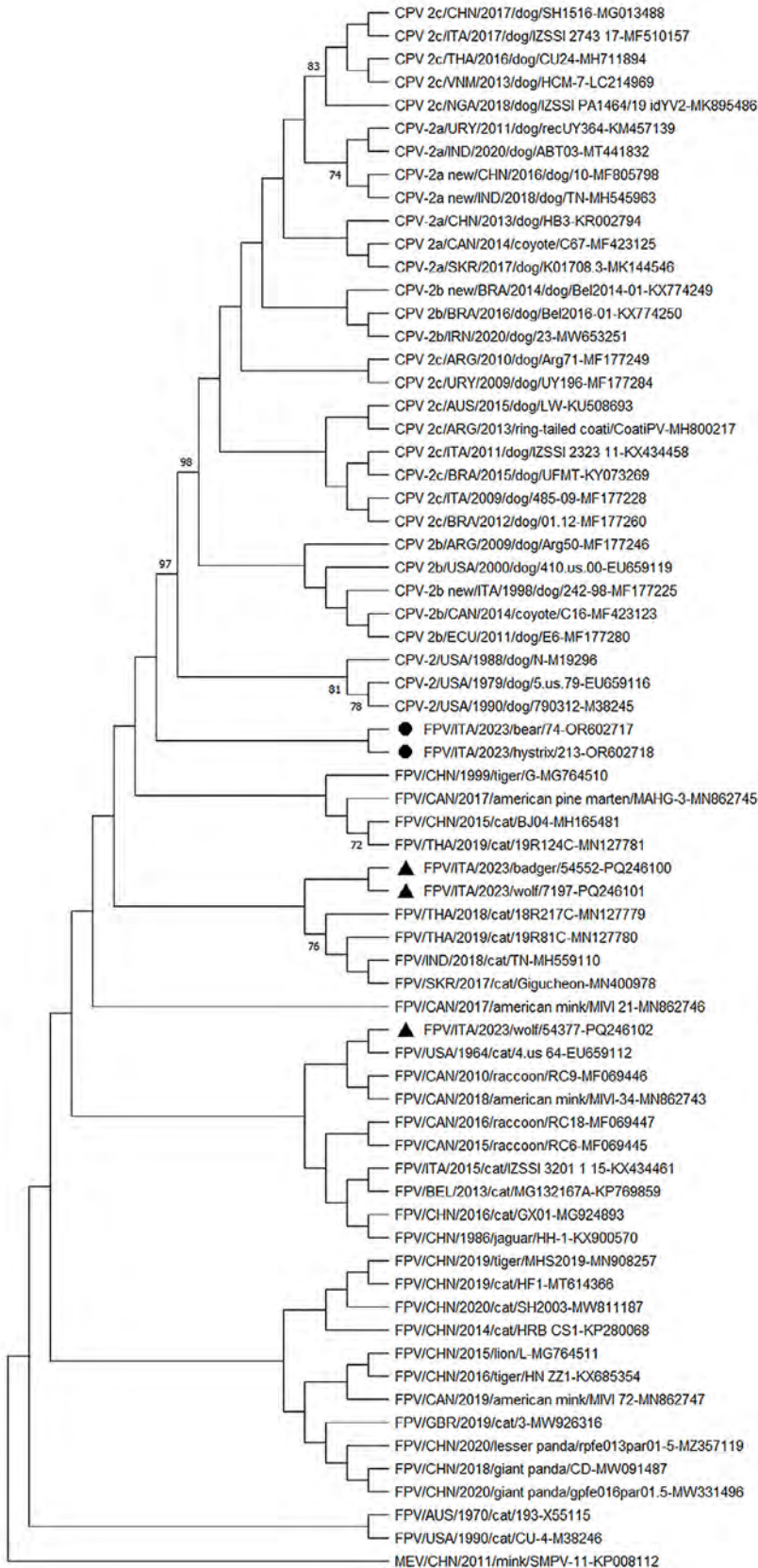
Figure. Neighbor-joining capsid protein 2 (VP2)–based phylogenetic tree of *Protoparvovirus carnivoran 1* from study of feline panleukopenia virus (FPV) in wild animals, Abruzzo and Molise, Italy, January 2022–May 2023. The tree was elaborated by using a 584-aa long alignment of the VP2 sequences of the FPV strains generated in the study and the cognate sequences of *Protoparvovirus carnivoran 1* strains retrieved from GenBank. The tree was constructed by using MEGA X version 10.0.5 software (https://www.megasoftware.net) and the maximum-likelihood method, the Jones-Taylor-Thornton substitution model, and bootstrapping up to 1,000 replicates. Bootstrap values >70% are shown. Black bullets indicate FPV strains from a Marsican brown bear (ITA/2023/bear/74 (GenBank accession no. OR602717) and a crested porcupine ITA/2023/hystrix/213 (accession no. OR602718). The black triangles indicate FPV strains from other wildlife animals in the same study: ITA/2023/badger/54552 (accession no. PQ246100), ITA/2023/wolf/7197 (accession no. PQ246101), and ITA/2023/wolf/54377 (accession no. PQ246102). MEV (accession no. KP008112) was used as an outgroup. Scale bar indicates number of amino acid substitutions per site. CPV, canine parovirus; MEV, mink enteritis virus; FPV, feline panleukopenia virus.

under accession no. OR602718). Sequence alignment of the complete VP2 genomic region revealed 2 aa mutations, 103-Val to Ala in both capsid sequences and 232-Val to Ile in the porcupine capsid, which are 2 key residues defining the biological properties and host range of CPV and FPV (2). VP2 residues 103- and 232- are Val in reference FPV strains, and they are replaced by Ala and Ile in CPV-2 strains. Phylogenetic analysis of the complete amino acid sequence of the VP2 gene indicated that the 2 FPV strains ITA/2023/bear/74 and ITA/2023/hystrix/213 were segregated together but separately from other FPV and CPV strains. Of note, sequencing of the FPV strains detected in other species (wolf and badger) evidenced circulation of ≥3 different FPV subclades/strains in the sampled animals (Figure). Also, based on our results and the geographic areas where the samples were collected, we can hypothesize that there could be an epidemiologic connection via either direct/indirect contact between porcupines and bears or other cohabiting wild animal species.

Immunofluorescence analysis of the mesenteric lymph node tissues of the crested porcupine detected parvovirus antigens (Appendix Figure, https://wwwnc.cdc.gov/EID/article/30/12/24-0505-App1.pdf). However, immunofluorescence analysis conducted on the bear samples did not allow correct interpretation because of advanced postmortem degradation of the intestinal tissue.

Conclusions

Serologic studies performed for several bear species (members of the family Ursidae) have shown evidence of exposure to FPV/CPV (6–8). Two serologic studies involving Marsican brown bears reported seroprevalences as high as 40% (7) and 100% (8) for FPV/CPV, although those tests do not differentiate between CPV-2 and FPV. The possibility that FPV and CPV can infect bears has also been confirmed by detection and molecular characterization of FPV and CPV-2a from giant pandas in China (9,10). In both of those instances, the VP2-coding region presented unusual amino acid mutations (i.e., 299-Gly to Glu in the FPV virus and 370-Arg to Gln in the CPV-2a strain). Whether those unique amino acid variations affected the host range of the parvovirus strains remains unknown.

A case report from 1984 in Canada described a suspected parvovirus infection in porcupines that exhibited clinical signs suggestive of parvoviral infection (11). However, electron microscopy, serologic tests, and virologic investigations did not confirm the etiology.

Recently, several new parvoviruses (e.g., bocaparvoviruses and bufaviruses) have been discovered in domestic and wild animals (12). CPV and FPV seem to be endemic to wildlife populations and have shown continuous evolution over the years; CPV/FPV-like strains have emerged with a broadened host range (3,13). Domestic pets are regarded as a source of FPV and CPV strains for wildlife carnivores through spillover infections (3,14). However, wildlife hosts may also serve as virus reservoirs and sources of infection for the domestic animal population in a perpetual cycle involving 2-way transmission among susceptible hosts. In our study, prevalence of CPV and FPV virus in wildlife was higher than expected (3,15). Genome sequencing of FPV strains detected from nonconventional FPV/CPV hosts, the Marsican brown bear and the crested porcupine, revealed amino acid mutations in key residues controlling host range and receptor affinity. Our detection of FPV strains in a Marsican brown bear and in a crested porcupine in Italy extends the known host range of this virus.

About the Author

Dr. Diakoudi is a researcher at the University of Bari, Bari, Italy. Her research interests cover virus discovery in animals, with particular focus on viruses with zoonotic potential.

References

1. Cotmore SF, Agbandje-McKenna M, Canuti M, Chiorini JA, Eis-Hubinger AM, Hughes J, et al.; ICTV Report Consortium. ICTV virus taxonomy profile: Parvoviridae. J Gen Virol. 2019;100:367–8. https://doi.org/10.1099/jgv.0.001212
2. Callaway HM, Welsch K, Weichert W, Allison AB, Hafenstein SL, Huang K, et al. Complex and dynamic interactions between parvovirus capsids, transferrin receptors, and antibodies control cell infection and host range. J Virol. 2018;92:e00460-18. https://doi.org/10.1128/JVI.00460-18
3. Ndiana LA, Lanave G, Desario C, Berjaoui S, Alfano F, Puglia I, et al. Circulation of diverse protoparvoviruses in wild carnivores, Italy. Transbound Emerg Dis. 2021;68:2489–502. https://doi.org/10.1111/tbed.13917
4. Decaro N, Desario C, Lucente MS, Amorisco F, Campolo M, Elia G, et al. Specific identification of feline panleukopenia virus and its rapid differentiation from canine parvoviruses using minor groove binder probes. J Virol
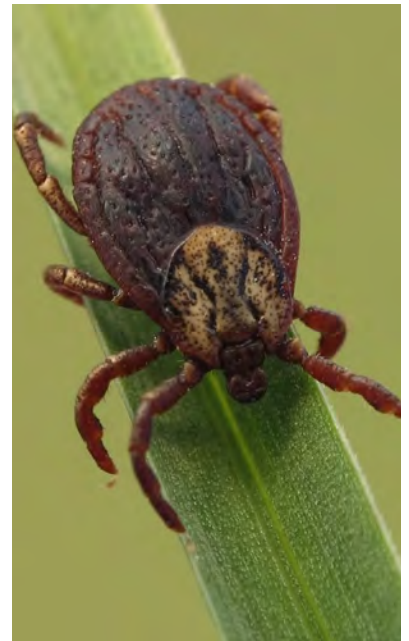
Methods. 2008;147:67–71. https://doi.org/10.1016/j.jviromet.2007.08.006

5. Quick J, Grubaugh ND, Pullan ST, Claro IM, Smith AD, Gangavarapu K, et al. Multiplex PCR method for MinION and Illumina sequencing of Zika and other virus genomes directly from clinical samples. Nat Protoc. 2017;12:1261–76. https://doi.org/10.1038/nprot.2017.066

6. Dunbar MR, Cunningham MW, Roof JC. Seroprevalence of selected disease agents from free-ranging black bears in Florida. J Wildl Dis. 1998;34:612–9. https://doi.org/10.7589/0090-3558-34.3.612

7. Marsilio F, Tiscar PG, Gentile L, Roth HU, Boscagli G, Tempesta M, et al. Serologic survey for selected viral pathogens in brown bears from Italy. J Wildl Dis. 1997;33:304–7. https://doi.org/10.7589/0090-3558-33.2.304

8. Di Francesco CE, Gentile L, Di Pirro V, Ladiana L, Tagliabue S, Marsilio F. Serologic evidence for selected infectious diseases in Marsican brown bears (*Ursus arctos marsicanus*) in Italy (2004–09). J Wildl Dis. 2015;51:209–13. https://doi.org/10.7589/2014-01-021

9. Yi S, Liu S, Meng X, Huang P, Cao Z, Jin H, et al. Feline panleukopenia virus With G299E substitution in the VP2 protein first identified from a captive giant panda in China. Front Cell Infect Microbiol. 2022;11:820144. https://doi.org/10.3389/fcimb.2021.820144

10. Guo L, Yang SL, Chen SJ, Zhang Z, Wang C, Hou R, et al. Identification of canine parvovirus with the Q370R point mutation in the VP2 gene from a giant panda (*Ailuropoda melanoleuca*). Virol J. 2013;10:163. https://doi.org/10.1186/1743-422X-10-163

11. Frelier PF, Leininger RW, Armstrong LD, Nation PN, Povey RC. Suspected parvovirus infection in porcupines. J Am Vet Med Assoc. 1984;185:1291–4.

12. Jager MC, Tomlinson JE, Lopez-Astacio RA, Parrish CR, Van de Walle GR. Small but mighty: old and new parvoviruses of veterinary significance. Virol J. 2021;18:210. https://doi.org/10.1186/s12985-021-01677-y

13. Hoelzer K, Parrish CR. The emergence of parvoviruses of carnivores. Vet Res. 2010;41:39. https://doi.org/10.1051/vetres/2010011

14. Behdenna A, Lembo T, Calatayud O, Cleaveland S, Halliday JEB, Packer C, et al. Transmission ecology of canine parvovirus in a multi-host, multi-pathogen system. Proc Biol Sci. 1899;2019:286.

15. Miranda C, Santos N, Parrish C, Thompson G. Genetic characterization of canine parvovirus in sympatric free-ranging wild carnivores in Portugal. J Wildl Dis. 2017;53:824–31. https://doi.org/10.7589/2016-08-194

Address for correspondence: Nicola Decaro, Department of Veterinary Medicine, University of Bari, Italy, S.p. per Casamassima Km 3, 70010, Valenzano, Bari, Italy; email: nicola.decaro@uniba.it

Lobomycosis in Amazon Region, Bolivia, 2022

Maria I. Méndez, Rony Colanzi, Jose A. Suárez, Homero Penagos,
Carolina Hernandez, Ruth Garcia-Redondo, Juan D. Ramirez, Alberto Paniz-Mondolfi

We report a patient with lobomycosis caused by *Paracoccidioides loboi* fungi in the Andes-Amazon region of Bolivia. We examined clinical, epidemiologic, and phylogenetic data and describe potential transmission/environmental aspects of infection. Continued surveillance and identification of lobomycosis cases in South America are crucial to prevent the spread of this disease.

Lobomycosis, also known as lacaziosis, is a rare chronic fungal infection primarily involving the skin and subcutaneous tissues caused by the dimorphic Onygenales fungus *Paracoccidioides loboi* (also known as *Lacazia loboi*). It is endemic to Central and South America, particularly within the Amazon rainforest, although its precise geographic boundaries remain poorly delineated and appear to be expanding (*1*). The first documented case of lobomycosis in Bolivia was reported in 1982 (*2*). Since then, 2 additional cases have been reported, distributed across the department of Pando in Bolivia in close proximity to Brazil (*3*).

Despite an increasing number of case reports, gaps persist in understanding the eco-epidemiologic and biogeographic aspects of lobomycosis, especially across the vast regions of the Andes. We report a patient from Cobija, located in the Pando Department of Bolivia, who had lobomycosis caused by *P. loboi*. We also describe the epidemiology and phylogeography of lobomycosis and the need for continued research to determine the geographic reach of this fungal infection across regions of the Andes in South America.

Author affiliations: Centro Nacional de Enfermedades Tropicales, Santa Cruz, Bolivia (M.I. Méndez); Laboratorio Catedral, Santa Cruz (R. Colanzi); Universidad Internacional Sek Quito, Quito, Ecuador (J.A. Suárez); Universidad Autónoma de Chiriquí, Chiriquí, Panama (H. Penagos); Icahn School of Medicine at Mount Sinai, New York, New York, USA (C. Hernandez, R. Garcia-Redondo, J.D. Ramirez, A. Paniz-Mondolfi)

The Study

A 71-year-old man, originally from Cobija in northern Bolivia, sought care at Centro Nacional de Enfermedades Tropicales (CENETROP) in Santa Cruz, Bolivia, in December 2022. He reported longstanding cutaneous lesions on his left ear, associated with pruritus and a chronic, insidious headache. He recalled that the lesions began when he was 11 years of age after he was bitten by a mosquito while playing in the Arroyo Virtudes river in his hometown in Pando Department, Bolivia. The lesions slowly progressed from single nodules to a confluent, enlarged nodular plaque. Despite multiple consultations with local shamans and healthcare providers, including 2 instances of surgical removal by otolaryngologists for presumed pinna perichondritis, a precise etiologic diagnosis remained elusive, and the patient remained untreated for 60 years with invariable recurrence of lesions.

Physical examination revealed that the entire left ear was replaced by keloid-like confluent nodular lesions, which appeared infiltrated and hyperpigmented with overriding telangiectasias (Figure 1, panel A). Patchy squamous crusted and eroded areas were noted on the helix and lobule. No noticeable lymphadenopathy existed, and the rest of the physical examination was unremarkable. Differential diagnoses included diffuse cutaneous leishmaniasis, leprosy, sporotrichosis, chromoblastomycosis, dermatofibrosarcoma protuberans, dermatofibroma, sarcomas, and cutaneous tuberculosis. We performed a biopsy, and histopathologic examination revealed abundant lemon-shaped, refractile, yeast-like cells that were single and in chains within a background of granulomatous inflammation, consistent with *P. loboi* infection (Figure 1, panels B, C).

We extracted DNA from the formalin-fixed paraffin-embedded biopsy tissue sample. We used PCR and Oxford nanopore sequencing (Oxford Nanopore Technologies, https://nanoporetech.com)

to detect and identify *ITS1*, *ITS2*, *ADP-rf*, and *GP43* genes (*4*). We compared the sequences to a reference sequence dataset of various *Paracoccidioides* spp. from GenBank. We reconstructed a phylogenetic tree by using the maximum-likelihood method and IQ-TREE 2 (http://www.iqtree.org) and assessed node support by using bootstrap (1,000 replicates), abayes, and SH-aLRT methods in IQ-TREE (Figure 2). We selected substitution models according to the Bayesian information criterion. We deposited DNA sequences in the European Nucleotide Archive (https://www.ebi.ac.uk/ena; project no. PRJEB77911; submission no. ERA30711349).

The patient underwent treatment with itraconazole (200 mg/d for 3 months). After the first month of treatment, he experienced symptomatic improvement of the headache and resolution of ear pruritus, although the ear lobe deformation persisted. After 3 months of treatment, the patient chose to stop the medication because of intolerable gastric side effects and opted for surgical resection.

Lobomycosis is endemic in many Latin America countries; most cases have been reported from Brazil (*5*). However, the disease has also been reported across Andes regions in Venezuela, Colombia, Ecuador, Peru, and Bolivia (*3*). Limited knowledge exists about endemicity and ecologic factors driving disease occurrence in the Andes regions. Lobomycosis was first reported in Bolivia in 1982 in a 58-year-old farmer who had skin nodules on his earlobe, face, and extremities, and a diagnosis of lobomycosis was confirmed by direct smear and histological examination of lesions. That patient was treated with a combination of pharmacological agents, including amphotericin, flucytosine, and ketoconazole, along with surgical treatment, and invariable recurrence was observed (*2*). Since 1982, only 2 more cases of lobomycosis have been reported from Bolivia in the literature (*3*); those cases occurred in the department of Pando near the Amazon Region of Brazil.

Paracoccidioides spp., similar to many dimorphic fungi, usually exhibit geographic restrictions linked to specific environmental conditions (*6*). Although soil and vegetation are believed to be the primary habitats of *P. loboi*, human infections have also been associated with proximity to water, suggesting that *P. loboi* might be a hydrophilic microorganism (*1*). *P. ceti* is known to infect dolphins (*7*), *P. braziliensis* infections have been reported in fish (*8*), and the recently described *Emydomyces testavorans* has been reported to cause shell lesions in fresh water chelonians (*9*). *P. loboi* and other fungi in the order Onygenales exhibit ecologic traits that have shaped their evolutionary, ecologic, and pathogenic characteristics, enabling them to thrive in complex habitats (*10*). Thus, conditions such as wet soil and high acidity, which are commonly found in the tropical Andes regions bordering the Amazon rainforest, appear to be suitable niches for *P. loboi*.

Because of the high biodiversity of the Andes and the association of *P. loboi* fungus with aquatic and sylvatic environments (*1*), cases of lobomycosis might be substantially underreported in countries with Andes mountain regions, particularly those sharing territories overlapping the Amazon and regions of the broader Andes-Amazon basin. By 2022, a total of 907
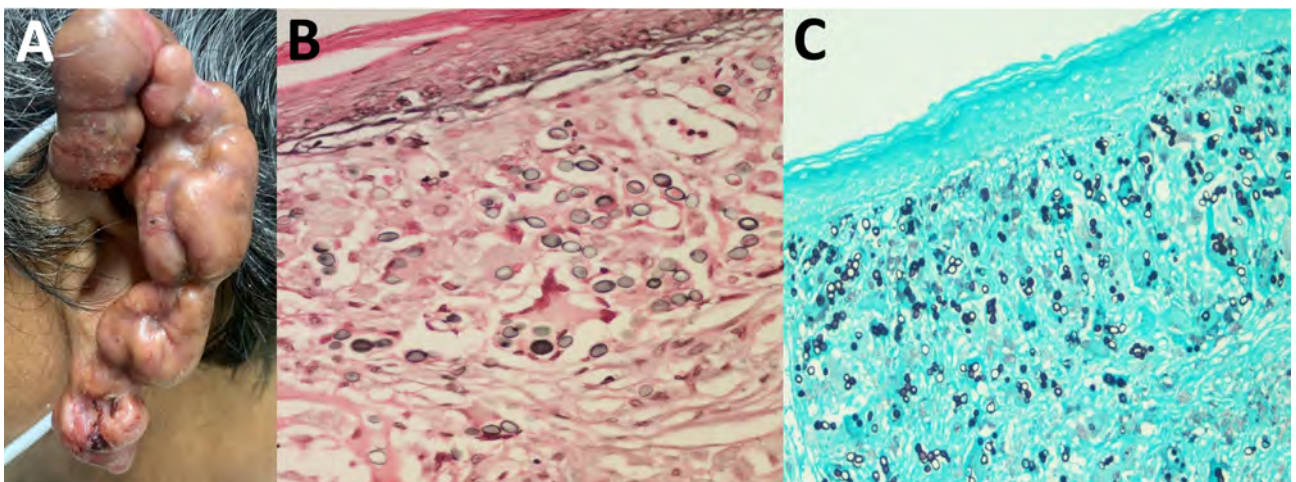
Figure 1. Clinical manifestations of lesions in patient with lobomycosis in Amazon Region, Bolivia, 2022. A) Multiple hyperpigmented, confluent keloid-like nodular lesions with overriding telangiectasias and patchy crusted and eroded squamous areas were noted on the helix and lobule of the left ear. B, C) Histologic examination of lesion specimens showed oval-to-round shaped cells that had connecting tubular projections organized in a string-of-pearls pattern, in pairs and individually. B) Fontana-Masson stain; original magnification ×1,000. C) Gömöri methenamine silver stain; original magnification ×400.
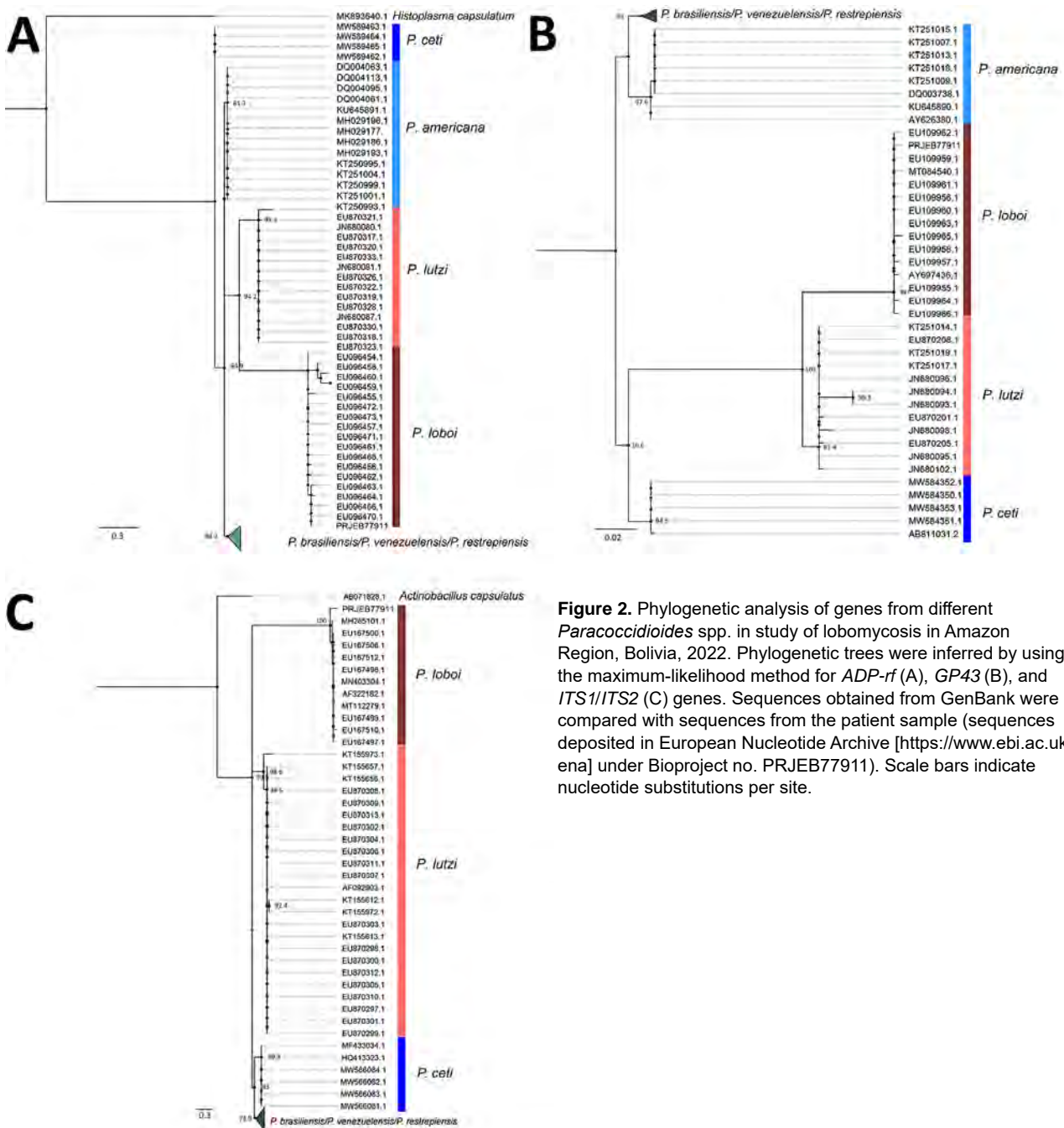
Figure 2. Phylogenetic analysis of genes from different *Paracoccidioides* spp. in study of lobomycosis in Amazon Region, Bolivia, 2022. Phylogenetic trees were inferred by using the maximum-likelihood method for *ADP-rf* (A), *GP43* (B), and *ITS1*/*ITS2* (C) genes. Sequences obtained from GenBank were compared with sequences from the patient sample (sequences deposited in European Nucleotide Archive [https://www.ebi.ac.uk/ena] under Bioproject no. PRJEB77911). Scale bars indicate nucleotide substitutions per site.

cases of lobomycosis had been reported worldwide (*5*). In the Andes regions, the total number of lobomycosis cases was 94, and a clear geographic trend toward occurrence eastward at the Andes-Amazon piedmont was observed for 84 of those cases. In contrast, the western regions accounted for only ≈10 cases (Appendix Table 1, https://wwwnc.cdc.gov/EID/article/30/12/24-1089-App1.pdf). Of the total number of cases reported worldwide, 496 (55%) cases have been reported from Acre State in Brazil

(Appendix Table 2) (*5*). Together with the departments of Madre de Dios (Peru) (*11*) and Pando (Bolivia) (*2*), where this case occurred, those 3 regions form a tri-border area harboring most lobomycosis cases in each country, making it a disease-endemic hotspot. Moreover, the stream where the patient recalled being exposed to the infection as a child is a tributary of the Acre River, the main waterway within this tri-border area. The patient recalled a mosquito bite during his childhood, which raises the longstanding

question about the potential transmission of this fungus through aquatic fauna, such as copepods, snails, or other aquatic insects (*12*). This topic warrants further research to decipher potentially unknown transmission mechanisms.

Conclusions

Lobomycosis cases have been reported in countries such as Colombia that are northwest of the Andes Mountain range (*13*), suggesting that geographic ranges of endemicity in the tropical Andes and Amazon might be expanding. Expansion might be occurring in other biogeographic regions northward into Central America through the moist tropical and deciduous forests of the Chocó-Darien region into Panama, where 1 case was reported in 2022 (*14*). Understanding ecologic niches and environmental variability is crucial for preventing transmission of infections caused by *P. loboi*. Ongoing climatic changes might also exert environmental pressures that lead to *P. loboi* emergence or spillover beyond known areas of disease endemicity. Continued surveillance and correct identification of lobomycosis cases in the Andes region and other parts of South and Central America are crucial to prevent the spread of this disease.

About the Author

Dr. Méndez is a clinician research scientist at the Centro Nacional de Enfermedades Tropicales (CENETROP), Santa Cruz, Bolivia. Her primary research interests are tropical medicine and fungal diseases.

References

1. Paniz-Mondolfi A, Talhari C, Sander Hoffmann L, Connor DL, Talhari S, Bermudez-Villapol L, et al. Lobomycosis: an emerging disease in humans and delphinidae. Mycoses. 2012;55:298–309. https://doi.org/10.1111/j.1439-0507.2012.02184.x
2. Recacoechea M, Vargas J. Experiencia con el ketoconazole en el primer caso de lobomicosis en Bolivia. Bol. inf CENETROP. 1982;8:23–6.
3. Brito AC, Quaresma JAS. Lacaziose (doença de Jorge Lobo): revisão e atualização. An Bras Dermatol. 2007;82:461–74. https://doi.org/10.1590/S0365-05962007000500010
4. Vilela R, Huebner M, Vilela C, Vilela G, Pettersen B, Oliveira C, et al. The taxonomy of two uncultivated fungal mammalian pathogens is revealed through phylogeny and population genetic analyses. Sci Rep. 2021;11:18119. https://doi.org/10.1038/s41598-021-97429-7
5. Gonçalves FG, Rosa PS, Belone AFF, Carneiro LB, de Barros VLQ, Bispo RF, et al. Lobomycosis epidemiology and management: the quest for a cure for the most neglected of neglected tropical diseases. J Fungi (Basel). 2022;8:494. https://doi.org/10.3390/jof8050494
6. Luberto ET, Ramsey ML, Kollath DR. The ecology of pathogenic Onygenales fungi and the impacts of climate change. Curr Clin Microbiol Rep. 2024;11:62–9. https://doi.org/10.1007/s40588-024-00223-y
7. Kanegae H, Sano A, Okubo-Murata M, Watanabe A, Tashiro R, Eto T, et al. Seroprevalences against *Paracoccidioides cetii*: a causative agent for paracoccidiomycosis ceti (PCM-C) and *Coccidioides posadasii*; for coccidioidomycosis (CCM) in Dall's porpoise (*Phocoenoides dalli*) and harbor porpoise (*Phocoena phocoena*) stranded at Hokkaido, Japan. Mycopathologia. 2022;187:423. https://doi.org/10.1007/s11046-022-00648-3
8. de Souza Suguiura IM, Macagnan R, Omori AM, Buck EL, Scarpassa JA, Pretto-Giordano LG, et al. First report of *Paracoccidioides brasiliensis* infection in fish. Med Mycol. 2020;58:737–43. https://doi.org/10.1093/mmy/myz120
9. Woodburn DB, Miller AN, Allender MC, Maddox CW, Terio KA. *Emydomyces testavorans*, a new genus and species of onygenalean fungus isolated from shell lesions of freshwater aquatic turtles. J Clin Microbiol. 2019;57:e00628-18. https://doi.org/10.1128/JCM.00628-18
10. Coleine C, Selbmann L, Guirado E, Singh BK, Delgado-Baquerizo M. Humidity and low pH boost occurrence of Onygenales fungi in soil at global scale. Soil Biol Biochem. 2022;167:108617. https://doi.org/10.1016/j.soilbio.2022.108617
11. Ramírez Soto MC, Malaga G. Subcutaneous mycoses in Peru: a systematic review and meta-analysis for the burden of disease. Int J Dermatol. 2017;56:1037–45. https://doi.org/10.1111/ijd.13665
12. Marsollier L, Sévérin T, Aubry J, Merritt RW, Saint André JP, Legras P, et al. Aquatic snails, passive hosts of *Mycobacterium ulcerans*. Appl Environ Microbiol. 2004;70:6296–8. https://doi.org/10.1128/AEM.70.10.6296-6298.2004
13. Rodriguez Toro G. Enfermedad de Jorge Lobo o *Blastomicosis queloidiana*. Nuevos aspectos de la entidad en Colombia. Revision. Biomedica. 1989;9:133–46
14. Suárez JA, Cerrud B, Pachar M, Patiño LH, Reidy J, Chace A, et al. Human lobomycosis caused by *Paracoccidioides* (*Lacazia*) *loboi*, Panama, 2022. Emerg Infect Dis. 2023;29:2513–7. https://doi.org/10.3201/eid2912.231092

Address for correspondence: Alberto Paniz-Mondolfi, Molecular Microbiology Laboratory, Icahn School of Medicine at Mount Sinai, 1428 Madison Ave, Atran Bldg, 2nd Fl, New York, NY 10029, USA; email: alberto.paniz-mondolfi@mountsinai.org

Experimental Infection of Reindeer with Jamestown Canyon Virus

Kayla J. Buhler, John Blake, Heather Fenton, Isaac H. Solomon, Emily Jenkins

Seroprevalence of Jamestown Canyon virus in free-ranging caribou in North America is high. We demonstrate serum antibodies and RNA of the virus in blood and tissues of experimentally exposed reindeer with no clinical illness and minimal histopathologic changes. Caribou and reindeer may play a role in emergence and dissemination of vectorborne zoonoses in Arctic regions.

California serogroup viruses (CSVs), including snowshoe hare virus and Jamestown Canyon virus (JCV), are mosquitoborne orthobunyaviruses present throughout northern North America (1). Infection typically causes influenza-like symptoms and rarely encephalitis, most commonly in children with snowshoe hare virus and adults with JCV infection (2). High CSV exposure has been documented in humans (27% of Alaska residents) and animals (64% of caribou with antibodies to JCV) in the Nearctic (3,4). Our serologic evidence suggests that caribou may be natural wildlife hosts for JCV, as has been suggested for white-tailed deer in temperate regions (5). Caribou and reindeer (*Rangifer tarandus*) play an essential role in northern ecosystems, are declining substantially in many regions, and are culturally significant to Indigenous populations (6). We conducted this study to gain more knowledge about the role of caribou in JCV disease ecology. Animal experimentation was approved by the University of Alaska Fairbanks Institutional Animal Care and Use Committee (IACUC

Author affiliations: Inland Norway University of Applied Sciences, Innlandet, Norway (K.J. Buhler); University of Saskatchewan, Saskatoon, Saskatchewan, Canada (K.J. Buhler, E. Jenkins); University of Alaska Fairbanks, Fairbanks, Alaska, USA (J. Blake); Australian Registry of Wildlife Health, Taronga Conservation Society, Mosman, New South Wales, Australia (H. Fenton); Ross University School of Veterinary Medicine, Basseterre, Saint Kitts and Nevis (H. Fenton); Brigham and Women's Hospital and Harvard Medical School, Boston, Massachusetts, USA (I.H. Solomon)

1552224, 1654054, and 1654058) and the University of Saskatchewan Animal Care Committee (20210075 and 20210076).

The Study

In May and December 2020, we screened 30 reindeer from the Large Animal Research Station (University of Alaska Fairbanks; UAF) for CSV antibodies by using cELISA (4,7) (Appendix Figure 1, https://wwwnc.cdc.gov/EID/article/30/12/24-0757-App1.pdf). After a summer of insect activity, seroprevalence remained the same among the adults (91%; n = 10/11), but 84% (n = 16/19) of young animals had seroconverted. We housed a control group (1 infected and 1 naive female) in a separate pen from experimentally exposed naive reindeer (2 females, 1 male) and a superinfected group (2 females, 1 male) (Figure 1). Exposed animals received 10^6 PFU of JCV in 1 mL of sterile phosphate buffered saline (PBS), pH 7.2, administered subcutaneously in the right shoulder. The control group received 1 mL PBS without virus, administered identically.

We disinfected handling facilities daily with a 10% bleach solution and collected rectal temperatures, weights, and jugular blood samples daily. We manually differentiated and quantified leukocytes on EDTA blood smears stained with EASY III (Azer Scientific, https://www.azerscientific.com). We anesthetized animals with intramuscular ketamine (7–10 mg/kg) and xylazine (0.6 mg/kg) before we euthanized them with intravenous pentobarbital (60–80 mg/kg) (Euthasol; Virbac, https://us.virbac.com) (Figure 1). During necropsy, we collected cerebral spinal fluid in red top BD Vacutainer tubes (https://www.bd.com) and placed oral, nasal, and conjunctival swab samples in tubes containing 1.0 mL sterile PBS, stored at −80°C until shipping. We subdivided tissues (liver, kidney, spleen, lung, gonad, brain, spinal cord, quadriceps, heart, muscle under the injection site, tonsils, parotid lymph nodes, retropharyngeal and mesenteric lymph

Figure 1. Study design for experimental infection of reindeer with JCV. JCV, Jamestown Canyon virus; PBS, phosphate-buffered saline.

nodes) and stored them frozen (−20°C) and fixed in 10% neutral buffered formalin. We also collected heart blood, chest fluid, abdominal fluid, urine, and feces if present. We disinfected instruments between each animal. We transferred all samples to the Zoonotic Parasite Research Unit (Western College of

Veterinary Medicine, Saskatoon, SK, Canada) and stored at −20°C until testing.

We extracted RNA from tissues and fluids by using the RNeasy Mini Kit (QIAGEN, https://www.qiagen.com) and performed reverse transcription PCR with JCV primers and probe (4). We considered
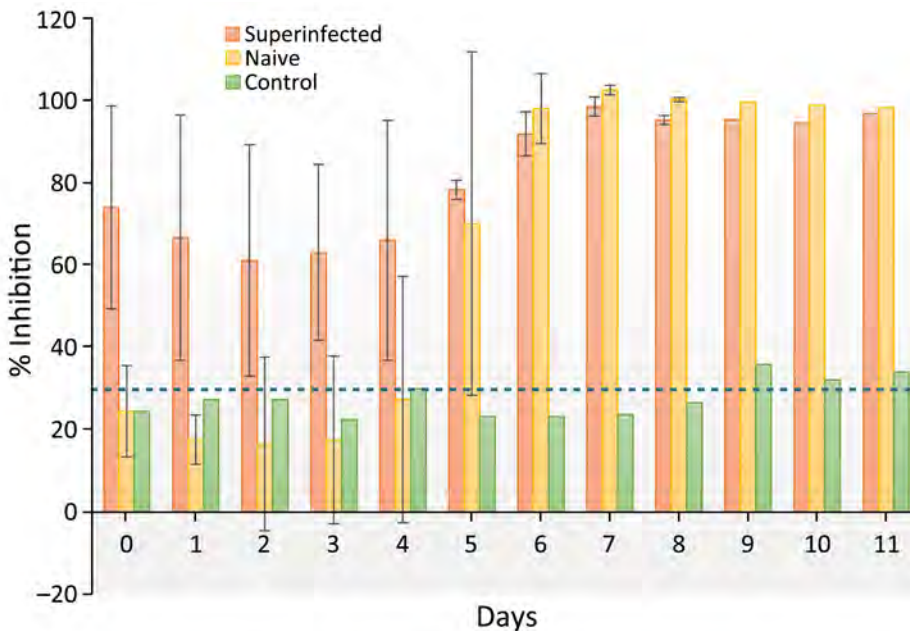
Figure 2. Average antibody response for naive and superinfected groups of reindeer experimentally infected with Jamestown Canyon virus. The titer of the naive control animal is provided for comparison. SD (error bars) are included when groups contained >1 animal. The dashed blue line indicates the positive cutoff value of the competitive ELISA (30% inhibition).
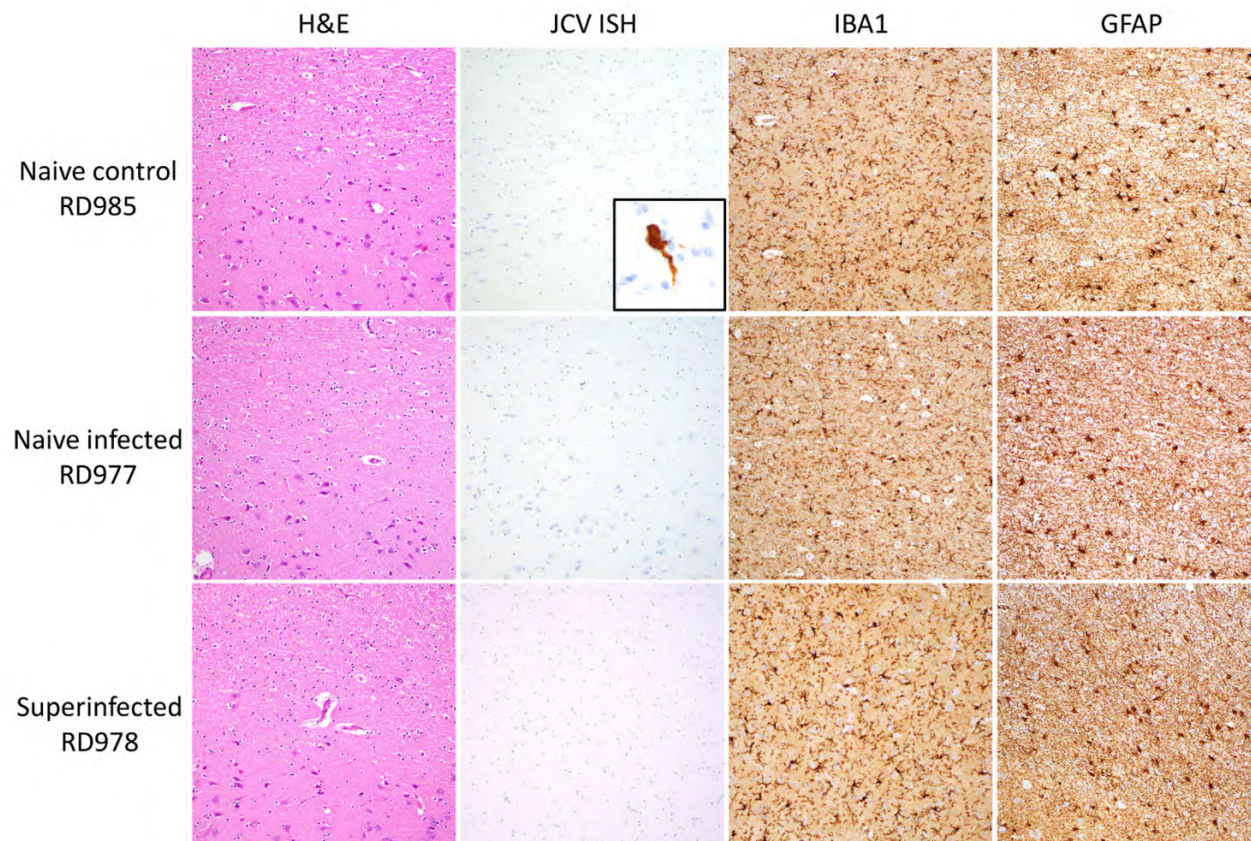
Figure 3. Histopathology of samples from reindeer experimentally infected with JCV. Representative brain sections from naive control (RD985), naive infected (RD977), and superinfected (RD978) animals shows H&E-stained sections of cerebral cortex and subcortical white matter with minimal diagnostic abnormalities, negative JCV RNA ISH staining, scattered IBA1-positive microglia/macrophages, and mild-to-moderate astrocytosis highlighted by GFAP immunohistochemistry. JCV ISH naive control inset panel demonstrates positive cytoplasmic staining in a cortical neuron from a positive control case of fatal JCV encephalitis in a human. All images taken with 20× objective with exception of the JCV ISH inset, taken with 60× objective. GFAP, glial fibrillary acidic protein; H&E, hematoxylin and eosin; IBA, allograft inflammatory factor 1; ISH, in situ hybridization; JCV, Jamestown Canyon virus.

samples at <30 quantification cycles (Cq) to be positive. Positive controls were gBlocks gene fragments (Integrated DNA Technologies, https://www.idtdna.com) created from the small (S) segment of JCV (GenBank accession no. MN135989.1).

Tissues were trimmed, embedded in paraffin, cut, and stained with hematoxylin and eosin after 30 days in formalin at Prairie Diagnostic Services Inc. (Saskatoon). Slides were read by a blinded, board-certified, veterinary pathologist. Paraffin-embedded sections of brain (cerebrum, cerebellum, and obex), cranial lymph node, tonsil, and a gastrointestinal section with myenteric plexus were sent to Brigham and Women's Hospital and Harvard Medical School (Boston, MA, USA) for in situ hybridization (ISH) and immunohistochemistry (Appendix Table 1). RNA ISH was performed on a Leica BOND-III system (Leica Biosystems, https://www.leicabiosystems.com) with RNAScope probes

V-JCV-LMS-O1 (1187658-C1) (Advanced Cell Diagnostics, https://www.acdbio.com) according to manufacturer protocols and 14 ZZ probes targeting JCV isolate 11497-03; segments tested were 52–814 bp of the S segment (GenBank accession no. EF681845.1), 2–462 bp of the medium (M) segment (accession no. EF687121.1), and 227–337 bp of the large (L) segment (accession no. EF687059.1). We performed immunohistochemistry by using the Leica-BOND-III system with rabbit polyclonal GFAP antibody (1:3,000 dilution; abcam, https://www.abcam.com) and rabbit polyclonal IBA1 antibody (1:100 dilution; FUJIFILM Wako Chemicals Corp., https://www.fujifilm.com). Slides were reviewed by a blinded, board-certified, medical neuropathologist.

Throughout the experiment, we observed no changes in behavior or body temperature of the reindeer (Appendix Table 2). The naive exposed group

seroconverted on postinfection day 5, and antibody titers for all exposed reindeer peaked at postinfection day 7 (Figure 2). Lymphocytes were consistently elevated for reindeer in the naive and superinfected exposed groups but not in the control group. Viral RNA was detected in blood on days 1 (Cq = 13.80; naive animal) and 5 (Cq = 10.08; superinfected animal). Viral RNA was detected in chest fluid (Cq = 11.47), urine (Cq = 20.26), spleen (Cq = 22.04), parotid lymph node (Cq = 16.26), obex (Cq = 28.03), and uterus (Cq = 11.66) from exposed but not control animals (Appendix Table 1).

Histopathology revealed subtle, nonspecific neuronal changes in the brains of all animals except the naive control. Mild congestion and lymphoplasmacytic inflammation were detected in kidneys (n = 8), urinary bladder (n = 1, naive control), liver (n = 4, including previously infected control), and conjunctiva (n = 1, previously infected control). In situ hybridization did not reveal viral RNA within lesions. Immunohistochemistry for GFAP (glial fibrillary acidic protein) showed mild to moderate astrogliosis and for IBA1 (allograft inflammatory factor 1) showed mild microgliosis in brain sections (Figure 3).

Conclusions

We demonstrate JCV experimental infection in reindeer with no clinical signs of illness and minimal, nonspecific histological changes, similar to what has been reported for other animal arbovirus infections (8). Our results are consistent with those of a previous experiment in which white-tailed deer were infected with JCV and were viremic for 2–4 days but showed no clinical illness (9). We detected RNA in blood in the chest cavity of 1 animal at postinfection day 11, suggesting that that reindeer may be viremic for longer. The high rate of seroconversion in the naturally exposed herd of 30 reindeer suggests that reindeer and caribou may play a role in the ecology of CSVs in northern ecosystems, especially given that most young animals seroconverted within a single summer (11%–84%). Further studies focusing on isolation of live virus from experimentally infected animals in addition to vector competence would provide more information about the potential for reindeer to be maintenance hosts of the virus (10).

In humans, neuroinvasive disease is a strong component of JCV disease (11). We note that genetic material was found in the obex of 1 reindeer, suggesting potential infection, but ISH and immunohistochemistry results did not demonstrate neuronal invasion, despite a potential glial response. Although JCV was detected in the uterus, the implications for potential vertical spread or other effects are unknown. Single-stranded RNA viruses are not stable in the environment, and multiple freeze–thaw events probably affected genetic detection of virus in our study (12).

Our detection of JCV in blood and tissues of experimentally exposed reindeer, together with high seroprevalence in free-ranging animals in North America, suggests that Rangifer spp. caribou and reindeer could play a role in disease ecology of JCV in Arctic and sub-Arctic North America (4).

About the Author

Dr. Buhler is a postdoctoral researcher at the Inland Norway University of Applied Sciences. Her research interests include the epidemiology and ecology of zoonotic pathogens, with a focus on foodborne and vectorborne pathogen transmission in wildlife across northern ecosystems.

References

1. Drebot MA. Emerging mosquito-borne bunyaviruses in Canada. Can Commun Dis Rep. 2015;41:117–23. https://doi.org/10.14745/ccdr.v41i06a01
2. Evans AB, Winkler CW, Peterson KE. Differences in neuropathogenesis of encephalitic California serogroup viruses. Emerg Infect Dis. 2019;25:728–38. https://doi.org/10.3201/eid2504.181016
3. Miernyk KM, Parkinson AJ, Stoddard RA, Wilkins PP, Kersh GJ, Drebot MA, et al. Human seroprevalence to 11

zoonotic pathogens in the US Arctic, Alaska. Vector Borne Zoonotic Dis. 2019;19:563–75. https://doi.org.10.1089/vbz.2018.2390

4. Buhler KJ, Dibernardo A, Pilfold NW, Harms NJ, Fenton H, Carriere S, et al. Widespread exposure to mosquitoborne California serogroup viruses in caribou, Arctic fox, red fox, and polar bears, Canada. Emerg Infect Dis. 2023;29:54–63. https://doi.org/10.3201/eid2901.220154

5. Hollis-Etter KM, Montgomery RA, Etter DR, Anchor CL, Chelsvig JE, Warner RE, et al. Environmental conditions for Jamestown Canyon virus correlated with population-level resource selection by white-tailed deer in a suburban landscape. PLoS One. 2019;14:e0223582. https://doi.org/10.1371/journal.pone.0223582

6. Festa-Bianchet M, Ray JC, Boutin S, Côté SD, Gunn A. Conservation of caribou (*Rangifer tarandus*) in Canada: an uncertain future. Can J Zool. 2011;89:419–34. https://doi.org/10.1139/z11-025

7. Rocheleau JP, Michel P, Lindsay LR, Drebot M, Dibernardo A, Ogden NH, et al. Emerging arboviruses in Quebec, Canada: assessing public health risk by s erology in humans, horses and pet dogs. Epidemiol Infect. 2017;145:2940–8. https://doi.org/10.1017/S0950268817002205

8. Agliani G, Giglia G, Marshall EM, Gröne A, Rockx BHG, van den Brand JMA. Pathological features of West Nile and Usutu virus natural infections in wild and domestic animals and in humans: a comparative review. One Health. 2023;16:100525. https://doi.org/10.1016/j.onehlt.2023.100525

9. Watts DM, Tammariello RF, Dalrymple JM, Eldridge BF, Russell PK, Top FH Jr. Experimental infection of vertebrates of the Pocomoke Cypress Swamp, Maryland with Keystone and Jamestown Canyon viruses. Am J Trop Med Hyg. 1979;28:344–50. https://doi.org/10.4269/ajtmh.1979.28.344

10. Kuno G, Mackenzie JS, Junglen S, Hubálek Z, Plyusnin A, Gubler DJ. Vertebrate reservoirs of arboviruses: myth, synonym of amplifier, or reality? Viruses. 2017;9:185. https://doi.org/10.3390/v9070185

11. Solomon IH, Ganesh VS, Yu G, Deng XD, Wilson MR, Miller S, et al. Fatal case of chronic Jamestown Canyon virus encephalitis diagnosed by metagenomic sequencing in patient receiving rituximab. Emerg Infect Dis. 2021;27:238–42. https://doi.org/10.3201/eid2701.203448

12. Tang JW. The effect of environmental parameters on the survival of airborne infectious agents. J R Soc Interface. 2009;6(Suppl 6):S737–46. https://doi.org/10.1098/rsif.2009.0227.focus

Address for correspondence: Kayla Buhler, Inland Norway University of Applied Sciences, Anne Evenstads Vei 80, 2480 Koppang, Norway; email: kayla.buhler@inn.no

etymologia revisited

Neospora caninum

[ne-os' pə-rə ca-nin' um]

From the *neo-* (Latin, "new") + *spora* (Greek, "seed")and *canis* (Latin, "dog"), *Neospora caninum* is a sporozoan parasite that was first described in 1984. It is a major pathogen of cattle and dogs but can also infect horses, goats, sheep, and deer. Antibodies to *N. caninum* have been found in humans, predominantly in those with HIV infection, although the role of this parasite in causing or exacerbating illness is unclear.

Originally published in June 2019

References:

1. Bjerkås I, Mohn SF, Presthus J. Unidentified cyst-forming sporozoon causing encephalomyelitis and myositis in dogs. Z Parasitenkd. 1984;70:271–4. http://dx.doi.org/10.1007/BF00942230

2. Dubey JP. Review of *Neospora caninum* and neosporosis in animals. Korean J Parasitol. 2003; 41:1–16. http://dx.doi.org/10.3347/kjp.2003.41.1.1

3. Lobato J, Silva DA, Mineo TW, Amaral JD, Segundo GR, Costa-Cruz JM, et al. Detection of immunoglobulin G antibodies to *Neospora caninum* in humans: high seropositivity rates in patients who are infected by human immunodeficiency virus or have neurological disorders. Clin Vaccine Immunol. 2006;13:84–9. http://dx.doi.org/10.1128/CVI.13.1.84-89.2006

https://wwwnc.cdc.gov/eid/article/25/6/et-2506_article

Transmission of Swine Influenza A Viruses along Pig Value Chains, Cambodia, 2020–2022

Arata Hidano, Dina Koeut, Hannah Holt, William T.M. Leung, Sokhom Krean, Vutha Chhim, Bunnary Seng, Sovanncheypo Chao, Wong Foong Ying, Pov Son, Sina Vor, Sokchea Huy, Ty Chhay, Sothyra Tum, San Sorn, Monidarin Chou, Yvonne C.F. Su, Gavin J.D. Smith, James W. Rudge

We analyzed >4,000 pig samples from slaughterhouses in Cambodia and found higher influenza A seroprevalence (40.0%) and prevalence (1.5%) among pigs from commercial farms than smallholder farms (seroprevalence 8.9%; prevalence 0.6%). Multivariable analyses revealed evidence of transmission after leaving farms. Findings have implications for influenza risk and surveillance in emerging livestock systems.

Swine influenza A viruses (IAVs) contribute to risk for pandemic emergence in humans. Emerging livestock systems in low- and middle-income countries (LMICs) have been proposed as hotspots for novel viruses because of the proximity between avian, swine, and human host populations, high densities of smallholder and multispecies farming systems with poor biosecurity, and rapid growth in livestock industries (*1–3*). However, systematic surveillance of swine IAVs in those settings is nearly nonexistent, limiting our understanding of IAV epidemiology and evolution. We conducted slaughterhouse sampling of pigs over a 2-year period in Cambodia to compare IAV circulation in smallholder versus commercial farms and identify risk factors

associated with active IAV infection at slaughterhouses. By performing IAV surveillance in slaughterhouses, we assessed the role of transmission during transport and at slaughterhouses and examined implications for epidemiologic inference of IAV risk along pig value chains, the series of interconnected activities encompassing the production, distribution, and processing of pigs.

The Study

We selected 18 slaughterhouses in 4 provinces in Cambodia to encompass pigs from smallholder (<100 pigs) and commercial farms (≥100 pigs), after conducting a rapid assessment survey among 52 slaughterhouses to characterize their operations (Appendix; https://wwwnc.cdc.gov/EID/article/30/12/24-0695-App1.pdf). We sampled pigs monthly at each slaughterhouse during March 2020–July 2022 (*4*). We based sample sizes for each batch (i.e., pigs from the same source sampled on the same day at a given slaughterhouse) on 95% probability of detecting ≥1 positive animal if prevalence within an infected batch was ≥20% (*5*). We extracted RNA from nasal swab samples and screened for active IAV shedding using real-time RT-PCR targeting the IAV M gene (*6*). We screened blood serum samples for IAV nucleoprotein antibodies using ID Screen Influenza A Multi-species ELISA (Innovative Diagnostics, https://www.innovative-diagnostics.com). We collected data on pig breed, age, type, and origin during each sampling visit.

Our study was approved by ethics committees at the London School of Hygiene and Tropical Medicine Institutional Review Board (approval no. 16635) and the Animal Welfare and Ethical Research Board (reference no. 2019-12), National Ethics Committee for Health Research in Cambodia (reference no. 105), Human Research Protection Office (reference no.

A-21055), and Animal Care and Use Review Office of the US Army Medical Research and Development Command Office of Research Protections.

To account for chronological and other directional relationships between variables, we developed a directed acyclic graph assuming IAV antibodies are detectable ≥ 7 days after exposure (7). ELISA-determined serostatus likely represented IAV exposure on farms because pigs stayed at slaughterhouses only ≤ 6 days in this study; virus shedding by pigs starts as early as 1 day after IAV infection and can last ≥ 5 days (7). Thus, positive PCR results (i.e., positive infection status) might indicate IAV exposure on the farm shortly before departure to a slaughterhouse, during transport, or at the slaughterhouse.

We developed Bayesian hierarchical logistic regression models to estimate the direct effect of each exposure, adjusted for confounding and batch-clustering effects. We used batch size and duration of stay at a slaughterhouse as continuous variables using fractional polynomial and generalized additive models and categorical variables. We selected functional forms with the largest Bayes factors. We estimated posterior adjusted odds ratios (aOR) using Stan version 2.26.1 (8). We explored spatial trends in seroprevalence based on location of batch origin. We conducted a sensitivity analysis to quantify the potential effects of imperfect diagnostic tests (Appendix).

We sampled 616 batches from 18 slaughterhouses, which provided 4,089 swab and 4,069 serum samples; 340 (55.2%) batches were from commercial and 204 (33.1%) were from smallholder farms in Cambodia, 59 (9.6%) batches were imported from Thailand, and 13 batches were of unknown origin. Estimated transport durations within Cambodia were 0.1–10.1 hours. At slaughterhouses, pigs were penned in groups of 3–30 and kept an average of 3–36 hours before slaughter, depending on the slaughterhouse. Most slaughterhouses reported that pigs were kept 1–6 days. Pens were cleaned daily in 15 slaughterhouses, weekly in 2, and monthly in 1. At least 1 pig tested positive for active infection in 37 (6.0%) batches and for seroconversion in 355 (59.1%) batches (Table).

Seroprevalence among commercial farm pigs was 40.0%, considerably higher than among pigs from smallholders (8.9%). In multivariable analyses, pigs from smallholders were less likely to test seropositive (aOR 0.07; 95% credible interval [CrI] 0.04–0.11) than pigs from commercial farms. Infection prevalence was also lower among smallholder (0.6%) than commercial farm pigs (1.5%), although that association was not statistically significant after adjusting for confounders (Figure 1). Odds of active infection were lower among seropositive pigs (aOR 0.39; 95% CrI 0.18–0.83) and among sows. Several associations provided evidence of transmission at

Table. Batch- and slaughterhouse-level results from pig sampling, stratified by slaughterhouse province in a study of transmission of swine influenza A viruses along pig value chains, Cambodia, 2020–2022*

Characteristics	Overall	Slaughterhouse province			
		Kampong Speu	Kandal	Takeo	Phnom Penh
Slaughterhouses	18	5	6	4	3
Batches	616	200	136	175	105
From commercial farms	397 (64.4)	137 (68.5)	97 (71.3)	94 (53.7)	71 (67.6)
PCR-positive	37 (6.0)	1 (0.5)	15 (11.0)	12 (6.9)	9 (8.6)
ELISA-positive	355 (59.1)	127 (63.5)	75 (55.1)	95 (54.3)	58 (55.2)
Batch size, median (range)	6 (1–120)	5 (1–110)	5 (1–32)	6 (1–31)	20 (2–120)
Samples per batch, median (range)	6 (1–16)	5 (1–16)	5 (1–15)	6 (1–13)	12 (2–16)
Within-batch prevalence, median (range)†	20 (6.7–100)	50	33.3 (6.7–100)	14.3 (10–66.7)	12.5 (7.1–55.6)
Within-batch seroprevalence, median (range)‡	50 (6.7–100)	50 (6.7–100)	58.3 (9.1–100)	50 (10–100)	50 (6.7–100)
Male percentage per batch, median (range)	50 (0–100)	42.9 (0–100)	50 (0–100)	50 (20–100)	50 (0–100)
Finisher percentage per batch, median (range)	100 (0–100)	100 (0–100)	100 (100–100)	100 (0–100)	100 (100–100)
Batches by cleaning frequency of slaughterhouse					
Daily	536 (87.0)	176 (88)	111 (84.1)	175 (100)	74 (70.5)
Weekly	45 (7.3)	24 (12)	21 (15.4)	0	0
Monthly	31 (5.0)	0	0	0	31 (29.5)
Transport duration, h, median (range)	0.8 (0.1–10.1)	0.5 (0.2–7.9)	1.5 (0.5–9.9)	0.3 (0.1–10.0)	2.1 (0.9–10.1)
Duration at slaughterhouse, h, median (range)	12 (2–144)	10 (2–48)	12 (5–48)	12 (5–144)	8 (5–20)
Batches by location of originating farm					
Kampong Speu Province	329 (53.4)	177 (88.5)	69 (52.3%)	39 (22.3)	44 (41.9)
Takeo Province	133 (21.6)	2 (1.0)	0 (0)	125 (71.4)	6 (5.7)
Kampong Chhnang Province	42 (6.8)	14 (7.0)	0 (0)	0 (0)	28 (26.7)
Cambodia, other province	53 (8.6)	6 (3.0)	36 (27.3)	3 (1.7)	4 (3.8)
Imported from Thailand	59 (9.6)	1 (0.5)	27 (20.5)	8 (4.6)	23 (21.9)

*Values are no. (%) except as indicated.
†PCR confirmed. Within-batch prevalence and seroprevalence were calculated among positive batches (i.e., with ≥ 1 positive pig). Range is not provided for Kampong Speu for within-batch prevalence because only a single batch tested PCR-positive.
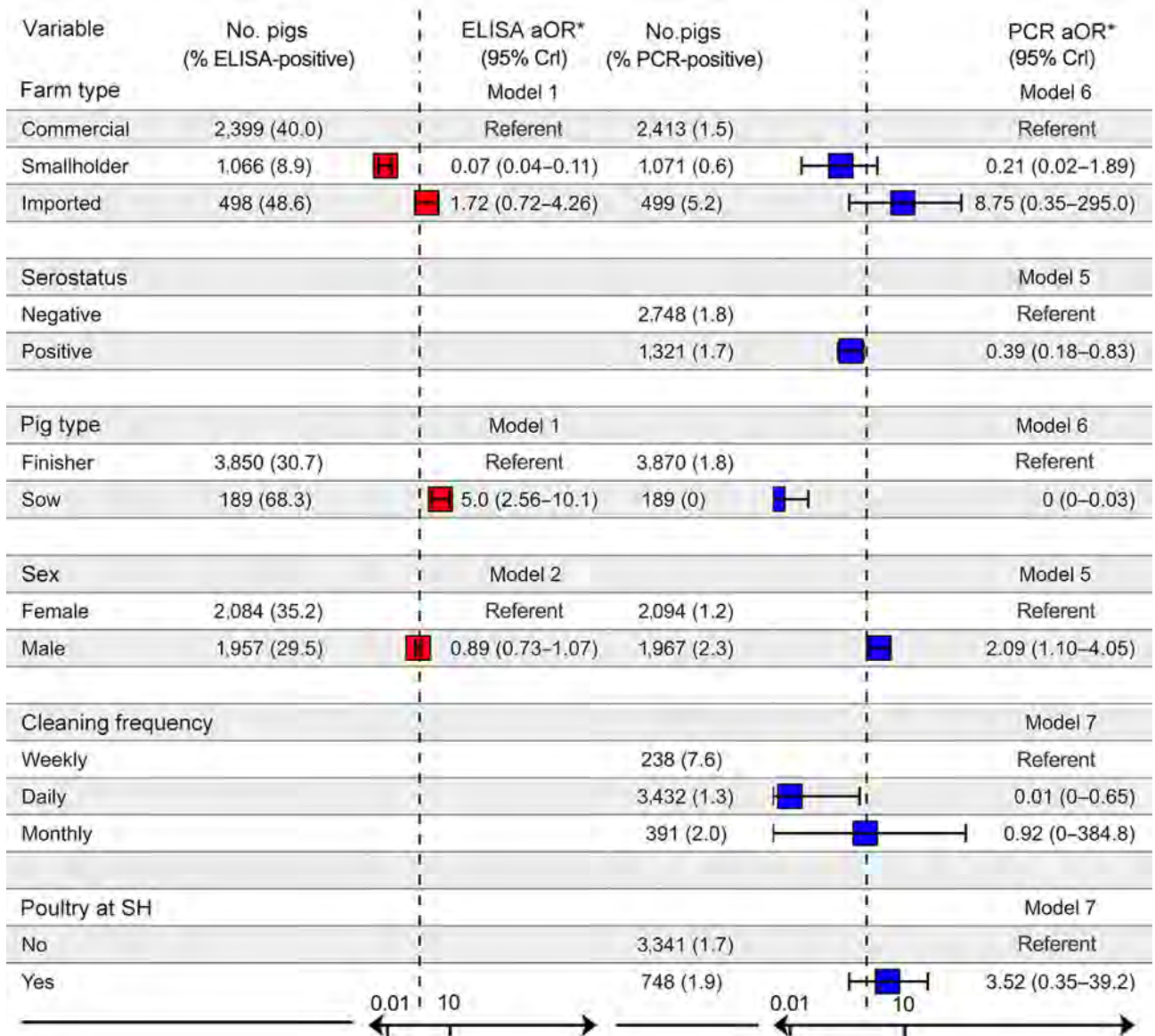‡ELISA confirmed.

Figure 1. Multivariable analyses in a study of transmission of swine influenza A viruses along pig value chains, Cambodia, 2020–2022. We analyzed exposure variables for associations with ELISA-confirmed influenza A serostatus (red) and PCR-confirmed active infection (blue) at the individual-pig level. Boxes indicate mean, horizontal bars attached to boxes indicate 95% CrI, vertical dotted lines indicate aOR = 1. We estimated posterior aORs and 95% CrI, shown on a log scale, using Bayesian hierarchical regression models derived from a directed acyclic graph. *Model numbers indicated in aOR columns correspond to models described in Appendix Table 1. 95% CrI, 95% credible interval; aOR, adjusted odds ratios; SH, slaughterhouse.

slaughterhouses; specifically, active infection was substantially lower among pigs sampled at slaughterhouses that cleaned pens daily compared with slaughterhouses that cleaned weekly, and increased with duration at the slaughterhouse. We also noted a positive trend between a longer stay at slaughterhouses and seroprevalence (Figure 2 panel A), possibly reflecting risk for exposure shortly before or during transport to the slaughterhouse. The presence of poultry at slaughterhouses did not affect active

infection status. Associations were not substantially affected by potential underdetection of infection in a sensitivity analysis (Appendix Table 4). For commercial but not smallholder farms, seroprevalence averaged across batches varied among districts (Figure 3).

Conclusions

Our findings demonstrate higher IAV circulation among pigs from commercial than from smallholder farms, adding information to limited studies on
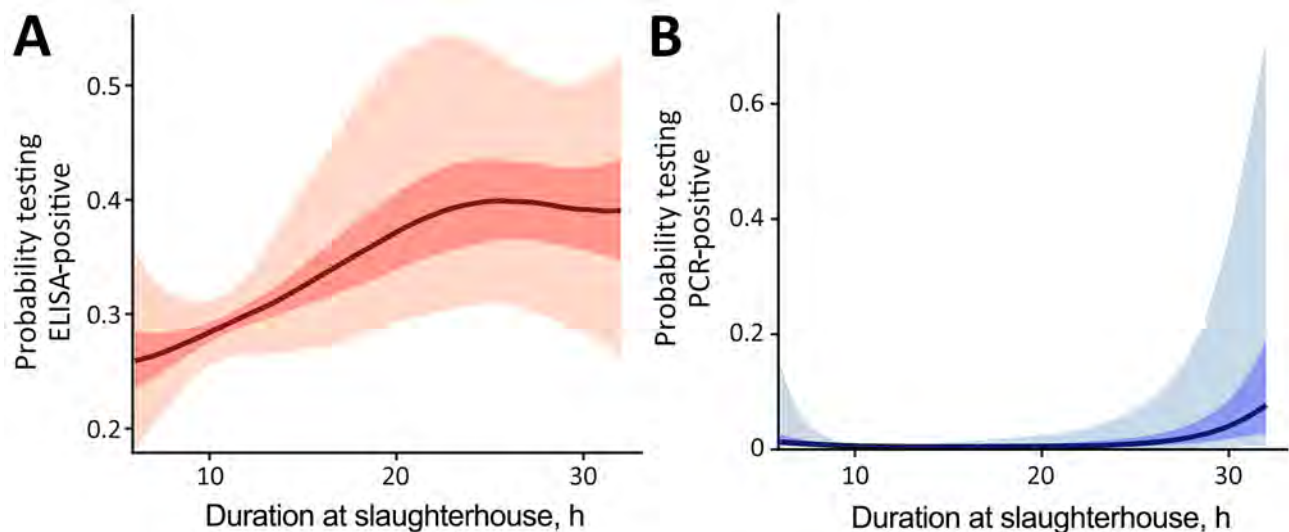
Figure 2. The adjusted probability of testing positive in a study of transmission of swine influenza A viruses along pig value chains, Cambodia, 2020–2022. A) Probability of ELISA-positive; B) probability of PCR-positive. Adjustments are a function of the duration at slaughterhouses, but other variables are kept at baseline. Solid lines indicate predicted means; dark shading indicates 50% CrI and light shading, 95% CrI.

swine IAV epidemiology in LMICs. The seroprevalence at commercial farms in Cambodia was comparable to that in high-income countries (*9*). The large variation in seroprevalence among batches from commercial farms, even farms owned by the same company, might reflect spatiotemporal variation in transmission, but warrants further investigation of the contribution of farm management practices. Literature provides evidence of IAV persistence and evolution through successive reassortments on commercial farms (*10*). Our findings highlight how increased livestock population and density in LMICs might increase risk for novel IAV emergence and amplification. As reported elsewhere, phylogenetic inferences from our samples from Cambodia identified 9 distinct swine IAV lineages, with human H1N1/pdm09 virus lineages predominating (*4*). The novel European avian-like H1N2 reassortant variant, possessing G4-like H1 sequences, was also present in 2 batches. Those batches, which we sampled within 24 hours of shipment, originated from different commercial farms at different timepoints, indicating the potential spread of this novel swine IAV variant among commercial farms in Cambodia.
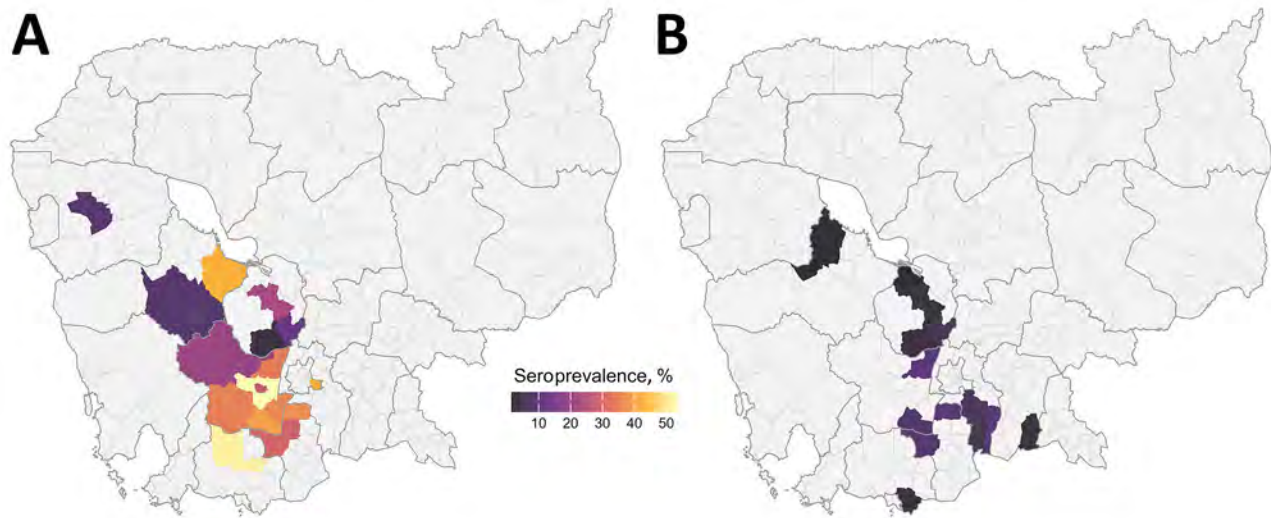
Figure 3. Spatial distributions of adjusted seroprevalence in a study of transmission of swine influenza A viruses along pig value chains, Cambodia, 2020–2022. Distribution by district of origin among commercial farms (A) and small-scale farms (B). Average seroprevalence was estimated for districts that had ≥2 batches of pigs from the same source sampled on the same day at a given slaughterhouse.

Although little is known about IAV transmission during transport and at slaughterhouses (*11*), our results indicate traders and slaughterhouse workers might be at heightened risk for swine IAV exposure. We are currently developing novel microbead-based serologic assays to distinguish antibodies to different IAV subtypes among pigs and humans, which will augment our understanding of IAV dynamics within and between different farm types and host species. In addition, reduced time from farm to slaughterhouse, less stressful pig handling, and improved slaughterhouse hygiene may ameliorate both enzootic and zoonotic transmission risks during the final stages of the pig value chain.

In summary, our analyses indicate that active infections among pigs sampled at slaughterhouses might reflect exposure immediately before or during transport to or at slaughterhouses. Thus, slaughterhouse surveillance data should be interpreted with caution when inferring risk from farm types or geographic origin, even when data on pig origin are available. In LMICs, surveillance at slaughterhouses rather than farms may be the only sustainable option (*12*). That surveillance should be coupled with monitoring of the status of pig value chains, which can change rapidly because of pig sector growth and outbreaks of diseases, such as African swine fever. Those findings contain implications for influenza risk and surveillance in emerging livestock systems.

About the Author

Dr. Hidano is a veterinary epidemiologist and assistant professor at the London School of Hygiene and Tropical Medicine, UK, based in Cambodia. He conducts interdisciplinary, One Health–focused research and his interests focus on how local behaviors are constructed in different contexts.

References

1. Coker RJ, Hunter BM, Rudge JW, Liverani M, Hanvoravongchai P. Emerging infectious diseases in southeast Asia: regional challenges to control. Lancet. 2011; 377:599–609. https://doi.org/10.1016/S0140-6736(10)62004-1
2. Liverani M, Waage J, Barnett T, Pfeiffer DU, Rushton J, Rudge JW, et al. Understanding and managing zoonotic risk in the new livestock industries. Environ Health Perspect. 2013;121:873–7. https://doi.org/10.1289/ehp.1206001
3. Li HY, Zhu GJ, Zhang YZ, Zhang LB, Hagan EA, Martinez S, et al. A qualitative study of zoonotic risk factors among rural communities in southern China. Int Health. 2020;12:77–85. https://doi.org/10.1093/inthealth/ihaa001
4. Zeller MA, Ma J, Wong FY, Tum S, Hidano A, Holt H, et al. The genomic landscape of swine influenza A viruses in Southeast Asia. Proc Natl Acad Sci U S A. 2023; 120:e2301926120. https://doi.org/10.1073/pnas.2301926120
5. Mastin A, Alarcon P, Pfeiffer D, Wood J, Williamson S, Brown I, et al.; COSI Consortium. Prevalence and risk factors for swine influenza virus infection in the English pig population. PLoS Curr. 2011;3:RRN1209. https://doi.org/10.1371/currents.RRN1209
6. Van TT, Miller J, Warshauer DM, Reisdorf E, Jernigan D, Humes R, et al. Pooling nasopharyngeal/throat swab specimens to increase testing capacity for influenza viruses by PCR. J Clin Microbiol. 2012;50:891–6. https://doi.org/10.1128/JCM.05631-11
7. Canini L, Holzer B, Morgan S, Dinie Hemmink J, Clark B, Woolhouse MEJ, et al.; sLoLa Dynamics Consortium. Timelines of infection and transmission dynamics of H1N1pdm09 in swine. PLoS Pathog. 2020;16:e1008628. https://doi.org/10.1371/journal.ppat.1008628
8. Bürkner PC. brms: Bayesian regression models using Stan [cited 2018 May 27]. https://CRAN.R-project.org/package=brms
9. Baudon E, Peyre M, Peiris M, Cowling BJ. Epidemiological features of influenza circulation in swine populations: a systematic review and meta-analysis. PLoS One. 2017; 12:e0179044. https://doi.org/10.1371/journal.pone.0179044
10. Chastagner A, Bonin E, Fablet C, Quéguiner S, Hirchaud E, Lucas P, et al. Virus persistence in pig herds led to successive reassortment events between swine and human influenza A viruses, resulting in the emergence of a novel triple-reassortant swine influenza virus. Vet Res. 2019;50:77. https://doi.org/10.1186/s13567-019-0699-y
11. Cheung JTL, Lau EH, Jin Z, Zhu H, Guan Y, Peiris M. Influenza A virus transmission in swine farms and during transport in the swine supply chain. Transbound Emerg Dis. 2022;69:e3101–10. https://doi.org/10.1111/tbed.14667
12. Baudon E, Chu DKW, Tung DD, Thi Nga P, Vu Mai Phuong H, Le Khanh Hang N, et al. Swine influenza viruses in Northern Vietnam in 2013–2014. Emerg Microbes Infect. 2018;7:123. https://doi.org/10.1038/s41426-018-0109-y

Address for correspondence: James W. Rudge, London School of Hygiene & Tropical Medicine, Department of Global Health and Development, 15–17 Tavistock Place, London, WC1E 7HT, UK; email: james.rudge@lshtm.ac.uk

Transboundary Movement of Yezo Virus via Ticks on Migratory Birds, Japan, 2020–2021

Ayano Nishino, Kango Tatemoto, Keita Ishijima, Yusuke Inoue, Eun-sil Park, Tsukasa Yamamoto, Masakatsu Taira, Yudai Kuroda, Milagros Virhuez-Mendoza, Michiko Harada, Noboru Nakamura, Gen Morimoto, Hiroki Yamaguchi, Takuma Ariizumi, Ai Takano, Hiroshi Shimoda, Keita Matsuno, Ken Maeda

Migratory birds carry ticks harboring various pathogens, including the zoonotic Yezo virus. In Hokkaido, Japan, we collected ticks from migratory birds during 2020–2021. Eight of 385 pools, comprising 2,534 ticks, tested positive for Yezo virus RNA, suggesting Yezo virus might be spread through the flyways of migratory birds.

Yezo virus (YEZV), in the order Bunyavirales, family Nairoviridae, genus *Orthonairovirus*, possesses a negative-sense single-stranded RNA genome comprising 3 segments: large (L), medium (M), and small (S) (*1*). Each segment contains a single open reading frame encoding the RNA-dependent RNA polymerase (L segment), glycoprotein precursor (M segment), and nucleoprotein (S segment) (*1*). YEZV infection is an emerging infectious disease, detected in Hokkaido, Japan, in 2019 among patients who had febrile illness after a tick bite (*1*); ≥9 patients infected with YEZV have been reported in Hokkaido (*1–3*). Among those patients, fever, myalgia, thrombocytopenia, leukopenia, and increasing liver enzymes were commonly reported after a tick bite (*1–3*). One patient who had a YEZV infection after a tick bite has also reported in Inner Mongolia in northeastern China (*4*).

Migratory birds carry ticks harboring various pathogens, such as Crimean-Congo hemorrhagic fever virus, belonging to the family *Nairoviridae* (*5–7*). Phylogenetic analysis of tickborne severe fever with thrombocytopenia syndrome virus indicated that this virus might be carried by ticks found on migratory birds that fly between China, South Korea, and Japan (*8,9*). Increasing evidence suggests that migratory birds play a critical role in spreading tickborne pathogens. In archipelagos, such as Japan, understanding transmission of pathogens by migratory birds is critical; however, information on tickborne pathogens carried by migratory birds is lacking. We investigated the prevalence of YEZV in ticks found on migratory birds in Japan to determine virus transmission pathways.

The Study

We conducted this research under approval by the animal research review board of Yamashina Institute for Ornithology, Chiba, Japan (approval nos. 2020-004 and 2021-002). We collected ticks infesting birds that mostly fly from Sakhalin and the Kuril Islands to Hokkaido, Japan. We collected the ticks during October 2–12, 2020, and October 2–13, 2021, in Lake Kutcharo, Hamatonbetsu Town, and Lake Furen, Nemuro City, Japan (Figure 1). We analyzed YEZV genes in the ticks to clarify virus spread. Because migratory birds at these locations in autumn are considered to have just arrived from Sakhalin (Sakhalin route) and the Kuril Islands (Kuril Islands route) (Figure 1), it is likely that the ticks crossed the sea attached to the birds.

We collected 2,534 ticks from 15 species of birds in October 2020 and 2021 (Appendix Tables 1, 2; https://wwwnc.cdc.gov/EID/article/30/12/24-0539-App1.pdf). All ticks were morphologically identified and pooled according to their species, life stage, and host species. Each pool consisted of ≤10 larval or 5 nymphal ticks (Appendix).
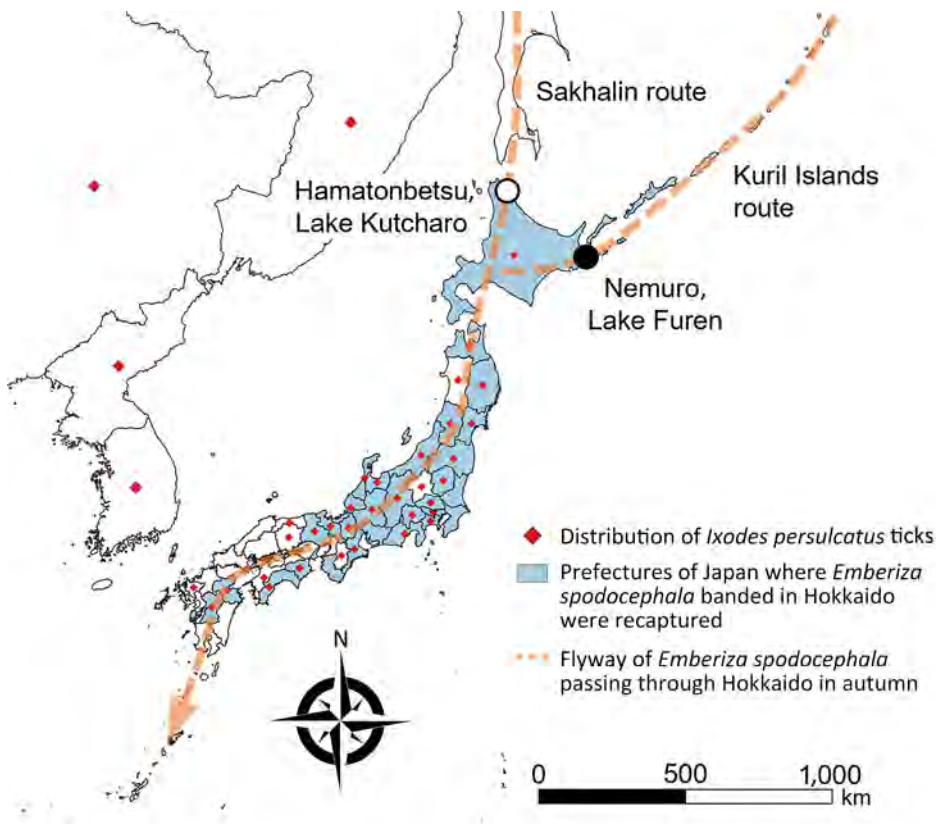
Figure 1. Migratory bird flyways and distribution of *Ixodes persulcatus* ticks in study of transboundary movement of Yezo virus via ticks on birds, Japan, 2020–2021. Distribution of *I. persulcatus* ticks (red rhombus), prefectures of Japan where black-faced buntings (*Emberiza spodocephala*) banded in Hokkaido were recaptured (light blue), and flyway of *E. spodocephala* passing through Hokkaido during autumn (orange dotted line). Distribution outside Japan is indicated at the country level. Black circle shows Lake Furen, Nemuro City, Hokkaido; white circle shows Lake Kutcharo, Hamatonbetsu Town, Hokkaido.

We examined 2,323 *Ixodes persulcatus* ticks (1,727 larvae and 596 nymphs), 203 *I. pavlovskyi* ticks (169 larvae and 34 nymphs), 1 *I. turdus* tick (nymph), 3 *Haemaphysalis megaspinosa* ticks (larvae), and 4 *H. concinna* ticks (3 larvae and 1 nymph) by using quantitative reverse transcription PCR (Appendix). Of those, 8 pools of *I. persulcatus* ticks were positive for YEZV RNA; no pools for the other tick species were YEZV positive (overall minimum infection rate 0.3%) (Table 1). Seven of 8 positive pools showed low cycle threshold (Ct) values of 22.08–30.08; 1 pool had a high Ct value of 39.19. Seven pools with low Ct values were used for further analysis. Ticks in all positive pools were *I. persulcatus* collected from black-faced buntings (*Emberiza spodocephala*) (Table 2). Five pools were collected in Lake Furen, Nemuro City, Hokkaido, and the other pools were collected in Lake Kutcharo, Hamatonbetsu Town, Hokkaido. Results indicated that ticks with YEZV were transferred by migratory birds along both the Sakhalin and Kuril Islands routes.

In *I. persulcatus* ticks, the minimum infection rate of YEZV was 0.2% in larvae and 0.8% in nymphs (Table 1). YEZV has been reported in 3 adult tick species, *H. megaspinosa*, *I. ovatus*, and *I. persulcatus*, found on vegetation in Hokkaido (*1*). In addition, 4 YEZV–positive pools consisted of only unfed ticks

(Appendix Table 3), indicating that *I. persulcatus* might transmit Yezo virus.

We sequenced 7 complete genomes of YEZV: YEZV/tick/BT-1821/Japan/2020, YEZV/tick/BT-1826/Japan/2020, YEZV/tick/BT-1844/Japan/2020, YEZV/tick/BT-1864/Japan/2020, YEZV/tick/BT-1968/Japan/2020, YEZV/tick/BT-2135/Japan/2021, and YEZV/tick/BT-2155/Japan/2021 (Appendix) and deposited those sequences into the DNA Data Bank of Japan (https://www.ddbj.nig.ac.jp) (Table 2). For 1 pool that had a high Ct value, YEZV/tick/BT-1822/Japan/2020, we could not determine the complete genome sequence; however, we amplified a short fragment of the S segment by nested reverse transcription PCR and deposited that sequence in the DNA Data Bank of Japan (Table 2).

We analyzed the nucleotide and amino acid sequences of the RNA-dependent RNA polymerase, glycoprotein precursor, and nucleoprotein among YEZV strains and compared those sequences to Sulina virus IxriSL16–01 sequences (*10*) (Appendix Tables 4–6). Sequence identity between YEZV strains was 93.0%–100.0% at the nucleotide level and 99.2%–100.0% at the amino acid level.

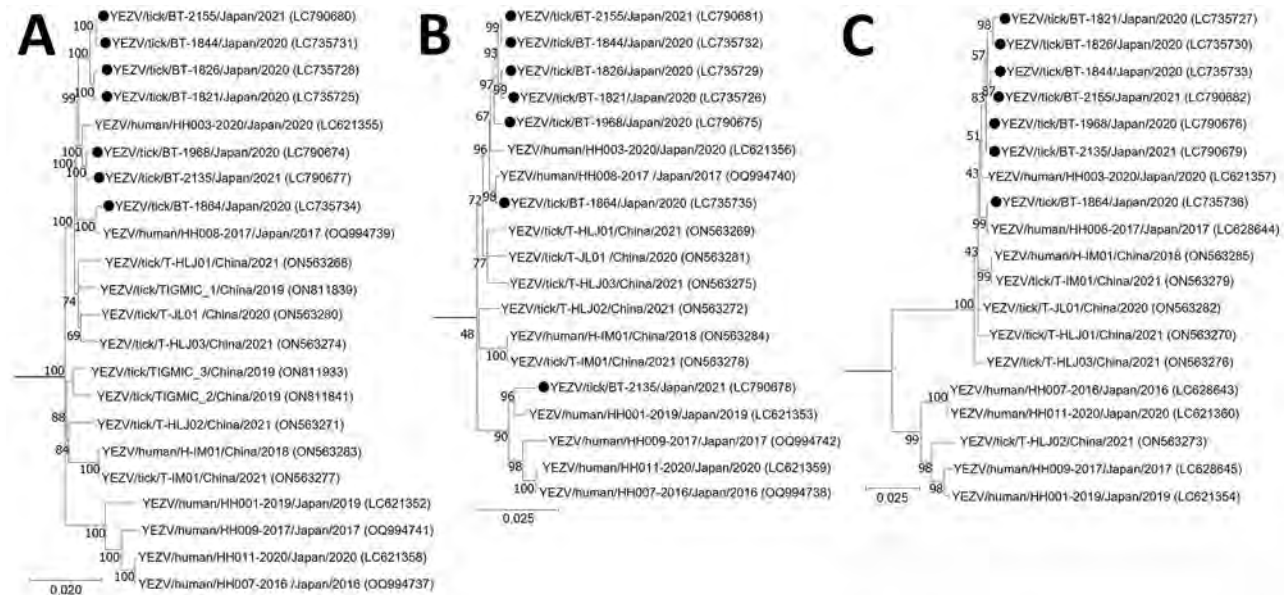We also performed phylogenetic analysis of YEZV strains by using the nucleotide sequences of the

Figure 2. Phylogenetic analysis of Yezo virus strains in study of transboundary movement of Yezo virus via ticks on migratory birds, Japan, 2020–2021. Trees were constructed by using the maximum-likelihood method in MEGA X (https://www.megasoftware.net) and 1,000 bootstrap replicates for nucleotide sequences. A) Large segment; B) medium segment; C) small segment. Black circles indicate sequences from this study. The number at each branch indicates the bootstrap value. GenBank accession numbers for nucleotide sequences are shown in parentheses. Sulina virus IxriSL16-01 was used as the outgroup to determine the root of Yezo virus trees but is not shown. Scale bars indicate nucleotide substitutions per site.

open reading frames of the L, M, and S segments (Figure 2). All tick-derived strains detected in this study belonged to the same cluster as the strains obtained from patients in Hokkaido, YEZV/human/HH003-2020/Japan/2020 and YEZV/human/HH008-2017/Japan/2017 (*1*). In addition, our tick-derived strain, YEZV/tick/BT-2135/Japan/2021, and the tick-derived strain from Heilongjiang, China, YEZV/tick/T-HLJ02/People's Republic of China/2021, were reassortment strains; both were generated through reassortment with the strains found in patients in Hokkaido, Japan. We also confirmed the events of genetic reassortment by using a recombination detection program (A. Nishino and K. Maeda, unpub. data), which suggested that YEZV might be transferred between China and Hokkaido, Japan.

Conclusions

We successfully detected YEZV in *I. persulcatus* ticks from migratory birds (*E. spodocephala* buntings) flying to Hokkaido, Japan, from Sakhalin and the Kuril Islands (*5,11*). The distribution of *I. persulcatus* ticks partially overlapped with the flyway of *E. spodocephala* buntings passing through Hokkaido in autumn (*12–15*). Together

Table 1. Virus prevalence in tick species collected in an investigation of transboundary movement of Yezo virus via ticks on migratory birds, Japan, 2020–2021

Species	No. ticks examined	No. pools examined	No. positive pools	Minimum infection rate, %
Ixodes persulcatus				
Larva	1,727	193	3	0.2
Nymph	596	137	5	0.8
I. pavlovskyi				
Larva	169	30	0	0
Nymph	34	19	0	0
I. turdus				
Larva	0	0	0	0
Nymph	1	1	0	0
Haemaphysalis megaspinosa				
Larva	3	2	0	0
Nymph	0	0	0	0
H. concinna				
Larva	3	2	0	0
Nymph	1	1	0	0
Total	2,534	385	8	0.3

Table 2. Genomic sequences in an investigation of transboundary movement of Yezo virus via ticks on migratory birds, Japan, 2020–2021*

Virus strain	Tick stage	No. ticks in pool	Collection site	Collection date	Segment	Accession nos.†
YEZV/tick/BT-1821/Japan/2020	Nymph	5	Lake Kutcharo, Hamatonbetsu	2020 Oct 6–7	L	LC735725
					M	LC735726
					S	LC735727
YEZV/tick/BT-1822/Japan/2020	Nymph	5	Lake Kutcharo, Hamatonbetsu	2020 Oct 6–7	S	LC737964, partial sequence
YEZV/tick/BT-1826/Japan/2020	Nymph	5	Lake Kutcharo, Hamatonbetsu	2020 Oct 7	L	LC735728
					M	LC735729
					S	LC735730
YEZV/tick/BT-1844/Japan/2020	Larva	10	Lake Furen, Nemuro	2020 Oct 8	L	LC735731
					M	LC735732
					S	LC735733
YEZV/tick/BT-1864/Japan/2020	Larva	10	Lake Furen, Nemuro	2020 Oct 8	L	LC735734
					M	LC735735
					S	LC735736
YEZV/tick/BT-1968/Japan/2020	Larva	10	Lake Furen, Nemuro	2020 Oct 11	L	LC790674
					M	LC790675
					S	LC790676
YEZV/tick/BT-2135/Japan/2021	Nymph	5	Lake Furen, Nemuro	2021 Oct 13	L	LC790677
					M	LC790678
					S	LC790679
YEZV/tick/BT-2155/Japan/2021	Nymph	5	Lake Furen, Nemuro	2021 Oct 13	L	LC790680
					M	LC790681
					S	LC790682

*All ticks collected were *Ixodes persulcatus* and all birds collected were black-faced buntings (*Emberiza spodocephala*). L, large segment; M, medium segment; S, small segment.
†DNA Data Bank of Japan (https://www.ddbj.nig.ac.jp) accession numbers.

with the possible genetic reassortment event between YEZV strains from Japan and China, this finding indicated that YEZV might be carried by migratory birds from other countries to Japan and from Hokkaido to other prefectures in Japan. To elucidate the distribution area and transmission routes of YEZV, further surveillance of YEZV infection should be conducted in ticks, birds, and wild and domestic animals.

Acknowledgments

About the Author

Ms. Nishino is a PhD candidate at the Joint Graduate School of Veterinary Medicine, Yamaguchi University, and a researcher at the Department of Veterinary Science, National Institute of Infectious Diseases. Her primary research interest focuses on transboundary tickborne diseases carried by migratory birds.

References

1. Kodama F, Yamaguchi H, Park E, Tatemoto K, Sashika M, Nakao R, et al. A novel nairovirus associated with acute febrile illness in Hokkaido, Japan. Nat Commun. 2021;12:5539. https://doi.org/10.1038/s41467-021-25857-0
2. Suzuki K, Suzuki S, Yamaguchi H, Kakinoki Y. Tick-borne disease with Yezo virus and *Borrelia miyamotoi* coinfection. Intern Med. 2024;63:2861–4. https://doi.org/10.2169/internalmedicine.3225-23
3. Ogata Y, Sato T, Kato K, Kikuchi K, Mitsuhashi K, Watari K, et al. A case of tick-borne Yezo virus infection: concurrent detection in the patient and tick. Int J Infect Dis. 2024;143:107038. https://doi.org/10.1016/j.ijid.2024.107038
4. Lv X, Liu Z, Li L, Xu W, Yuan Y, Liang X, et al. Yezo virus infection in tick-bitten patient and ticks, northeastern China. Emerg Infect Dis. 2023;29:797–800. https://doi.org/10.3201/eid2904.220885
5. Ishiguro F, Takada N, Masuzawa T, Fukui T. Prevalence of Lyme disease *Borrelia* spp. in ticks from migratory birds on the Japanese mainland. Appl Environ Microbiol. 2000;66:982–6. https://doi.org/10.1128/AEM.66.3.982-986.2000
6. Waldenström J, Lundkvist A, Falk KI, Garpmo U, Bergström S, Lindegren G, et al. Migrating birds and tickborne encephalitis virus. Emerg Infect Dis. 2007;13:1215–8. https://doi.org/10.3201/eid1308.061416
7. Lindeborg M, Barboutis C, Ehrenborg C, Fransson T, Jaenson TGT, Lindgren PE, et al. Migratory birds, ticks, and Crimean-Congo hemorrhagic fever virus. Emerg Infect Dis. 2012;18:2095–7. https://doi.org/10.3201/eid1812.120718
8. Yoshikawa T, Shimojima M, Fukushi S, Tani H, Fukuma A, Taniguchi S, et al. Phylogenetic and geographic relationships of severe fever with thrombocytopenia syndrome virus in China, South Korea, and Japan. J Infect Dis. 2015;212:889–98. https://doi.org/10.1093/infdis/jiv144
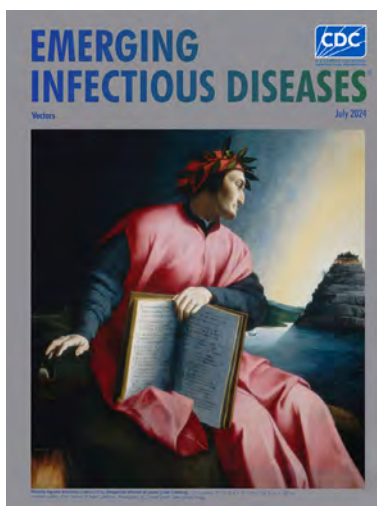9. Yun Y, Heo ST, Kim G, Hewson R, Kim H, Park D, et al. Phylogenetic analysis of severe fever with thrombocytopenia

syndrome virus in South Korea and migratory bird routes between China, South Korea, and Japan. Am J Trop Med Hyg. 2015;93:468–74. https://doi.org/10.4269/ajtmh.15-0047

10. Tomazatos A, von Possel R, Pekarek N, Holm T, Rieger T, Baum H, et al. Discovery and genetic characterization of a novel orthonairovirus in *Ixodes ricinus* ticks from Danube Delta. Infect Genet Evol. 2021;88:104704. https://doi.org/10.1016/j.meegid.2021.104704

11. BirdLife International. East Asia/Australasia Flyway [cited 2023 Feb 26]. http://datazone.birdlife.org/userfiles/file/sowb/flyways/8_East_Asia_Australasia_Factsheet.pdf

12. St. John HK, Masuoka P, Jiang J, Takhampunya R, Klein TA, Kim HC, et al. Geographic distribution and modeling of ticks in the Republic of Korea and the application of tick models towards understanding the distribution of associated pathogenic agents. Ticks Tick Borne Dis. 2021;12:101686. https://doi.org/10.1016/j.ttbdis.2021.101686

13. Yamashina Institute for Ornithology. Atlas of Japanese migratory birds from 1961 to 1995 [in Japanese] [cited 2024 Apr 15]. https://www.biodic.go.jp/banding_en/banding/atlas.html

14. Swanson SJ, Neitzel D, Reed KD, Belongia EA. Coinfections acquired from *Ixodes* ticks. Clin Microbiol Rev. 2006;19:708–27. https://doi.org/10.1128/CMR.00011-06

15. Takada N, Takahashi M, Fujita H, Natsuaki M. Tick & tick-borne infectious diseases. In: Takada N, editor. Medical acarology in Japan [in Japanese]. Tokyo: Hokuryukan; 2019. p. 114–249.

Address for correspondence: Ken Maeda, Department of Veterinary Science, National Institute of Infectious Diseases, 1-23-1 Toyama, Shinjuku-ku, Tokyo 162-8640, Japan; email: kmaeda@niid.go.jp

July 2024

Vectors

EMERGING INFECTIOUS DISEASES®

To revisit the July 2024 issue, go to:

https://wwwnc.cdc.gov/eid/articles/issue/30/7/table-of-contents

Chikungunya Outbreak Risks after the 2014 Outbreak, Dominican Republic

Gideon Loevinsohn,[1] Cecilia Then Paulino,[1] Jessica Spring, Holly R. Hughes, Angela Cadavid Restrepo, Helen Mayfield, Michael de St. Aubin, Janeen Laven, Amanda Panella, William Duke, Marie Caroline Etienne, Gabriela Abdalla, Salome Garnier, Naomi Iihoshi, Beatriz Lopez, Lucia de la Cruz, Bernarda Henríquez, Margaret Baldwin, Farah Peña, Adam J. Kucharski, Marietta Vasquez, Emily Zielinski Gutiérrez, Aaron C. Brault, Ronald Skewes-Ramm, Colleen L. Lau, Eric J. Nilles

The 2014 chikungunya outbreak in the Dominican Republic resulted in intense local transmission, with high postoutbreak seroprevalence. The resulting population immunity will likely minimize risk for another large outbreak through 2035, but changes in population behavior or environmental conditions or emergence of different virus strains could lead to increased transmission.

In early 2023, a substantial increase in chikungunya disease cases in South America prompted an alert from the Pan American Health Organization (1). Although most chikungunya virus (CHIKV) transmission has occurred in Paraguay and Brazil, the proximity of nearby regions, including the Caribbean, with histories of intense arboviral transmission raises the prospect of epidemic spread. The Caribbean is an ecologically receptive setting for CHIKV and was heavily impacted by a 2014 epidemic (2). The epidemic was particularly severe in the Dominican Republic, where >539,000 cases and more deaths per capita than any other country in the Americas were reported (3,4). Given that vulnerability, we conducted a study to assess the risks for future CHIKV outbreaks in the Dominican Republic by evaluating post-2014 CHIKV transmission, estimating current population-level immune protection, and modeling future epidemic risks. Our research aims to inform public health interventions and preparedness strategies in anticipation of potential regional CHIKV resurgence.

Data and specimens were collected as part of a US Centers for Disease Control and Prevention–funded acute febrile illness (AFI) research program. The studies were approved by the Dominican Republic National Council of Bioethics in Health (#013-2019); the institutional review board of Pedro Henríquez Ureña National University (Santo Domingo, Dominican Republic), and the Massachusetts General Brigham Human Research Committee (Boston, MA, USA) (#2019P000094).

The Study

To understand local CHIKV epidemiology and transmission after the 2014 outbreak, we first performed reverse transcription PCR (RT-PCR) on acute-phase serum samples from patients enrolled as part of a prospective AFI surveillance program at Dr. Toribio Benosme Hospital in Espaillat Province in northwestern

Author affiliations: Massachusetts General Hospital, Boston, Massechusetts, USA (G. Loevinsohn); Brigham and Women's Hospital, Boston (G. Loevinsohn, M. de St. Aubin, M.C. Etienne, G. Abdalla, S. Garnier, N. Iihoshi, M. Baldwin, E.J. Nilles); Ministry of Health and Social Assistance, Santo Domingo, Dominican Republic (C. Then Paulino, L. de la Cruz, B. Henríquez, F. Peña, R. Skewes-Ramm); Centers for Disease Control and Prevention, Fort Collins, Colorado, USA (J. Spring, H.R. Hughes, J. Laven, A. Panella, A.C. Brault); University of Queensland, Brisbane, Queensland, Australia (A. Cadavid Restrepo, H. Mayfield, C.L. Lau); Harvard Humanitarian Initiative, Cambridge, Massachusetts, USA (M. de St. Aubin, M. Baldwin. E.J. Nilles); Pedro Henríquez Ureña National University, Santo Domingo (W. Duke); Centers for Disease Control and Prevention, Central America Regional Office, Guatemala City, Guatemala (B. Lopez, E. Zielinski Gutiérrez); London School of Hygiene and Tropical Medicine, London, UK (A.J. Kucharski); Yale School of Medicine, New Haven, Connecticut, USA (M. Vasquez); Harvard Medical School, Boston (E.J. Nilles)

Dominican Republic and Dr. Antonio Musa Hospital in San Pedro de Macorís Province in southeastern Dominican Republic, using study processes described elsewhere (5). We invited patients ≥2 years of age with measured (≥38°C) or reported undifferentiated fever to participate. All adult participants and parents or legal guardians of child participants provided written consent; children 7–17 years of age provided assent. During November 2019–June 2023, we enrolled and tested 2,792 persons for a range of pathogens, including CHIKV, by RT-PCR (Appendix Table 1, https://wwwnc.cdc.gov/EID/article/30/12/24-0824-App1.pdf). We detected no cases of acute CHIKV infection, which aligns with national reported surveillance data that suggest minimal post-2014 transmission (Appendix Figure 1).

Next, to estimate population-level chikungunya seroprevalence, we conducted serologic screening among asymptomatic persons enrolled in a cross-sectional household cluster survey during July–October 2021 that included San Pedro de Macoris and Espaillat Provinces, which aligned with locations from the AFI surveillance program. The 3-stage cross-sectional sampling strategy, which enrolled household members ≥5 years of age, has been described elsewhere (6). We screened 201 serum samples using plaque reduction neutralization tests (PRNT) and 196 using ELISA IgG tests (Appendix). Of 397 persons enrolled from the 2 provinces, 319 (80.4%) were seropositive (Table). After adjusting for sex, age, and urban/rural setting, the estimated population sero-

prevalence across all age groups was 69.6% (95% CI 64.5%–74.8%) in 2021. That estimate based on national surveillance data assumed that persons born after 2014 were seronegative (Appendix Figure 1). To further assess that assumption, and because few participants enrolled in the serologic survey were born after the 2014 outbreak, we conducted serologic screening on serum samples from children enrolled through the prospective AFI surveillance platform (5). That testing enabled us to assess seropositivity derived from infection after the 2014 outbreak. Date of birth relative to the 2014 outbreak strongly predicted serostatus. Of 275 children screened using PRNT, 110 were born during 2009–2013 (60 [55%] seropositive), 14 in 2014 (1 [7%] seropositive), and 151 after 2014 (1 [0.7%] seropositive) (Table; Figure 1).

We then used our seroprevalence estimates to model population-level immune protection from 2012 through 2045 using methods reported elsewhere (7). We considered that infection generates lifelong immune protection and adjusted population immune protection over time to account for new births adding susceptible persons to the population and deaths reducing the pool of immune persons (Figure 2). Given minimal post-2014 transmission, we assumed no additional population immunity was generated after 2014. Based on our seroprevalence values, we calculated a basic reproduction number (R_0) of 2.0 (95% CI 1.84–2.33). We calculated the effective reproduction number (R_{eff}) over time using the R_0 and population immune protection (Figure
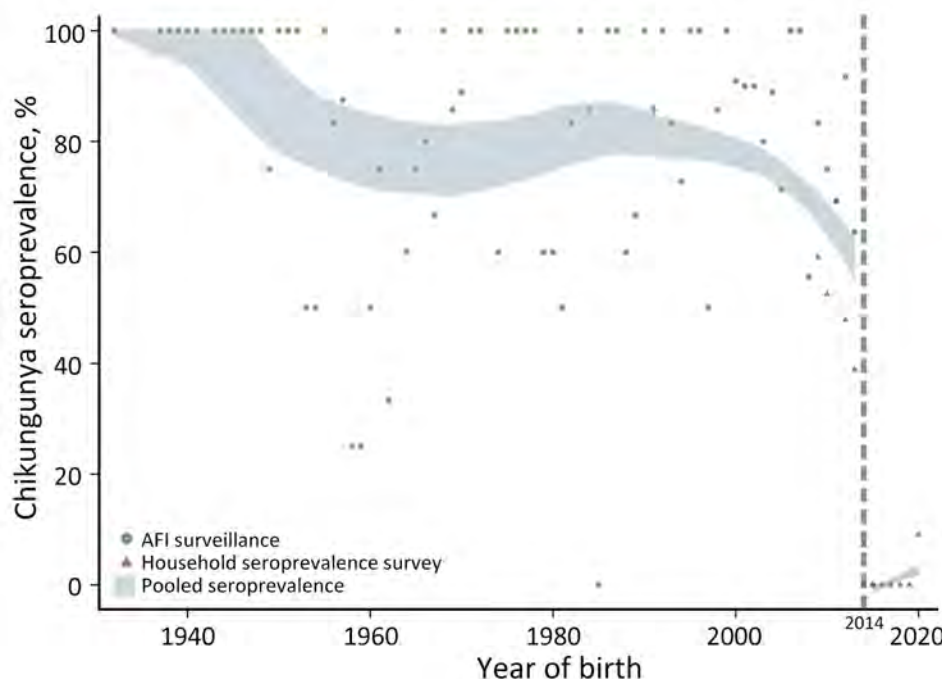

Figure 1. Chikungunya seroprevalence by year of birth in study of chikungunya outbreak risks after the 2014 outbreak, Dominican Republic. Blue band represents the 95% CI for pooled seroprevalence, which combined data from acute febrile illness and serosurvey cohorts. Estimates were obtained using kernel-weighted local polynomial smoothing weighted by the size of each birth cohort. AFI, acute febrile illness.

2, panel A). Our findings suggest that the R_{eff} will remain <1.0 through 2035, indicating that, although clusters of CHIKV infection may occur, widespread and intense community transmission is unlikely. Finally, for comparison, we performed similar analyses for other Caribbean settings, including Jamaica and Puerto Rico, that have reported on CHIKV seroprevalence since the 2014 outbreak. Those analyses suggest that although postoutbreak seroprevalence and R_0 values differ between settings (Appendix Table 2), the risk of widespread regional transmission will remain low through 2035 (Appendix, Appendix Figure 2, panels A, B).

Conclusion

We found serologic evidence of intense CHIKV transmission in study sites in northwestern and southeastern Dominican Republic during the 2014 outbreak but little subsequent transmission. Those findings were corroborated across a range of sources, including national surveillance, sentinel AFI surveillance, and a cross-sectional serologic survey. Our postoutbreak seroprevalence estimates provide key public health data for the Dominican Republic; the estimate (69.6%) was slightly lower than estimates from Jamaica (83.6%) and Haiti (78.7%) but higher than in other countries in the region (8–11). However, when

Table. Population characteristics and prevalence information from study of future risks for chikungunya outbreaks in the Dominican Republic*

	Household serologic survey†			Acute febrile infection illness‡		
Category	All study participants, n = 397	CHIKV seropositive, n = 319	CHIKV seronegative, n = 78	All study participants, n = 275	CHIKV seropositive, |n = 62	CHIKV seronegative, n = 213
Province						
San Pedro de Macorís	311	260 (84)	51 (16)	131	34 (26)	97 (74)
Espaillat	86	59 (69)	27 (31)	135	25 (19)	110 (81)
Other	0	0	0	9	3 (33)	6 (67)
Year of birth						
Before 2014	392	319 (81)	73 (19)	110	60 (55)	50 (45)
2014	3	0	3 (100)	14	1 (7)	13 (93)
After 2014	2	0	2 (100)	151	1 (1)	150 (99)
Median age, y (IQR)	32 (17.4–55.5)	31.9 (18–55.5)	32.7 (13–56.3)	6.7 (4.0–10.0)	10.7 (9.5–11.4)	5.3 (3.7–7.5)
Age group, y						
1–5	0	0	0	118	1 (1)	117 (99)
6–10	43	28 (65)	15 (35)	114	37 (32)	77 (68)
11–20	95	81 (85)	14 (15)	43	24 (56)	19 (44)
21–40	99	81 (82)	18 (18)	0	0	0
41–60	87	68 (78)	19 (22)	0	0	0
≥61	73	61 (84)	12 (16)	0	0	0
Sex						
F	250	206 (82)	44 (18)	131	37 (28)	94 (72)
M	147	113 (77)	34 (23)	144	25 (17)	119 (83)
Place of birth						
Dominican Republic	384	309 (80)	75 (20)	270	61 (23)	209 (77)
Other	13	10 (77)	3 (23)	5	1 (20)	4 (80)
Educational attainment						
No formal education	23	17 (74)	6 (26)	153	12 (8)	141 (92)
Primary	112	95 (85)	17 (15)	119	49 (41)	70 (59)
Secondary	123	104 (85)	19 (15)	2	1 (50)	1 (50)
Technical	13	11 (85)	2 (15)	0	0	0
University	37	26 (70)	11 (30)	0	0	0
Missing or not available	89	66 (74)	23 (26)	1	0	1 (100)
Occupation						
Active worker	91	67 (74)	24 (26)	1	1 (100)	0
Houseperson	82	72 (88)	10 (12)	0	0	0
Student	130	102 (78)	28 (22)	161	58 (36)	103 (64)
Retired	12	10 (83)	2 (17)	0	0	0
Unemployed	79	67 (85)	12 (15)	3	0	3 (100)
Preschool	0	0	0	110	3 (3)	107 (97)
Other	3	2 (67)	2 (67)	0	0	0
Self-reported prior infection						
Chikungunya	108	97 (90)	11 (10)	NA	NA	NA
Dengue	14	14 (100)	0	NA	NA	NA
Zika	3	3 (100)	0	NA	NA	NA

*Values are no. (%) except as inidicated. CHIKV, chikungunya virus; NA, not applicable.
†Serologic status was assessed for household serologic survey participants using chikungunya plaque reduction neutralization test (n = 202) and ELISA to detect CHIKV IgG (n = 195).
‡Serologic status for all acute febrile illness surveillance participants was assessed using chikungunya plaque reduction neutralization test.
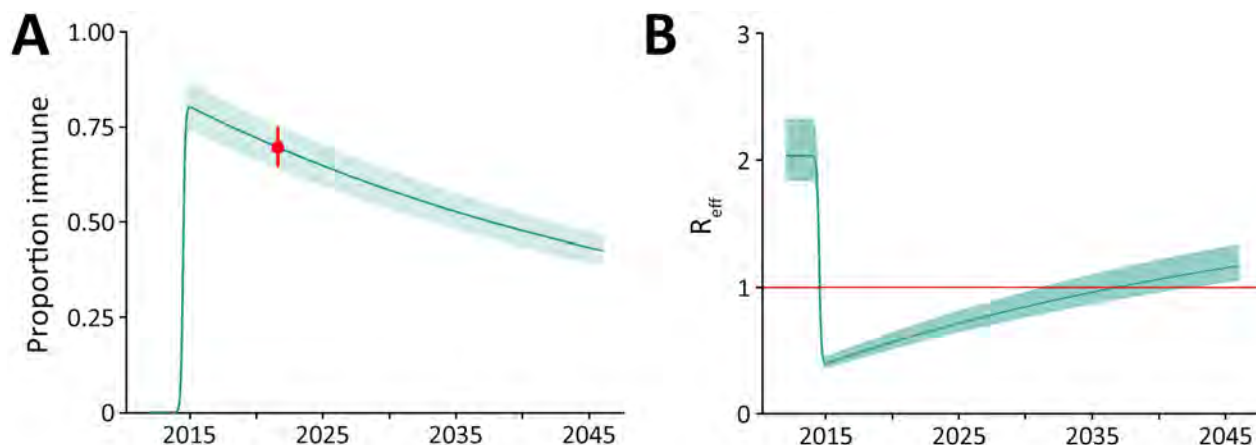
Figure 2. Projected chikungunya population immunity and R_{eff} in study of chikungunya outbreak risks after the 2014 outbreak, Dominican Republic. A) Estimated population immunity from 2012 through 2045 using a simulated population parameterized to the current population seroprevalence (red dot). Solid line represent point estimates and shading 95% CIs. Changes in population immunity over time reflect the introduction of new susceptible persons through births and decrease in immune persons through deaths. B) Projected changes in effective reproductive number over time calculated from the basic reproduction number R_0 and population immunity. Solid line represents change in R_{eff} and shading 95% CIs, based on the simulated proportion of the immune population. The solid red horizontal line at $R_{eff} = 1$ represents the threshold for sustained transmission; values above this line indicate $R_{eff} >1$, suggesting potential for ongoing transmission, wheras values below this line indicate $R_{eff} <1$, suggesting a decline in transmission. R_{eff}, effective reproduction number.

differences in the timing of the serological surveys in relation to the 2014 outbreak are considered, and interval decreases in seroprevalence accounted for, post-2014 outbreak seroprevalence estimates across the 3 countries were broadly similar, and all were >80%.

We concluded that the 2014 outbreak generated high levels of population immune protection. However, in the absence of meaningful ongoing transmission, population protection will decrease. Because new births add susceptible persons to the population and deaths reduce the pool of immune persons, the ratio of susceptible to immune persons increases over time. As this ratio increases, so does the risk for a sustained outbreak. Awareness of when population immune protection falls below a threshold that could allow widespread transmission is critical for public health forecasting and response, both in the Dominican Republic and in settings with similar immunologic and epidemiologic profiles.

Our analyses suggest that population immune protection derived from the 2014 outbreak is likely to minimize the risk for another large outbreak through at least 2035 (Figure 2, panel A) if other factors remain unchanged. However, changes in population behavior or environmental conditions, or emergence of new strains, could lead to increased transmission, as documented in the 2022–2023 outbreak in Paraguay, when transmission expanded to multiple previously unaffected regions (*12*).

Limitations included lack of generalizability of the data sources. We largely addressed this limitation by using multiple data sources to confirm key findings, with the exception of population seroprevalence estimates, for which we relied on a single source. The number of study participants was limited, and data were restricted to 2 provinces; therefore, our point estimates might not be representative of national seroprevalence. In addition, the specificity of CHIKV immunoassays may be affected by other circulating alphaviruses (*13*), although substantially lower seroprevalence among those born after 2014 suggests that effect was unlikely.

In conclusion, chikungunya immune protection generated during the 2014 outbreak in the Dominican Republic will likely minimize the risk for widespread and intense transmission in the next decade, similar to findings from Jamaica and Puerto Rico. However, changes in behaviors, environmental conditions, or emergence of new strains could affect those predictions. Therefore, public health authorities should closely monitor chikungunya activity and develop preparedness plans to mitigate effects of future outbreaks.

About the Author

Dr. Loevinsohn is chief resident in the Department of Emergency Medicine at Massachussets General Hospital and Brigham and Women's Hospital in Boston, Massachusetts, USA. His clinical and research interests focus on emergency care in resource-limited settings, epidemiology of acute illnesses, and multifaceted determinants of health.

References

1. Pan American Health Organization/World Health Organization. Epidemiological alert: increase in cases and deaths from chikungunya in the region of the Americas [cited 2024 Apr 7]. https://www.paho.org/en/documents/epidemiological-alert-increase-cases-and-deaths-chikungunya-region-americas

2. Gutierrez-Saravia E, Gutierrez CE. Chikungunya virus in the Caribbean: a threat for all of the Americas. J Pediatric Infect Dis Soc. 2015;4:1–3. https://doi.org/10.1093/jpids/piv002

3. Pan American Health Organization. Chikungunya [cited 2024 Apr 7]. https://www3.paho.org/data/index.php/en/mnu-topics/chikv-en.html

4. Freitas ARR, Alarcón-Elbal PM, Paulino-Ramírez R, Donalisio MR. Excess mortality profile during the Asian genotype chikungunya epidemic in the Dominican Republic, 2014. Trans R Soc Trop Med Hyg. 2018;112:443–9. https://doi.org/10.1093/trstmh/try072

5. Nilles EJ, de St Aubin M, Dumas D, Duke W, Etienne MC, Abdalla G, et al. Monitoring temporal changes in SARS-CoV-2 spike antibody levels and variant-specific risk for infection, Dominican Republic, March 2021–August 2022. Emerg Infect Dis. 2023;29:723–33. https://doi.org/10.3201/eid2904.221628

6. Nilles EJ, Paulino CT, de St Aubin M, Restrepo AC, Mayfield H, Dumas D, et al. SARS-CoV-2 seroprevalence, cumulative infections, and immunity to symptomatic infection—a multistage national household survey and modelling study, Dominican Republic, June–October 2021. Lancet Reg Health Am. 2022;16:100390. https://doi.org/10.1016/j.lana.2022.100390

7. Kucharski AJ, Funk S, Eggo RM, Mallet HP, Edmunds WJ, Nilles EJ. Transmission dynamics of Zika virus in island populations: a modelling analysis of the 2013–14 French Polynesia outbreak. PLoS Negl Trop Dis. 2016;10:e0004726. https://doi.org/10.1371/journal.pntd.0004726

8. Anzinger JJ, Mears CD, Ades AE, Francis K, Phillips Y, Leys YE, et al.; ZIKAction Consortium1,2. Antenatal seroprevalence of Zika and chikungunya viruses, Kingston metropolitan area, Jamaica, 2017–2019. Emerg Infect Dis. 2022;28:473–5. https://doi.org/10.3201/eid2802.211849

9. Adams LE, Sánchez-González L, Rodriguez DM, Ryff K, Major C, Lorenzi O, et al. Risk factors for infection with chikungunya and Zika viruses in southern Puerto Rico: a community-based cross-sectional seroprevalence survey. PLoS Negl Trop Dis. 2022;16:e0010416. https://doi.org/10.1371/journal.pntd.0010416

10. Poirier MJP, Moss DM, Feeser KR, Streit TG, Chang GJJ, Whitney M, et al. Measuring Haitian children's exposure to chikungunya, dengue and malaria. Bull World Health Organ. 2016;94:817–25A. https://doi.org/10.2471/BLT.16.173252

11. Gallian P, Leparc-Goffart I, Richard P, Maire F, Flusin O, Djoudi R, et al. Epidemiology of chikungunya virus outbreaks in Guadeloupe and Martinique, 2014: an observational study in volunteer blood donors. PLoS Negl Trop Dis. 2017;11:e0005254. https://doi.org/10.1371/journal.pntd.0005254

12. Giovanetti M, Vazquez C, Lima M, Castro E, Rojas A, Gomez de la Fuente A, et al. Rapid epidemic expansion of chikungunya virus East/Central/South African lineage, Paraguay. Emerg Infect Dis. 2023;29:1859–63. https://doi.org/10.3201/eid2909.230523

13. Fischer C, Bozza F, Merino Merino XJ, Pedroso C, de Oliveira Filho EF, Moreira-Soto A, et al. Robustness of serologic investigations for chikungunya and Mayaro viruses following coemergence. MSphere. 2020;5:5. https://doi.org/10.1128/mSphere.00915-19

Address for correspondence: Eric J. Nilles, Brigham and Women's Hospital, 75 Francis St, Boston, MA 02115, USA; email: enilles@bwh.harvard.edu

Replication-Competent Oropouche Virus in Semen of Traveler Returning to Italy from Cuba, 2024

Concetta Castilletti,[1] Ralph Huits,[1] Rebeca Passarelli Mantovani, Silvia Accordini, Francesca Alladio, Federico Gobbi

Author affiliations: IRCCS Sacro Cuore Don Calabria Hospital, Negrar di Valpolicella, Italy (C. Castilletti, R. Huits, R. Passarelli Mantovani, S. Accordini, F. Alladio, F. Gobbi); University of Brescia, Brescia, Italy (F. Gobbi)

DOI: https://doi.org/10.3201/eid3012.241470

A febrile man in Italy who had traveled to Cuba in July 2024 was diagnosed with Oropouche fever. Reverse transcription PCR detected prolonged shedding of Oropouche virus RNA in whole blood, serum, urine, and semen. Sixteen days after symptom onset, replication-competent virus was detected in semen, suggesting risk for sexual transmission.

Oropouche virus (OROV) is an emerging zoonotic arbovirus that belongs to the Simbu serogroup of the genus *Orthobunyavirus*, family Peribunyaviridae. Natural hosts include nonhuman primates, some wild bird species, and pale-throated sloths (*1*). OROV is primarily transmitted by biting midges (e.g., *Culicoides paraensis*) and *Culex quinquefasciatus* mosquitoes. Clinical appearance of symptomatic Oropouche fever is similar to that of influenza-like illness (*1*). Self-limiting meningitis or meningoencephalitis can occur (*1*).

OROV has been endemic to the Amazon Region (*1*). Through September 6, 2024, a total of 9,852 confirmed Oropouche cases had been reported in Brazil, Bolivia, Colombia, Cuba, Peru, and the Dominican Republic (*2*). Travel-associated cases have been identified in Europe and the United States (*3*,*4*). In Brazil, identification of adverse pregnancy outcomes associated with OROV infection led to ongoing investigations of possible vertical transmission of the virus (*2*). In the 1980s, spontaneous abortions in pregnant women with OROV antibodies already suggested that OROV infection might be harmful during pregnancy (*5*).

On August 2, 2024, a 42-year-old man from Italy was evaluated for an acute febrile illness at the IRCCS Sacro Cuore Don Calabria Hospital, Negrar di Valpolicella, Italy. He had visited Cuba during July 19–29, 2024. The day before returning home, he experienced high fever (39.0°C), headache, and general malaise (Figure 1). After 2 days, his fever subsided, but it recurred on day 4 after symptom onset. Neurologic examination was unremarkable; no meningeal irritation was noted. The patient did not have a rash or lymphadenopathy and did not report testicular discomfort. Laboratory evaluation showed a leukocyte count within reference limits and no thrombocytopenia. Blood culture results were negative, and specific real-time reverse transcription PCR (RT-PCR) of whole blood and serum were negative for dengue, chikungunya, and Zika viruses (Appendix, https://wwwnc.cdc.gov/EID/article/30/12/24-1470-App1.pdf). We diagnosed Oropouche fever by using 2 OROV-specific RT-PCRs that both target the small (S) genomic segment (*6*,*7*), which was positive in serum, whole blood, and urine samples collected on day 4 after symptom onset. The patient recovered and was free of symptoms on day 10.

RT-PCR remained positive in whole blood and urine samples obtained on days 10, 16 and 32 after symptom onset. Serum was positive for OROV RNA (cycle threshold [Ct] 37.7) on day 10 but not day 16 (Ct >45). We detected OROV RNA in fresh, unfractionated semen samples on days 16 ([Ct 25.4], 32 [Ct 28.9], and 58 [Ct 34.1]). Viral RNA levels were higher in semen than in urine or whole blood (Figure 1). On day 58, OROV was still detectable in whole blood and in semen but not in urine.

On day 16 after symptom onset, we obtained infectious OROV from semen in cell culture under Biosafety Level 3 conditions (Appendix). Virus replication was confirmed by the appearance of clear cytopathic effects (CPE) after 5 days (Figure 2) and increased OROV-RNA levels in spent cell growth medium (Ct values decreased from 25.4 to 14.0). We harvested the virus and performed subsequent passages. On day 32, we still detected shedding of OROV RNA at higher levels in semen (Ct 28.9) than in urine (Ct 32.5) and whole blood (Ct 37.1) but could no longer demonstrate replication competence.

Virus persistence and shedding in semen has been documented for 40 viruses from various virus families and have been most thoroughly studied for Zika and Ebola viruses (*8*,*9*). Viruses in the family Phenuiviridae, order Bunyavirales, have also been detected in human semen: Rift Valley fever virus (day 117 after symptom onset), Toscana virus (day 59), and severe fever with thrombocytopenia syndrome virus (day 30) (*8*,*9*). Orchitis and reduced fertility have been observed in association with Toscana virus infection.
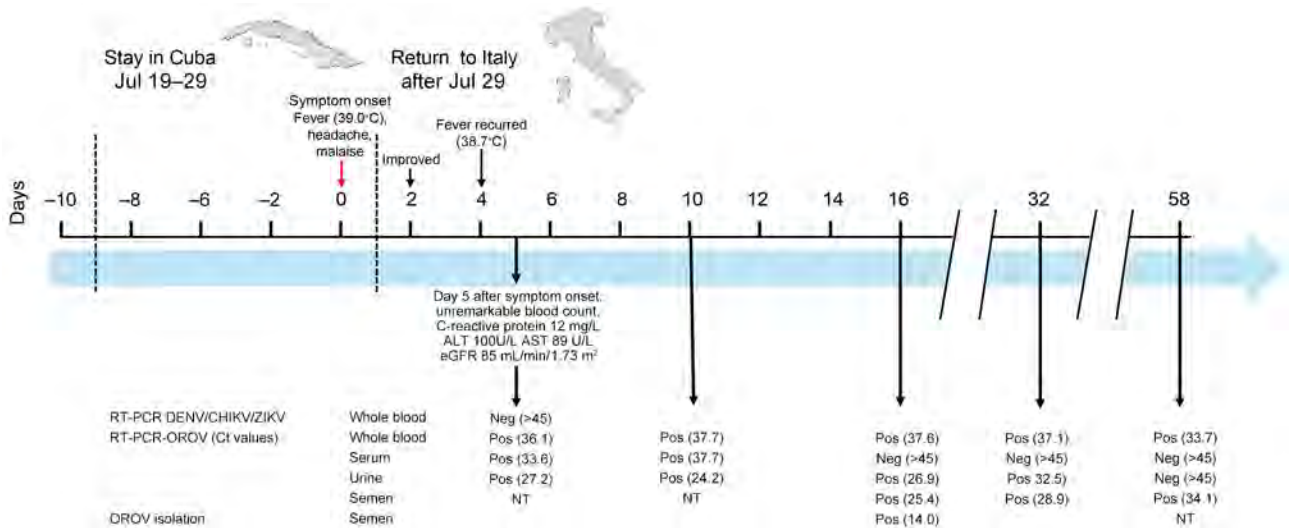
Figure 1. Clinical events and laboratory findings associated with OROV infection in a 42-year-old man from Italy who visited Cuba during July 19–29, 2024. Shown is clinical timeline of patient's OROV infection, with key days indicating the onset of symptoms and the results of both endpoint and real-time RT-PCR tests of whole blood, serum, urine, and semen samples. ALT, alanine aminotransferase; AST, aspartate aminotransferase; CHIKV, chikungunya virus; Ct, cycle threshold; DENV, dengue virus; eGFR, estimated glomerular filtration rate; NT, not tested; neg, negative; OROV, Oropouche virus; pos, positive; RT-PCR, reverse transcription PCR; ZIKV, Zika virus.

Infectious Schmallenberg virus has been isolated from bovine semen up to 3 months after infection (*10*), and infection in a pregnant animal can lead to severe congenital infections in the fetus.

Detectable OROV RNA in semen could result from replication in the male genital tract but also from passive diffusion of OROV. In the patient we report, blood could not be excluded as a cause for a positive RT-PCR in semen, but cross-contamination from urine seems unlikely because OROV RNA shedding persisted longer in semen than in urine.

We report prolonged shedding of Oropouche virus RNA in whole blood, serum, urine and semen and detection of replication-competent virus in 1 patient but caution against overinterpretation of our findings. Because we did not separate seminal fractions, we cannot establish an association with the cellular fraction or spermatozoa. Failure to isolate RT-PCR–detectable OROV from semen does not exclude the possibility of prolonged shedding of infectious virus.

Our findings raise concerns over the potential for person-to-person transmission of OROV via
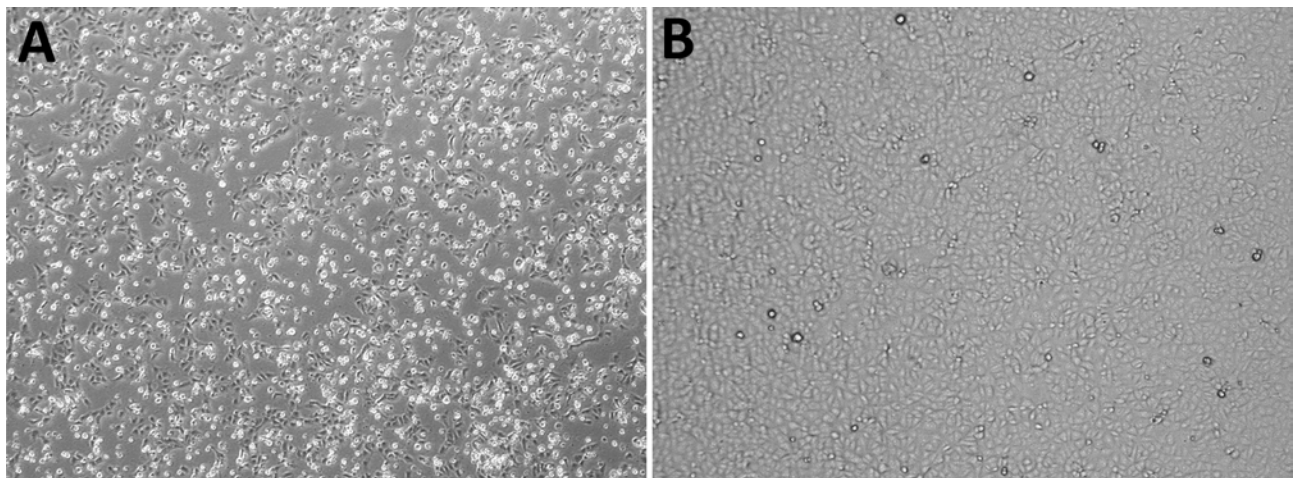
Figure 2. Cytopathic effect associated with Oropouche virus infection in a 42-year-old man from Italy who visited Cuba during July 19–29, 2024, observed by using light microscopy on Vero E6 cells monolayer after 5 days of incubation. A) Semen sample from patient (Appendix, https://wwwnc.cdc.gov/EID/article/30/12/24-1470-App1.pdf). B) Semen sample from uninfected control. Original magnification ×10.

sexual encounters and may have implications for sperm banking and assisted reproductive technologies. Pending further evidence (e.g., longitudinal studies to establish the frequency and kinetics of infectious OROV shedding in semen to assess its clinical relevance), we recommend use of barrier protection when engaging in sexual intercourse if OROV is confirmed or suspected.

About the Author

Dr. Castilletti is head of the Virology and Emerging Pathogens Unit of the Department of Infectious Tropical Diseases and Microbiology at the IRCCS Sacro Cuore Don Calabria Hospital, Negrar di Valpolicella, Italy. Her research interests are viral pathophysiology, molecular epidemiology of emerging and re-emerging viruses, as well as design and validation of innovative diagnostic methods.

References

1. Wesselmann KM, Postigo-Hidalgo I, Pezzi L, de Oliveira-Filho EF, Fischer C, de Lamballerie X, et al. Emergence of Oropouche fever in Latin America: a narrative review. Lancet Infect Dis. 2024;24:e439–e452.
2. Pan American Health Organization/World Health Organization. Epidemiological update: Oropouche in the Americas Region, 6 September 2024 [cited 2024 Oct 3]. https://www.paho.org/en/documents/epidemiological-update-oropouche-americas-region-6-september-2024
3. Morrison A, White JL, Hughes HR, Guagliardo SAJ, Velez JO, Fitzpatrick KA, et al. Oropouche virus disease among U.S. travelers—United States, 2024. MMWR Morb Mortal Wkly Rep. 2024;73:769–73. https://doi.org/10.15585/mmwr.mm7335e1
4. Huits R, Waggoner JJ, Castilletti C. New insights into Oropouche: expanding geographic spread, mortality, vertical transmission, and birth defects. J Travel Med. 2024;29:taae117.
5. Borborema CA, Pinheiro FP, Albuquerque BC, da Rosa AP, da Rosa JF, Dourado HV. First occurrence of outbreaks caused by Oropouche virus in the State of Amazona [in Portuguese]. Rev Inst Med Trop Sao Paulo. 1982;24:132–9.
6. Lambert AJ, Lanciotti RS. Consensus amplification and novel multiplex sequencing method for S segment species identification of 47 viruses of the *Orthobunyavirus, Phlebovirus*, and *Nairovirus* genera of the family *Bunyaviridae*. J Clin Microbiol. 2009;47:2398–404. https://doi.org/10.1128/JCM.00182-09
7. Naveca FG, Nascimento VAD, Souza VC, Nunes BTD, Rodrigues DSG, Vasconcelos PFDC. Multiplexed reverse transcription real-time polymerase chain reaction for simultaneous detection of Mayaro, Oropouche, and Oropouche-like viruses. Mem Inst Oswaldo Cruz. 2017;112:510–3. https://doi.org/10.1590/0074-02760160062
8. Blitvich BJ, Magalhaes T, Viridiana Laredo-Tiscareño S, Foy BD. Sexual transmission of arboviruses: a systematic review. Viruses. 2020;12:933.
9. Le Tortorec A, Matusali G, Mahé D, Aubry F, Mazaud-Guittot S, Houzet L, et al. From ancient to emerging infections: the odyssey of viruses in the male genital tract. Physiol Rev. 2020;100:1349–414. https://doi.org/10.1152/physrev.00021.2019
10. Schulz C, Wernike K, Beer M, Hoffmann B. Infectious Schmallenberg virus from bovine semen, Germany. Emerg Infect Dis. 2014;20:338–40 https://doi.org/10.3201/eid2002.131436

Address for correspondence: Ralph Huits, IRCCS Sacro Cuore Don Calabria Hospital, Department of Infectious Tropical Diseases and Microbiology, Via Don A. Sembreboni, 5 Verona Negrar 37024, Italy; email: rhuits@geosentinel.org

Bacteriologic and Genomic Investigation of *Bacillus anthracis* Isolated from World War II Site, China

Yarong Wu,[1] Yuan Yuan,[1] Bing Yuan, Jiaxin Li, Jinglin Wang, Yujun Cui

Author affiliation: State Key Laboratory of Pathogen and Biosecurity, Academy of Military Medical Sciences, Beijing, China

Records suggest *Bacillus anthracis* was used in biowarfare during World War II, but evidence remains limited. We isolated *B. anthracis* from soil at the remains of a World War II–era laboratory in China. Phenotypic and genomic analyses confirmed the finding, highlighting the value of microbial forensics in biothreat investigation.

Bacillus anthracis, the etiologic agent of anthrax, is a gram-positive bacterium that can cause life-threatening disease among wild and domestic mammals, including humans (*1*). *B. anthracis* can form spores, enabling long-term survival under adverse conditions. Isolation of *B. anthracis* from soil stored up to 60 years has been reported previously (*2*). Because of its pathogenic features, *B. anthracis* is considered one of the most serious and threatening agents for conducting biowarfare or bioterrorism (*3,4*).

In our previous study, 3 of 24 soil samples collected from a World War II (WWII) site in northeastern China (Appendix Figure 1; https://wwwnc.cdc.gov/EID/article/30/12/23-1520-App1.pdf) tested positive for *B. anthracis* using RPA/CRISPR-Cas12a, real-time PCR, and metagenomic analysis (*5*). Of note, those positive samples were obtained from the site of Unit 731 (45°36′55.940″N, 126°38′33.738″E), a former bacteria laboratory run by the army of Japan (*5*). We collected an additional 24 samples from 12 collection sites located within radii of 0.5 km, 3 km, and 5 km from the remains of the WWII laboratory (Appendix Figure 2). However, we detected no trace of *B. anthracis* in the newly collected samples, implying that the positive samples we previously found likely did not originate from a local natural source.

Using polymyxin B-lysozyme-EDTA-thallous acetate agar and API 50CHB-API 50CH biochemical reagents (BioMérieux, https://www.biomerieux.com), we successfully isolated and identified a *B. anthracis* strain (named BA20200413YY) from one of the soil samples. Morphologic, hemolytic, and biochemical

analyses revealed classic *B. anthracis* phenotypes: gray, opaque, medium-sized, irregular-shaped colonies with a ground glass surface and no surrounding hemolytic rings (Figure, panel A). In addition, Gram staining revealed a bamboo-like arrangement of bacilli (Figure, panel B). We sequenced the whole genome of strain BA20200413YY using MiSeq (Illumina, https://www.illumina.com) and Sequel I (PacBio, https://www.pacb.com) platforms. We assembled reads into a complete
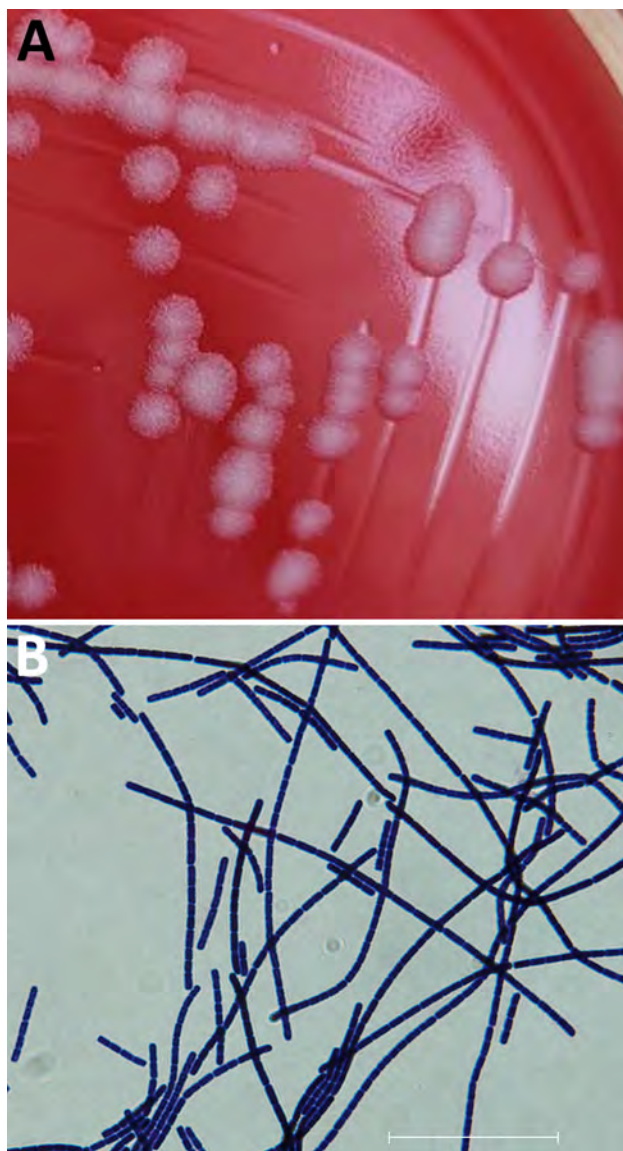

Figure. Preserved isolate from a bacteriologic and genomic investigation of *Bacillus anthracis* from World War II site, China. A) Morphological analysis of *B. anthracis* isolated on Columbia blood agar plate showing classic *B. anthracis* features: gray, opaque, medium sized, irregular-shaped colonies with a ground glass surface and no surrounding hemolytic rings. B) Gram staining showing *B. anthracis* bamboo-like arrangement. Scale bar represents 30 μm. Isolate data are available in GenBank (accession no. CP135587–89).

[1]These first authors contributed equally to this article.

genome totaling 5.5 Mbp, including the chromosome (5,228,177 bp) and 2 plasmids, pXO1 (181,765 bp) and pXO2 (94,821 bp). Functional genetic analysis revealed that BA20200413YY carries the 5 natural resistance genes of *B. anthracis*, which confer resistance to fosfomycin, β-lactamase, streptothricin, and macrolide, as well as 33 virulence genes associated with anthrax toxin and other exotoxins, exoenzymes, capsular synthesis, type VII secretion systems, and adherence (Appendix Table 1).

To infer the evolutionary association between BA20200413YY and other known *B. anthracis* strains, we rebuilt the phylogeny between BA20200413YY and 1,552 publicly available *B. anthracis* genomes from GenBank (https://www.ncbi.nlm.nih.gov/genbank) and Sequence Reads Archive (https://www.ncbi.nlm.nih.gov/sra) databases, based on 11,967 core genome single nucleotide polymorphisms (SNPs). Our results revealed that BA20200413YY belongs to subcluster 5.2 described elsewhere (6), corresponding to the classic categorization of subbranch A.Br.081 of the A.Br.002 lineage (7) (Appendix Figure 3, panel A). Further analysis of subcluster 5.2 strains revealed a close clustering of BA20200413YY with 9 other strains, forming a sublineage characterized by 5 lineage-specific SNPs (Appendix Table 2; Appendix Figure 3, panel B). Given the large observed genetic difference ($\approx$35–78 SNPs) between BA20200413YY and the limited number of its close relatives (Appendix Figure 3, panel B), precisely tracing its origin was challenging. We identified 20 unique SNPs and 6 unique indels in the chromosome of BA20200413YY (Appendix Table 2). We confirmed those identifications by metagenomic sequencing of DNA extracted from the anthrax-positive soil samples from which we also isolated strain BA20200413YY. We observed no notable genomic gains or losses in either the chromosome or 2 plasmids of BA20200413YY when compared with the 9 closely related strains.

The Fell report (8) described human experiments conducted at Unit 731 involving anthrax, plague, typhoid, paratyphoid A and B, shigellosis, cholera, and melioidosis using direct oral infection, infection by injection, or exposure to environmental pathogens. Moreover, the human experimental anatomy reports of anthrax (9) and glanders (10), decoded by the United States, contain information about the *B. anthracis* and *B. mallei* experiments completed at Unit 731. In this study, we isolated a strain of *B. anthracis* from soil samples collected at the former site of the bacteria laboratory of Unit 731 in Heilongjiang Province, China. Of note, all other samples collected from surrounding sites in the same region tested negative for *B. anthracis*. By analyzing the distribution of the positive samples, qualities of the isolated strain, and historical documents, we established a chain of evidence supporting the hypothesis that *B. anthracis* was misused in inhumane medical experiments and likely for developing biologic weapons during WWII.

In conclusion, our study offers a model approach for investigating sites of historical biologic agent research related to biowarfare activities during WWII. Our findings highlight the role of microbial forensics in tracing biologic warfare and providing insights into biothreats. In addition, our results indicate that the environmental remains of hardy biologic agents pose a long-term biosecurity risk at similar WWII sites potentially contaminated with highly pathogenic biothreat agents, posing potential threats to the surrounding natural environment, and nearby humans and animals if the site is not well protected.

Author contributions: Y.C., Y.Y., and Y.W. designed the study; Y.Y., Y.W., and Y.C. wrote the paper; Y.W. and Y.C. performed core genome single nucleotide polymorphism analysis; Y.Y. isolated BA20200413YY from soil samples; Y.Y., J.L., and J.W. collected soil samples from the location of World War II site. B.Y. performed DNA extraction and *Bacillus anthracis* identification.

About the Author

Dr. Wu is a postdoctoral fellow at Academy of Military Medical Sciences, Beijing, China. Her research interests focus on the evolution and population genomic analysis of pathogenic bacteria. Dr. Yuan is an associate researcher at Academy of Military Medical Sciences. Her primary research interests are pathogen identification and microbe-host interaction.

References

1. Spencer RC. *Bacillus anthracis*. J Clin Pathol. 2003;56:182–7. https://doi.org/10.1136/jcp.56.3.182
2. Wilson JB, Russell KE. Isolation of *Bacillus anthracis* from soil stored 60 years. J Bacteriol. 1964;87:237–8. https://doi.org/10.1128/jb.87.1.237-238.1964
3. Zilinskas RA. Iraq's biological weapons. The past as future? JAMA. 1997;278:418–24. https://doi.org/10.1001/jama.1997.03550050080037

4. Inglesby TV, Henderson DA, Bartlett JG, Ascher MS, Eitzen E, Friedlander AM, et al.; Working Group on Civilian Biodefense. Anthrax as a biological weapon: medical and public health management. JAMA. 1999;281:1735–45. https://doi.org/10.1001/jama.281.18.1735

5. Xu J, Bai X, Zhang X, Yuan B, Lin L, Guo Y, et al. Development and application of DETECTR-based rapid detection for pathogenic *Bacillus anthracis.* Anal Chim Acta. 2023; 1247:340891. https://doi.org/10.1016/j.aca.2023.340891

6. Bruce SA, Schiraldi NJ, Kamath PL, Easterday WR, Turner WC. A classification framework for *Bacillus anthracis* defined by global genomic structure. Evol Appl. 2020;13:935–44. https://doi.org/10.1111/eva.12911

7. Sahl JW, Pearson T, Okinaka R, Schupp JM, Gillece JD, Heaton H, et al. A *Bacillus anthracis* genome sequence from the Sverdlovsk 1979 autopsy specimens. MBio. 2016;7:2–10. https://doi.org/10.1128/mBio.01501-16

8. Fell NH. Brief summary of new information about Japanese BW activities. 1947; Location: 290/03/19/02, RG#175, ENTRY#67A4900, Box 196. National Archives and Records Administration, Washington DC, USA.

9. Report of "A" [Anthrax]. 1949; Location: 2910, RG#IWG reference collection. National Archives and Records Administration, Washington DC, USA.

10. Report of "G" [Glanders]. 1949; Location: 2910, RG#IWG reference collection. National Archives and Records Administration, Washington DC, USA.

Canine Multidrug-Resistant *Pseudomonas aeruginosa* Cases Linked to Human Artificial Tears–Related Outbreak

Emma R. Price, Darby McDermott, Adrienne Sherman, Lakisha Kelley, Jason Mehr, Rebecca Greeley, Stephen D. Cole

Author affiliations: Centers for Disease Control and Prevention, Atlanta, Georgia, USA (E.R. Price); New Jersey Department of Health, Trenton, New Jersey, USA (E.R. Price, D. McDermott, A. Sherman, L. Kelley, J. Mehr, R. Greeley); University of Pennsylvania School of Veterinary Medicine, Philadelphia, Pennsylvania, USA (S.D. Cole)

We report 2 canine cases of carbapenemase-producing *Pseudomonas aeruginosa* within a United States veterinary hospital associated with a human outbreak linked to over-the-counter artificial tears. We investigated veterinary hospital transmission. Veterinary antimicrobial resistance surveillance and infection prevention and control enhancements are needed to reduce transmission of carbapenemase-producing organisms.

Carbapenem antimicrobial drugs are reserved for highly resistant gram-negative bacterial infections. Carbapenemase enzymes, which hydrolyze and inactivate carbapenems, are commonly encoded on mobile genetic elements that can spread among bacterial genera and species and amplify resistance. Therefore, carbapenemase-producing organisms (CPOs) are a major public health concern (*1*). Although less commonly documented compared with humans, CPOs have been identified in companion animals and suspected transmission reported between humans and animals (*2–4*).

In March and June 2023, New Jersey Department of Health (NJDOH) was notified of carbapenemase-producing *Pseudomonas aeruginosa* (CP-PsA) isolated from 2 separately owned pet dogs treated at the same New Jersey, USA, small animal specialty veterinary hospital. The isolates were closely genetically related to the multistate cluster of Verona integron-mediated metallo-β-lactamase (VIM)–producing and Guiana-extended spectrum-β-lactamase (GES)–producing carbapenem-resistant *P. aeruginosa* (VIM-GES-CRPA) isolated from multiple human clinical cultures and associated with contaminated over-the-counter artificial tears products (*5,6*). The combination of VIM-80 and GES-9 in a single organism had not been identified in the United States before that outbreak. By May 2023, that outbreak was associated with 81 human cases and 4 deaths in 18 states; no other animal cases were reported.

NJDOH interviewed the dog owners, reviewed veterinary medical and hospital purchase records, and conducted an onsite infection prevention and control (IPC) assessment 1 month after the second case identification. The investigation was reviewed by Centers for Disease Control and Prevention (CDC) and conducted consistent with federal law and CDC policy.

The first canine case was identified in March 2023 in a spayed female Labrador retriever 7 years of age that had a 3-month history of cough. VIM-GES-CRPA was isolated from a bronchoalveolar lavage specimen. The second canine case was identified in June 2023 in a neutered male cocker spaniel 6 years of age with a chronic history of otitis externa and keratoconjunctivitis sicca; VIM-GES-CP-PsA was isolated from

Table. Clinical characteristics and genetic relatedness of *Pseudomonas aeruginosa* infections in canines during outbreak in humans linked to artificial tears*

Case no.	Sample collection month, 2023	Isolate location	Isolate no.	BioSample ID†	SNP difference from human outbreak strain
Dog 1	March	Bronchial alveolar lavage	13494-23	SAMN33902373	2
Dog 2	June	External ear canal	30793-23	SAMN35751022	5

*ID, identification; SNP, single nucleotide polymorphism.
†National Center for Biotechnology Information (https://www.ncbi.nlm.nih.gov).

the external ear canal along with methicillin-resistant *Staphylococcus pseudintermedius*. Clinical specimens were submitted to the clinical microbiology laboratory of the PennVet Diagnostic Laboratory, University of Pennsylvania (Philadelphia, PA, USA), for culture and antimicrobial susceptibility testing (AST).

AST was performed using AST-GN98 cards on Vitek 2 (bioMérieux, https://www.biomerieux.com), according to manufacturer instructions. Isolates tested were resistant to aminoglycosides amikacin and gentamicin, fluoroquinolones enrofloxacin and marbofloxacin, and ceftazidime. Isolate 13494-23 was resistant to imipenem. Although isolate 30793-23 was susceptible (MIC 2 µg/mL), ceftazidime resistance still prompted PCR by Carba-R (Cepheid, https://www.cepheid.com) for carbapenemase genes. Phenotypically susceptible isolates producing carbapenemases are a well-described phenomenon and prompt further investigation (7). Short-read whole-genome sequencing was performed using Nextera Library Prep chemistry and HiSeq 2500 (Illumina, https://www.illumina.com) platform and uploaded to National Center for Biotechnology Information (https://www.ncbi.nlm.nih.gov) prokaryotic genomic annotation pipeline for deposit in the pathogen detection database (8). The isolates were 2 and 5 single-nucleotide polymorphism differences from the closest related human isolate (Table)

Neither dog owners nor household members reported outbreak-associated ophthalmic product exposures since March 2022, but the second dog had received different over-the-counter artificial tears. The veterinary hospital did not stock the outbreak-associated products. Both dogs had received recent antimicrobial drug treatment. The first dog lived with 3 other dogs; the second dog was the only household pet. No dogs, owners, or household members had travel history (domestic or international) or healthcare setting exposures. Epidemiologic links between the 2 canine cases included treatment in the veterinary facility's surgical preparation and recovery areas for both dogs and ophthalmology department visits by either the affected dog or another animal in the same household. The NJDOH onsite visit identified IPC gaps in hand hygiene, personal protective equipment use, and equipment and environmental cleaning and disinfection. Surgical scrub and instrument sink drains, shared equipment, and ophthalmic product cultures did not grow the outbreak strain. NJDOH provided IPC resources and recommendations to the facility and owners.

CPO identification in dogs linked to a human outbreak but with an unknown transmission route necessitates consideration of the role of companion animals and veterinary hospitals in transmitting and acting as reservoirs for CPOs and underscores the need for veterinary public health action. To clarify veterinary-associated CPO transmission and enhance CPO identification, veterinarians should request diagnostic laboratories perform carbapenem susceptibility testing for gram-negative bacteria resistant to third-generation cephalosporins (e.g., ceftazidime), if clinical history suggests CPO infection risk, and, upon carbapenem-resistant organism identification, request resistance mechanism confirmation. CPO infection risk can include recent antimicrobial use, international travel, hospitalization, raw food diet, close contact with humans or animals carrying CPOs, or exposure to contaminated products (9,10). Veterinarians and pet owners are encouraged to maintain awareness of outbreaks in persons associated with products used in multiple species, such as through Food and Drug Administration medical product recall notifications.

In conclusion, identifying CPOs in companion animals associated with a human outbreak serves as an urgent call to veterinarians to identify and prevent CPO transmission. Veterinarians should request carbapenem susceptibility testing when appropriate, veterinarians and pet owners should maintain awareness of CPO outbreaks, and veterinary hospitals should establish and implement IPC protocols. By following those recommendations, veterinarians can identify and prevent CPO transmission to protect animal and human health.

Acknowledgments

About the Author

Dr. Price is a veterinary epidemiologist at the Centers for Disease Control and Prevention assigned to New Jersey Department of Health, Trenton, New Jersey, USA. Her research interests focus on healthcare-associated infections and antimicrobial stewardship strategies in companion animals.

References

1. Centers for Disease Control and Prevention. 2019 Antibiotic resistance threats report [cited 2023 Dec 6]. https://www.cdc.gov/antimicrobial-resistance/data-research/threats
2. Hyun JE, Chung TH, Hwang CY. Identification of VIM-2 metallo-β-lactamase-producing *Pseudomonas aeruginosa* isolated from dogs with pyoderma and otitis in Korea. Vet Dermatol. 2018;29:186–e68. https://doi.org/10.1111/vde.12534
3. Fernandes MR, Sellera FP, Moura Q, Carvalho MPN, Rosato PN, Cerdeira L, et al. Zooanthroponotic transmission of drug-resistant *Pseudomonas aeruginosa*, Brazil. Emerg Infect Dis. 2018;24:1160–2. https://doi.org/10.3201/eid2406.180335
4. Wang Y, Wang X, Schwarz S, Zhang R, Lei L, Liu X, et al. IMP-45-producing multidrug-resistant *Pseudomonas aeruginosa* of canine origin. J Antimicrob Chemother. 2014;69:2579–81. https://doi.org/10.1093/jac/dku133
5. US Food and Drug Administration. FDA warns consumers not to purchase or use EzriCare Artificial Tears due to potential contamination [updated 8/25/2023] [cited 2023 Dec 6]. https://www.fda.gov/drugs/drug-safety-and-availability/fda-warns-consumers-not-purchase-or-use-ezricare-artificial-tears-due-potential-contamination
6. Grossman MK, Rankin DA, Maloney M, Stanton RA, Gable P, Stevens VA, et al; Multistate Pseudomonas Outbreak Investigation Group. Extensively drug-resistant *Pseudomonas aeruginosa* outbreak associated with artificial tears. Clin Infect Dis. 2024;79:6–14. https://doi.org/10.1093/cid/ciae052
7. Livermore DM, Andrews JM, Hawkey PM, Ho PL, Keness Y, Doi Y, et al. Are susceptibility tests enough, or should laboratories still seek ESBLs and carbapenemases directly? J Antimicrob Chemother. 2012;67:1569–77. https://doi.org/10.1093/jac/dks088
8. Tatusova T, DiCuccio M, Badretdin A, Chetvernin V, Nawrocki EP, Zaslavsky L, et al. NCBI prokaryotic genome annotation pipeline. Nucleic Acids Res. 2016;44:6614–24. https://doi.org/10.1093/nar/gkw569
9. Dazio V, Nigg A, Schmidt JS, Brilhante M, Mauri N, Kuster SP, et al. Acquisition and carriage of multidrug-resistant organisms in dogs and cats presented to small animal practices and clinics in Switzerland. J Vet Intern Med. 2021;35:970–9. https://doi.org/10.1111/jvim.16038
10. van den Bunt G, Fluit AC, Spaninks MP, Timmerman AJ, Geurts Y, Kant A, et al. Faecal carriage, risk factors, acquisition and persistence of ESBL-producing Enterobacteriaceae in dogs and cats and co-carriage with humans belonging to the same household. J Antimicrob Chemother. 2020;75:342–50. https://doi.org/10.1093/jac/dkz462

Address for correspondence: Emma R. Price, New Jersey Department of Health, 135 E State St, Trenton, NJ 08625, USA; email: emma.price@doh.nj.gov

Zoonotic Potential of Chronic Wasting Disease after Adaptation in Intermediate Species

Tomás Barrio, Sylvie L. Benestad, Jean-Yves Douet, Alvina Huor, Séverine Lugan, Naïma Aron, Hervé Cassard, Juan Carlos Espinosa, Alicia Otero, Rosa Bolea, Juan María Torres, Olivier Andréoletti

Author affiliations: Unité Mixte de Recherche de l'Institut National de Recherche pour l'Agriculture, l'Alimentation, et l'Environnement 1225 Interactions Hôtes-Agents Pathogènes, École Nationale Vétérinaire de Toulouse, Toulouse, France (T. Barrio, J.-Y. Douet, A. Huor, S. Lugan, N. Aron, H. Cassard, O. Andréoletti); Norwegian Veterinary Institute, Ås, Norway (S.L. Benestad); Consejo Superior de Investigaciones Científicas, Madrid, Spain (J.C. Espinosa, J.M. Torres); Universidad de Zaragoza, Zaragoza, Spain (A. Otero, R. Bolea)
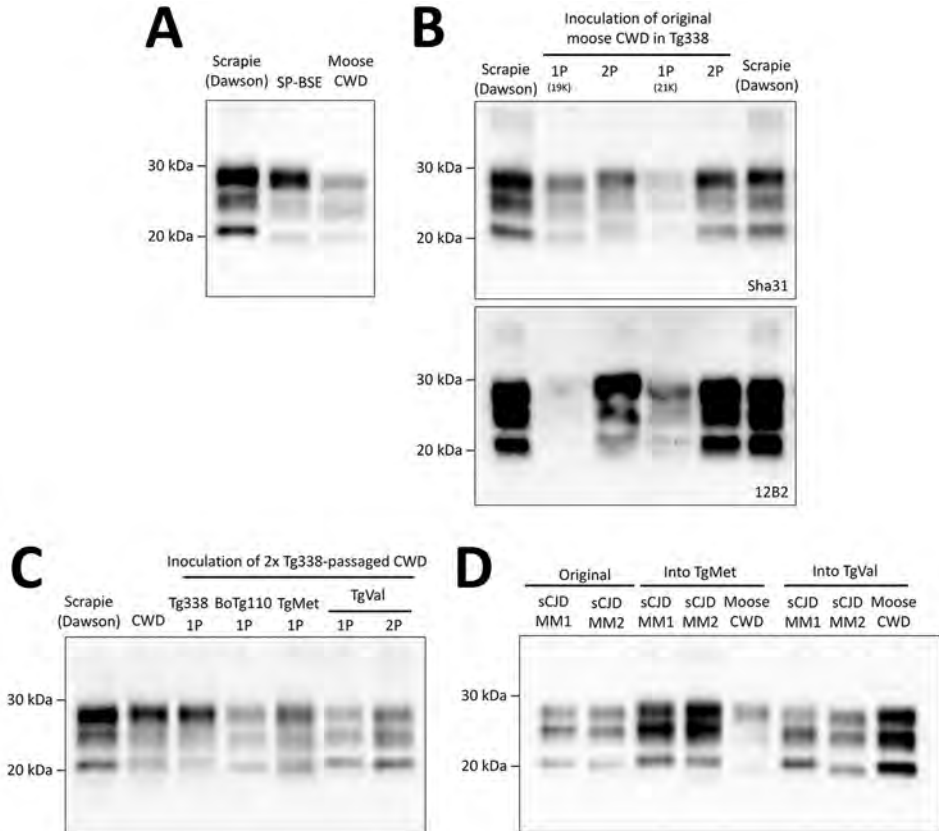
DOI: https://doi.org/10.3201/eid3012.240536

Chronic wasting disease (CWD) is an emerging disease in Europe. We report an increase in interspecies transmission capacity and zoonotic potential of a moose CWD isolate from Europe after passage in an ovine prion protein–expressing host. Those results indicated some CWD prions could acquire enhanced zoonotic properties following adaptation in an intermediate species.

Chronic wasting disease (CWD) is a highly contagious prion disease affecting members of the Cervidae family. CWD is widely spread across North America, where it endangers the survival of free-ranging cervid populations. In Europe, CWD was reported in a reindeer (*Rangifer tarandus tarandus*) from Norway in 2016 (*1*). Since 2016, several cases have been reported in Norway, Sweden, and Finland in multiple species, including reindeer, red deer (*Cervus elaphus*), and moose (*Alces alces*) (*2*).

Whereas CWD strains circulating in North America exhibit some uniformity (*3*), the cases found in Europe are more variable. Transmission into rodent models has revealed multiple CWD strains that are apparently different than strains in North America, and moose cases in Norway have demonstrated biochemical patterns distinct from previous cases in Europe (*4*). We characterized the interspecies transmission potential of 1 moose CWD isolate from Norway (Norwegian Veterinary Institute identification no. 16–60-P153) (*4*) by intracerebral injection of mouse models expressing the normal prion protein (PrP^C) sequences from several species (Figure, panel A).

Figure. Western blot analysis in a study of zoonotic potential of chronic wasting disease after adaptation in intermediate species. Results show PK-resistant PrP (PrP^res) banding patterns of a moose CWD isolate from Europe after transmission to transgenic PrP models. A) Original 16–60-P153 CWD isolate compared with reference Dawson and sheep-passaged BSE. B) Transmission of the original moose CWD isolate to mice ovine PrP^C genotype VRQ (Tg338), resulting in positive transmission with either 19 or 21 kDa PrP^res on first passage and 21 kDa PrP^res on second passage; PrP Sha31 antibodies (right panel) and PrP 12B2 antibodies (left panel). C) Transmission of Tg338-adapted (second passage) moose CWD isolate to Tg338, BoTg110, TgMet, or TgVal. D) Comparison of PrP^res banding patterns in TgMet and TgVal inoculated with the Tg338-adapted moose CWD isolate or with M1^CJD and V2^CJD reference sCJD strains. Immunodetection was performed by using either the Sha31 antibody to detect the amino acid sequence YEDRYYRE (145–152), or the 12B2 antibody to detect the amino acid sequence WGQGG (89–93). Dawson (a reference 21-kDa scrapie strain) is included on all panels except D for molecular weight reference. 1P, 1st passage; 2P, 2nd passage; BoTg110, bovine PrP^C-expressing mice; BSE, bovine spongiform encephalopathy; CJD, Creutzfeldt-Jakob disease; CWD, chronic wasting disease; PK, proteinase K; PrP, prion protein; PrP^C, normal prion protein; PrP^res, PK-resistant prion protein. TgMet, Tg340 mice expressing methionine; TgVal, Tg361 mice expressing valine.

We anesthetized and inoculated 6-to-10-week-old mice with 2 mg of equivalent tissue (20 µL of 10% brain homogenate) in the right parietal lobe. We monitored the inoculated animals daily and humanely euthanized animals at the onset of clinical signs or after the preestablished endpoint of 700 days postinfection (dpi). We conducted a systematic proteinase K–resistant prion protein (PrP^res) detection by using Western blot.

Inoculation of the original CWD isolate did not cause the propagation of detectable prions in Tg340 mice expressing methionine (TgMet) or Tg361 mice expressing valine (TgVal) at position 129 of human PrP^C. We did not observe PrP^res in brain tissue or disease occurrence in bovine PrP^C-expressing mice (BoTg110) after intracerebral inoculation of the CWD isolate (Table; Figure, panel B).

We inoculated the CWD isolate in Tg338 mice, which overexpress ovine PrP ≈8 times. At 612 and 717 dpi (Table), 2 of 12 animals showed clinical signs of prion disease, and we detected PrP^res accumulation in their brain tissue (Figure, panel B). Of note, the 2 animals showed different PrP^res banding patterns, with the nonglycosylated band migrating to 19 kDa in the first mouse and to 21 kDa in the second. Both PrP^res-containing brains transmitted disease with 100% efficacy to second-passage Tg338 mice, which contained 21-kDa PrP^res in their brains (Figure, panel B). A third passage resulted in the incubation period shortening (95 ± 5 dpi). Our observations are consistent with a progressive adaptation of the moose CWD prion to the ovine-PrP^C expressing model and suggest moose CWD prions in Europe may have an intrinsic capability to propagate in ovine species with the VRQ genotype.

We next determined whether adaptation of this moose CWD agent to Tg338 altered its capacity to cross species barriers. For that purpose, we inoculated Tg338-adapted moose CWD prions (passaged twice in Tg338) to the same panel of PrP^C-

Table. Transmission of a moose CWD isolate in a study of zoonotic potential of chronic wasting disease after adaptation in intermediate species*

Model characteristics	TgMet			TgVal			Tg338			BoTg110		
	No./no.†	Mean dpi (SD)	PrPres band type	No./no.†	Mean dpi (SD)	PrPres band type	No./no.†	Mean dpi (SD)	PrPres band type	No./no.†	Mean dpi (SD)	PrPres band type
Prion strains												
M1CJD (sCJD MM1)												
1st passage	6/6	219 (17)	21 kDa	6/6	327 (19)‡	21 kDa	ND			ND		
2nd passage	6/6	239 (8)‡	21 kDa	6/6	286 (16)‡	21 kDa	ND			ND		
V2CJD (sCJD VV2)												
1st passage	6/6	618 (81)‡	21 kDa	6/6	168 (12)‡	19 kDa	ND			ND		
2nd passage	6/6	509 (41)‡	21 kDa	6/6	169 (12)‡	19 kDa	ND			ND		
Classical BSE												
1st passage	1/12	739‡	BSE§	0/12	≥750‡	NA	6/6	≥750¶	BSE§	6/6	295 (12)#	BSE§
2nd passage	9/12	613 (43)‡	BSE§	0/12	≥750‡	NA	6/6	682 (52)¶	BSE§	6/6	265 (35)#	BSE§
Sheep-adapted BSE												
1st passage	6/6	690 (83)#	BSE§	ND			6/6	≥750¶	BSE§	6/6	254 (19)¶	BSE§
2nd passage	5/5	564 (39)#	BSE§	ND			6/6	653 (32)¶	BSE§	6/6	234 (12)¶	BSE§
Tg338-adapted BSE												
1st passage	6/6	596 (92)	BSE§	0/6	≥700	BSE§	5/5	224 (37)	BSE§	6/6	222 (22)	BSE§
2nd passage				ND			ND			ND		
Moose CWD (16–60-P153)												
1st passage	0/12	≥700	NA	0/12	≥700	NA	2/12	612, 717	19 kDa, 21 kDa	0/12	≥700	NA
2nd passage	0/6 ND	≥700	NA	ND ND			5/5 6/6	167 (4)** 244 (33)††	21 kDa 21 kDa	ND		
Tg338-adapted moose CWD‡‡												
1st passage	1/8	561	19+21 kDa	5/6	483 (35)	21 kDa	7/7	95 (5)	21 kDa	5/5	431 (32)	20 kDa
2nd passage	ND			4/4	311 (12)	21 kDa	ND			ND		

*Results show moose isolate (16–60-P153) from Norway and reference prion strains (human sCJD strains M1CJD and V2CJD, cattle strain c-BSE) in transgenic mouse models expressing human PrPC 129M (TgMet) and 129V (TgVal), ovine VRQ PrPC (Tg338) and bovine PrPC (BoTg110). BSE, bovine spongiform encephalopathy; dpi, days post-inoculation; NA, not available; ND, not done; PrP, prion protein; PrPres, PK-resistant prion protein; VRQ, valine136-arginine154-glutamine171 ovine PrPC variant.
†No. affected mice/total no. inoculated.
‡Transmissions reported in (5)
§Transmissions reported in (6)
¶Transmissions reported in (7)
#Transmissions reported in (8)
**Transmission was performed from the brain of the first-passage mouse that showed a 19 kDa banding pattern.
††Transmission was performed from the brain of the first-passage mouse that showed a 21 kDa banding pattern.
‡‡The Tg338-adapted isolate corresponds to the brain of a second-passage Tg338 mouse that was culled at 170 dpi after infection with first-passage 19K brain.

expressing mice models. Inoculation of the Tg338-adapted isolate to BoTg110 resulted in 100% disease transmission that showed a banding pattern and intermediate molecular weight from 19–21 kDa (Figure, panel C; Appendix Figure, https://wwwnc.cdc.gov/EID/article/30/12/24-0536-App1.pdf) and an incubation period of 431 ± 32 dpi (Table), which suggested the lack of a major transmission barrier. In addition, 1 of 8 inoculated TgMet mice showed clinical signs at 561 dpi (Table). PrPres in the brain of that mouse was revealed by a mixed 19 + 21–kDa banding pattern (Figure, panel C). A second passage in TgMet is underway.

Inoculation of TgVal resulted in efficient transmission (5/6 animals); the mean incubation period was 483 ± 35 dpi (Table) and accumulation was 21–kDa PrPres (Figure, panel C). On second passage, transmission was 100% and we observed a shorter incubation period (311 ± 12 dpi).

The incubation periods and PrPres biochemical profiles of the CWD prions that propagated in the TgMet and TgVal mice greatly differed from those observed in mice inoculated with the most prevalent human prion strains or with classic bovine spongiform encephalopathy (BSE), sheep-adapted BSE, or Tg338-adapted c-BSE (Table; Figure, panel D). Those results might suggest this CWD-derived prion strain differs from other strains documented in those models. Further investigation is necessary.

The evolution of moose CWD zoonotic potential after its passage in an ovine PrPC-expressing host is reminiscent of the well-documented altered capacities of the c-BSE agent to cross the human species barrier after adaptation in sheep and goats (9). The codon 129-dependent response to infection of humanized mice with Tg338-adapted CWD is also compatible with studies demonstrating

the role of this polymorphism in susceptibility to prions (10).

In summary, our results demonstrate the potential capacity of some CWD agents to transmit to sheep or other farmed animals. Our results highlight the need to experimentally assess and monitor this transmission risk under natural exposure conditions. In addition, the dramatic changes of the zoonotic capacity of the CWD isolate we documented from Europe clearly demonstrate the risk adaptation and propagation of cervid prions into farmed animals represents. Although additional studies are needed to characterize these emerging agents, our findings have major potential implications for animal and public health.

About the Author

Dr. Barrio is a research scientist with Institut National de Recherche pour l'Agriculture, l'Alimentation et l'Environnement. His research interests include animal and human prion diseases and other neurodegenerative disorders linked to misfolded proteins.

References

1. Benestad SL, Mitchell G, Simmons M, Ytrehus B, Vikøren T. First case of chronic wasting disease in Europe in a Norwegian free-ranging reindeer. Vet Res. 2016;47:88. https://doi.org/10.1186/s13567-016-0375-4
2. Tranulis MA, Gavier-Widén D, Våge J, Nöremark M, Korpenfelt SL, Hautaniemi M, et al. Chronic wasting disease in Europe: new strains on the horizon. Acta Vet Scand. 2021;63:48. https://doi.org/10.1186/s13028-021-00606-x
3. Nonno R, Di Bari MA, Pirisinu L, D'Agostino C, Vanni I, Chiappini B, et al. Studies in bank voles reveal strain differences between chronic wasting disease prions from Norway and North America. Proc Natl Acad Sci U S A. 2020;117:31417–26. https://doi.org/10.1073/pnas.2013237117
4. Pirisinu L, Tran L, Chiappini B, Vanni I, Di Bari MA, Vaccari G, et al. Novel type of chronic wasting disease detected in moose (*Alces alces*), Norway. Emerg Infect Dis. 2018;24:2210–8. https://doi.org/10.3201/eid2412.180702
5. Cassard H, Torres JM, Lacroux C, Douet JY, Benestad SL, Lantier F, et al. Evidence for zoonotic potential of ovine scrapie prions. Nat Commun. 2014;5:5821. https://doi.org/10.1038/ncomms6821
6. Hill AF, Joiner S, Wadsworth JD, Sidle KC, Bell JE, Budka H, et al. Molecular classification of sporadic Creutzfeldt-Jakob disease. Brain. 2003;126:1333–46. https://doi.org/10.1093/brain/awg125
7. Huor A, Espinosa JC, Vidal E, Cassard H, Douet JY, Lugan S, et al. The emergence of classical BSE from atypical/Nor98 scrapie. Proc Natl Acad Sci U S A. 2019;116:26853–62. https://doi.org/10.1073/pnas.1915737116
8. Torres JM, Espinosa JC, Aguilar-Calvo P, Herva ME, Relaño-Ginés A, Villa-Diaz A, et al. Elements modulating the prion species barrier and its passage consequences. PLoS One. 2014;9:e89722. https://doi.org/10.1371/journal.pone.0089722
9. Padilla D, Béringue V, Espinosa JC, Andreoletti O, Jaumain E, Reine F, et al. Sheep and goat BSE propagate more efficiently than cattle BSE in human PrP transgenic mice. PLoS Pathog. 2011;7:e1001319. https://doi.org/10.1371/journal.ppat.1001319
10. Deslys JP, Marcé D, Dormont D. Similar genetic susceptibility in iatrogenic and sporadic Creutzfeldt-Jakob disease. J Gen Virol. 1994;75:23–7. https://doi.org/10.1099/0022-1317-75-1-23

Address for correspondence: Tomás Barrio, Unité Mixte de Recherche de l'Institut National de Recherche pour l'Agriculture, l'Alimentation et l'Environnement 1225 Interactions Hôtes-Agents Pathogènes, , 23 chemin des Capelles 31076 Toulouse, France; email: tomas.barrio@envt.fr

Salmonella sp. Tied to Multistate Outbreak Isolated from Wastewater, United States, 2022

Zoe S. Goldblum, Nkuchia M. M'ikanatha,
Erin M. Nawrocki, Nicholas Cesari, Jasna Kovac,
Edward G. Dudley

Author affiliations: The Pennsylvania State University, University
Park, Pennsylvania, USA (Z.S. Goldblum, N.M. M'ikanatha,
E.M. Nawrocki, J. Kovac, E.G. Dudley); Pennsylvania Department
of Health, Harrisburg, Pennsylvania (N.M. M'ikanatha, N. Cesari)

We isolated *Salmonella enterica* serovar Senftenberg in raw wastewater from 2 Pennsylvania wastewater treatment facilities during June 2022. Whole-genome sequencing revealed 4 isolates separated by <4 single nucleotide polymorphisms from *S. enterica* Senftenberg in a cluster from the 2022 nationwide outbreak linked to contaminated peanut butter.
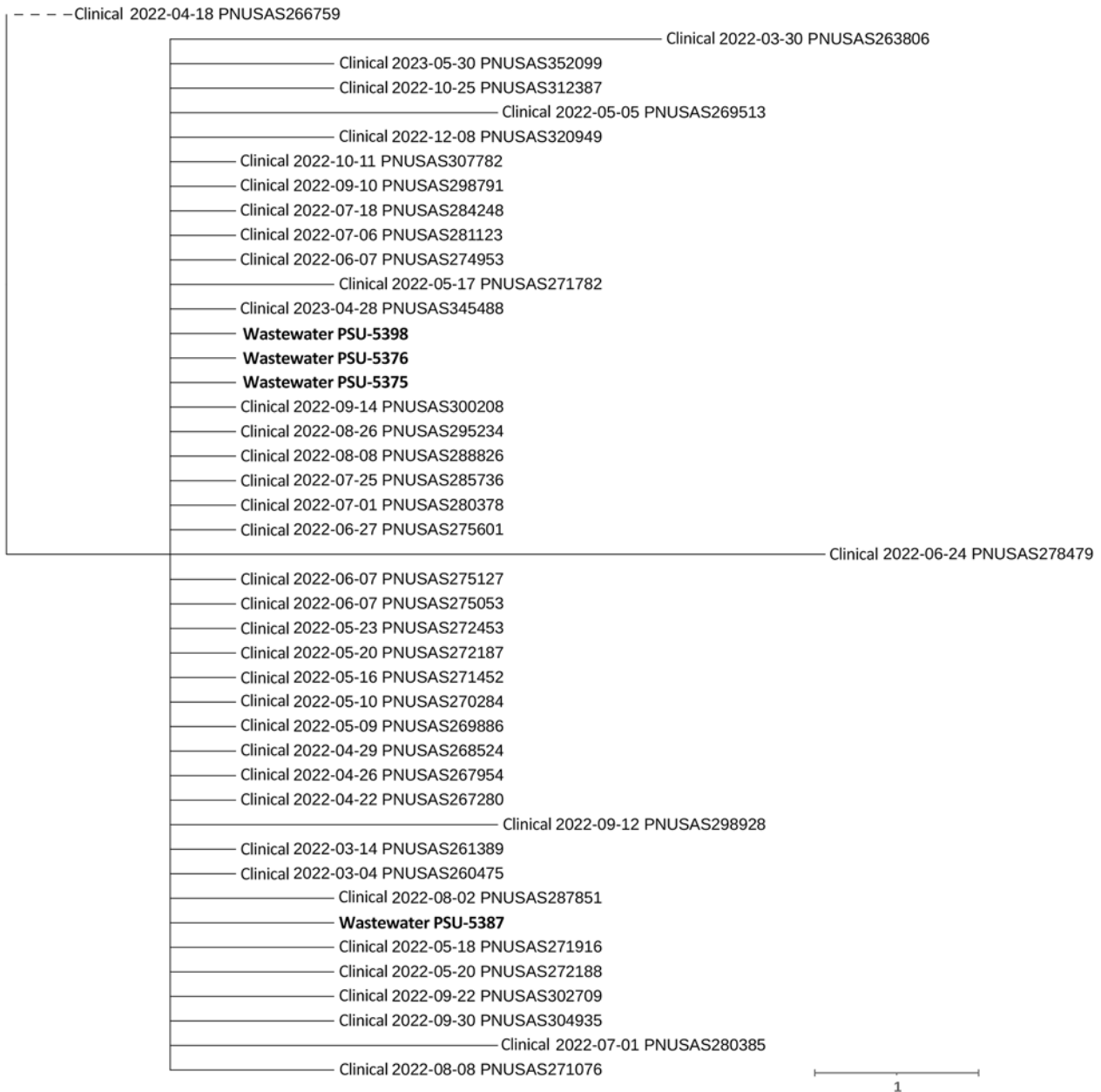
Table. Data for *Salmonella* sp. linked to multistate outbreak isolated from wastewater treatment facilities, United States, 2022*

Isolate no.	Isolation date, 2022	Location	Biosample accession no.
PSU-5375	June 15	WWTP-1	SAMN33902330
PSU-5376	June 15	WWTP-1	SAMN33902331
PSU-5387	June 22	WWTP-1	SAMN33902342
PSU-5398	June 16	WWTP-2	SAMN34154796

*WWTP-1, wastewater treatment plant 1; WWTP-2, wastewater treatment plant 2. Accession nos. from National Center for Biotechnology Information's Sequence Read Archive (https://www.ncbi.nlm.nih.gov/sra).

The COVID-19 pandemic showcased the power of wastewater-based surveillance (WBS) to infer viral loads in communities (*1*). Health officials have also used WBS to track antimicrobial resistance (*2*,*3*), and some researchers have made associations between bacterial pathogens (e.g., *Salmonella enterica*) from domestic wastewater and those from clinical sources (*4*–*7*). The extent to which routine surveillance for bacterial pathogens would benefit public health is unclear. To evaluate possible benefits, we screened samples from 2 wastewater facilities for *S. enterica* during June 2022, concurrent with a study investigating SARS-CoV-2 in wastewater (*8*). Our study also included a broader investigation into whether we could isolate *S. enterica* that matched human isolates from ongoing outbreaks.

We collected composite wastewater samples twice a week during June 2022 from 2 wastewater (sewage) treatment facilities in central Pennsylvania, designated WWTP-1 and WWTP-2 (Table). We selected the 2 facilities based on their convenience and suitability: both were within a 1-hour driving radius from our laboratory and water treatment in both facilities focused solely on domestic sewage. WWTP-1 received wastewater from a population of ≈3,600 persons, and WWTP-2 received wastewater from a population of ≈13,600 persons. We adapted protocols from the US Food and Drug Administration's Bacteriological Analytical Manual (https://www.fda.gov/food/laboratory-methods-food/bacteriological-analytical-manual-bam) to identify *S. enterica* isolates. In brief, we centrifuged 120 mL of wastewater at 5,000 *g* for 20 minutes at 4°C to precipitate solids. We then passed the supernatant through a 0.45-µm filter, and the filter was added to the pellet along with 40 mL of buffered peptone water supplemented with 20 mg/L of novobiocin. After a 24-hour recovery at 35°C, we subcultured the samples into selective media (tetrathionate and Rappaport-Vassiliadis broths) and incubated them at 42°C for 24 hours. We plated 10-µL aliquots of each enrichment culture on xylose lysine deoxycholate and Hektoen enteric agars and monitored them for growth and colonies characteristic of *Salmonella* sp. We restreaked putative *S. enterica* colonies to purify them and confirmed identity by PCR targeting *invA*. We constructed libraries by using the Nextera XT DNA Library Preparation Kit (Illumina, https://www.illumina.com) and used the MiSeq Reagent Kit v3 (Illumina) to perform sequencing at 500 (2 × 250) cycles.

We uploaded short sequence reads to the National Center for Biotechnology Information Pathogen Detection site (https://www.ncbi.nlm.nih.gov/pathogens) for genomic comparison to human clinical isolates and to identify molecular serovars. We deposited all sequencing data in the National Center for Biotechnology Information's Sequence Read Archive (https://www.ncbi.nlm.nih.gov/sra) under BioProject PRJNA357723. We constructed an annotated phylogenetic tree by importing the Newick data from the National Center for Biotechnology Information's Pathogen Detection database into the Interactive Tree of Life (https://itol.embl.de). We verified clusters on the Centers for Disease Control and Prevention's System for Enteric Disease Response, Investigation, and Coordination (SEDRIC; https://www.cdc.gov/foodborne-outbreaks/php/foodsafety/tools/index.html).

During June 13–29, 2022, we isolated 42 *Salmonella* strains from wastewater samples. We conducted this *Salmonella* study alongside SARS-CoV-2 emergency response efforts, while new protocols were being validated, which affected its timing and duration.

Whole-genome sequencing rendered isolates that we aligned to various serovars; Panama was the most prevalent (16 [38.1%]), followed by Senftenberg (9 [21.4%]) and Baildon (8 [19.0%]). Other serovars included Agona (3 [7.1%]), Oranienburg (3 [7.1%]), Montevideo (2 [4.8%]), and Kintambo (1 [2.4%]). We noted 4 serovar Senftenberg isolates were separated by 0–4 single

nucleotide polymorphisms from a cluster of 40 clinical isolates uploaded to the Pathogen Detection database during March 2022–May 2023 (Table, Figure). Using SEDRIC, we verified that 21 (52.5%) of the clinical isolates matched a 2022 multistate foodborne outbreak of salmonellosis (designated cluster 2205MLJMP-1 in SEDRIC) that was sourced to contaminated peanut

Figure. Isolates of *Salmonella* sp. linked to multistate outbreak isolated from wastewater treatment facilities, United States, 2022. We detected *S. enterica* serovar Senftenberg from 2 Pennsylvania wastewater facilities genetically linked to those associated with a 2022 multistate outbreak. SNP-based tree constructed using Newick data generated by the National Center for Biotechnology Information's Pathogen Detection database (https://www.ncbi.nlm.nih.gov/pathogens), showing the relationship between 4 *S. enterica* Senftenberg isolates reported in this study (bold) and whole-genome sequence previously isolated from human cases within the same cluster. Note that dates indicate when data were uploaded to the pathogen detection database and are not necessarily the date of isolation. Scale bar indicates nucleotide substitutions per site. SNP, single-nucleotide polymorphism.

butter. Patients lived in 17 different states (https://www.cdc.gov/salmonella/senftenberg-05-22/map.html). Although Pennsylvania was not initially included, health officials eventually identified 3 additional Senftenberg isolates matching 2205MLJMP-1 in SEDRIC. Those isolates were from 3 Pennsylvania patients (PNUSAS320949, PNUSAS280385, PNUSAS280378 [Figure]), and researchers detected them after the outbreak investigation concluded on May 9, 2022. Researchers also connected 8 Baildon isolates to a previously documented outbreak of salmonellosis that occurred primarily in Pennsylvania (*9*).

In conclusion, we isolated *S. enterica* Senftenberg from 2 rural wastewater treatment facilities in Pennsylvania and found the isolates to be genomic matches to strains associated with a multistate salmonellosis outbreak. No human cases of salmonellosis were reported in Pennsylvania at the time of that outbreak, possibly because of underreporting of nontyphoidal *Salmonella* (*10*). Our results highlight *Salmonella* strains reported to public health authorities that were not initially recognized as part of a multistate outbreak. We were only able to uncover this connection by comparing the genetic relatedness of *Salmonella* Senftenberg isolates from clinical and wastewater sources. The results of our study underscore the value of wastewater testing and targeted sewerage monitoring, not only in facilitating outbreak investigations but also in identifying additional cases, even after an outbreak has been declared closed. Our findings also highlight the need for further research into how targeted sewage monitoring can inform outbreak duration, prevention efforts, and regulatory oversight related to foodborne illnesses.

Acknowledgments

About the Author

Ms. Goldblum is a student in the master's of public health program at Emory University. Her research interests focus on infectious disease epidemiology.

References

1. The potential of wastewater-based epidemiology. Nat Water. 2023;1:399. [Editorial]. https://doi.org/10.1038/s44221-023-00093-6
2. Pärnänen KMM, Narciso-da-Rocha C, Kneis D, Berendonk TU, Cacace D, Do TT, et al. Antibiotic resistance in European wastewater treatment plants mirrors the pattern of clinical antibiotic resistance prevalence. Sci Adv. 2019;5:eaau9124. https://doi.org/10.1126/sciadv.aau9124
3. Hutinel M, Huijbers PMC, Fick J, Åhrén C, Larsson DGJ, Flach CF. Population-level surveillance of antibiotic resistance in *Escherichia coli* through sewage analysis. Euro Surveill. 2019;24:1800497. https://doi.org/10.2807/1560-7917.ES.2019.24.37.1800497
4. Diemert S, Yan T. Clinically unreported salmonellosis outbreak detected via comparative genomic analysis of municipal wastewater *Salmonella* isolates. Appl Environ Microbiol. 2019;85:e00139–19. https://doi.org/10.1128/AEM.00139-19
5. Sahlström L, de Jong B, Aspan A. *Salmonella* isolated in sewage sludge traced back to human cases of salmonellosis. Lett Appl Microbiol. 2006;43:46–52. https://doi.org/10.1111/j.1472-765X.2006.01911.x
6. Diemert S, Yan T. Municipal wastewater surveillance revealed a high community disease burden of a rarely reported and possibly subclinical *Salmonella enterica* serovar Derby strain. Appl Environ Microbiol. 2020;86:e00814–20. https://doi.org/10.1128/AEM.00814-20
7. Vincent V, Scott HM, Harvey RB, Alali WQ, Hume ME. Novel surveillance of *Salmonella enterica* serotype Heidelberg epidemics in a closed community. Foodborne Pathog Dis. 2007;4:375–85. https://doi.org/10.1089/fpd.2007.0025
8. Timme RE, Woods J, Jones JL, Calci KR, Rodriguez R, Barnes C, et al.; GenomeTrakr Laboratory Consortium. SARS-CoV-2 wastewater variant surveillance: pandemic response leveraging FDA's GenomeTrakr network. mSystems. 2024;9:e0141523. https://doi.org/10.1128/msystems.01415-23
9. M'ikanatha NM, Goldblum ZS, Cesari N, Nawrocki EM, Fu Y, Kovac J, et al. Outbreak-associated *Salmonella* Baildon found in wastewater demonstrates how sewage monitoring can supplement traditional disease surveillance. J Clin Microbiol. 2024;62:e0082524. https://doi.org/10.1128/jcm.00825-24
10. Scallan E, Hoekstra RM, Angulo FJ, Tauxe RV, Widdowson MA, Roy SL, et al. Foodborne illness acquired in the United States—major pathogens. Emerg Infect Dis. 2011;17:7–15. https://doi.org/10.3201/eid1701.P11101

Address for correspondence: Edward G. Dudley, The Pennsylvania State University, 202 Rodney A. Erickson Food Science Building, University Park, PA 16802, USA; email: egd100@psu.edu

Possible New Focus of Diphyllobothriasis, Central Europe

Tomáš Scholz,[1] Roman Kuchta,[1] Jan Brabec

Author affiliation: Institute of Parasitology, Biology Centre of the Czech Academy of Sciences, České Budějovice, Czech Republic

Diphyllobothriasis is a human parasitic infection that is widespread in the Northern Hemisphere. Popular sport fish such as pike and perch are the source of human infection. We document the autochthonous origin of diphyllobothriasis in a popular tourist destination in Central Europe, which likely marks recent colonization of the parasite.

In contrast to most human parasitic infections, which occur mainly in tropical and subtropical regions that have lower standards of hygiene and less economic development, diphyllobothriasis (also known as dibothriocephalosis) is more common in temperate and cold latitudes. The disease, which is caused by the human broad tapeworm (*Dibothriocephalus latus*), is particularly prevalent in the Northern Hemisphere. The source of infection is the consumption of popular sport fish, such as pike and perch (*1–4*).

There are 4 main foci of diphyllobothriasis in Europe: Fennoscandia; Baltic region; the Alpine lakes; the Danube region; and certain areas in Russia (Figure). The number of cases decreased drastically after World War II (*4*). Today, only small foci remain, mainly in the Alpine lakes of northern Italy, Switzerland, and France, where diphyllobothriasis continues to circulate (*4,5*).

With the exception of a few imported cases, no cases of human diphyllobothriasis or of fish infected with parasite larvae have been reported in Central Europe (Czech Republic and neighboring countries such as Austria, Hungary, and eastern Germany), although the fish parasites have been intensively studied for over a century (*4,6,7*). In 2024, however, an autochthonous case of diphyllobothriasis caused by *D. latus* was documented in the Czech Republic.

A 37-year-old man, who had not traveled to known diphyllobothriasis-endemic areas and had not previously consumed raw or undercooked fish or fish products, obtained a pike (*Esox lucius*) caught in October 2023 near Horní Planá, the largest settlement on the Lipno reservoir (48.7 km²) in South Bohemia, Czech Republic (Figure). He consumed ≈1 teaspoon of raw salted roe (caviar) from the pike, which is the most common source of diphyllobothriasis in many parts of Russia (*8*). Two months later, he experienced occasional abdominal bloating. After another 2 months, he expelled a piece of tapeworm with dozens of proglottids. A coprologic examination confirmed the presence of the typical diphyllobothriid eggs. Treatment with mebendazole (Vermox, 6 tablets) (Johnson & Johnson, https://www.jnj.com) was unsuccessful, but the tapeworm was later completely expelled after a single dose of praziquantel (Biltricide) (Bayer, https://www.bayer.com). Sequencing of the complete mitochondrial cytochrome *c* oxidase subunit I gene (*cox*1) from the eggs (GenBank accession no. PQ270068) confirmed the species identity as *D. latus*. Because the patient could not have been infected elsewhere and his symptoms appeared after eating the pike roe, considering his infection as an autochthonous case of diphyllobothriasis is reasonable. Furthermore, raw products from fish that serve as second intermediate hosts for the human broad tapeworm (i.e., pike, perch, or ruffe) are not imported into the Czech Republic.

The Lipno Reservoir is a popular year-round tourist destination in the Czech Republic, attracting hundreds of thousands of visitors every year, including many local and foreign anglers. The fish parasites in that reservoir were intensively studied in the 1960s after the construction and filling of the reservoir (*9*). However, *D. latus* has never been found in Central Europe, apart from a single case in the 1960s in an angler from southwestern Slovakia who consumed raw perch from the Danube (*4,6,10*) (Figure). A presumably autochthonous, unpublished but molecularly identified (*cox*1; GenBank accession no. PQ270069) case from 2014 involved a 43-year-old angler from the Czech Republic who had consumed pike from northeastern and southern Bohemia, Czech Republic (as in this case) and had not traveled to diphyllobothriasis-endemic areas.

Given the intensive study of the reservoir and the popularity of the area, the parasite going undetected for decades seems unlikely. The reservoir has also never been stocked with fish imported from abroad, such as pike, perch, or ruffe, so it is unlikely that the tapeworm was imported from diphyllobothriasis-endemic areas through

---

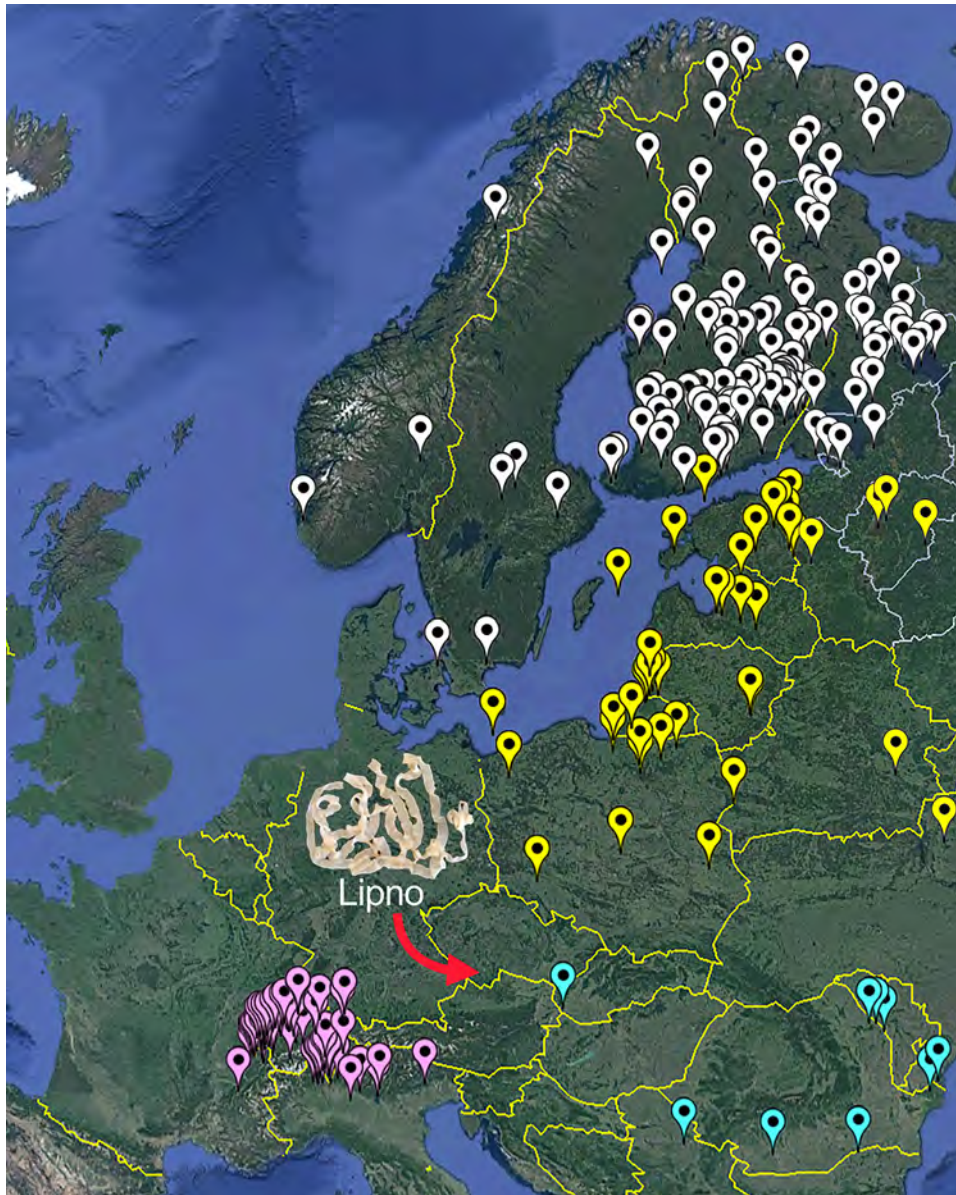[1]These authors contributed equally to this article.

Figure. Map of the distribution of *Dibothriocephalus latus* in Europe according to Králová-Hromadová et al. (*4*) and Kuecha et al. (*8*). Diphyllobothriasis-endemic areas in Europe are identified by different colors: white indicates Fennoscandia, yellow indicates Baltic region, purple indicates Alpine lake region, and turquoise indicates Danube region. Red arrow indicates the newly reported case from the Czech Republic.

fish. During the examination of 108 potential second intermediate hosts (10 pike [including the pike whose eggs caused the human infection], 53 perch, and 54 ruffe) from the Lipno Reservoir in May and August 2024, no plerocercoids of *D. latus* have been found. However, the prevalence of the fish infection might be low even in other known foci of diphyllobothriasis (*5*). Therefore, a plausible explanation for the possibly autochthonous occurrence of *D. latus* in Central Europe is a recent appearance of the parasite in this ecosystem, probably introduced by tourists from a diphyllobothriasis-endemic area, such as the lake regions of northwestern Russia (*8*).

Acknowledgments

About the Author

Dr. Scholz is a senior researcher at the Institute of Parasitology, Biology Centre of the Czech Academy of Sciences in České Budějovice, Czech Republic. He deals with fish parasites and the systematics, diversity, phylogeny, and life cycles of helminths, especially tapeworms (Cestoda) and trematodes (Digenea).

References

1. Dick T. Diphyllobothriasis: the *Diphyllobothrium latum* human infection conundrum and reconciliation with a worldwide zoonosis. In: Murrell KD, Fried B, editors. World Class Parasites, vol. 11. Boston: Springer; 2008. p. 151–184.
2. Scholz T, Kuchta R. Fish-borne, zoonotic cestodes (*Diphyllobothrium* and relatives) in cold climates: a never-ending story of neglected and (re)-emergent parasites. Food Waterborne Parasitol. 2016;4:23–28.
3. Scholz T, Kuchta R, Brabec J. Broad tapeworms (Diphyllobothriidae), parasites of wildlife and humans: recent progress and future challenges. Int J Parasitol Parasites Wildl. 2019;9:359–69. https://doi.org/10.1016/j.ijppaw.2019.02.001
4. Králová-Hromadová I, Radačovská A, Čisovská Bazsalovicsová E, Kuchta R. Ups and downs of infections with the broad fish tapeworm *Dibothriocephalus latus* in Europe from 1900 to 2020: Part I. Adv Parasitol. 2021; 114:75–166. https://doi.org/10.1016/bs.apar.2021.08.008
5. Gustinelli A, Menconi V, Prearo M, Caffara M, Righetti M, Scanzio T, et al. Prevalence of *Diphyllobothrium latum* (Cestoda: Diphyllobothriidae) plerocercoids in fish species from four Italian lakes and risk for the consumers. Int J Food Microbiol. 2016;235:109–12. https://doi.org/10.1016/j.ijfoodmicro.2016.06.033
6. Moravec F. Checklist of the Metazoan Parasites of Fishes of the Czech Republic and the Slovak Republic (1873–2000). Prague: Academia; 2001.
7. Konecny R, Sattmann H, Schabuss M, Jütte M, Lewis JW. A review of research studies on helminth parasites of fish from Austria. Acta ZooBot Austria. 2020;157:41–62.
8. Kuchta R, Radačovská A, Čisovská Bazsalovicsová E, Králová-Hromadová I. Ups and downs of infections with the broad fish tapeworm *Dibothriocephalus latus* in Europe (Part II) and Asia from 1900 to 2020. Adv Parasitol. 2023;122:1–69. https://doi.org/10.1016/bs.apar.2023.05.001
9. Ergens R. Results of parasitological investigation on the health of *Esox lucius* L. in the Lipno reservoir. Folia Parasitol. 1966;13:222–36.
10. Čatár G, Sobota K, Kvasz L, Hrúzik J. The 1st nonimported case of diphyllobothriasis in Czechoslovakia [in Slovak]. Bratisl Lék Listy. 1967;47:241–4.

Address for correspondence: Tomáš Scholz, Institute of Parasitology, Biology Centre of the Czech Academy of Sciences, Branišovská 31, 370 05 České Budějovice, Czech Republic; email: tscholz@paru.cas.cz

COMMENT LETTER

Sporotrichosis in Domestic Cat and Zoonotic Transmission

Sunil More, Timothy A. Snider, Akhilesh Ramachandran

Author affiliations: Oklahoma State University College of Veterinary Medicine, Stillwater, Oklahoma, USA (S. More, A. Ramachandran); University of Missouri College of Veterinary Medicine, Columbia, Missouri, USA (T.A. Snider)

To the Editor: Recent cases of feline sporotrichosis with zoonotic human infection have been highlighted in Kansas, USA (*1*). We describe a challenging feline sporotrichosis case in Oklahoma, USA, that emphasizes the critical need for early diagnostic strategies to mitigate the risk of further zoonotic transmission. Of note, the cat also scratched the veterinarian and owner and severe skin lesions subsequently developed on both of them; lesions resolved within 2 weeks (M. Carver, unpub. data, telephone report).

A 4-year-old domestic short-haired cat was taken for veterinary care with a raised, nodular, ulcerated mass on its right front foot. The mass was unresponsive to antibacterial treatment and progressively necrosed; the leg was subsequently amputated. A similar lesion developed on the left front foot. Skin biopsy samples from the cat's left front foot were submitted for analysis. Histopathology revealed dermal infiltrates of neutrophils and macrophages with edema, fibrin, and karyorrhectic debris. We observed numerous intrahistiocytic and extracellular round to oval, faint basophilic 4 to 10-µm diameter yeasts surrounded by a clear halo (Figure 1, panel A, black arrowhead). Gram and Grocott methenamine silver stains showed yeasts with occasional cigar-shaped morphology (Figure 1, panel B, magenta arrow). We identified the fungal culture colonies as *Sporothrix schenckii* by using matrix-assisted laser desorption/ionization time-of-flight (MALDI-TOF) mass spectrometry. We cultured and identified a large number of secondary bacterial contaminants from the lesions.

Sporotrichosis caused by dimorphic fungus of the genus *Sporothrix* presents potential diagnostic challenges because it can manifest in various clinical forms in human patients (*2*). The differential diagnoses for sporotrichosis in cats, because of overlapping clinical features, include feline leprosy, bartonellosis, atypical mycobacterial infections, *Staphylococcus* spp. pyoderma, dermatophytosis (ringworm), cutaneous lymphoma, deep mycoses (cryptococcosis,
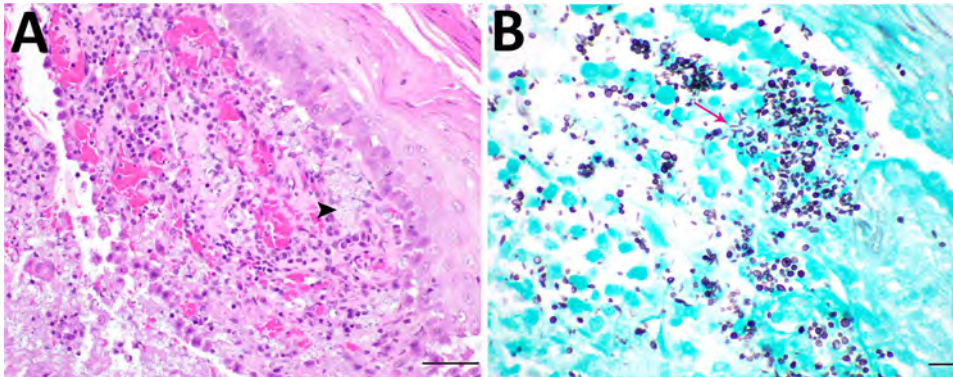
Figure. Skin lesions of sporotrichosis in a cat, Oklahoma, USA. A) Suppurative dermatitis with numerous 4 to 10-µm diameter intralesional yeasts (black arrowhead). Hematoxylin and eosin stain; scale bar indicates 50 µm. B) Occasional cigar-shaped morphology of *Sporothrix schenckii* (magenta arrow). Grocott methenamine silver stain; scale bar indicates 20 µm.

histoplasmosis, blastomycosis), and hypersensitivity reactions. Selecting appropriate diagnostic tests is crucial for accurately diagnosing sporotrichosis. Those multiple differential diagnoses emphasize the importance of incorporating histopathology, followed by fungal culture or PCR, for accurate diagnosis. To obtain reliable samples, deep punch or wedge biopsy specimens from intact nondraining lesions are recommended. Considering the zoonotic potential of *Sporothrix schenckii* infections (*1*,*3–5*), taking a One Health approach incorporating collaboration between veterinary and human healthcare sectors is essential for effective diagnosis and treatment of sporotrichosis cases.

About the Author

Dr. More, a diplomate of the American College of Veterinary Pathologists, is an assistant professor at Oklahoma State University's College of Veterinary Medicine. His research focuses on respiratory viral diseases and veterinary pathology.

References

1. Hennessee I, Barber E, Petro E, Lindemann S, Buss B, Santos A, et al. Sporotrichosis cluster in domestic cats and veterinary technician, Kansas, USA, 2022. Emerg Infect Dis. 2024;30:1053–5. https://doi.org/10.3201/eid3005.231563
2. Gutierrez-Galhardo MC, Freitas DFS, do Valle ACF. Clinical forms of human sporotrichosis and host immunocompetence. In: Zeppone Carlos I, editor. Sporotrichosis. Berlin: Springer International Publishing; 2015. p. 73–82.
3. Gallo S, Arias-Rodriguez C, Sánchez-Cifuentes EA, Santa-Vélez C, Larrañaga-Piñeres I, Gaviria-Barrera ME, et al. First three cases of cat-associated zoonotic cutaneous sporotrichosis in Colombia. Int J Dermatol. 2022;61:1276–9. https://doi.org/10.1111/ijd.16377
4. Gremião ID, Miranda LH, Reis EG, Rodrigues AM, Pereira SA. Zoonotic epidemic of sporotrichosis: cat to human transmission. PLoS Pathog. 2017;13:e1006077. https://doi.org/10.1371/journal.ppat.1006077
5. Rachman R, Ligaj M, Chinthapalli S, Serafino Wani R. Zoonotic acquisition of cutaneous *Sporothrix braziliensis* infection in the UK. BMJ Case Rep. 2022;15:e248418. https://doi.org/10.1136/bcr-2021-248418

Address for correspondence: Sunil More, Department of Veterinary Pathobiology, 250 McElroy Hall, Stillwater, OK 74078-1010, USA; email: sunil.more@okstate.edu

Perspectives of Infectious Disease Physicians on *Bartonella quintana* Cases, United States, 2014–2024

Souci Louis, Grace Marx, Alison F. Hinckley, Shannan N. Rich, Susan E. Beekmann, Philip M. Polgreen, Matthew Kuehnert, Jessica N. Ricaldi, Scott Santibañez

Author affiliations: Centers for Disease Control and Prevention, Atlanta, Georgia, USA (S. Louis, G. Marx, A.F. Hinckley, S.N. Rich, M. Kuehnert, J.N. Ricaldi, S. Santibañez); University of Iowa Carver College of Medicine, Iowa City, Iowa, USA (S.E. Beekmann, P.M. Polgreen)

In a US survey of infectious disease specialists, 61 respondents reported seeing >1 *Bartonella quintana* infection during 2014–2024. Diagnostic challenges included limited healthcare provider awareness, inadequate testing, and inconsistent healthcare access among affected populations. Early recognition of *B. quintana* infections is needed to improve outcomes among affected populations.

Bartonella quintana is a pathogenic bacterium carried and transmitted to humans by the body louse, *Pediculus humanus humanus*. Clinical manifestations of disease are relapsing fever, bacillary angiomatosis, chronic bacteremia, and endocarditis (*1*). *B. quintana* infections are not nationally notifiable and little is known regarding their incidence and geographic distribution. Barriers to healthcare access in affected human populations and inherent diagnostic challenges might both contribute to underdiagnosis of cases (*2*). However, recent cases have been reported among persons experiencing homelessness (PEH) in New York, New York, and Denver, Colorado, USA (*1,3*).

The Infectious Diseases Society of America's Emerging Infections Network (EIN) is a healthcare provider–based sentinel network that has >2,800 infectious disease specialists throughout North America (*4*). We evaluated provider-diagnosed *B. quintana* infections reported by EIN members to identify opportunities for improving disease awareness and patient diagnosis.

We sent a 6-question survey to EIN members to collect data regarding *B. quintana* cases, affected populations, and diagnostic challenges (Appendix, https://wwwnc.cdc.gov/EID/article/30/12/24-0655-App1.pdf). We distributed the questionnaire through an electronic mailing list on January 18, 2024,

and sent reminder emails on January 25 and February 7. A total of 240 members from 41 US states and the District of Columbia responded; 61 (25%) respondents from 24 states and the District of Columbia stated that they had seen >1 case of *B. quintana* infection within the previous 10 years (Table), and 47 (20%) noted that cases occurred primarily in PEH communities. Other, nonmutually exclusive affected populations included persons with substance use disorders, mental health disorders, HIV infection, and refugee or rural indigenous populations. The most frequently reported obstacles to earlier diagnosis of *B. quintana* infection were the lack of clinical suspicion (88%), knowledge about diagnostic tests (73%), and access to *B. quintana*-specific diagnostic tests (51%). Other challenges included long laboratory turnaround times and inconsistent access to healthcare among affected populations. Free-text responses indicated the value of general clinical knowledge about *B. quintana* infection. For example, one respondent commented, "I have a strong clinical suspicion that there is an association with other endovascular infections that we sometimes miss clinically. For example, a hemorrhagic stroke in someone with a history of homelessness should raise suspicion of this infection. Additionally, any mycotic aneurysm, particularly of the thoracic or abdominal aorta, should raise suspicion for *B. quintana* infection."

We believe that EIN members are seeing *B. quintana* cases in diverse geographic locations across the United States, including in the Southeast (Figure), where *B. quintana* has not been described in the literature (*2,5*). We also believe that those findings highlight the importance of increasing clinician awareness of possible *B. quintana* infections among patients at risk for body louse infestation across the United States.

Diagnosis of a *B. quintana* infection is challenging because of serologic cross-reactivity with other *Bartonella* spp. and the specific conditions required for a bacterial culture. Several studies suggest that laboratory confirmation could be improved by using molecular testing for detection instead of serologic and culture methods (*6,7*). Intentional collaboration between healthcare providers and clinical microbiology laboratories could result in earlier diagnosis and improved treatment outcomes, especially the use of reflexive *B. quintana* molecular diagnostic assays for PEH seeking care for fever of unknown etiology in emergency departments (*2*).

PEH are disproportionately affected by *B. quintana* infections, although several other communities are impacted in the United States (*1–3*). Co-existing medical conditions (e.g., behavioral health conditions) and socioeconomic barriers beyond housing

Table. Quantitative summary of responses from Emerging Infections Network members across the United States who reported seeing *Bartonella quintana* infection cases during 2014–2024*

Questions	Responses, no. (%)
Question 1. Have you seen any cases?	
a. Recently, 2019–2024, n = 240	
Yes	44 (18)
No	191 (80)
Not sure	5 (2)
b. More remotely, 2014–2018, n = 240	
Yes	34 (14)
No	174 (73)
Not sure	20 (8)
NA (not in practice)	12 (5)
Question 2a. Have you noticed cases within any of the following communities (persons experiencing homelessness, persons with substance use disorder, persons with mental health disorders)? n = 240	
Yes	47 (20)
No	17 (7)
Not sure	5 (2)
NA (no cases)	171 (71)
Question 2b. If yes, in which communities? n = 46 [select any that apply; numbers add up to >100%]	
Persons experiencing homelessness	42 (91)
Persons with substance use disorders	30 (65)
Persons with mental health disorders	29 (63)
Question 3. What do you see as obstacles(s) to earlier diagnosis for patients with *B. quintana* infections? n = 203 [select any that apply; numbers add up to >100%]	
Lack of clinical suspicion by providers	179 (88)
Lack of provider knowledge about optimal diagnostic tests for *B. quintana*	148 (73)
Lack of clinically available *B. quintana*–specific diagnostic tests	103 (51)
No obstacles selected	37 (18)

*Responses were collected from a questionnaire sent to Emerging Infections Network members in 2024 (Appendix, https://wwwnc.cdc.gov/EID/article/30/12/24-0655-App1.pdf). Free-text questions and responses are not shown. NA, not applicable.

instability, such as lack of medical insurance, can further complicate clinical management (*1*). Inconsistent access to running water, showers, and laundry facilities with hot water increases the risk for body lice infestation. Limited access to healthcare increases the risk for undiagnosed and untreated *B. quintana* infections that can lead to severe disease. Recognizing complex social determinants of health provides an opportunity to improve prevention, detection, and treatment of *B. quintana* infections.

The first limitation of our study is that, although querying EIN members is an efficient and convenient method to hear from infectious disease specialists, those members are not representative of all healthcare providers in the United States. Second, the EIN members who did respond might not have recalled all of their *B. quintana* cases. Also, reported case locations might have differed from the providers' current practice location.

In conclusion, we consider it critical to increase awareness of *B. quintana* infection risk among certain
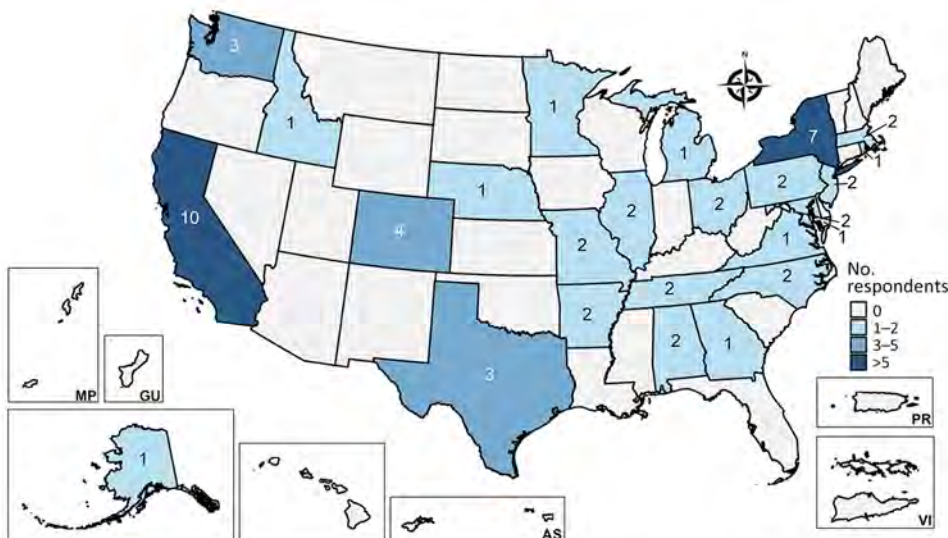
Figure. Map indicating numbers and locations of infectious disease physicians responding to survey regarding *Bartonella quintana* infection cases, United States, 2014–2024. US states and territories are indicated. The survey was sent to members of The Infectious Diseases Society of America's Emerging Infections Network in 2024. AS, American Samoa; G, Guam; MP, Northern Marianis Islands; PR, Puerto Rico; VI, Virgin Islands.

patient populations, such as PEH, across the United States and increase awareness of diagnostic testing that would most effectively detect active *B. quintana* infections. Promoting early recognition and diagnosis of *B. quintana* infections could result in earlier treatment and improve health outcomes among affected populations.

About the Author

Dr. Louis is an Epidemic Intelligence Service fellow assigned to the Division of Infectious Disease Readiness and Innovation, National Center for Emerging and Zoonotic Infectious Diseases at the Centers for Disease Control and Prevention, Atlanta, GA, USA. Her research interests focus on zoonotic diseases and integrating One Health approaches to enhance disease prevention and response across diverse populations.

References

1. Rich SN, Beeson A, Seifu L, Mitchell K, Wroblewski D, Juretschko S, et al. Notes from the field: severe *Bartonella quintana* infections among persons experiencing unsheltered homelessness—New York City, January 2020–December 2022. MMWR Morb Mortal Wkly Rep. 2023;72:1147–8. https://doi.org/10.15585/mmwr.mm7242a3
2. Boodman C, Gupta N, Nelson CA, van Griensven J. *Bartonella quintana* endocarditis: a systematic review of individual cases. Clin Infect Dis. 2024;78:554–61. https://doi.org/10.1093/cid/ciad706
3. Shepard Z, Vargas Barahona L, Montalbano G, Rowan SE, Franco-Paredes C, Madinger N. *Bartonella quintana* infection in people experiencing homelessness in the Denver metropolitan area. J Infect Dis. 2022;226:S315–21. https://doi.org/10.1093/infdis/jiac238
4. Pillai SK, Beekmann SE, Santibanez S, Polgreen PM. The Infectious Diseases Society of America Emerging Infections Network: bridging the gap between clinical infectious diseases and public health. Clin Infect Dis. 2014;58:991–6. https://doi.org/10.1093/cid/cit932
5. Lam JC, Fonseca K, Pabbaraju K, Meatherall BL. Case report: *Bartonella quintana* endocarditis outside of the Europe–African gradient: comprehensive review of cases within North America. Am J Trop Med Hyg. 2019;100:1125–9. https://doi.org/10.4269/ajtmh.18-0929
6. McCormick DW, Rassoulian-Barrett SL, Hoogestraat DR, Salipante SJ, SenGupta D, Dietrich EA, et al. *Bartonella* spp. infections identified by molecular methods, United States. Emerg Infect Dis. 2023;29:467–76. https://doi.org/10.3201/eid2903.221223
7. Motzer AR, Mudroch S, Schultz S, Sullivan KV, Altneu E. The brief case: *Bartonella quintana* aortic and mitral valve endocarditis identified through 16S rRNA sequencing. J Clin Microbiol. 2024;62:e0040223. https://doi.org/10.1128/jcm.00402-23

Address for correspondence: Souci Louis, Centers for Disease Control and Prevention, 1600 Clifton Rd NE, Mailstop H24-11, Atlanta, GA 30329-4027, USA; email: qfb8@cdc.gov

EID Podcast
Streptococcus dysgalactiae Bloodstream Infections, Norway, 1999–2021
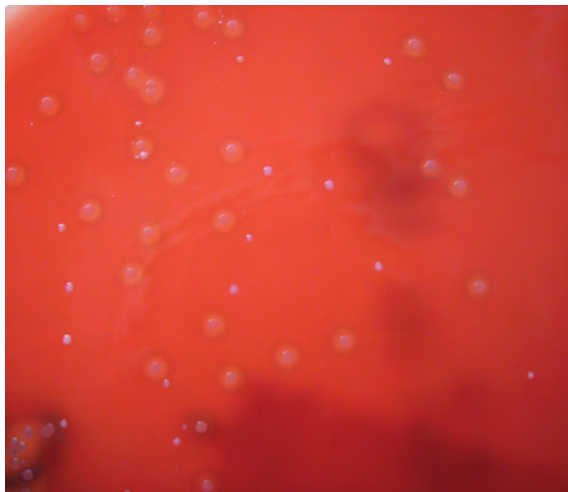
Streptococcus dysgalactiae increasingly is recognized as a pathogen of concern for human health. However, longitudinal surveillance data describing temporal trends of *S. dysgalactiae* are scarce. In this large epidemiologic study of invasive *S. dysgalactiae* bloodstream infections in western Norway, researchers found that *S. dysgalactiae* is rapidly emerging as a potent pathogen and currently is the fifth most common cause of bloodstream infections in the Bergen health region.

In this EID podcast, Dr. Oddvar Oppegaard, an infectious disease specialist at Haukeland University Hospital and an associate professor at the University of Bergen discusses *Streptococcus dysgalactiae* bloodstream infections in Norway.

Visit our website to listen: https://bit.ly/3Ynwt4q

EMERGING INFECTIOUS DISEASES®

On Call: A Doctor's Journey in Public Service

Anthony S. Fauci; Viking [imprint of Penguin Random House LLC], New York, NY, USA 2024;ISBN-13: 9780593657478; Pages: 480; Price: $36.00

For readers engaged in the prevention and treatment of infectious diseases, Dr. Anthony Fauci's recent memoir, in which he shares not only his triumphs and achievements but also his mistakes and challenges, provides a rich resource of leadership lessons. Fauci adds depth and color to his memoir by including discussions regarding his sports interests and Italian heritage, as well as moving and deeply personal stories of his family.

During his Jesuit schooling and subsequent medical training at Cornell University, Fauci exhibited a commitment to excellence. Starting as a focused research clinician at the National Institute of Allergy and Infectious Diseases (NIAID) at the National Institutes of Health, he soon pivoted to an enhanced leadership role in addressing the emerging HIV/AIDS epidemic, demonstrating self-confidence and superior insight. Fauci's sharp intellect and enormous energy allowed him to successfully wear many hats: productive clinical researcher, skillful administrator, effective communicator, and inspiring leader. That multifaceted prowess has made him one of the most influential physicians and public health leaders of our time.

As NIAID Director, Fauci steadily expanded the size and scope of the institute; the annual budget increased from $370 million in 1984 to well over $6 billion when he stepped down in early 2023 (1). In addition to overseeing unprecedented scientific, medical, and public health progress in addressing multiple infectious disease threats (e.g., HIV, tuberculosis, influenza, anthrax, Ebola, Zika, West Nile, and SARS-CoV-2), Fauci recruited, mentored, and supported many productive research scientists.

To support the NIAID research agenda, Fauci realized that he needed to engage and communicate effectively, noting "how important it was to cultivate relationships with people who are in a position to make things happen." Fauci not only fostered close ties with leaders in academia, industry, and government, including 7 American presidents, but also established himself as an engaging public spokesperson.

Despite these efforts, Fauci navigated criticism, controversy, and outright hostility, especially during the HIV/AIDS and COVID-19 pandemics. With regard to HIV, Fauci effectively managed denial and criticism by engaging decision makers, activists, and the community at large to garner support for HIV research, prevention, and treatment. With the strong backing of President George W. Bush, Fauci was a principal architect for the President's Emergency Plan for AIDS Relief (PEPFAR), on which he reflects with pride that "after more than 20 years, over $100 billion has been spent on the PEPFAR program in more than 50 countries, resulting in the saving of 25 million lives and counting."

In the context of COVID-19, Fauci became a lightning rod for segments of society that distrusted science and the government. Although Fauci acknowledges mistakes made in the COVID-19 response, especially when information was incomplete and evolving, he emphasizes that science is an iterative process. Describing "the spread of egregious misinformation and disinformation enabled by the internet and social media" as "one of the true enemies of public health," Fauci goes on to applaud the efforts put forth in developing highly effective vaccines, noting that "the payoff was that millions of lives were saved."

Fauci concludes by stating that his main motivation for writing his memoir was "to share my experiences with the world and particularly the younger generation…as an example and hopefully an inspiration for some to pursue a life serving others…" The lessons shared in this book undoubtedly provide such inspiration, along with thoughtful, intelligent strategies for combatting ongoing global infectious threats.

Reference

1. National Institute of Allergy and Infectious Diseases. Congressional Justification FY 2023 [cited 2024 Oct 22] https://www.niaid.nih.gov/sites/default/files/fy2023cj.pdf

Dale J. Hu

Author affiliations: US Public Health Service, Bethesda, Maryland, USA (retired); US Centers for Disease Control and Prevention, Atlanta, Georgia, USA (1992–2013); Department of Health and Human Services, Washington, DC, USA, (2013–2015), National Institutes of Health, Bethesda, Maryland (2015–2021)

Email for correspondence: djh9cdc@gmail.com

Unknown artist, *Tomb painting identified as Nebamun Fowling in the Marshes* **fragment (circa 1350 BCE).** Painted plaster, 38.6 in × 38.6 in × 8.7 in/98 cm × 98 cm × 22 cm. © Trustees of the British Museum, London, United Kingdom. Shared under a Creative Commons Attribution-NonCommercial-ShareAlike 4.0 International (CC BY-NC-SA 4.0) license.

Rough Edges, Meticulous Attention

Byron Breedlove

This month's cover features a well-known example of ancient Egyptian tomb art. The tomb walls were first plastered with a thick mixture of mud and straw, followed by a thinner, smooth layer suitable for painting. According to the British Museum, a team of artists created the images, initially sketching outlines for each scene, then adding details, using for pigments a range of natural materials, including soot and various ground stones and minerals. Despite being more than 3,000 years old, the paintings are well-preserved, in measure because of the dry air in the sealed tomb.

This painting, which is known as Nebamun Fowling in the Marshes, is among the artifacts that

antiquities hunters removed from the tomb chapel of Nebamun in 1820.[1] Richard Parkinson, professor of Egyptology and curator with the British Museum, explains that archaeological methods and practices were then quite primitive and the workers who removed the art "probably cut into the plaster surface of the walls with knives and saws, outlining rectangular pieces which they then pried off the walls with implements such as crowbars. Sometimes they removed the full depth of the mud plaster, but sometimes they carried away only a very thin layer, and the edges inevitably suffered cracking and disintegration."

The British Museum, which subsequently acquired many of those artifacts, notes that "The wall paintings from Nebamun's tomb chapel show an idealised vision of daily ancient Egyptian life," and adds that "Nebamun's tomb chapel was a place for people to come and commemorate Nebamun and his wife after his death with prayers and offerings. Nebamun himself was buried somewhere beneath the floor of the innermost room of the tomb chapel in a hidden burial chamber."

Nebamun, the subject of these paintings, has been identified as a wealthy government official who served as an accountant and scribe overseeing the collection and accounting of grain supplies. This marsh hunting scene depicts him standing on a small boat hunting birds, gripping a throw stick on one hand and decoy herons in the other. His young daughter, sitting beneath him on the skiff, is shown clutching his leg. Nebamun's wife, Hatshepsut, dressed in finery, stands behind him. Parkinson wrote that "With his black wig and beaded collar, holding his snake-headed throwing stick, he strikes an athletic, dynamic, almost heroic pose, as master of the whole proceedings."

The marsh teems with wildlife. Fish swim below the part of the waterline that remains intact. An array of startled birds emerging from a thicket of papyrus fills the left side of the panel. Several lotus flowers, considered symbols of rebirth and everlasting life, appear. A tabby cat capturing one bird in its claws and another with its teeth shows that Nebamun is not the only hunter here. The British Museum also notes that the gold leaf gilding on the cat's eye is the only example of such gilding to be found on wall paintings in Theban tomb

chapels. Details, such as finely rendered scales, speckles, feathers, and fins attest to meticulous attention by the artists. The British Museum notes that the painting also includes "remains of eight vertical registers of hieroglyphs" visible on the right half of the panel.

Nebamun's cause of death is not known or suggested by any of the extant rough-edged panels from his tomb. After Giovanni d'Athanasi discovered the tomb in 1820, he kept the tomb's exact location, somewhere on the west bank of the Nile, secret because he wished to protect it from rival antiquities hunters and because of a dispute with Henry Salt, the British Consul General in Egypt who had hired him. What else might remain in the tomb, including clues about Nebamun's cause of death, continues to be a mystery. A recently published meta-analysis by Piers D. Mitchell in Advances in Parasitology examines evidence of parasitic and zoonotic infections found in Egyptian mummies, and considering his research, some of the imagery from this panel could tempt conjecture. For instance, could the prominently featured tabby cat have transmitted toxoplasmosis to Nebamun? Was he possibly infected with malaria transmitted by mosquitos that flourished near the Nile River or schistosomiasis acquired from contaminated fresh water in the marsh? Might he have acquired leishmaniasis after being bitten by infected female sand flies?

Although such questions cannot be answered, the scope and impact of zoonotic infections are well known. According to the Centers for Disease Control and Prevention, "Scientists estimate that more than 6 out of every 10 known infectious diseases in people can be spread from animals, and 3 out of every 4 new or emerging infectious diseases in people come from animals." A number of articles in this issue of Emerging Infectious Diseases document outbreaks and case reports of zoonotic diseases emerging around the world. Applying the same sort of meticulous attention to detail that those ancient artists lavished on Nebamun's tomb paintings is a crucial component of the public health efforts to mitigate such diseases.

Bibliography
1. British Museum. The story of Nebamun's tomb chapel [cited 2024 Oct 25]. https://www.britishmuseum.org/collection/galleries/egyptian-life-and-death#nebamuns-story
2. British Museum. Tomb-painting [cited 2024 Oct 25]. https://www.britishmuseum.org/collection/object/Y_EA37977
3. Centers for Disease Control and Prevention. About zoonotic diseases [cited 2024 Nov 2]. https://www.cdc.gov/one-health/about/about-zoonotic-diseases.html

---

[1]Giovanni d'Athanasi, who discovered Nebanum's tomb, to excavate and remove objects. Parkinson briefly noted how antiquity hunters competed among each other and kept locations of discoveries secret, a practice that has obscured the provenance of these panels and of other items.

4. McCouat P. Lost masterpieces of ancient Egyptian art from the Nebamun tomb-chapel [cited 2024 Oct 28]. https://www.artinsociety.com/lost-masterpieces-of-ancient-egyptian-art-from-the-nebamun-tomb-chapel.html
5. McKie R. Raiders of the lost art [cited 2024 Oct 28]. https://www.theguardian.com/artanddesign/2009/jan/04/british-museum-egyptian-nebamun-tomb
6. Mitchell PD. Parasites in ancient Egypt and Nubia: malaria, schistosomiasis and the pharaohs. Adv Parasitol. 2024;123:23–49. https://doi.org/10.1016/bs.apar.2023.12.003
7. Parkinson R. The painted tomb-chapel of Nebamun. London: The British Museum Press; 2008
8. World Health Organization. Schistosomiasis [cited 2024 Nov 2]. https://www.who.int/news-room/fact-sheets/detail/schistosomiasis

April 2024

High-Consequence Pathogens

EMERGING INFECTIOUS DISEASES®

To revisit the April 2024 issue, go to:

EMERGING INFECTIOUS DISEASES®

Emerging Infectious Diseases **thanks the following reviewers for their support through thoughtful, thorough, and timely reviews in 2024. Please contact us if your name is missing from this list.**

Joseph Abrams
Carly Adams
Laura Adams
Linda Adams
Paul Adamson
Bishwa Adhikari
Susan Adkins
Amos Adler
Cornelia Adlhoch
Yaw Afrane
Abhimanyu Aggarwal
Megha Aggarwal
Elfriede Agyemang
Faruque Ahmed
Andrei Akhmetzhanov
Alexandre Alanio
Cesar Albariño
Bo Albinsson
Afsar Ali
Ibne Ali
Sheikh Ali
Lao-Tzu Allan-Blitz
Valerie Allendorf
Jaffar Al-Tawfiq
Gerardo
   Alvarez-Hernandez
Brian Amman
Yaw Amoako
M. Anderson
Marcos Andre
Jason Andrews
Kristina Angelo
Benjamin Ansa
Joshua Anzinger
Charles Apperson
Matthew Arduino
Mohammad Asadzadeh
Meredith Avalos
Malik Aydin
Andrew Azman
P. Backenson
Oliver Bader
Justin Bahl
Nathan Bahr
Frank Baiden
Madhava Balakrishnan
Valerie Bampoe

Sapna Bamrah
Ananda Bandyopadhyay
Arinjay Banerjee
Gad Baneth
Rémi Barbieri
Galileu Barbosa Costa
Christopher Barker
Timothy Barkham
Aaron Barnes
Terence Barnhart
Ian Barr
Joel Barratt
Roberto Barrera
Alan Barrett
Casey Barton Behravesh
Jason Bartz
Sridhar Basavaraju
Aneesh Basheer
Soumava Basu
Erik Bathoorn
Michael Batz
Wolfgang Baumgaertner
Jenna Bayne
Mariana Baz
Michael Bazaco
Bernard Beall
Ben Beard
Julia Beatty
Jeffery Becasen
Josh Beck
Garrett Beeler Asay
Martin Beer
Cari Beesley
Jessica Belser
Kaitlin Benedict
John Bennett
Shannon Bennett
Béatrice Berçot
Sven Bergstrom
Yohannes Berhane
Justin Berk
Caryn Bern
Kyle Bernstein
Gregory Berry
Stephen Bertke
Jeanne Bertolli
Darlene Bhavnani

Scott Biering
Adam Birkenheuer
Aaron Bivins
Allison Black
Jason Blackburn
Anna Blackstock
David Blair
Romain Blaizot
David Blaney
Lucas Blanton
Amanda Bleichrodt
Bradley Blitvich
Evan Bloch
Jesse Bloom
Emily Bloss
Alexandria Boehm
Sameh Boktor
Daniel N.A. Bolon
Marco Bongiovanni
Denise Bonilla
Manuel Borca
Carles M. Borrego
María Laura Boschiroli
Angela Bosco-Lauth
Danilo Boskovic
Hervé Bourhy
Vincent Bourret
Andrew Bowman
David Boxrud
Ross Boyce
Richard Bradbury
Steven Bradfute
Robert Bradsher
Aaron Brault
Andrew Breed
Matthew Breed
Byron Breedlove
David Brett-Major
Thomas Briese
Melissa Briggs-Hagen
Lauren
   Brinkley-Rubinstein
Kari Brisolara
Sylvain Brisse
Egan Brockhoff
William Brode
Victoria Brookes

John Brooks
Richard Brostrom
Philippe Brouqui
Corrie Brown
Daniel Brown
Ian Brown
Joe Brown
Justin Brown
Josephine Bryant
Laura Bubba
Udo Buchholz
Hannah Bullock
Dora Buonfrate
Antonio
   Riccardo Buonomo
Eric Burrough
Felicity Burt
Jay Butler
Nate Byers
Rafael Calero-Bernal
Ruxandra Calin
Charles Calisher
Sébastien
   Calvignac-Spencer
Emmanuelle Cambau
Jonathon Campbell
Lindsay Campbell
Brian Campfield
Chase Cannon
Avrom Caplan
Yehuda Carmeli
Christine Carrington
Filipe Carvalho Costa
Cristina Casalone
Kenneth Castro
Jordan Cates
Sean Cavany
Catherine Cetre-Sossah
Muge Cevik
Leonor Chacin-Bonilla
Chrispin Chaguza
Henry F. Chambers
Thomas Chambers
Martin Chi-Wai Chan
Howard Chang
Michelle Chang
Hannah Charles

Kelly Charniga
Rémi Charrel
Vishnu Chaturvedi
Liang Chen
Zhuo "Adam" Chen
Qu Cheng
Cedric Chesnais
Harrell Chesson
Preeti Chhabra
Chien-Shun Chiou
Andrew Cho
Bo-Hyun Cho
James Chodosh
Mary Choi
Min Hyuk Choi
Samuel Choice
B. B. Chomel
Terence Chorba
Eric P. Chow
Eric J. Chow
Nancy Chow
Rajib Chowdhury
Gerardo Chowell
Rebecca Christofferson
Daniel Chu
Shimin Chung
Alexander Ciota
Filip Claes
Kristie Clarke
Jean-Michel Claverie
Joshua Clayton
Adam Cohen
Vito Colella
Frances Colles
Sarah Collier
Jennifer Collins
Emilyn Conceicao
FranzJ Conraths
Constantin
 Constantinoiu
Caitlin Contag
Shane Conyers
Ryland Corchis-Scott
Susan Cork
Victor Corman
Hernán Correa
Sofia Cortes
Stephane Corvec
Caitlin Cossaboom
Solenne Costard
Samira Costa-Silva
Alexia Couture
Allen Craig

James Crainey
Adam Crawley
Miria Criado
Caelin Cubenas
Kathryn Curran
Bart Currie
Daniel Czyz
Mara Dacso
Ron Dagan
Clarissa Damaso
David Dance
M. Carolina
 Danovaro-Holliday
Mihaela Dascalu
Nishi Dave
Michael David
Mark Davies
Emily Davis
Bernard Davoust
Patrick Dawson
Marcos de Almeida
Kevin de Cock
Gabrielle
 de Crombrugghe
Brechje de Gier
Bouke de Jong
Steven de Keukeleire
Vanise de Medeiros
Marie de Perio
Dziedzom de Souza
William de Souza
Annabelle de St. Maurice
Nicola Decaro
Pascal Del Giudice
Thomas Deliberto
Zygmunt Dembek
John Dennehy
Peter Deplazes
David Deshazer
Guillaume Desoubeaux
Rita Desousa
Nerlyne Desravines
Amélie Desvars-Larrive
Megan Dewar
Cristina Di Francesco
Barbara Di Martino
Ndongo Dia
Georges Diatta
Maureen Diaz
Tim Dickerson
Seydina Diene
Kai Ding
Tanis Dingle

Michel Drancourt
Jan Drexler
Jan Drobeniuc
Christian Drosten
Jitender Dubey
Jennifer Dubois
Edward Dudley
Jonathan Duffy
Philippe Dufresne
Vivien Dugan
Nisha K. Duggal
Erwin Duizer
Jean-Claude Dujardin
Roger Dumke
John Stephen Dumler
Emily Duncan
Christopher Dunphy
Nicolas Dupin
Alan Dupuis
Lizette Durand
Clare Dykewicz
David Eads
Giulia Earle-Richardson
David Eastlund
Gregory Ebel
Chrissy Eckstrand
Paul H. Edelstein
Chris Edens
Anne Eder
Kathryn M. Edwards
Leslie Edwards
Paul Effler
Lars Eisen
Christopher Elkins
Katherine Ellingson
Sascha Ellington
Ivo Elliott
Marc Eloit
Hanne-Dorthe Emborg
Jacob Ende
Andrea Endimiani
Saron Ephraim
Jonathan Epstein
Lauren Epstein
Dean Erdman
Marina Eremeeva
Roser Escrig
Saber Esmaeili
Juan Carlos Espinosa
Peter Evans
Thomas Fabrizio
Anna Fagre
Klinger Faíco-Filho

Geroncio Fajardo
Joseph Falkinham
Andrea Farnham
Eileen Farnon
Heinz Feldmann
Claire Fellman
Florence Fenollar
Natalia
 Fernandez Borges
Christopher
 Fernandez Prada
Gianmarco Ferrara
Helena Ferreira
Iris Finci
Anthony Fiore
Jay Fishman
Dustin Flannery
Seth Flaxman
Anthony Flores
Anthony Fooks
Laura Ford
Andrea Forde
Taya L. Forde
Brett Forshey
Erik Foster
Ron Fouchier
Pierre-Edouard Fournier
Ashley Fowlkes
Cornel Fraefel
Maria Frank
John Frean
David Freedman
Nigel French
Sagan Friant
Thomas Frieden
Yezhi Fu
Kentaro Fukushima
Kiyoharu Fukushima
James Fuller
Isaac Chun-Hai Fung
Alice Fusaro
Aldo Gaggero
Sebastien Gagneux
Mario Gajdacs
Romeo Galang
John Galgiani
Carmina Gallardo
Danielle Galvin
Hector H. Garcia
Dea Garcia-Hermoso
James Garnett
Joy Gary
Paul Gastanaduy

Yang Ge
Thomas Geisbert
Marike
  Geldenhuys-Venter
Irina Gelmanova
Kathleen Gensheimer
Peter Gerner-Smidt
Antoine Gessain
Ana Gheller
Giovanni Ghielmetti
Susanta Ghosh
Connie Gibas
Laura Giese
Crystal Gigante
Robert Gilmore
Christopher Gilpin
Federica Giorda
Carol Glaser
Sherry Glied
Jeremy Gold
Tony Goldberg
Paul Goldwater
Gabriel Gonzalez
Moisés Gonzálvez
Laura B. Goodman
Uri Gophna
Maria Gori
Lara Gosce
Carolyn Gould
Stephanie Goya
David Graham
Rikki Graham
Jen Granick
William E. Grant
Gregor Grass
Stephen Graves
William Greendyke
Bradford Greening
Justin Greenlee
Luisa Gregori
Alexander Greninger
Daniel Griffin
Patricia Griffin
Charles Grose
Sarah Anne Guagliardo
Milehna Guarido
Jeannette Guarner
Larisa Gubareva
Duane Gubler
Lorenzo Guglielmetti
Alice Guh
Steve Guillouzic
Sarah Gunter

Emily Gurley
Bernardo Gutierrez
Rebecca Guy
Rosa Gynthersen
Dana Haberling
Nicole Hackman
Andrew Haddow
Liesl Hagan
Ferry Hagen
Nicholas Haley
Michael Hall
Eric Halsey
Davidson Hamer
Michelle Hämmerle
Margaret Hammerschlag
Christian Hanson
Josh Hanson
Jennifer Harcourt
Timm Harder
Susan Hariri
Jeffrey Harris
Heli Harvala Simmonds
Ben Hause
Jonathon Heale
Craig Hedberg
Benoit Heid-Picard
Kelley Henderson
Emily Henkle
Ian Hennessee
Timothy Henrich
Benoit Henriet
Meghan Hermance
Brenda Hernandez
David Hewitt
David Heymann
Joseph Hicks
Lauri Hicks
Anke Hildebrandt
Verity Hill
Susan Hills
Alison Hinckley
Takahiro Hiono
Robert Hirt
Matt Hitchings
Wolfgang Hladik
Mengfei Ho
Charlotte Hobbs
Martin Hoenigl
Nicole Hoff
Mike Holbrook
Peter Holloway
Iris Holmes
Tomoyuki Honda

Amanda Honeycutt
Steven Hong
Sarah Hook
Margaret Hosie
Sasan Hosseini
Benjamin Howell
Ana Hoxha
Wenbiao Hu
Xinyi Hua
Randolph Hubach
Katie Hufstetler
Lucas Huggins
Christine Hughes
Holly Hughes
Ralph Huits
David Hunstad
Rezhan Hussein
Christina Hutson
Yuichi Imanaka
Munir Iqbal
Nicholas A. T. Irwin
Kazuhiro Ishikawa
Sadequl Islam
Shamim Islam
Claire Italiano
Masaaki Iwaki
Radosław Izdebski
Arezki Izri
Arnaud Jabet
Alan Jackson
Anne Jackson
Yunho Jang
Marjan Javanbakht
Barbara Javor
Radke Jay
Seonghye Jeon
Kwang Cheol Jeong
Samuel Jeyasingh
Anders Johansson
Daniel Johnson
Nick Johnson
Alyce Jones
Jefferson Jones
Jessica Jones
T. Stephen Jones
Lisa Jones-Engel
Colleen Jonsson
Heesoo Joo
Jaume Jorba
Kathleen Julian
Jessica Justman
Achim Kaasch
Rebekah Kading

Charlene Kahler
Emily Kahn
Masahiro Kajihara
Adriana Kajon
Aley Kalapila
Mary Kamb
Bryan Kaplan
Neera Kapoor
Jacek Karamon
Erik Karlsson
Haru Kato
Louis Katz
Carol A. Kauffman
Ghazi Kayali
Karen Helena Keddy
Eben Kenah
Francis Kengne
Stephen Kennedy
Joan Kenney
Jing Kersey
Asad Khan
Aisha Khatib
Sarah Kidd
Kelly Kilburn
Do Young Kim
Nina Kim
Jason Kindrachuk
Christopher King
Emily Kirby
Russell Kirby
Martyn Kirk
Robert Kirkcaldy
Peter Kirkland
Alexander Kirpich
Stephen Kissler
Tomoya Kitamura
Anne Kjemtrup
Jonas Klingstrom
Marisa Klopper
Keith Klugman
Barbara Knust
Miwako Kobayashi
Gary Kobinger
Marleen Kock
Anson Koehler
Cristian Koepfli
Jules Koffi
Aaron Kofman
Qingzhong Kong
Milena Kordalewska
Mark Kortepeter
Michael Kosoy
Stephanie Kovacs

Nataliia Kovalenko
Barbara Kowalcyk
Colleen Kraft
Peter Krause
Barry N. Kreiswirth
Alexander Kreuter
Jerry Krishnan
Andi Krumbholz
Matthew Kuehnert
Amy Kuenzi
Thijs Kuiken
Suvi Kuivanen
Shu-Chen Kuo
Brenda
   Kwambana-Adams
Yatwah Kwan
Kin On Kwok
Bernard La Scola
Tinja Lääveri
Marcelo Labruna
Sarah Labuda
Alvaro Laga
Jean-Christophe Lagier
Katrien Lagrou
Monica Lahra
Jianyu Lai
Seema Lakdawala
Cristiane Lamas
Amy Lambert
Scott Lambert
Patrick Lammie
Daryl Lamson
Ruiting Lan
Andrew Lang
Jan Langermans
Fanny Lanternier
Pascal Lapierre
Karine Laroucau
Colleen Lau
Eric Lau
Yiu Chung Lau
Douglas Lauffenburger
Kevin Laupland
Adam Lauring
Kirsty Le Doare
Luz Angela Le Van
Tan Le Van
Thuy Le
Fabian Lean
David Lebeaux
John Lednicky
James Leduc
Brian Lee

Dong-Hun Lee
Theodore Lee
Youn-Jeong Lee
John Lees
David Lefebvre
Jessica Leibler
Eva Leidman
Manigandan Lejeune
Jacob Lemieux
Eyal Leshem
Daniel Leung
Kent Lewandrowski
Bryan Lewis
Yuan Li
Yuejin Liang
Chun-Hsing Liao
Laurens Liesenborghs
Anthony Lieu
Marshall Lightowlers
Ajit Limaye
Jiun-Nong Lin
Meng-Yun Lin
Erica Lindroth
Julian Lindsay
Mark Lindsley
W. Ian Lipkin
John LiPuma
Anastasia Litvintseva
Yang Liu
Janice Lo
Shawn Lockhart
Ann Loeffler
Gideon Loevinsohn
Kenneth Long
S. Long
Benjamin Lopman
Natalie Lorent
Jacob Lorenzo-Morales
Stephen Luby
Jay Lucidarme
Martin Ludlow
Ulzii-Orshikh
   Luvsansharav
Patrick Lypaczewski
Miriam Maas
Duncan MacCannell
Kimberly Mace
Ryan Maddox
Nyashadzaishe
   Mafirakureva
Tereza Magalhaes
Shelley Magill
Krisztian Magori

Siddhartha Mahanty
Nicole Maison
Akiko Makino
Richard Malik
Arshpreet Kaur Mallhi
Jennifer Malmberg
Nina Marano
Mona Marin
Mateusz Markowicz
Guy Marks
Adriana Marques
Solene Marquine
Theodore Marras
Jonas Marschall
Rachel Marschang
Fulvio Marsilio
Michael Martin
Valeria Paula Martinez
Jaime Martinez-Urtaza
Sandra Regina
   Maruyama
Grace E. Marx
Nazish Masud
Thomas Mather
Blaine Mathison
Larissa Matos
Wasin Matsee
Yasufumi Matsumura
Matthew Mauldin
Anthony Maurelli
Max Maurin
Carla Mavian
Maurizio Mazzei
Denise McAloose
William McBride
Andrea McCollum
Zachary McCormic
David McCormick
Robert McDonald
Anita McElroy
Peter McElroy
Juan McEwen
Lesley McGee
David McGovern
Gerald McGwin
Debbie McKenzie
Heather McLaughlin
Brendan McMullan
Lucy McNamara
Tristan McPherson
Jennifer McQuiston
John McQuiston
Samir Mechai

Oleg Mediannikov
Jennifer Meece
Martin Meltzer
Nicole Mendell
Thangam Menon
Dick Menzies
Nicolas Menzies
Kirsten Mertz
Raphaëlle Métras
Ella Meumann
Abhishek Mewara
Patrick Meyer Sauteur
Claire Midgley
Nkuchia M'ikanatha
Malgorzata Mikulska
Michele Miller
Mathieu Million
Faisal Minhaj
Francesco Mira
Julia Miranda
Ali Mirazimi
Mautusi Mitra
Kenji Mizumoto
Abdinoor Mohamed
Noelle-Angelique
   Molinari
Abelardo Moncayo
Dinesh Mondal
Isabella Monne
Joel Montgomery
Julia Moody
Patrick Moonan
Susan Moore
Eric Mooring
Rodrigo Morales
Maria Morales-Betoulle
Jacob Moran-Gilad
Konosuke Morimoto
J. Glenn Morris
Amy Morrison
Tem Morrison
Marinda Mortlock
Eric Mossel
Heba Mostafa
Vladimir Motin
Alexandra Moura
Barbara Mühlemann
Brendan Mullen
Ananda Müller
Marcel Müller
Vincent Munster
Shin Murakami
David Murdoch

Edward L. Murphy
Trudy Murphy
Gemma Murray
Kristy Murray
Nedzad Music
Joseph Myers
Maria Nagel
So Nakagawa
Satosi Nakano
Hannah Nam
Subhi Nandakumar
Ranjan Nandy
Pontus Naucler
Felipe Naveca
Anoma Nellore
Eric Nelson
Ciara Nestor
Gabriele Neumann
Katherine Newell
Laura Newman
Paul Newton
Johan Neyts
Terry Fei Fan Ng
Popchai
  Ngamskulrungroj
Hai Nguyen-Tran
Emanuele Nicastri
Tracy A. Nichols
Ainsley Nicholson
Christina Nielsen
Kirsten Nielsen
Eric Nilles
Eric Niqueux
Hidekazu Niwa
Romolo Nonno
Norbert Nowotny
Patrick Obermeier
Carolyn O'Brien
Kevin O'Callaghan
Eric Ochomo
David O'Connor
Max O'Donnell
Clarissa Oeser
Norio Ohmagari
Tochi Okwor
Liset Olarte
Tricia Oliveira
Sonja Olsen
Enoma Omoregie
Ryosuke Omori
Clayton Onyango
Samuel Opoku
Francesco Origgi

Lucia Ortiz
Stephen Ostroff
José A. Oteo
Domenico Otranto
Nao Otsuka
Kevin Outterson
Christopher Overton
Hannah Padda
Christopher Paddock
Slobodan Paessler
Gustavo Palacios
Prasit Palittapongarnpim
Mitchell Palmer
Alberto Paniz Mondolfi
Nivedha Panneer
Daniela Paolotti
Costas Papagiannitsis
Igor Paploski
John Papp
Sarah Park
Lindsay Parnell
Colin Parrish
W. Clyde Partin
Sally Partridge
Daniel Pastula
Monica Patton
Prabasaj Paul
Jean-Michel Pawlotsky
Gabriela Paz-Bailey
David Pegues
Sen Pei
Gisele Peirano
Malik Peiris
Andrew Pekosz
Andrew Peregrine
Marcus Pereira
Ranawaka Perera
Daniel Perez
Carlos Perez-Velez
Kiran Perkins
Lívia Perles
Stanley Perlman
Julia Pescarini
Ted Pestorius
Barbara Petersen
Christine Petersen
Jeannine Petersen
Karin Peterson
Brittany Petros
Klara Petrzelkova
Martin Pfeffer
Pearl Philip
Anne Piantadosi

Brad Pickering
Emily Pieracci
Jamison Pike
Kelsey Pilewski
Allan Pillay
Nils Pilotte
Benjamin Pinsky
Johann Pitout
Alberto Piubello
Nottasorn Plipat
Ian Plumb
Veronica Poggio
Jason M. Pogue
Anne Pohlmann
Stefan Pöhlmann
Laurent Poirel
Maciej Polak
Drew Posey
Jeffrey Post
Stephanie Pouch
Keith Poulsen
Ann Powers
John Powers
Pravata Pradhan
Wolfgang Preiser
D. Rebecca Prevots
Bobbi S. Pritt
Diann Prosser
Christine Prue
Joanna Pulit-Penaloza
Mirja Puolakkainen
Michael Purdy
Wendy Puryear
Wenbao Qi
Flávio Queiroz-Telles
Peter Rabinowitz
Brent Race
Sumathi Ramachandran
Aditya Ramadona
Andrew Ramey
Didier Raoult
Sonja A. Rasmussen
Heather Reese
Andrew Reeves
Scott Reid
Sharon Reisfeld
Mary Reynolds
Guilherme Ribeiro
Stephen Rich
Gabriele Richardson
Martin Heinrich Richter
Erin Ricketts
Mark S. Riddle

Alison Ridpath
Agustina Rimondi
Alice Risely
Jana Ritter
Antonio Rivero-Juarez
Caitlin Rivers
Annapaola Rizzoli
Suelee
  Robbe-Austerman
Jeffrey Roberts
Sarah Robinson
Ilia Rochlin
Daniel Rockey
Roxana Rodriguez
Sergio Rodriguez
Paulo Roehe
Dawn Roellig
P. David Rogers
Adelaide Roguet
Alicia Rojas
Pierre Rollin
Daniel Romero-Álvarez
Antonio Rosales-Castillo
Elena Cecilia Rosca
Stacey Rose
Eli Rosenberg
Benjamin Rosenthal
John Ross
Shannan Rossi
Paul Rota
Raymond Rowland
James Rudge
Maria Cristina Rulli
Jonathan Runstadler
Stephen Ruoss
Kay Russo
Thomas Russo
Daniel Ruzek
Gerard Ryan
Sadie Ryan
Jeffrey Rybak
Sukhyun Ryu
Gilberto Sabino-Santos
Ryuichi Sada
Farzin Sadeghi
David Safronetz
Masayuki Saijo
Prasanta Saini
Yoshihiro Sakoda
Enrique Saldarriaga
Johanna Salzer
Jeanne Samake
Alexandra Sanchez

Liliana Sanchez-Gonzalez
Sokani Sánchez-Montes
Maria Paz Sanchez-Seco
John Sanders
Justin Sanders
Sarah Sansom
Brock Santi
Gilberto Santiago
Monica Santin
Amanda Santos
Huarrisson Santos
Sarah Sapp
Derek Sarovich
Delight Satter
Paul Saunderson
Amy Saupe
Sharon Saydah
Elaine Scallan Walter
Maria Scaturro
Ilana Schafer
Elizabeth Schiffman
Jonas Schmidt-Chanasit
Tony Schountz
Peter Schreiber
Caroline Schrodt
Krysten Schuler
David Schwartz
Ilan Schwartz
David Scollard
Isaac See
James Sejvar
Zuzana Sekeyova
Tara Sell
Teri Senn
Nuno Sepúlveda
Joe Sexton
Soufien Sghaier
Giovanni Sgroi
Sean Shadomy
Ami Shah
Marc Shamier
Andi Shane
Tyler Sharp
Kirill Sharshov
Frederic Shaw
Jessica Sherman
Kayoko Shioda
Paul Sigala
Rachel Silva
Frédy Brice Simo Nemg
Gaelle Simon
Les Sims
Nagendra Singanallur

Brajendra (Braj) Singh
Om Singh
Alyson Singleton
Gilman Kit Hang Siu
Beth Skaggs
Kurt Sladky
Jan Slapeta
Jonathan Sleeman
Larry Slutsker
Dallas Smith
Hunter Smith
Jessica Smith
Todd Smith
Eveline Snelders
Jumari Snyman
Louwrens Snyman
Benjamin Sobkowiak
Vanete Soccol
Heidi Soeters
Woon-Mok Sohn
Lola Solebo
Isaac Solomon
Michal Solomon
Gail Sondermeyer
    Cooksey
Mark Sonderup
Ying Song
Lynn Sosa
Massimo Spedicato
Barbara Spellerberg
Jessica R. Spengler
Christina Spiropoulou
Jessica Spring
Kirsten St. George
David Stallknecht
Claire Standley
Manuela Staneva
Anne Stangl
J. Staples
James Stark
Leith States
Arjan Stegeman
Eike Steinmann
Christen Stensvold
David Stephens
Brian Stevenson
Guppy Stott
Jason Stout
Anne Straily
Tomas Strandin
Marc Strassburg
Franc Strle
Jason Stull

Kanta Subbarao
David Sugerman
Rebekah Sutter
Melissa Sutton
Troy Sutton
Annika Sweetland
Brett Swierczewski
Christine Szablewski
Fikadu Tafesse
Don Bambino Geno Tai
Shigeru Tajima
Saki Takahashi
Emi Takashita
Makoto Takeda
Howard Takiff
Carolina Talhari
Kathrine Tan
Arthur Tang
Phillip Tarr
Thuy-Huong Ta-Tang
Jacqueline Tate
Ahmad Tavakoli
Christopher Taylor
Pete D. Teel
Marcio Teixeira Nunes
Sam Telford
Glenn Telling
Nigel Temperton
Janjira Thaipadungpanit
Harsh Thaker
Saravanan Thangamani
Grant Theron
Beth Thielen
Fabiano Thompson
Peter Thompson
Sharmi Thor
Bruce Thorley
Natalie Thornburg
Julie Thwing
Simon Tiberi
Boghuma Titanji
Paolo Tizzani
James Tobias
Farrell Tobolowsky
Mitsuru Toda
Rafael Toledo
Mahmoud Torabi
Noel Tordo
Gabriela Torrea
Alfredo Torres
A. Tortorano
Vi Tran Thuy
David Tribble

Richard Truman
Raymond Tsang
Jean Tsao
Sarah Tschudin-Sutter
Clement Tsui
Thomas Tu
Wei Tu
Kenneth Tyler
Gregory Tyrrell
Elizabeth Unger
Juliette Unwin
David Ussery
Ronald Valdiserri
M. A. Valero
Steven van Borm
Kate van Brussel
Tjip van der Werf
H. Rogier van Doorn
N. M. van Sorge
Ralph Vanstreels
Andrea S. Varela-Stokes
Gilberto Vaughan
Everardo Vega
Paschalis Vergidis
Guilherme Verocai
Juan Vesga
Winston Vickers
Carlos Villa
Lorenzo Villa-Zapata
Mark Viney
Chantal Vogels
Michael von Fricken
Neil Vora
Duc Vugia
Jesse Waggoner
David Wagner
Milton Wainberg
Samantha Wales
David Walker
Ryan Wallace
Gabriel Wallau
Dayan Wang
Leyi Wang
Lin-Fa Wang
Thomas Ward
Gamal Wareth
Matthew Watts
Scott Weaver
Richard Webby
J. Todd Weber
Stefan Weber
Scott Weese
Michael Weigand

EMERGING INFECTIOUS DISEASES®

Upcoming Issue • Antimicrobial Resistance

- Cluster of Legionellosis Cases Associated with Manufacturing Process, South Carolina, USA, 2022

- *Rickettsia sibirica mongolitimonae* Infections in Spain and Case Review of the Literature

- Ongoing Evolution of Middle East Respiratory Syndrome Coronavirus, Saudi Arabia, 2023–2024

- Social Contact Patterns and Age-Mixing before and during COVID-19 Pandemic, Greece, January 2020–October 2021

- Novel *Trichuris incognita* with Low Albendazole/Ivermectin Sensitivity Identified through Fecal DNA Metabarcoding of Patient Samples from Côte d'Ivoire

- Case Reports of Human Monkeypox Virus Infections in Uganda, 2024

- Detection and Genomic Characterization of Novel Mammarenavirus in European Hedgehogs, Italy

- Influenza A(H5N1) Virus Clade 2.3.2.1a in Traveler Returning to Australia from India, 2024

- Equine Encephalomyelitis Outbreak, Uruguay, 2023–2024

- Cocirculation of 4 Dengue Virus Serotypes, Putumayo Amazon Basin, 2023–2024

- Low IgG Seroconversion among Persons Vaccinated against Measles, Republic of the Congo

- Fatal Mixed *Plasmodium* Infection in Traveler Returning to Colombia from Comoros Islands, 2024

- Identification and Characterization of Vancomycin-Resistant *Staphylococcus aureus* CC45/USA600, North Carolina, USA, 2021

- Evidence of H5N1 Influenza Spillover Infections in Horses, Mongolia

- Spread of Antifungal-Resistant *Trichophyton indotineae*, United Kingdom, 2017–2024

- Research and Development of Medical Countermeasures for Emerging Infectious Diseases, China

- Fatal Case of Crimean-Congo Hemorrhagic Fever, Portugal, 2024

Complete list of articles in the January issue at
https://wwwnc.cdc.gov/eid/#issue-317

Earning CME Credit

To obtain credit, you should first read the journal article. After reading the article, you should be able to answer the following, related, multiple-choice questions. To complete the questions (with a minimum 75% passing score) and earn continuing medical education (CME) credit, please go to http://www.medscape.org/journal/eid. Credit cannot be obtained for tests completed on paper, although you may use the worksheet below to keep a record of your answers.

You must be a registered user on http://www.medscape.org. If you are not registered on http://www.medscape.org, please click on the "Register" link on the right hand side of the website.

Only one answer is correct for each question. Once you successfully answer all post-test questions, you will be able to view and/or print your certificate. For questions regarding this activity, contact the accredited provider, CME@medscape.net. For technical assistance, contact CME@medscape.net. American Medical Association's Physician's Recognition Award (AMA PRA) credits are accepted in the US as evidence of participation in CME activities. For further information on this award, please go to https://www.ama-assn.org. The AMA has determined that physicians not licensed in the US who participate in this CME activity are eligible for *AMA PRA Category 1 Credits™*. Through agreements that the AMA has made with agencies in some countries, AMA PRA credit may be acceptable as evidence of participation in CME activities. If you are not licensed in the US, please complete the questions online, print the AMA PRA CME credit certificate, and present it to your national medical association for review.

Article Title
Ophthalmic Sequelae of Ebola Virus Disease in Survivors, Sierra Leone

CME Questions

1. What percentage of Ebola virus disease (EVD) survivors in the current study had ophthalmic findings on examination?

A. 12%
B. 34%
C. 51%
D. 71%

2. What was the most common ophthalmic finding among survivors of EVD in the current study?

A. Uveitis
B. Dry eyes
C. Chorioretinal scar
D. Cataract

3. All the following clinical variables were associated with a higher rate of uveitis among survivors of EVD in the current study except

A. Higher number of days treated in the Ebola treatment unit
B. Female sex
C. Older age
D. Having a previous history of cataracts

4. Which of the following concomitant ophthalmic findings was most associated with a higher rate of uveitis in the current study?

A. Cataract
B. Corneal scar
C. Chorioretinal scar
D. Optic neuropathy

2024
CDC YELLOW BOOK

Health Information for International Travel

CS 330909-P

Launch of CDC Yellow Book 2024 – A Trusted Travel Medicine Resource

CDC is pleased to announce the launch of the CDC Yellow Book 2024. The CDC Yellow Book is a source of the U.S. Government's recommendations on travel medicine and has been a trusted resource among the travel medicine community for over 50 years. Healthcare professionals can use the print and digital versions to find the most up-to-date travel medicine information to better serve their patients' healthcare needs.

The CDC Yellow Book is available in print through Oxford University Press and online at www.cdc.gov/yellowbook.